UNIVERSITE DE STRASBOURG

Ecole Doctorale des Sciences de la Vie et de la Santé

THESE

présentée pour obtenir le grade de

Docteur de l'Université de Strasbourg

Discipline : Sciences du Vivant

Domaine : Aspects Moléculaires et Cellulaires de la Biologie

par

Volodymyr SHVADCHAK

SONDES FLUORESCENTES A EMISSION DUALE POUR LA CARACTERISATION D'INTERACTIONS IMPLIQUANT DES PROTEINES: APPLICATION AUX PROTEINES RETROVIRALES

Soutenue le 20 avril 2009 devant la commission d'examen :

Dr. Eric DEPREZ	**Rapporteur externe**
Pr. Ludovic JULLIEN	**Rapporteur externe**
Dr. Sylviane MULLER	**Rapporteur interne**
Pr.Vasyl PIVOVARENKO	**Examinateur**
Pr. Yves MELY	**Directiur de thèse**
Dr. Hugues de ROCQUIGNY	**Co-Directeur de thèse**

CONTENTS

ABBREVIATIONS

3HC	3-Hydroxychromone
3HF	3-Hydroxyflavone
3HQ	3-Hydroxyquinolone
Ch	Cholesterol
DLS	Dynamic Light Scattering
DMF	Dimethyl formamide
DMSO	Dimethyl sulfoxid
DOPC	Dioleoylphosphatidylcholine
DOPG	Dioleoylphosphoglycerol
DOPS	Dioleoylphosphatidylserine
DPPC	Dipalmitoylphosphatidylcholine
ESIPT	Excited State Intramolecular Proton Transfer
LUV	Large Unilamellar Vesicles
MLV	Multilamellar Vesicles
N*	Normal form
NMP	N-methylpyrrolidone
SM	Sphingomyelin
SPPS	Solid Phase Peptide Synthesis
T*	Tautomer form
TFA	Trifluoroacetic acid
THF	Tetrahydrofuran
λ_{abs}	Position of absorbtion maximum
λ_{ex}	Excitation wavelength
λ_{em}	Emission wavelength
λ_{N^*}	N* form emission maximum
λ_{T^*}	T* form emission maximum
N*/T*	Intensity ratio of the N* and T* forms

1. BIBLIOGRAPHICAL REVIEW

1.1. Principles of fluorescence spectroscopy and protein labeling

1.1.1. Advantages of fluorescence

The wide applications of fluorescence techniques in biological studies are related to its three major advantages over other investigation methods:

- **Sensitivity.** Detection of single molecules is possible with proper dye selection and experimental conditions. Whereas absorbance measurements can reliably be used at concentrations down to several tenths of micromole, fluorescence techniques can currently be used at picomolar concentrations- and even femtomolar for up-to-date developments.
- **High speed of response**. Using fluorescence, it is possible to monitor very rapid processes, since the response is limited only by the fluorescence lifetime within the range 10^{-8}–10^{-10} s.
- **Non-destructive character** Due to its non-invasive character, the sample is not destroyed. Thus, fluorescence can be used in living cells and tissues with limited adverse effects.

As a consequence, fluorescence appeared as a versatile tool for a large range of applications, as for instance:

— binding of ligands to biomolecules, including *in vivo*

— measurement of distances within macromolecules and biological assemblies

— study of the dynamics of proteins folding

— measurement of ion concentrations inside living cells

— study of membrane structure and function

— cell imaging

Fluorescence is a powerful tool for studying molecular interactions in analytical chemistry, biochemistry, cell biology, physiology, photochemistry, environmental science…

1.1.2. Fluorescence principles

Fluorescence belongs to the general photophysical phenomenon called luminescence, which corresponds to the emission of light from electronically excited states of atoms and molecules. Concerning molecules two types of luminescence can be considered depending on the nature of their excited state. If the emission occurs from the singlet excited state, the process is called *fluorescence*. The emission rates of fluorescence are typically about 10^8-10^9 s^{-1}. If the emission occurs from the triplet excited state, the process is called *phosphorescence*. In this case, transitions to the ground state are forbidden and the emission rates are slow, about 10^6-$10\ s^{-1}$.

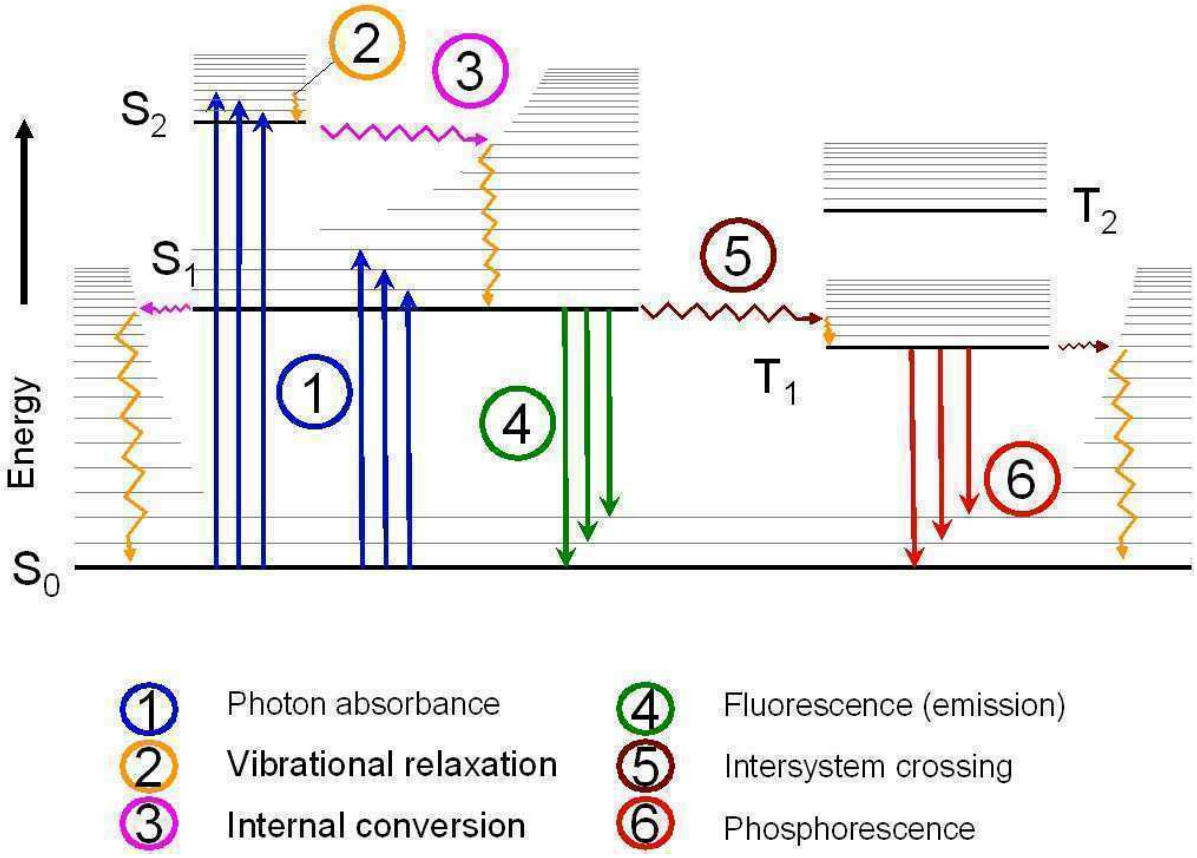

Figure 1.1. Jablonski diagram.

Fluorescence occurs in a limited number of molecules (generally polyaromatic hydrocarbons or heterocycles) called fluorophores or fluorescent dyes. A fluorescent probe is a fluorophore designed to localize within a specific region of a biological specimen and/or to respond to a specific stimulus. The process responsible for fluorescence is illustrated by the Jablonski diagram (**Fig. 1.1**). Three main steps are important in the fluorescence process [1].

Step 1 Excitation

A photon of energy $h\nu_{ex}$ supplied by an external source such as a lamp or a laser is absorbed by the fluorophore, creating an excited electronic singlet state (S_n). This process distinguishes fluorescence from other types of luminescence like radioluminescence, electroluminescence, thermoluminescence, chemiluminescence, bioluminescence, triboluminescence and sonoluminescence in which the excited state is induced by an ionizing radiation (X-ray, α, β, γ), electric field, heating, chemical reaction, biological process, electrostatic forces and ultrasounds, respectively.

Step 2 Non-radiative relaxation

The fluorophore is typically excited to one of the excited vibrational states of the first electronic singlet state (S_1). The excess of vibrational energy is rapidly transferred to the solvent, through collisions with the solvent molecules. This nonradiative process is called vibrational relaxation and occurs in the sub-picosecond range. If the fluorophore is excited to the second electronic singlet state (S_2), it rapidly falls down to the S_1 state due to internal conversion that corresponds to a non-radiative transition between two electronic states of the same spin multiplicity. From S_1, internal conversion to S_0 is also possible but is less efficient than conversion from S_2 to S_1, due to the much larger energy gap between S_1 and S_0. Therefore, internal conversion from S_1 to S_0 can compete with emission of photons (fluorescence, see below).

Intersystem crossing is another non-radiative transition that occurs between two isoenergetic vibrational levels belonging to electronic states of different multiplicities. Thus, an excited molecule in the lowest vibrational level of the S_1 state can move to the isoenergetic vibrational level of the T_1 triplet state; then vibrational relaxation brings it to the lowest vibrational level of T_1. It is important to mention that according to the selection rules of quantum mechanics, the crossing between two states with different multiplicities is forbidden. However, due to spin-orbital coupling between the orbital magnetic moment and the spin magnetic moment, such crossing can take place.

Other processes such as collisional quenching and fluorescence resonance energy transfer (FRET) may also depopulate S_1 and thus, together with internal conversion and intersystem crossing, compete with fluorescence.

Step 3 Fluorescence Emission

Fluorescence emission is a radiative process in which a photon of energy $h\nu_{em}$ is emitted, with the fluorophore going back to its ground state S_0. As a consequence of the energy loss due to vibrational relaxation during the excited-state lifetime, the energy of the photon of fluorescence is lower, and therefore of longer wavelengths, than the excitation photon. The difference in energy or wavelength represented by ($h\nu_{ex} - h\nu_{em}$) is called the Stokes shift. The Stokes shift is an important parameter for the sensitivity of fluorescence techniques because it allows detecting emission photons with a low background, as they are easily discriminated from the excitation photons. In contrast, absorption spectrometry requires the measurement of transmitted light relative to high incident light levels at the same wavelength. An important characteristic of fluorescence is the fluorescence quantum yield, which is the ratio of the number of fluorescence photons emitted to the number of photons absorbed.

A) Fluorescence Spectra

Unless an irreversible reaction such as photobleaching occurs, the same fluorophore can repeatedly emit photons under constant illumination. The fact that a single fluorophore can generate a large amount of photons is of main importance for the high sensitivity of fluorescence detection techniques. For polyatomic molecules in solution, the discrete electronic transitions represented by $h\nu_{ex}$ and $h\nu_{em}$ are replaced by rather broad energy spectra called fluorescence excitation spectrum and fluorescence emission spectrum, respectively. The bandwidths of these spectra are important parameters for applications in which two or more different fluorophores are simultaneously detected. With only a few exceptions, the fluorescence excitation spectrum of a single fluorophore species in dilute solution is identical to its absorption spectrum. Under the same conditions, the fluorescence emission spectrum is nearly independent of the excitation wavelength, due to the partial dissipation of excitation energy during the excited-state lifetime (**Fig. 1.1**).

B) Lifetimes and quantum yields

The processes that lead to the deactivation of the S_1 excited state of a fluorophore are usually characterized by their rate constants. Thus, k^S_r is the rate constant for the radiative deactivation of S_1 to S_0 with emission of fluorescence; k^S_{ic} is the rate constant of internal conversion from S_1 to S_0 and k_{isc} is the rate constant of intersystem crossing from S_1 to T_1 state. The general non-radiative constant can thus be presented as: $k^S_{nr} = k^S_{ic} + k_{isc}$

If intermolecular interactions are not taken into account, the rate of disappearance of the excited molecules M* from the excited state S_1 (that appeared from M after very short pulses of light) can be expressed by:

$$-dM^*/dt = (k_r^s + k_{nr}^s)M^* \quad (1)$$

Integration of this equation yields the time evolution of the concentration of excited molecules M*. Assuming that M^*_0 is the concentration of excited molecules at time 0 resulting from pulse light excitation then, integration of 1 leads to:

$$M^* = M_0^* \times \exp(-t/\tau_s) \quad (2)$$

where τ_s is the lifetime of the excited state S_1 given by:

$$\tau_s = 1/(k_r^s + k_{nr}^s) \quad (3)$$

The fluorescence intensity is defined as the amount of photons (in mol) emitted per unit time (s) and per unit volume of solution (liter: L). At time t after excitation by a very short pulse of light, the fluorescence intensity i_F is proportional to the instantaneous concentration of molecules still excited:

$$i_F(t) = k_r^s \times M^* = k_r^s \times M_0^* \times \exp(-t/\tau_s) \quad (4)$$

The fluorescence quantum yield φ is the fraction of excited molecules that returns to the ground state S_0 with emission of fluorescence photons:

$$\varphi = k_r^s/(k_r^s + k_{nr}^s) \quad (5)$$

C) Solvent relaxation

The fluorescence process described above does not take into consideration the influence of the solvent that can strongly modify the fluorescence of the fluorophore. Solvent effects shift the emission to still lower energies owing to the stabilization of the excited state by the solvent molecules. Typically, the fluorophore shows a larger dipole moment in the excited state (μ_e) than in the ground state (μ_g) due to a photoinduced charge transfer (PCT). Following excitation, the solvent dipoles can reorient or relax around μ_e, which lowers the energy of the excited state thus leading to a relaxation called solvent relaxation (**Fig. 1.2**). This effect becomes larger with increasing solvent polarity, resulting in emission at lower energies or longer wavelengths. In general, only fluorophores that have high dipole moment in the ground or excited state display a large sensitivity to solvent polarity. Apolar molecules, such as unsubstituted aromatic hydrocarbons, are much less sensitive.

It is important to note that the rate of solvent relaxation depends on the solvent viscosity. If the time required for the reorganization of solvent molecules around the solute is short with respect to the excited-state lifetime, fluorescence will essentially be emitted from molecules in equilibrium with their solvation shell. After emission, the solute recovers its ground state dipole moment and a new relaxation process restores the stable initial configuration of the solute–solvent system in the ground state.

In contrast, if the medium is too viscous to allow solvent molecules to reorganize, emission will not be affected by solvent and no shift of the fluorescence spectrum will be observed. Finally, if the solvent reorganization time is of the order of the excited-state lifetime, the first emitted photons will correspond to wavelengths shorter than those emitted at longer times. In this case, the fluorescence spectrum observed under continuous illumination will be shifted but the position of the maximum cannot be directly related to the solvent polarity.

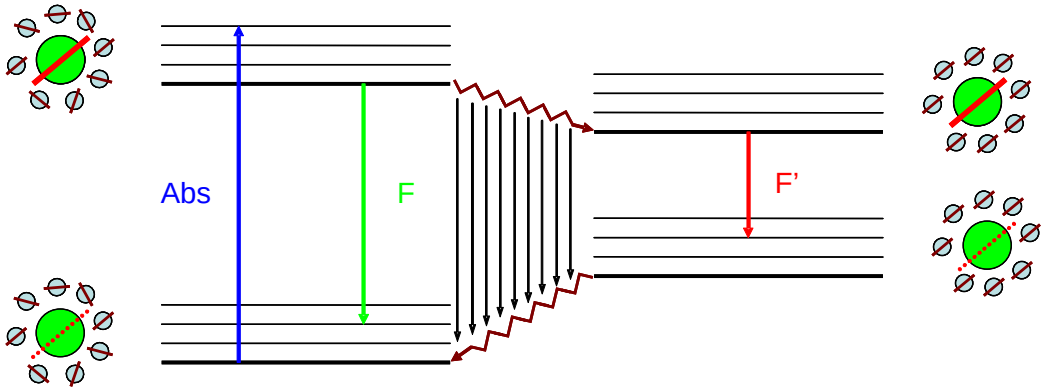

Figure 1.2. Solvent relaxation around a probe with a small dipole moment in its ground state and a large dipole moment in its excited state.

In the description of general solvent effects, the fluorophore is considered to be a dipole in a continuous medium of uniform dielectric constant. The interactions between the solvent and fluorophore affect the energy difference between the ground and the excited state. To a first approximation, this energy difference is a property of the refractive index (n) and dielectric constant (ε) of the solvent and is described by the Lippert-Mataga equation:

$$\bar{\nu}_a - \bar{\nu}_f = \frac{2}{hc}(\mu_e - \mu_g)^2 a^{-3} \Delta f + const \quad (6)$$

where h is the Planck's constant, c is the velocity of light, a is the radius of the cavity in which the solute resides, *const* is a constant taking into account the non-radiative relaxation and Δf is the orientation polarizability defined as:

$$\Delta f = f(\varepsilon) - f(n^2) = \frac{\varepsilon - 1}{2\varepsilon + 1} - \frac{n^2 + 1}{2n^2 + 1} \quad (7)$$

Specific solvent-fluorophore interactions produce deviations from the theory.

D) Excited-state reactions

An excited-state reaction can be defined as a molecular process which occurs subsequent to excitation and which changes the structure of the excited-state fluorophore [1]. Such reactions occur because light absorption frequently changes the electron distribution within a fluorophore, which in turn changes its chemical or physical properties. An example of excited-state reaction is that of phenol, which in neutral solution can loose its phenolic proton in the excited state. Deprotonation occurs more readily in the excited state because the electrons on the phenolic hydroxyl groups are shifted to the phenol ring, making this hydroxyl group more acidic.

Another example of excited-state reaction is the aforementioned photoinduced charge transfer (PCT) that found a large range of applications in the construction of polarity sensitive fluorophores including labels for proteins. Among the well-known polarity sensitive probes are ANS (1-anilino-8-naphthalene sulfonate), TNS (p-toluidinyl-6-naphthalene sulfonate), Prodan (6-propionyl-2-dimethylaminonaphthalene) and theirs derivatives. More detail about them and their applications will be discussed in following chapters.

Excimer and exciplex formation can also be considered as excited-state reactions, as for example pyrene excimer formation, or 2-phenylindole and anthracene exciplexes through interaction with dimethylaniline. Intramolecular charge transfer (ICT) and twisted intramolecular charge transfer (TICT) accompanied with internal rotation are other examples of excited-state reactions that found numerous applications in the design of viscosity sensitive fluorescent probes (molecular rotors). Examples of molecular rotors are DMABN (p-N,N-dimethylamino-benzylidenemalononitrile) and its analogues.

Finally, an interesting example of excited-state reaction is the excited state intramolecular proton transfer (ESIPT) reaction. This ESIPT reaction is on the basis of the probes used in this PhD work. Its characteristics and applications will be developed in the following chapters.

1.1.3. Fluorescent labels for proteins

Fluorescent labels are common tools in protein science. Many organic dyes have been used to label proteins in order to investigate their dynamics, conformational changes and interactions. The selection of the label and the peculiar fluorescence technique depends entirely on the system and problem under study. Here, we will highlight only the most important examples of chromophores and their applications.

A) Intrinsic chromophores

The first fluorescent protein "labels" are the intrinsic chromophores constituted by the aromatic amino acids: tryptophan (Trp), tyrosine (Tyr) and phenylalanine (Phe), (**Fig. 1.3**). The indole group of the Trp residue is the dominant chromophore responsible for UV absorbance and emission in proteins. In native proteins, the emission of Tyr is often quenched due to its interaction with the peptide chain or to energy transfer to Trp. Denaturation of proteins frequently results in an increased Tyr emission. Emission from Phe is observed only when the sample protein lacks both Tyr and Trp residues, which is a rare occurrence.

The main advantage of Trp label is that it is constitutively present in the native protein. Thus, in contrast to extrinsic chromophores, there is no concern with the degree of labeling, as well as with the proper folding and the activity of the protein. In addition, the emission of Trp is highly sensitive to its local environment. For this reason, it is often used as for monitoring protein conformational changes. Spectral shifts have been observed as a result of several phenomena, such as binding of ligands and in some cases, in protein-protein interactions. However, the presence of more than one Trp in the system complicates the interpretation of steady-state data. In this case, time-resolved spectroscopy and (time-resolved) anisotropy are widely used [1].

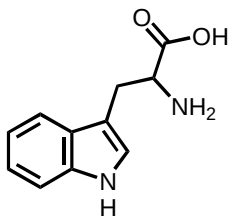

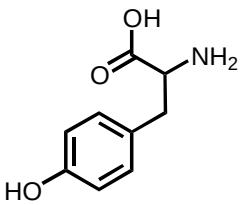

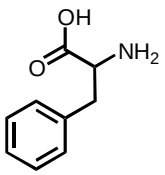

	Tryptophan (Trp, **W**)	Tyrosine (Tyr, **Y**)	Phenylalanine (Phe, **F**)
λ_{ex}/ε	295 nm / 5700 $M^{-1}cm^{-1}$	275 nm / 1400 $M^{-1}cm^{-1}$	260 nm / 195 $M^{-1}cm^{-1}$
λ_{em} /QY	350 nm / 0.13	304 nm / 0.14	282 nm / 0.02
τ	3 ns	3-4 ns	7 ns

Figure 1.3. Natural fluorescent amino acids. λ_{ex}, λ_{em} , ε, QY and τ are typical absorbtion and emission maxima, extinction coefficients, fluorescence quantum yields and lifetimes respectively.

Among the main limitations of the natural fluorescent amino acids, including Trp, are their UV-range absorption, and their rather small absorption coefficient. In addition, the complex photophysics of Trp often impairs the interpretation of the fluorescence data [1]. Moreover, proteins usually contain more than one Trp residue, making it difficult (if not impossible) to assign changes in the fluorescence signal to a particular site and interpret spectral changes that result from intermolecular protein–ligand association [2]. To overcome these problems, two approaches were applied. The first one consists in removing Trp residues by site-directed mutagenesis, to reduce the complexity of the signal. The second approach consists in the biosynthetic substitution of Trp by Trp analogs. Among the non-coded Trp analogues studied so far, the most representative are 7-azatryptophan (7AW), 5-hydroxytryptophan (5HW) and 4-fluorotryptophans (4FW) (**Fig. 1.4**).

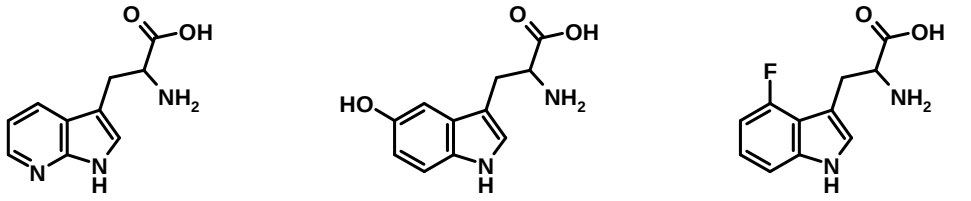

7-azatryptophan (7AW) **5-hydroxytryptophan (5HW)** **4-fluorotryptophan (6FW)**

Figure 1.4. Most representative analogues of tryptophan.

These analogues display absorption and fluorescence properties that are red-shifted in respect with the Trp ones. These analogues have been used to study ligand recognition and protein conformational changes [3]. Nevertheless, their absorption and emission are still in the UV range, and site-selective substitution of natural aminoacids by these Trp analogues is limited to peptides.

B) GFP and other Fluorescent Proteins

In 1964 a natural green fluorescent protein (later called GFP) was isolated from jellyfish. This protein undergoes a post-synthetic modification that leads to the formation of a chromophore. The addition of the GFP coding nucleic acid sequence to the one of the target protein allows the expression of this protein with a GFP fluorescent tag.

One of the most important advantages of such an approach is the possibility to label almost any cell-expressible proteins and to track them in vivo. (For a review see [4])

The rapid increase of fluorescent proteins (FPs) as a fundamental tool of biological research began about 15 years ago. The wild type (wtGFP) was quickly modified to produce variants emitting in the blue (BFP), cyan (CFP) and yellow (YFP) regions [5-7] (**Fig. 1.5**). In 1999, the first red FP from a non-bioluminescent reef coral was isolated and introduced in cell biology research.

Despite the recent advances in FP technology, most groups still use the enhanced version of wild-type GFP (EGFP), as well as the original cyan and yellow derivatives (ECFP and EYFP), for most of their imaging applications.

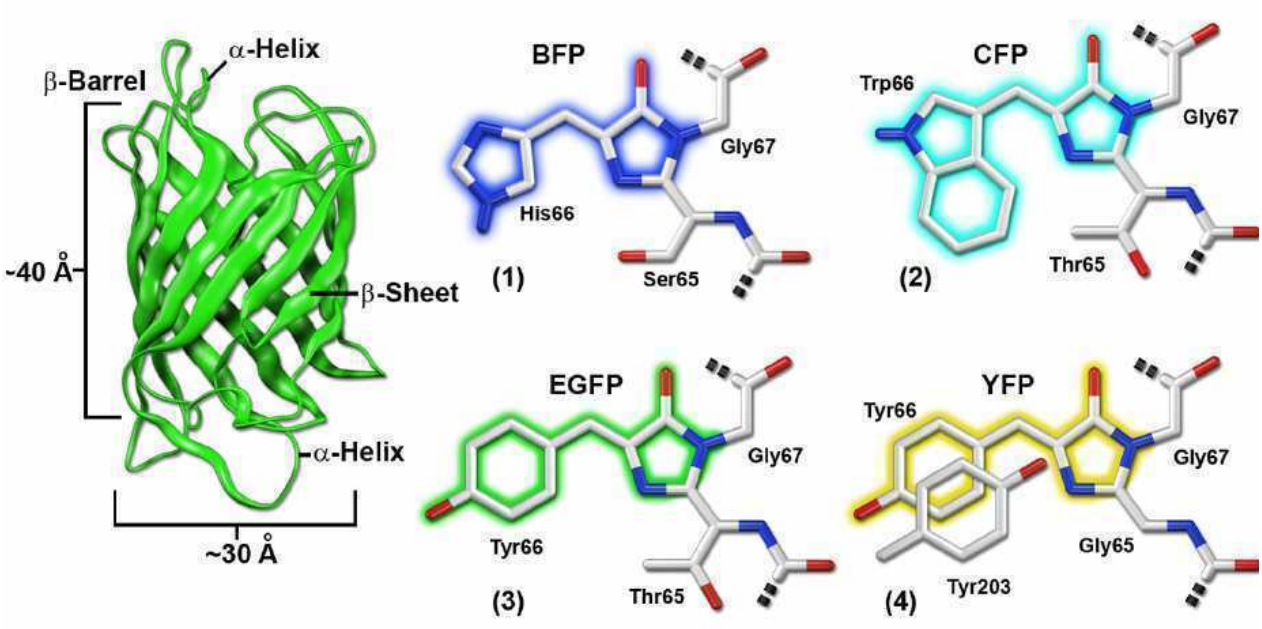

Figure 1.5. Model of GFP protein (left) and fluorophore structures of different fluorescent proteins.

Although most attention now focuses on the orange-to-far-red spectral regions, recent BFP and CFP variants have dramatically strengthened the potential for imaging because of the possibility of multi-color imaging and protein-protein interaction sensing by using two different FP simultaneously.

Fluorescence proteins are perfect tools for in vivo labeling of large proteins expressed in cells. Nevertheless, their applications are essentially limited by their large size (about 3.5 nm) that modify the folding and activity of a number of proteins. Moreover, the need to overexpress the tagged proteins can induce irrelevant sub-cellular expression of the target and force interactions with non natural targets.

C) Labels for FRET

Fluorescence resonance energy transfer (FRET) is a powerful tool for analyzing the structure and dynamics of proteins and their interactions. This technique allows the determination of the distance between two chromophores [1, 9]. FRET can take place when the emission spectrum of one chromophore (donor) overlaps with the excitation spectrum of the other (acceptor) (**Fig. 1.6**). The distances accessible by this technique range from ~2 nm to ~10 nm. These distances are comparable with the sizes of most biological molecules, thus explaining why FRET has been widely used in a variety of biological applications. The efficiency of energy transfer shows a very steep dependence on the distance separating the two chromophores:

$$E = R_0^6 /(R_0^6 + R^6) \qquad (8)$$

where E is the energy transfer efficiency, R_0 is a parameter characteristic for a given donor–acceptor pair corresponding to a distance of 50% energy transfer efficiency, and R is the donor–acceptor distance.

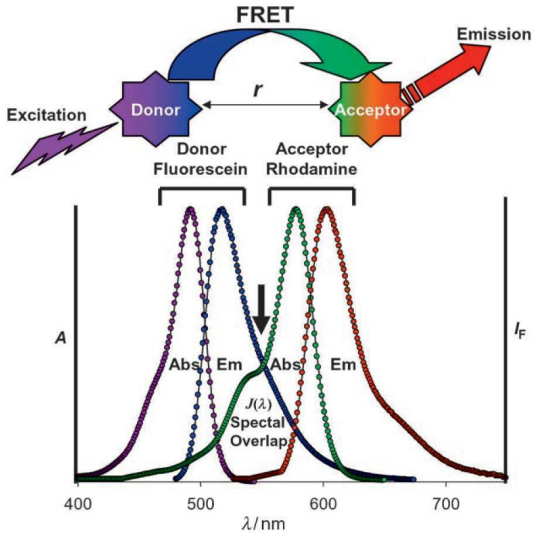

Figure 1.6. Scheme of the FRET process [8]: Upon excitation, the excited donor molecule transfers its energy non-radiatively to a proximal acceptor molecule located at distance R from the donor. Then, the acceptor releases the energy either through fluorescence or nonradiatively. The spectra show the absorption (Abs) and emission (Em) profiles of one of the most commonly used FRET pairs: fluorescein as donor and rhodamine as acceptor. Fluorescein can be efficiently excited at 480 nm and emits at around 520 nm. The spectral overlap between fluorescein emission and rhodamine absorption is observed at 500–600 nm. The Förster distance R_0 for this pair is 5.5 nm. Thus, in an optimal configuration ($0.5R_0<R<1.5R_0$), excitation of fluorescein below 500 nm can result in a significant FRETemission of rhodamine above 600 nm. A: normalized absorption, I_F : normalized fluorescence.

FRET requires an appropriate selection and incorporation of both chromophores. In case of intramolecular FRET (a single biopolymer is labeled by both chromophores), conformational changes could be monitored. Intermolecular interactions are detected when one biopolymer is labeled with the donor and another one with the acceptor.

The most important properties for dyes applied in FRET system are

- suitable excitation and emission wavelengths
- high extinction coefficients
- sufficient photostability

Several families of dyes were developed to meet those criteria [10] (**Fig. 1.7- 1.12**, **Table 1.1**).

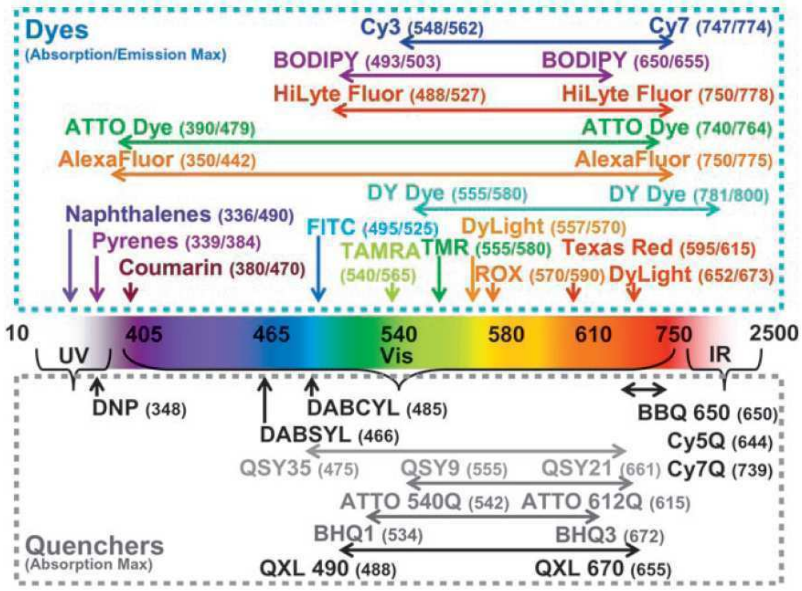

Figure 1.7. Examples of available fluorescent dyes and quencher molecules used for FRET measurements. Absorbance and emission maxima along with spectral regions for a series of dyes are highlighted. The most common D/A combinations are coumarin/fluorescein, fluorescein/rhodamine, and Cy3/Cy5. Common dye/quencher combinations include rhodamine/Dabcyl and Cy3/QSY9.

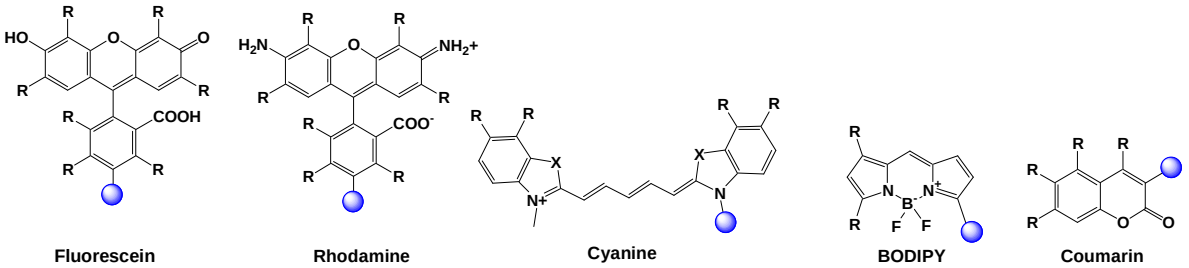

Figure 1.8. Common fluorescent dyes. Typical substituents at the R position include COOH, SO_3H, OH, OMe and Me. Blue balls mark the typical position of the bioconjugation linker. For cyanine, X could be CH_2, CMe_2, O, S.

Table 1.1. Selected families of dyes

Family	Name	ε, $M^{-1}cm^{-1}$	λ_{ABS}, nm	λ_{EM}, nm	Comments
Fluorescein	Fluorescein	88000	490	515	Medium environment sensitivity, self-quenching, moderate photostability
Rhodamine	TAMRA	99000	502	524	Positive, stacks with DNA, almost not environment sensitive
	Carboxy-X-Rhodamine (ROX)	113000	570	590	
	Sulpho-Rhodamine (Texas Red)	84000	580	600	
BODIPY	BODIPY (see below)	≈90000	505	515	Neutral
	BODIPY (see below)	≈100000	555	590	Neutral
Cyanine dyes	Cy3	150000	550	570	Highly photostable
	Cy3.5	150000	581	596	
	Cy5	250000	650	670	
Coumarines	Coumarin 1	23500	375	430	Small size
	Coumarin 314	47000	435	480	Small size

Fluorescein and Rhodamine

The Fluorescein-Rhodamine dye pair is frequently used for FRET. Fluorescein was first synthesized by Baeyer in 1871 and remains one of the most popular dyes. Rhodamine is an amino-containing analog of fluorescein. It bears a positive charge delocalized between two amino groups through a conjugated aromatic system. Rhodamines are much more photostable and less environment-sensitive than fluorescein. Tetramethylrhodamine (TMR), carboxytetramethylrhodamine (TAMRA), and carboxy-X-rhodamine (ROX) are the most used rhodamine-based dyes (**Fig. 1.9**).

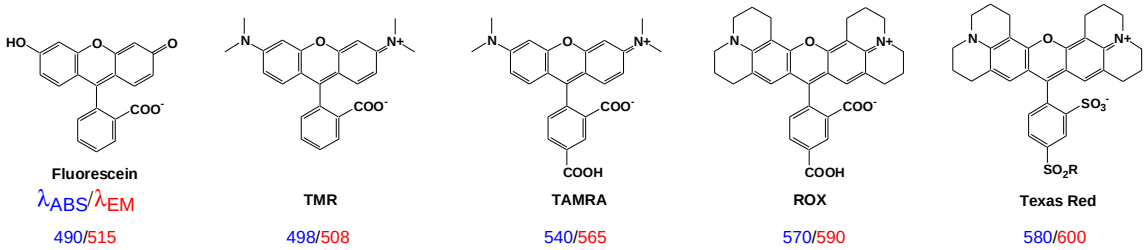

Figure 1.9. Common fluorescein and rhodamine dyes.

BODIPY

BODIPY dyes were first discovered in 1968 by Treibs and Kreuzer. They are strongly UV-absorbing small molecules that emit a relatively narrow fluorescence with high quantum yields. BODIPY dyes are relatively insensitive to the polarity and pH of their environment and are

reasonably stable in physiological conditions. Meantime, they have some disadvantages like poor water solubility and small Stokes shift (**Fig. 1.10**). Nowadays, the chemistry and application of BODIPY dyes are increasingly developing [11].

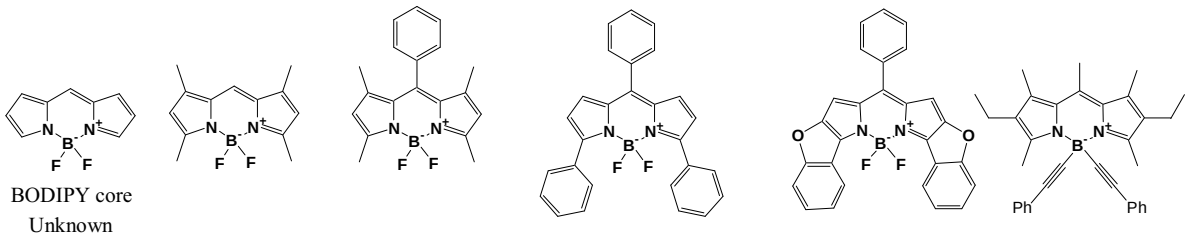

Figure 1.10. BODIPY dyes with different spectroscopic properties.

Cyanine dyes

Cyanine dyes are based on a polymethine chain ending by two amino groups. (**Fig. 1.11**) Most popular cyanine dyes contain heterocyclic rings that increase the stability and make synthesis easier. This family of dyes is characterized by high extinction coefficients and red-shifted absorption maxima. Both parameters depend strongly on the length of the polymethine chain.

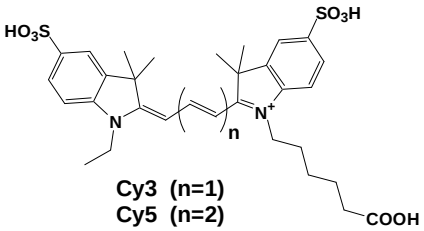

Figure 1.11. Examples of cyanine dyes.

"Alexa"

The ALEXA dye family is a trademark for different common dyes sulfonated at different positions (**Fig. 1.12**). Introduction of a negatively charged acceptor group dramatically increased both the hydrophilicity and stability of the dyes [12].

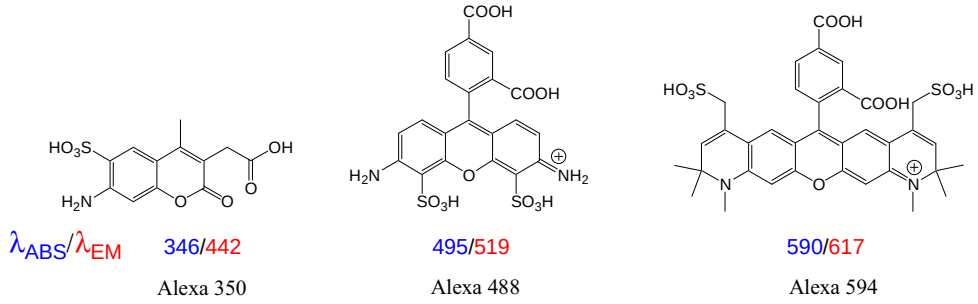

Figure 1.12. Examples of ALEXA dyes derived from coumarine (left) and rhodamines (middle and right).

It is also possible to mention other families of dyes provided by commercial companies such as DyLight, ATTO and HiLyte Fluors.

Quenchers

A particular case of FRET consists in energy transfer to non-fluorescent molecules (quenchers). In this case, only the donor fluorescence can be observed and its fluorescence intensity increases with the donor-acceptor distance. The most used quencher is Dabcyl (**Fig. 1.13**). Other frequently used quenchers include the QSY, QXL, ATTO, BlackBerry, and Black Hole quenchers. They generally tend to exhibit broad absorption spectra, which allow them to function as acceptors for many different dyes. Quenchers are often applied to DNA analysis and more particularly in molecular beacons [13, 14], though in this case, exciton coupling between the chromophore and the quencher also appears, due to the very close interchromophore distance (< 1 nm) [15].

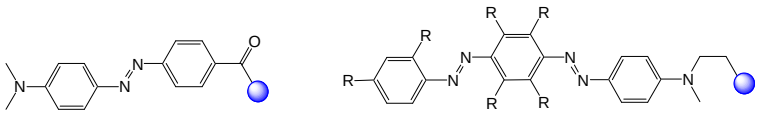

Figure 1.13. Commonly used fluorescence quenchers. Blue ball shows conjugation position.

FRET could be used for sensing almost any type of biomolecular interactions. The main disadvantage of this method holds in the necessity to introduce two labels into the investigated system. Intermolecular FRET assay needs labeling of both components, which is difficult to realize when a large set of compounds should be tested. Moreover, labeling of the biomolecules by probes that are usually bulkier than any aminoacid or nucleotide could strongly affect the folding or the activity of the labeled biomolecule, and perturb its interaction with ligands. Site-specific introduction of two synthetic fluorophores into proteins is a multistep and complicated task [16] which could be replaced by GFP-labeling [17].

D) Environment-sensitive (solvatochromic) dyes

A single-label technique for protein studies can be based on environment-sensitive dyes. Physicochemical parameters, such as hydration, polarity and electrostatics, which condition the interactions with other proteins, substrates and ligands, are critical for the protein structure, stability and activity. In this respect, environment-sensitive fluorophores are of great interest due to their spectroscopic behavior that depends on these physicochemical properties.

The environment-sensitive dyes report on changes of their environment by fluorescence emission maxima shifts and/or changes of fluorescence intensity.

The most common solvatochromic fluorophore that displays sensitivity to the polarity of its local environment is Prodan (2-propionyl-6-dimethylaminonaphthalene, **Fig. 1.14**) [18]. Prodan shows suitable fluorescence properties for monitoring molecular events since the fluorophore displays dramatic changes in fluorescence intensity and emission wavelength maxima with changes in the environment. The fluorophore is also excited at wavelengths longer than those of most intrinsic chromophores are and presents a high quantum yield. The solvent-dependent shifts of its fluorescence spectrum are due to a charge-transfer in its excited state [1] as well as to specific H-bonding interactions with protic solvents [19-21]. Prodan has been used in many biological systems, notably in lipid bilayers and proteins presenting a binding site for this fluorophore [22-24]. Derivatives of Prodan have also been attached covalently to proteins *via* reaction of thiols with Acrylodan (6-acryloyl-2-dimethylamino-naphthalen) [25-27] or Badan (6-bromoacetyl-2-dimethylaminonaphthalene) [28]. These methods provide useful information about biopolymers of interest but are limited to systems having a single reacting amino acid. Furthermore, labeling of the aminoacid side-chains increases the distance between the fluorophore and the protein backbone, which may reduce the sensitivity of the label to the local changes in the environment of the labeling site.

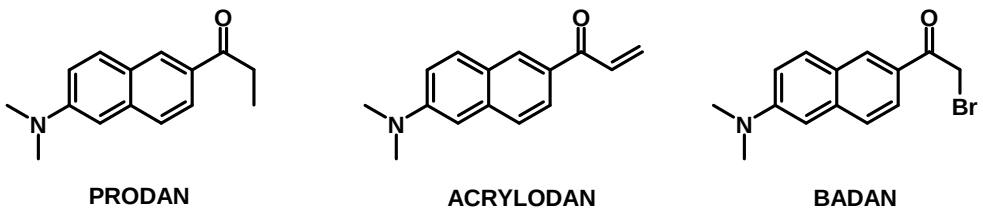

Figure 1.14. Structure of Prodan and its reactive derivatives.

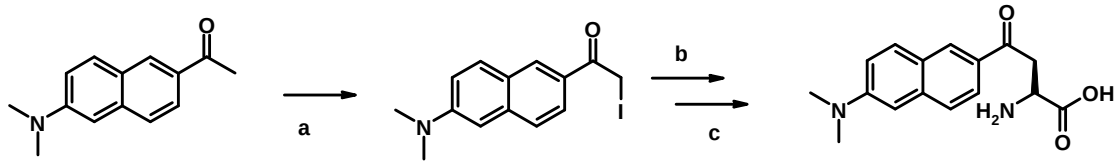

Figure 1.15. Scheme of the Aladan (6-dimethylaminonaphtoyl alanine) synthesis.
(a) $LiN(SiMe_3)_2$/THF, -78°C, then I_2; (b), $Ph_2C{=}NCH_2CO_2$-*t*-Bu, catalyst, CsOH, DCM, -70°C; (c), TFA, EDT.

To overcome this problem of non-specificity, a Prodan-based amino acid, 6-dimethylaminonaphtoyl alanine (Aladan), was synthesized by two independent research groups [29, 30]. In both cases, the substituted amino acid was prepared via an enantioselective synthesis as shown on **Fig. 1.15** and specifically introduced by solid-phase synthesis into peptides. The probe allowed to monitor binding of S-peptide with ribonuclease S [30] and to estimate the local dielectric constant of the B1 domain of the staphylococcal protein G at different sites [29]. Later, this amino acid was successfully applied in the study of δ-opioid receptor antagonist binding [31].

In order to shift the absorbance of Prodan to the red, Lu et al [32] have synthesized its benzo-analogue, 2-propionyl-6-dihexylaminoanthracene (Anthradan). The main advantage of this red-shifted dye is the possibility to avoid interference from the autofluorescence of many biological components and allow a more favorable excitation wavelength for fluorescence microscopy applications.

Prodan and its derivatives are not the only dyes that can be used as solvatochromic labels for proteins. A large number of environment-sensitive dyes is known, but only some of them can be used as protein labels because of either their large size or their strong quenching in aqueous media [33]. One of the first solvatochromic labels applied for protein labeling was dansyl (DNS) (**Fig. 1.16**), that can be excited at 350 nm, where proteins do not absorb. The emission spectrum of the dansyl moiety is also highly sensitive to solvent polarity, and emission maximum appears typically near 520 nm [10]. Its derivatives, ANS and TNS (p-toluidineyl-6-naphtalene sulfonate) have been extensively used for probing proteins [1]. Meantime the small size of DNS label makes it appropriate for biological applications. Recently DNS1-labelled amino acid was introduced into proteins through the aminoacyl-tRNA / nonsens codon technique [34].

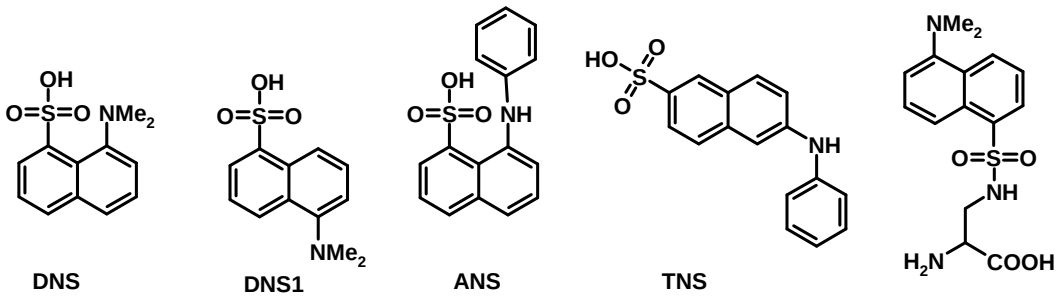

Figure 1.16. Structures of dansyl, its analogues and DNS1-labelled amino acid.

Another example of a label highly sensitive to solvent polarity is 7-nitrobenz-2-oxa-1,3-diazol-4-yl chloride (NBD-Cl) (**Fig. 1.17**), which absorbs at 470 nm and emits at ca 550 nm. NBD, due to its reactive chlorine group can be readily conjugated with the amino groups of proteins allowing probing polarity at the level of the labeling site [1].

Recently, a red-shifted Cys-reactive probe, aminophenoxazone maleimide (APM), was designed for reporting protein conformational changes [35]. APM has a short linker between the probe and the protein, ensuring that it can closely follow the motions of the side chain to which it is attached. It undergoes large polarity-dependent changes in its Stokes shift, as well as large bathochromic shifts. The spectral characteristics of APM provided information on the conformation changes of the water-exposed domain of the β2 adrenergic receptor during its interactions with ligands [35].

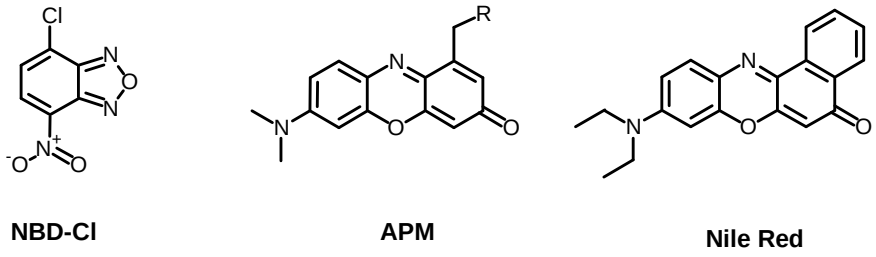

Figure 1.17. Structures of NBD-Cl, APM and Nile Red.

AMP is a smaller version of the well-known polarity-sensitive dye Nile Red dye, which shows good solvatochromism but has tendency to aggregate due to its high hydrophobicity. Nile Red is frequently used for non-covalent labeling of lipophilic systems [36].

Recently a family of dyes based on phtalimido-like fluorophores was applied for peptide labeling. The smallest of them, 4-dimethylaminophthalimide (4DMP) can be considered as one the fist chromophores for polarity sensing. This relatively small and rigid molecule presents a shift of its emission from 400 nm in heptane to 600 nm in water. Application of 4DMP for protein-protein investigation was shown in recent papers [37]. Fmoc-protected amino acid based

on 4DMP (**Fig. 1.18**) was synthesized and introduced into an octapeptide using standard Fmoc SPPS. The label was able to sense phosphorylation-dependent binding of the synthesized peptide to 14-3-3bp protein [37].

The fluorophore of 4DMP was extended, giving a new environment-sensitive dye [38], 6-N,N-dimethylamino-2,3-naphthalimide (6DMN), (**Fig. 1.18**). This chromophore exhibits interesting fluorescent properties with emission in the 500-600 nm range and combined (fluorescence intensity and position) response to changes in the environment polarity. The applications of the 6DMN probe were further expanded with the synthesis of an Fmoc-protected amino acid derivative (**Fig. 1.18**), containing the fluorophore. Peptides labeled with this new residue were used for monitoring protein-protein interactions as exemplified in studies with the SH2 phosphotyrosine binding domains [38]. The same labelled amino acid was used for sensing peptide binding to proteins of a major histocompatibility complex (MHC) at the cell surface [39].

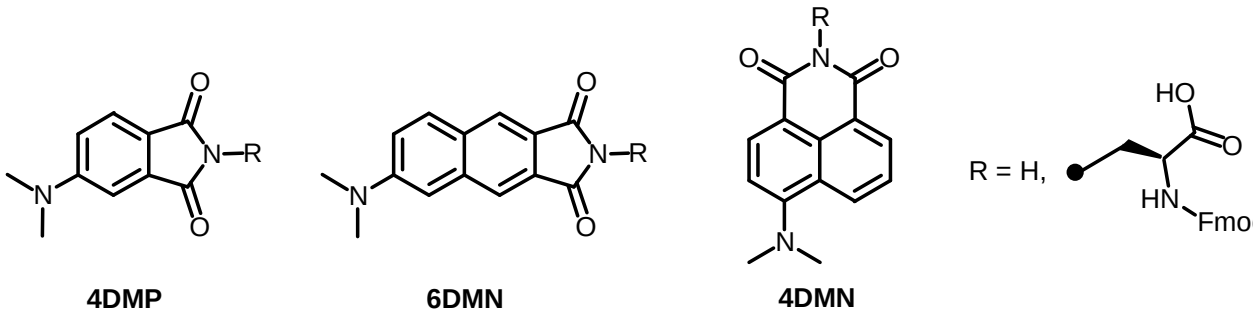

Figure 1.18. Structure of dyes of the "dimethylaminonaphthalimide family", which were applied to peptide synthesis through Fmoc-protected labelled amino acids.

Recently, this class of environment-sensitive fluorophores was expanded by 4DMN [40] that presents better spectral properties (50 nm red shift in absorption in respect with 6DMN, **Table 1.2**) being more easily synthesized and easily transformed to corresponding Fmoc amino acid than 4DMP and 6DMP. Moreover, it was found to be much more stable in presence of amines, which is crucial for Fmoc peptide synthesis because of the repetitive piperidine-deprotection steps.

Fluorescent labels of this family report on peptide interactions with relatively apolar proteins through a strong increase in their fluorescence quantum yields and blue shift in their fluorescence emission maxima.

Table 1.2. Properties of solvatochromic fluorescent dyes

Dye	ε, $M^{-1}\times cm^{-1}$	λ_{ABS}, nm	Quenching in water	Reference
Prodan	20000	390	low (<10x)	[29]
Dansyl	5300	337	medium (≈10x)	[34]
NBD	22000	465	low (<10x)	
APM	48000	590	medium (≈10x)	[35]
4DMP	6500	421	high (>100x)	[37]
6DMN	8000	390	high (>100x)	[38]
4DMN	8800	440	high (>100x)	[40]

These examples clearly demonstrate that environment-sensitive probes are of great interest for protein investigation. Nevertheless, there is still a lack of probes with optimal parameters. Most of the dyes described in this chapter absorb in the UV range that is often not suitable for biological applications. Excitation at longer wavelengths would decrease significantly the photo-damage of the biological samples and the photo-degradation of the dye itself. Moreover, the low fluorescence quantum yield in aqueous media of some of the described dyes limits their application for the investigation of small peptides for which the label is exposed to water. Finally, all these dyes exhibit only a single emission band and respond to an environment change merely by a shift of their maximum. As a consequence, these dyes provide only limited information on local conformational changes. As it will be shown in the present work, a new class of environment-sensitive labels exhibiting dual fluorescence presents important advantages for protein research.

In conclusion, fluorescent labels are powerful tools for investigating biomolecular events. Their utility is amplified when their emission spectrum is sensitive to the environment. They allow real-time monitoring of binding events and studying conformational changes of biomolecules of interest by using a single labeling approach. For sensitivity enhancement, dye incorporation in close proximity of the interaction site is commonly required. Several site-specific protein labeling methods are established.

1.1.4. Chromophore incorporation

In many cases, the intrinsic fluorescence is not adequate to obtain the desired information. In addition, the molecules of interest are frequently non-fluorescent. In these cases, the only way to study the corresponding systems by fluorescence spectroscopy is to label the proteins or the molecules of interest with extrinsic fluorescent probes, which allow a shift to higher excitation and emission wavelengths in comparison with Trp fluorescence.

There are several ways to label a protein:

1. Direct labeling of native proteins
2. Indirect labeling
3. Incorporation of a labeled amino acid by peptide synthesis
4. Incorporation of non-coded amino acid by recombinant DNA technology.

A) Direct labeling of native proteins

Choosing the appropriate method to functionalize a protein is not an easy task. It strongly depends on the accessibility of the targeted functional group on the protein. The target group should be exposed at the surface of the protein. When two or more amino acid side chains are exposed, it becomes very difficult to control the conjugation reaction in such a way that only one site is labelled. Moreover, the reactions are rarely selective and more than one type of reactive groups is generally targeted. Of course, the modification should have little or no effect on the protein conformation, function and specificity. This in mind, the most useful protein functionalities for specific chemical modification are the natural amino acid side chains of cysteine (Cys), lysine (Lys), tyrosine (Tyr), and together with the α-N-terminus of the peptide backbone [41]. Depending on the targeted amino acid, different labeling methods are used

Lysine and the free amino group of the protein backbone are common candidates for labeling. They could be modified by several types of reactions (**Fig. 1.19**).

- Active ester reactions are relatively specific for primary amino groups, easily controlled, and occur over a period of a few minutes. The amino-labeling reaction competes favorably with hydrolysis of the active ester, but the rates of both reactions depend on pH. Higher pH favors the $-NH_2$ form of lysine groups, which reacts well with active

esters and isothiocyanates. Most of the labeling reactions with active esters or isothiocyanate are carried out between pH 8.5 and 9.5 over a period of 15 min to several hours (active esters generally react faster than isothiocyanates). If this pH range is used, it is important to be sure that the protein conformation is not irreversibly altered. If denaturation could occur, active ester reactions can be performed at neutral pH but over a longer period of time [42].

- Reaction with aldehydes results in the reversible formation of a Schiff base (imide), which can in turn be reduced with $NaCNBH_3$ to form a secondary amine linker. As the ε-amine group of Lys and the α-N terminus have different pKa values, (about 10 and 7.8, respectively), their difference in reactivity could be used for the selective functionalization of the α-N-ternimus. Only the α-N terminus will react with aldehydes at pH=5.
- Sulfonyl chlorides are very reactive with amino groups, but they react non-selectively. It is essential to have no any other primary amines in solution than those of the target biomolecule. Dichlorotriazine derivatives have been used as similar amino-reactive groups.
- Isothiocyanates also allow efficient labeling of proteins [43].

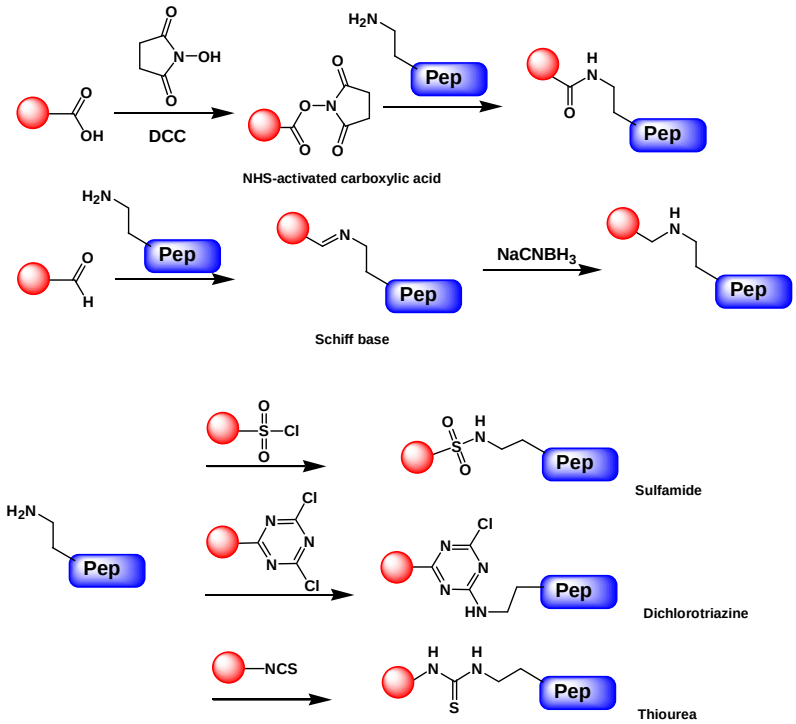

Figure 1.19. Lysine labeling methods. Red balls correspond to labels

Cysteine contains a mild nucleophilic thiol group in their side chain. Under appropriate conditions, Cys can be modified selectively, rapidly, and quantitatively (**Fig. 1.20**). Another advantage of the Cys residue is that it is rather rare in proteins, so that many proteins contain only one accessible Cys.

- Alkylation of Cys can be achieved using α-halo (usually iodine) carbonyl compounds. The reaction can be performed in a pH range (pH 7.0-8.0) where alkylation of cysteines is much more efficient than alkylation of Lys amino groups that are protonated in this pH range.
- Maleimide-functionalized groups react as Michael acceptors with Cys. This method gives mild conditions (proteins can be modified at neutral pH) and greater specificity (side-reaction with amines will occur only at pH >8).
- Disulfide formation, especially with dyes and heterofunctional spacers terminated with the o-pyridyldisulfide group, is the most specific method for functionalization of Cys. It is also a fully reversible reaction through the use of standard reducing agents such as dithiothreitol (DTT)

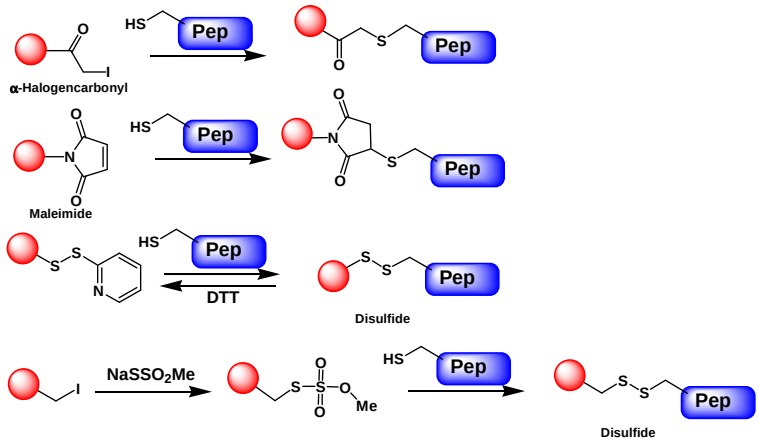

Figure 1.20. Cysteine labeling methods.

Tyrosine also gives some possibilities for specific protein functionalization. It contains a hydroxyl-substituted phenyl ring, which could be deprotonated under mild basic conditions (pH >8.5) that facilitates aromatic substitution reactions (**Fig. 1.21**).

- Reaction with diazonium salts allows labeling Tyr selectively in the presence of almost any other exposed amino acids.
- palladium-catalysed coupling of π-allyl species to Tyr under mild basic conditions is a new and prospective method for protein modification [44].
- Mannich-type reaction between Tyr, an aliphatic aldehyde and an aniline derivative proceeds smoothly and at nearly neutral pH (6.5), but needs large excess of the label.

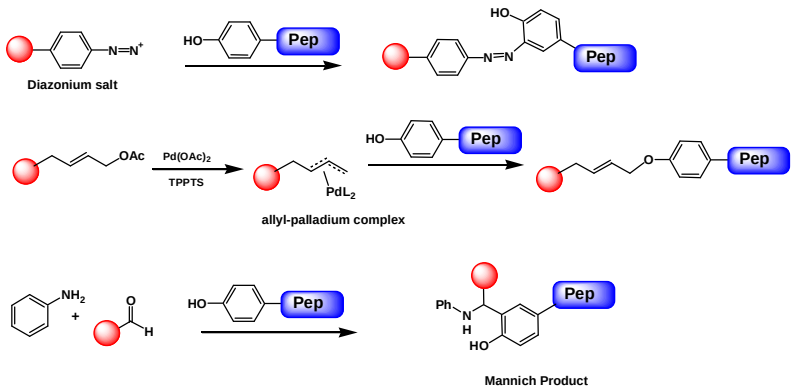

Figure 1.21. Tyrozine labeling methods.

Direct labeling is the best choice for introducing fluorescence labels into relatively large natural proteins exhibiting a limited number of accessible reactive groups

B) Indirect labeling by click chemistry reactions

Click chemistry is the easiest way to functionalize peptides and proteins. It requires the incorporation of a non-natural amino acid containing a group suitable for click chemistry (like azides or alkynes) or grafting of such groups to protein in other way. Two types of click chemistry reactions are used in protein labeling: azide-alkyne [3 + 2] cycloaddition reaction and Staudinger ligation

[3 + 2] cycloaddition reaction with acetylene or azide derivatives. Since this method involves a cycloaddition rather than a nucleophilic substitution, proteins can be modified with an extremely high selectivity. This reaction can be carried out at room temperature under aqueous conditions with an excellent regioselectivity (1,4 > 1,5) by the addition of catalytic amounts of Cu(I) salts to the reaction mixture [45, 46]. Moreover, Cu-free methods and reagents were developed recently [47] (**Fig. 1.22**).

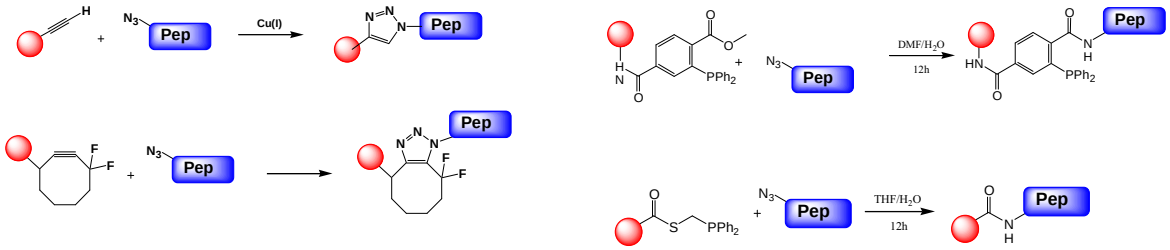

Figure 1.22. Azide-alkyne [3 + 2] cycloaddition reaction (left) and Staudinger reaction (right).

Staudinger ligation exploits the smooth reaction between an azide and a phosphane to form a phospha–aza-ylide. This ylide can be trapped by an acyl group with formation of a stable amide bond (**Fig. 1.22**). Since the azide moiety is absent in almost all naturally occurring compounds, this reaction could be widely used in chemical biology [48].

C) "Tag-labeling"

Short tag sequences of amino acids can be expressed with the protein of interest in fusion proteins. These short sequences can then be recognized by a fluorescent ligand, in order to obtain labeled proteins [49, 50].

This approach has been notably used with the tetracysteine-biarsenical pair. The basic components are a peptide tag with the consensus sequence CCXXCC and a chemical probe, with two arsenic atoms positioned so that each arsenic atom binds with two thiol groups on adjacent cysteines (**Fig. 1.23**). The bidentate nature of the complex results in an extremely high (~10 pM) affinity. Incorporations of the green fluorophore FlAsH or the red fluorophore ReAsH are the most known application of this scheme [51].

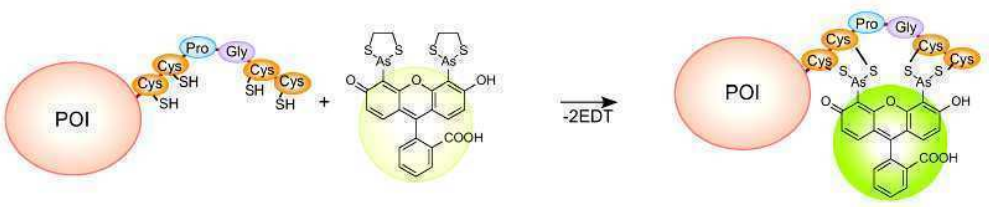

Figure 1.23. Interaction of the FlAsH dye with a protein of interest (POI) containing a tetracysteine tag.

Two other specific tags are oligo-histidine and oligo-aspartate. Oligohistidine sequences (generally $(His)_n$, $n \geq 6$) called His-tag strongly interact with transition-metal complexes, including nitrilotriacetic acid (NTA) complex of Ni^{2+}, and thereby these sequences are widely used for purification of expressed proteins by affinity chromatography. The selective interaction between His-tag and the metal complexes can also be used for site-specific fluorescent labeling of proteins.

Oligoaspartate tags (D4 tag; $(D4)_n$, n = 1-3) interact with multinuclear Zn^{2+} complexes, as shown on **Fig. 1.24**.

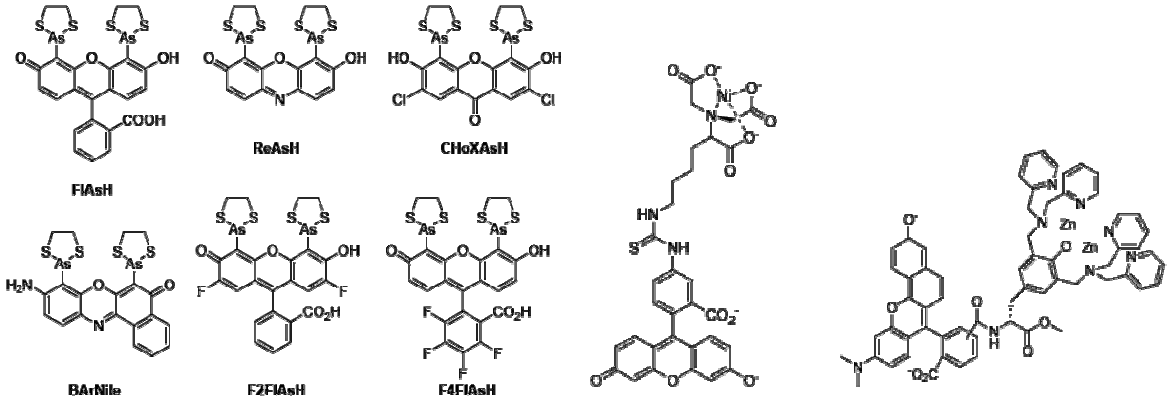

Figure 1.24. Structures of the fluorescent dyes reacting with tetracysteine (left) , oligo-histidine (middle) and Oligo-aspartate (right) tags.

D) Synthesis of labelled peptides

Relatively short peptides and proteins could be prepared synthetically. This method is faster than "in vivo production" and has no limitation concerning the use of non natural amino acids and post-synthetical modifications.

Nowadays, solid-phase peptide synthesis (SPPS), pioneered by Merrifield [52], allows to synthesize almost any peptide or protein of less than 100 amino acids. In SPPS, the peptide remains covalently attached to the solid bead until the end of the synthesis. The general principle of SPPS consists in repeated coupling-deprotection cycles. The free N-terminal amine of the solid-phase attached peptide is coupled to a single N-protected amino acid unit. This unit is then deprotected, revealing a new N-terminal amine to which a further amino acid may be attached. Unlike ribosome protein synthesis, solid-phase peptide synthesis proceeds from the C-terminus to the N-terminus.

There are mainly two ways for SPPS to proceed, using either **Fmoc** or **Boc** chemistry. In Boc chemistry, deprotection is performed in acidic conditions and peptide removal from support by using hydrofluoric acid (**Table 1.3**). In contrast to Boc, Fmoc could be removed in basic conditions as the peptide is attached to the resin by more labile bonds. Thus, the removal can be done in mild conditions and no hydrofluoric acid is needed. Due to this advantage, Fmoc chemistry is used for most peptide synthesis.

Table 1.3. Two strategies of SPPS

	Protective group	Coupling agents	Deprotection conditions	Cleavage conditions
Boc		DCC	H^+	HF
Fmoc	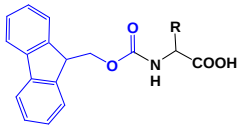	HBTU	Piperidine/DMF	TFA/H_2O

Typically, synthesis of peptides with unmodified C-terminus is most frequently performed on an HMP resin. The cleavage with TFA/H_2O simultaneously removes the peptide from the resin as well as the side-chain protective groups. When cleavage should be performed in mild conditions (for example to protect side-chain to protective groups) trityl or chlorotrityl resin should be used (**Fig. 1.25**). Application of oxime resin allows the synthesis of differently C-modified peptides such as peptide amides, alcohols, esters or even cyclic peptides.

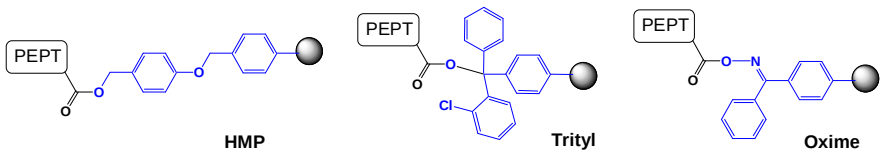

Figure 1.25. Resins for Fmoc synthesis. Grey ball represents polymer.

Recent methods of peptide backbone building are based on the use of amino acid activation reagents, among the most widely used of them are carbodiimides and uronium/phosphonium salts (**Fig. 1.26**).

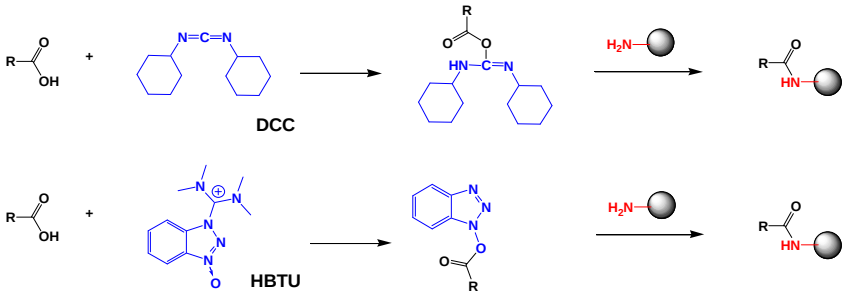

Figure 1.26. Peptide backbone building. RCOOH is protected amino acid that to be coupled to peptidyl-resins.

To remove the Fmoc from a growing peptide chain, basic conditions (usually 20% piperidine in DMF) are used. Fmoc deprotection is usually slow because the anionic nitrogen produced at the end is not a particularly favorable product, although the whole process is thermodynamically driven by the evolution of the carbon dioxide.

Removal of side-chain protecting groups and peptide from the resin is achieved by incubation in TFA, deionized water, and triisopropylsilane (scavenger to protect side-chains of peptide).

Incorporation of the labels during SPPS could be done in one of the following ways:

Synthetic fluorescent amino acid could be incorporated into any position of the peptide during the SPPS. Such a synthesis is useful for relatively small fluorophores incorporated instead of hydrophobic amino acids to limit the perturbation of the natural structure of the peptide.

On-resin labeling of the side chain is a complementary approach to introduce non-natural amino acids. To do it in a proper way, one should operate with orthogonally protected amino acids. A number of protecting groups stable towards both acids and bases exist, which are removable at special conditions. Representative examples are thio-tert-butyl (removable by reduction) and Alloc (Pd-catalyzed removal). Another possibility is to introduce amino acids with labile protective groups (like Mtt), which removal does not affect the protection of the other groups. The easiest of these approaches consists in coupling the fluorophore to the terminal amino group after a Fmoc-deprotection step.

1.2. 3-Hydroxychromone dyes

Chromones (chromen-4-ones) are natural dyes, which are widespread in the vegetal kingdom. Most natural chromones, containing phenyl (aryl) substituents in position 2 of the heterocycle, are commonly called flavones (**Fig. 1.27**). Moreover, the flavone derivatives bearing a hydroxyl group in position 3 of the heterocycle are called 3-hydroxyflavones (3HF). These compounds attracted the attention of spectroscopists after the discovery of their dual fluorescence by Frolov and colleagues [53]. Later, Sengupta and Kasha have explained this phenomenon by an excited state intramolecular proton transfer (ESIPT) reaction [54].

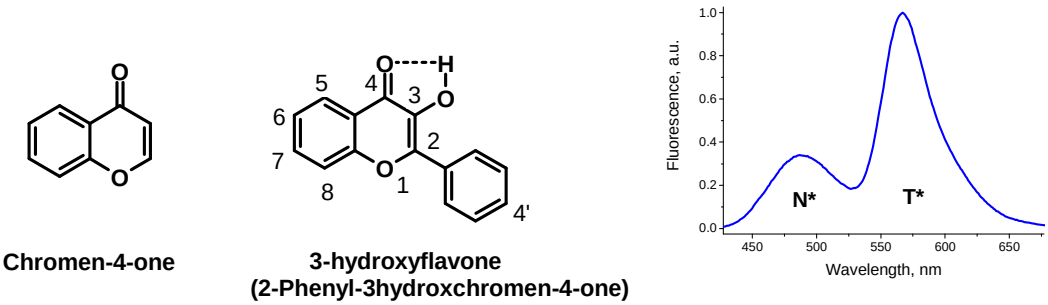

Figure 1.27. Structures of chromones (chromen-4-ones) and example of 3-hydroxyflavone spectrum.

3-hydroxyflavone and its derivatives exhibit two bands in their fluorescence emission spectra. The short-wavelength band corresponds to the emission of the normal excited state (N*) and the long-wavelength band to the photo-tautomer product (T*) formed during the ESIPT reaction. The ratio of these two bands depends on the properties of the environment. While classical solvatochromic dyes shift their emission maximum and fluorescence intensity in response to changes in their environment, for example in their polarity, 3HC dyes change also the ratio of their two emission bands intensities. Measuring the intensity ratio of the two emission bands is more precise and convenient than measuring band position or absolute intensity, since this ratio is independent from dye concentration and instrumental settings. Moreover, the environment sensitivity of ESIPT-based dyes depends not only on static properties as sensed by classical solvatochromic dyes, but also on dynamic properties through the proton transfer rate. Here, we will present the current status on ESIPT dyes with a particular focus on 3-hydroxychromones.

1.2.1. ESIPT and ESIPT dyes

Excited State Intramolecular Proton Transfer (ESIPT) reaction was observed and characterized for the first time in salicylic acid ester (**Fig. 1.28**) [55]. The methylsalicylate ion displays an unusual large Stokes shift in comparison to its methylated analog methyl 2-methoxybenzoate. This unusual spectral property was attributed to an excited state proton transfer from the hydroxyl to the carbonyl group that decreases the energy of the excited state species, giving a red-shifted emission band. Later, similar spectroscopic properties were observed for different carbonyl and heterocyclic compounds.

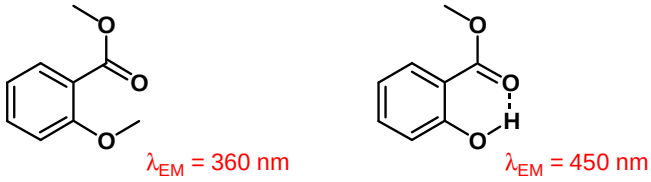

Figure 1.28. Structures of methyl 2-methoxybenzoate (λ_{fl}= 360 nm) and methylsalicylate (λ_{fl}= 450 nm).

The main governing force for the ESIPT reaction depends on the charge redistribution occurring in the excited state. Due to this charge redistribution, a strongly basic center appears in close proximity of the hydroxyl group, which involves the shift of the proton to give the tautomer form (T*). Both the rate and the equilibrium of such a process are controlled by the proton transfer energy barrier and the energy difference between the normal (N*) and tautomer (T*) forms of the excited molecule (**Fig. 1.29**).

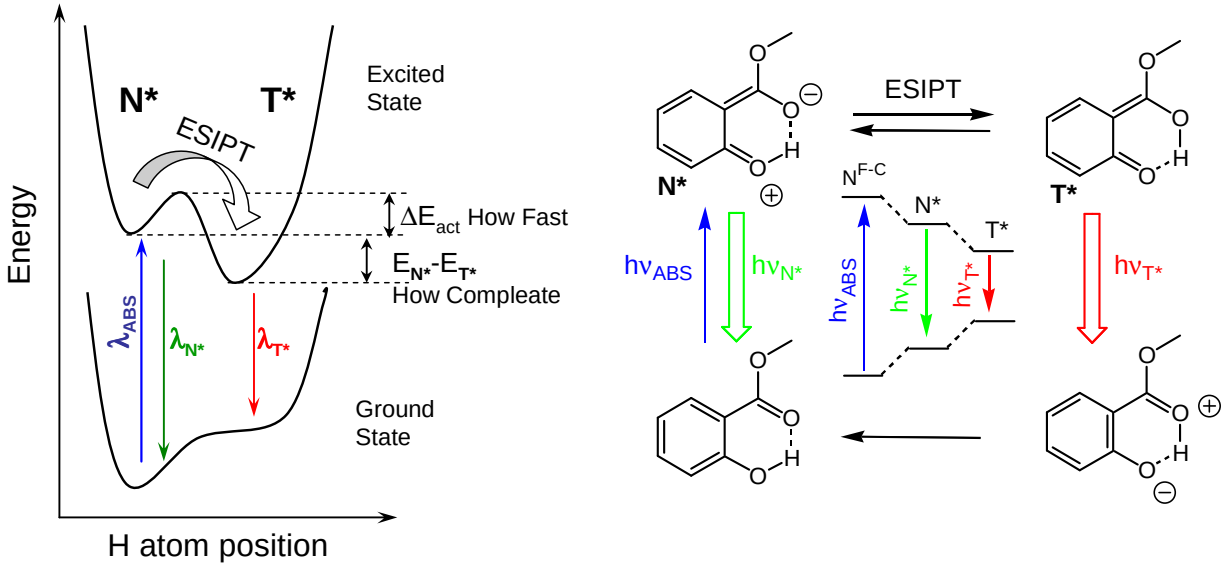

Figure 1.29. Energy diagram of the ESIPT reaction. In the ground state, the "Normal" form is strongly favored since molecules with shifted proton are unstable. In contrast, after excitation, the T* form with a shifted proton presents a lower energy. Some molecules undergo a proton transfer in the excited state (ESIPT) and their emission is shifted to higher wavelengths as compared to the initial normal form (N*). This proton transfer reaction could be characterized by a) rate, which depends on the energy barrier (ΔE_{act}) and b) equilibrium constant, which depends on the energy level difference between the two excited states (E_{N^*}-E_{T^*}). If ΔE_{act} is too high, the ESIPT will not occur within the "fluorescence time frame". In contrast, if ΔE_{act} is low, only the fluorescence of the T* form will be observed. When ΔE_{act} is low and the equilibrium between the N* and T* forms can be reached during the short lifetime of the excited state, E_{N^*}-E_{T^*} governs the ratio of the two forms and consequently, the ratio of corresponding emission bands intensities.

The ESIPT reaction is probably one of the fastest chemical processes. Its rate can vary in a rather large time-scale range (from 10^{-14} to 10^{-8} s). Only in the 90s, new instrumental methods appeared which allow to study such processes with enough precision, namely the so-called "ultra-fast laser spectroscopy" methods, which include the ultra-fast transient absorption (TA) and the time-correlated single photon counting (TCSPC) methods.

In most of cases described so far, the ESIPT reaction occurs between the hydroxyl group and the oxygen atom of the carbonyl [56] or the sp3 hybridized nitrogen atom [57].

In salicylic acid, the hydrogen bond results in the formation of a six-member cycle. The short length of this bond (~2 Å) is optimal for proton transfer, explaining the low energy barrier of the process (< 10 kJ/mol) and its very high rate (k~ 10^{13} s^{-1}) [58]. In most cases, the salicylic acid derivatives exhibit only one fluorescence band that belongs to the tautomer form, due to the large energy difference between the two excited–state forms (~ 8 kJ/mol).

The influence of electron-donating substituents on the ratio of the emission bands was investigated with 4- and 5-methoxysalicylic acid esters. In these derivatives, the methoxy group increases the electron density on the substituent in the *para*-position. As a result, the basicity of the carbonyl group increases for the 4-methoxy derivative while the acidity of the hydroxyl group decreases in the case of the 5-methoxy derivative. In cyclohexane, the band of the tautomer form dominates in the fluorescence spectrum of 4-methoxy-methylsalicylate, while in the case of 5-methoxy-methylsalicylate, the band of the normal form dominates [59] (**Fig. 1.30**). Thus, the ratio of the two emission bands could be modulated by substitution.

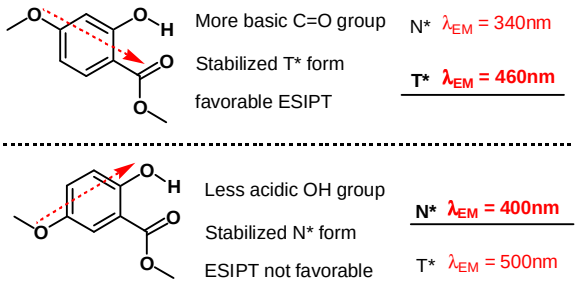

Figure 1.30. Effect of substituents on ESIPT in 4-methoxy and 5-methoxy methylsalicylate.

Ortho-hydroxyarylbenzoazines [60], including *ortho*-hydroxybenzoazoles [61], correspond to a large class of compounds that exhibit an ESIPT reaction to a nitrogen atom (**Fig. 1.31**). Due to their relatively easy synthesis, they were thoroughly investigated [62, 63]. The common feature of these molecules is their fast and irreversible ESIPT reaction. As a result, their fluorescence spectra exhibit only a tautomer emission band (T*).

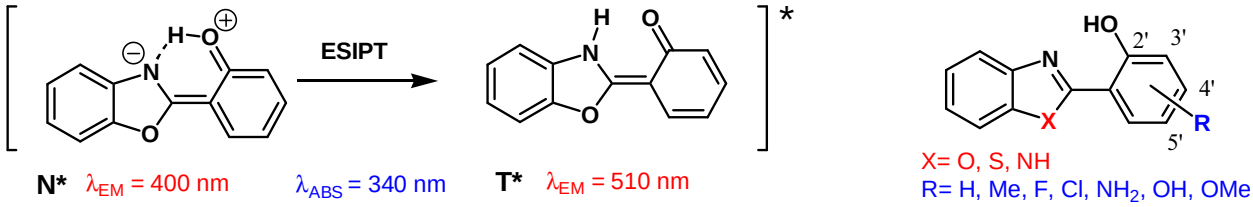

Figure 1.31. ESIPT in *Ortho*-hydroxyarylbenzoazole and main substitutions for this class of dyes.

All these compounds exhibit similar fluorescence properties and undergo an ESIPT reaction in aprotic media. In protic solvents, the ESIPT reaction is blocked due to intermolecular hydrogen bonds, thus resulting in the emission of only the N* band. The normal and tautomer forms have their emission maxima around 400 nm and 510 nm, respectively. In most cases, the quantum yields do not exceed 20%, with the only exception of benzimidazoles [64] for which they reach 50-80%.

The effect of substituents at the aryl ring of *ortho*-hydroxyarylbenzotriazols on the fluorescence properties was investigated [62]. The fluorescence was shown to depend on the position and electron donating properties of the substituent on the side ring of the dye. For example, an amino group in position 5' of the aromatic ring gives a bathochromic shift, while a dialkylamino group in position 4' induces a hypsochromic shift. Interestingly, the 4'-dialkylamino derivative undergoes a relatively slow ESIPT rate (~ 5.4×10^{11} s^{-1}) compared to the parent unsubstituted compound (> 2.9×10^{13} s^{-1}) [65]. Unfortunately, neither electron donating nor electron-withdrawing groups are inducing a high quantum yield of the chromophore, which remains low in all cases.

Of particular interest are 3-hydroxychromones (3HC), which form an intramolecular H-bond through a 5-membered cycle (**Fig. 1.32**). In comparison with a 6-membered cycle (for instance their close analogues 5-hydroxychromones), the hydrogen bond in the 5-membered cycle is longer and leads to a slowdown of the ESIPT reaction [66]. As a result, the emission of both N* and T* forms can be observed in solvents with different polarity.

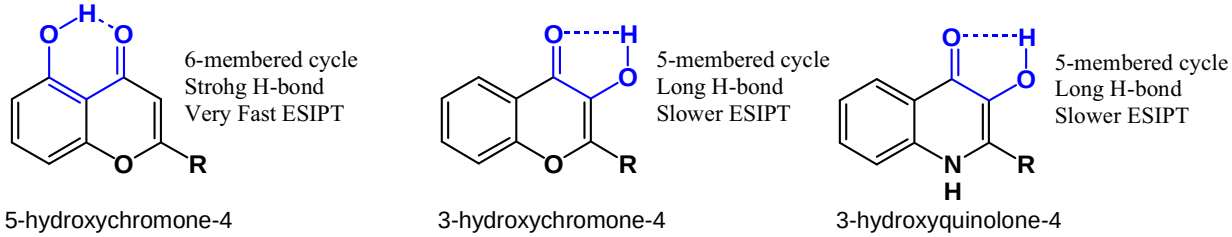

Figure 1.32. Structures of 5-hydroxychromone-4 (5HC), 3-hydroxychromone-4 (3HC) and 3-hydroxyquinolone-4 (3HQ).

Recently aza-analogs of 3HC were also shown to undergo ESIPT (**Fig. 1.32**) [67]. In the case of 3-hydroxyquinolones (3HQs), combination of both the relatively long H-bond in a 5-membered cycle and the presence of an electron-donating nitrogen atom makes ESIPT reaction much slower than in other systems [68]. This makes 3HQs prospective molecules for studying the ESIPT mechanism and the influence of different factors on the proton transfer kinetics.

1.2.2. Spectroscopic properties of 3HC derivatives

The non-substituted 3HF shows only T* band emission in aprotic solvents, while a dual fluorescence is observed in protic environment [69] (**Fig. 1.33**). The ratio of emission bands intensities (N*/T*) is higher in more polar alcohols making possible to sense the environment polarity just by recording the fluorescence spectrum. Meanwhile, in aprotic media the N* band intensity is too low, thus rendering the environment sensing difficult to perform through ratiometric measurements.

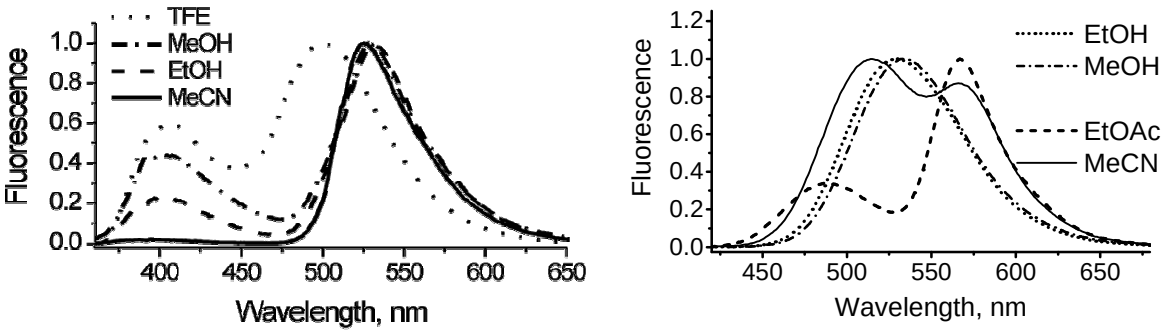

Figure 1.33. Fluorescence of 3HF (left) and its dimethylamino derivative (right) in protic and aprotic solvents.

A significant progress in this direction was done after dialkylamino derivatives of 3HF were synthesized [70, 71] (**Fig**. **1.34**). Since the dialkylamino group acts as an electron donor to the chromone moiety, increasing both molecule polarizability and excited state dipole moment, two bands in emission were observed in most solvents. It is important that the four states, N, T, N* and T*, possess different distribution of charges and interact differently with the environment (**Fig. 1.35**). The strongest dipole moment corresponds to the N* state [72] where the electronic charge is transferred from the dialkylamino group to the chromone moiety. Therefore, it shows a significant solvatochromism.

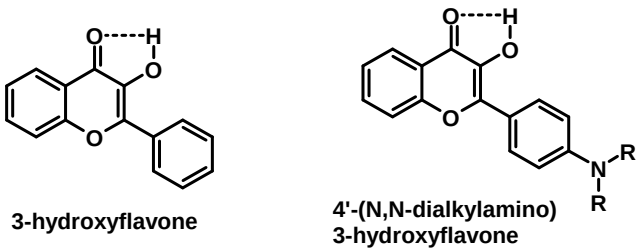

Figure 1.34. Structures of 3-hydroxyflavone (3HF) and 4'-(N,N-dialkylamino)-3-hydroxyflavone.

Meanwhile, the separation of charges in the T* state due to proton transfer is significantly smaller (**Fig. 1.35**), in line with the reported low solvatochromism of the T* band [73, 74]. Due to this significant difference, the positions of the two bands can be considered as independent variables. An important parameter is the ratio of intensities of the N* and T* bands in emission, I_{N*}/I_{T*} , which is a very sensitive indicator of solvent polarity [75-79]. Thus, these molecules allow the simultaneous determination of four parameters, ν_{abs}, ν_{N*}, ν_{T*} and I_{N*}/I_{T*}, which can differently characterize the physical properties of the microenvironment. An algorithm using these four spectroscopic parameters was proposed to simultaneously estimate three microenvironment characteristics: polarity, polarizability and H-bond donor ability [80]. This algorithm was successfully applied in binary solvent mixtures, AOT reverse micelles and proteins.

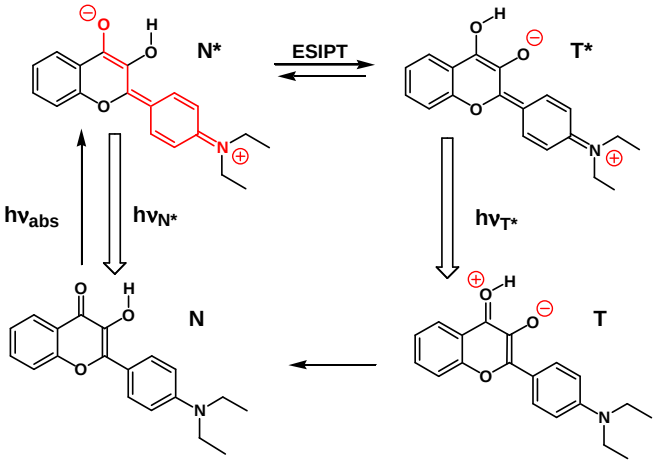

Figure 1.35. Photophysical cycle of dye FE.

Hydrogen bonding

A particularly attractive feature of 3HFs is their high sensitivity to hydrogen bonding. The ESIPT reaction site is strictly localized between the 3-hydroxyl and 4-carbonyl groups, which form an H-bond that closes a low-stable five-member ring [54]. Therefore, this reaction shows an extreme sensitivity to intermolecular H-bond perturbation [69]. 3HFs show two emission bands in alcohols; meanwhile in aprotic solvents of similar polarity, the T* band strongly dominates. This effect could be better observed in dialkylamino derivatives of 3HCs, namely 4'-diethylamino-3-hydroxyflafone (FE) [80]. The I_{N*}/I_{T*} ratio of FE was shown to be up to 10 times higher in protic solvents than in aprotic solvents of the same polarity. This high sensitivity was related to the H-bonding of solvent proton donors with the 4-carbonyl group of FE acting as an H-bond proton acceptor (**Fig. 1.36**).

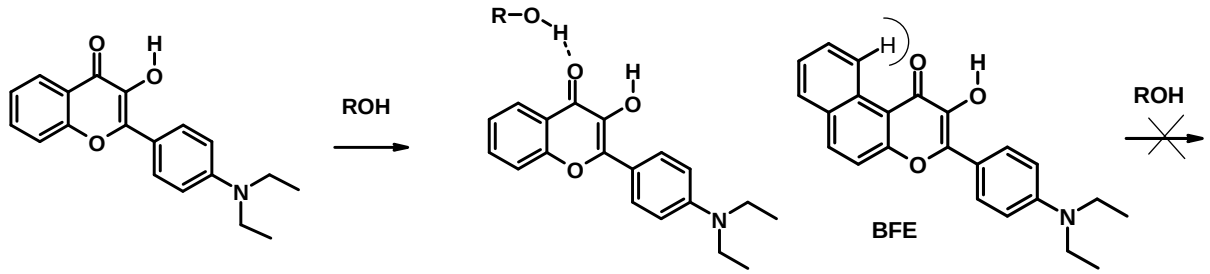

Figure 1.36. Formation of an H-bonding complex of FE with alcohol is blocked by the additional benzene ring in BFE.

Interestingly, using a benzo-analogue of FE, 3-(4-diethylamino-phenyl)-2-hydroxy-benzo[f]chromen-1-one (BFE), with a 4-carbonyl group spatially protected from intermolecular H-bonding, it was demonstrated that only H-bonding of the solvents with the carbonyl group affects the dual emission of dialkylamino substituted 3HFs, while H-bonding of the solvents with the 3-hydroxy group are not detected in the fluorescence spectra [81].

The mechanism of H-bonding of 4'-dimethylamino-3-hydroxyflavone (F) was investigated by steady-state and time-resolved fluorescence studies in protic and aprotic solvents as well as in their mixtures. These studies showed the appearance of a new form emitting at 500 nm and distorting the excitation spectrum. This new form corresponds to the H-bonded form of the dye. It appears in the ground state and is in equilibrium with the non-H-bonded form. The two ground-state forms, N and H-N, are excited separately and their corresponding excited-state forms, N* and H-N*, do not interconvert, as was shown by time-resolved fluorescence [82].

Recently the influence of H-bonding was studied for non-substituted 3HF [83]. It was found that an increase in the H-bond donor concentration increases the N*/T* ratio but does not affect the position of the emission bands. Meantime, the increase in the H-bond donor ability of the solvents results both in an increase of the N*/T* emission band ratio and a shift of the emission bands. These effects are related to the increase in the strength of the H-bonds between the solvents and the 4-carbonyl group of dyes with intact intramolecular H-bonds.

1.2.3. Kinetics study of 3-hydroxyflavones

ESIPT in non substituted 3HFs was an object of intensive kinetic studies in the 1980s. The first dynamic studies of ESIPT in non-substituted 3HFs by picosecond time-resolved spectroscopy revealed that [54, 84] ESIPT occurs very rapidly, usually in less than 10 ps, and that the kinetic constants of the proton-transfer reaction are temperature-

dependent. Moreover, Mc Morrow et al. observed that the ESIPT reaction time is less than 8 ps [85] in degassed ultra-dry hydrocarbon solutions at 293 K.

Kinetic two-state models were developed for describing excited-state processes, in particular intramolecular proton transfer. Pioneer works on the analysis of two-state excited-state reactions were from Birks [86] and Brand et al. [87]. The latter focused on the time-resolved study of the intermolecular proton transfer in the excited-state of naphthol molecules. In further research works [88-90], an excited-two-state model was applied for describing the intramolecular proton transfer in 3HF molecules. This became possible due to the development of ultrafast time-resolved fluorescence spectroscopy that allowed measuring the time constants of ESIPT processes [91]. Brown et al. found that ESIPT for 3HF in methylcyclohexane and acetonitrile is extremely fast, showing estimated time constant of 35 fs [92]. In ethanol, they found a time constant of 60 fs. The slower ESIPT in this solvent was attributed to the greater strength of the solute-solvent interactions. Introducing new techniques for measuring the decay curves and new methods for treating the lifetime data allowed revisiting the results of previous experiments and building new concepts.

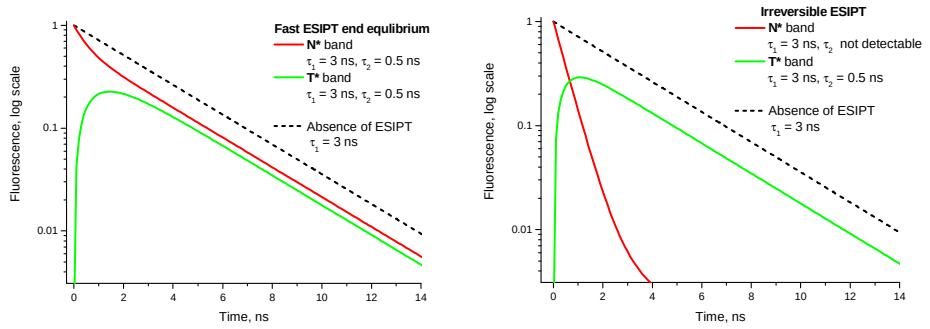

Figure 1.37. Theoretical fluorescence intensity decay in systems with reversible (left) and irreversible (right) ESIPT. Fluorescence decay of fluorophore not undergoing excited state reactions is shown for the comparison.

Picosecond time-resolved fluorescence study of the ESIPT dynamics of dialkylamino 3HF derivatives helped to understand the differences in the spectroscopic properties of dialkylamino 3HFs as compared to their parent 3HF [93]. In parent 3HF, slow ESIPT kinetics (in the picosecond time range) occurs only in protic solvents where the solvent hydrogen bonding with the dye leads to an activation barrier. In this case, the reaction is *irreversible* [94, 95]. Later, the fluorescence decay kinetics of both the short-wavelength normal (N*) and long-wavelength

tautomer (T*) bands of dialkylamino 3HF derivatives were shown to be characterized by the same two lifetime components, which were constant over the whole wavelength range of emission [93] (**Fig. 1.37**). Meantime, the pre-exponential factor of the short-lifetime component changed its sign, being positive for the N* and negative for the T* emission band. Moreover, the two pre-exponential factors of the T* emission decay were of the same magnitude but opposite in sign. All together, these features pointed to a fast *reversible* two-state ESIPT reaction in dialkylamino 3HFs. A detailed kinetic model was applied for the analysis of these data, enabling the determination of radiative and nonradiative decay rate constants of both N* and T* forms and of forward and reverse rate constants for transitions between them [96]. The ESIPT reaction occurs on the scale of tens of picoseconds and thus is uncoupled with the dielectric relaxation of the solvent occurring at sub-picosecond times. Moreover, the radiative and nonradiative deactivation processes were found to be much slower than the ESIPT reaction, suggesting that the relative intensities of the two emission bands are mainly governed by the ESIPT equilibrium. Therefore, both electrochromic and solvatochromic effects on the relative intensities of the two emission bands in 4′-(dialkylamino)-3-hydroxyflavones were shown to result from shifts in the ESIPT equilibrium.

Comprehensive studies of excited state dynamics and its dependence on different factors in 3HCs is complicated by its fast rate. In some respect, this type of study could be facilitated by using dyes of the 3HQ family that shows much higher N*/T* emission band ratios, likely due to an about one order of magnitude slower ESIPT reaction rates [67].

1.2.4. 3HC fluorophore design: Substitution effect

Further improvement of the 3HC molecules to obtain good fluorophores requires to increase their quantum yield, shift their emission/absorption spectra to longer wavelengths and increase the sensitivity of their ratiometric response to solvent polarity.

Extension of the π-electron system is a common way to increase the absorption wavelength of dyes. This approach was applied to 3HFs by substitution of the phenyl by a benzofuryl ring leading to the corresponding 2-(2-benzo[b]furanyl)-3-hydroxychromone (HC2; **Fig. 1.38**). Absorbance and emission of this new dye was red-shifted by about 20 nm in comparison to the parent one (HC1) [97].

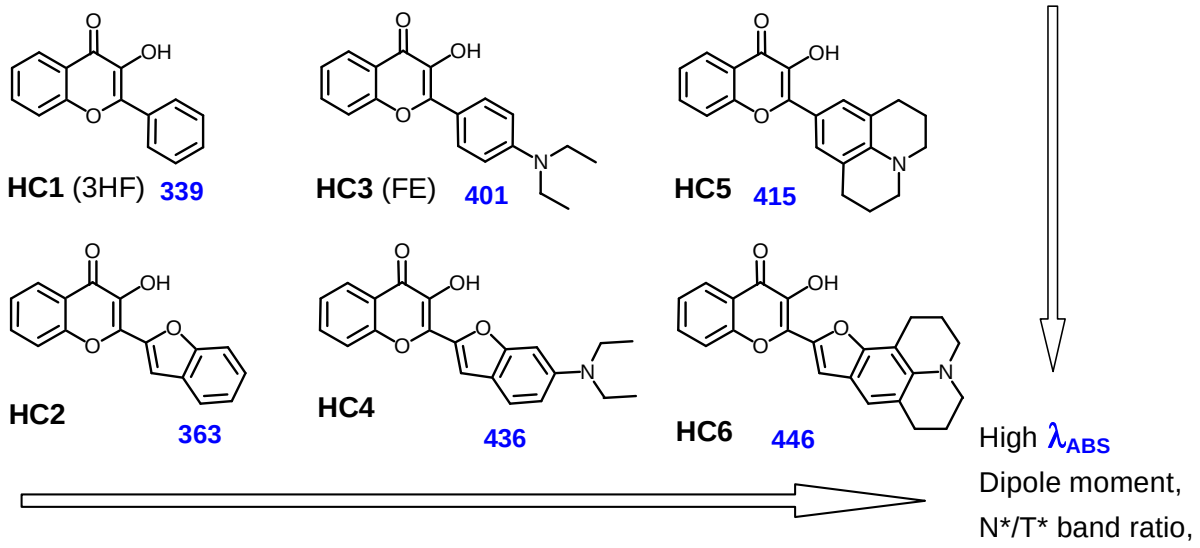

Figure 1.38. Structures and absorption maxima of several 3HCs.

In a following step, by analogy with 4-diethylamino-3-hydroxyflavone, a π-electron donor group, diethylamino, was introduced to the 6-position of the benzofuran ring. This increases the charge-transfer character of 3-hydroxychromone in the N* state, leading to a dramatic bathochromic shift (30 nm) of HC4 as compared to 4-diethylamino-3-hydroxyflavone HC3, (**Fig. 1.38**). In addition, chromones HC2 and HC4 in apolar solvents showed much higher fluorescence quantum yields than their corresponding phenyl analogues. Presumably, this is due to their more planar structure as compared with the non-planar 3HF [98] that shows an angle of ca. 28° between the chromone and phenyl units. The increase of the donor strength leads to molecules with even higher dipole moment HC5 and HC6, that show higher absorption wavelengths and N*/T* fluorescence band intensity ratios [99]. Moreover, all the studied 3HC dyes demonstrated a linear increase of log(N*/T*) with the solvent polarity parameter $E_T(30)$.

Thus, substitution of 2-phenyl for 2-(2-benzo[b]furanyl) or introduction of electron donors on the 2-aryl group in 3HC increases the sensitivity of their N*/T* ratio to solvent polarity and shifts the optimal range of ratiometric polarity sensing to less polar solvents. Opposite effects were observed for 7-methoxy derivatives. Altogether, these results show that by using proper substituents, the photophysical properties of 3HCs can be optimized for sensing a given polarity range (**Fig. 1.39**).

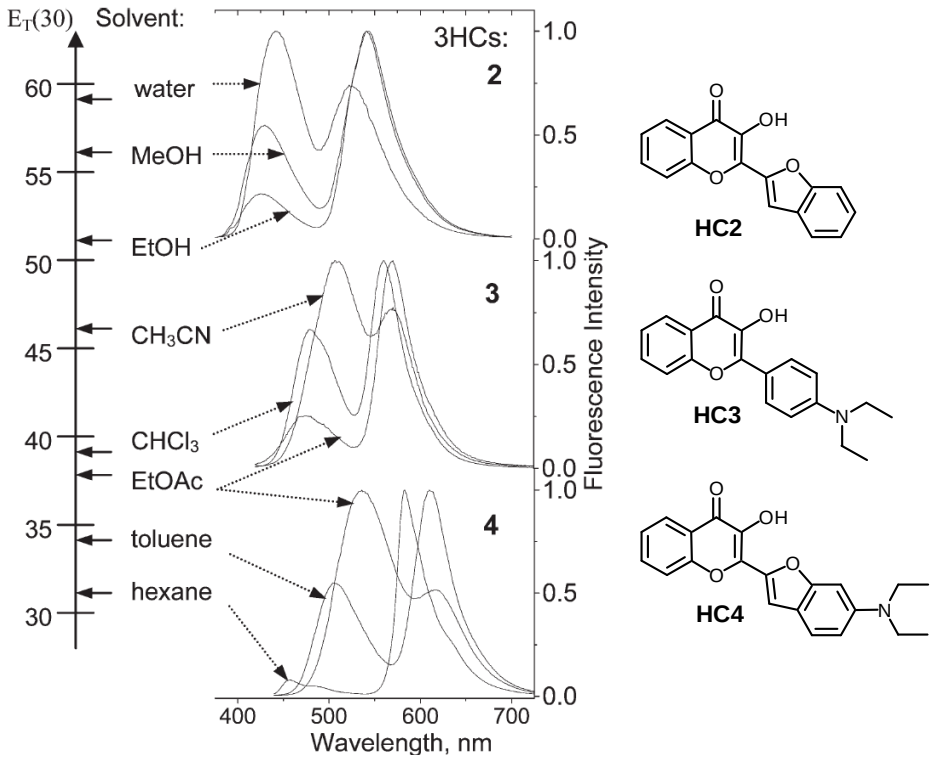

Figure 1.39. Two-band fluorescence ratiometric responses of HC2, HC3 and HC4 for three different ranges of solvent polarity: polar, medium-polar and low-polar, respectively.

It could be concluded that the increase of the 2-aryl ring donating ability not only shifts the absorption and fluorescence spectra to the red, but also modulates the ESIPT behaviour, resulting in a dramatic increase of the N*/T* ratio of the two emission bands intensities. This λ_{ABS}-N*/T* relationship makes difficult to conceive environment-sensitive dyes for polar media with red-shifted absorption spectra just by a simple extension of the 2-aryl ring donating ability.

Further extension of this "dipole principle" was realized by the synthesis of 7-(2-methoxycarbonylvinyl)-3-hydroxychromones [100] (HC7 and HC8, **Fig. 1.40**). These compounds show a 30-40 nm red-shift in absorption (giving absorption maxima at 480 nm) and > 50 nm red-shifts of both bands in emission. Moreover, HC7 and HC8 demonstrate a significantly stronger solvatochromism than their parent analogues, due to the acceptor group at 7-position, which increases the charge transfer character of their excited state. Due to their spectroscopic properties, these new dyes are thus highly prospective for developing new fluorescent probes for apolar environment, namely membrane probes.

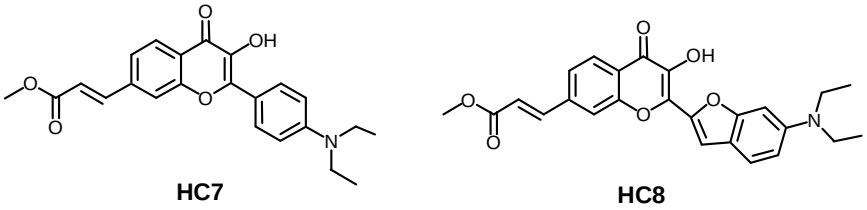

Figure 1.40. Structures of 7-(2-Methoxycarbonylvinyl)-3-hydroxychromones HC7 and HC8

A very illustrative example of acceptor substituent influence is the reaction of 7-isothiocyano-3-hydroxychromone with amines [101]. Transformation of an isothiocyano-group to a non electron-acceptor thiourea group leads to a decrease of the molecular dipole moment, especially in the excited state. This is reflected by a 20 nm blue shift in the absorption spectrum and a strong decrease of the N*/T* emission band ratio (**Fig. 1.41**).

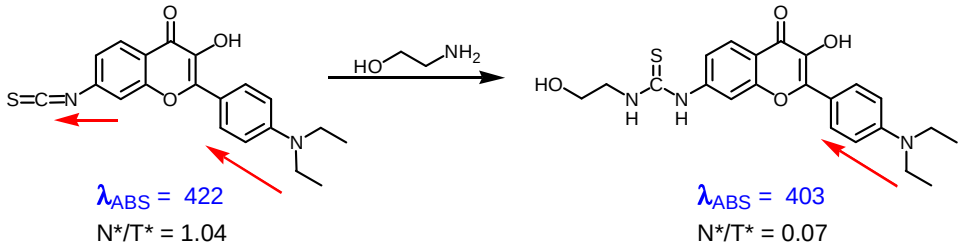

Figure 1.41. Switching of ESIPT by changing the dipole moment. Absorption position and emission band ratio are for ethyl acetate. Red arrows shows shifts of the electron density.

Moreover, substitution of an acceptor group in position 7 of 3HC by a donor one could strongly decrease the dipole moment. 7-methoxy analogues of HC3 and HC4 present a blue-shift in their absorption spectra (about 10 nm) and an important decrease in their N*/T* band ratio [99]. Addition of a 7-dialkylamino-group leads to a much stronger perturbation in the electronic properties of the fluorophore making the N* form thermodynamically less stable than the T* one, thus inducing a strong decrease of the N*/T* band ratio [102] (**Fig. 1.42**). Meantime, in contrary to the N*/T* band ratio, the absorption maxima depend mostly on the effective length of the conjugation system.

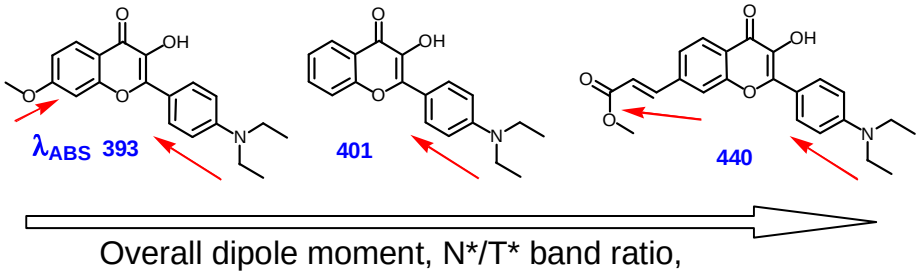

Figure 1.42. Influence of substituents on the dipole moment and the absorption maxima in 3HCs.

An environment-sensitive probe with proper excitation and environment sensitivity could be achieved by varying the substituents on both sides of the fluorophore. Meantime, many probes presenting large dipole moments show low quantum yields in water. The development of probes suited for aqueous media was based on 2-furyl-3-hydroxychromone (HC9, **Fig. 1.43**). These new dyes are a good alternative to dialkylamino flavones because they combine increased donating properties of 2-aryl substituents with the absence of charge transfer in the excited state.

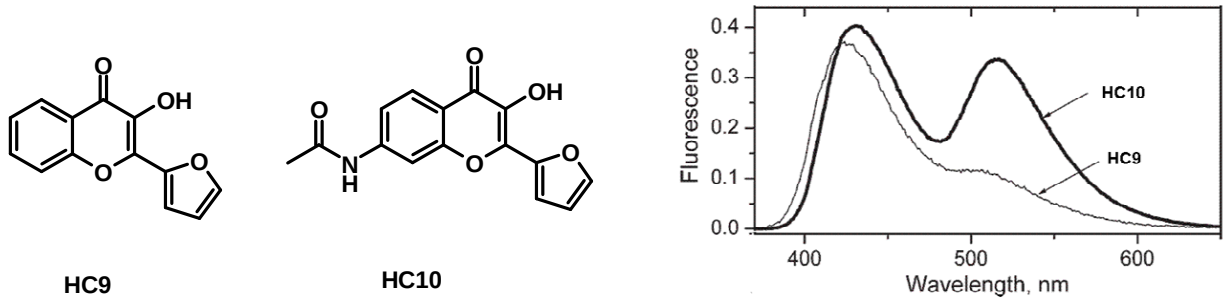

Figure 1.43. Structures of 2-furyl 3HCs and their fluorescence emission spectra in water.

A further improvement of 3HCs dyes was achieved by introduction of an acetamido group in position 7 of 2-furyl 3HCs [103] (**Fig. 1.43**). The 7-acetamido-3-hydroxychromone (HC10), as well as its parent compound HC9, exhibits ESIPT in polar protic media including water, resulting in two well-resolved fluorescence bands. Among all 3HCs reported so far, HC10 and its benzofuryl analog show the highest quantum yields ever reported in water (4-13%), while maintaining a sensitive ratiometric response to solvent polarity [103]. Together with their relatively small size, this makes them very promising precursors for the development of two-band fluorescent labels for peptide and proteins.

1.2.5. Protein studies by 3HC labels

One of the first application of 3HF derivatives for proteins was described by Sytnik et al. [104]. In this work, the interaction of 4'-diethylamino-3-hydroxyflavone (HC3) with serum albumin (SA) was investigated. SA is the major transporter in blood of non-esterified fatty acids as well as of many other low-polar metabolites and drugs. Albumin binds a huge variety of ligands, most of them being hydrophobic and low-soluble in aqueous media. The ligand affinities are determined not only by their hydrophobicity, but also by a number of other factors including steric ones. 3-Hydroxyflavone (HC1) was shown to bind to SA, leading to a strong fluorescence increase. However, the protein-bound form of HC1 does not exhibit two well-separated emission bands, probably due to the too polar character of this dye, which prevents an optimal interaction with the apolar binding sites of SA.

Later, the 2-(6-diethylaminobenzo[b]furan-2-yl)-3-hydroxychromone (HC4) probe was found to bind with strong affinity and high specificity to a single binding site of bovine SA [105]. Multiparametric analysis of the spectroscopic properties of the bound probe revealed that the binding site is characterized by very low polarity, high screening from aqueous environment and unusually high electronic polarizability, suggesting the participation of aromatic amino acids in the binding site. Furthermore, comparison of the binding of HC4 to SA of different species revealed that FA binds efficiently to all these proteins [106]. Binding occurs apparently at the same binding site and the properties of this site are similar in all species. Combination of FRET and ESIPT was used for investigating the binding sites of 3-hydroxyflavone (HC1) on human SA [107]. Energy transfer experiments from tryptophan to HC1 showed that two binding sites were involved in the human SA- HC1 interaction.

The first covalent labeling of protein with a flavone dye has been recently described [108]. A reactive derivative of HC3, 6-bromomethyl-4'-diethylamino-3-hydroxyflavone (BMFE) (**Fig. 1.44**) was used to label the bovine eye lens α-crystallin. This protein is characterized by a rather flexible three-dimensional structure, which allows its functioning as a heat-shock protein and its binding to various unfolded proteins. The thiol group of its sole Cys and probably also one or several amino groups of Lys located in low polar environment were the targets of the bromomethyl derivative BMFE (**Fig. 1.44**).

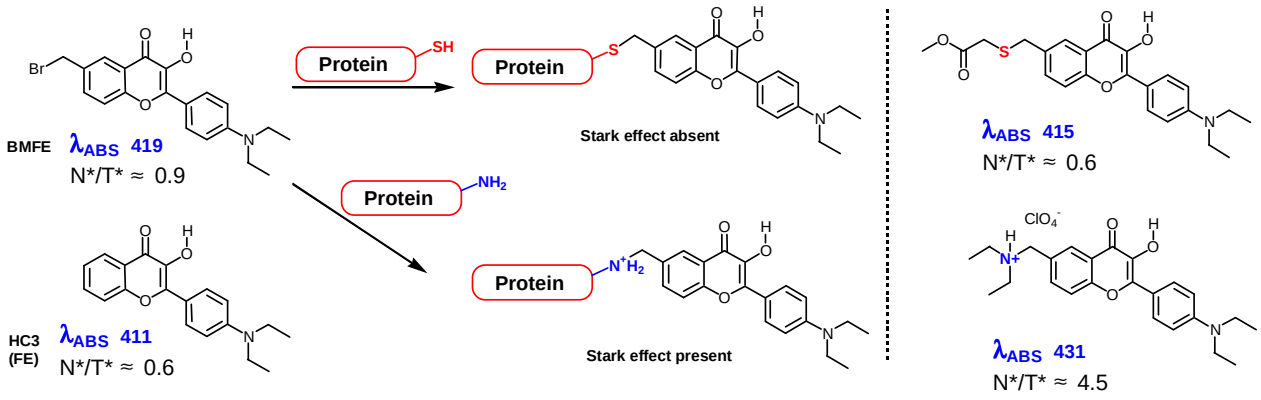

Figure 1.44. Structure of BMFE and its reaction with the SH/NH_2 groups of proteins (left) and model compounds for SH and NH_2 conjugates of BMFE (right). Absorption maxima and N*/T* band ratios are shown for solutions in dichloromethane.

To understand the spectroscopic behavior of the label attached to the protein, the fluorescence and absorption properties of model compounds were studied. Thus, for modeling the conjugation with the ε-amino group of Lys with formation of an ammonium group, a cationic derivative of the probe was used (**Fig. 1.44**). Conjugation with SH groups of Cys residues was modeled by alkylation of a small thiol-containing molecule.

The SH conjugate was found to exhibit absorption and fluorescence properties that are very close to those of BMFE and the parent fluorophore HC3 (FE), thus demonstrating that ESIPT is not affected by conjugation. Thus, the spectroscopic properties of the SH-labelled proteins can be analyzed using the published solvatochromic data on the HC3 dye. In contrast, the absorption and fluorescence spectra of the cationic derivative were shown to be red shifted about 15 nm as compared to dye HC3, probably due to an internal Stark effect induced by the positively charged ammonium group [109, 110].

Analysis of the spectral properties of α-crystallin labeled with BMFE showed the presence of two types of labeled species that differ in both excitation and emission spectra. These species correspond to the labeling of both SH and NH_2 groups. The contributions of both species to the spectra can be resolved by excitation-dependent fluorescence analysis that consists in comparison of the fluorescence spectra of the labeled protein at different excitation wavelengths.

Finally, the heat perturbation of α-crystallin [111] labelled by BMFE was investigated using excitation-dependent fluorescence analysis. It was shown that at room temperature, the environment of the SH-attached dye is rigid and low polar while at 60^0C it became more polar and highly flexible, exposing the dye to bulk water.

Nevertheless, though BMFE gave interesting results, it exhibits some drawbacks, like the significant overlap of its emission bands and the low relative intensity of the T* emission in polar media. To limit these drawbacjs, an improved reactive dye 6-bromomethyl-2-(2-furanyl)-3-hydroxychromone (BMFC) was introduced [112].

Like BMFE, it is a two-band ratiometric probe, but with much better resolved (by more than 100 nm) N* and T* emission bands, and larger relative intensity of the T* band, making the analysis of the spectral changes more simple. Application of BMFC allowed further characterizing the changes of the Cys microenvironment in α-crystallin. A decrease of the number of H-bonds near the Cys residue on heating up to 60^0 C was observed with this label. The lack of full reversibility of the observed effects within several hours suggested that the changes in the H-bond network in the vicinity of the Cys may be connected with structure rearrangements.

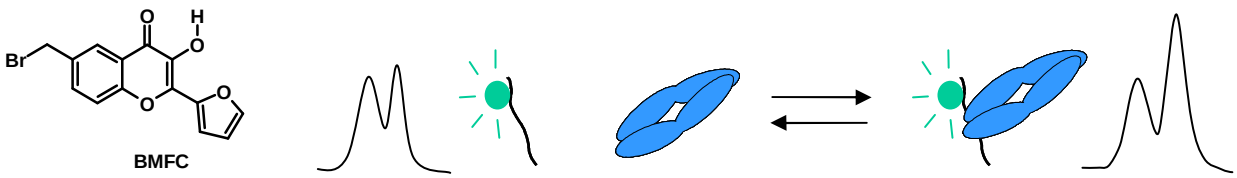

Figure 1.45. Schematic representation of sensing peptide-protein binding by BMFC label.

Recently, a first example of site-specific introduction of BMFC label into a short peptide was described [113]. The authors have designed and synthesized by solid-phase synthesis two peptide-based fluorescent biosensors for protein detection. Upon binding of the labelled peptides to the corresponding antibody, a decrease of the polarity of label environment through a change in the N*/T* intensity ratio was observed (**Fig. 1.45**).

Taken together, the aforementioned examples showed the interest of 3HC probes in protein studies. Nevertheless, further progress in this field requires to control the selectivity of labeling. One additional key point for the successful applications of these probes is the correspondence of the polarity range in the labeling site with the sensitivity of the fluorophore. For labeling and sensing protein interactions with relatively hydrated peptides in protic media, 2-furyl-3-hydroxychromone derivatives are the most appropriate.

1.2.6. Membrane studies by 3HF probes

Another important field of biological applications of fluorescent probes concerns biomembranes. Cellular membranes are dynamic systems, basically composed of a lipid bilayer, that play a crucial role in the cell life. Depending on its lipid composition, the membrane bilayer could differ in its charge as well as in its phase and hydration level. Lipid bilayers can exist either in a rigid **gel phase** with highly packed fatty acid chains (corresponding essentially to saturated lipids) or in a more fluid **liquid crystalline phase**. Lipid bilayers composed of saturated lipids can be characterized by their transition temperature between gel and liquid-crystalline phases (for example, 41 °C for bilayers composed of dipamitoylphosphatidylcholine). Saturated phospholipids and sphingomyelin can form also the so-called liquid ordered phase which requires cholesterol. This phase can co-exist together with the liquid-crystalline phase and is believed to be responsible for the formation of raft domains in cell membranes. Microviscosity, hydration and electrostatics are the key physicochemical properties of biomembranes defining their structure and function. Fluorescent probes are a powerful tool to monitor these properties.

Like in proteins, membrane investigation requires fluorescent probes not only bound to the membrane but also properly localized. Most of the probes are quite lipophilic molecules and their binding is essentially driven by hydrophobic interactions, sometimes together with an electrostatic contribution. This is the case when a positively charged group attached to the probe allows its location at the bilayer interface due to an interaction of this group with the negative charge of the phospholipid phosphate groups [114]. Additional stabilization and orientation of

the probe can be achieved by introduction at proper places of aliphatic hydrocarbon chains of different lengths, making the probe properties close to that of a lipid. This was realized with several new flavone derivatives [115], that contain a quaternary ammonium group as an attached positive charge, and hydrocarbon chains at different positions (**Fig. 1.46**). Better-defined probe localization was obtained by addition of negatively charged groups. The short three-carbon connector of F2N12S and PPZ (**Fig. 1.46**) between positive and negative charges appears complementary to the zwitterionic polar-head of phosphatidylcholines. In all cases, the chromophore was not modified and was still able to undergo ESIPT, and thus to provide two-band ratiometric fluorescence response to the environment.

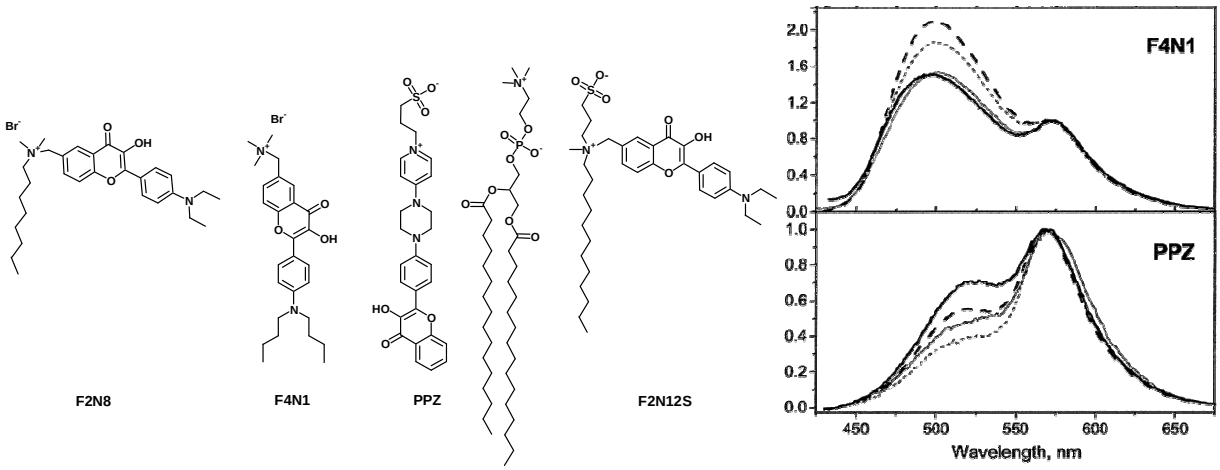

Figure 1.46. Localization of several 3HF- based membrane probes and examples of their fluorescence spectra in neutral (solid lines) and negatively charged (dashed lines) phospholipids [115].

The probes presented in **Fig. 1.46** were used for sensing membrane properties. Interestingly, these probes show different spectra in membranes. This can be explained by their different localization in the membrane bilayer, as determined by the parallax quenching method measuring the probe fluorescence quenching by shallow, medium, or deep nitroxide-labeled lipids incorporated into DOPC vesicles [115]. According to this method, F2N8 is located at the level of the ester groups and glycerol residues of phospholipids while F4N1 and PPZ probes are embedded deeper (**Fig. 1.46**). As it could be inferred from the location of the charged group of F4N1 and PPZ, their identical chromophore is inversely oriented in the bilayer. This explains the different influence of the membrane surface charge on their fluorescence response. In negatively charged vesicles, F4N1 shows higher N*/T* band ratio while in neutral vesicles PPZ shows a lower ratio. The strong sensitivity of the N*/T* ratio to the electric field (Stark effect) allows using these dyes to sense the membrane dipole potential [116], created by various dipoles (carbonyl groups of the phospholipids and bound water molecules) between the top and the middle of the phospholipid bilayer. Moreover, due to their strong binding to the external leaflet

of the plasma membranes, F4N1 and the benzo-analogue of PPZ were shown to be applicable for imaging the cellular membrane dipole potential [117].

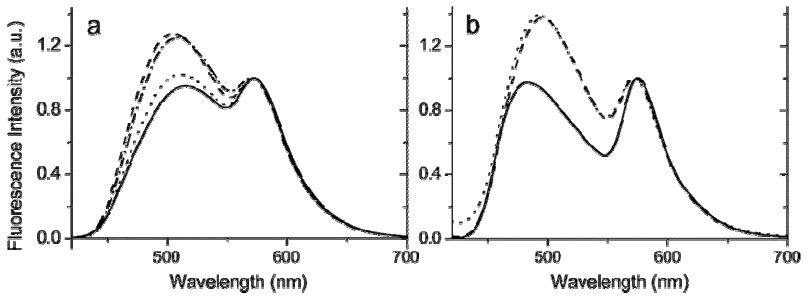

Figure 1.47. Fluorescence spectra of F2N12S in lipid vesicles (a) and cells (b). In (a), the lipid vesicles are composed of EYPC (solid), EYPE (dot), EYPG (dash dot), or PS (dash). In (b), the spectrum of F2N12S was recorded in normal (solid) or apoptotic cells (dash).

Sensitivity of the probes to surface charge [115, 118-121] was applied for the detection of apoptosis. During this process which precedes cell death, the two leaflets of the cellular membrane mix and the surface potential is modified, essentially because the negative phosphatidylserine molecules migrate from the inner to the outer leaflet. Probe F2N12S was found to be very sensitive to monitor such changes in living cells (**Fig. 1.47**) [122], giving a response similar to that observed in model systems. The ratiometric response of this probe allowed discrimination of normal and apoptotic cells by confocal microscopy as well as by flow cytometry using two-color detection. The fluorescence response of F2N12S probe is similar to that of F2N8 [123, 124] but its more strict localization in the external leaflet of the lipid bilayer allows proper apoptosis sensing in the living cells.

Noticeably, 4'-dialkylaminoflavone-based dyes that show low quantum yields in water with only one fluorescence emission band, exhibit strong dual emission in lipid membranes. This property enables to conceive protein and peptide labels able to monitor protein binding to membranes and to report on environment properties of the labelled site.

Dyes of the 3-hydroxychromone family have found wide applications as a tool for studies of biomolecular systems. Their concentration-independent two-band ratiometric response facilitates studies of membrane properties and protein conformation changes. Their diversity allows the selection of dyes sensitive in the appropriate polarity range. Thus, 3HCs are prospective candidates for construction of biomolecule labels.

1.3. Human immunodeficiency virus type 1 (HIV-1)

The first case of Acquired ImmunoDeficiency Syndrome (AIDS) was registered in USA in 1981. Patients presented symptoms and opportunistic infections resulting from the damage to the human immune system. In 1983, the causative agent of AIDS, Human Immunodeficiency Virus (HIV, type 1) was discovered by Luc Montagnier and his Team in France. For this achievement, in 2008, he received the Nobel Prize of Medecine together with Françoise Barré-Sinoussi.

In the 2008 report of the global AIDS epidemic, it was estimated that 30 million–36 million people world-wide are living with the HIV. In more than 20 years, about 25 million of people died due to AIDS (about 1.9–2.4 million in 2007) and it has been estimated that 1.8–4.1 millions became newly infected with HIV in 2007. In some countries more then 10% of adults are infected (**Fig. 1.48**)

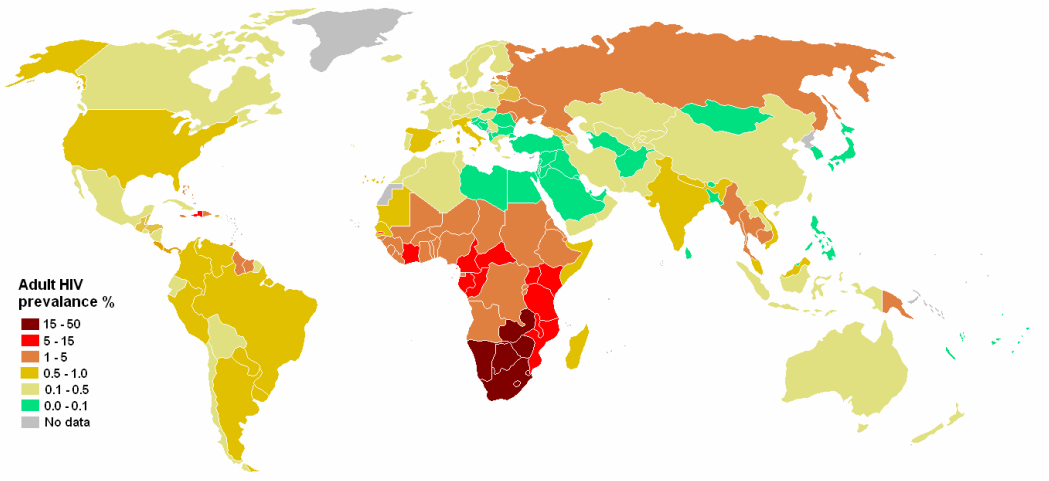

Figure 1.48. Prevalence of HIV among young adults (15-50) per country in 2008.

HIV is a lentivirus, a member of the retrovirus family. It infects cells from the human immune system such as lymphocytes CD4+, but also macrophages and dendritic cells, leading to their death. When the number of immune system cells declines below a critical level, the cell-mediated immunity is lost, and the body becomes progressively more susceptible to opportunistic infections. HIV is transmitted by sexual contact, through blood and from infected mother to child.

There are two types of HIV, type 1 (HIV-1) and type 2 (HIV-2). HIV-1 is the most prevalent in the worldwide pandemic. HIV-2 is present mainly in West Africa, where it was discovered in 1986 and it is slowly but continuously spreading to Europe, Asia and America.

Compared to HIV-1, HIV-2 is less transmissible and less pathogenic, with lower viral loads and giving an asymptomatic and a slower progression to AIDS.

Due to this variability, HIV-1 variants are classified into three major phylogenetic groups: group M (Main), group O (Outlier, restricted to west-central Africa), and group N (Non-M/Non-O. Rare group discovered in 1998 in Cameroon). Group M, which is responsible for the majority of infections in the worldwide HIV-1 epidemic, can be further subdivided into ten recognized phylogenetic subtypes, or clades (A to K, excluding E, which is actually a CRF (circulating recombinant form)

1.3.1. Genetic organization and structure of the virus

A) Genetic organization

a. Proviral DNA (Fig. 1.49)

Genomic DNA is flanked by two LTRs (Long Terminal Repeats) that are non coding region. However these LTRs are important for the integration of the viral DNA and for the transcription of viral RNA. In addition, these sequences play a role in the viral RNA context (see below)

HIV-1 genomic DNA encodes for three polyproteins, Gag, Pol and Env that are clived either by cellular or viral protease.

Gag gene (group-specific antigen) generates a precursor $Pr55^{Gag}$. After clivage by viral protease, it produces structural components that make up the core of the virion: MA (matrix), CA (capsid), NC (nucleocapsid). Peptides p1, p2 and p6 are also generated from Gag polyprotein but their function is less clear.

* ***Pol*** gene encodes a precursor that generates three enzymatic proteins: PR (protease) that is cleaved by self-catalysis, RT (reverse transcriptase), and IN (integrase). These two proteins are clived by the viral protease. Pol precursor is obtained by a -1 ribosomal frameshift mechanism that occurs at a frequency of 5 to 10% of Gag translation events [125].

* ***Env*** gene encodes a precursor $Pr160^{env}$. This Env polyprotein is cleaved by the cellular protease to produce a transmembrane protein (TMgp41) and a surface protein (SUgp120).

In addition HIV-1 encodes six regulatory/accessory proteins (Tat, Rev, Vif, Vpr, Vpu, and Nef) required for the viral pathology [126].

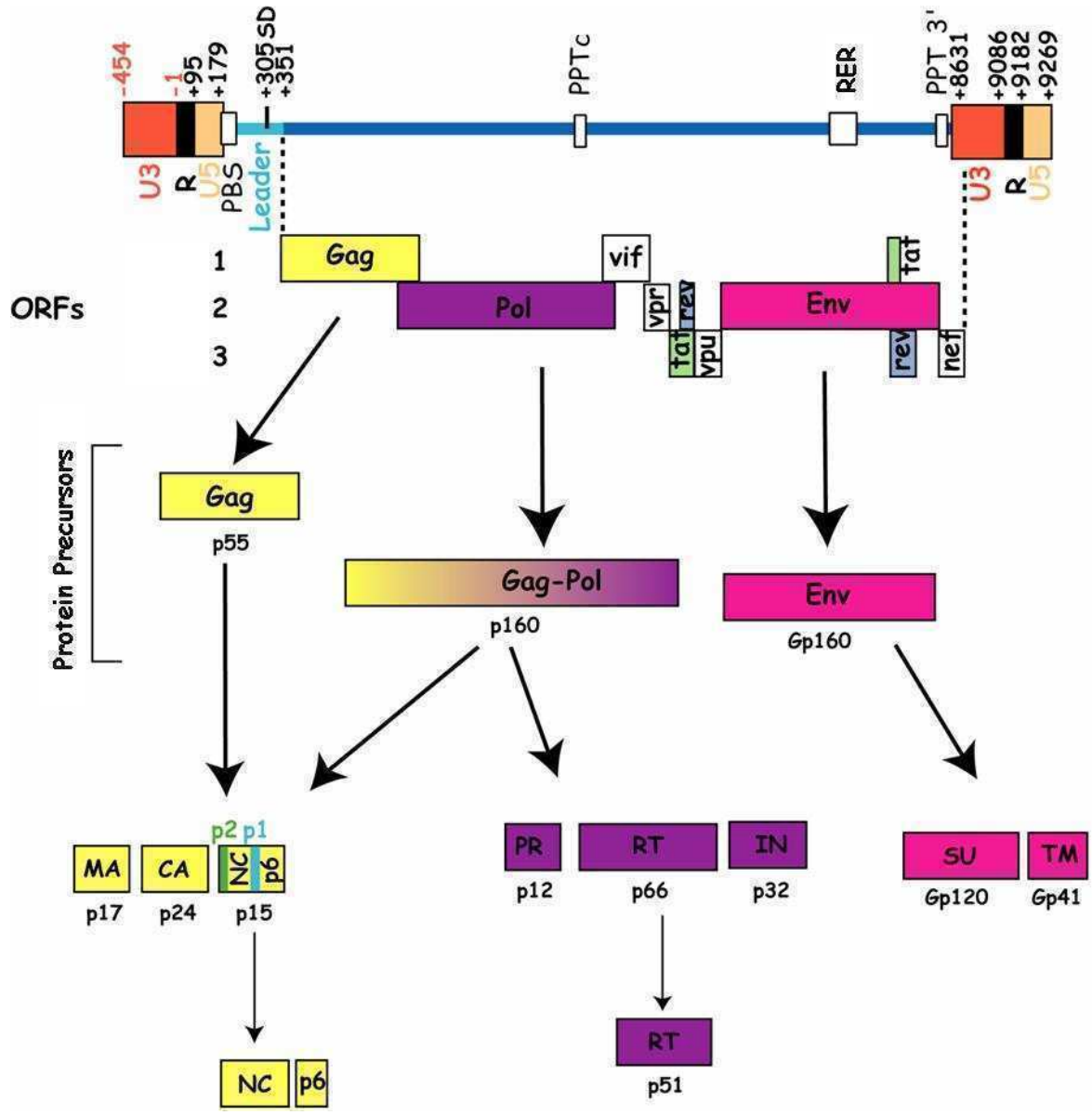

Figure 1.49. Genetic organization of HIV-1. The proviral DNA is flanked by two LTR (Long Terminal Repeats : U3RU5) sequence that contain transcriptional regulatory elements.

b. Viral RNA

The HIV-1 genomic RNA is diploid, consisting of two copies of homologous single-stranded RNA of 9.2 kb that are linked non covalently near their 5' end. This RNA is capped and polyadenylated. It is produced after the integration of provirus into the host cell genome and transcripted by the cellular machinery. Transcription of the viral RNA begins in 5' of the R sequence located in the 5' LTR and ends in 3' of the R sequence located in the 3' LTR.

Viral RNA contains coding regions encoding 14 viral proteins (see below for the details) and also non-coding regions that are important in the HIV-1 replication cycle. Non coding regions are located in the 5' and 3' parts of the viral RNA and inside the RNA.

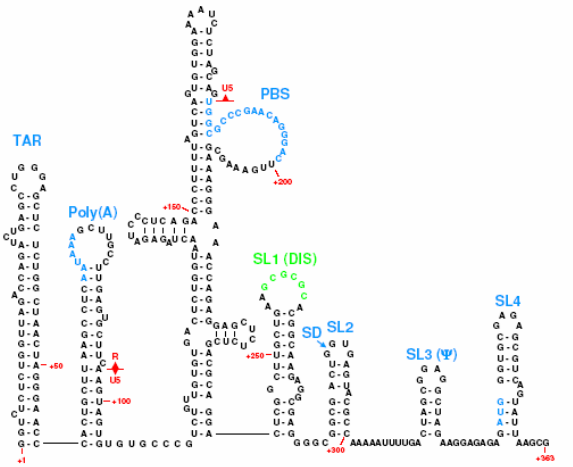

Figure 1.50. Sequence and structure of the non-coding regions of the 5' region of HIV-1 RNA. (From [127]).

- **5' region of the viral RNA** (**Fig. 1.50**)

Many stem-loops are found in the 5' region of the RNA genome and are involved in different steps of the replicative cycle, such as transcription, splicing, translation, dimerization and encapsidation of genomic RNA as well asin the reverse transcription and recombination.

- **Region R** contains two hairpins- like sequences. The TAR hairpin binds Tat and several cellular proteins [128] and allows the transcriptional regulation of the viral genome [129]. The second hairpin contains a polyadenilation signal AAUAAA in the loop and is only effective in the 3' end of the viral RNA. It allows clivage of the viral RNA and addition of a poly A tail.

- Primer Binding Site (PBS) is a sequence of 18-nucleotides complementary to the 3' end of a specific tRNA : $tRNA^{Lys3}$, which is important to initiate the reverse transcription [130].

- The leader region (between the PBS and the starting codon). It contains four stem loops (SL1 – SL4) crucial for genome recognition and RNA dimerization [131]. It was shown that viral genome dimerization starts from the DIS (Dimerization Initiation Site) sequence [131], SL1 (**Fig. 1.50**). SL2 contains the major Splicing Donor (SD) site [132] that is used to generate all subgenomic spliced mRNAs. Viral RNA recognition during encapsidation mostly depends on the SL3 sequence [133] and plays a role in the virus assembly [134, 135]. Finally, SL4 serves as an initiation codon for the Gag gene.

- **Internal elements :**

- Splicing sites allow alternative splicing and the production of more than 30 different viral RNAs.

Rev Response Element (RRE), close to the 3' end of the viral genome [126], contains about 200 nucleotides structured in hairpins. REV protein binds to the RRE sequence found in non- or mono-spliced viral RNA and regulates their export.

Polypurine tract (ppt)

There are 2 PPT sequences (PPTc and 3' PPT), that are rich in guanines and adenines and serve as primer during synthesis of (+)DNA (one of the steps of reverse transcription) due to their resistance to the degradation by the RNAse H activity of HIV RT [126].

B) Viral particle

The mature HIV virion shows a spherical morphology of 100–120 nm in diameter (**Fig. 1.51**) [136]. The lipid bilayer, which forms the virion envelope comes from the host cell plasma membrane and contains viral glycoproteins, Env (TMgp41 and SUgp120: 300-500 copies per particle). During the maturation of the virus, the viral capsid protein (CA) oligomerizes and forms a capsid or "core" of the virus, of conical shape, which surrounds a ribonucleoprotein complex.

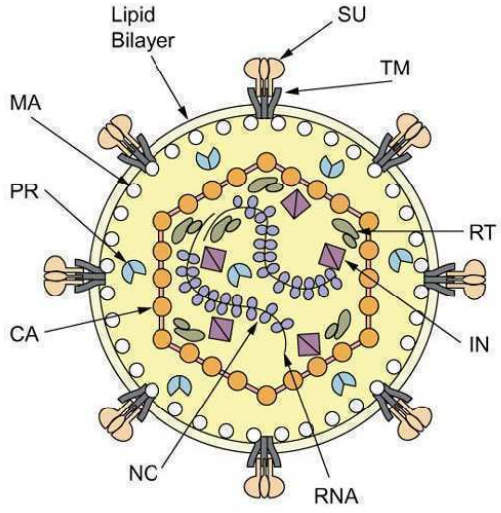

Figure 1.51. Schematic structure of the mature virion of HIV-1.

The core contains two genomic RNA molecules covered and protected by the nucleocapsid protein (NC), and all the enzymes necessary for viral replication as retrotranscriptase (RT), protease (PR) and integrase (IN). In addition, viral (Vpu, Vif, Vpr, Nef) and cellular proteins (UNG) and tRNAs of cellular origin, including in majority $tRNA^{Lys3}$, are encapsidated. A matrix composed of an association of the viral MA protein serves as interface between the lipid bilayer and the core, ensuring the integrity of the virion particle.

1.3.2. HIV proteins

Depending of their function, viral proteins could be classified in four groups:

- Envelop proteins - Transmembrane (TM) and Surface (SU) proteins
- Structural proteins - Matrix (MA), Capsid (CA) and Nucleocapsid (NC)
- Enzymatic proteins - Protease (PR), Reverse transcriptase (RT) and Integrase (IN)
- Regulatory/accessory proteins - Vpu, Vif, Vpr, Nef, Tat and Rev

A) Envelop proteins

The HIV-1 envelope glycoproteins are the product of the Env gene. After a clivage mediated by the cellular protease, the Env precursor (gp160) allows the production of the surface envelope glycoprotein (SUgp120) and the transmembrane glycoprotein (TMgp41). On the surface of the viral particle, the envelope glycoproteins TMgp41 form as a trimer in which each monomer is linked non-covalently to a glycoprotein envelope SUgp120.

Surface protein (SUgp120) is a highly glycosylated 515 amino acids protein which is located on the outside of the viral particle by being non-covalently attached to the TMgp41. Gp120 contains five variable regions (V1 to V5) of which four loops are exposed on the surface of the cell. These variable regions and notably the V3 region are critical. In fact, after a specific recognition between gp120 and the CD4 receptor at the surface of the target cell, a conformational change of gp120 allows the exposition of the V3 loop that could interact with co-receptors CCR5 or CXCR-4.

Transmembrane protein (TMgp41) is a 345–amino acid glycosylated protein located in the viral membrane. In the virus, TMgp41 forms two antiparallel helices that combine to form a trimer (**Fig. 1.52**). The protein TMpg41 contains three domains: an intracellular (endodomain), a transmembrane (TM) and an extracellular (ectodomain) domain. The N-terminus of the ectodomain is called the fusion domain and is important for the fusion between the virion membrane

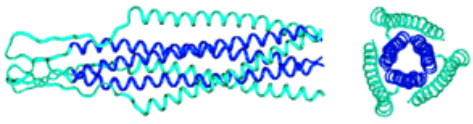

Figure 1.52.: Side and top views of HIV-1 TMgp41 trimer. C-terminal (residues 1–77) and N-terminal domains (residues 117–154) are blue and cyan, respectively.

and the plasma membrane of the host cell. This step takes place after the interaction between gp120/CD4 and the coreceptor.

B) Structural proteins

The Gag gene encodes a polyprotein (55kDa) that self-assemble to the membrane cell to form the immature virion. Gag particles can form virus-like particles (VLP) in the absence of other viral proteins. During virion maturation, Gag is cleaved by protease into three structural proteins (matrix, capsid and nucleocapsid) and other products of lower molecular weight: p1 (SP2), p2 (SP1) and p6 (**Fig. 1.53)**

Matrix (MA) is the N-terminal component of the Gag polyprotein (**Fig. 1.53**). MA is important for targeting the Gag and Gag-Pol precursors to the plasma membrane prior to viral assembly. In the mature viral particle, the 132-residue MA protein lines the inner surface of the virion membrane forming an interface between the envelop and the capsid (**Fig. 1.51**). Two distinct features of MA are involved in membrane targeting: an N-terminal myristate group and basic residues located within the first 50 amino acids. The trimeric form is presumed to be biologically relevant because mutation of residues involved in trimerization (residues 42–77) abolishes viral assembly [138] and because basic residues important for membrane localization are arranged on the putative membrane-binding surface of the trimer. Moreover, the monomeric form of MA can also interact with the pre-integration complex (PIC) and play a role in its nuclear localization.

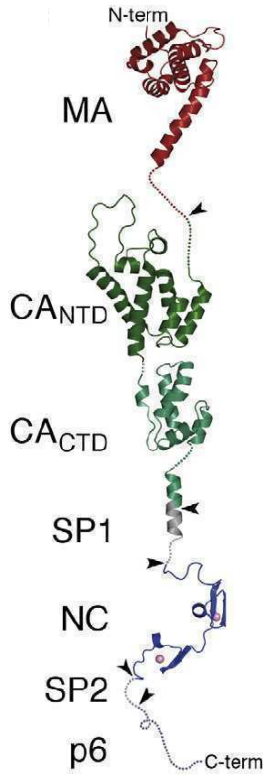

Figure 1.53. Structural model of the extended Gag polypeptide, derived from high-resolution structures and models of isolated domains. Unstructured and linker regions are represented by dashed lines. PR cleavage sites are indicated by the arrowheads [137].

Capsid (CA) is the second component of the Gag polyprotein produced during virion maturation. About 2000 molecules of CA form the capsid core of the virus particle. The C-terminal domain (CTD, aa 152–231) consists of four α-helixes (**Fig. 1.54**) primarily involved

in assembly, but also in CA dimerization and Gag oligomerization. The N-terminal domain (NTD, aa 1–151) plays a major role for infectivity, apparently by participating in viral uncoating through its association with a putative cellular chaperone, cyclophilin A (CypA) [139]. It is also important in the morphogenesis of the capsid.

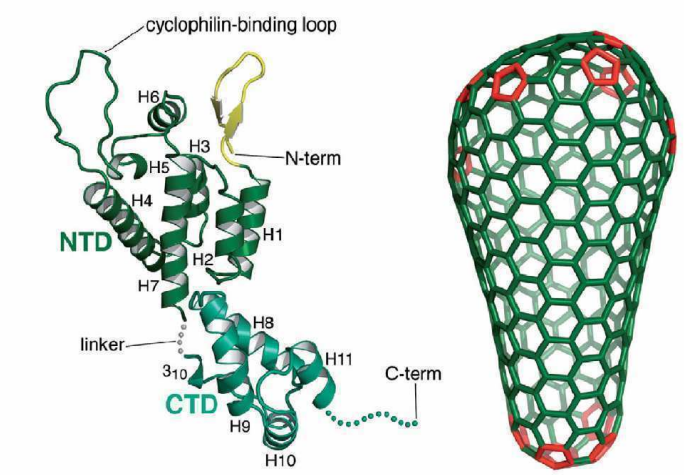

Figure 1.54. Proposed structure of the capsid protein [137] predicted from the structures of the N-terminal domain (NTD) and C-terminal one (CTD) determined separately [140]. α-helixes are marked as H1 – H11. The right figure shows the model for the conical capsid, with CA hexamers (green) and pentameric declinations (red) [137].

Nucleocapsid (NC) is the third component of the Gag polyprotein (**Fig. 1.53**). NC is a small (55 amino acid) basic protein characterized by two highly conserved zinc finger motifs, connected by a basic sequence.

NC binds to nucleic acids via two zinc fingers motifs and is involved in many processes such as:

- Encapsidation of the viral RNA (by binding specifically to the packaging signal) and the assembly of the viral particle by promoting the oligomerization of the Gag precursor
- Coating of the genomic RNA that presumably protects it from nucleases and compact it within the core.
- Stabilization of the RNA dimer
- Reverse transcription and integration, which are likely promoted through the nucleic acid chaperone properties of NC.

Functions and structure of NC will be described in more detail in Chapter 1.3.4.

p6 is a small 6kDa protein consisting of 51 amino acids, that is present in mature virions. On the C-terminus it contains a L-X-S-L-F-G sequence that is important for Vpr binding and

incorporation into viral particles. The p6 protein plays also a role in the budding of the viral particle.

SP1 and **SP2** also known as p2 and p1, respectively are small proteins formed after clivage of the Gag precursor (**Fig. 1.53**). They are required during the assembly of the Gag and Gag-Pol polyproteins, and contribute to the recognition of the encapsidation signal of the viral genomic RNA.

C) Enzymatic proteins

Enzymatic proteins are products of the ***pol*** gene. After self catalysis, the viral protease (that belong to the Gag-Pol precursor) cleaves the polyprotein precursor Gag-Pol and allows the production of protease, reverse transcriptase and integrase.

Protease (PR) is 99 amino acid homodimer. (**Fig. 1.55**) Its active site is at the interface between the two subunits. PR is produced from the Gag-Pol precursor by a self-catalysis mechanism. It cleaves Gag and Gag-Pol polyproteins that are encapsidated into immature virions. This induces conformational rearrangements within the particle, to produce the mature infectious viruses. Some of these "maturation" events may occur simultaneously with assembly and budding. PR cleaves at several polyprotein sites to produce the final MA, CA, NC, and p6, p2, p1 proteins from Gag and PR, RT, and IN proteins from Pol (See **Fig. 1.47** and **1.50**).

.

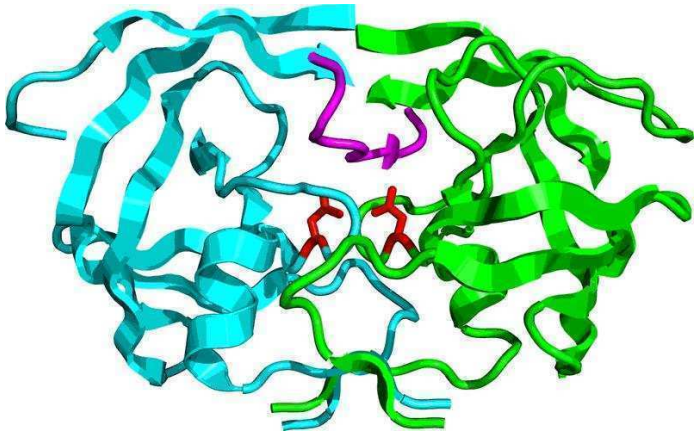

Figure 1.55. Structure of the HIV-1 protease homodimer (PDB file 1KJF). The two monomers are colored in blue and green, respectively.

Reverse Transcriptase (RT) is first produced as a homodimer composed of two p66 subunits. After a maturation step, a heterodimer containing two subunits p66 and p51 is obtained

(**Fig. 1.56**). P66 subunit is composed of 5 domains. The RNase H domain, corresponding to the C-terminus of p66 and is absent in p51. Three domains called fingers, palm and thumb form the polymerase catalytic site. The last domain is called the connexion domain since it connects the polymerase catalytic site and the RNase H domain. Although the four domains are structurally very similar in both sub-units, their relative position differs from one subunit to another, so that p51 has no polymerase activity but plays a structural role. RT is an RNA- and DNA-dependent DNA polymerase and contains also an endonuclease activity (RNaseH) that is polymerase dependent or independent. The RNaseH activity cleaves specifically the RNA in the DNA/RNA duplexes formed during reverse transcription.

One of the most important properties of RT is that it lacks proofreading activity. As a result, RT has a high error rate and generates a large number of mutations, leading to a large number of HIV-1 variants.

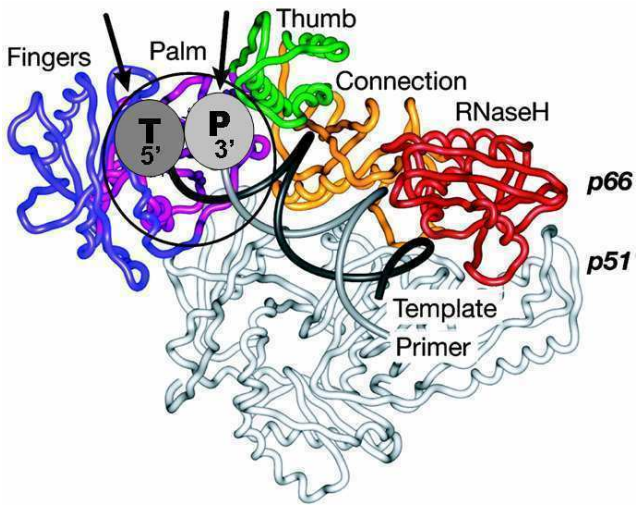

Figure 1.56. Structure of HIV-1 RT with a DNA primer/template The DNA primer (light gray) and template (dark gray); the fingers (blue), palm (purple), thumb (green), connection (yellow), and RNaseH (red) subdomains of the p66 subunit of HIV-1 RT; and p51 subunit (white) are in ribbon representation. The region circled includes the polymerase active site.

Integrase (IN) is a 32-kDa (288 amino acids) protein encoded by the end of the *pol* gene. IN is composed of three structurally and functionally distinct domains and all three domains are required for each step of the integration reaction. 1) The N-terminal domain contains a conserved "HH-CC" motif that binds zinc and possibly favors protein oligomerization. 2) The central catalytic core domain contains the catalytic site. This domain is also needed for binding to viral DNA. 3) The C-terminal domain contributes to DNA binding and oligomerization necessary for the integration

This enzyme is responsible for the two consecutive reactions that constitute the overall process of viral DNA integration [142]. The first of these two reactions is 3'-processing, which involves cleavage of the 3'-terminal GT dinucleotide at each extremity of the viral DNA. The hydroxyl groups of the newly recessed 3'-ends are then used in the strand transfer reaction, for the covalent joining of viral and target DNAs, resulting in the full-site integration [143]. Integrase is active as an oligomer (**Fig. 1.57**). A single IN dimer at each extremity of viral DNA molecules is required for 3'-processing, while a dimer of dimers is responsible for the subsequent full integration [144, 145]. Additionally, aggregation, mediated by nonspecific IN-IN interactions, occurs in presence of DNA [146].

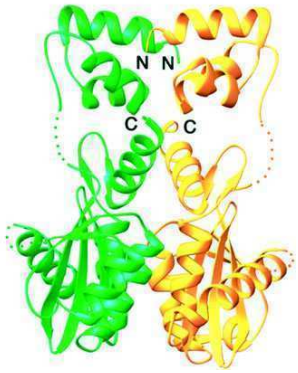

Figure 1.57. Structure of the HIV-1 integrase dimer. The two monomers are in green and yellow, respectively. (From [141]).

D) Regulatory and accessory proteins

Transactivating regulatory protein (Tat) protein is a 101 amino-acid protein that also exists as an 86 amino acid form in some virus strains [147]. The main role of the viral Tat protein is to trans-activate the HIV-1 gene expression [148]. The absence of Tat decreases the trans-activation rate several hundred times. The Tat protein is composed of five domains (**Fig. 1.58**). The first three domains (aa 1-47) form the transcriptional activation and cofactor binding region that is functionally autonomous [149]. It consists of the N-terminal region, a cysteine rich region and region rich in hydrophobic residues. The two other domains (Arg-rich and Glu-rich regions) are involved in RNA binding [150, 151]. The arginine-rich RNA-binding motif is essential for the recognition and the binding to the TAR loop and acts as the nuclear localization signal allowing the protein to enter in the nucleus. The cysteine-rich fragment of Tat is able to bind Zn. This binding is thought to modulate the Tat activity, especially on microtubule assembly [152].

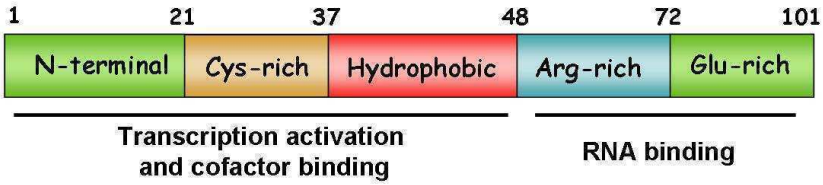

Figure 1.58. Functional domains of Tat protein.

The flexible structure of Tat may well account for its ability to interact with multiple proteins and nucleic factors in a manner similar to other chaperones such as the HIV-1 nucleocapsid protein. It was also found that the Tat (44-61) peptide encompassing the Tat basic domain is the smallest known peptide with nucleic acid chaperone activities [153].

Virion Infectivity Factor (Vif) is a small highly basic, 192 amino acid protein. The requirement for Vif in HIV-1 replication is cell-type dependent. Vif is essential for *in vivo* infectivity and pathogenesis, functioning as an auxiliary protein. One of the functions of Vif is to impair an innate antiviral defense mediated by the cytidine deaminases APOBEC-3G and 3F encoded by non permissive cell lines.

In the absence of Vif, APOBEC-3G and 3F are packaged into the HIV-1 particles through formation of a complex with the viral NC domain of the Gag precursor [154, 155]. It causes extensive C-to-U mutations during synthesis of the (–) DNA strand, leading to either degradation of viral DNA or introducing a number of mutations into the viral DNA that could be detrimental for virus replication. In addition, Vif interacts with Gag, the viral protease and the genomic RNA. These interactions are likely important for the correct particle assembly. Moreover, a chaperone activity was also reported for Vif [156, 157].

Viral protein U (Vpu) is an 81-residue integral membrane protein with an N-terminal hydrophobic membrane-spanning domain and a C-terminal cytoplasmic tail (**Fig. 1.59**) [157, 158]. Vpu promotes the degradation of cellular CD4. This is needed because newly synthesized Env proteins are sometimes held in the endoplasmic reticulum through interactions with the newly synthesized CD4 molecules leading to their degradation. The C-terminal domain of Vpu interacts with CD4 (to direct them to a degradation pathway), liberating the Env proteins that could be transported to the cell surface for assembly into viral particles In addition, Vpu can also stimulate the virion release, and it has been proposed to be an ion channel [136].

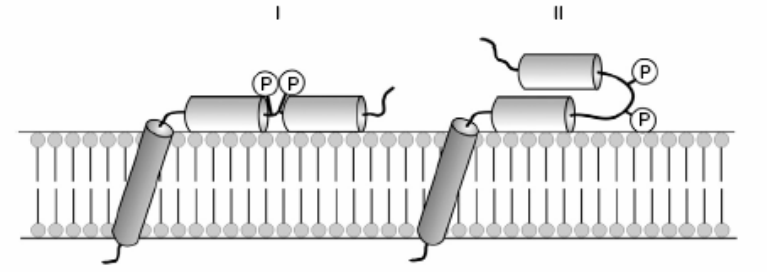

Figure 1.59. Proposed secondary structure of the Vpu protein in two modes of orientation. Symbol (P) shows the positions of the phosphorylated serines 52 and 56 infolved in the promotion of the degradation of the CD4 receptors. (From [157])

Negative Factor (Nef) is a 206–amino acid protein that, like Vpu, reduces the levels of cellular CD4. In contrast to Vpu, Nef acts on CD4 molecules that have already reached the cell surface. Nef-induced CD4 downregulation involves an acceleration of CD4 endocytosis followed by its degradation through the endo-lysosomal pathway [159]. This prevents the surinfection of infected cells and their premature death. Nef can also downregulate the expression of the MHC (major histocompatibility complex) class I and II molecules [160, 161], which help to protect infected cells from killing by cytotoxic T cells.

Regulatory of Virion Expression (Rev) is an essential accessory protein whose function is to transport mRNA to the cytoplasm. This 116 amino acid phosphoprotein binds to RRE ("Rev-response element", a cis-acting element) within the Env gene of all unspliced mRNAs. Binding is mediated by an arginine-rich domain that forms an α-helix and specifically recognizes an internal loop in the IIB stem (**Fig. 1.60**). The RRE contains several hairpins and binds several Rev monomers. Oligomeric binding is important for the Rev function, presumably because it increases the concentration of leucine-rich nuclear export signal sites on a single mRNA.

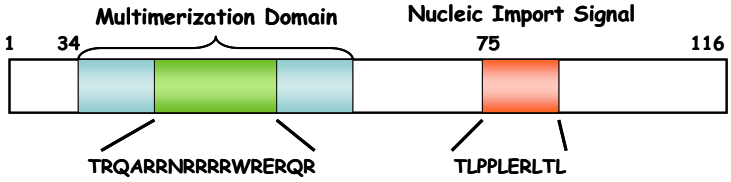

Figure 1.60. Functional domains of the Rev protein. The arginine-rich domain (34-50) is essential for nucleic acid binding. The nucleic import signal is within the leucine-rich domain (in red) [162].

Viral protein R (Vpr) is an 96–amino acid protein involved in the nuclear transport of the preintegration complexes [143]. In addition to its nuclear uptake function, Vpr can also induce G2 cell cycle arrest as well as cell apoptosis. Sustained expression of Vpr was shown to kill T cells through apoptosis.

Functions and properties of Vpr are described in more detail in Chapter 1.3.5

1.3.3. HIV-1 life cycle

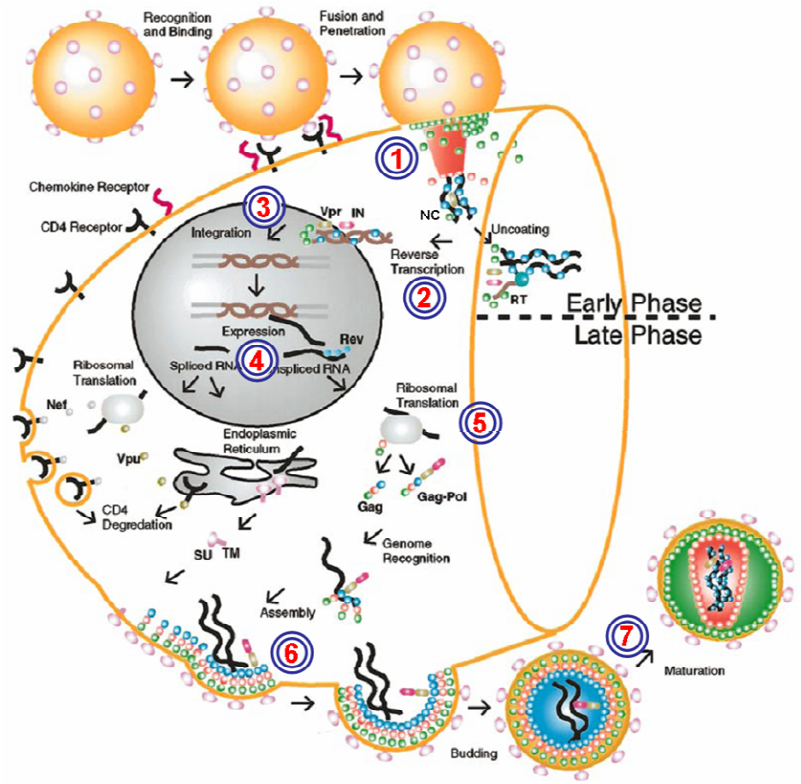

Figure 1.61. HIV-1 replication cycle. During the early phase of replication (upper portion), the virus binds to CD4 and chemokine receptors on the cell surface, triggering fusion of the viral and cellular membranes. During or after uncoating of the core (red), the viral RNA genome is reverse-transcribed to proviral DNA, which is transported to the nucleus and integrated into the cellular DNA. Late phase (bottom portion) consists of transcription, translation, assembling, budding and maturation. (Figure adopted from [163])

The HIV-1 life cycle (**Fig. 1.61**) could be divided in two main phases [164, 165]:

- **A pre-integration phase**, which begins with the recognition of the host cell, entry of the virus and its decapsidation followed by the reverse transcription step, the nuclear import of the viral genome, and ends with the integration of proviral DNA. These steps are carried out mainly by the viral proteins present in the virion.
- **A post-integration phase**, including the transcription of integrated provirus, translation of viral proteins, assembly, budding and maturation of the virion. During this phase, the virus diverts the cellular machinery of transcription, splicing, transport, and translation, which are regulated by viral proteins (Tat, Rev ...).

A) Pre-integration phase

1) Binding to cell and virion core uncoating

The infection begins with the attachment of the virions to the cell surface. This step is promoted by the envelope glycoproteins on the surface of the virus. The SU proteins bind to CD4 and chemokine receptors (CCR5 ou CXCR-4) (**Fig. 1.61**). This interaction allows a conformational change of the TM protein that promotes virus-cell membrane fusion and the entry of the core into the cell. The core is then released into the cytoplasm of the host cell where it is uncoated to expose the nucleoprotein complex, containing the viral RNA, $tRNA^{Lys3}$, cellular and viral proteins. This step is called decapsidation.

2) Reverse transcription

After uncoating of the core, the viral RNA genome is reverse-transcribed by the viral RT to proviral DNA.

Transcription starts after the annealing of $tRNA^{Lys3}$ to the complementary primer binding site (PBS) near the 5' end of the viral RNA genome (**Fig. 1.62**, step 1). Minus-strand strong-stop DNA (ss-DNA) synthesis starts at the 3 'end of $tRNA^{Lys3}$ and continues to the 5' end of the RNAv, while the polymerase-dependent RNase H concomitantly degrades the RNA template (step 2). ss-DNA is then transferred to the 3 'end of the genome (step 3). This transfer is mediated through the repeated R sequences at both ends of viral RNA and reverse transcription is resumed to generate the cDNA(−) (step 4).

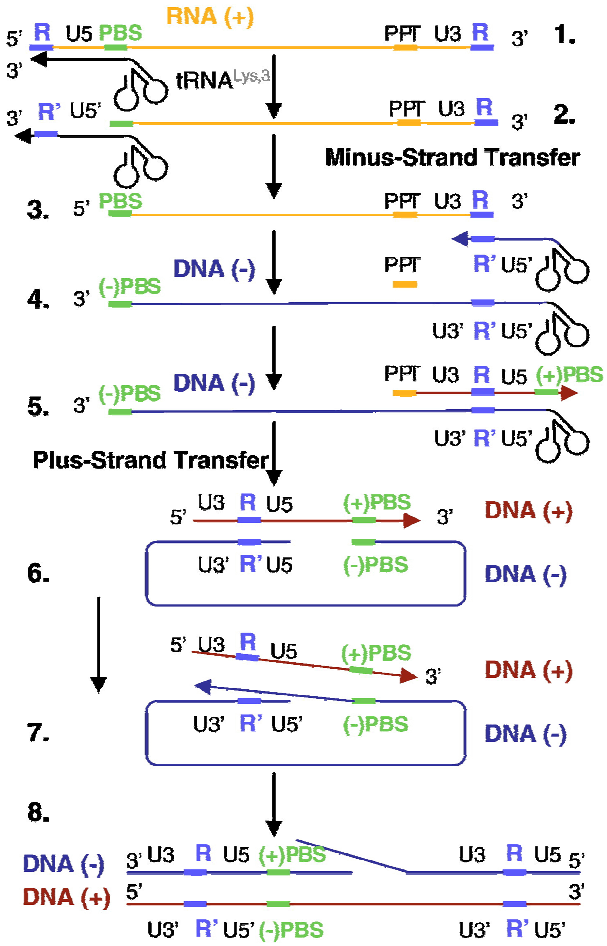

Figure 1.62. Reverse transcription scheme. The different steps are detailed in the text.

During the synthesis of this strand, the RNase H activity of RT degrades the RNA template with the exception of two resistant identical 15 nt sequences rich in purines called PPT3' and PPTc. Plus-strand DNA synthesis is primed by the PPT sequences, and continues to the end of the minus-strand template (step 5). The $tRNA^{Lys3}$

primer is specifically removed by the RNase H activity of RT and the second strand transfer occurs (step 6) to allow the completion of the proviral DNA (steps 7 and 8).

3) Transport to nucleus and integration

The synthetized proviral DNA, associated with viral (NC, Vpr, MA and IN [143]) and cellular proteins is transported to the nucleus. This complex is called the preintegration complex (PIC). The molecular mechanism by which retroviral PICs cross the nuclear envelope is still poorly understood.

After nuclear import, the proviral DNA is integrated into the host cell genome. This reaction is catalyzed by the viral integrase, which specifically recognizes the two LTR ends of viral DNA.

B) Post-integration phase

1) Transcription

The proviral DNA is transcribed by the cellular RNA polymerase II, starting from the promoter located in the 5' long terminal repeat . Tat largely enhances the rate of transcription. Then, a set of spliced and genomic-length RNAs are transported from the nucleus to the cytoplasm, where they can be translated or packaged. This step is regulated by Rev, the regulator of viral protein expression.

2) Translation

In the cytoplasm, the cellular machinery is diverted by the virus to allow viral protein synthesis.

Translation of the unspliced RNA by the cellular polysomes produces the viral Gag and Gag-Pol proteins. Mono- and multi-spliced mRNAs encode the Env, and Regulatory/accessory proteins.

3) Assembling and budding [137, 165]

The formation of a viral particle requires as a first step, the transport of the Gag precursor at the plasma membrane and its association with various viral and cellular partners. Specific interaction between the NC domain of Gag precursor and a region located 5 'of viral RNA is responsible for its selection and its encapsidation during assembly [165]. A dimeric RNA is encapsidated in a viral particle. Each virion is made of 1500 to 2000 molecules of Gag and 100 polyproteins Gag-Pol, and two copies of genomic RNA. The Env precursor is synthesized in the

endoplasmic reticulum. It leads to complex glycoproteins, which are transported to the membrane of the infected cells to form the viral particles.

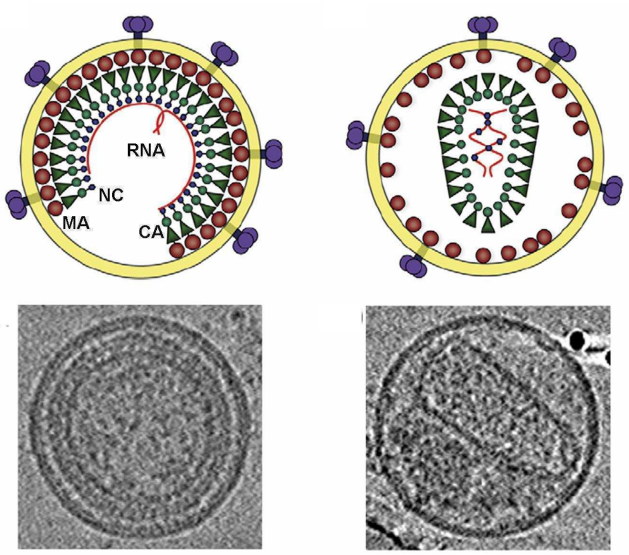

Figure 1.63. Immature (left) and mature (right) HIV-1 virions. Schematic models (top) and central slices through tomograms of HIV-1 particles derived by electron cryotomography (bottom). (From [137])

4) Maturation

The last step of the replicative cycle is the maturation of virions, which takes place at the same time or shortly after budding. Maturation leads to changes in the morphology of the viral particles.

The immature virion is a roughly spherical shell of radially extended Gag molecules (**Fig. 1.63**). The N-terminal MA domains of the Gag polyproteins are bound to the inner viral membrane, and the C-termini of the Gag molecules project into the center of the virus. Maturation involves proteolytic cleavage of Gag and Gag-Pol polyproteins by the viral protease (PR). These newly processed proteins then reassemble to form the distinct layers of the mature virion: MA remains associated with the inner viral membrane (the 'matrix' layer), NC coats the viral RNA genome (the 'nucleocapsid' layer), and CA assembles into the conical capsid that surrounds the nucleocapsid and its associated enzymes, reverse transcriptase (RT) and integrase (IN) [165].

1.3.4. NC

Genomes of retroviruses are protected by nucleocapsid proteins (NC). In all orthoretroviruses, NC are small (<100 amino acids), highly basic nucleic acid-binding proteins (**Fig. 1.64**). In addition, these proteins contain either one (gammaretroviruses) or two strictly conserved zinc fingers of the sequence C-X_2-C-X_4-H-X_4-C, also named CCHC fingers [163, 166-168] In all retroviruses containing zinc fingers, the spacing between the zinc-binding residues is absolutely conserved. The only exceptions are the nucleocapsid proteins of spumaviruses, which do not contain zinc fingers. The nucleocapsid protein of HIV-1 is one of the smallest ones among the different retroviruses. This 55 amino acid protein contains two zinc fingers. NC proteins of various HIV-1 strains differ mainly by their N-terminus while changes in the other parts of the protein are mostly restricted to Arg/Lys substitutions (**Fig 1.64 C**) [163]. It is important to note that in several studies, a 72 amino acid precursor of NC that contains also the p2 fragment (**Fig. 1.53**) was used. This protein is a result of the non complete PR processing of GAG and could be found in viral particles at low concentrations.

A) Structure

HIV-1 NC is a partially folded protein, with two rigid retroviral-type zinc fingers connected by a flexible basic linker and flanked by poorly folded N- and C-terminal basic domains [169]. Zinc fingers bind Zn^{2+} ions with high affinity (K=10^{-13} – 10^{-14} M) [170, 171] and play an important role in the protein activity.

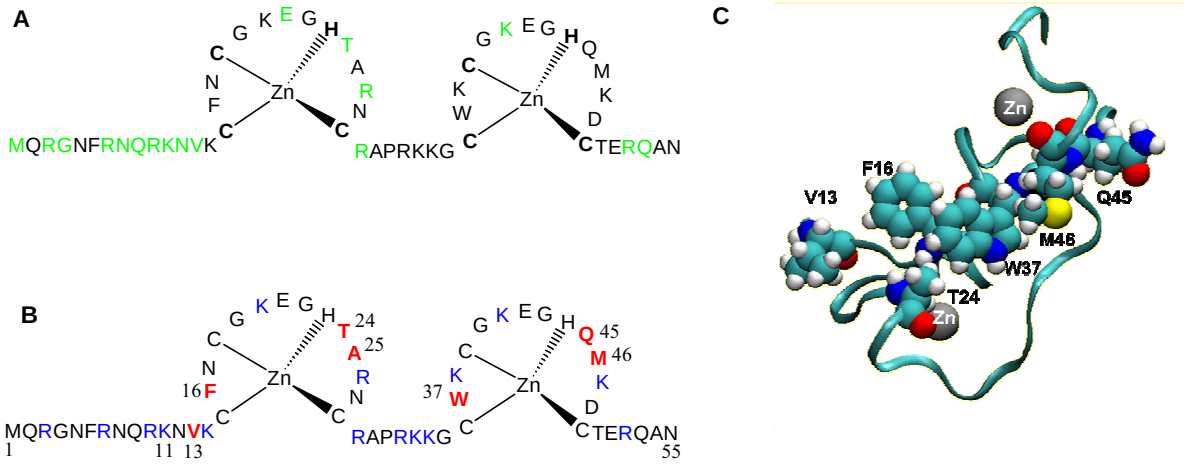

Figure 1.64. Structure of HIV-1 NC. (A) Variation map. The amino acids shown in green are not conserved over different strains of HIV-1.
(B) Distribution of the positively charged amino acids (blue) and the amino acids of the hydrophobic plateau (red).
(C) 3D structure of the NC(13-55) fragment based on NMR data [167]. Amino acids of the hydrophobic plateau are highlighted.

The structures of the individual zinc fingers, as well as that of the full - length NC protein were determined by nuclear magnetic resonance (NMR) spectroscopy [166-168]. As one can see from the NMR-derived 3D structure of the NC(13-55) fragment, the two zinc fingers are spatially close (**Fig. 1.64**). The hydrophobic amino acids of both fingers are forming a hydrophobic platform where, for example Phe16 is close to Trp37. These two amino acids are extremely important for binding of NC to nucleic acids. Their spatial proximity allows them to stack with neighbour nucleic bases (**Fig. 1.65** and **1.70**). Other non-charged amino acids especially Thr(Ile)24, Ala25, Gln45 and Met46 were reported to participate in nucleic acid binding [172]. The hydrophobic plateau in combination with the flexible basic linker between the two Zn fingers plays a key role in NC-nucleic acids interactions.

B) Role of NC in genome protection. Non specific RNA/DNA binding

Viral particles contains about 2000 molecules of NC proteins associated with RNA [173]. This interaction leads to RNA condensation that is necessary for formation of the viral particle [174, 175]. It has been observed *in vitro* that nucleic acids coated with NC are protected against nucleases [176-179]. Infection experiments confirm that NC stabilizes nascent vDNA in the cytoplasm.

NC is able to bind to nearly any sequence of five to seven nucleotides length [181]. As it was mentioned above, this interaction is promoted by its hydrophobic plateau and the basic amino acids in the interfinger linker. The structural aspects of this kind of complexes were determined by NMR using a short oligonucleotide d(ACGCC) as a model [180]. In the complex, the pentanucleotide sugar-phosphate axis is almost perpendicular to the interfinger linker (**Fig. 1.65**). This interaction is directed by the stacking of Trp37 with G (guanine) that plays a major role in the complex stability. The key role of the Trp-G stacking has been confirmed, using variants of the d(ACGCC) sequence, where each nucleotide has been systematically varied [179, 182].

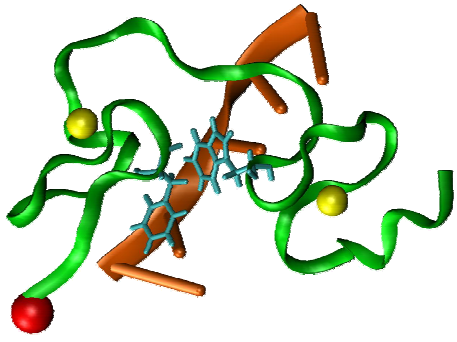

Figure 1.65. NMR-derived structure of NC(13-55) bound to the d(ACGCC) oligonucleotide. Atom coordinates are from [180].

C) Role of NC in the virus assembly. Selective RNA binding

RNA packaging

During virus assembly, NC is present mainly as a part of the Gag polyprotein (**Fig. 1.53**). Genetic analyses have demonstrated that the NC domain in the Gag precursor is critical for specific recognition and packaging of gRNA. Mutations of the NC domain from Gag prevent specific packaging of HIV-1 gRNA. NMR experiments have shown that the NC zinc fingers are responsible for specific interactions with the encapsidation Ψ sequence of the gRNA, while the basic residues contribute more to non-specific nucleic acid binding [183, 184]. Specific binding to the ψ sequence is required for the selective recognition of viral RNA among the large excess of cellular RNAs [185]. NC binds specifically to three of the four stem - loop sequences (SL1, SL2 and SL3) [182, 185-187] that constitute the Ψ sequence.

Structures of NC-SL2 and NC-SL3 complexes were determined by NMR [188, 189] (**Fig. 1.66**). In both complexes, the main driving forces are the interactions of the loop residues at the top of the stem-loops with the conservatively substituted hydrophobic residues Val13, Phe16, Thr (Ile)24 and Ala25 at the top of the proximal finger and the Trp37 and Met46 residues at the top of the distal finger. In the NC-SL2 complex, the nucleotide bases of G11 and G9 bind to the hydrophobic cleft of the N and C-terminal knuckles, respectively [190]. The GXG motif of the SL3 loop is also crucial for NC binding [191]. Moreover, the N-terminal fragment (1-11) folds in form of a 3_{10} helix, providing additional binding in the NC-SL3 complex but not in the NC-SL2 complex (**Fig. 1.66**).

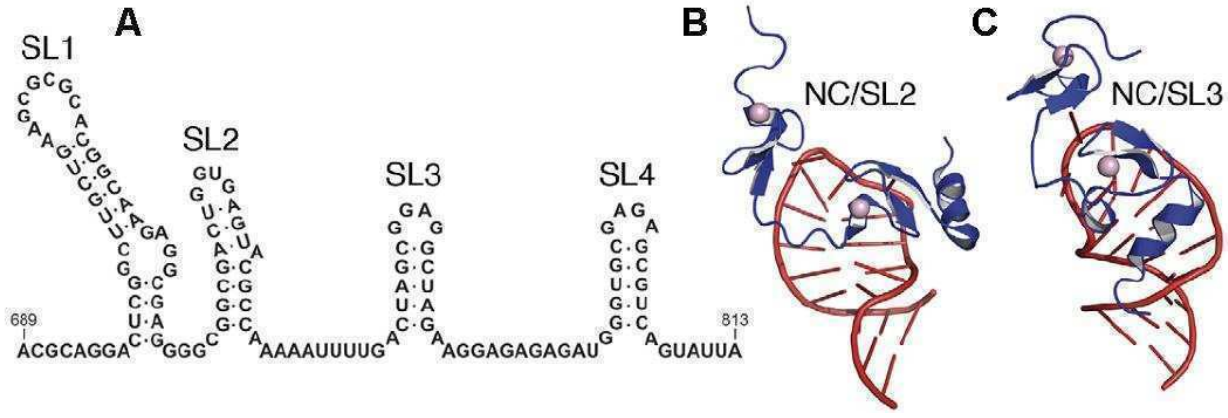

Fig 1.66. (A) Encapsidation sequence of the HIV-1 genome recognized by the Gag polyprotein. (B) and (C) 3D structure of NC complexes with SL2 and SL3. (Figure adopted from [165])

Genome dimerization

A necessary step for virus particle maturation is the formation of a stable dimer between the two molecules of gRNA present in the retrovirus particle [165]. It has been demonstrated that NC is critical for the formation of this complex. The mechanism of its stabilization is thought to begin with a limited base pairing between the genomes, termed a "kissing loop structure", which, with the assistance of NC expands to form a more extended duplex. This process, termed "dimer maturation," results in the formation of a more thermostable RNA dimer, and occurs during the maturation of the virus particle, after budding. NC facilitates the RNA maturation via its nucleic acid chaperone activity, which assists the RNA to find the most thermodynamically stable annealed structure. The formation of the RNA dimer probably facilitates the complex events of reverse transcription, such as the obligatory strand transfer steps and the high degree of recombination observed between genomes [169, 192].

D) Role of NC in Reverse Transcription. Chaperone properties

The conversion of gRNA to full-length dsDNA is an essential early step in retroviral replication, but it is a complex process requiring at least two strand-transfers [193], and the RNA- and DNA-dependent polymerase transcription of RNA and cDNA sequences, respectively (**Fig. 1.62**). Reverse transcriptase (RT) alone can accomplish many of these steps, albeit inefficiently.

In the context of the virus, RT is not the only protein present, and it must perform its functions in the context of gRNA being completely coated with NC [194]. Through its chaperone properties, NC can initiate RNA conformational changes by directing the rearrangement of nucleic acid molecules into their most stable conformation [195]. Due to these properties, NC is notably thought to assist the reverse transcriptase to convert the HIV-1 RNA genome into a linear double-stranded DNA [196]. NC plays key functions in several steps of reverse transcription:

Initiation

Before reverse transcription can begin, the 3' 18 nt of a cellular tRNA must be annealed to the complementary 18-nt primer binding site (PBS) near the 5' end of the viral RNA genome. It has been observed that HIV-1 NC can greatly enhance the rate of tRNA primer annealing to the PBS of the gRNA (**Fig. 1.62**) [195, 197-203]. This annealing step involves the partial disruption of the tRNA structure so that its 3' 18 nucleotides can form base pairs with the PBS region on

the gRNA. Similar annealing can also be performed using heat to destabilize the intramolecular base pairing of these sequences, indicating that NC acts as "melting energy" decreasing agent. Mechanism of such activity is connected with the fact that binding of NC to single stranded RNA (or DNA) is energetically favored over double stranded RNA (or DNA). It means that in the NC-bound form, the energy needed for RNA or DNA unpairing is decreased (**Fig 1.67**).

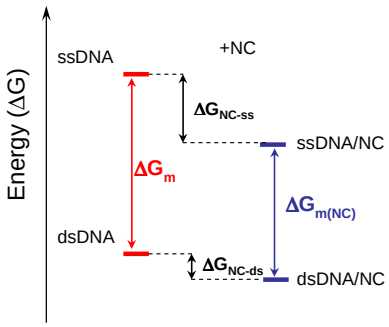

Figure 1.67. Energy diagram of NC-DNA systems. Energy needed for base unpairing in the DNA/NC complex is lower than for free DNA because of difference in binding energies of NC to single- and double-strand DNA (ssDNA and dsDNA).

Minus-strand-transfer

As the minus-strand strong-stop DNA is being synthesized, the RNase H domain of RT digests the RNA template of the newly synthesized heteroduplex into small fragments. The RnaseH digestion allows the transfer of the cDNArepeat (R) region, facilitated by NC, to the RNA R region at the 3'-end of the genome, an event termed minus-strand-transfer (**Fig. 1.62**, Step 3). This strand-transfer is greatly enhanced by NC, both through promoting the annealing of 5'-R cDNA to the 3'-R region of the genome and stimulating the RNase H activity. The RNase H activity will result in the cDNA R region being bound to fragments of gRNA Since NC facilitates the formation of nucleic acid structures having the maximum number of base pairs; it will favor the displacement of the RNA fragments by the 3'-R region. Hybridization of the TAR sequence (3' of viral RNA) with the complementary cTAR sequence on ss(-)DNA is the rate-limiting step of the transfer [179, 204, 205].

These two stem–loops are folded in similar stable structures, limiting the efficiency of the minus strand transfer reaction. Due to its chaperone ability, NC promotes this transfer by increasing the rate and extent of annealing and by preventing non-specific self-primed cDNA synthesis by reverse transcriptase (RT). The initial and rate-limiting step of minus-strand transfer is thought to be destabilization of the TAR and cTAR structures upon binding of NC. In fact, NC activates the transient opening (fraying) of cTAR terminal base-pairs, leading to a partial melting of the cTAR ends [206]. In its free form, TAR is in equilibrium between closed and partially melted forms. NC binds preferentially to single strands and shifts the equilibrium toward the "open" form.

Biophysical studies of this system showed that the NC-promoted cTAR/TAR annealing [197, 207] involves two pathways (**Fig. 1.68**), of which only one is productive.

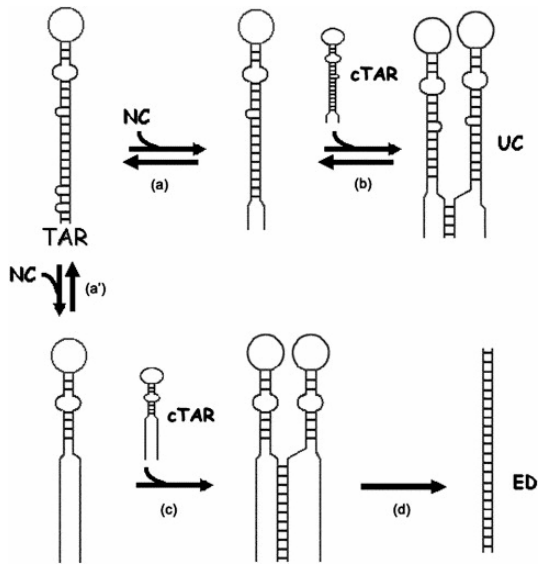

Fgure 1.68. Proposed mechanism for NC-promoted cTAR-TAR annealing. The upper pathway (steps a and b) is associated with the fast kinetic formation of an unproductive complex (UC). In this pathway, NC melts the terminal double-stranded segments of the TAR stem (step a) and promotes a limited annealing with the corresponding segments of cTAR stem (step b). The lower pathway (steps a′, c and d) corresponds to the slow formation of the extended duplex (ED). In this pathway, NC propagates the melting up to the middle of the stem (step a′) and nucleates ED through residues located mainly within the central double-stranded segment of both cTAR and TAR stems (step c). Formation of the rate-limiting nucleus is followed by a fast zipping reaction (step d). (From [197])

Several model assays have been developed to determine the structure–activity relationships of NC nucleic acid binding and chaperone activities. A simple but efficient model system is based on TAR (or cTAR) hairpin doubly labelled with FRET pair of dyes [200, 201], that allows measuring the mean distance between the 3' and 5' ends of the oligonucleotide. It was found that the NC destabilizing activity is strongly related on the proper folding of the Zn fingers. [174, 196]

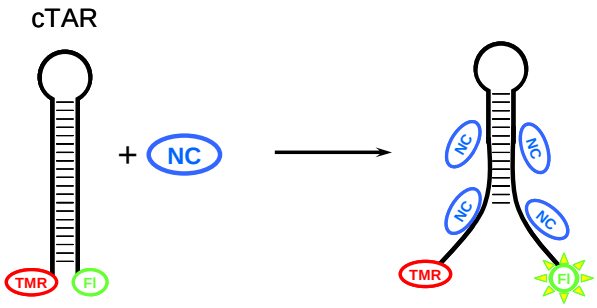

Figure 1.69. Scheme of the FRET-based assay for studying the NC chaperone activity on cTAR hairpin. The sequence was labelled at its 3' and 5' ends by 5(6)-carboxyfluorescein (Fl) and 5(6)-carboxytetramethylrhodamine (TMR), respectively. In the absence of NC, cTAR is mainly in a non-fluorescent closed form where the Fl and TMR labels are close together, giving excitonic coupling. NC led to a concentration dependent melting of the bottom of cTAR stem [201], which increases the distance between the two fluorophores and thus, restores the Fl fluorescence.

Experiments with NC mutants lacking destabilization activity (without Zn fingers) show that they are still able to promote cTAR/TAR hybridization in vitro. This suggests that NC lowers the energy cost of bringing the hairpins together in the encounter complex by screening the negative charges of the hairpins and probably also through specific interactions [207-210].

Second Strand Transfer

During the second strand transfer, NC chaperones the (+) strand transfer [212, 213] by promoting the annealing of (+)PBS to its (−)PBS complement present at the 3′ end of minus strand DNA (**Fig. 1.62** step 8). This annealing reaction relies on the ability of NC to destabilize the PBS stem–loops (SLs), [213, 214] exposing nucleotides that are sequestered in the stem and activating the fraying of the terminal G–C base pair [213]. NC likely changes also the structure of the PBS loops, since NC was shown to promote the (−)PBS/(+)PBS annealing mainly through the loops [214]. According to the structure of NC/PBS complex determined by NMR, the protein binds to the 5-CTG -7 motif of the PBS loop mainly through the Trp37 and Phe16 residues (**Fig. 1.70**) [211].

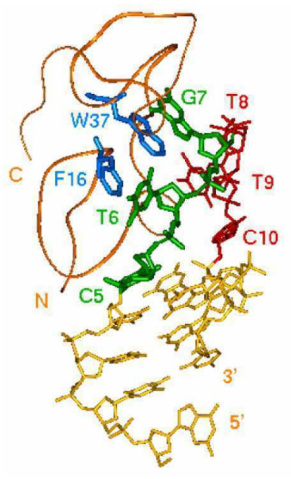

Figure 1.70. NMR structure of the ΔP(−)PBS/NC(12–55) complex. Phe16 and Trp37 are in blue. The ΔP(−)PBS stem is in yellow. Bases involved in the interaction (5-CTG -7) are in green; the remaining bases from the loops are in red. (From [211])

E) Role of NC in Integration

Integration of full-length vDNA into the chromosomal DNA of the infected cell to form the provirus is the final step of early infection. *In vitro*, only three components are strictly required for integration; the integrase (IN), the viral LTR ends containing the requisite attachment sites, and a DNA substrate in which to integrate the vDNA [215]. Nevertheless, *in vivo* infection experiments performed with NC mutant viruses have provided indirect evidence for the involvement of NC in integration. Disruption of the first NC Zn finger by H23C mutation leads to replication defective virus. Meantime, only minor defects in reverse transcription were observed, which implies that the integration step itself is affected [216]. This idea was strongly

supported by the fact that until recently, the phenotypes of NCH23C could not be readily distinguished from IND116N, which is an active site mutant of IN that cannot catalyze the 3' processing or strand-transfer reactions [217]. The role of NC in the integration process is not yet determined precisely and three main hypothesis are under discussion [163] (1) NC enhances the enzymatic steps of integration; (2) NC is involved the formation of a functional intasome, possibly by assisting IN to bind the LTR ends or by stabilizing the IN nucleoprotein complex at the LTR ends; (3) NC may be important for the proper structure of the preintegration complex.

The role of NC in the early steps of retroviral replication appears largely that of a facilitator in reverse transcription and integration [163]. NC is greatly enhancing the efficiency of both strand transfers and the initiation of reverse transcription, thereby increasing the probability of productive virus replication. NC also likely controls the RT activity, by direct interaction with the enzyme [218]. Moreover, NC as a part of the Gag polyprotein controls viral genome recognition, dimerization and packing.

1.3.5. Vpr

The HIV-1 accessory protein Vpr is a 96 amino acid basic protein (14kDa). This small protein is incorporated into the virus particle through interaction with the p6 domain of Gag and is present in relatively low amounts. Vpr is a multifunctional protein for HIV-1 replication that has been reported to be involved in the G2–M cell-cycle arrest, apoptotic cell death and transcription activity.

A) Structure

The structure of the full length protein was obtained by NMR in water with addition of solvent or lipids. All these studies indicate the formation of three long amphipathic α-helices (17-33), (38-50) and (56-77) [210, 219-221]. Two loops spanning residues 34-37 and 51-55 allow a mutual orientation (**Fig. 1.71**) of these helices that promotes the formation of a hydrophobic core made by the spatial proximity of numerous hydrophobic amino acids dispersed in the primary sequence. This globular conformation is surrounded by flexible N- and C- terminal sequences [210, 220, 222]. The difficulties to obtain structural elements could be explained by the potency of Vpr to oligomerize [222] through formation of leucine zippers both at the C- and N- terminus [220, 223].

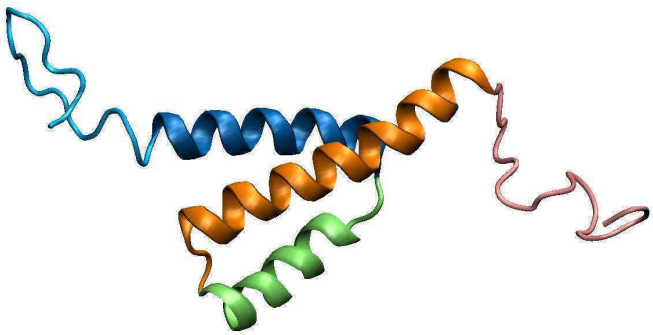

Figure 1.71. 3D structure of Vpr derived from NMR experiments [207]. α-Helices (17-33), (38-50) and (56-77) are shown in blue, green and orange respectively.

Vpr-Vpr interaction

It was shown by biochemical techniques [224] and NMR studies [222] that Vpr can oligomerise. A theoretical model of a coiled-coil (52-96)Vpr dimer was proposed with a parallel orientation in the presence of TFE [225-227] and antiparallel orientation in the presence of CH_3CN [228]. In our lab, Vpr-Vpr interaction was recently investigated in HeLa cells by a combination of FLIM and FCS experiments [229]. Mutations carried out in the central hydrophobic core are characterized by a loss of oligomerization in contrast with mutations outside the core. This phenotype could arise from a global reorganization of the 3D structure, local helix destabilization or a loss of the appropriate side chains involved in the protein-protein interaction.

B) Role

The C-terminal domain of Vpr (52-96), contains a Leu/Ile-rich domain (amino acids 60–81) and a basic flexible domain. It shows similarity with the domains of arginine-rich protein transduction domains (PTD), and may explain the transducing properties of Vpr, including its ability to cross the cell membrane [222]. The C-terminal part is also involved in the G2 cell cycle arrest, apoptosis and the interaction with NC and nucleic acids [222, 224]. The N-terminal part of the protein (1-51) is more acidic and is required for virion incorporation, nuclear localization and Vpr oligomerization [220, 230].

Vpr is incorporated in the virus through interaction with the C-terminus of Gag [231, 232] in a ratio of one Vpr for seven Gag [232-235]. Deletion of p6 and point mutation of the LXLL p6 conserved motif in the context of Gag abolish the interaction with Vpr and prevent Vpr incorporation in the particle [226]. Nevertheless, biochemical and double hybrid analysis evidenced a stronger affinity for mature NC zinc fingers than for p6 [225, 227].

Interaction of Vpr with many cellular proteins could explain most cellular and viral features attributed to this protein [228]. Vpr co-activates several transcription factors such as the glucocorticoid receptor and TFIII3B [236-240] and transactivates the long terminal repeat (LTR) of HIV [241-243]. Up regulation of LTR transcription correlates with Vpr-induced G2 phase cell cycle arrest [244-246]. This arrest, normally characterized by a down regulation of cap-dependent translated proteins, elicits an up regulation of protein translation from the viral internal ribosome entry (IRES) [247, 248]. This burst of viral products is followed by an apoptosis event [249-251]. These two activities are intricately related even though several studies suggest the opposite. Another function ascribed to Vpr is the nuclear import of the pre-integration complex (PIC) by disruption of the nuclear envelope [252]. This last function is reinforced by the nuclear envelop (NE) localization of Vpr, which is probably mediated by the nucleoporin [253-255] and by accumulation of Vpr in the nucleus [256]. As the PIC presents a too important size for nuclear penetration through channels, its uptake could be explained by a local Vpr-dependent architectural membrane disruption or formation of larger channels.

Subsequently, Vpr was reported to be involved in the nuclear localization of HIV-1 DNA in non-dividing cells, particularly in macrophages. It can interact with nucleoporins and importin and accumulates at nucleopore complexes on the outer face of the nuclear envelope. Vpr has also been proposed to mediate an unconventional mode of nuclear entry by disrupting the nuclear envelope [143].

1.3.6. Anti-HIV drug targets

Although vaccines have helped to control several of the most important viral pathogens, there is currently little prospect of an effective vaccine for HIV. High virus type diversity and ability to easily mutate complicated dramatically the design of anti-HIV drugs and vaccines. Nevertheless, drug discovery based on advances in the understanding of the viral life cycle, has transformed what used to be a rapid and lethal infection into a chronic condition that can be controlled for many years through combination therapies with different classes of antiviral drugs — known as Highly Active AntiRetroviral Therapy (HAART)

At present, at least 25 compounds have been formally licensed for the therapy of HIV infections. These compounds fall into six categories [257] (**Fig. 1.72**):

1) **Nucleoside and nucleosite reverse transcriptase inhibitors (NRTIs and NtRTIs)** [Zidovudine (Retrovir®); Didanosine (Videx®); Zalcitabine (Hivid®); Stavudine (Zerit®); Lamivudine (Epivir®, Zeffix®); Abacavir (Ziagen®); Emtricitabine (Emtriva®, Tenofovir disoproxil fumarate (TDF) (Viread®))]
2) **Non-nucleoside reverse transcriptase inhibitors (NNRTIs)** [Nevirapine (Viramune®); Delavirdine (Rescriptor®); Efavirenz (Sustiva®, Stocrin®) ; Etraverine (Interlence®)]
3) **Protease inhibitors (PIs)** [Saquinavir (Invirase®, Fortovase®); Ritonavir (Norvir®); Indinavir (Crixivan®); Nelfinavir (Viracept®); Amprenavir (Agenerase®, Prozei®); Lopinavir (in Kaletra®); Atazanavir (Reyataz®); Fosamprenavir (Lexiva®, Telzir®); Tipranavir (Aptivus®); Darunavir (Prezista®)]
4) **Integrase inhibitor** [Raltegravir (Isentress®)]
5) **Fusion inhibitors (FIs)** [Enfuvirtide (Fuzeon®)]
6) **Co-receptor inhibitors (CRIs)** [Maraviroc (Selzentry®)]

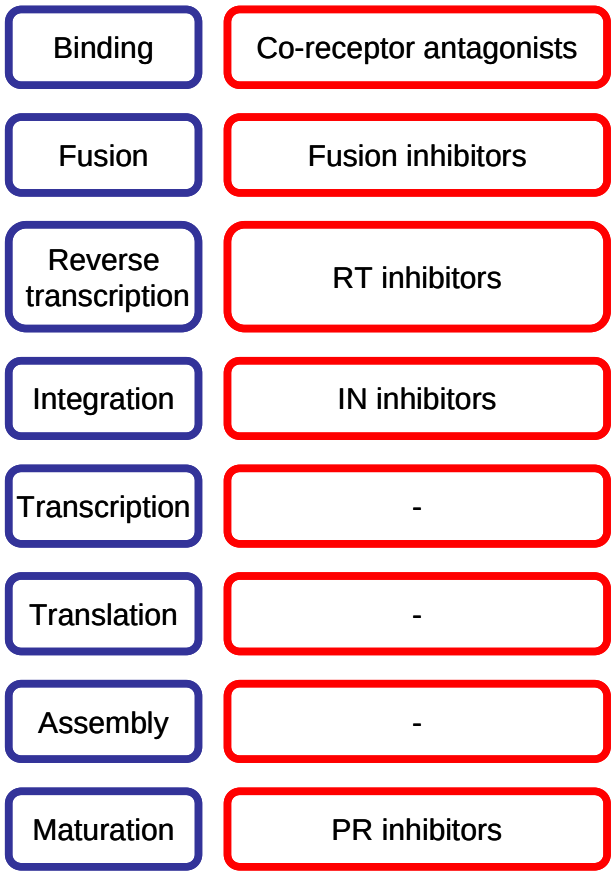

Figure 1.72. Steps of the HIV-1 life cycle that are targeted in clinical therapy.

Starting from the various, currently available, anti-HIV drugs, numerous drug combinations could be conceived, containing two, three, four, five or more drugs. The drug combinations which have been extensively pursued contain one or two NRTIs (or one NtRTI instead of one of the NRTIs), and one NNRTI (or instead of the NNRTI, one or two PIs).

Reverse transcriptase Inhibitors. The first anti-HIV drug AZT (Zidovudine, Retrovir®) was introduced in 1987 [258]. It belongs to NRTIs, (**Fig. 1.73**) that target the HIV reverse transcriptase and block viral genome replication. NRTIs mimic natural nucleosides but lack the 3′-OH group that is required for nucleic acid chain elongation. Thus, they act as a chain terminator in the reverse transcriptase reaction. To be active, they have to be phosphorylated by cell-derived kinases.

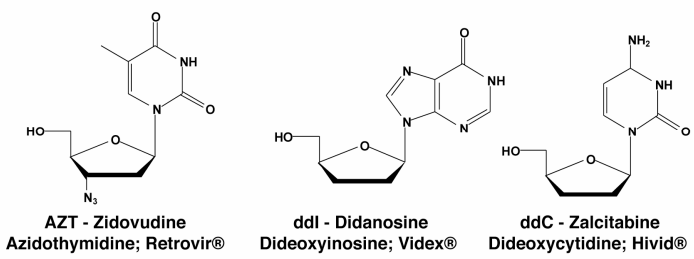

Figure 1.73. Examples of nucleoside reverse transcriptase inhibitors.

NtRTIs exhibit a similar mode of action to NRTIs, but the presence of the phosphonate group, which is analogous to a phosphate group, means that only two phosphorylation steps by cellular kinases are required for conversion to the active metabolite. NtRTIs are therefore able to bypass the nucleoside-kinase reaction, which can limit the activity of the dideoxynucleoside analogues against HIV. In addition, unlike phosphate, phosphonate can no longer be cleaved by the esterases that would normally convert nucleoside monophosphates back to their nucleoside form. At present, only one NtRTI, Tenofovir (**Fig. 1.74**), has been approved for the treatment of HIV.

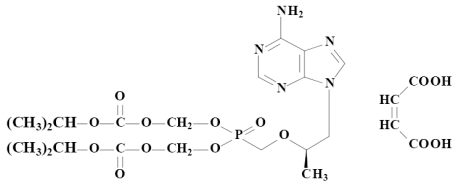

Figure 1.74. Example of NtRTI: Tenofovir disoproxil fumarate (TDF), Viread®.

NNRTIs target also the RT but show a different mechanism of action. They are allosteric non-competitive inhibitors that decrease reverse transcription activity by interaction with an allosteric binding site on HIV-1 reverse transcriptase that becomes exposed upon ligand binding [259]. All drugs of this class including the recently approved Etravirine [260] are bulky compounds having "clef"-motif (**Fig. 1.75**).

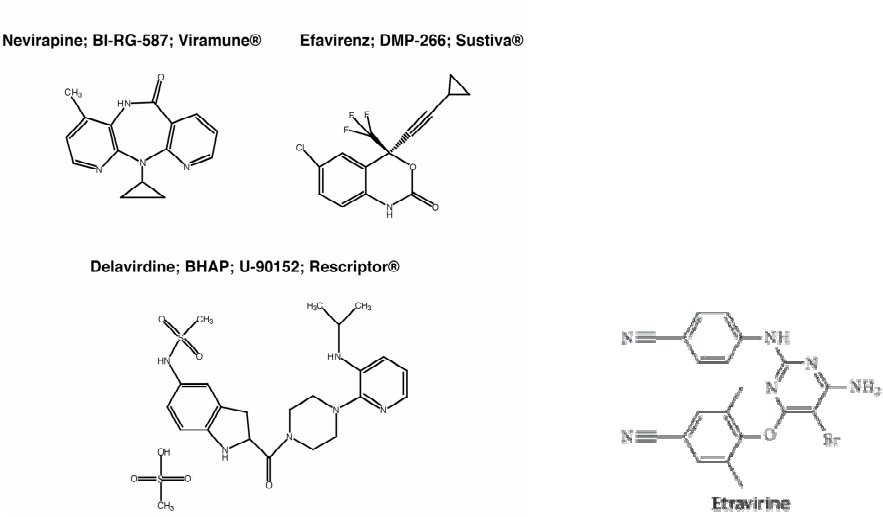

Figure 1.75. Non-nucleoside reverse transcriptase inhibitors (NNRTIs) used in clinics.

Protease inhibitors. Most of the currently available HIV protease inhibitors can be considered as peptidomimetics (**Fig. 1.76**). They are built upon a hydroxyethylene group, which mimics the peptide linkage in the polyprotein precursor Gag–Pol, which is cleaved by the HIV protease into the mature capsid proteins and enzymes. The protease inhibitors compete with binding of the regular substrate, thus blocking the protease activity.

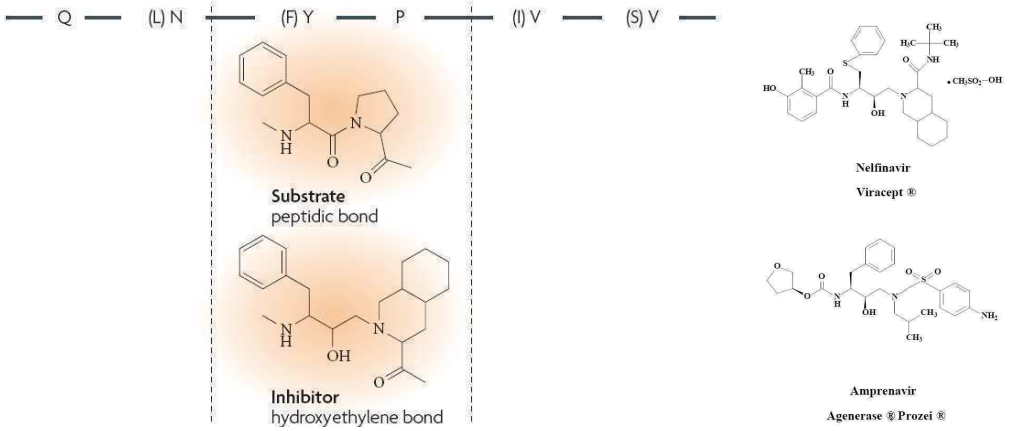

Figure 1.76. Substrate of HIV protease and examples of inhibitors that mimic the substrate but lack the peptide bond.

Integrase inhibitors inhibit the strand transfer reaction in the integration process, a crucial step in the stable maintenance of the viral genome, as well as for efficient viral gene expression

and replication. They are represented by relatively small polycyclic organic molecules (**Fig. 1.77 A**). This class of drugs was established recently and has an impressive potency in respect to other anti-HIV agents.

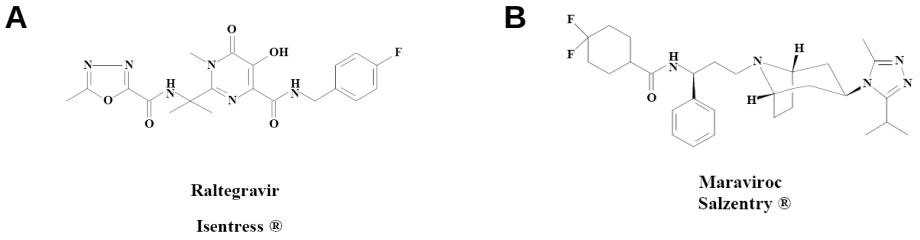

Figure 1.77. (A) Integrase inhibitor Raltegravir (Isentress®) (**B**) Co-receptor antagonists Maraviroc (Selzentry®).

Fusion inhibitors (FIs) in clinical use are represented by Enfuvirtide (Fuzeon®). This drug of peptide nature [261] corresponds to the amino-acid residues 643–678 of the HIV‑1 envelope precursor glycoprotein gp160. HIV easily undergoes mutations to give resistance to Enfuvirtide, thus this drug is used mostly in combinations with others.

Co-receptor antagonists bind to the CCR5 co-receptor and change its shape so that gp120 cannot recognize it. This approach is prospective for construction of small anti-HIV drugs because the human co-receptor is not as variable as viral components. Several drugs of this class were developed but only Maraviroc (Selzentry®) is used to date (**Fig. 1.77 B**).

Several other directions are included in the development of anti-HIV drugs. The most prospective are the ones that target highly conserved elements of the virus and thus have high genetic barrier to resistance. Combination of drugs acting on several targets strongly decreases the possibility of drug-resistance mutations. Thus, thorough studies of the virus, detection of highly conserved sequences and development of drugs targeting them is of extreme importance for future improvements in anti-HIV therapy.

In the frame of this thesis work, inhibitors of the nucleocapsid protein (NC) were developed. A review of the HIV-1 NC inhibitors is presented in the Appendix.

1.4. Conclusions to introduction and research objectives

Fluorescent labeling is of paramount importance to study protein interactions. Environment-sensitive fluorophores combine small size with ability to report biomolecular interactions by monitoring changes in the environment at the specific labeling site. Small proteins and peptides with precise label position could be prepared by the solid-phase peptide synthesis. Two-band ratiometric dyes based on 3-hydroxychromone are highly promising for the proteins studies by a single-label approach, because, they provide a convenient ratiometric signal and additional information channels for the analysis of the labeling site properties.

The aim of the present work is to develop methodology for sensing interactions of proteins with DNA, membranes and other proteins based on environment-sensitive labels from the 3-hydroxychromone family. In this work, a variety of 3-hydroxychromone and 3-hydoxyquinolone derivatives were characterized in order to evaluate their environment sensitivity and applicability for sensing biomolecular interactions. The most promising dyes were derivatized to obtain amino-group reactive labels for N-terminal modification of the peptides prepared by solid-phase peptide synthesis.

Our target peptides for labeling were HIV-1 NC and C-terminal domain of HIV-1 Vpr. The HIV-1 NC protein combines the relatively small size with ability to binds various DNA/RNA targets, while Vpr protein exhibit high affinity to biological membrane and tendency to oligomerization. In this work, the NC and Vpr peptides labeled 3-hydroxychromone dyes were synthesized and their interactions with corresponding biological targets (DNA/RNA and lipid membranes, respectively) were characterized using fluorescence spectroscopy techniques. The obtained results suggest 3-hydroxychromone labeles as a universal tool for sensing biomolecular interactions.

2. Development of two-color dyes for peptide labeling

As it was shown in the bibliographical overview, ESIPT-based two-color ratiometric fluorophores are promising labels for protein systems, due to their high sensitivity to the environment polarity. Strong response to the biomolecular interactions is the key property of the good label. Best signal collection for the ratiometric dyes is achieved when the two emission bands are of comparable intensity. Thus, selection of the dye with proper sensitivity range is extremely important for the successful use of the labeled biomolecules.

Recently 3-hydroxychromones were shown to be prospective dyes for sensing protein conformation changes [111] and peptide-protein interactions [262]. Dyes of this family have also been successfully applied as membrane probes [122, 124].

In the present work we constructed improved two-color ratiometric labels applicable for sensing peptide interactions with oligonucleotides and lipid membranes. For this purpose, we initially studied environment sensitivity of 3-hydroxychromones and newly described similar class of fluorophores, 3-hydroxyquinolones, and compared their applicability in different polarity ranges.

2.1. 3-Hydroxyquinolones (3HQ)

3-hydroxyquinolones (3HQs) are the aza-analogues of 3-hydroxychromones (3HCs) dyes. This class of compounds was described in 1970th but theirs ability to undergo ESIPT reaction was discovered only recently [67].

Structure of 3HQs allows us to expect higher chemical stability of the nitrogen-containing heterocycle than of oxygen-containing one of 3HCs. Free valence of the nitrogen atom provides an additional possibility for fluorophore modifications and linker introduction.

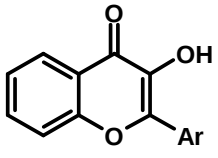

3HC

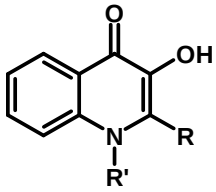

3HQ

To evaluate 3HQs as potential fluorescent labels, systematic studies of their fluorescent properties were performed. Two key questions were addressed: (1) the influence of chemical substituents on fluorescence of 3HQ dyes and (2) sensitivity of the fluorescence properties of 3HQ dyes to the environment.

2.1.1. Fluorescent properties of 3HQs. Structural Effects

The major difference of 3HQs compared with 3HCs is presence of the heterocyclic nitrogen. Therefore, we focused our attention on influence of its substitution and substitution at position 2.

Emission spectra of 2-aryl 3HQs and especially the intensity ratio of their two emission bands are highly dependent on the substituents at the heterocyclic nitrogen (**Fig. 2.1**). Presence of methyl group disturb planarity of the molecule, which slows down the ESIPT reaction and consequently leads to the increase in the N*/T* band ratio. Non-planar conformation of N-methyl-substituted 3HQs was proved by quantum mechanical calculations.

Variation of the substituents in the 2-aryl group of 3HQs leads to moderate changes in the fluorescence. Electron-donating groups in this position induce increase in the N*/T* band ratio proportionally to their Hammett constant. Meantime, the spectroscopic effects of these substituents are much smaller than in the 3HC dye family. Based on these observations we concluded that electronic conjugation of 2-aryl with the quinolone part does not play major role for 3HQs fluorescence.

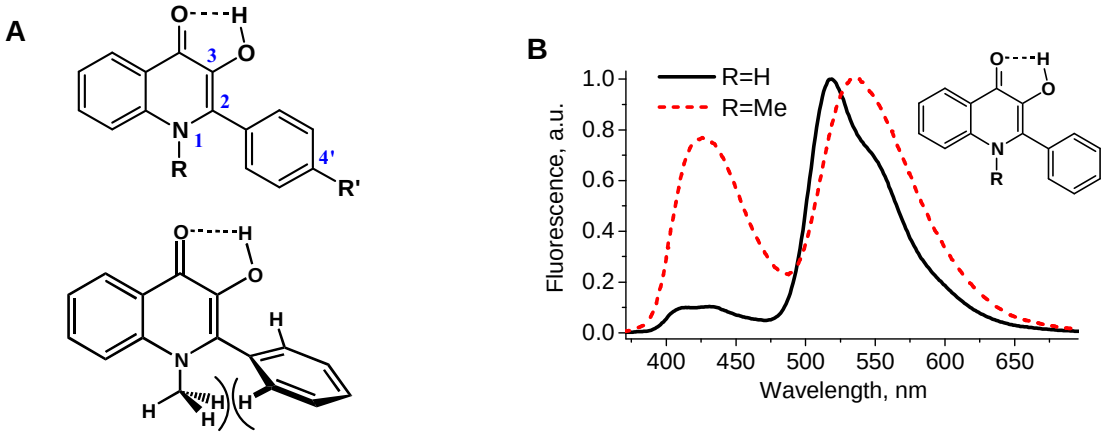

Figure 2.1. (**A**) Atom numeration in 3HQs and scheme of planarity disturbtion by N-methyl group. (**B**) Normalized fluorescence emission spectra of 2-phenyl-3HQs (red) and 1-methyl2-phenyl-3HQs (black) in DMF (λ_{ex}= 360 nm).

To check this hypothesis and to better understand the effect of conjugation with the 2-aryl group in 3HQs on the fluorescence properties, we have synthesised 3HQs bearing 2-methyl group instead of 2-aryl. While the dual emission of 2-aryl-3HQs was significantly affected by the presence of N-methyl group, the dual emission the new dyes was nearly unaffected by this substituent (**Fig. 2.2**). To better discriminate steric and electronic effects on 3HQ fluorescence, we performed time-resolved fluorescence measurements and calculated ESIPT reaction rate constants. Proton transfer in 2-methyl 3HQs is much slower than in 2-aryl analogues. Moreover

planar 2-aryl-3HQ, lacking N-methyl group, undergoes faster ESIPT than flat N-methyl derivative (**Fig. 2.3**). This allows us to conclude that ESIPT reaction is accelerated by steric interaction between 3-OH group and 2-aryl ring.

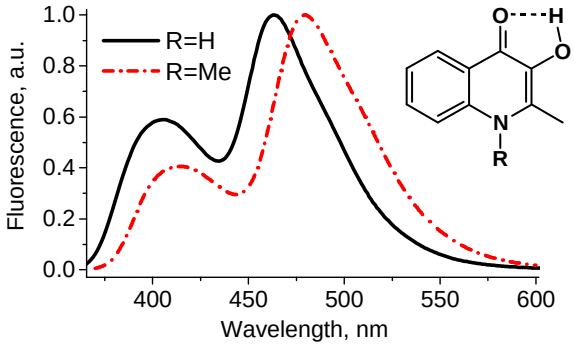

Figure 2.2. Normalized fluorescence emission spectra of 2-methyl-3HQs (black) and 1,2-dimethyl-3HQs (red) in DMF (λ_{ex}= 360 nm).

Finally, 2-methyl-3HQs were found to be highly fluorescent in contrast to the corresponding 2-methyl-3HCs. Their quantum yields are much higher than those of the 2-aryl-3HQs and in some solvents exceed 60% likely due to the lower level of the non-radiative transitions in the absence of vibrations of the aryl ring. This makes 2-methyl-3HQs prospective for constructing of very compact two-band environment-sensitive dyes.

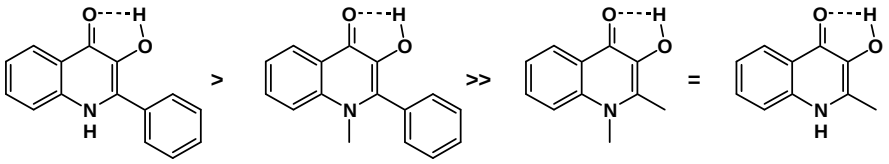

Figure 2.3. The ESIPT reaction rate in 3HQs. Rate constants were calculated based on time-resolved measurements in the acetonitrile.

The detailed description of this work is presented in Articles 1 and 2.

Article 1

2-Aryl-3-hydroxyquinolones, a new class of dyes with solvent dependent dual emission due to excited state intramolecular proton transfer

2-Aryl-3-hydroxyquinolones, a new class of dyes with solvent dependent dual emission due to excited state intramolecular proton transfer

Dmytro A. Yushchenko,*[ab] Volodymyr V. Shvadchak,[b] Andrey S. Klymchenko,[b] Guy Duportail,[b] Yves Mély[b] and Vasyl G. Pivovarenko*[a]

Received (in Montpellier, France) 30th January 2006, Accepted 23rd February 2006
First published as an Advance Article on the web 20th March 2006
DOI: 10.1039/b601400c

Herein, the fluorescence properties of a series of 2-aryl-3-hydroxyquinolones (3HQs) were investigated and compared with the properties of well-studied 3-hydroxyflavone. All these compounds were found to display dual fluorescence with well-separated bands in organic solvents and aqueous solutions. Using steady-state and time-resolved fluorescence spectroscopy, we showed that their dual fluorescence is due to an excited state intramolecular proton transfer reaction. Moreover, the absorption spectra of most 3HQs tested were found to be similar, indicating that they are not sensitive to the substituent at the 2-aryl ring. This was related by quantum chemical calculations to the non-planarity of these molecules which prevents conjugation between the two aromatic moieties. The only exception was the 3HQ derivative with a thiophene ring at position 2 which exhibited a red-shifted spectrum due to its more planar structure. In sharp contrast, the emission spectra and especially the intensity ratio of the two emission bands were highly dependent on the substituents at the 2-aryl ring and at the heterocyclic nitrogen. Moreover, *N*-methyl substituted 3HQs (N–Me 3HQs) demonstrate strong solvatochromic properties, with large changes in their fluorescence band intensity ratio as a function of the solvent polarity. In addition, the logarithm of these intensity ratios varied linearly with the Hammett constant associated with the substituent in the 2-aryl ring, enabling the design of 3HQ dyes with optimized intensity ratios in a given range of solvent polarities. Thus, 3HQs preserve the unique properties of 3-hydroxyflavones, namely dual emission that is highly sensitive to solvent polarity and to chemical substituents. Moreover, in comparison to 3-hydroxyflavones, 3HQ dyes exhibit higher fluorescence quantum yields and 10-fold increased photostability. These properties of the 3HQ derivatives make them prospective candidates for application as polarity-sensitive fluorescent labels for biomolecules.

Introduction

Due to its exquisite sensitivity, fluorescence is one of the most used techniques for investigating molecular events in biological systems. However, this technique relies strongly on the availability of fluorescent probes with optimal properties. In cells and tissues, probes are generally distributed inhomogeneously. As a consequence their fluorescence intensity is dependent on their local concentration. To avoid this limitation, probes with a ratiometric response are strongly desirable. In this respect, dual fluorescence probes exhibiting two well separated emission bands are of particular interest, since they provide a reliable ratiometric signal independent of the probe concentration.[1]

Excited state intramolecular proton transfer (ESIPT) reaction[2] is very effective for the design of probes with dual fluorescence.[3] ESIPT results in the formation of two tautomeric forms in the excited state of the probe: N*—normal and T*—tautomer form. Due to their different photophysical properties, these tautomeric forms exhibit widely separated emission bands on the wavelength scale. The most interesting and characterized representatives of this class of probes are the 3-hydroxyflavone derivatives (3HFs) that have been shown to be highly effective tools for investigating polarity,[3,4] hydration and electronic polarizability,[4] electrostatic effects in different media including lipid membranes[5,6] and proteins.[7,8] Moreover, these dyes were shown to be useful to determine the nature and concentration of cations[9] and anions[10] in solution. However, despite their significant advantages compared to common single-band probes, 3HFs exhibit relatively low photostability and quantum yields that limit their application. As a consequence, the development of new dual fluorescence probes with improved fluorescent parameters is strongly required.

It has been reported[11,12] that 2-aryl-3-hydroxyquinolones (3HQs), which are structural analogs of 3HFs, also undergo ESIPT reaction in organic solvents and thus exhibit two bands in the emission spectrum (Scheme 1). Remarkably, the ratio of the intensities of the two bands changes with the solvent, indicating that these dyes are sensitive to their microenvironment. However, a detailed study of the fluorescent properties

[a] *Department of Chemistry, Kyiv National Taras Shevchenko University, 01033 Kyiv, Ukraine*
[b] *Photophysique des Interactions Biomoléculaires, UMR 7175-LC1 du CNRS, Institut Gilbert Laustriat, Faculté de Pharmacie, Université Louis Pasteur, 67401 Illkirch, France. E-mail: dmytro@pharma.u-strasbg.fr; Fax: +33 390 244313; Tel: +33 390 244262*

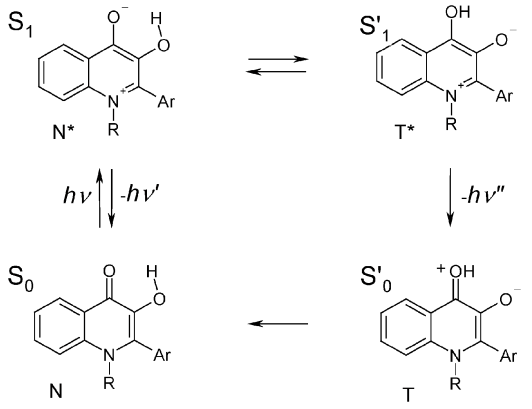

Scheme 1

of this new class of dyes has not yet been done. Moreover, it would be of high interest to compare the properties of 3HQs with the properties of 3HF analogs which have already found a variety of applications. Therefore, the present paper is focused on studies of structure–fluorescence property relationships, solvatochromism and photostability of 3HQs with respect to 3HFs.

Experimental

Materials and methods

All the solvents and chemicals were purchased from Aldrich. The solvents were of analytical grade. Melting points were determined using a Gallenkamp Melting Point Apparatus. Mass spectra were measured using Mass Spectrometer Mariner System 5155. ^{1}H-NMR spectra were recorded on a Bruker 300 MHz spectrometer. Absorption spectra were recorded on a Cary 4 spectrophotometer (Varian) and fluorescence spectra on a FluoroMax 3.0 (Jobin Yvon, Horiba) spectrofluorimeter. Time-resolved fluorescence measurements were performed with the time-correlated, single-photon counting technique using the frequency doubled output of a Ti-sapphire laser (Tsunami, Spectra Physics) pumped by a Millenia X laser (Tsunami, Spectra Physics).[13] The excitation wavelength was set at 320 nm. The fluorescence decays were collected at the magic angle (54.7°) of the emission polarizer. Data were analyzed by the Maximum Entropy method (MEM) using the Pulse 5.0 software.[14]

The pK_a values of quinolones were calculated by the Fletcher–Pawl algorithm using a nonlinear least squares method, as developed in Doroshenko's program,[15] which minimizes the sum of squared deviations of the experimental and calculated absorbance or fluorescence data (A) assuming a one-step protonation process for each transition. The program utilizes the common expression eqn (1):[16]

$$A = \frac{A_{HA}10^{-pH} + A_A10^{-pK_a}}{10^{-pH} + 10^{-pK_a}}, \qquad (1)$$

where A_{HA} is the absorbance or fluorescence intensity of 3HQ in its neutral form and A_A is the absorbance or fluorescence intensity of the 3HQ anion.

The photostability of the dyes was determined on a FluoroMax 3.0 apparatus. Solutions of 3HQs and 3HF of equal absorbance were irradiated at the excitation wavelength (360 nm) in the same conditions. Emission decays were collected at 520 nm. The intensity of the irradiating light was 2.94 mW cm^{-2} in all cases. Acetonitrile was used because the emission spectra of 3HQs and 3HFs in this solvent are similar in their shape and the ratio of their two bands. This limits errors due to possible differences in the photodegradation rates of the two emission states. Concentrations of the dyes were about 10^{-6} mol L^{-1}. The quantum yields of photodegradation were calculated using eqn (2):[17]

$$\Phi_{pd} = (1 - F_T/F_0)/\{I_0\sigma(\lambda_{exc})\int_0^T [F(t)/F_0]\,dt\}, \qquad (2)$$

where F_0 and F_T are the fluorescence intensities expressed in counts s^{-1} at time 0 and at the end of the measurements, respectively. I_0 is the intensity of the irradiating light expressed in photons cm^{-2} s^{-1}, $\sigma(\lambda_{exc})$ is the one-photon absorption cross-section at λ_{exc} expressed in cm^2 and t is the time in seconds.

Fluorescence quantum yields φ were determined with quinine sulfate in 0.5 M sulfuric acid (φ = 0.577[18]), taken as a reference.

Quantum-chemical calculations of 3HQ and 3HF torsional enthalpy were performed by the AM1 semi-empirical method using the MOPAC 6.0 program.[19]

Syntheses

3HQs synthesized in this work are given in Scheme 2 and Table 1. To synthesize them we have used condensation of anthranilic acid esters in polyphosphoric acid as described earlier.[20] The general procedure of synthesis is provided on the example of dye **5**.

1-Methyl-2-(4-(trifluoromethyl)phenyl)-3-hydroxy-4(1*H*)-quinolone (5). A solution of anthranilic acid (3.2 g, 21 mmol) and 4′-(trifluoromethyl)phenacyl bromide (6.38 g, 20 mmol) in 10 ml of DMF was stirred in the presence of dried potassium carbonate (3 g, 21.7 mmol) at 80 °C during 2 h. The solution was poured into water (100 ml), and the 4′-(trifluoromethyl)-phenacylanthranilate formed was filtered off and dried. Then 0.5 g (1.48 mmol) of the latter compound was added to polyphosphoric acid (3.3 g) and stirred at 120° during 2 h. After that, the mixture was poured into 20 g of ice and neutralized by 10% aqueous sodium carbonate. The filtered precipitate after washing, drying and recrystallization from DMF provided the dye **5**. (0.42 g, 89.0%). δ_H(300 MHz; DMSO-d$_6$; Me$_4$Si): 8.34 (d, J 8, 1H, ArH), 7.98–7.73

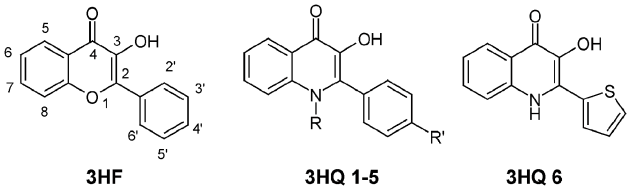

3HF 3HQ 1-5 3HQ 6

Scheme 2

Table 1 Spectroscopic properties of the synthesized 3HQs in acetonitrile and phosphate buffer[a]

	No	**1a**	**1b**	**2**	**3**	**4**	**5**	**6**
	Ar			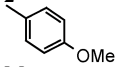	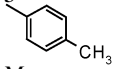		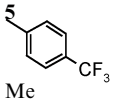	
	R	H	Me	Me	Me	Me	Me	H
Phosphate buffer	λ_{abs}/nm	352	351	356	353	353	353	364
	λ_{N^*}/nm	413	422	423	423	422	429	419
	λ_{T^*}/nm	495	499	492	498	496	518	501
	I_{N^*}/I_{T^*}	0.12	0.72	1.60	1.12	0.76	0.46	0.14
	$\varepsilon \times 10^{-3}$/l mol^{-1} cm^{-1}	13.0	13.3	13.1	12.3	15.1	9.9	11.5
	φ	0.45	0.13	0.096	0.13	0.12	0.13	0.31
Acetonitrile	λ_{abs}/nm	362	366	366	366	366	366	375
	λ_{N^*}/nm	424	419	419	422	418	433	433
	λ_{T^*}/nm	510	525	521	523	523	541	518
	I_{N^*}/I_{T^*}	0.02	0.10	0.17	0.11	0.11	0.12	0.03
	$\varepsilon \times 10^{-3}$/l mol^{-1} cm^{-1}	11.5	11.5	10.6	12.0	12.0	9.6	10.5
	φ	0.32	0.14	0.078	0.12	0.14	0.17	0.31
	Φ_{pd} (%)[b]	0.28	0.12	0.11	0.11	0.11	0.14	0.23

[a] Ar and R are the 3HQ substituents at position 2 and the heterocyclic nitrogen, respectively. λ_{abs} is the position of the absorption maximum (nm), λ_N* and λ_T* are the positions of the fluorescence maxima of the N* and T* forms, respectively (nm), ε is the molar extinction coefficient (l mol^{-1} cm^{-1}), φ is the fluorescence quantum yield, Φ_{pd} is the quantum yield of photodegradation. [b] For 3HF, Φ_{pd} = 1.2%.

(m, 6H, ArH, Ar′H), 7.42 (t, *J* 7, 1H, ArH), 3.54 (s, 3H, NCH_3); *m*/*z* 342.21 ($M^+ + H$); mp 234 °C.

2-Phenyl-3-hydroxy-4(1*H*)-quinolone (1a). Prepared by using the experimental procedure described above for **5**. δ_H(300 MHz; DMSO-d_6): 11.59 (br s, 1H, NH), 8.15 (d, *J* 8.5, 2H, ArH), 7.81 (d, *J* 7, 2H, Ar′H), 7.72 (d, *J* 8, 1H, ArH), 7.57 (m, 4H, ArH, Ar′H), 7.27 (t, *J* 7, 1H, Ar′H); *m*/*z* 238.24 ($M^+ + H$); mp 276 °C.

1-Methyl-2-phenyl-3-hydroxy-4(1*H*)-quinolone (1b). Prepared by using the experimental procedure described above for **5**. δ_H(300 MHz; DMSO-d_6): 8.31 (d, *J* 8, 1H, ArH), 7.74 (m, 2H, ArH), 7.57 (m, 3H, Ar′H), 7.45 (d, *J* 7, 2H, Ar′H), 7.38 (dd, *J* 7, 1H, ArH), 3.52 (s, 3H, NCH_3); *m*/*z* 252.22 ($M^+ + H$); mp 262 °C.

1-Methyl-2-(4-methoxyphenyl)-3-hydroxy-4(1*H*)-quinolone (2). Prepared by using the experimental procedure described above for **5**. δ_H(300 MHz; DMSO-d_6): 8.33 (d, *J* 8, 1H, ArH), 7.79 (m, 2H, ArH), 7.35 (m, 3H, ArH, Ar′H), 7.09 (d, *J* 7, 2H, Ar′H), 3.87 (s, 3H, OCH_3), 3.58 (s, 3H, NCH_3); *m*/*z* 282.31 ($M^+ + H$); mp 259 °C.

1-Methyl-2-(4-methylphenyl)-3-hydroxy-4(1*H*)-quinolone (3). Prepared by using the experimental procedure described above for **5**. δ_H(300 MHz; DMSO-d_6): 8.31 (d, *J* 8, 1H, ArH), 7.69 (m, 2H, ArH), 7.33 (m, 5H, ArH, Ar′H), 3.55 (s, 3H, NCH_3), 2.44 (s, 3H, 4′-CH_3); *m*/*z* 266.30 ($M^+ + H$); mp 224 °C.

1-Methyl-2-(4-fluorophenyl)-3-hydroxy-4(1*H*)-quinolone (4). Prepared by using the experimental procedure described above for **5**. δ_H(300 MHz; DMSO-d_6): 8.30 (d, *J* 6.9, 1H, ArH), 7.70 (m, 2H, ArH), 7.50 (m, 2H, ArH), 7.40 (m, 2H, ArH), 3.53 (s, 3H, NCH_3); *m*/*z* 270.11 ($M^+ + H$); mp 238 °C.

2-(2-Thienyl)-3-hydroxy-4(1*H*)-quinolone (6). Prepared by using the experimental procedure described above for **5**. δ_H(300 MHz; DMSO-d_6): 11.35 (br s, 1H, NH) 8.14 (d, *J* 8.5, 1H, ArH), 8.06 (d, *J* 4, 1H, Het), 7.86 (m, 2H, ArH, HetH), 7.63 (t, *J* 7.5, 1H, ArH), 7.32 (m, 2H, ArH, HetH); *m*/*z* 244.16 ($M^+ + H$); mp 296 °C.

Results and discussion

Light absorption properties

The absorption spectra for all tested 3HQs with an aromatic ring at position 2 were found to be marginally dependent on the nature of the substituents at this ring and on the quinolone nitrogen atom (Fig. 1). The absorption maximum in acetonitrile of all these derivatives is 365 ± 2 nm. This constitutes a major difference with 3HFs, where the absorption properties are very sensitive to the donor substituents at position 2.[3]

The only exception is compound **6** with a five-membered aromatic ring substituent that differs significantly from the other compounds by its absorption maximum being red-shifted by 9 nm and by the appearance of a shoulder at 394 nm. These differences may be attributed to the lower steric hindrance provided by the smaller ring in compound **6**. To further assess this hypothesis, quantum chemical calculations were performed for compounds **1a**, **1b** and **6** in comparison with 3HF (Fig. 2). Like 3HF, the 3HQ derivatives are

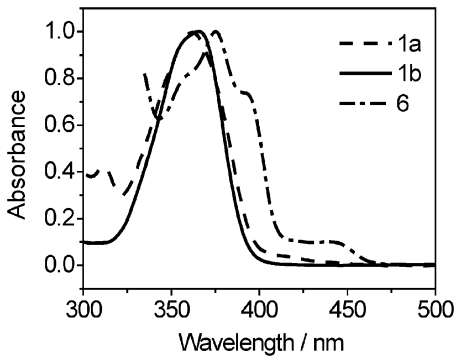

Fig. 1 Absorption spectra of 3HQs in acetonitrile. Spectra of compounds **2–5** are superimposed on that of compound **1b**.

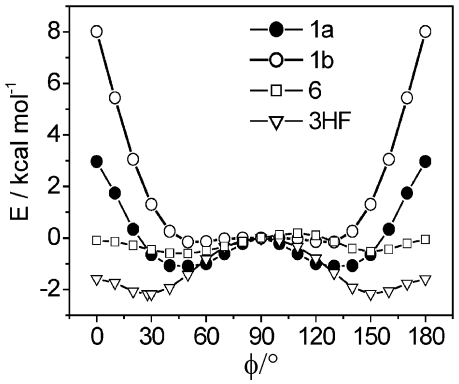

Fig. 2 Torsional enthalpy profiles (superimposed at $\phi = 90°$) of 3HF and 3HQ derivatives.

characterized by two planar moieties that can adopt non-planar conformations with dihedral angles between the two moieties governed by steric factors. Depending on these angles, substantial differences on the conjugation of the rings and thus in the absorption properties are expected. Crystallographic data show that in flavones the dihedral angle ϕ between the aryl and heterocycle moieties is in the range 5–30° depending whether a hydrogen atom or a more bulky hydroxyl group is at position 3 of the molecule.[21] According to our quantum chemical calculations, this angle is close to 30° and the energy of the planar conformation ($\phi = 0°$) is much lower than that of the twisted ($\phi = 90°$) conformation (Fig. 2). This relatively small angle still allows good conjugation between the two moieties and as a consequence, the possibility of controlling the absorption and fluorescence properties of 3HF by changing the substituents on the aryl ring. In contrast, the torsion energy profiles for 3HQ derivatives **1a**, **1b** (Fig. 2) suggest that the favorable dihedral angles are close to 45°, in line with recent X-ray data.[22] Moreover, in contrast to the energy profiles of 3HF, the planar conformation of 3HQ derivatives is of much higher energy than the twisted one (Fig. 2). These large angles and the high energy of the planar conformation likely prevent conjugation between the two aromatic moieties and explain the limited influence of the aromatic ring at position 2 on the light absorption properties.

In sharp contrast, conformations with smaller dihedral angles can be populated in the derivative **6** with a thiophene ring at position 2 (Fig. 2). Moreover, the energy differences between the various conformations of compound **6** are much lower than for the other 3HQ compounds (for instance, compare **6** with **1a** in Fig. 2). Consequently, better conjugation between the moieties is possible. This should enable us to adjust the absorption and fluorescence properties by varying the substituents on the five-membered ring at position 2.

Fluorescence properties: evidence of ESIPT in 3HQs

Due to their structural similarities with 3HFs, the 3HQ derivatives are also expected to exhibit an ESIPT reaction. In line with our previous results,[11] all the synthesized compounds exhibit two emission bands in phosphate buffer (Fig. 3a) and organic solvents (Fig. 4, Tables 1 and 2). Moreover, the excitation spectra of 3HQs recorded at the two emission band maxima are the same and match well with the corresponding absorption spectra. These observations on excitation and emission spectra are strongly indicative of an excited state process. Since in addition, the positions of the two maxima are close to those observed for 3HF, it is strongly suggested that 3HQ derivatives also undergo ESIPT. Additional experiments were performed to exclude other photophysical reactions such as excimer formation or photodissociation. Experiments performed with dye **4** demonstrated a stable ratio of the two band intensities I_{N*}/I_{T*} in the 10^{-7}–10^{-5} M concentration range and a linear growth of the fluorescence intensities with the dye concentration in this range. Both observations exclude excimer formation as the cause of the observed dual fluorescence.

Moreover, the intensity ratio of the two bands of dye **4** displayed only limited changes in the pH range 5–8. Formation of dye **4** anion was observed only at pH > 8 as monitored

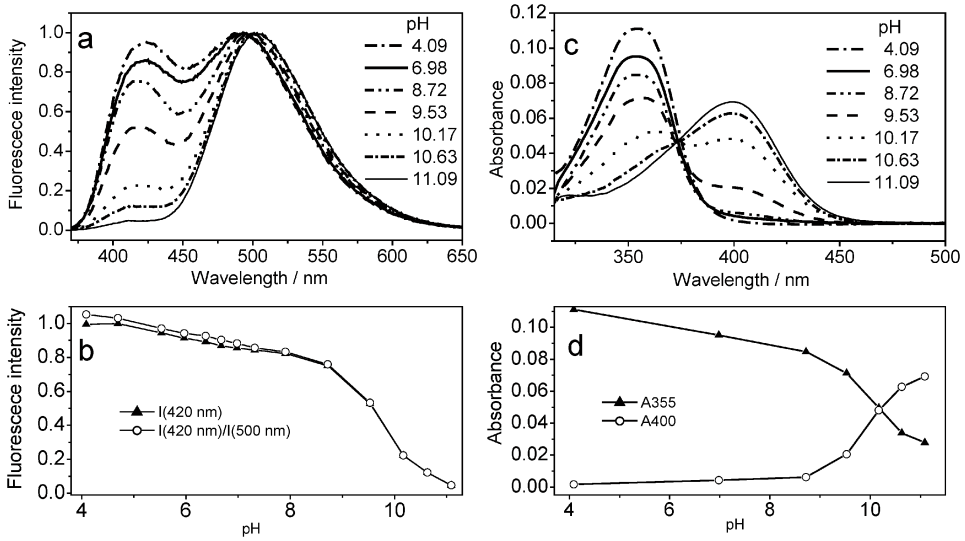

Fig. 3 pH dependence of the fluorescence and absorption spectra of dye **4**. **a** Emission spectra. **b** Fluorescence intensity at 420 nm and I_{420}/I_{500} intensity ratio. **c** Absorption spectra. **d** Absorbances at 355 and 400 nm.

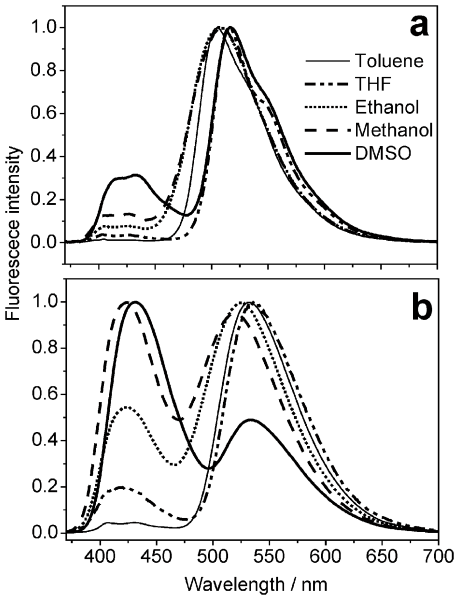

Fig. 4 Normalized emission spectra of 3HQ **1a** (R = H, panel a) and **1b** (R = Me, panel b) in organic solvents.

from the disappearance of the short wavelength band (Fig. 3a). Evaluation of the excited state pK_a by the dependence of the fluorescence intensity at 420 nm or the intensity ratio I_{420}/I_{500} on pH gives a value of 9.58 ± 0.04 (Fig. 3b). This excludes the possibility that photodissociation of dye **4** occurs at neutral pH in aqueous solutions and thus provides additional support for the ESIPT mechanism of the dual emission in 3HQs. Moreover, both the absence of excited state photodissociation in aqueous solutions and the preference of 3HQ molecules to undergo ESIPT are fully in line with previous observations on 3HF derivatives.[23]

Acid–base properties in the ground state are an additional important characteristic of fluorescence probes. In aqueous solutions, the anionic form of **4** appears only at pH ≥ 9 and exhibits an absorption maximum at 400 nm (Fig. 3c). A pK_a value of 10 ± 0.1 was calculated using the dependences of the absorbances at 355 and 400 nm *versus* pH (Fig. 3d). The fluorescence spectrum of the pure anionic form of dye **4** was obtained at pH > 11 using an excitation wavelength of 400 nm and exhibited a single band with a maximum at 504 nm (not shown).

To further characterize the ESIPT reaction in aqueous medium, time-resolved measurements of compound **4** were performed with a 320 nm excitation wavelength. The fluorescence decay of the N* form recorded at 400 nm was mono-exponential with a 0.38 ns lifetime. The fluorescence decay of the T* form recorded at 530 nm was bi-exponential with two lifetime values, 0.38 and 1.16 ns. These two lifetimes were associated with negative and positive pre-exponential coefficients, respectively. The negative pre-exponential coefficient for the long-wavelength band is a clear indication of an excited state reaction.[24] Moreover, the identity of the short lifetime components of the two emission bands suggests that the long-wavelength emissive species is generated from the short-wavelength emissive species. These results provide additional evidence for the ESIPT reaction being the mechanism for the dual emission of compound **4**. However, the observed ESIPT related lifetime component is much longer than that observed for 3HFs in organic solvents, which indicates that in this particular case the ESIPT reaction is relatively slow. The latter could be connected both with an intrinsic property of the 3HQ fluorophore and with the solvation effect of water. The absence of long lifetime component in the case of the N* band suggests that in the present case the ESIPT reaction is probably an irreversible process,[24] which is in contrast with reversible ESIPT in 3HF derivatives observed in organic solvents.[13]

Taken together, our data indicate that the long-wavelength band of 3HQs in aqueous solution at neutral pH results from an emission of the ESIPT product. This behavior being similar to that of 3HFs, 3HQs appear as prospective two-color fluorescent dyes for biological applications.

Dependence of the emission spectra on the substituent at the heterocyclic nitrogen

The ratio of the two band intensities and the sensitivity of this ratio to the solvent were found to depend on the substituent at the heterocyclic nitrogen. For instance, compounds **1a** and **6** with R = H are characterized by a low intensity of the short

Table 2 Spectroscopic properties of 3HQs in organic solvents

Solvent	PPS[a]	3HQ	**1a**	**1b**	**2**	**3**	**4**	**5**	**6**
Toluene	0.655	I_{N*}/I_{T*}	0.01	0.03	0.03	0.02	0.02	0.11	0.02
		φ	0.38	0.22	0.16	0.22	0.23	0.22	0.34
Chloroform	0.786	I_{N*}/I_{T*}	0.02	0.07	0.10	0.07	0.06	0.09	0.03
		φ	0.44	0.23	0.14	0.21	0.23	0.27	0.40
THF	0.838	I_{N*}/I_{T*}	0.04	0.2	0.25	0.19	0.20	0.45	0.08
		φ	0.28	0.13	0.07	0.11	0.12	0.13	0.22
Ethanol	0.853	I_{N*}/I_{T*}	0.09	0.51	1.02	0.58	0.59	0.42	0.11
		φ	0.36	0.13	0.08	0.12	0.12	0.18	0.33
Methanol	0.857	I_{N*}/I_{T*}	0.34	1.01	2.10	1.12	1.18	0.60	0.16
		φ	0.35	0.13	0.07	0.11	0.11	0.17	0.30
DMF	0.954	I_{N*}/I_{T*}	0.16	0.77	1.14	0.78	0.84	0.87	0.23
		φ	0.39	0.19	0.12	0.17	0.37	0.2	0.34
DMSO	1	I_{N*}/I_{T*}	0.34	2.00	3.66	2.13	2.14	1.12	0.48
		φ	0.51	0.32	0.25	0.31	0.37	0.28	0.39

[a] PPS and φ designate the solvent polarity–polarizability scale and the fluorescence quantum yield, respectively.

wavelength band and thus a limited sensitivity of its intensity ratio to the nature of the solvent (Fig. 4a, Table 2). In contrast, compounds **1b–5** with R = Me display a pronounced variation of their intensity ratio in different solvents (Fig. 4b, Table 2).

One possible explanation for the increase of the N* form intensity in N–Me 3HQs in comparison with N–H derivatives is the decrease of the acidity of their 3-OH group in the excited state. This acidity can decrease due to the higher electron-donating properties of Me as compared to H. Alternatively, the higher relative intensity of the N* band in the case of N–Me substituted 3HQs can also be assigned to the larger size of the methyl group which disrupts the planarity of the molecule in the excited state due to steric hindrance (see above). This conclusion is in line with previous reports on 3-hydroxychromones, showing that an *ortho*-methyl group on the 2-aryl ring produced similar steric effects and increased the N* form emission.[25]

Dependence of the emission spectra of *N*-methyl substituted 3HQs on the substituent at position 2

Though N–Me 3HQ derivatives exhibit similar absorption spectra, their emission spectra were found to depend on the nature of the aromatic group at position 2. Indeed, the electron-donor properties of this aromatic group substantially influence the I_{N*}/I_{T*} intensity ratio. For example, in phosphate buffer at pH 7.0 the I_{N*}/I_{T*} ratio varies from 0.46 for dye **5** containing an electron-withdrawing CF_3 group to 1.6 for dye **2** with an electron-donating OMe group in the *para* position of the aromatic ring (Fig. 5).

To evaluate the electronic influence of substituents on the chemical reaction rates of aromatic compounds, the Hammett equation can be used:[26]

$$\log k/k_0 = \sigma^+\rho$$

where k_0 and k are the rate constants of a given reaction with a non-substituted (R′ = H) and a substituted compound, respectively. The constant ρ characterizes the type of reaction and σ^+ characterizes the electron-withdrawing properties of the substituent, taking into account a high level of π-conjugation.

Interestingly, the dependence of the logarithm of the I_{N*}/I_{T*} intensity ratio *versus* the σ^+ value of the substituent R′ (Scheme 2) was found to be linear (Fig. 6), indicating that the same reaction, namely ESIPT, takes place for all studied

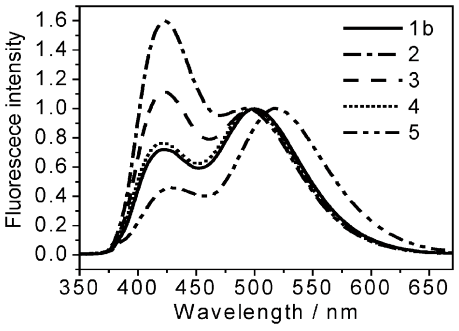

Fig. 5 Emission spectra of 3HQs **1b–5** in phosphate buffer (pH 7.0) normalized at the long-wavelength band maximum: **1b** (–), **2** (--), **3** (···), **4** (-·-) and **5** (– · ·).

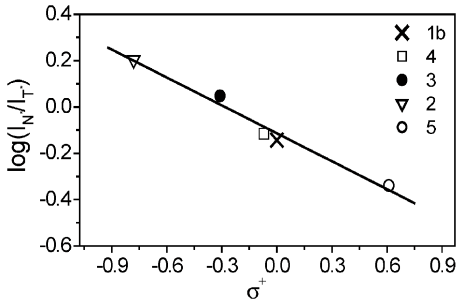

Fig. 6 Dependence of $\log(I_{N*}/I_{T*})$ of N–Me 3HQs on the Hammett constant in phosphate buffer. The data are fitted to: $\log(I_{N*}/I_{T*}) = -0.114\sigma^+ - 0.402$ ($r^2 = 0.98$).

N–Me 3HQs and that its rate increases with the electron-withdrawing property σ^+ of the substituent. The gradual increase in the ESIPT rate can be explained by the increase in the excited state acidity of the 3-OH group with the electron-withdrawing ability of the substituent. Moreover, since the I_{N*}/I_{T*} value is controlled by the relative rates of the various photophysical processes taking place in the excited state,[13] this linear dependence indicates that the other processes (radiative and non-radiative) were not significantly affected by these substituents. Moreover, the effect of the substituent on the emission of 3HQs together with its poor influence on the absorption spectra indicate that the conjugation between the 2-aryl group and the 3HQ moiety is much more pronounced in the excited state than in the ground state.

Thus, the I_{N*}/I_{T*} ratio can be modulated by the substituents on the aromatic ring of N–Me 3HQs. Moreover, using the Hammett equation, one can predict the I_{N*}/I_{T*} ratio of N–Me 3HQ for various groups in the *para* position. This feature is of high interest for developing 3HQs with programmed fluorescence properties.

Dependence of the I_{N*}/I_{T*} ratio and quantum yield of N–Me 3HQs on the solvent polarity

One unique property of 3HF dyes with dual fluorescence is the dependence of their I_{N*}/I_{T*} ratio on the environment.[3–5] To check whether this dependence also exists for N–Me 3HQs, we have determined their I_{N*}/I_{T*} ratio and quantum yield in different organic solvents (Table 2).

The correlations between the I_{N*}/I_{T*} ratios and the solvent polarity were established on the basis of the empirical solvent polarity–polarizability scale (PPS).[27] This scale is based on the solvatochromic shifts undergone by the long-wavelength absorption maximum of two indicators—DMANF and FNF. This scale excludes specific solvent–solute interactions and thus reflects 'pure' polarity.[27]

The I_{N*}/I_{T*} ratios of all N–Me 3HQs are highly sensitive to solvent polarity (Table 2). In Fig. 7, it can be seen that for the representative compound **1b**, the logarithm of the I_{N*}/I_{T*} ratio linearly increases with the PPS index in aprotic solvents. In contrast, the I_{N*}/I_{T*} ratio in the two protic solvents (methyl and ethyl alcohol) was much higher than expected from the PPS scale. This indicates that, as in the case of 3HF derivatives,[5] the hydroxyl groups of protic solvents probably form

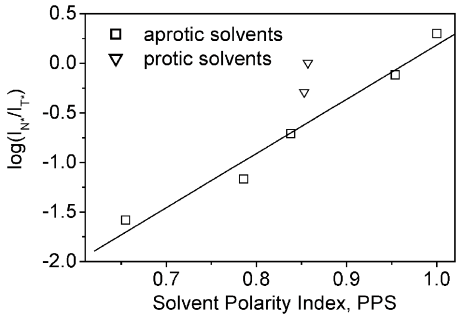

Fig. 7 Dependence of $\log(I_{N^*}/I_{T^*})$ of the dye **1b** on the solvent polarity index PPS. The aprotic solvents are toluene, chloroform, THF, DMF and DMSO. The protic solvents are ethyl alcohol and methyl alcohol. For aprotic solvents, data are fitted to $\log(I_{N^*}/I_{T^*}) = 5474 \times \text{PPS} - 5289$ ($r^2 = 0.97$).

hydrogen bonds with 3HQs, decreasing the ESIPT rates and therefore increasing the I_{N^*}/I_{T^*} ratio.

Comparison of the polarity dependences of all studied N–Me 3HQs in aprotic solvents is given in Fig. 8. Interestingly, the dyes exhibit different sensitivities to polarity, as can be seen from the different slopes. These different sensitivities are probably dependent on the electronic properties of the 2-aryl substituents. For instance, compound **5** with the electron-withdrawing *p*-(trifluoromethyl)phenyl group is less sensitive than **1b** with an unsubstituted phenyl group.

In contrast to the I_{N^*}/I_{T^*} ratio, only limited differences in 3HQ quantum yields were observed as a function of the solvent polarity. Moreover, as in the case of 3HFs, [3,4] no clear correlation could be established between the quantum yields of 3HQs and the solvent polarity (Table 2). For instance, similar quantum yields were found for all 3HQs in toluene and DMSO, though these solvents differ largely in polarity. However, the quantum yield was found to depend upon the structure of the 3HQs. For instance, N–H 3HQs **1a** and **6** exhibit higher quantum yields than the *N*-methyl derivatives in all solvents studied. This could be explained by an increase in the non-radiative rate constants due to a steric effect of the *N*-methyl group on the 2-aryl substituent that decreases the planarity of the *N*-methyl derivatives. Most interestingly, the quantum yields of the studied 3HQs are

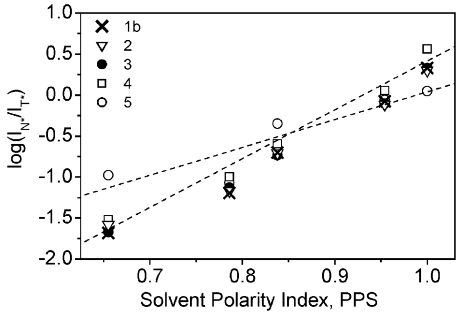

Fig. 8 Dependence of $\log(I_{N^*}/I_{T^*})$ on the solvent polarity index PPS for the N–Me 3HQs. Linear fits are presented for the most and the least sensitive dyes, **2** and **5**, respectively. The solvents are toluene, chloroform, THF, DMF and DMSO.

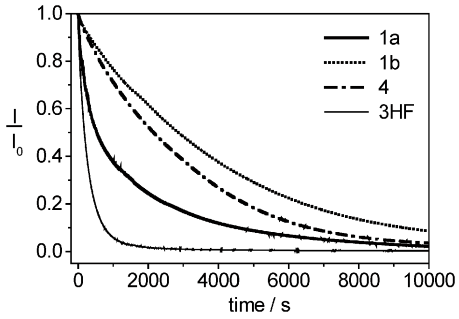

Fig. 9 Dynamics of photodestruction of 3HQs **1a**, **1b**, **4** and 3HF.

generally higher than those reported for 3HFs.[3] This constitutes an additional advantage of 3HQs over 3HFs.

Photostability

Photostability is an important property of fluorescent probes designed for biological applications. This property is notably important for investigating the dynamic properties of biomolecules such as proteins or nucleic acids, when the samples are irradiated for a long time. As could be seen from the quantum yields of photodegradation (Table 1) or the kinetic curves of photodestruction (Fig. 9), all studied 3HQs are one order of magnitude more photostable than 3HF. Moreover, comparison of compounds **1a**, **6** and **1b–5** indicates that N–Me 3HQs are about three times more photostable than the N–H derivatives (Table 1 and Fig. 9).

Conclusions

In this study, a new class of dyes, the substituted 2-aryl-3-hydroxyquinolones, has been shown to exhibit dual fluorescence in organic solvents as well as in aqueous solutions due to an excited state intramolecular proton transfer reaction. We observe that the substituent at the 2-aryl ring does not modify the absorption spectra of 3HQs, probably due to its twisted orientation with respect to the 3HQ moiety. Only the compound with a five-membered aryl substituent exhibits an increased planarity and thus differs considerably in its absorption properties. In contrast, the fluorescence properties of the dyes show a systematic dependence on the substituent. Indeed, a linear correlation of the logarithm of the intensity ratio of the two emission bands *versus* the Hammett constant (electron-withdrawing ability) associated with the substituent in the 2-aryl ring is observed for N–Me 3HQs. Moreover, the fluorescence properties of 3HQs are modulated by the nature of the substituent at the nitrogen heteroatom. While the dual fluorescence of N–H derivatives exhibits limited sensitivity to the polarity of their surroundings, N–Me 3HQs demonstrate strong solvatochromic properties, with large and systematic changes in the relative intensities of the two emission bands as a function of the solvent polarity. Finally, the 3HQ derivatives were found to exhibit higher fluorescence quantum yield and photostability than 3HFs. Consequently, 3HQ derivatives appear as prospective polarity-sensitive fluorescent labels for biomolecules, with fluorescence properties and sensitivity to solvent that can be tuned by the substituents at the 2-aryl ring and the nitrogen heteroatom.

Acknowledgements

This work was supported by the Agence Française contre les Myopathies (contract #LHSB-CT 2003-50311480), the TRIoH European program and the Eco-Net program from the Ministère des Affaires Etrangères. DAY is a member of the European Doctoral College and is supported by an Eiffel fellowship. VVS is supported by TRIoH. The laboratory of Drs André Mann and Jean Suffert is acknowledged for providing support for organic synthesis.

References

1 (*a*) G. R Bright, G. W. Fisher, J. Rogowska and D. L. Taylor, *Methods Cell Biol*., 1989, **30**, 157–192; (*b*) Z. R. Grabowski, K. Rotkiewicz and W. Rettig, *Chem. Rev*., 2003, **103**, 3899–4031.
2 (*a*) S. J. Formosinho and L. G. Arnaut, *J. Photochem. Photobiol., A*, 1993, **75**, 21–48; (*b*) D. Le Gourrierec, S. M. Ormson and R. G. Brown, *Prog. React. Kinet*., 1994, **19**, 211–275.
3 (*a*) T. C. Swinney and D. F. Kelley, *J. Chem. Phys*., 1993, **99**, 211–221; (*b*) A. S. Klymchenko, T. Ozturk, V. G. Pivovarenko and A. P. Demchenko, *Can. J. Chem*., 2001, **79**, 358–363; (*c*) A. S. Klymchenko, T. Ozturk, V. G. Pivovarenko and A. P. Demchenko, *Tetrahedron Lett*., 2001, **42**, 7967–7970; (*d*) A. S. Klymchenko, T. Ozturk and A. P. Demchenko, *Tetrahedron Lett*., 2002, **43**, 7079–7082; (*e*) A. S. Klymchenko, T. Ozturk, V. G. Pivovarenko and A. P. Demchenko, *New J. Chem*., 2003, **27**, 1336–1343.
4 (*a*) S. Ercelen, A. S. Klymchenko and A. P. Demchenko, *Anal. Chim. Acta*, 2002, **464**, 273–287; (*b*) A. S. Klymchenko, V. G. Pivovarenko and A. P. Demchenko, *J. Phys. Chem. A*, 2003, **107**, 4211–4216; (*c*) A. S. Klymchenko and A. P. Demchenko, *Phys. Chem. Chem. Phys*., 2003, **5**, 461–468.
5 (*a*) A. S. Klymchenko, G. Duportail, T. Ozturk, Y. Mély and A. P. Demchenko, *Proc. Natl. Acad. Sci. USA*, 2003, **100**, 11219–11224; (*b*) O. P. Bondar, V. G. Pivovarenko and E. S. Rowe, *Biochim. Biophys. Acta*, 1998, **1369**, 119–130.
6 (*a*) S. M. Dennison, J. Guharay and P. K. Sengupta, *Spectrochim. Acta, Part A*, 1999, **55**, 1127–1132; (*b*) V. V. Shynkar, A. S. Klymchenko, G. Duportail, A. P. Demchenko and Y. Mely, *Biochim. Biophys. Acta*, 2005, **1712**, 128–136.
7 (*a*) S. Ercelen, A. S. Klymchenko and A. P. Demchenko, *FEBS Lett*., 2003, **538**, 25–28; (*b*) A. S. Klymchenko, S. V. Avilov and A. P. Demchenko, *Anal. Biochem*., 2004, **329**, 43–57.
8 A. Sytnik, D. Gormin and M. Kasha, *Proc. Natl. Acad. Sci. USA*, 1994, **91**, 11968–11972.
9 (*a*) D. Roshal, A. V. Grigorovich, A. O. Doroshenko, V. G. Pivovarenko and A. P. Demchenko, *J. Phys. Chem*., 1998, **102**, 5907–5914; (*b*) X. Poteau, G. Saroja, C. Spies and R. G. Brown, *J. Photochem. Photobiol., A*, 2004, **162**, 431–439.
10 V. G. Pivovarenko, O. B. Vadzyuk and S. O. Kosterin, *J. Fluoresc*., 2006, DOI: 10.1007/s10895-005-0020-5.
11 D. A. Yushchenko, M. D. Bilokin, O. V. Pyvovarenko, G. Duportail, Y. Mely and V. G. Pivovarenko, *Tetrahedron Lett*., 2006, **47**, 905–908.
12 F. Gao, K. F. Johnson and J. B. Schlenoff, *J. Chem. Soc., Perkin Trans. 2*, 1996, **2**, 269–273.
13 (*a*) V. V. Shynkar, Y. Mély, G. Duportail, E. Piémont, A. S. Klymchenko and A. P. Demchenko, *J. Phys. Chem. A*, 2003, **107**, 9522–9529; (*b*) A. D. Roshal, J. A. Organero and A. Douhal, *Chem. Phys. Lett*., 2003, **379**, 53–59.
14 (*a*) K. Livesey and J.-C. Brochon, *Biophys. J*., 1987, **52**, 693–706; (*b*) J.-C. Brochon, *Methods Enzymol*., 1994, **240**, 262–311.
15 (*a*) A. O. Doroshenko, L. B. Sychevskaya, A. V. Grygorovych and V. G. Pivovarenko, *J. Fluoresc*., 2002, **12**, 455–464; (*b*) D. M. Himmelblau, *Applied Nonlinear Programming*, McGraw-Hill Book Company, 1972 (Russian edn, Moscow, Mir, 1975).
16 I. J. Berstein and Y. L. Kaminskij, *Spectrophotometric Analysis in Organic Chemistry*, Khimija, Leningrad, 1986.
17 K. D. Belfield, M. V. Bondar, Y. Liu and O. V. Przhonska, *J. Phys. Org. Chem*., 2003, **16**, 69–78.
18 J. R. Lakovicz, *Principles of Fluorescence Spectroscopy*, Kluwer Academic/Plenum Publishers, New York, 2nd edn, 1999, p. 52.
19 M. J. S. Dewar, E. G. Zoebich, E. F. Healy and J. P. Stewart, *J. Am. Chem. Soc*., 1985, **107**, 3902–3908.
20 P. Hradil and J. Jirman, *Collect. Czech. Chem. Commun*., 1995, **60**, 1357–1366.
21 (*a*) S. Ozbei, E. Kendi, G. K. Ayhan and R. Eltan, *Acta Crystallogr., Sect. C: Cryst. Struct. Commun*., 1999, **55**, 678–680; (*b*) G. Smith, J. P. Bartley, E. Wang and R. C. Bott, *Acta Crystallogr., Sect. C: Cryst. Struct. Commun*., 2001, **57**, 1336–1337; (*c*) I. Lippai, G. Speier, J. Huttner and L. Zsolnai, *Acta Crysallogr., Sect. C: Cryst. Struct. Commun*., 1997, **53**, 1547–1549.
22 P. Hradil, P. Krejci, J. Hlavac, I. Wiedermannova, A. Lycka and V. Bertolasi, *J. Heterocycl. Chem*., 2004, **41**, 375.
23 A. S. Klymchenko and A. P. Demchenko, *New J. Chem*., 2004, **28**, 687–692.
24 W. R. Laws and L. Brand, *J. Phys. Chem*., 1979, **83**, 795–802.
25 (*a*) A. S. Klymchenko, V. G. Pivovarenko and A. P. Demchenko, *Spectrochim. Acta, Part A*, 2003, **59**, 787–792; (*b*) A. J. G. Strandjord, D. E. Smith and P. F. Barbara, *J. Phys. Chem*., 1985, **89**, 2362.
26 F. A. Carey and R. J. Sundberg, *Advanced Organic Chemistry, Part A*, Kluwer Academic/Plenum Publishers, New York, 4th edn, 2000, pp. 204–215.
27 J. Catalan, V. Lopez, P. Pçerez, R. Martın-Villamil and J. G. Rodrıguez, *Liebigs Ann*., 1995, 241.

Article 2

Steric control of the excited state intramolecular proton transfer in 3-hydroxyquinolones: steady-state and time-resolved fluorescence study

Steric Control of the Excited-State Intramolecular Proton Transfer in 3-Hydroxyquinolones: Steady-State and Time-Resolved Fluorescence Study

Dmytro A. Yushchenko,*[,†,‡] Volodymyr V. Shvadchak,[†,‡] Andrey S. Klymchenko,*[,‡] Guy Duportail,[‡] Vasyl G. Pivovarenko,[†,‡] and Yves Mély[‡]

Department of Chemistry, Kyiv National Taras Shevchenko University, 01033 Kyiv, Ukraine, and Photophysique des Interactions Biomoléculaires, UMR 7175-LC1 du CNRS, Institut Gilbert Laustriat, Faculté de Pharmacie, Université Louis Pasteur, 67401 Illkirch, France

Received: February 7, 2007; In Final Form: May 7, 2007

3-Hydroxyquinolones (3HQs), similarly to their 3-hydroxychromone analogs, undergo excited state intramolecular proton transfer (ESIPT) resulting in dual emission. In the ground state, 2-phenyl-3HQ derivatives are not flat due to a steric hindrance between the 2-phenyl group and the 3-OH group that participates in the ESIPT reaction. To study the effect of this steric hindrance on the ESIPT reaction, a number of 3HQ derivatives have been synthesized and characterized in different organic solvents by steady-state and time-resolved fluorescence techniques. According to our results, 2-phenyl-3HQ derivatives undergo much faster ESIPT (by nearly 1 order of magnitude) than their 2-methyl-3HQ analogs. Moreover, 1-methyl-2-phenyl-3HQ having a strongly twisted 2-phenyl group undergoes a two- to three-fold slower ESIPT compared to 2-phenyl-3HQ. These results suggest that the flatter conformation of 2-phenyl-3HQ, which allows a close proximity of the 2-phenyl and 3-OH groups, favors a fast ESIPT reaction. The absorption and fluorescence spectra of the 3HQ derivatives additionally confirm that the steric rather than the electronic effect of the 2-phenyl group is responsible for the faster ESIPT reaction. Based on the spectroscopic studies and quantum chemical calculations, we suggest that the 2-phenyl group decreases the rotational freedom of its proximal 3-OH group in the more planar conformation of 2-phenyl-3HQ. As a result, the conformations of 3HQ, where the 3-OH group orients to form an intramolecular H-bond with the 4-carbonyl group, are favored over those with a disrupted intramolecular H-bond. Therefore, the 2-phenyl group sterically favors the intramolecular H-bond and thus accelerates the ESIPT reaction. This conclusion provides a new understanding of the ESIPT process in 3-hydroxyquinolones and related systems and suggests new possibilities for the design of ESIPT based molecular sensors and switchers.

1. Introduction

The mechanism of the excited-state intramolecular proton transfer (ESIPT) in 3-hydroxyflavones (3HFs) is a matter of debate since its introduction by Sengupta and Kasha.[1,2] These authors suggested that ESIPT occurs without energetic barrier so that it is essentially a tunneling process. Moreover, they proposed a critical role for the motion of the 2-phenyl group in the ESIPT reaction. This interpretation was critically revised by Woolfe and Thistlethwaite who claimed that ESIPT in apolar solvents exhibits a high activation barrier but does not depend much on the phenyl motion.[3] The role of the 2-phenyl ring in 3HF was further investigated by Barbara et al. who showed that modification of the phenyl group with a methyl group in its ortho position decreases the intensity of the tautomer emission.[4] A similar effect was observed later with 2-benzofuranyl derivatives.[5] These results point out that a planar configuration of 3HF is required for fast ESIPT reaction.[4,6] The observed phenomenon was explained by the electronic effect of the 2-phenyl group on 3-hydroxychromone moiety. Thus, this planar configuration and, therefore, the optimized conjugation of the phenyl group with the 3-hydroxychromone ring increases the basicity of the 4-carbonyl group and thus strengthens the intramolecular H-bond. This in turn accelerates the ESIPT reaction in line with the very fast ESIPT kinetics (30 fs) recently measured for 3HF in aprotic solvents.[7,8]

Recently, a new class of dyes, 2-aryl-3-hydroxy-4(*1H*)-quinolones (3HQs), which are structural analogs of 3HFs, was introduced[9,10] (Chart 1). The 3HQ dyes exhibit also two emission bands due to ESIPT.[11] Because 3HFs already found a large range of applications as fluorescent probes in biology,[12−17] the 3HQ dyes form a new promising class of dyes, especially due to their higher photostability as compared to the 3HF analogs.[18] However, the development of improved 3HQ dyes for particular applications requires a better understanding of their ESIPT mechanism. In this respect, we have recently shown that the dual emission of 3HQs is highly sensitive to solvent properties, especially polarity and H-bonding basicity. In addition, the introduction of a methyl group at the nitrogen heteroatom was found to increase dramatically the N* emission, so that both bands are of comparable intensities in a number of organic solvents.[11,18]

This strong effect of the N-methyl group, which actually does not change considerably other spectroscopic properties, could be mainly due to changes of the orientation of the 2-phenyl group with respect to the 3HQ heterocycle. A somewhat similar

* To whom correspondence should be addressed. E-mail: (D.A.Y.) dmytro@pharma.u-strasbg.fr; (A.S.K.) aklymchenko@pharma.u-strasbg.fr. Phone: +33 390 244255. Fax: +33 390 244313.
† Kyiv National Taras Shevchenko University.
‡ Université Louis Pasteur.

10.1021/jp071075t CCC: $37.00
Published on Web 08/24/2007 PAGE EST: 6.5

CHART 1: Structures of 3HF and 3HQ Derivatives.

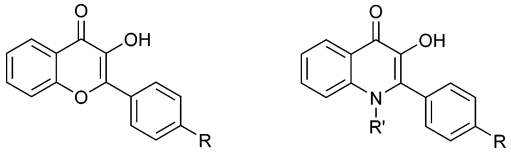

CHART 2: Structures of Studied 3HQs.

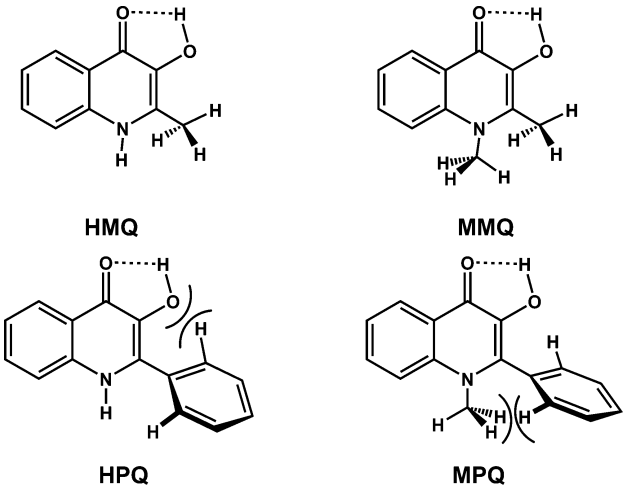

effect was observed with ortho-substituted 3HF,[4] but in both cases the mechanism of the effect of the phenyl group remains unclear. To further understand this phenomenon, we synthesized substituted 3HQs without 2-phenyl group and compared their properties with 2-phenyl-substituted derivatives (Chart 2). Our results show that the steric interaction of 2-phenyl and 3-OH groups is of key importance. Indeed, 2-phenyl-3-hydroxy-4(*1H*)-quinolone (HPQ), the 2-phenyl-3HQ with the most flat structure, undergoes the fastest ESIPT, while the 2-methyl-3-hydroxy-4(*1H*)-quinolone (HMQ) and 1-methyl-2-methyl-3-hydroxy-4(*1H*)-quinolone (MMQ) dyes without 2-phenyl group exhibit the slowest ESIPT. These results suggest that the flat structure of HPQ freezes the rotation of the 3-OH group, stabilizing the intramolecular H-bond and thus accelerating the ESIPT reaction.

2. Materials and Methods

HPQ, 1-methyl-2-phenyl-3-hydroxy-4(*1H*)-quinolone (MPQ), HMQ, and MMQ were synthesized by condensing the corresponding anthranilic acid ester in polyphosphoric acid as previously described.[10,11] All the solvents and chemicals were purchased from Aldrich. The solvents were of spectroscopic grade. Absorption spectra were recorded on a Cary 4 spectrophotometer (Varian) and fluorescence spectra on a FluoroMax 3.0 (Jobin Yvon, Horiba) spectrofluorometer. For the steady-state fluorescence measurements, the excitation wavelength was 360 nm. Fluorescence quantum yields were determined by taking quinine sulfate in 0.5 M sulfuric acid (quantum yield, $\varphi = 0.577$)[19] as a reference.

Time-resolved fluorescence measurements were performed with the time-correlated, single-photon counting technique using the frequency-doubled output of a Ti-Sapphire laser (Tsunami, Spectra Physics), pumped by a Millenia X laser (Tsunami, Spectra Physics).[20] The excitation wavelength was set at 320 nm. The fluorescence decays were collected at the magic angle (54.7°) of the emission polarizer. The single-photon events were detected with a microchannel plate Hamamatsu R3809U photomultiplier coupled to a Philips 6954 pulse preamplifier and were recorded on a multichannel analyzer (Ortec 7100) calibrated at 25.5 ps/channel. The instrumental response function was recorded with a polished aluminum reflector, and its full-width at half-maximum was 50 ps. Time-resolved decays were analyzed both by the iterative reconvolution method and the maximum entropy method (MEM).[21] The goodness of the fit was evaluated from the χ^2 values, the plots of the residuals, and the autocorrelation function. Quantum chemical calculations of 3HQs were performed with the AM1 semiempirical method[22] using the MOPAC 6.0 program. To estimate the mean dihedral angle between 2-phenyl and 3HQ rings, we first calculated with AM1 method the dependence of energy versus the dihedral angle and then applied Boltzmann statistics for room temperature to calculate the probability of each conformation.

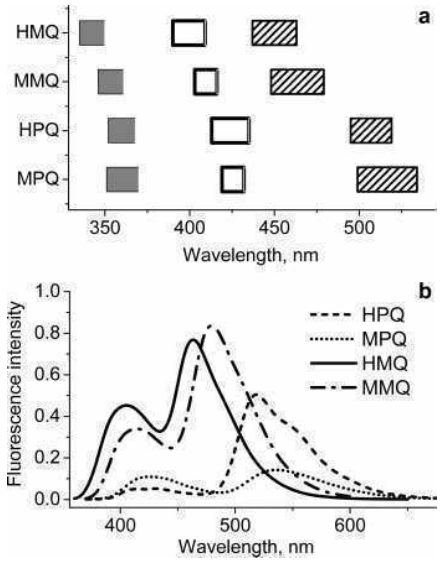

Figure 1. (a) Ranges of absorption and fluorescence maxima of 3HQs in the studied organic solvents. (b) Fluorescence spectra of 3HQs in DMF. The excitation wavelength was 360 nm.

3. Results and Discussion

3.1. Spectroscopic Properties of 3HQ Dyes. Absorption spectra of the four studied dyes in different organic solvents are composed of a single band with the maximum slightly varying with the dye structure. In 2-methyl-3HQ, introduction of a N-methyl group (MMQ) results in a ca. 10 nm red shift of the absorption maximum (Figure 1, Table 1), which is probably related to the electron donor property of the methyl group.

In contrast, the N-methyl group does not shift the absorption maximum of 2-phenyl-3HQ. This absence of red shift is probably related to the decrease of planarity of the 3HQ molecule in the presence of the N-methyl group[18] that compensates the red shift effect of this group. Indeed, a similar decrease of the planarity of a 3HF molecule by modification of its 2-phenyl ring with an ortho-methyl group was previously shown to shift the absorption band by ca. 20 nm to the blue,[4] due to the decrease of the electronic conjugation between the 2-phenyl and chromone rings.

The fluorescence spectra of all dyes in the studied solvents show two emission bands, which according to our previous studies[11,18] can be assigned to the emission of the normal- (N*) and tautomeric- (T*) excited states. For all the dyes, the excitation spectra recorded at these two emission band maxima are very close to the corresponding absorption spectrum, indicating that both emission forms originate from the same

TABLE 1: Spectroscopic Properties of 3HQs in Different Organic Solvents[a]

solvent	3HQ	λabs nm	λN* nm	λT* nm	I_{N^*}/I_{T^*}	Φ
chloroform	MMQ	360	405	466	0.07	0.37
	MPQ	368	418	518	0.07	0.23
	HMQ	343	390	453	0.08	0.41
	HPQ	364	422	503	0.02	0.44
ethyl acetate	MMQ	354	403	475	0.07	0.42
	MPQ	368	420	532	0.09	0.15
	HMQ	343	394	459	0.09	0.44
	HPQ	363	403	513	0.03	0.36
acetonitrile	MMQ	352	403	471	0.11	0.45
	MPQ	366	419	525	0.10	0.12
	HMQ	341	397	456	0.12	0.49
	HPQ	362	424	510	0.02	0.32
ethanol	MMQ	353	403	470	0.26	0.54
	MPQ	366	424	523	0.51	0.13
	HMQ	340	390	448	0.18	0.63
	HPQ	362	425	514	0.09	0.36
methanol	MMQ	352	404	467	0.45	0.52
	MPQ	364	423	519	1.01	0.13
	HMQ	340	396	448	0.37	0.54
	HPQ	361	425	512	0.34	0.35
DMF	MMQ	361	413	478	0.52	0.72
	MPQ	368	426	536	0.77	0.19
	HMQ	348	406	463	0.59	0.71
	HPQ	367	432	519	0.16	0.39
DMSO	MMQ	360	416	479	0.92	0.80
	MPQ	370	432	534	2.00	0.32
	HMQ	350	409	463	1.05	0.86
	HPQ	368	435	519	0.34	0.51
H_2O (phosphate	MMQ	346		448		0.61
buffer pH 7)	MPQ	351	422	499	0.72	0.13
	HMQ	335		437		0.54
	HPQ	352	413	495	0.12	0.45

[a] λ_{abs}: position of absorption maxima. λ_{N^*} and λ_{T^*}: position of fluorescence maxima of N* and T* forms. I_{N^*}/I_{T^*}: ratio of the intensities of the two emission bands at their peak maxima. φ: fluorescence quantum yield.

ground-state species. The position of these two emission bands varies with the substituents. Introduction of a N-methyl group in 2-methyl-3HQ shifts the emission maxima to a small extent. These shifts are close to those observed in the absorption spectra, so that the Stokes shifts of the N* and T* bands remain unchanged. Meantime, introduction of a 2-phenyl group shifts the N* and T* bands to a different extent. While the N* band shifts slightly to the red similarly to the absorption band, the T* band is strongly red-shifted. As a result, the Stokes shift of the T* band of MPQ is 13 nm (1380 cm^{-1}) larger than that of MMQ. A similar shift is observed when HPQ is compared with HMQ. This significant increase in the Stokes shift of the T* band on introduction of the 2-phenyl group can be assigned to the flattening of the HPQ and MPQ molecules in the T* state. Indeed, it was previously shown that the 2-phenyl-3HQ dyes are not planar in their ground states,[18] so that the 2-phenyl group is tilted with respect to the quinolone heterocycle. As a consequence, a flattening of the molecule in the excited state would decrease the energy of the S_1 state (due to increased electronic conjugation) and increase the energy of the nonrelaxed S_0 state due to the unfavored flat conformation in the ground state. Therefore, this flattening of the dye in the excited state leads to the observed larger Stokes shift for HPQ and MPQ. Because this phenomenon is only observed to the T* emission band, we conclude that the studied 2-phenyl-3HQs are probably more flat in the T* state than in the N* state. The importance of this conclusion becomes clearer when the intensity ratio of the two emission bands as well as their time-resolved decays are analyzed.

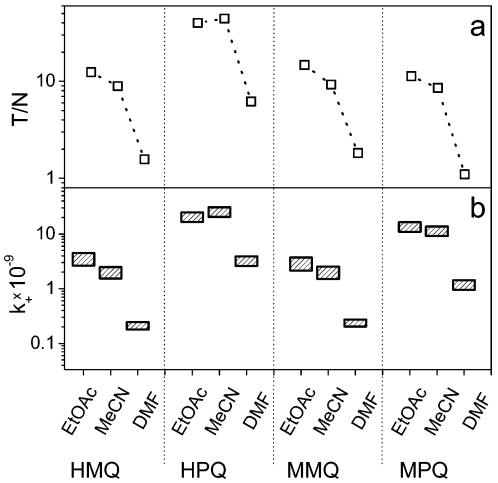

Figure 2. Intensity ratio of T* to N* bands (a) and the ESIPT rate constants (b) of the four 3HQs in ethyl acetate (EtOAc), acetonitrile (MeCN) and dimethylformamide (DMF).

Substitution of the 2-methyl group in HMQ by a 2-phenyl group in HPQ strongly increases the relative intensity of the T* emission, that is, the I_{T^*}/I_{N^*} ratio (Figure 2a). Further attachment of the N-methyl group in MPQ decreases the I_{T^*}/I_{N^*} ratio back to the values of the nonsubstituted dye HMQ. Meanwhile, introduction of the N-methyl group in the dye without 2-phenyl group (MMQ) does not change significantly the relative intensities of the two emission bands (Figure 2a, Table 1). Thus, we conclude that introduction of the 2-phenyl group favors the T* emission of the 3HQ dyes. In contrast, the N-methyl group switches off this effect, likely by twisting the phenyl ring out of the quinolone plane, due to steric hindrance. This conclusion is substantiated by the lower quantum yield of MPQ in respect with HPQ, in line with a less planar conformation in MPQ with a lower conjugation of the aromatic units. Similar changes in the intensity ratio were previously reported for 3HFs when the 2-phenyl group is methylated in the sterically hindered ortho position.[4] Thus, it appears that the more planar conformation of HPQ favors the T* emission.

Noticeably, in contrast to the absorption and emission maxima that do not change considerably with the solvent, the intensity ratios vary strongly, especially in solvents of different basicity. For instance, the relative intensity of the T* emission in dimethylformamide (DMF) is much lower than that in acetonitrile, a solvent of similar polarity but much lower basicity. This strong effect of solvent basicity is in line with our recent studies with other 3HQ derivatives and suggests that it is a general property of 3HQ dyes.[23]

3.2. Time-Resolved Fluorescence Measurements. To analyze whether the changes in the I_{N^*}/I_{T^*} ratios are connected with the rates of the ESIPT reaction, the time-resolved decays of both emission bands of the 3HQ dyes were measured in different solvents. In both HMQ and HPQ dyes, the fluorescence decays of the N* band are clearly faster than those of the T* band (Figure 3). Moreover, the T* decay curves contain a raising component, which indicates that the T* species is formed due to an excited-state process. The fluorescence decay times and the corresponding pre-exponential coefficients of the four studied dyes in various organic solvents are given in Table 2.

The identical short-lived decay times τ_1 for the N* and T* forms and their negative amplitudes α_1 for the T* form confirm that the T* state is produced from the N* state through an ESIPT reaction.[20] The long-lived lifetime τ_2 is systematically observed for the T* emission, but for the N* band, it is either not observed

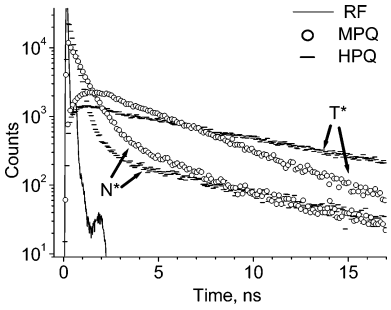

Figure 3. Fluorescence decays of N* and T* forms of 3HQs in DMF. The decays of the N* and T* forms were recorded at 420 and 540 nm, respectively. The response function (RF) of the instrument is also presented. The excitation wavelength was 320 nm.

or shows a small amplitude (Table 2). According to previous studies,[20,24] these results suggest an irreversible ESIPT reaction for all four compounds in the studied solvents. HMQ and MMQ dyes show relatively high τ_2 values in line with their high-fluorescence quantum yields (Tables 1 and 2). Within this couple of compounds, the N-methyl group does not significantly affect the emission kinetics. Introduction of the 2-phenyl group decreases considerably τ_2 and this decrease is especially strong in the MPQ dye, which contains the N-methyl group. The decrease in τ_2 correlates well with the decrease in the quantum yield (Tables 1 and 2), suggesting that the 2-phenyl group probably due to its rotational motion opens new deactivation channels in the dye. This effect appears especially strong when the phenyl ring is twisted with respect to the quinolone heterocycle due to the steric hindrance of the N-methyl group.

The effect of substituents is even stronger on the short-lived decay time τ_1, which is related to the kinetics of the ESIPT reaction (Table 2). Indeed, τ_1 is the longest in 3HQs without 2-phenyl group and does not depend much on the N-methyl group in this case. Introduction of the 2-phenyl group decreases τ_1 up to 12-fold in the absence of the N-methyl group and up to 5-fold in the presence of the N-methyl group (Table 2). To evaluate quantitatively the effect of the substituents on the ESIPT kinetics, we used the model of irreversible phototautomerization,[24] which is in line with the observed low amplitudes of τ_2 at the N* band. This model allows us to neglect the backward kinetic rate constant (k_-) and to estimate the ESIPT rate constants k_+ of the four 3HQs.[20,23]

Through the use of this model, the quantum yields of the N* and T* bands (Q_{N^*} and Q_{T^*}) can be expressed as

$$Q_{N^*} = k_R^{N^*}\,\tau_1 \tag{1}$$

$$Q_{T^*} = k_R^{T^*}\,\tau_2(k_+\tau_1) \tag{2}$$

where τ_1 and τ_2 are the short-lived and long-lived decay times, respectively, given by the following

$$\tau_1 = 1/(k_R^{N^*} + k_{NR}^{N^*} + k_+);\ \tau_2 = 1/(k_R^{T^*} + k_{NR}^{T^*})$$

where $k_R^{N^*}$, $k_R^{T^*}$, $k_{NR}^{N^*}$, $k_{NR}^{T^*}$ are the radiative and nonradiative rate constants of the N* and T* forms, respectively, and k_+ is the forward rate constant of ESIPT. Calculation of Q_{N^*} from the steady-state fluorescence spectra (Table 1) and τ_1 from time-resolved measurements (Table 2) allows us to obtain the values of the radiative decay constant $k_R^{N^*}$ from eq 1 for the four 3HQs in different solvents (Table 2).

The value of $k_R^{N^*}$ for HMQ and MMQ is similar in different solvents and is not sensitive to the introduction of the N-methyl group. In contrast, introduction of the 2-phenyl group increases $k_R^{N^*}$ probably by increasing the size and thus the oscillator strength of the fluorophore. Subtraction of $k_R^{N^*}$ from $1/\tau_1$ gives the sum of the nonradiative and ESIPT rate constants, $k_{NR}^{N^*} + k_+$ (Table 2). To estimate the contribution of the forward ESIPT rate constant k_+ to this sum, we used the following approach.

The ratio of eqs 1 and 2 gives us a simplified expression of k_+ as

$$k_+ = \frac{k_R^{N^*}}{k_R^{T^*}}\frac{Q_{T^*}}{Q_{N^*}}\frac{1}{\tau_2} \tag{3}$$

Because the $k_R^{N^*}$ value does not vary significantly with the solvent, we can reasonably assume that the radiative rate constant of the T* state, $k_R^{T^*}$, shows a similar behavior. As a consequence, the ratio $k_R^{N^*}/k_R^{T^*}$ can be considered as constant in different solvents. Thus, k_+ is proportional to the relative intensities of the N* and T* bands and to $1/\tau_2$. Consequently, dividing eq 3 in one solvent by that in another solvent allows us to estimate the relative changes of k_+ from solvent to solvent as

$$\frac{k_+^1}{k_+^2} = a \tag{4}$$

where k_+^1 and k_+^2 are the forward ESIPT rate constants in the first and the second solvent, respectively, calculated from eq 3.

The values of k_+ can be directly obtained from the experimentally obtained sum $k_{NR}^{N^*} + k_+$ in the case if $k_+ \gg k_{NR}^{N^*}$. To check this last assumption, we calculated the ratio of $k_{NR}^{N^*} + k_+$ for a pair of solvents as

$$\frac{k_+^1 + k_{NR}^{N^*1}}{k_+^2 + k_{NR}^{N^*2}} = b \tag{5}$$

where $k_{NR}^{N^*1}$ and $k_{NR}^{N^*2}$ are the nonradiative rate constants for the N* form in the first and the second solvent, respectively.

Then, from the combination of eqs 4 to 5, we can express the $k_+/k_{NR}^{N^*}$ ratio for a particular solvent as

$$\frac{k_+^1}{k_{NR}^{N^*1}} = \frac{a - b\dfrac{k_{NR}^{N^*2}}{k_{NR}^{N^*1}}}{b - a} \tag{6}$$

Considering a pair of solvents with a low value of b, like DMF−ethyl acetate or DMF−acetonitrile and assuming that $k_{NR}^{N^*1}$ and $k_{NR}^{N^*2}$ values are of the same order (which is in line with the values of the fluorescence quantum yields), we can neglect $b\,k_{NR}^{N^*2}/k_{NR}^{N^*1}$ and express the ratio of the rate constants as

$$k_+^1/k_{NR}^{N^*1} \approx \frac{a}{b - a} \tag{7}$$

Using eq 7, we estimated the $k_+/k_{NR}^{N^*1}$ ratio for all four 3HQs in the three studied solvents. This ratio always exceeds 2.5, so that $k_+ > 0.7(k_{NR}^{N^*} + k_+)$. Therefore, the value of k_+ varies between $0.7(k_{NR}^{N^*} + k_+)$ and $k_{NR}^{N^*} + k_+$, which allows us to estimate k_+ for all four compounds and calculate the error of this estimation (Table 2). When different compounds are compared in the same solvent, it appears that the 2-phenyl group increases the ESIPT rate constant dramatically (Table 2). The

TABLE 2: Time-Resolved Fluorescence Parameters of the Two Emission Bands of 3HQs in Organic Solvents

		τ_1[a], ns (α_1[c])		τ_2, ns (α_2[c])						
dye	solvent	N*	T*	N*	T*	Q_{N^*}[a]	Q_{T^*}[a]	$k_R^{N^*}$[b]	$k_+ + k_{NR}^{N^*}$[b]	k_+[b]
HPQ	EtOAc	0.044 (1.00)	0.041 (−0.57)		6.80 (0.43)	0.0056	0.36	0.13	23.1	20 ± 3
	MeCN	0.032 (0.98)	0.049 (−0.48)	0.032 (0.02)	7.30 (0.52)	0.0044	0.30	0.13	28.5	24 ± 4
	DMF	0.283 (1.00)	0.258 (−0.41)		8.28 (0.59)	0.061	0.40	0.24	3.61	3.1 ± 0.6
MPQ	EtOAc	0.063 (1.00)	0.080 (−0.57)		4.23 (0.43)	0.0093	0.15	0.14	15.2	13 ± 2
	MeCN	0.079 (0.98)	0.073 (−0.50)	4.20 (0.02)	4.20 (0.50)	0.011	0.14	0.15	12.7	11 ± 2
	DMF	0.700 (0.9)	0.700 (−0.49)	2.85 (0.1)	3.64 (0.51)	0.088	0.13	0.13	1.32	1.1 ± 0.2
HMQ	EtOAc	0.250 (1.00)	0.264 (−0.53)		8.4 (0.47)	0.027	0.41	0.13	4.64	3.9 ± 0.7
	MeCN	0.392 (0.95)	0.340 (−0.42)	8.6 (0.05)	8.6 (0.58)	0.035	0.46	0.09	2.54	2.2 ± 0.4
	DMF	2.73 (0.99)	2.90 (−0.43)	8.2 (0.01)	12.4 (0.57)	0.25	0.47	0.08	0.25	0.21 ± 0.04
MMQ	EtOAc	0.207 (1.00)	0.231 (−0.40)		8.1 (0.60)	0.021	0.40	0.08	3.84	3.3 ± 0.6
	MeCN	0.383 (1.00)	0.335 (−0.40)		8.8 (0.60)	0.032	0.42	0.09	2.62	2.2 ± 0.4
	DMF	2.90 (0.78)	3.36 (−0.74)	6.5 (0.22)	11.8 (0.74)	0.22	0.50	0.08	0.28	0.24 ± 0.04

[a] τ_1, τ_2 (ns) are the short-lived and long-lived decay times respectively, α_1, α_2 are the relative amplitudes; Q_{N^*},Q_{T^*} are the quantum yields of the N* and T* forms, respectively; $k_R^{N^*}$, $k_{NR}^{N^*}$ ($\times 10^{-9}$ s^{-1}) are, respectively, the radiative and nonradiative rate constants of the N* form; k_+ ($\times 10^{-9}$ s^{-1}) is the forward rate constant of the ESIPT reaction. [b]The error for all values is ±10% due to the precision of the measurements. [c]α_1 and α_2 values were normalized according to $|\alpha_1| + |\alpha_2| = 1$.

highest k_+ value is observed for HPQ. Introduction of the N-methyl group in MPQ results in a 2-fold decrease of k_+ as compared to HPQ. Thus, our data directly evidence that the 2-phenyl group favors the ESIPT reaction, while twisting this group from the quinolone plane by the N-methyl group decreases this effect.

Besides the structure of the 3HQ dye, the nature of the solvent also influences the ESIPT kinetics. Indeed, the ESIPT rate is much lower in DMF than in acetonitrile and ethyl acetate. Taking into account that DMF and acetonitrile are of close polarity but differ by their basicity, we conclude that the ESIPT rate slows down in basic solvents. This conclusion is in line with recent time-resolved studies[23,25] and suggests that basic solvents perturb the intramolecular hydrogen bond in 3HQs through the formation of an intermolecular H-bond of the dye 3-OH group with the solvent. This intermolecular H-bond blocks or slows down the ESIPT reaction.

Importantly, the variations of the k_+ values correlate well with the variations of the relative intensity of the T* emission (Figure 2), suggesting that the ESIPT kinetics is responsible for the strong variations of the intensity ratios. Noticeably, a deviation is observed for the MPQ dye, which exhibits a somewhat lower relative intensity of the T* emission. This may be due to an increase of the nonradiative deactivation rate from the T* state, which is supported by the observed lower quantum yield of MPQ (Table 1).

3.3. Mechanism of the Substituent Effect on the ESIPT Rate. Both electronic and steric effects can be considered to explain the increase of the ESIPT rate constant by the 2-phenyl group in 3HQ. In previous studies, a planar conformation was shown to be required in 2-phenyl-3HF for a fast ESIPT process.[4] This was explained by the electronic effect of the phenyl group, which in a planar conformation increases the basicity of the 4-carbonyl group and thus accelerates the ESIPT. However, this explanation does not consider that the phenyl group can also decrease the acidicity of the 3-OH group and thus, slow down the ESIPT process. Moreover, modification of the 2-phenyl ring by electron donor groups that further increase the basicity of the carbonyl oxygen of 3HFs dramatically slows down the ESIPT reaction, further questioning the interpretation based on the electronic effect.[20] In 3HQs, the electronic effects of the 2-phenyl group also do not explain the variations of the ESIPT rate. Indeed, according to our recent studies, an analog of MPQ containing an electron donor methoxy group on the 2-phenyl ring shows an ESIPT rate close to that of MPQ in the same solvents. This indicates that the electron donor properties of the 2-phenyl group do not strongly affect the ESIPT kinetics. Moreover, when 2-methyl and 2-phenyl-subsituted 3HQ are compared, it appears that the introduction of the 2-phenyl group does not modify the Stokes shift of the N* band (Figure 1a). This is likely because the 2-phenyl group is out of the quinolone plane, so that the aromatic moieties probably form a large dihedral angle that prevents electronic conjugation between them in both ground and excited states. In contrast, the T* state of HPQ shows a much larger Stokes shift than its 2-methyl analog MPQ (Figure 1a, Table 1), suggesting a more planar configuration for the T* state of HPQ (Table 2). Addition of the N-methyl group that decreases the planarity of the MPQ dye does not affect the positions of the absorption and fluorescence bands but strongly modulates the ESIPT rate (Figures 1 and 2). Thus, the orientation of the 2-phenyl group with respect to the

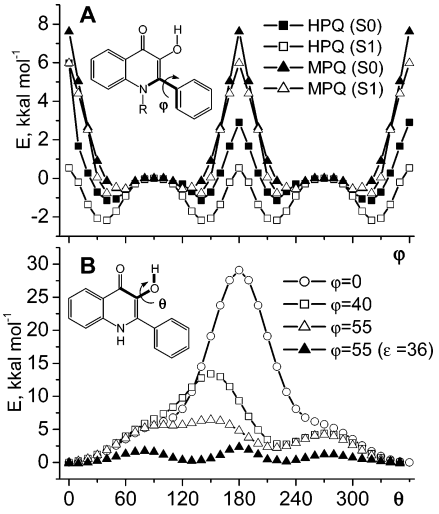

Figure 4. Calculated energies of the 3HQs in the ground (S_0) and Franck−Condon excited (S_1) states at different torsional angles of the 2-phenyl (φ) and 3-OH (θ) groups. (A) Calculated energies of HPQ and MPQ as a function of φ. (B) Calculated energies of HPQ in the S_1 Franck−Condon state as a function of θ for different fixed values of φ. Calculations were done with the AM1 method in vacuum and in acetonitrile ($\epsilon = 36$).

SCHEME 1: (a) The Interaction between the 3-Hydroxy Group and the 2-Phenyl Moiety in N−H Substituted 3HQs Limits Considerably the Rotational Motion of the Hydroxyl Group; (b) the Steric Effect of the Proximal *N*-Methyl Group Decreases the Planarity of the Dye, Enabling a Larger Rotational Freedom of the 3-OH Group.

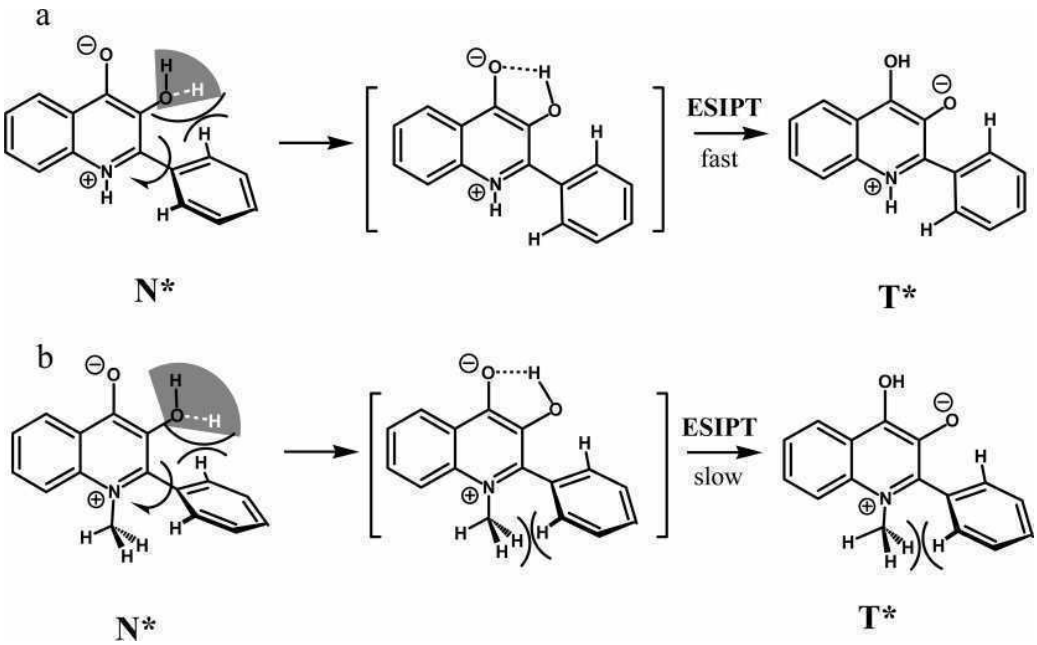

3HQ plane affects directly the ESIPT kinetics, and this effect does not seem to correlate with the energies of the electronic transitions.

To understand better the observed phenomena, we performed quantum chemical calculations of the energies of the 2-phenyl-3HQ dyes in both their ground state and excited state as a function of the 2-phenyl orientation using the AM1 method.[22] In the ground state, a flat conformation is not favorable for both HPQ and MPQ dyes, so that the mean angle between the 2-phenyl and quinolone rings is 49 and 61°, respectively (Figure 4). In the excited state, the planar conformation becomes slightly more favorable so that the corresponding angle decreases to 38 and 54°, respectively. Thus, according to our calculations, both HPQ and MPQ are not flat, while the excited state favors some flattening. Moreover, the twist between 2-phenyl and 3HQ rings is larger in the MPQ molecule probably due to the steric effect of the N-methyl group. Evidently, HPQ is not flat due to the steric interaction of the 2-phenyl group with the 3-OH group. This interaction may in turn affect the rotational motion of the 3-OH group. We analyzed the motion of the 3-OH group in the excited state of HPQ with the AM1 method, and we found that its rotational freedom depends strongly on the orientation of the 2-phenyl ring. Thus, in the case of the relatively flat conformation of HPQ (with the φ angle between the 2-phenyl and quinolone rings being lower than 40°) the rotation of 3-OH is restricted, favoring the H-bonding of the 3-OH group with the 4-carbonyl group. When φ is increased to 55°, the energy barrier of rotation of the 3-OH group decreases significantly, thus favoring the disruption of the intramolecular H-bond. Because the mean φ angle in MPQ in the excited state is close to 55°, the intramolecular H-bond is likely disrupted in this dye. If the solvent (acetonitrile, $\epsilon = 36$) is taken into account in the calculations (at $\varphi = 55°$), the energy barrier of the 3-OH group rotation is almost absent, so that at room temperature a large population of the dye with disrupted intramolecular H-bond is expected.

These calculations allow us to conclude that in the excited state flattening of the HPQ molecule restricts the rotational motion of the 3-OH group so that its proton is forced to be directed toward the 4-carbonyl group (Scheme 1a). This in turn stabilizes the intramolecular hydrogen bond and thus increases the ESIPT rate constant.

In contrast, introduction of the N-methyl group twists the 2-phenyl moiety out of the quinolone plane and thus increases the rotational freedom of the 3-OH group (Scheme 1b). As a consequence, it weakens the intramolecular H-bond and decreases the ESIPT rate. The largest rotational freedom is probably observed for 3HQs without 2-phenyl group, which show the lowest rates of ESIPT reaction (Table 2). In 3HFs, the ortho-methyl group in 2-phenyl, which also decreases significantly the planarity of the fluorophore, was also reported to decrease the strength of the intramolecular H-bond between 3-OH and 4-carbonyl groups, so that a fraction of the molecules exists without intramolecular H-bond.[4] These data strongly support our hypothesis that the 3-OH group in the nonplanar species of 3HQs (and 3HFs) exhibits higher rotational freedom and thus lower binding to the 4-carbonyl group. In basic solvents, which can form H-bond with 3-OH group, the decrease in the ESIPT rate is especially strong, so that for 2-methyl-3HQ dyes in DMF we observe an extremely slow ESIPT process (Table 2, Figure 2b). Such unusually slow ESIPT is likely the consequence of the large rotational freedom of the 3-OH group that allows the basic solvent to disrupt the intramolecular H-bond and thus to slow down the ESIPT reaction.

4. Conclusions

Our results show that substitution of 2-methyl with 2-phenyl group in 3HQs accelerates significantly the ESIPT reaction, while twisting of the 2-phenyl group out of the 3HQ plane by a proximal substituent slows down the ESIPT reaction. These data together with the absorption and fluorescence spectra of the dyes suggest that the ESIPT reaction in 2-phenyl-3HQ is accompanied by a flattening of the molecule (i.e., a decrease in the dihedral angle between the 2-phenyl and 3-hydroxyquinolone rings). On the basis of our data, we hypothesize that the steric

influence of the phenyl ring on the ESIPT reaction dominates over its electronic influence. According to our model, the 2-phenyl group being close to the plane of the 3HQ heterocycle sterically limits the rotational motion of the 3-OH group, stabilizing the intramolecular H-bond of the 3-OH group with the 4-carbonyl group and thus accelerating the ESIPT reaction.

Acknowledgment. This work was supported by the ECO-NET program from the French Ministére des Affaires Etrangères between France, Ukraine, and Russia. D.A.Y. is a member of the European Doctoral College. V.V.S. is supported by the TriOH European Program. D.A.Y. is the recipient of a high-level Eiffel Fellowship. The laboratory of Drs. André Mann and Jean Suffert is acknowledged for providing support for organic synthesis, and we are grateful to Professor Andrey Doroshenko for his kind assistance in quantum-chemical calculations.

Supporting Information Available: All the recorded fluorescence decay curves (PDF). This material is available free of charge via the Internet at http://pubs.acs.org.

References and Notes

(1) Sengupta, P. K; Kasha, M. *Chem. Phys. Lett.* **1979**, *68*, 382.
(2) McMorrow, D.; Kasha, M. *J. Phys. Chem.* **1984**, *88*, 2235−2243.
(3) Woolfe, G. J.; Thistlethwaite, P. J. *J. Am. Chem. Soc.* **1981**, *103*, 6916−6923.
(4) Strandjord, J. G.; Smith, D. E.; Barbara, P. F. *J. Phys. Chem.* **1985**, *89*, 2362−2366.
(5) Klymchenko, A. S.; Pivovarenko, V. G.; Demchenko, A. P. *Spectrochim. Acta, Part A* **2003**, *59*, 787−792
(6) Itoh, M.; Fujiwara, Y.; Sumitani, M.; Yoshihara, K. *J. Phys. Chem.* **1986**, *90*, 5672−5678.
(7) Ameer-Beg, S.; Ormson, S. M.; Brown, R. G.; Matousek, P.; Towrie, M.; Nibbering, E. T. J.; Foggi, P.; Neuwahl, F. V. R. *J. Phys. Chem. A* **2001**, *105*, 3709−3718.
(8) Bader, A. N.; Ariese, F.; Gooijer, C. *J. Phys. Chem. A* **2002**, *106*, 2844−2849.
(9) Gao, F.; Johnson, K. F.; Schlenoff, J. B. *J. Chem. Soc., Perkin Trans. 2* **1996**, *2*, 269−273.
(10) Hradil, P.; Jirman, J. *Collect. Czeh. Chem. Commun.* **1995**, *60*, 1357−1366.
(11) Yushchenko, D. A.; Bilokin, M. D.; Pyvovarenko, O. V.; Duportail, G.; Mély, Y.; Pivovarenko, V. G. *Tetrahedron Lett.* **2006**, *47*, 905.
(12) Klymchenko, A. S.; Duportail, G.; Oztürk, T.; Pivovarenko, V. G.; Mély, Y.; Demchenko, A. P. *Chem. Biol.* **2002**, *9*, 1199.
(13) Klymchenko, A. S.; Duportail, G.; Mély, Y.; Demchenko, A. P. *Proc. Natl. Acad. Sci. U.S.A.* **2003**, *100*, 11219.
(14) Bondar, O. P.; Pivovarenko, V. G.; Rowe, E. S. *Biochim. Biophys. Acta* **1998**, *1369*, 119.
(15) Shynkar, V. V.; Klymchenko, A. S.; Duportail, G.; Demchenko, A. P.; Mély, Y. *Biochim. Biophys. Acta* **2005**, *1712*, 128.
(16) Klymchenko, S. A.; Avilov, S. V.; Demchenko, A. P. *Anal. Biochem.* **2004**, *329*, 43.
(17) Ercelen, S.; Klymchenko, S. A.; Demchenko, A. P. *FEBS Lett.* **2003**, *538*, 25.
(18) Yushchenko, D. A.; Shvadchak, V. V.; Klymchenko, A. S.; Duportail, G.; Mély, Y.; Pivovarenko, V. G. *New. J. Chem.* **2006**, *30*, 774.
(19) Lakovicz, J. R. *Principles of Fluorescence Spectroscopy*; Kluwer Academic/Plenum Publishers: New York, 1999; p 52.
(20) Shynkar, V. V.; Mély, Y.; Duportail, G.; Piémont, E.; Klymchenko, A. S.; Demchenko, A. P. *J. Phys. Chem. A* **2003**, *107*, 9522.
(21) Livesey, A. K.; Brochon, J.-C. *Biophys. J.* **1987**, *52*, 693.
(22) Dewar, M. J. S.; Zoebich, E. G.; Healy, E. F.; Stewart, J. J. P. *J. Am. Chem. Soc.* **1985**, *107*, 3902.
(23) Yushchenko, D. A.; Shvadchak, V. V.; Bilokin, M. D.; Klymchenko, A. S.; Duportail, G.; Mély, Y.; Pivovarenko, V. G. *Photochem. Photobiol. Sci.* **2006**, *5*, 1038.
(24) Laws, W. R.; Brand, L. *J. Phys. Chem.* **1979**, *83*, 795.
(25) Douhal, A.; Sanz, M.; Tormo, L.; Organero, J. A. *ChemPhysChem* **2005**, *6*, 419.

2.1.2. Effect of basicity on ESIPT in 3-hydroxyquinolones

To better characterize the sensitivity of 3HQ dyes to the environment, we selected QMOM dye and performed its fluorescent studies in a wide range of solvents. It was found that the fluorescence of QMOM, particularly the N*/T* emission band ratio, depends strongly on the solvent polarity. Moreover, an additional effect of solvent basicity was observed (**Fig. 2.4 A**). We hypothesized that the hydrogen-bond acceptors (H-bond basic) solvents disrupt intramolecular hydrogen bond and slow down the ESIPT reaction.

Time-resolved fluorescence measurements showed that ESIPT reaction in QMOM is irreversible and emission band ratio is controlled by kinetics of ESIPT and the non-radiative deactivation (**Fig. 2.5**). In contrary, 3HC analogues, which are not sensitive to the solvent basicity, 3HQs undergo fast reversible ESIPT and their dual emission is controlled by the thermodynamic equilibrium between the N* and T* states [96].

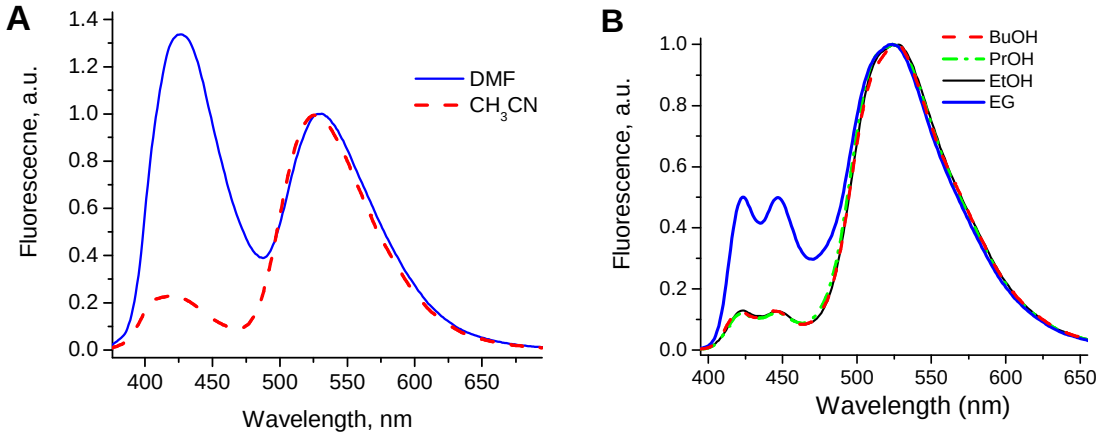

Figure 2.4. (**A**) Comparison of QMOM fluorescence in DMF(ε=37.2, β=0.74, blue line) and acetonitrile (ε=35.7, β=0.32, dashed red line) (ε and β are dielectric constant and Abraham's hydrogen bond basicity respectively).
(**B**) Normalized fluorescence spectra of 3HQ-Bf in alcohols of different polarity (ε) and basicity (β). Ethanol (ε=24.9, β=0.48, black curve), propanol (ε=20.5, β=0.48, green dash dot curve) and buthanol (ε=17.3, β=0.51, red dash curve) are different by polarity but similar by basicity and shows almost identical spectra. While ethylene glycol (ε=40.2, β=0.78 blue thick curve) is more polar and more basic. Excitation wavelength was 360 nm in all the cases.

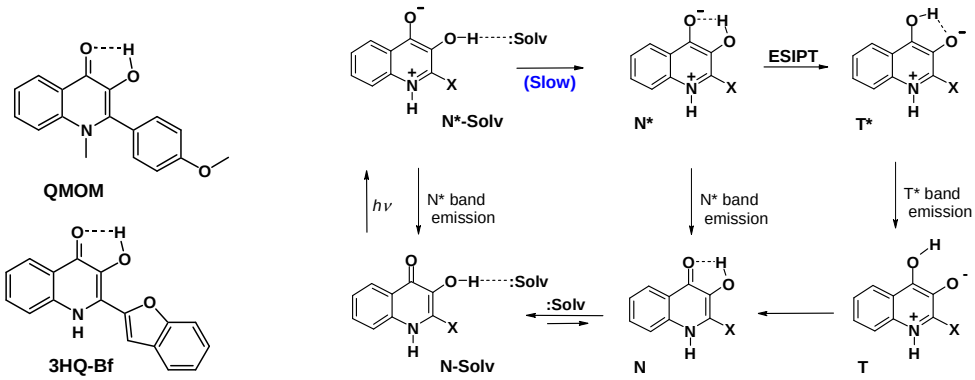

Figure 2.5. Structures of QMOM and 3HQ-Bf dyes and scheme of the ESIPT in 3HQs accounting formation of intermolecular bond with basic solvents.

All studied 3HQ show similar sensitivity to solvent basicity. Nevertheless, their practical application for sensing of hydrogen-bond acceptors is limited, because the basicity and polarity effects overlapping. To achieve selective response to hydrogen-bond basicity of the environment, the effects of polarity and basicity should be separated. For this, a new dye, 3HQ-Bf, with decreased polarity sensitivity was designed and characterized. We found that 3HQ-Bf has no direct sensitivity to solvent polarity in protic media meanwhile is sensitive to solvent basicity (**Fig. 2.4 B**). Unfortunately in aprotic media effect of polarity is decreased but not eliminated.

Studies of the effects of solvent basicity on 3HQs fluorescence are presented in Articles 3 and 4.

Article 3

Modulation of dual fluorescence in a 3-hydroxyquinolone dye by perturbation of its intramolecular proton transfer with solvent polarity and basicity

Photochemical & Photobiological Sciences

An international journal

www.rsc.org/pps

Volume 5 | Number 11 | November 2006 | Pages 985–1088

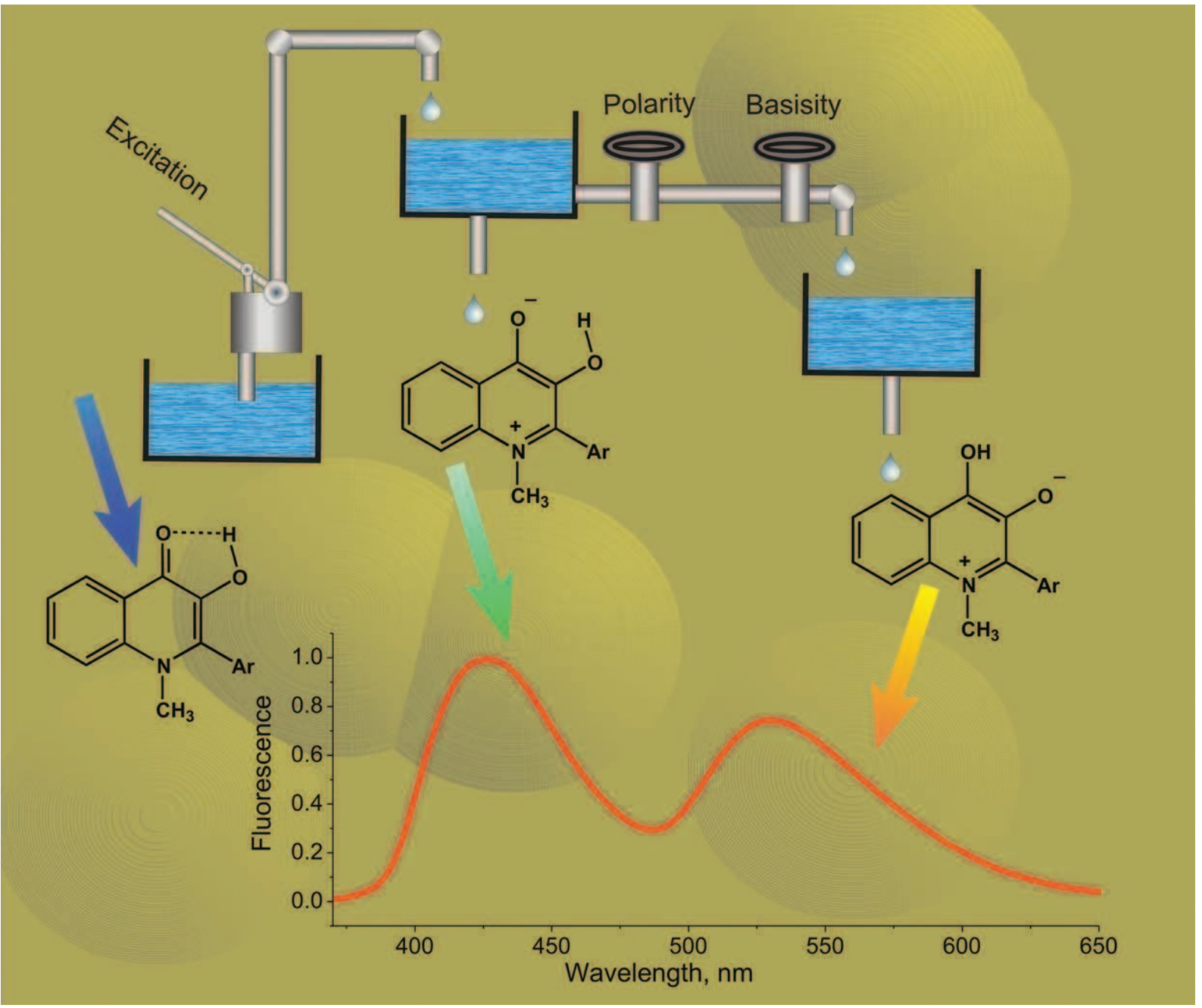

ISSN 1474-905X

RSC Publishing

1474-905X(2006)5:11;1-D

Modulation of dual fluorescence in a 3-hydroxyquinolone dye by perturbation of its intramolecular proton transfer with solvent polarity and basicity

Dmytro A. Yushchenko,*[a,b] Volodymyr V. Shvadchak,[b] Mykhailo D. Bilokin',[a] Andrey S. Klymchenko,[b] Guy Duportail,[b] Yves Mély[b] and Vasyl G. Pivovarenko[a]

Received 13th July 2006, Accepted 4th August 2006
First published as an Advance Article on the web 16th August 2006
DOI: 10.1039/b610054f

A representative of a new class of dyes with dual fluorescence due to an excited state intramolecular proton transfer (ESIPT) reaction, namely 1-methyl-2-(4-methoxy)phenyl-3-hydroxy-4(1*H*)-quinolone (QMOM), has been studied in a series of solvents covering a large range of polarity and basicity. A linear dependence of the logarithm of its two bands intensity ratio, $\log(I_{N^*}/I_{T^*})$, upon the solvent polarity expressed as a function of the dielectric constant, $(\varepsilon - 1)/(2\varepsilon + 1)$, is observed for a series of protic solvents. A linear dependence for $\log(I_{N^*}/I_{T^*})$ is also found in aprotic solvents after taking into account the solvent basicity. In contrast, the positions of the absorption and the two emission bands of QMOM do not noticeably depend on the solvent polarity and basicity, indicating relatively small changes in the transition moment of QMOM upon excitation and emission. Time-resolved experiments in acetonitrile, ethyl acetate and dimethylformamide suggest an irreversible ESIPT reaction for this dye. According to the time-resolved data, an increase of solvent basicity results in a dramatic decrease of the ESIPT rate constant, probably due to the disruption of the intramolecular H-bond of the dye by the basic solvent. Due to this new sensor property, 3-hydroxyquinolones are promising candidates for the development of a new generation of environment-sensitive fluorescence dyes for probing interactions of biomolecules.

Introduction

Fluorescence spectroscopy is one of the most used techniques for investigating molecular events in biological systems due to its exquisite sensitivity. However, this technique strongly relies on the availability of fluorescent probes with optimal properties. In cells and tissues, probes are generally distributed inhomogeneously. As a consequence their fluorescence intensity depends on their local concentration. To avoid this limitation, fluorescence ratio imaging techniques have been developed,[1,2] which require probes with a ratiometric response. In this respect, dual fluorescence probes[3] exhibiting two well separated emission bands are of particular interest, since they provide a reliable ratiometric signal independent on the probe concentration.

Among the best approaches for designing dyes with dual fluorescence is the utilization of the excited state intramolecular proton transfer (ESIPT) reaction.[4–10]

ESIPT results in the formation of two tautomeric forms in the excited state of the probe. Due to their different photophysical properties, these tautomeric forms exhibit largely separated emission bands on the wavelength scale. Some of the most interesting representatives of the dyes undergoing ESIPT are the 3-hydroxyflavone derivatives (3HFs), which exhibit dual emission highly sensitive to the environment.[11–15] These dyes have already been used as efficient tools for investigating the polarity,[16–21] electronic polarizability,[22] and electrostatic effects[23] in different media[24–30] including lipid membrane, biomembranes and proteins.[23,26–33] Moreover, these dyes have been shown to be useful to determine the nature and concentration of cations[34,35] and anions[36] in solution. However, despite their significant advantages compared to common single-band probes, 3HFs exhibit low photostability and quantum yields that limit their application. As a consequence, the development of a new generation of dual fluorescence probes with improved properties is required.

Previously, it has been reported that 2-aryl-3-hydroxyquinolones (3HQs), which are structural analogs of 3HFs, also display dual emission.[37,38] Examination of the excitation spectra and time resolved measurements allowed us to conclude that similarly to 3-hydroxyflavones, 3HQ dyes exhibit ESIPT reaction, resulting in two excited states.[39] Both the normal (N*) and tautomer (T*) forms (Scheme 1) are highly emissive giving rise to two well separated bands in the fluorescence spectra. Moreover, we showed that *N*-methyl derivatives exhibit better separation of their emission bands than *N*-H derivatives.[38,39] In addition, the ratio of the intensities of the two emission bands (I_{N^*}/I_{T^*}) varies broadly with the solvent, indicating that the *N*-methyl derivatives are sensitive to the nature of the environment. However, a systematic study of the dependence of their spectroscopic properties on the physicochemical parameters of the environment has not been performed and the mechanism of the I_{N^*}/I_{T^*} variations is not clear. Interestingly, their close 3-hydroxyflavone analog, 4′-(diethylamino)-3-hydroxyflavone (FET) and its homologs show reversible ESIPT reaction, so that in the exited state an equilibrium between the two tautomeric forms is obtained.[22,40,41] In this case, polar solvents stabilize the N* state dielectrically having a large

[a]*Department of Chemistry, Kyiv National Taras Shevchenko University, 01033, Kyiv, Ukraine*
[b]*Photophysique des Interactions Biomoléculaires, UMR 7175 du CNRS, Institut Gilbert Laustriat, Faculté de Pharmacie, Université Louis Pasteur, 67401, Illkirch, France*

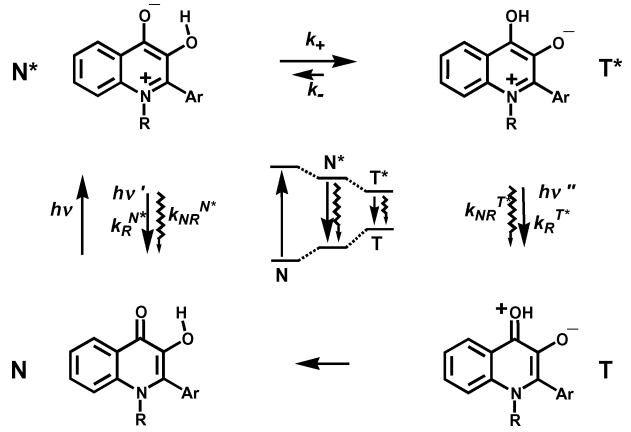

Scheme 1 Four-state diagram of the excited state intramolecular proton transfer (ESIPT) in 3-hydroxyquinolones; k_+ and k_- are the forward and reverse kinetic rate constants of ESIPT respectively; $k_R{}^{N^*}$ and $k_{NR}{}^{N^*}$ are the radiative and non-radiative rate constants of the N* form, respectively; $k_R{}^{T^*}$ and $k_{NR}{}^{T^*}$ are the radiative and non-radiative rate constants of the T* form, respectively.

dipole moment, and thus shift the N*↔T* ESIPT equilibrium towards the N* state.[17,22,40,41] Therefore, in FET and its analogs, the solvent dependent increase of the N* emission is accompanied by a spectral shift to the red.[17,22] In contrast, the solvent dependent variation of the two emission bands of 3HQs is not accompanied by considerable shifts of its N* band,[38] so that a different mechanism may be responsible for these variations. To further understand the photophysical properties of 3HQs, we have performed herein a steady-state and time-resolved fluorescence investigation of a representative quinolone dye, namely 1-methyl-2-(4-methoxy)phenyl-3-hydroxy-4(1*H*)-quinolone (QMOM) in comparison with its 3-hydroxyflavone analog FET, which has already been well characterized. QMOM was chosen because its intensity ratio (I_{N^*}/I_{T^*}) is measurable within a large range of organic solvents. Our results show that the ESIPT of this dye in the studied solvents is an irreversible process and that its rate is highly sensitive to solvent basicity. These results explain the strong variations of the relative intensities of the two emission bands in solvents of different basicity and provide insights for the development of new environment-sensitive fluorescence ratiometric probes for biological and polymer sciences.

Experimental

Structure of FET and QMOM are shown on Scheme 2. QMOM was synthesized by condensing the corresponding anthranilic acid ester in polyphosphoric acid as previously described.[38] All the solvents and chemicals were purchased from Aldrich. The solvents were of spectroscopic grade. Absorption spectra were recorded on a Cary 4 spectrophotometer (Varian) and fluorescence spectra on a FluoroMax 3.0 (Jobin Yvon, Horiba) spectrofluorometer. Fluorescence spectra were corrected for the internal function of the instrument. Decomposition of fluorescence spectra into two bands when these bands are overlapped was performed using the program Siano, kindly provided by the author (Dr A. O. Doroshenko from the Karazin University, Kharkov, Ukraine). The program uses an iterational non-linear least-squares method based on the Fletcher–Powell algorithm. The shape of the individual emission bands was approximated by a lognormal function,[42] which accounts for the asymmetry of the spectral bands. This method of band separation was also used for determination of fluorescence quantum yield of each of the two bands φ_{N^*} and φ_{T^*} separately.

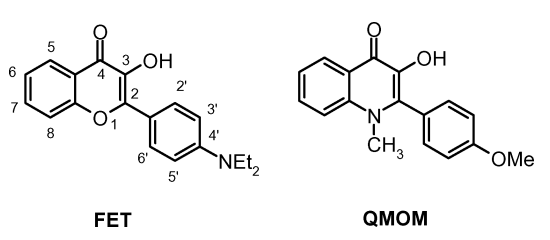

Scheme 2

For the determination of the fluorescence quantum yields φ, φ_{N^*} and φ_{T^*} quinine sulfate in 0.5M sulfuric acid ($\varphi = 0577$[43]) was taken as a reference.

Time-resolved fluorescence measurements were performed with the time-correlated, single-photon counting technique using the frequency doubled output of a Ti-Sapphire laser (Tsunami, Spectra Physics), pumped by a Millenia X laser (Tsunami, Spectra Physics).[40] The excitation wavelength was set at 320 nm. The fluorescence decays were collected at the magic angle (54.7°) of the emission polarizer. The single-photon events were detected with a microchannel plate Hamamatsu R3809U photomultiplier coupled to a Philips 6954 pulse preamplifier and recorded on a multichannel analyzer (Ortec 7100) calibrated at 25.5 ps channel^{-1}. The instrumental response function was recorded with a polished aluminium reflector, and its full-width at half-maximum was 50 ps.

The time-resolved decays were analyzed both by the iterative reconvolution method[43] and the Maximum Entropy Method (MEM).[44] The goodness of the fit was evaluated from the χ^2 values, the plots of the residuals and the autocorrelation function.

Quantum-chemical calculations of FET and QMOM dipole moments were performed by the AM1 semi-empirical method using the MOPAC 6.0 program.[45]

Results and discussion

Dependence of the I_{N^*}/I_{T^*} ratio on the characteristics of the environment

Previous studies on FET have shown that the logarithm of the I_{N^*}/I_{T^*} ratio exhibits a linear dependence on the solvent polarity expressed as a function of the dielectric constant, $f(\varepsilon) = (\varepsilon - 1)/(2\varepsilon + 1)$.[22] In order to check whether QMOM presents a similar sensitivity to solvent polarity, we studied its fluorescence properties in different organic solvents (Fig. 1, Table 1).

In protic solvents a linear correlation of $\log(I_{N^*}/I_{T^*})$ as a function of $f(\varepsilon)$ is observed for QMOM (Fig. 2). Interestingly, the I_{N^*}/I_{T^*} ratio in protic solvents does not deviate to higher values as compared to aprotic solvents. This is a remarkable difference with the FET dye, which shows in protic solvents nearly 10-fold higher I_{N^*}/I_{T^*} values as compared to aprotic solvents of the same polarity.[22] Moreover, in aprotic solvents the polarity dependence of QMOM appears to be more complex. Indeed, in solvents of similar $f(\varepsilon)$ values such as tributylphosphate and tetrahydrofuran or acetonitrile and dimethylformamide, QMOM exhibits very different I_{N^*}/I_{T^*} ratios. Since the mentioned solvents

Table 1 Spectroscopic properties of QMOM in different solvents

No.	Solvent	ε^a	$f(\varepsilon)$	α^a	β^a	λ_{abs}/nm	λ_{N^*}/nm	λ_{T^*}/nm	I_{N^*}/I_{T^*}	φ
1	Water	78.4	0.490	—	—	355	420	480	1.6	0.16
2	DMSO	46.8	0.484	0	0.88	370	431	522.5	3.7	0.39
3	Sulfolan	44.0	0.483	0	0.88	373	434	516	1.1	0.18
4	*N*,*N*-Dimethylacetamide	37.8	0.480	0	0.78	370	426	532.5	0.9	0.20
5	*N*,*N*-Dimethylformamide (DMF)	37.2	0.480	0	0.74	370	426	530	1.3	0.16
6	Acetonitrile	35.7	0.479	0.07	0.32	371	420	519	0.2	0.10
7	Methanol	32.6	0.477	0.43	0.47	364	422	499.5	1.9	0.12
8	*N*-Methyl-pyrrolidone	32.6	0.477	0	0.76	369	428	534	1.1	0.24
9	Hexamethyl phosphoramide (HMPA)	29.0	0.475	0	1	370	432	540.5	2.1	0.25
10	Ethanol	24.9	0.470	0.37	0.48	367	423	515	1.0	0.14
11	1,1,3,3-Tetra-methylurea	24.5	0.470	0	0.78	368	426	534.5	0.6	0.16
12	1-Propanol	20.5	0.464	0.37	0.48	366	423	509.5	0.7	0.17
13	Acetone	20.5	0.464	0.04	0.49	368	421	526	0.2	0.09
14	2-Propanol	19.3	0.462	0.33	0.56	367	423	510	0.6	0.14
15	Butanone	18.2	0.460	0	0.51	369	415	527	0.2	0.11
16	1-Butanol	17.3	0.458	0.37	0.48	368	424	510.5	0.6	0.19
17	2-Pentanone	15.2	0.452	0	0.51	369	421	523	0.4	0.12
18	1-Octanol	9.86	0.428	0.37	0.48	369	424	513	0.4	0.03
19	Tributylphosphate	8.18	0.414	0	1.21	367	419	534	0.7	0.24
20	Tetrahydrofuran	7.43	0.405	0	0.48	370	422	532	0.3	0.16
21	Ethyl acetate	5.99	0.384	0	0.45	369	420	526	0.1	0.14
22	Diisopropyl ether	3.38	0.307	0	0.41	370	421.5	533	0.1	0.14

[a] ε is the dielectric constant at 298 K; $f(\varepsilon) = (\varepsilon - 1)/(2\varepsilon + 1)$; α and β are Abraham's hydrogen bond acidity and basicity, respectively;[46,47] λ_{abs} is the position of the absorption maximum (nm); λ_{N^*}, λ_{T^*} and I_{N^*}, I_{T^*} are positions of the fluorescence maxima and fluorescence intensities of the N* and T* forms, respectively; φ is the fluorescence quantum yield; I_{N^*}/I_{T^*} is the intensity ratio at the peak maxima of the N* and T* bands, respectively.

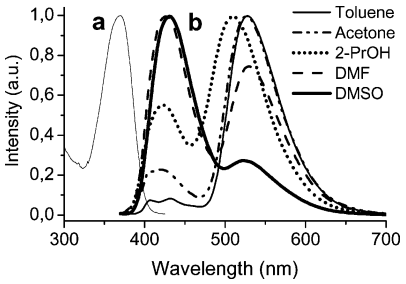

Fig. 1 Examples of absorption and emission spectra of QMOM: a—normalized absorption spectrum in DMSO and b—normalized fluorescence spectra in toluene, acetone, 2-propanol, DMF and DMSO (excitation wavelength: 360 nm).

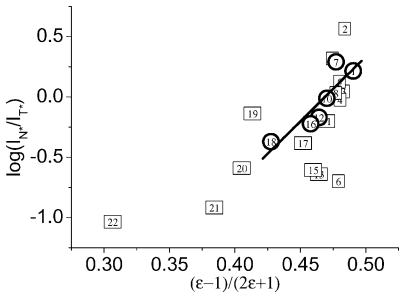

Fig. 2 Dependence of $\log(I_{N^*}/I_{T^*})$ of QMOM on the polarity function $f(\varepsilon)$ for protic solvents (○) and aprotic basic solvents (□). For protic solvents the data were fitted to a linear function: $\log(I_{N^*}/I_{T^*}) = 10.73f(\varepsilon) - 5.03$. Correlation parameter $r^2 = 0.89$.

differ significantly in terms of their basicity index β (see Table 1), we took into account this parameter and using a regression technique we found a good correlation by plotting $\log(I_{N^*}/I_{T^*})$ *versus* the sum of the basicity and polarity indexes: $(\varepsilon - 1)/(2\varepsilon + 1) + 0.3\beta$ (Fig 3). At the same time, no systematic dependence of $\log(I_{N^*}/I_{T^*})$ was found as a function of the solvent basicity index alone.

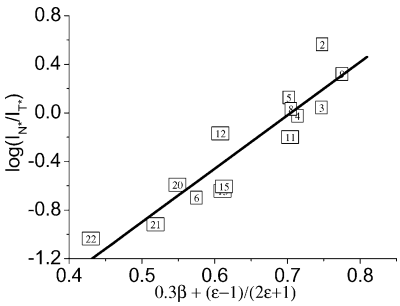

Fig. 3 Dependence of $\log(I_{N^*}/I_{T^*})$ of QMOM on the sum of the polarity $f(\varepsilon)$ and the basicity β functions for aprotic basic solvents.

Thus, in contrast with the 3-hydroxyflavone derivative FET,[22] the basicity of aprotic solvents has a pronounced influence on the fluorescence intensity ratio I_{N^*}/I_{T^*} of the quinolone dye QMOM, indicating an important role of the solvent basicity on the ESIPT reaction in 3-hydroxyquinolones. In protic solvents, the specific effects of solvent acidity and basicity overlap and thus we observe I_{N^*}/I_{T^*} values close to those in highly basic solvents (Table 1, Fig. 2).

Dependence of the absorption and fluorescence band position on the solvent properties

As in the case of FET, the absorption spectra of QMOM are independent on the solvent polarity. However, in contrast to FET, the absorption maximum of QMOM is nearly independent on the solvent polarizability (its position in aprotic solvents changes by

less than 5 nm, Table 1), indicating that the electronic excitation does not change noticeably the dye dipole moment.

In addition, it was shown[48] that, due to its large dipole moment, the N* excited state of FET is highly solvatochromic and displays a linear correlation of the position of its emission maximum as a function of $f(\varepsilon)$.[22] Surprisingly, no pronounced shifts of the N* and T* emission bands of QMOM are observed in all studied solvents (Fig. 4), so that QMOM appears to be insensitive to the solvent polarity and basicity.

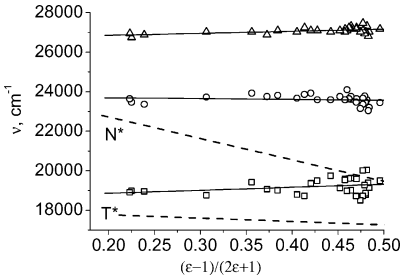

Fig. 4 Dependence of the positions of the absorption (△), N* (○) and T* (□) emission band maxima of QMOM on the polarity function $f(\varepsilon)$ for different solvents. Solid lines represent the linear fits of these dependences. Dashed lines correspond to the linear fits with the data for the N* and T* bands of the FET probe (taken from ref. 22).

The absence of solvatochromism for the N* and T* states of QMOM probably reflects negligible changes of the dipole moments of QMOM during the transition to the ground state. Indeed, according to the Onsager cavity model[49–53] the energy corresponding to the N* or T* emission depends on the difference in the dipole moments of their excited and ground states, and is given by:

$$\nu_{N^*} = \nu^0_{N^*} - \frac{2(\Delta\mu)^2}{a_0^3 hc}\,\frac{\varepsilon - 1}{2\varepsilon + 1}$$

where $\Delta\mu$ is the change of the amplitude of the dipole moment upon the transition, a_0 is the dielectric cavity radius, $\nu_{N^*}{}^0$ is the position of the N* band emission maximum *in vacuo*, h is the Planck constant and c is the speed of light.

We calculated the amplitude difference of the dipole moments of QMOM in its ground (S_0) and non-relaxed excited (S_1) states by the AM1 method[54] and compared it with the values obtained previously for FET *in vacuo* by using the same method, or by direct measurements for the FET homolog, 4′-(dimethylamino)-3-hydroxyflavone in dioxane (Table 2).[48] The obtained data show a significantly smaller increase of the QMOM dipole moment during the S_0–S_1 transition in comparison with that of FET. This feature is probably connected with the non-planar conformation of *N*-methyl-3HQs dyes,[39] which decreases the charge transfer character of the excited state due to a lower conjugation between the two parts of the molecule. Moreover, this lower conjugation may also explain the lower molar extinction coefficients of *N*-methyl-3HQs as compared to FET.[19]

Table 2 Dipole moments of the S_0–S_1 transition (debye) *in vacuo*

	FET		QMOM
	Calculated	Data from literature	Calculated
$\Delta\mu$	7.84	7.17[a]; 13.5[b]	1.84

[a] Ref. 54. [b] Ref. 48, measured in dioxan.

Time-resolved measurements

In contrast to FET, the large changes in the intensity ratio of the two emission bands of QMOM are not accompanied by spectral shifts. In the case of FET, the energies of the emission states vary strongly with the solvent polarity that affects the thermodynamic ESIPT equilibrium between the two states.[22,40,41] Since the energies of the two excited states of QMOM probably do not vary significantly as a function of $f(\varepsilon)$, the mechanism of the strong I_{N^*}/I_{T^*} ratio changes should be different. To understand the mechanistic differences in the ESIPT reaction between FET and QMOM, time-resolved fluorescence measurements were performed. The time-resolved fluorescence parameters for FET and QMOM in organic solvents of different polarity and basicity are presented in Table 3. Identical short lifetimes τ_1 are found for the N* and T* forms together with negative values of the corresponding a_1 pre-exponential coefficients for the T* form. These features clearly indicate an intramolecular proton transfer reaction for FET[28] and QMOM dyes.

In the set of lifetime data in Table 3, two main features have to be underlined. First, in ethyl acetate, the negligibly low value of the pre-exponential coefficient a_2 for the emission at 400 nm (N* band) for QMOM as compared to FET suggests that the ESIPT reaction in QMOM is an irreversible process,[55] while in contrast, the ESIPT reaction of FET in a number of organic solvents is reversible.[28] Another noticeable difference concerns the one order of magnitude higher value of τ_1 for QMOM in basic dimethylformamide as compared to acetonitrile. To understand why these two solvents of similar polarity ($\varepsilon = 37.2$ and 35.7 respectively) display such a large difference in the τ_1 value, we analyzed the contributions of the different processes described in Scheme 1 to the τ_1 value.[43]

Assuming that the ESIPT reaction in QMOM is an irreversible process, we can neglect the backward kinetic rate constant (k_-) Then for an excited-state reaction between the N* and T* forms (Fig. 1), the differential equations of the changes of the concentrations of the N* and T* species, [N*] and [T*], with time can be given by:[40,55]

$$\mathrm{d[N^*]}/\mathrm{d}t = -(k_R{}^{N^*} + k_{NR}{}^{N^*} + k_+)[\mathrm{N^*}] \quad (1)$$

$$\mathrm{d[T^*]}/\mathrm{d}t = -(k_R{}^{T^*} + k_{NR}{}^{T^*})[\mathrm{T^*}] + k_+[\mathrm{N^*}] \quad (2)$$

where $k_R{}^{N^*}$, $k_{NR}{}^{N^*}$, $k_R{}^{T^*}$, $k_{NR}{}^{T^*}$ are the N* and T* form radiative and non-radiative rate constants respectively, and k_+ is the rate constant of the forward proton transfer reaction.

Integration of eqn (1) and (2) with the initial boundary condition that only N* is directly excited and populated at time zero (*i.e.*, at $t = 0$, $[\mathrm{N^*}] = [\mathrm{N^*}]_0$ and $[\mathrm{T^*}] = 0$), yields the following equations for [N*] and [T*]:

$$[\mathrm{N^*}] = [\mathrm{N^*}]_0\, \mathrm{e}^{-t/\tau_1} \quad (3)$$

$$[\mathrm{T^*}] = a[\mathrm{N^*}]_0\, (\mathrm{e}^{-t/\tau_1} - \mathrm{e}^{-t/\tau_2}) \quad (4)$$

where τ_1 and τ_2 are short-lived and long-lived lifetimes given by: $\tau_1 = 1/(k_R{}^{N^*} + k_{NR}{}^{N^*} + k_+)$; $\tau_2 = 1/(k_R{}^{T^*} + k_{NR}{}^{T^*})$. The pre-exponential amplitude a is given by: $a = k_+\tau_1\tau_2/(\tau_1 - \tau_2)$.

Table 3 Time-resolved fluorescence parameters of the two emission bands of QMOM and FET in various organic solvents

Dye	Solvent	Band	τ_1[a,b]	a_1[a,c]	τ_2[a,b]	a_2[a,c]	φ_{N^*}[a]	φ_{T^*}[a]	$k_R^{N^*}$[a,b]	$k_{NR}^{N^*} + k_+$[a,b]	k_+[a,b]
QMOM	Ethyl acetate	N*	0.062	0.98	1.8	0.02	0.01	0.13	0.18	17	15 ± 2
		T*	0.056	−0.47	1.8	0.53					
	Acetonitrile	N*	0.065	0.99	1.3	0.01	0.012	0.088	0.18	15	13 ± 2
		T*	0.069	−0.48	1.3	0.52					
	DMF	N*	0.45	0.98	1.4	0.02	0.08	0.08	0.18	2.0	1.7 ± 0.3
		T*	0.45	−0.46	1.4	0.54					
FET	Ethyl acetate	N*	0.038	0.87	0.31	0.13	0.014	0.047	0.19	—	22.0
		T*	0.038	−0.49	0.33	0.51					
	Dichloromethane	N*	0.061	0.78	0.65	0.22	0.049	0.102	0.26	—	13.2
		T*	0.053	−0.47	0.65	0.53					

[a] τ_1, τ_2 (ns) are the short-lived and long-lived decay times respectively; a_1, a_2 are the relative amplitudes; φ_{N^*}, φ_{T^*} are the N* and T* form quantum yields; $k_R^{N^*}$, $k_{NR}^{N^*}$ ($\times 10^{-9}$ s^{-1}) are the N* form radiative and non-radiative rate constants respectively; k_+ ($\times 10^{-9}$ s^{-1}) is the forward rate constant of the ESIPT reaction. [b] The error for all values is ±10% due to the precision of lifetimes measurements. [c] a_1 and a_2 values were normalized according to $|a_1| + |a_2| = 1$.

Moreover, integration of eqn (3) and (4) with time gives the following quantum yields for the N* and T* bands respectively:

$$\varphi_{N^*} = k_R^{N^*}\tau_1 \quad (5)$$

$$\varphi_{T^*} = \frac{k_R^{T^*}}{k_R^{T^*} + k_{NR}^{T^*}} k_+\tau_1 \quad (6)$$

Using eqn (5), we calculated the rate of the radiative process $k_R^{N^*}$ (Table 3). The obtained values are close to those reported previously for FET (Table 3).[40] Moreover, $k_R^{N^*}$ appears to be independent of the nature of the solvent. This was expected, because $k_R^{N^*}$ is mainly affected by the electronic polarizability of the medium, a property that does not significantly vary in the studied solvents.[56] Then, subtraction of $k_R^{N^*}$ from $1/\tau_1$ gives us the sum of non-radiative and ESIPT rate constants, $k_{NR}^{N^*} + k_+$ (Table 3). To estimate the contribution of the ESIPT rate constant to this sum, we used the following approach.

The ratio of eqn (5) and (6) gives us a simplified expression of k_+:

$$\frac{\varphi_{N^*}}{\varphi_{T^*}} = \frac{k_R^{N^*}}{k_R^{T^*}} \frac{k_R^{T^*} + k_{NR}^{T^*}}{k_+} = \frac{k_R^{N^*}}{k_R^{T^*}} \frac{1}{\tau_2 k_+} \quad (7)$$

As we have already shown, the $k_R^{N^*}$ value does not vary significantly with the solvent. Assuming that the radiative constant of the T* state shows a similar behavior, the ratio $k_R^{N^*}/k_R^{T^*}$ can be considered as constant in different solvents. Thus, the variation of the relative intensities of the N* and T* bands is defined mainly by the ESIPT rate constant k_+ and τ_2. Then dividing eqn (7) for one solvent by that in another solvent allows us to estimate the relative changes of k_+ from solvent to solvent. While the ESIPT rate constant does not change significantly with the solvent polarity from ethyl acetate to acetonitrile, k_+(acetonitrile)/k_+(ethyl acetate) = 0.79, the increase in solvent basicity from acetonitrile to DMF decreases the ESIPT rate constant by a factor of six, *i.e.* k_+(DMF)/k_+(acetonitrile) = 0.13. Moreover, the ratio of k_+ in a pair of solvents is close to the ratio of $k_{NR}^{N^*} + k_+$ in these solvents, calculated independently from τ_1. Indeed, ($k_{NR}^{N^*} + k_+$ in acetonitrile)/($k_{NR}^{N^*} + k_+$ in ethyl acetate) = 0.88, while ($k_{NR}^{N^*} + k_+$ in DMF)/($k_{NR}^{N^*} + k_+$ in acetonitrile) = 0.14. This indicates that the ESIPT rate constant k_+ is much larger than the non-radiative rate $k_{NR}^{N^*}$, namely $k_+ > 5k_{NR}^{N^*}$. Therefore, the value of k_+ varies between $0.8(k_{NR}^{N^*} + k_+)$ and $k_{NR}^{N^*} + k_+$ (Table 3). The results show that, in ethyl acetate and acetonitrile, the estimated k_+ values are similar and close to the ESIPT rate of FET in dichloromethane (Table 3). In contrast, the ESIPT rate constant in the basic solvent DMF is much lower than in the other two solvents, suggesting that the solvent basicity uncouples the ESIPT process. These results are in line with our steady-state data which indicate that the solvent basicity favors the increase of the intensity of the N* band with respect to the T* band (Table 1), so that it should be accounted in the linear correlations with the solvent polarity (Fig. 3).

Thus, the behaviors of FET and QMOM in basic solvents are very different. Since QMOM undergoes an irreversible ESIPT reaction that is a kinetically controlled process, the I_{N^*}/I_{T^*} ratio for this dye is directly controlled by the rate of the forward ESIPT reaction (see eqn (7)). Moreover, the basic solvent DMF slows down the ESIPT reaction of QMOM in comparison to acetonitrile and ethyl acetate, and thus we observe a much larger I_{N^*}/I_{T^*} ratio in DMF. The slow-down of ESIPT in DMF can be assigned to the formation of an intermolecular hydrogen bond between the 3-hydroxyl group of the dye with the solvent (Scheme 3(a)), that disrupts the intramolecular H-bond with the carbonyl oxygen. In contrast, in FET and other 3-hydroxyflavones, the formation of intermolecular H-bonds with basic solvents decreases their fluorescence quantum yield, suggesting that intermolecular H-bonded species are probably not emissive.[22,57] The increase of the non-radiative decay rate constants in FET due to intermolecular H-bonding with basic solvents does not change significantly the

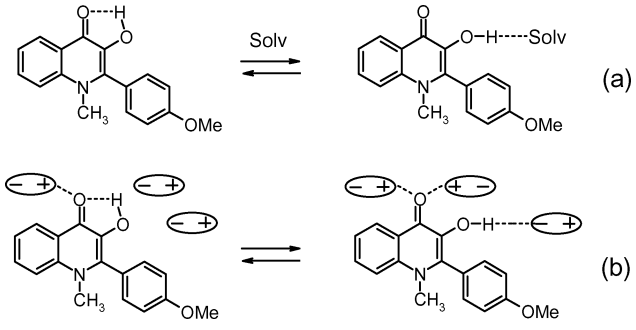

Scheme 3 Mechanism of the influence of basicity (a) and polarity (b) of surroundings on the ESIPT rate in 3-hydroxyquinolone QMOM.

I_{N^*}/I_{T^*} ratio, because in FET this ratio is controlled by the thermodynamic equilibrium between the two states.[22,40] As a result, basic solvents quench the fluorescence of FET but do not modify its I_{N^*}/I_{T^*} ratio. Thus, an important novel feature of QMOM as compared to FET is that its intermolecular H-bonded species in basic solvents is probably emissive and thus contributes to increase the relative intensity of the N* band.

Since QMOM exhibits negligible changes of its dipole moment upon transition to the excited state and back, how to explain then the contribution of polarity to the changes in the I_{N^*}/I_{T^*} ratio in protic and aprotic solvents (Fig. 3)? By interacting with the carbonyl oxygen and the hydroxyl group, polar solvent molecules likely promote the breaking of the intramolecular hydrogen bond of the dye (Scheme 3(b)). As a result, polar solvents, similarly to basic solvents, should slow down the ESIPT reaction leading to an increase in the relative intensity of the N* band. Meantime, the I_{N^*}/I_{T^*} ratio of FET is controlled by the dielectric stabilization of the large dipole of the N* state, which shifts the ESIPT equilibrium toward the N* state.[22,40] Thus, in contrast to FET, QMOM changes its I_{N^*}/I_{T^*} ratio mainly due to a direct perturbation caused by the solvent in a small volume, near the carbonyl and hydroxyl groups of the dye. Due to this property, QMOM exhibits an extremely high spatial resolution in sensing the polarity of the medium.

Conclusions

In the present work, the spectroscopic properties of QMOM, a new 3-hydroxyquinolone dye which undergoes an ESIPT reaction, have been studied in a series of organic solvents and compared with those of its 3-hydroxyflavone analog. We observe that the ratio of the two emission bands of QMOM depends not only on the solvent polarity but also on the solvent basicity, which is different from the behavior of its 3-hydroxyflavone analog. Moreover, in further contrast to 3-hydroxyflavone dyes, the position of the absorption and emission bands of QMOM does not noticeably depend on the solvent properties. This was attributed to limited changes of the QMOM dipole moments upon excitation. Time-resolved experiments demonstrate an irreversible mechanism of the ESIPT reaction for the 3-hydroxyquinolone dye in ethyl acetate, acetonitrile and dimethylformamide. Kinetic analysis of the lifetime data further suggests that basic solvents decrease dramatically its ESIPT rate constant, due to the formation of a hydrogen bond between its 3-hydroxyl group and the solvent. This unique sensor property makes 3-hydroxyquinolone dyes promising building blocks for the development of a new generation of environment-sensitive fluorescent dyes for probing the intermolecular interactions in biological and polymer systems.

Acknowledgements

This work was supported by the ECO-NET program from the French Ministére des Affaires Etrangères between France, Ukraine and Russia. DAY is a member of the European Doctoral College and recipient of a high-level Eiffel Fellowship. VVS is supported by the TriOH European Program. The laboratory of Dr André Mann and Dr Jean Suffert is acknowledged for providing support for organic synthesis. We are also thankful to Professor Andrey Doroshenko for useful discussions.

References

1 G. R. Bright, G. W. Fisher, J. Rogowska and D. L. Taylor, Fluorescence ratio imaging microscopy, *Methods Cell Biol.*, 1989, **30**, 157.
2 R. B. Silver, Ratio imaging: practical considerations for measuring intracellular calcium and pH in living tissue, *Methods Cell Biol.*, 1998, **56**, 237.
3 Z. R. Grabowski, K. Rotkiewicz and W. Rettig, Structural changes accompanying intramolecular electron transfer: focus on twisted intramolecular charge-transfer states and structures, *Chem. Rev.*, 2003, **103**, 3899.
4 S. J. Formosinho and L. G. Arnaut, Excited-state proton transfer reactions II. Intramolecular, reactions, *J. Photochem. Photobiol., A*, 1993, **75**, 21.
5 D. Le Gourrierec, S. M. Ormson and R. G. Brown, Excited state intramolecular proton transfer. Part 2. ESIPT to oxygen, *Prog. React. Kinet.*, 1994, **19**, 211.
6 A. Douhal, F. Lahmani and A. H. Zewail, Proton-Transfer Reaction Dynamics, *Chem. Phys.*, 1996, **207**, 477.
7 M. Henary and C. Fahrni, Excited state intramolecular proton transfer and metal ion complexation of 2-(2′-hydroxyphenyl)benzazoles in aqueous solution, *J. Phys. Chem. A*, 2002, **106**, 5210.
8 C. R. Mateo and A. Douhal, A coupled proton-transfer and twisting-motion fluorescence probe for lipid bilayers, *Proc. Natl. Acad. Sci. U. S. A.*, 1998, **95**, 7245.
9 S. Santra, G. Krishnamoorthy and S. K. Dogra, Excited state intramolecular proton transfer in 2-(2′-benzamidophenyl) benzimidazole: effect of solvents, *Chem. Phys. Lett.*, 1999, **311**, 55.
10 D. Le Gourrierec, V. A. Kharlanov, R. G. Brown and W. Rettig, Excited-state intramolecular proton transfer (ESIPT) in 2-(2′-hydroxyphenyl)-oxazole and -thiazole, *J. Photochem. Photobiol., A*, 2000, **130**, 101.
11 P. K. Sengupta and M. Kasha, Excited state proton-transfer spectroscopy of 3-hydroxyflavone and quercetin, *Chem. Phys. Lett.*, 1979, **68**, 382.
12 D. McMorrow and M. Kasha, Proton-transfer spectroscopy of 3-hydroxyflavone in an isolated-site crystal matrix, *J. Phys. Chem.*, 1984, **88**, 2235.
13 T. C. Swiney and F. D. Kelley, Proton transfer dynamics in substituted 3-hydroxyflavones: Solvent polarization effects, *J. Chem. Phys.*, 1993, **99**, 211.
14 P.-T. Chou, M. L. Martinez and J. H. Clements, Reversal of excitation behavior of proton-transfer *vs.* charge-transfer by dielectric perturbation of electronic manifolds, *J. Phys. Chem.*, 1993, **97**, 2618.
15 M. S. Ormson, R. Brown, G. F. Vollmer and W. Rettig, Switching between charge- and proton-transfer emission in the excited state of a substituted 3-hydroxyflavone, *J. Photochem. Photobiol.*, 1994, **81**, 65.
16 A. S. Klymchenko, T. Oztürk, V. G. Pivovarenko and A. P. Demchenko, Synthesis and spectroscopic properties of benzo- and naphthofuryl-3-hydroxychromones, *Can. J. Chem.*, 2001, **79**, 358.
17 A. S. Klymchenko, V. G. Pivovarenko, T. Oztürk and A. P. Demchenko, Modulation of the solvent-dependent dual emission in 3-hydroxychromones by substituents, *New J. Chem.*, 2003, **27**, 1336.
18 A. S. Klymchenko, T. Oztürk and A. P. Demchenko, Synthesis of furanochromones: a new step in improvement of fluorescence properties, *Tetrahedron Lett.*, 2002, **43**, 7079.
19 A. S. Klymchenko, T. Oztürk, V. G. Pivovarenko and A. P. Demchenko, A 3-hydroxychromone with dramatically improved fluorescence properties, *Tetrahedron Lett.*, 2001, **42**, 7967.
20 S. Ercelen, A. S. Klymchenko and A. P. Demchenko, Ultrasensitive fluorescent probe for the hydrophobic range of solvent polarities, *Anal. Chim. Acta*, 2002, **464**, 273.
21 A. S. Klymchenko, V. G. Pivovarenko and A. P. Demchenko, Elimination of the hydrogen bonding effect on the solvatochromism of 3-hydroxyflavones, *J. Phys. Chem. A*, 2003, **107**, 4211.
22 A. S. Klymchenko and A. P. Demchenko, Multiparametric probing of intermolecular interactions with fluorescent dye exhibiting excited state intramolecular proton transfer, *Phys. Chem. Chem. Phys.*, 2003, **5**, 461.
23 A. S. Klymchenko and A. P. Demchenko, Electrochromic modulation of excited-state intramolecular proton transfer: The new principle in design of fluorescence sensors, *J. Am. Chem. Soc.*, 2002, **124**, 12372.
24 M. Sarkar, J. G. Ray and P. K. Sengupta, Effect of reverse micelles on the intramolecular excited state proton transfer (ESPT) and dual luminescence behaviour of 3-hydroxyflavone, *Spectrochim. Acta, Part A*, 1996, **52**, 275.

25 J. R. Dharia, K. F. Johnson and J. B. Schlenoff, Synthesis and characterization of wavelength-shifting monomers and polymers based on 3-hydroxyflavone, *Macromolecules*, 1994, **27**, 5167.
26 A. S. Klymchenko and A. P. Demchenko, Probing AOT reverse micelles with two-color fluorescence dyes based on 3-hydroxychromone, *Langmuir*, 2002, **18**, 5637.
27 A. S. Klymchenko, G. Duportail, T. Oztürk, V. G. Pivovarenko, Y. Mély and A. P. Demchenko, Novel two-band ratiometric fluorescence probes with different location and orientation in phospholipid membranes, *Chem. Biol.*, 2002, **9**, 1199.
28 A. S. Klymchenko, G. Duportail, Y. Mély and A. P. Demchenko, Ultrasensitive two-color fluorescence probes for dipole potential in phospholipid membranes, *Proc. Natl. Acad. Sci. U. S. A.*, 2003, **100**, 11219.
29 A. Sytnik, D. Gormin and M. Kasha, Interplay between excited-state intramolecular proton transfer and charge transfer in flavonols and their use as protein-binding-site fluorescence probes, *Proc. Natl. Acad. Sci. U. S. A.*, 1994, **91**, 11968.
30 O. P. Bondar, V. G. Pivovarenko and E. S. Rowe, Flavonols-new fluorescent membrane probes for studying the interdigitation of lipid bilayers, *Biochim. Biophys. Acta*, 1998, **1369**, 119.
31 V. V. Shynkar, A. S. Klymchenko, G. Duportail, A. P. Demchenko and Y. Mély, Two-color fluorescent probes for imaging the dipole potential of cell plasma membranes, *Biochim. Biophys. Acta*, 2005, **1712**, 128.
32 S. Ercelen, A. S. Klymchenko and A. P. Demchenko, Novel two-color fluorescence probe with extreme specificity to bovine serum albumin, *FEBS Lett.*, 2003, **538**, 25.
33 A. S. Klymchenko, S. V. Avilov and A. P. Demchenko, Application of two-color ratiometric site-selective fluorescence probes and labels in protein research, *Anal. Biochem.*, 2004, **329**, 43.
34 A. D. Roshal, A. V. Grigorovich, A. O. Doroshenko, V. G. Pivovarenko and A. P. Demchenko, Flavonols and crown-flavonols as metal cation chelators. The different nature of Ba^{2+} and Mg^{2+} complexes, *J. Phys. Chem. A*, 1998, **102**, 5907.
35 X. Poteau, G. Saroja, C. Spies and R. G. Brown, The photophysics of some 3-hydroxyflavone derivatives in the presence of protons, alkali metal and alkaline earth cations, *J. Phys. Chem. A*, 2004, **162**, 431.
36 V. G. Pivovarenko, O. B. Vadzyuk and S. O. Kosterin, Fluorometric detection of adenosine triphosphate with 3-hydroxy-4′-(dimethylamino)flavone in aqueous solutions, *J. Fluoresc.*, 2006, **16**, 9.
37 F. Gao, K. F. Johnson and J. B. Schlenoff, Ring closing and photooxidation in nitrogen analogues of 3-hydroxyflavone, *J. Chem. Soc., Perkin Trans. 2*, 1996, **2**, 269.
38 D. A. Yushchenko, M. D. Bilokin, O. V. Pyvovarenko, G. Duportail, Y. Mély and V. G. Pivovarenko, Synthesis and fluorescence properties of 2-aryl-3-hydroxyquinolones, a new class of dyes displaying dual fluorescence, *Tetrahedron Lett.*, 2006, **47**, 905.
39 D. A. Yushchenko, V. V. Shvadchak, A. S. Klymchenko, G. Duportail, Y. Mély and V. G. Pivovarenko, 2-Aryl-3-hydroxyquinolones, a new class of dyes with solvent dependent dual emission due to excited state intramolecular proton transfer, *New J. Chem.*, 2006, **30**, 774.
40 V. V. Shynkar, Y. Mély, G. Duportail, E. Piémont, A. S. Klymchenko and A. P. Demchenko, Picosecond time-resolved fluorescence studies are consistent with reversible excited-state intramolecular proton transfer in 4′-(dialkylaminoe)-3-hydroxyflavones, *J. Phys. Chem. A*, 2003, **107**, 9522.
41 A. D. Roshal, J. A. Organero and A. Douhal, Tuning the mechanism of proton-transfer in a hydroxyflavone derivative, *Chem. Phys. Lett.*, 2003, **379**, 53.
42 D. B. Siano and D. E. Metzler, Band shapes of the electronic spectra of complex molecules, *J. Chem. Phys.*, 1969, **51**, 1856.
43 Joseph R. Lakovicz, in *Principles of Fluorescence Spectroscopy*, Kluwer Academic/Plenum Publishers, New York, 2nd edn, 1999, p. 52.
44 A. K. Livesey and J.-C. Brochon, Analyzing the distribution of decay constants in pulse-fluorimetry using the maximum entropy method, *Biophys. J.*, 1987, **52**, 693.
45 M. J. S. Dewar, E. G. Zoebisch, E. F. Healy and J. J. P. Stewart, AM1. A New General Purpose Quantum Mechanical Molecular Model, *J. Am. Chem. Soc.*, 1985, **107**, 3902.
46 M. J. Kamlet, J. L. M. Abboud, M. H. Abraham and R. W. Taft, Linear salvation energy relationships. 23. A comprehensive collection of the solvatochromic parameters, π^*, α, and β, and some methods for simplifying the generalized solvatochromic equation, *J. Org. Chem.*, 1983, **48**, 2877.
47 M. H. Abraham, H. S. Chadha, G. S. Whiting and R. C. Mitchell, Hydrogen bonding. 32. An analysis of water–octanol and water–alkane partitioning and the delta log *P* parameter of seiler, *J. Pharm. Sci.*, 1994, **83**, 1085.
48 N. A. Nemkovich, W. Baumann and V. G. Pivovarenko, Dipole moments of 4′-aminoflavonols determined using electro-optical absorption measurements or molecular Stark-effect spectroscopy, *J. Photochem. Photobiol., A*, 2002, **153**, 19.
49 L. J. Onsager, Electric moments of molecules in liquids, *Am. Chem. Soc.*, 1936, **58**, 1486.
50 E. L. Lippert, in *Organic molecular photophysics*, Wiley, New York, 1975, vol. 2, p. 1.
51 W. Liptay, in *Excited States*, Academic Press, New York, 1974, p. 129.
52 N. Mataga and T. Kubata, in *Molecular interactions and electronic spectra*, Marcel Dekker, New York, 1970.
53 N. G. Bakhshiev, in *Spectroscopy of intermolecular interactions*, Nauka, Leningrad, 1972.
54 S. O. Yesylevsky, A. S. Klymchenko and A. P. Demchenko, Semiempirical study of two-color fluorescent dyes based on 3-hydroxychromone, *J. Mol. Struct. (THEOCHEM)*, 2005, **755**, 229.
55 W. R. Laws and L. Brand, Analysis of two-state excited-state reactions. The fluorescence decay of 2-naphthol, *J. Phys. Chem.*, 1979, **83**, 795.
56 C. A. Parker, in *Photoluminescene in Solutions*, Elsevier Publishing Company, Amsterdam, 1968, p. 23.
57 A. S. Klymchenko, V. G. Pivovarenko and A. P. Demchenko, Perturbation of planarity as the possible mechanism of solvent-dependent variations of fluorescence quantum yield in 2-aryl-3-hydroxychromones, *Spectrochim. Acta, Part A*, 2003, **59**, 787.

Article 4

Dual-fluorescence probe of environment basicity (hydrogen bond accepting ability) displaying no sensitivity to polarity

J Fluoresc
DOI 10.1007/s10895-008-0443-x

ORIGINAL PAPER

Dual-Fluorescence Probe of Environment Basicity (Hydrogen Bond Accepting Ability) Displaying no Sensitivity to Polarity

Mykhailo D. Bilokin' · Volodymyr V. Shvadchak · Dmytro A. Yushchenko · Guy Duportail · Yves Mély · Vasyl G. Pivovarenko

Received: 11 October 2008 / Accepted: 11 November 2008

Abstract 3-Hydroxyquinolones (3HQs) are a new class of water soluble dual fluorescence probes that can monitor both polarity and basicity (H-bond accepting ability) parameters. Both parameters play an important role in proteins and lipid membranes. Nevertheless, no method exists actually to measure the basicity parameter separately from the polarity. To achieve this aim, we synthesized 2-benzofuryl-3-hydroxy-4(1H)-quinolone (3HQ-Bf) and characterized its photophysical properties by UV, steady-state and time-resolved fluorescence spectroscopy. Due to its extended conjugation and totally planar conformation, 3HQ-Bf is characterized by a high fluorescence quantum yield. In solution, this dye shows an excited state intramolecular proton transfer (ESIPT) reaction resulting in two tautomer bands in the emission spectra. The ESIPT reaction can be considered as irreversible and is governed by rate constants from 0.6 to 8×10^9 s^{-1}, depending on the solvent. The analysis of the spectral properties of 3HQ-Bf in a series of organic solvents revealed a marginal sensitivity to the solvent polarity, but an exquisite sensitivity to solvent basicity, as shown by the linear dependence of the logarithm of the emission bands intensity ratio, $\log(I_{N*}/I_{T*})$, as well as the absorption or emission maxima wavenumbers as a function of the solvent basicity parameter. This probe may find useful applications through coupling to a protein ligand, for characterizing the H-bond acceptor ability at the ligand binding site as well as for studying the basicity changes of lipid membranes during their chemo- and thermotropic conversions.

Keywords Fluorescence probes · Solvent basicity · Hydrogen-bond acceptor · Ratiometric sensors · Intramolecular proton transfer · 3-hydroxyquinolones

M. D. Bilokin' · V. V. Shvadchak · D. A. Yushchenko · V. G. Pivovarenko (✉)
Organic Chemistry Department, Chemistry Faculty, National Taras Shevchenko University of Kyiv, Kyiv 01601, Ukraine
e-mail: pvg_org@mail.ru

V. V. Shvadchak · D. A. Yushchenko · G. Duportail · Y. Mély · V. G. Pivovarenko
Photophysique des Interactions Biomoléculaires, UMR 7175 du CNRS, Institut Gilbert Laustriat, Faculté de Pharmacie, Université Louis Pasteur, Illkirch 67401, France

Introduction

Fluorescence methods are powerful for investigating molecular interactions and especially protein/ligand interactions in complex biological systems [1]. For this reason, there is a strong demand for the development of new fluorescent probes that could sense, for example, in the protein binding site not only the electric field of the surrounding atoms, but also the H-bond donating and H-bond accepting ability. In this respect, probes with a dual emission (two-channel emitters) present the strong advantage over intensiometric probes (single-channel emitters) to give a ratiometric response independent of the probe concentration. Excited state intramolecular proton transfer (ESIPT) [2–4] procures a very effective basis for the design of probes with dual fluorescence. The ESIPT reaction leads to the formation of two isomers (normal N* and tautomer T* forms) in the excited state of the probe. Due to their different photophysical properties, these tautomeric forms exhibit highly separated emission bands. The most interesting and characteristic representatives of ESIPT probes are 3-hydroxyflavones and their derivatives (3HFs) [5, 6]. They

have been shown to be effective tools for investigating the polarity [6–12], H-bond donor ability [12, 13], electronic polarizability [14] and electrostatic effects in different media [15,16] including model lipid membranes [16–19], cell membranes [20] and proteins [21–23]. Moreover, these dyes were shown to be useful to determine the nature and concentration of cations and anions [24–27]. However, despite their advantages over common single-band probes, 3HFs exhibit relatively low photostability and low quantum yields in water that limit their application. As a consequence, the development of new dual-fluorescence probes with improved fluorescent parameters is strongly required.

3-hydroxyquinolones (3HQs) are structural aza-analogs of the 3HFs. They also display a well-expressed dual emission in most tested media [28] due to an ESIPT reaction [28–30]. Spectral properties of 3HQs were up to now less investigated since they are a relatively new class of dyes with more complex synthetic pathways. But importantly, in comparison to 3HFs, most of the synthesized 3HQs are more photostable and have higher fluorescence quantum yields in aqueous solutions [28]. They were shown to be effective in sensing the viscosity of protic solvents [31] as well as both the polarity and basicity of organic media [32]. The last two properties are provided by intra– and intermolecular processes that play a key role in the functions of proteins and lipid membranes. However, in contrast to polarity [33, 34] and H-bond donor ability [12,13], no fluorescence probe reports selectively on the basicity (H-bond acceptor ability) of the surrounding molecules. Thus, it would be important to develop a probe able to sense the basicity independently from the polarity.

In this respect, we present herein the design, synthesis and fluorescence properties of a new dye of the 3HQ series, namely 2-benzofuryl–3-hydroxy–4(1H)-quinolone (3HQ-Bf, Scheme 1). This probe has been designed based on more simple analogs–3HQ-Ph and 3HQ–Th - which, being water soluble and possessing good fluorescence quantum yields, exhibit a mixed sensitivity to both solvent polarity and basicity [32]. According to the principles of solvatochromism [33], the sensitivity of a dye to polarity is due to the difference in stabilization of its S_0 and S_1 states by the solvent. Thus, to lower the sensitivity to solvent polarity, this difference should be reduced. In the case of the ESIPT dyes, a decrease of the sensitivity of the ratiometric response to solvent polarity should be achieved by limiting the reorganization of the solvation shell around the proton transfer system. In principle, this requires to minimize the changes in the dipole moment of the dye during its transition from the S_0 to S_1 states. According to quantum chemical calculations [28], this should be achieved by substituting the electron acceptor phenyl or thiophenyl rings by an electron donor benzofuryl ring. In addition, the decrease of the effective size of the five atoms cycle caused by the replacement of the sulfur atom in 3HQ-Th by the oxygen atom in 3HQ-Bf should favor the disruption of the intramolecular H-bond by the solvent [35], thus increasing the sensitivity of the N* emission band to basic molecules. In line with our expectations, all these features brought together resulted in the development of a fluorescence probe that reports about the basicity of the environment, independently from the polarity. As a consequence, we obtained for the first time a pure basicity sensitive fluorescence probe that can find interesting applications in the study of protein binding sites or lipid membranes.

Experimental

Materials and methods

All reagents were purchased from Sigma-Aldrich. Solvents for synthesis were of reagent quality and appropriately dried if necessary. For absorption and fluorescence studies, the solvents were of spectroscopic grade. Melting points were determined on a "VEB Analytik", Dresden hostage microscope melting point apparatus, and were uncorrected. Proton NMR spectra were recorded on a Varian Mercury–400 MHz spectrometer. Tetramethylsilane (TMS) was used as an internal standard in $CDCl_3$ or DMSO−d_6. Mass spectra were measured with a Mass Spectrometer Mariner System 5155.

Absorption spectra were recorded on a Cary 4 spectrophotometer (Varian) and fluorescence spectra on a FluoroMax 3.0 (Jobin Yvon, Horiba) spectrofluorimeter at room temperature. In case of a structured emission spectrum, the middle emission peak which usually was the highest one was chosen to determine the position of the maximum emission wavelength. Fluorescence quantum yields φ were

Scheme 1 Chemical structures of the studied 3-hydroxyquinolones

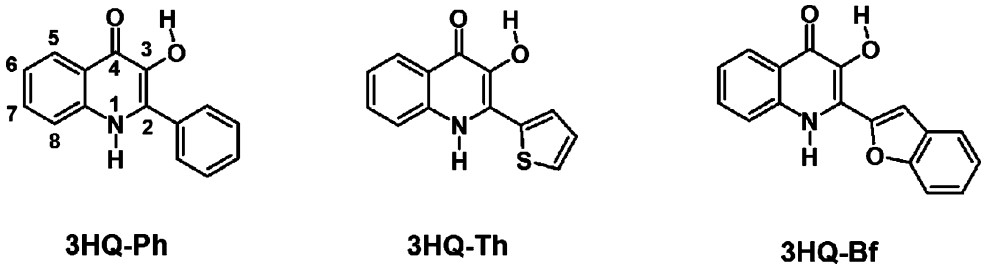

determined with quinine sulfate in 0.5 M sulfuric acid (φ= 0.577) as a reference [36]. All measurements were carried out in a temperature-controlled cell at 20±0.1°C. Quantum-chemical calculations were performed by the AM1 semi-empirical method [37] using the MOPAC 2007 program [38]. Configuration interactions in different combinations were taken into account during the calculations of the S_1 state parameters.

Time-resolved fluorescence measurements were performed with the time-correlated, single-photon counting technique using the frequency tripled output of a Ti-Sapphire laser (Tsunami, Spectra Physics), pumped by a Millenia X laser (Tsunami, Spectra Physics) [11]. The excitation wavelength was set at 320 nm. The fluorescence decays were collected at the magic angle (54.7°) of the emission polarizer. The single-photon events were detected with a microchannel plate Hamamatsu R3809U photomultiplier coupled to a Philips 6954 pulse preamplifier and recorded on a multichannel analyzer (Ortec 7100) calibrated at 25.5 ps/channel. The instrumental response function was recorded with a polished aluminum reflector, and its full-width at half-maximum was 50 ps.

The time-resolved decays were analyzed both by the iterative reconvolution method and the Maximum Entropy Method (MEM) [39]. The goodness of the fit was evaluated from the χ^2 values, the plots of the residuals and the autocorrelation function.

Synthesis

Synthesis (Scheme 2) and purification of 3HQ-Ph and 3HQ-Th were performed as previously described [28]. For the preparation of 2–(2-benzofuryl)-3-hydroxy-4(1H)-quinolone (3HQ-Bf) 0.5 ml of 30% aqueous solution of KOH was slowly added to a solution of 2-aminoacetophenone (0.675 g, 5 mmol) and 2-formylbenzofurane (0.759 g, 5.2 mmol) in 2 ml of ethanol. The resulting solution was stirred at room temperature during 45 min. Then, water (10 ml) was added to the reaction mixture, resulting in a yellow precipitate which was isolated by filtration and recrystallized from ethanol to give i as light yellow needles (96% yield). On the next step, the obtained product was dissolved in a mixture of ethanol and 10% aqueous NaOH (1:1 in v/v). 0.5 ml of 30% hydrogen peroxide was added drop-wise to the resulting mixture at 0°C up to the formation of the corresponding epoxide ii (TLC-controled). The resulting mixture was poured into 10 g of ice and neutralized by diluted aqueous acetic acid. The filtered precipitate was dissolved in 20 ml ethanol and refluxed during 20 h, until the precipitate of 3HQ-Bf was formed (TLC-controled). The crude product after washing and recrystallization from ethanol, gives light yellow needles of 3HQ-Bf. Yield 0.381 g (47%), m.p. 265–266°C (from ethanol), LC/MSD:%, m/z 278 $[M+1]^+$, ^1H -NMR data (TMS, DMSO−d_6) δ, (J, Hz): 7.27t, J=8.1 Hz, 1H(H-5′); 7.35t, J=6.9 Hz, 1H(H-6′); 7.61dd, J_1=8.3 Hz, J_2=3.1 Hz, 2H(H−7′, H-4′); 7.74 m, 2H(H-3′, H-8); 7.95d, J=2.1 Hz, 1H(H-6); 8.05d, J=8.7 Hz 1H(H-5); 11.07c, 1H (NH).

Results and discussion

Absorption properties

The absorption spectra of 3HQ-Bf and 3HQ-Ph exhibit dramatic differences in their profiles as well as in the

Scheme 2 Synthesis of 3HQ-Bf

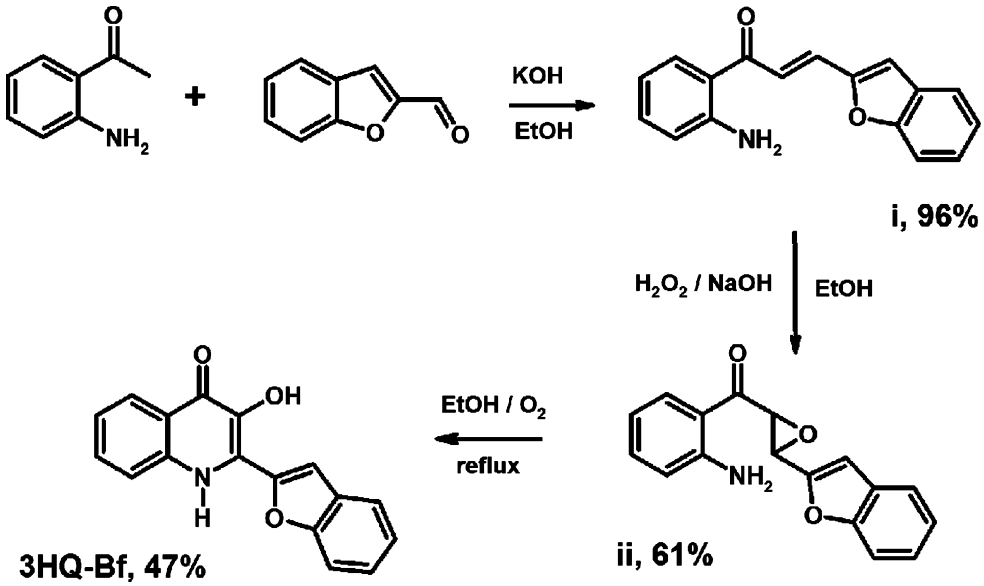

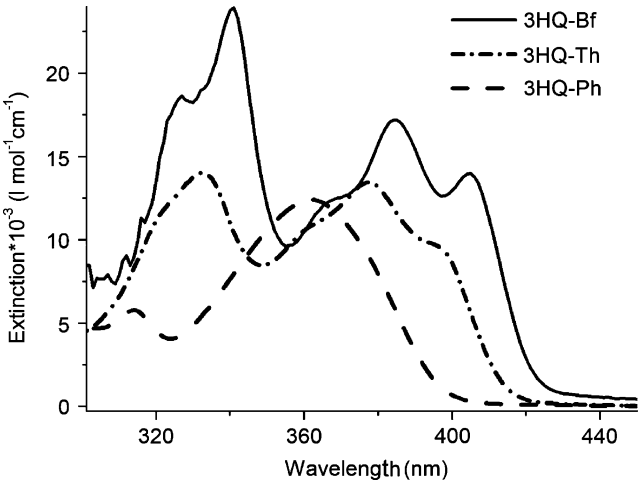

Fig. 1 Absorption spectra of 3HQs in ethanol

positions of their bands (Fig. 1), evidencing strong conformational differences between the two compounds. For 3HQ-Ph, the structureless profile and the short-wavelength position of the bands are in line with a distribution of nonplanar conformations with a low degree of π-conjugation between the rings [28]. On the contrary, the absorption spectrum of 3HQ-Bf is well structured and presents a 30 nm red-shift suggesting a distribution of more planar conformations and a larger degree of π-conjugation. In further line with this conclusion, 3HQ-Bf shows a ~1.5-fold higher molar extinction coefficient in solution as compared to 3HQ−Ph and other dyes of the 3HQ series [28] (Table 1). The absorption spectrum of 3HQ-Th shows an intermediate behavior, being less structured than the 3HQ-Bf one, indicating that 3HQ-Th exhibits less planar conformations than 3HQ-Bf.

To further strengthen our conclusions on the conformations of the 3HQ derivatives, quantum-chemical calculations were performed. In good agreement with the above spectral data, the calculated torsional enthalpy values show that the 3HQ derivatives with thiophene and phenyl rings are favoring non-planar conformations ([28], Fig. 2) with optimal angle values between the aromatic rings of 28° for 3HQ-Th and 42° for 3HQ-Ph, respectively. Meantime, the deep energy minimum observed for 3HQ-Bf indicates a narrow distribution of totally planar conformations at room temperature, in full agreement with the well-structured absorption spectrum. Thus, 3HQ-Th and 3HQ-Bf are a good example of molecules with close chemical structures, but with markedly different distribution of conformations. The main reason for this difference is likely the smaller size of the more compact oxygen-containing furyl ring that limits the steric hindrance with the 3HQ moiety.

Fluorescence properties

3HQ-Bf was found to exhibit high quantum yield in all types of solvents (Table 1), in full line with its highly planar structure. Furthermore, 3HQ-Bf displayed dual fluores-

Table 1 Spectroscopic properties of 3HQ-Bf in different solvents

№	Solvent	ε	β	λ_{abs}	$E \cdot 10^{-3}$	λ_{N^*}	λ_{T^*}	I_{N^*}/I_{T^*}	φ
1	Water	78.4	0.35	381	18.2	443	503	0.296	0.102
2	DMSO	46.8	0.88	391	15.3	453	532	1.433	0.408
3	Ethane-1,2-diol	40.2	0.78	389	18.6	447	524	0.500	0.462
4	DMFA	37.2	0.74	387	19.5	449	532	0.633	0.294
5	Acetonitrile	35.7	0.32	381	16.9	436	523	0.086	0.263
6	Methanol	32.6	0.47	384	17.7	444	526	0.213	0.143
7	N-methyl-pyrrolidone	32.6	0.76	389	17.5	450	536	0.523	0.309
8	HMPA	29.0	1.00	392	17.9	453	541	0.892	0.302
9	Ethanol	24.9	0.48	386	17.2	444	527	0.128	0.288
10	1,1,3,3-Tetra-methylurea	24.5	0.78	388	15.0	448	535	0.326	0.315
11	1-Propanol	20.5	0.48	385	17.5	447	524	0.121	0.310
12	Acetone	20.5	0.49	384	14.7	438	528	0.116	0.134
13	1-Butanol	17.3	0.51	385	16.8	446	525	0.130	0.374
14	Dichlormethane	9.02	0.05	383	17.1	437	521	0.050	0.320
15	Tetrahydrofuran	7.43	0.48	386	13.9	444	531	0.135	0.422
16	Ethyl acetate	5.99	0.45	383	16.9	438	527	0.068	0.250
17	Bromobenenzene	5.41	0.09	379	14.2	437	530	0.038	0.425
18	1,2-Dibromoethane	4.93	0.17	380	18.9	441	527	0.040	0.453
19	Diisopropyl ether	3.38	0.41	383	17.3	435	530	0.060	0.306
20	Dioxan	2.27	0.64	386	17.8	449	531	0.235	0.274

[a] ε – dielectric constant at 298 K. β – Abraham's hydrogen bond basicity [42], λ_{abs}: position of the absorption maximum (nm), E – molar extinction coefficient $l\ mol^{-1}\ cm^{-1}$ at λ_{abs}, λ_{N^*}, λ_{T^*} and I_{N^*}/I_{T^*}–positions of the fluorescence maxima and fluorescence intensity ratio of the N* and T* forms, respectively, φ is the fluorescence quantum yield.

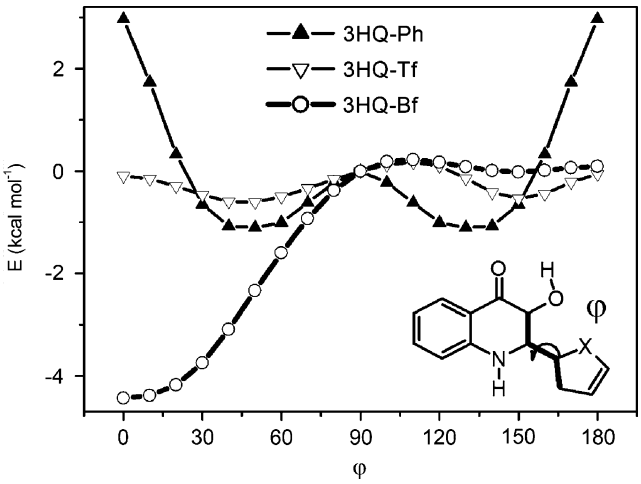

Fig. 2 Torsion enthalpy profiles of 3HQ derivatives

cence in all tested media (Fig. 3). Both emission bands are well resolved, with a separation between their maxima of 60-100 nm (2700−4200 cm^{-1}). Appearing in the blue and yellow-green regions of the visible spectrum, both emission bands showed only limited solvatochromic shifts, suggesting that the dipole moment values in the S_1 and S_0 electronic states are close. In spite of its poor solubility in low polar solvents, we succeeded to obtain solutions of monomeric dye starting from bromobenzene and dioxane. The excitation spectra of 3HQ-Bf recorded at the maximum emission wavelengths of the N* and T* bands were found to superimpose with the absorption spectrum, proving that the two emission bands belong to excited tautomeric forms. In addition, the ESIPT reaction for 3HQ-Bf was further confirmed by the identical fluorescence lifetimes values τ_1 for both N* and T* bands as well as by the appearance of a negative amplitude associated with the τ_1 value in the time-resolved fluorescence decay of the T* band (see below).

Due to the weak solvatochromism exhibited by 3HQ-Bf in its absorption as well as in its emission spectra, the positions of the band maxima are clearly non-effective parameters for characterizing the solvent polarity. In contrast, the ratio of the emission intensities of the two tautomers I_{N*}/I_{T*} displays dramatic changes in protic as well as in aprotic solvents (Fig. 3, Table 1). In contrast to 3-hydroxyflavones [12,13] and N-methyl-3HQs [30,32], where the I_{N*}/I_{T*} intensity ratio was largely governed by the solvent polarity, the I_{N*}/I_{T*} ratio of 3HQ-Bf showed no regular dependency on either the empirical $E_T(30)$ [33] or SPP [34] polarity parameters or the theoretical Lippert [40,41] polarity-polarisability function (Fig. 4a). Meantime, a linear relationship was found when $\log(I_{N*}/I_{T*})$ was plotted as a function of the H-bond acceptor ability expressed by the Abraham's basicity parameter β [42,43] (Fig. 4b, $log(I_{N*}/I_{T*}) = -1.59 + 1.62\beta$, r^2=0.9). In addition, in spite of their limited variations, the positions of the maxima of both absorption and emission spectra were also found to linearly depend on the β value (Fig. 5). Thus, in line with our expectations, the spectroscopic properties of 3HQ-Bf appear to be strongly sensitive to the basicity parameter β, but not to the polarity.

An additional demonstration of the sensitivity of 3HQ-Bf emission to solvent basicity was obtained from the study of its spectral properties in mixtures of two solvents with close dielectric constant, but different basicity. For this purpose, acetonitrile (ε=35.7, β=0.32) and dimethylformamide (ε=37.2, β=0.74) were chosen as an appropriate pair of solvents. A linear relationship was found when the logarithm of the intensity ratio changes $\log(\Delta I_{N*}/I_{T*})$ was plotted as a function of the logarithm of the concentration of dimethylformamide in the mixture (Fig. 4c, r^2=0.990) or when the intensity ratio I_{N*}/I_{T*} was plotted as a function of the proportion of dimethylformamide in the mixture (Fig. 4 d,

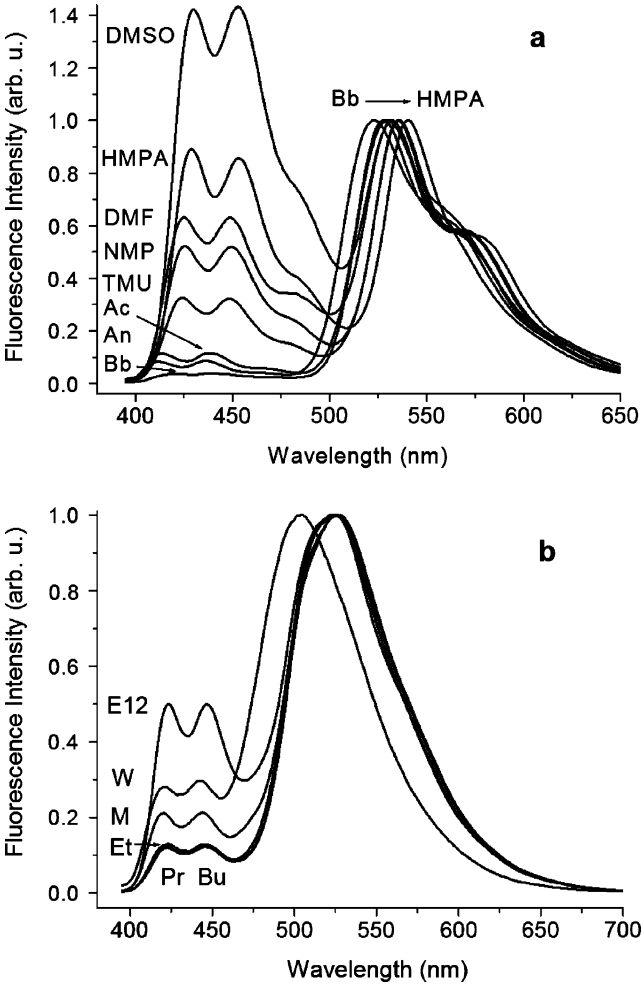

Fig. 3 Normalized fluorescence emission spectra of 3HQ-Bf in aprotic **a** and protic **b** solvents. Abbreviations: NMP - N-methylpyrrolidone, TMU - tetramethylurea, Ac - acetone, An - acetonitrile, Bb - bromobenzene, E12 - Ethane-1,2-diol, W - water, M - methanol, Et - ethanol, Pr - 1-propanol, Bu - 1-butanol

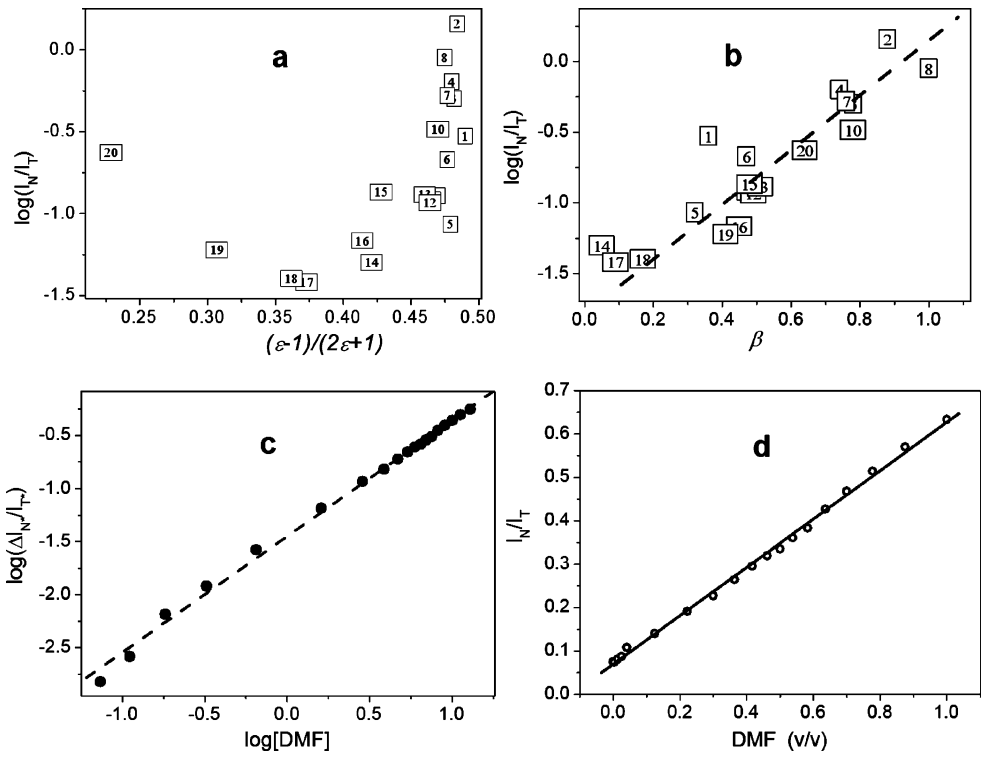

Fig. 4 Dependence of $\log(I_{N*}/I_{T*})$ on the polarity function **a** and the Abraham's hydrogen bond acceptor basicity parameter **b**. Numbering of solvents is as in Table 1. Influence of the solvent basicity in MeCN-DMF mixtures on the I_{N*}/I_{T*} ratio **c**, **d**. $\Delta I_{N*} = I_{N*}(\text{mixture}) - I_{N*}(\text{pure acetonitrile})$

$r^2=0.999$). This shows the absence of preferential solvation of 3HQ-Bf by DMF in acetonitrile and points on the close values of the solvation energies of 3HQ-Bf in acetonitrile and DMF. The two linear relationships unambiguously confirmed the direct dependence of the 3HQ-Bf fluorescence properties on the solvent basicity.

Noticeably, several solvents show some deviations from the linear plot of $\log(I_{N*}/I_{T*})$ as a function of the solvent basicity β (Fig. 4b). For instance, the $\log(I_{N*}/I_{T*})$ values where found to be below the linear fit in 8–HMPA, 10–TMU, and 19–diisopropyl ether, while in contrast, $\log(I_{N*}/I_{T*})$ values significantly above the fit were observed in 1–water, 2–DMSO, 4–DMF, and 6 – methanol. In the former solvents (8, 10 and 19), the low $\log(I_{N*}/I_{T*})$ values could result from the poor accessibility of the spatially hindered basic (H-bond acceptor) center of the solvent molecules to the proton-transfer system. The relatively low concentrations of these basic centers (from 5.6 to 9.8 mole·l^{-1}) resulting from the high molar volume of these solvents should also contribute to this behaviour. In contrast, in the latter solvents (1, 2, 4 and 6), the high $\log(I_{N*}/I_{T*})$ values may be related to their comparatively higher molar concentrations (from 13 to 55 mole·l^{-1}). The deviation observed with dichloromethane (14) is less clear and may result from the cooperative effect of the two basic chlorine atoms localized in close proximity.

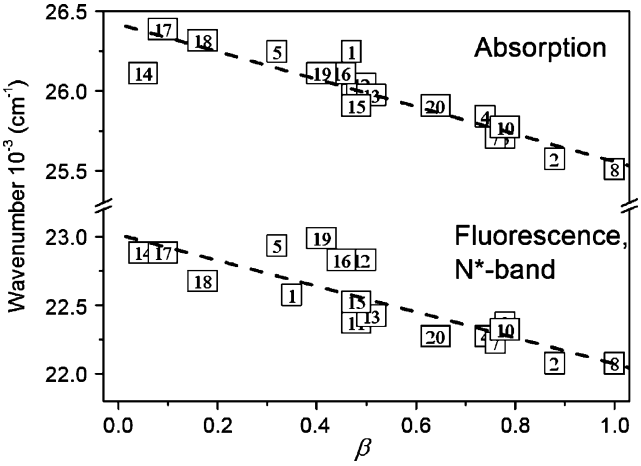

Fig. 5 Dependence of the band maxima positions (cm^{-1}) of the absorption and fluorescence emission spectra of 3HQ-Bf as a function of the Abraham's hydrogen bonding basicity parameter of the solvent. Solvent numbering is as in Table 1

Time-resolved fluorescence measurements

To further characterize the molecular basis of the spectral properties of 3HQ-Bf in comparison with 3HQ-Th, their ESIPT mechanism was investigated by time-resolved fluorescence measurements in methanol, taken as a protic solvent and in aprotic solvents of various basicity. In all cases, the fluorescence decays were biexponential and, both N* and T* forms exhibited the same fluorescence lifetimes (τ_1 and τ_2) but different pre-exponential coefficients (α_1 and α_2). The negative α_1 values for the T* form confirmed that it is produced from the N* state through an ESIPT

Table 2 Time-resolved fluorescence parameters of N* and T* emission bands in organic solvents for the two considered dyes

Dye	Solvent	Band	τ_1 [a,b]	α_1 [a,c]	τ_2 [a,b]	α_2 [a,b]	φ_{N^*} [a]	φ_{T^*} [a]	k_+ [a]	I/I_{T^*}
3HQ-Bf	DMSO	N^*	1.34	0.91	7.51	0.09	0.240	0.168	0.6	1.43
		T^*	1.27	−0.44	7.57	0.56				
	DMF	N^*	0.82	0.99	6.49	0.01	0.114	0.180	1.0	0.63
		T^*	0.75	−0.66	6.42	0.33				
	MeOH	N^*	0.28	0.99	5.62	0.01	0.025	0.118	3.0	0.21
		T^*	0.27	−0.77	5.64	0.23				
	MeCN	N^*	0.11	0.98	6.01	0.02	0.019	0.244	8.1	0.08
		T^*	0.12	−0.66	5.95	0.33				
3HQ-Th	DMSO	N^*	0.98	0.97	4.79	0.03	0.126	0.264	0.9	0.48
		T^*	0.55	−0.33	7.65	0.66				
	DMF	N^*	0.56	0.99	4.02	0.01	0.064	0.276	1.5	0.23
		T^*	0.32	−0.51	7.76	0.49				
	MeOH	N^*	0.23	0.98	6.07	0.02	0.041	0.259	3.8	0.16
		T^*	0.21	−0.78	6.61	0.22				
	MeCN	N^*	0.06	0.98	5.59	0.02	0.009	0.301	15	0.03
		T^*	0.08	-0.51	5.76	0.49				

[a] τ_1 and τ_2 (ns) are the short-lived and long-lived fluorescence lifetimes respectively; α_1 and α_2 are the corresponding relative amplitudes; φ_{N^*}, φ_{T^*} are the fluorescence quantum yields of the N* and T* forms, respectively. $k_R^{N^*}$, $k_{NR}^{N^*}$ ($\times 10^{-9}$ s^{-1}) are respectively the radiative and non-radiative rate constants of the N^* form; k_+ ($\times 10^{-9}$ s^{-1}) is the forward rate constant of the ESIPT reaction. [b] The error for all lifetime values is ± 10%. The excitation wavelength was 320 nm. The time-resolved data for the N* and T* emission bands were recorded at 425 and 540 nm, respectively. α_1 and α_2 values were normalized according to $|\alpha_1| + |\alpha_2| = 1$.

reaction (Table 2). Furthermore, the very small contribution (< 5%) of the long-lived lifetime τ_2 for the N* form provides a strong argument to consider the ESIPT reaction as an irreversible process. Thus, the ESIPT rate constant k_+ could be calculated as recently described [32, 35].

For the two dyes, the slowest ESIPT reaction within the series of aprotic solvents is observed for the most basic solvent DMSO, while the ESIPT reaction rate is one order of magnitude faster in the non-basic acetonitrile. The k_+ values were inversely correlated with the I_{N^*}/I_{T^*} ratio, confirming the direct control of this ratio by the forward ESIPT reaction rate in 3HQs [32, 35]. In this respect, the slow reaction rates in basic solvents like DMSO or DMF may be explained by the rate-limiting disruption of the intermolecular H-bond of the N* form [32] between the basic atoms of DMSO or DMF and the proton of the 3HQ hydroxyl group (Fig. 6). This rate-limiting disruption step is required to allow the formation of the intramolecular H bond between the carbonyl oxygen O-4 and the hydroxyl group, which is needed for the ESIPT reaction. The

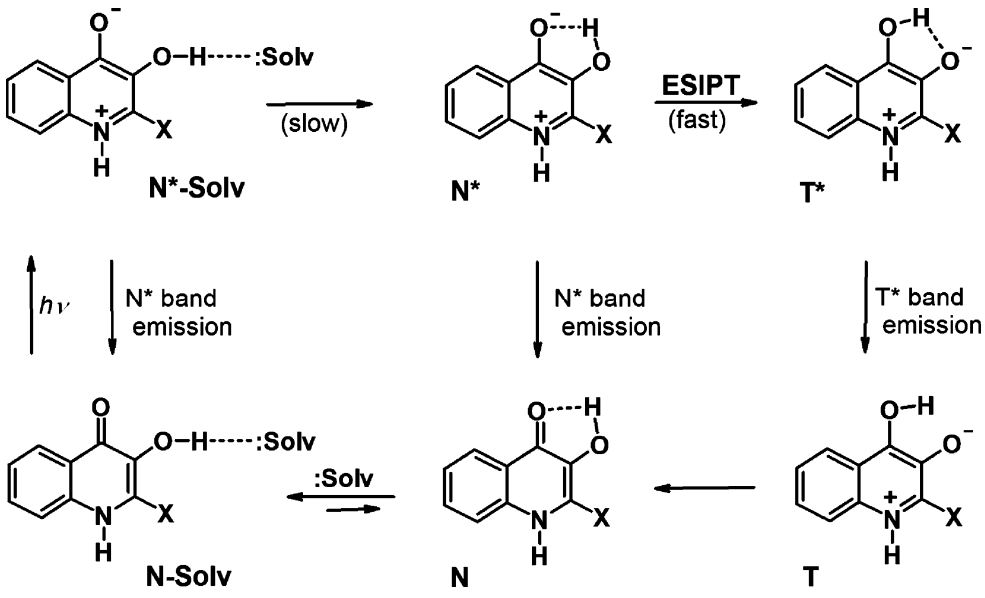

Fig. 6 Proposed excited-state reactions for 3HQ-Bf in basic solvents. In the ground state, 3HQ-Bf is mainly in a solvated form (N-solv) with an intermolecular H-bond between the solvent and the hydroxyl group of 3HQ-Bf. After excitation, the increase of basicity of the O-4 oxygen due to charge displacement in the excited state allows it to compete with the solvent for H-bonding with the hydroxyl group. This results in the rate-limiting formation of the N* form and, its subsequent and irreversible transformation into the T* form by ESIPT. After emission, the T form is thought to rapidly transform into N and finally, N-Solv forms

disruption of the H-bond with the solvent is likely more favored in the excited state than in the ground state, due to the increased basicity of the carbonyl oxygen O-4 in the excited state that allows this oxygen to compete with the solvent for H-bonding with the hydroxyl group. Thus, the excited state reaction rates and the ratio of the emission intensities I_{N*}/I_{T*} of the 3HQ-Bf dye are mainly controlled by the solvent basicity.

Interestingly, 3HQ-Bf exhibits lower ESIPT rate constants than 3HQ-Th in all aprotic solvents. This may result from the smaller steric hindrance provided by the less bulky furyl ring as compared with the thiophene ring on the formation of the intermolecular H-bond between the 3-OH group and the solvent (Fig. 6). As it was shown recently [35], the contact of bulky rings with the 3-OH group of 3HQs increases the ESIPT reaction rate by preserving the intramolecular H-bond for a longer time.

Finally, while the ESIPT reaction rates are different for the two quinolones in aprotic solvents, they appear similar in methanol, indicating that the side ring of the 3HQ derivatives has no influence on the ESIPT reaction in methanol and that the H-bonded complexes are likely different in protic and aprotic solvents.

Conclusions

A novel fluorescent dye, 2-benzofuryl-3-hydroxy-4(1H)-quinolone (3HQ-Bf), was synthesized and studied by absorption, steady-state and time-resolved fluorescence spectroscopy. Due to its totally planar conformation, 3HQ-Bf is characterized by a high fluorescence quantum yield. In solution, this dye demonstrates an excited state intramolecular proton transfer (ESIPT) reaction giving a dual emission resulting from the existence of the two tautomers, N* and T*. The ESIPT reaction in 3HQ-Bf is an irreversible process characterized by rate constants of $0.6–8\times10^{9}$ s^{-1}, depending on the solvent nature. The spectral properties of 3HQ-Bf were found to be exquisitely sensitive to basicity, while being almost non sensitive to polarity. The strong sensitivity of 3HQ-Bf to basicity results from the disruption of its intramolecular H-bond by basic molecules that prevent the ESIPT reaction. As a consequence, since the environment basicity (H-bond acceptor ability) is thought to play an important role in proteins and lipid membranes, 3HQ-Bf appears as a promising fluorophore for the design of probes for studying intermolecular interactions in lipid membranes and proteins.

Acknowledgments This work was supported by the ECO-NET and ARCUS programs from the French Ministère des Affaires Etrangères. DAY and VVS are recipients of a high-level Eiffel Fellowship. VGP was supported by a fellowship from University Louis Pasteur. We are also thankful to Andrey Klymchenko for useful discussion and to Etienne Piémont for help with time-resolved measurements.

References

1. Giuliano KA, Post PL, Hahn KM, Taylor DL (1995) Fluorescent protein biosensors: measurement of molecular dynamics in living cells. Annu. Rev. Biophys. Biomol. Struct. 24:405–434. doi:10.1146/annurev.bb.24.060195.002201
2. Kasha M (1986) Proton-transfer spectroscopy. Perturbation of the tautomerization potential. J. Chem. Soc., Faraday Trans. II 82:2379–2392. doi:10.1039/f29868202379
3. Le Gourrierec D, Ormson SM, Brown RG (1994) Excited-State Intramolecular Proton-Transfer. 2. ESIPT To Oxygen. Prog. React. Kinet. 19:211—275
4. Formosinho SJ, Arnaut LG (1993) Excited state proton transfer reactions. II. Intramolecular reactions. J. Photochem. Photobiol. Chem. 75:21—48. doi:10.1016/1010-6030(93)80158-6
5. Klymchenko A, Oztürk T, Pivovarenko V, Demchenko A (2001) Synthesis and spectroscopic properties of benzo- and naphtho-furyl-3-hydroxychromones. Can. J. Chem. 79:358–363. doi:10.1139/cjc-79-4-358
6. Klymchenko A, Oztürk T, Pivovarenko V, Demchenko A (2001) A 3-hydroxychromone with dramatically improved fluorescence properties. Tetrahedron Lett. 42:7967–7970. doi:10.1016/S0040-4039(01)01723-3
7. Klymchenko A, Oztürk T, Demchenko A (2002) Synthesis of furanochromones: a new step in improvement of fluorescence properties. Tetrahedron Lett. 43:7079–7082. doi:10.1016/S0040-4039(02)01547-2
8. Klymchenko A, Pivovarenko V, Oztürk T, Demchenko A (2003) Modulation of the solvent-dependent dual emission in 3-hydroxychromones by substituents. New J. Chem. 27:1336–1343. doi:10.1039/b302965d
9. Klymchenko A, Demchenko A (2004) 3-Hydroxychromone dyes exhibiting excited-state intramolecular proton transfer in water with efficient two-band fluorescence. New J. Chem. 28:687–692. doi:10.1039/b316149h
10. Klymchenko AS, Pivovarenko VG, Demchenko AP (2003) Perturbation of planarity as the possible mechanism of solvent-dependent variations of fluorescence quantum yield in 2-aryl-3-hydroxychromones. Spectrochim. Acta A Mol. Biomol. Spectrosc. 59:787–792. doi:10.1016/S1386-1425(02)00233-0
11. Shynkar V, Mély Y, Duportail G, Piemont E, Klymchenko A, Demchenko A (2003) Picosecond time-resolved fluorescence studies are consistent with reversible excited-state intramolecular proton transfer in 4'-(dialkylamino)-3-hydroxyflavones. J. Phys. Chem. A 107:9522–9529. doi:10.1021/jp035855n
12. Klymchenko A, Demchenko A (2003) Multiparametric probing of intermolecular interactions with fluorescent dye exhibiting excited state intramolecular proton transfer. Phys. Chem. Chem. Phys. 5:461–468. doi:10.1039/b210352d
13. Pivovarenko V, Wroblewska A, Blazejowski J (2005) 2–[4–(Dimethylamino)phenyll-3-hydroxy-4H-chromene-4-one: A H-bond-sensitive fluorescent probe for investigating binary mixtures of organic solvents. Anal. Chim. Acta 545:74–78. doi:10.1016/j.aca.2005.04.042
14. Ercelen S, Klymchenko A, Demchenko A (2002) Ultrasensitive fluorescent probe for the hydrophobic range of solvent polarities. Anal. Chim. Acta 464:273–287. doi:10.1016/S0003-2670(02)00493-2
15. Nemkovich N, Baumann W, Pivovarenko V (2002) Dipole moments of 4'-aminoflavonols determined using electro-optical absorption measurements or molecular Stark-effect spectroscopy. J. Photochem. Photobiol. Chem. 153:19–24. doi:10.1016/S1010-6030(02)00270-8
16. Klymchenko A, Duportail G, Mély Y, Demchenko A (2003) Ultrasensitive two-color fluorescence probes for dipole potential

in phospholipid membranes. Proc. Natl. Acad. Sci. USA 100:11219–11224. doi:10.1073/pnas.1934603100
17. Bondar O, Pivovarenko V, Rowe E (1998) Flavonols - new fluorescent membrane probes for studying the interdigitation of lipid bilayers. Biochim. Biophys. Acta 1369:119–130. doi:10.1016/S0005-2736(97)00218-6
18. Dennison S, Guharay J, Sengupta P (1999) Excited-state intramolecular proton transfer (ESIPT) and charge transfer (CT) fluorescence probe for model membranes. Spectrochim. Acta A Mol. Biomol. Spectrosc. 55:1127–1132. doi:10.1016/S1386-1425(99)00013-X
19. Shynkar V, Klymchenko A, Duportail G, Demchenko A, Mély Y (2005) Two-color fluorescent probes for imaging the dipole potential of cell plasma membranes. Biochim. Biophys. Acta 1712:128–136. doi:10.1016/j.bbamem.2005.03.015
20. Shynkar V, Klymchenko A, Kunzelmann C, Duportail G, Muller CD, Demchenko A, Freyssinet J, Mély Y (2007) Fluorescent biomembrane probe for ratiometric detection of apoptosis. J. Am. Chem. Soc. 129:2187–2193. doi:10.1021/ja068008h
21. Ercelen S, Klymchenko A, Demchenko A (2003) Novel two-color fluorescence probe with extreme specificity to bovine serum albumin. FEBS Lett. 538:25–28. doi:10.1016/S0014-5793(03)00116-9
22. Klymchenko A, Avilov S, Demchenko A (2004) Resolution of Cys and Lys labeling of alpha-crystallin with site-sensitive fluorescent 3-hydroxyflavone dye. Anal. Biochem. 329:43–57 . doi:10.1016/j.ab.2004.02.031
23. Sytnik A, Gormin D, Kasha M (1994) Interplay between excited-state intramolecular proton transfer and charge transfer in flavonols and their use as protein-binding-site fluorescence probes. Proc. Natl. Acad. Sci. USA 91:11968–11972. doi:10.1073/pnas.91.25.11968
24. Roshal A, Grigorovich A, Doroshenko A, Pivovarenko V, Demchenko A (1998) Flavonols and crown-flavonols as metal cation chelators. The different nature of Ba^{2+} and Mg^{2+} complexes. J. Phys. Chem. 102:5907–5914
25. Poteau X, Saroja G, Spies C, Brown R (2004) The photophysics of some 3-hydroxyflavone derivatives in the presence of protons, alkali metal and alkaline earth cations. J. Photochem. Photobiol., A 162:431–439
26. Pivovarenko V, Vadzyuk O, Kosterin S (2006) Fluorometric detection of adenosine triphosphate with 3-hydroxy-4'-(dimethylamino)flavone in aqueous solutions. J. Fluoresc. 16:9–15. doi:10.1007/s10895-005-0020-5
27. Yushchenko D, Vadzyuk O, Kosterin S, Duportail G, Mély Y, Pivovarenko V (2007) Sensing of adenosine-5'-triphosphate anion in aqueous solutions and mitochondria by a fluorescent 3-hydroxyflavone dye. Anal. Biochem. 369:218–225. doi:10.1016/j.ab.2007.05.005
28. Yushchenko D, Shvadchak V, Klymchenko A, Duportail G, Mély Y, Pivovarenko V (2006) 2-Aryl-3-hydroxyquinolones, a new class of dyes with solvent dependent dual emission due to excited state intramolecular proton transfer. New J. Chem. 30:774–781. doi:10.1039/b601400c
29. Gao F, Johnson KF, Schlenoff JB (1996) Ring closing and photooxidation in nitrogen analogues of 3-hydroxyflavone. J. Chem. Soc., Perkin Trans. 2(2):269–273. doi:10.1039/p29960000269
30. Yushchenko D, Bilokin' M, Pyvovarenko O, Duportail G, Mély Y, Pivovarenko V (2006) Synthesis and fluorescence properties of 2-aryl-3-hydroxyquinolones, a new class of dyes displaying dual fluorescence. Tetrahedron Lett. 47:905–908. doi:10.1016/j.tetlet.2005.11.160
31. Yushchenko D, Shvadchak V, Klymchenko A, Duportail G, Pivovarenko V, Mély Y (2007) Modulation of excited-state intramolecular proton transfer by viscosity in protic media. J. Phys. Chem. A 111:10435–10438. doi:10.1021/jp074726u
32. Yushchenko D, Shvadchak V, Bilokin' M, Klymchenko A, Duportail G, Mély Y, Pivovarenko V (2006) Modulation of dual fluorescence in a 3-hydroxyquinolone dye by perturbation of its intramolecular proton transfer with solvent polarity and basicity. Photochem. Photobiol. Sci. 5:1038–1044. doi:10.1039/b610054f
33. Reichardt C (1994) Solvatochromic Dyes as Solvent Polarity Indicators. Chem. Rev. 94:2319–2358. doi:10.1021/cr00032a005
34. Catalán J (1997) On the ET (30), π*, Py, S'., and SPP Empirical Scales as Descriptors of Nonspecific Solvent Effects. J. Org. Chem. 62:8231–8234. doi:10.1021/jo971040x
35. Yushchenko D, Shvadchak V, Klymchenko A, Duportail G, Pivovarenko V, Mély Y (2007) Steric control of the excited-state intramolecular proton transfer in 3-hydroxyquinolones: Steady-state and time-resolved fluorescence study. J. Phys. Chem. A 111:8986–8992
36. Eastman JW (1967) Quantitative spectrofluorimetry-the fluorescence quantum yield of quinine sulfate. Photochem. Photobiol. 6:55–72. doi:10.1111/j.1751-1097.1967.tb08790.x
37. Dewar MJS, Zoebich EG, Healy EF, Stewart JP (1985) Development and use of quantum mechanical molecular models. 76. AM1: a new general purpose quantum mechanical molecular model. J. Am. Chem. Soc. 107:3902–3909. doi:10.1021/ja00299a024
38. Stewart JJP (2007) MOPAC2007. Stewart Computational Chemistry, Colorado Springs, CO, USA. http://OpenMOPAC.net
39. Livesey AK, Brochon J-C (1987) Analyzing the Distribution of Decay Constants in Pulse-Fluorimetry Using the Maximum Entropy Method. Biophys. J. 52:693–706
40. Lippert, EL (1975) in J. B. Birks (Ed), *Organic Molecular Photophysics*, Wiley, New York, 1975, vol. 2, p. 1-95.
41. Liptay, W (1974) in E. C. Lim (Ed), *Excited States*. Academic Press, New York, pp. 129-175
42. Abraham MH (1993) Hydrogen bonding. XXXI: Construction of a scale of solute effective or summation hydrogen-bond basicity. J. Phys. Org. Chem. 6:660–684. doi:10.1002/poc.610061204
43. Kamlet MJ, Dickinson C, Taft RW (1981) Linear solvation energy relationships Solvent effects on some fluorescence probes. Chem. Phys. Lett. 77:69–72. doi:10.1016/0009-2614(81)85602-3

2.1.3. Effect of viscosity

Fluorescence spectra of 3HQs in glycerol show about 3-fold higher N*/T* band ratio and could be expected basing on solvent polarity and basicity (**Fig. 2.6 A**). We attributed this effect to the viscosity of glycerol, which is about 1000-fold higher then that of water and other common solvents.

To study this phenomenon, 3HQ derivative, 3HQT, was selected. To vary viscosity, we used two alternative approaches, (a) solvent mixtures of different compositions and (b) neat viscous solvents at different temperatures (**Fig. 2.6 B**). Linear relationship between logarithm of viscosity and log(N*/T*) of the dye was found for all the studied solvent systems. The slope of this linear relation varied considerably from one system to another. As a general trend, we observed that, in experiments with temperature variation, the slope of the linear correlation was steeper than that in solvent mixtures. As a consequence, the temperature seems to additionally contribute to the increase in the relative emission of the tautomer (T*) form.

It is important to note that temperature-dependent variation of viscosity did not significantly modify the fluorescence spectrum of 3HQT in aprotic viscous solvents, such as triacetin. The viscosity dependence in the dual emission of 3HQT requires protic environments, and therefore, it is connected with the specific H-bonding interactions of the dye and solvent.

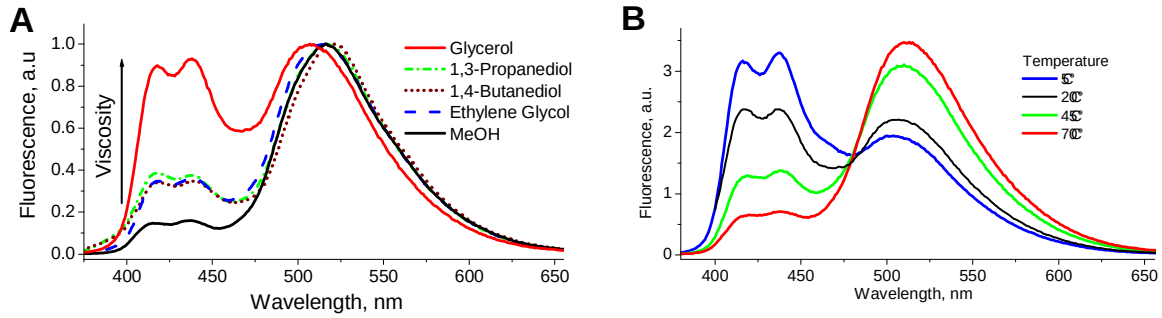

Figure 2.6. (**A**) Normalize Fluorescence spectra of 3HQT in solvents of different viscosity but similar polarity (**B**) Fluorescence spectra of 3HQT in glycerol at different temperatures. Note that overall fluorescence intensity remains almost constant. Excitation wavelength was 360 nm.

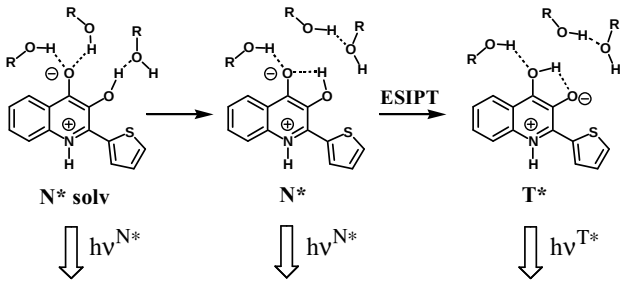

Figure 2.7. Model of excited state transformations of 3HQT in the presence of viscose protic solvent.

Time-resolved fluorescence studies suggest the presence in viscous media of solvated species characterized by decay times close to the slow solvent relaxation times. The intramolecular H-bond in these species is probably disrupted by the solvent (**Fig. 2.7**). Therefore, the ESIPT reaction requires a reorganization of their solvation shell for restoring this intramolecular H-bond. The rearrangement of the solvation shell is viscosity dependent, which explains the effect of viscosity on the ESIPT reaction and the dual emission of the dye. (Article 5)

Article 5

Modulation of excited-state intramolecular proton transfer by viscosity in protic media

THE JOURNAL OF PHYSICAL CHEMISTRY A LETTERS

2007, *111,* 10435−10438
Published on Web 10/02/2007

Modulation of Excited-State Intramolecular Proton Transfer by Viscosity in Protic Media

Dmytro A. Yushchenko,*,†,‡ Volodymyr V. Shvadchak,† Andrey S. Klymchenko,*,† Guy Duportail,† Vasyl G. Pivovarenko,‡ and Yves Mély†

Photophysique des Interactions Biomoléculaires, UMR 7175-LC1 du CNRS, Institut Gilbert Laustriat, Faculté de Pharmacie, Université Louis Pasteur, 67401 Illkirch, France, and Department of Chemistry, Kyiv National Taras Shevchenko University, 01033 Kyiv, Ukraine

Received: June 18, 2007; In Final Form: August 20, 2007

3-Hydroxyquinolones undergo excited-state intramolecular proton transfer (ESIPT), resulting in a dual emission highly sensitive to H-bonding perturbations. Here, we report on the strong effect of viscosity on the dual emission of 2-(2-thienyl)-3-hydroxyquinolone in protic solvents. An increase in viscosity significantly decreases the formation of the ESIPT product, thus changing dramatically the ratio of the two emission bands. Time-resolved studies suggest the presence of solvated species characterized by decay times close to the solvent relaxation times in viscous media. The intramolecular H bond in this species is probably disrupted by the solvent, and therefore, its ESIPT requires a reorganization of the solvation shell for restoring this intramolecular H bond. Thus, the ESIPT reaction of this dye and its dual emission depend on solvent relaxation rates and, therefore, on viscosity. The present results suggest a new physical principle for the fluorescence ratiometric measurement of local viscosity.

1. Introduction

Viscosity is a fundamental parameter in biological systems.[1−5] Since the viscosity distributes heterogeneously on the nanometer scale in living cells, molecular probes are efficient tools for its measurement. Specially designed fluorescent molecular rotors have notably been developed for this purpose.[6−11] These molecules are characterized by a high rotational mobility of their π-conjugated system so that their fluorescence quantum yield depends on this mobility and thus on the viscosity. In order to obtain a ratiometric fluorescent probe of viscosity, which is highly desirable for biological applications,[12,13] a combination of a molecular rotor fluorophore with a reference (environment-insensitive) fluorophore has been realized.[14] However, application of two fluorophores in one sensor complicates the data interpretation since factors like FRET, quenching, and photobleaching of individual fluorophores will interfere with the fluorescence response of this probe. A single fluorophore-based approach for ratiometric measurement of viscosity, which up to now has not been sufficiently explored, is to use the excited-state intramolecular proton-transfer (ESIPT) reaction. In protic environments, which are ubiquitous in biological systems, microviscosity can, in principle, be characterized through the dynamics of H bond exchange that may affect the proton-transfer rate. However, ESIPT is generally poorly dependent on viscosity. One exception is 7-azaindole,[15,16] which undergoes a "solvent assisted" proton transfer. This transfer requires appropriate solvent rearrangement so that the whole process depends on viscosity. Meanwhile, the application of this dye as a viscosity probe in protic media is limited because 7-azaindole exhibits a low fluorescence quantum yield (ca 1%) and a weak variation of the relative intensities of its two emission bands in response to viscosity. Most of other ESIPT dyes are not sensitive to solvent viscosity since their intramolecular H bond forms a stable six-membered ring. This stable intramolecular H bond cannot be readily disrupted by protic solvents, and therefore, no sensitivity to viscosity is observed.[17] In contrast, in dyes with a less stable five-membered H-bonded ring, such as 3-hydroxyflavones (3HF), the intramolecular H bond can be disrupted by protic solvents, leading to a decrease of the ESIPT rate. However, the dual emission of 3HF dyes is also not sensitive to viscosity,[18] probably because the dye forms with a disrupted intramolecular H bond are nonemissive at room temperature.[19] In this respect, the recently introduced 3-hydroxyquinolones (3HQs)[20] are highly promising since they exhibit high fluorescence quantum yields in protic solvents.[21] Moreover, the ESIPT in these dyes occurs (Figure 1) on a slower time scale (around 100 ps),[21,22] which is close to the time scale of solvent relaxation in viscous protic environments ($\geq$100 ps).[23] The ESIPT of 3HQs is highly sensitive to H-bonding perturbations since their intramolecular H bond forms a less stable five-membered ring.[20−22,24] An additional attractive feature of 3HQs is the independence of their fluorescence properties on pH in the biologically relevant range (pH 4−9).[21] However, nothing is reported so far on the effects of viscosity on the fluorescence of 3HQ dyes. Among the 3HQ dyes, *N*-methyl-substituted dyes show a significant sensitivity of their dual emission to solvent polarity, which is observed as an increase in the relative intensity of their normal (N*) emission band with respect to the long wavelength band, belonging to the ESIPT tautomer (T*)

* To whom correspondence should be addressed. E-mail: andrey.klymchenko@pharma.u-strasbg.fr (A.S.K.); dmytro.yushchenko@pharma.u-strasbg.fr (D.A.Y.). Fax: +33 390 244313. Tel: +33 390 24 42 55.
† Université Louis Pasteur. Fax: +33 390 244313. Tel: +33 390 244262.
‡ Kyiv National Taras Shevchenko University.

10.1021/jp074726u CCC: $37.00

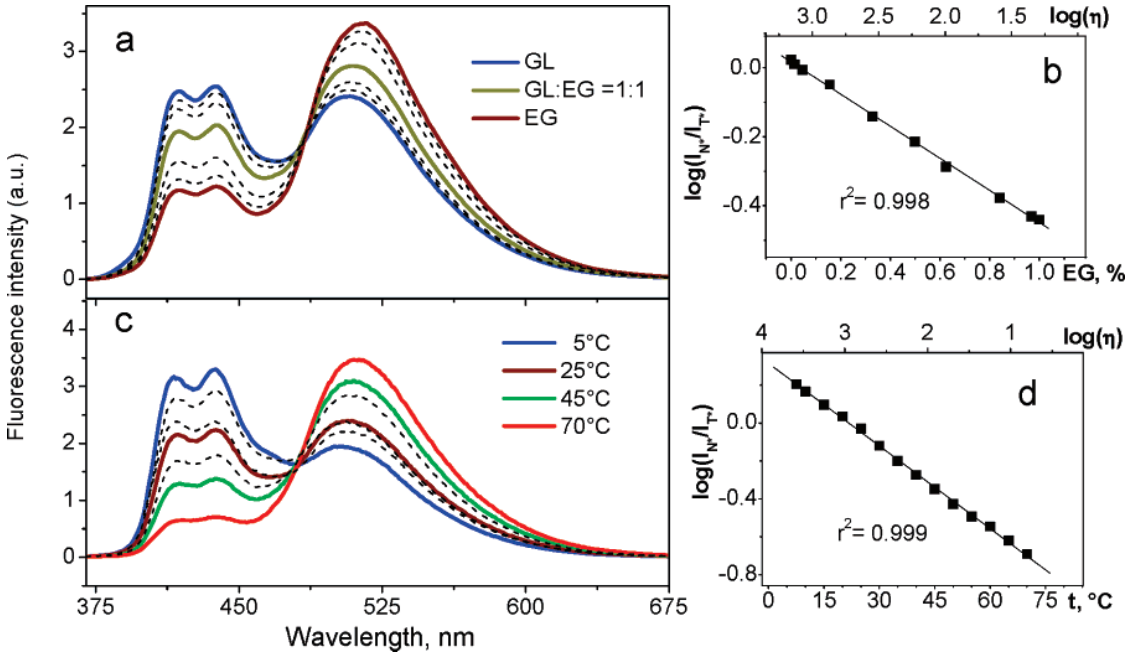

Figure 1. Viscosity dependence of 3HQT fluorescence. The spectra were performed (a and b) in mixtures of ethylene glycol (Eg) and glycerol (Gl) of various compositions at 20 °C and (c and d) in glycerol at various temperatures. The corresponding values of viscosity were taken from the literature.[14,25]

SCHEME 1: 3HQT Dye and Its Excited-State Transformation

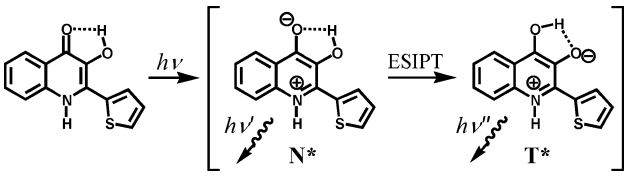

product.[20−22] Meanwhile, N-nonsubstituted 3HQs are poorly sensitive to polarity and show a low relative intensity of their short-wavelength band in most nonviscous organic solvents.[21] Therefore, to study the effect of viscosity independently of polarity, we selected a N-nonsubstituted 3HQ, namely, 2-(2-thienyl)-3-hydroxy-4(1H)-quinolone (3HQT, Scheme 1). Due to the 2-thienyl substituent, this molecule is flat in the ground state and therefore, unlike other 3HQs, exhibits a limited rotational mobility of its 2-aryl group and a rather constant fluorescence quantum yield in a variety of solvents.[21] The dual emission of this dye was found to be highly sensitive to viscosity in protic media, showing a dramatic decrease of the relative intensity of its T* band with increasing viscosities. Time-resolved data suggest that this phenomenon is connected with the viscosity-dependent reorganization of the solvation shell of the dye, which is required for the ESIPT reaction. We expect that the observed phenomenon can be used for the development of new fluorescence ratiometric probes of viscosity.

2. Experimental Section

3HQT dye (Scheme 1) has been synthesized by condensation of the corresponding anthranilic acid ester (prepared from phenacyl bromide and anthranilic acid) in polyphosphoric acid.[21] All of the solvents and chemicals were purchased from Aldrich. The solvents for fluorescence measurements were of spectroscopic grade. The viscosity values for different viscous solvents and their mixtures were taken from the literature.[14,25,26] Absorption spectra (for fluorescence quantum yield calculations) were recorded on a Cary 4 spectrophotometer (Varian) and fluorescence spectra on a FluoroMax 3.0 (Jobin Yvon, Horiba) spectrofluorometer. For fluorescence spectroscopy measurements, the excitation wavelength was systematically 360 nm. For determination of fluorescence quantum yields, quinine sulfate in 0.5 M sulfuric acid ($Q = 0.577$) was used as a reference.[27] In all of the spectroscopic measurements, the concentration of the dye was $\sim 5 \times 10^{-6}$ M.

Time-resolved fluorescence measurements were performed with the time-correlated, single-photon counting technique using the frequency-doubled output of a Ti−sapphire laser (Tsunami, Spectra Physics) pumped by a Millenia X laser (Tsunami, Spectra Physics).[28] The excitation wavelength was set at 320 nm. The fluorescence decays were collected at the magic angle (54.7°) of the emission polarizer. The single-photon events were detected with a microchannel plate Hamamatsu R3809U photomultiplier coupled to a Philips 6954 pulse preamplifier and recorded on a multichannel analyzer (Ortec 7100) calibrated at 25.5 ps/channel. The instrumental response function was recorded with a polished aluminum reflector, and its full-width at half-maximum was 50 ps. The time-resolved decays were analyzed by the iterative reconvolution method.[29] The goodness of the fit was evaluated from the χ^2 values, the plots of the residuals and the autocorrelation function.

3. Results and Discussion

Like other 3HQs, 3HQT shows two emission bands in organic solvents, and the excitation spectra recorded at these two bands are identical.[21,22] These data indicate that 3HQT also undergoes an ESIPT reaction, resulting in the emission of both a normal form (N*) and a phototautomer (T*) (Scheme 1).

To vary viscosity, we used two alternative approaches, (a) solvent mixtures of different compositions and (b) neat viscous solvents at different temperatures. The increase in the glycerol content of a glycerol−ethylene glycol mixture, which increases the solvent viscosity, resulted in a large increase of the intensity ratio of the two emission bands, I_{N^*}/I_{T^*} (Figure 1a). Moreover,

TABLE 1: Time-Resolved Data of 3HQT in Solvent Systems of Different Viscosities[a]

T,°C	Gl,%	τ_1^{N*}, ns	α_1^{N*}	τ_2^{N*}, ns	α_2^{N*}	τ_1^{T*}, ns	α_1^{T*}	τ_2^{T*}, ns	α_2^{T*}	*Q*
20	0	0.59 ± 0.06	1.00			0.51 ± 0.12	−0.40	8.02 ± 0.1	0.60	0.32
20	20	0.66 ± 0.06	0.81	0.69 ± 0.06	0.19	0.55 ± 0.13	−0.37	7.96 ± 0.1	0.63	0.32
20	40	0.59 ± 0.05	0.57	0.99 ± 0.07	0.43	0.55 ± 0.13	−0.32	7.84 ± 0.1	0.68	0.34
20	60	0.57 ± 0.05	0.50	1.22 ± 0.09	0.50					0.36
20	80	0.43 ± 0.05	0.38	1.29 ± 0.09	0.62	0.42 ± 0.11	−0.27	7.53 ± 0.1	0.73	0.36
20	100	0.38 ± 0.04	0.29	1.28 ± 0.09	0.71	0.40 ± 0.11	−0.27	7.53 ± 0.1	0.73	0.36
70	100	0.30 ± 0.04	1.00			0.30 ± 0.10	−0.37	6.38 ± 0.1	0.63	0.36
60	100	0.38 ± 0.04	0.95	0.67 ± 0.06	0.05	0.38 ± 0.11	−0.37	6.66 ± 0.1	0.63	0.39
50	100	0.33 ± 0.04	0.46	0.65 ± 0.06	0.54	0.43 ± 0.11	−0.34	6.91 ± 0.1	0.66	0.33
40	100	0.33 ± 0.04	0.38	0.80 ± 0.07	0.62	0.50 ± 0.12	−0.34	7.16 ± 0.1	0.66	0.37
30	100	0.40 ± 0.05	0.41	1.05 ± 0.08	0.59	0.50 ± 0.12	−0.30	7.35 ± 0.1	0.70	0.37
20	100	0.38 ± 0.04	0.29	1.28 ± 0.09	0.71	0.40 ± 0.11	−0.27	7.53 ± 0.1	0.73	0.36
methanol		0.25 ± 0.03	0.98	1.30 ± 0.09	0.02	0.24 ± 0.09	−0.43	6.73 ± 0.1	0.57	0.30

[a] *T*,°C temperature; Gl,% volume % of glycerol in the mixture with ethylene glycol; τ_1^{N*}, τ_2^{N*}, τ_1^{T*}, and τ_2^{T*} fluorescence decay times recorded at the N* (415 nm) and T* (520 nm) bands; α_1^{N*}, α_2^{N*}, α_1^{T*}, and α_2^{T*} amplitudes of the corresponding decay components; *Q* fluorescence quantum yield.

the logarithm of the intensity ratio ($\log(I_{N*}/I_{T*})$), which is a linear function of different solvent parameters in 3HQ and 3HF derivatives,[21,22,30] exhibited a linear relationship with the glycerol content (Figure 1b). Since the logarithm of the viscosity ($\log \eta$) of this solvent mixture depends linearly on the glycerol content,[14,26] $\log(I_{N*}/I_{T*})$ depends linearly on $\log \eta$ (Figure 1b). Remarkably, a linear correlation between the logarithm of the fluorescence intensity and the logarithm of viscosity was also reported for molecular rotors.[14,31] Variation of the viscosity of glycerol at different temperatures also led to strong I_{N*}/I_{T*} changes (Figure 1c). In this case, the dependence of $\log(I_{N*}/I_{T*})$ on temperature was linear (Figure 1d); therefore, $\log(I_{N*}/I_{T*})$ was also a linear function of $\log \eta$ ($\log \eta$ being a linear function of temperature; see ref 25).

In glycerol−water mixtures as well as in 1,2-propylenglycol and 1,3-propylenglycol at different temperatures, we observed similar linear increases of $\log(I_{N*}/I_{T*})$ as a function of $\log \eta$. The slope of these linear relations varied from one system to another. As a general trend, we observed that, in experiments with temperature variation, the slope of the linear correlation was steeper than that in solvent mixtures. As a consequence, the temperature seems to additionally contribute to the increase in the relative emission of the tautomer (T*) form.

It is important to note that in aprotic solvents (such as toluene, tetrahydrofuran, and acetonitrile), the I_{N*}/I_{T*} ratio was very low; therefore, the emission of the ESIPT product T* dominated.[21] Moreover, a temperature-dependent variation of viscosity in a viscos aprotic solvent triacetin did not significantly modify the fluorescence spectrum of 3HQT (data not shown). Therefore, we can conclude that the viscosity dependence in the dual emission of 3HQT requires protic environments, and therefore, it is connected with the specific H-bonding interactions of the dye and solvent. In order to understand the mechanism of the viscosity-dependent changes of the intensity ratio, we performed time-resolved fluorescence measurements. At relatively low viscosities (neat ethylene glycol and glycerol at 70 °C or methanol), the decay of the N* band was monoexponential. At higher viscosities (with a decrease in the temperature of neat glycerol or an increase in the content of glycerol in mixtures with ethylene glycol), a longer decay component (τ_2^{N*}) appeared, and its relative contribution (α_2^{N*}) increased with the viscosity (Table 1). Moreover, an increase in viscosity resulted in a substantial increase in the decay time τ_2^{N*}, while the shorter component τ_1^{N*} exhibited only slight changes. For the T* emission, the fluorescence decay of 3HQT in glycerol was biexponential. The short decay time τ_1^{T*} exhibited a negative amplitude and corresponded well to the short decay time τ_1^{N*}

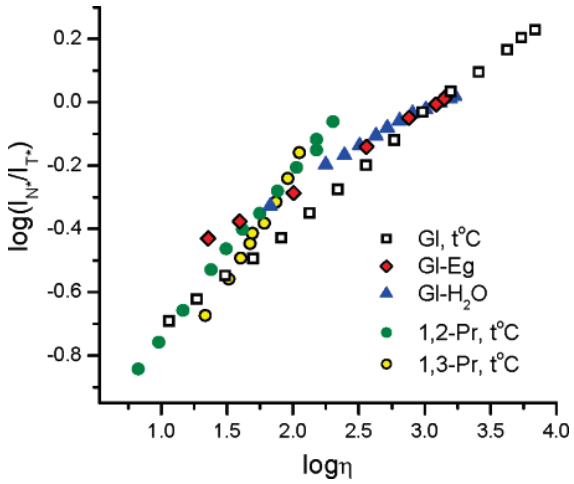

Figure 2. Dependences of $\log(I_{N*}/I_{T*})$ on $\log \eta$. Experiments were performed with glycerol at different temperatures and mixtures of glycerol (Gl) with ethylene glycol (Eg) at 20 °C. 1,2-Pr and 1,3-Pr correspond to 1,2- and 1,3-propylenglycol, respectively. The values of viscosity were taken from the literature.[14,25,26]

recorded at the N* band. This confirms that the T* form is generated from the N* form by an excited-state process (ESIPT).[32] Moreover, the second decay time τ_2^{T*} was more than 10-fold longer than τ_1^{T*} and was absent in the N* band. These results are in accordance with our previous measurements on 3HQs,[21,22] suggesting that the dye undergoes an irreversible ESIPT transformation N* → T* and the rate of this transformation is close to $1/\tau_1^{N*}$ (or $1/\tau_1^{T*}$).[32] Since τ_1^{N*} and τ_1^{T*} did not vary significantly with viscosity, we conclude that the ESIPT rate itself does not depend significantly on viscosity. The long decay time of the T* band τ_2^{T*} was also independent of viscosity, in line with the observed invariant quantum yields (Table 1). Thus, viscosity affects only the long-lived component of the N* emission. What is the origin of this decay time component and how it can be responsible for the strong dependence of the dual emission of the dye on viscosity? Since this component was observed only for the N* emission, we can attribute it to an additional N* form, which cannot undergo ESIPT. It is commonly accepted that the intramolecular H bond closing the five-membered ring in 3HQs and 3HFs can be easily disrupted by a protic solvent, resulting in an inhibition of the ESIPT reaction.[21,22,24] Therefore, the new lifetime observed in viscous solvents could be attributed to a solvated form of the dye (N*-solv) with a disrupted intramolecular H bond. In the excited state, the large increase of basicity of the 4-carbonyl

SCHEME 2: Model of Excited-State Transformations of 3HQT in Viscous Protic Solvents[a]

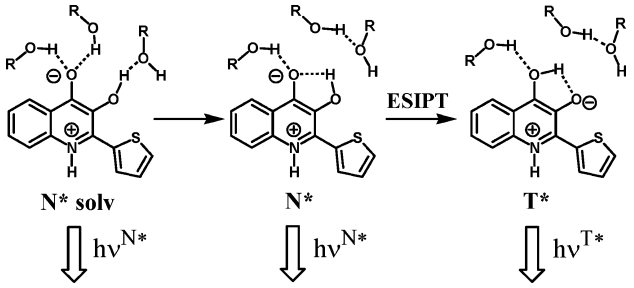

[a] In the solvated form (N*-solv), the intramolecular H bond of 3HQT is disrupted by the protic solvent. In the excited state, the increase of basicity of the 4-carbonyl group favors the intramolecular H bond and, thus, the N*-solv → N* reaction. In viscous solvents, the reorganization of the solvation shell is slowed down, preventing the formation of the N* form and its subsequent transformation into the T* form by ESIPT.

group should favor the intramolecular H bond of the dye and, thus, favor the transformation of the N*-solv form into the N* form. However, this transformation requires the reorganization of the H-bonding network of the solvation shell of the dye (Scheme 2). In relatively low viscosity environments, this process is much faster than ESIPT; therefore, the fluorescence decay of the N*-solv form cannot be detected, and only the decay of the N* form is observed (Table 1). However, with the increase in viscosity, the reorganization of H bonds slows down, and therefore, the decay of the N*-solv form can be resolved as an individual component. Importantly, the observed increase in the decay time of this new component (τ_2^{N*}) from 0.6 up to 1.5 ns upon increase in the solvent viscosity (Table 1) corresponds well to the viscosity-dependent increase in the solvent relaxation times reported in the literature for the relevant glycol systems.[23] Evidently, the decay time τ_2^{N*} and its amplitude α_2^{N*} are directly connected with the viscosity-dependent solvent reorganization rates. In this respect, the ESIPT transformation of 3HQT in viscous protic solvents may have an "activation" step which consists of the formation of the intramolecular H bond due to reorganization of the solvation shell (Scheme 2), which is a viscosity-dependent process. The increase in viscosity slows down this step, which was observed in the fluorescence spectra as an increase in the relative intensity of the short-wavelength emission (Figure 1). In the time-resolved measurements, this was observed as the increase of the τ_2^{N*} value and its amplitude α_2^{N*} (Table 1). A similar "solvent-assisted" two-step proton-transfer mechanism was previously reported for 7-azaindole, which also shows a clear correlation between the rates of proton transfer and the relaxation of the protic solvent.[15,16] Importantly, unlike 7-azaindole, the 3HQT dye shows a strong variation of its dual emission in response to viscosity as well as a high fluorescence quantum yield in protic media (Table 1). These properties make 3HQT and its derivatives attractive for development of fluorescence probes for ratiometric measurements of viscosity.

In conclusion, we report on the dramatic viscosity-dependent changes of the dual emission of a dye that undergoes ESIPT. Time-resolved data reveal an additional excited-state species of the dye in viscous protic solvents. This species is probably highly solvated and, thus, can undergo ESIPT only after an appropriate viscosity-dependent solvent rearrangement. This viscosity-dependent inhibition of the ESIPT reaction suggests a new principle in the design of ratiometric fluorescence probes of viscosity.

Acknowledgment. We thank to the laboratory of Drs. André Mann and Jean Suffert for providing support for the organic synthesis. Dr. A. P. Demchenko is acknowledged for fruitful discussions. D.A.Y. is a member of the European Doctoral College and recipient of an Eiffel Fellowship. V.V.S. is supported by the TriOH European Program.

References and Notes

(1) Luby-Phelps, K. *Int. Rev. Cytol.* **2000**, *192*, 189.
(2) Ohnishi, S. T.; Ohnishi, T. *Membrane Abnormalities in Sickle Cell Disease and in Other Red Blood Cell Disorders*; CRC Press: Boca Raton, FL, 1994.
(3) Moriarty, P. M.; Gibson, C. A.; Kensey, K. R.; Hogenauer, W. *Am. J. Cardiol.* **2004**, *93*, 1044.
(4) Moriarty, P. M.; Gibson, C. A.; Kensey, K. R.; Hogenauer, W. N. *Arterioscler. Thromb., Vasc. Biol.* **2002**, *22*, A47.
(5) Simon, A.; Gariepy, J.; Chironi, G.; Megnien, J. L.; Levenson, J. *J. Hypertens.* **2002**, *20*, 159.
(6) Haidekker, M. A.; Ling, T. T.; Anglo, M.; Stevens, H. Y.; Frangos, J. A.; Theodorakis, E. A. *Chem. Biol.* **2001**, *8*, 123.
(7) Akers, W.; Haidekker, M. A. *J. Biomech. Eng.* **2004**, *126*, 340.
(8) Benjelloun, A.; Geoffroy-Chapotot, C.; Brembilla, A.; Adrian, M.; Viriot, M. L.; Lochon, P. *Polym. Int.* **1999**, *48*, 293.
(9) Akers, W. J.; Haidekker, M. A. *J. Biomech. Eng.* **2005**, *127*, 450.
(10) Haidekker, M. A.; Tsai, A. G.; Brady, T.; Stevens, H. Y.; Frangos, J. A.; Theodorakis, E.; Intaglietta, M. *Am. J. Physiol. Heart Circ. Physiol.* **2002**, *282*, H1609.
(11) Damas, C.; Adibnejad, M.; Benjelloun, A.; Brembilla, A.; Carre, M. C.; Viriot, M. L.; Lochon, P. *Colloid Polym. Sci.* **1997**, *275*, 364.
(12) Demchenko, A. P. *Lab Chip* **2005**, *5*, 1210.
(13) Silver, R. B. *Methods Cell Biol.* **1998**, *56*, 237.
(14) Haidekker, M. A.; Brady, T. P.; Lichlyter, D.; Theodorakis, E. A. *J. Am. Chem. Soc.* **2006**, *128*, 398.
(15) McMorrow, D.; Aartsma, T. J. *Chem. Phys. Lett.* **1986**, *125*, 581.
(16) Moog, R. S.; Maroncelli, M. *J. Phys. Chem.* **1991**, *95*, 10359.
(17) Formosinho, S. J.; Arnaut, L. J. *J. Photochem. Photobiol., A.* **1993**, *75*, 21.
(18) Strandjord, A. J. G.; Barbara, P. F. *J. Phys. Chem.* **1985**, *89*, 2355−2361.
(19) Klymchenko, A. S.; Pivovarenko, V. G.; Demchenko, A. P. *Spectrochim. Acta, Part A* **2003**, *59*, 787.
(20) Yushchenko, D. A.; Bilokin', M. D.; Pyvovarenko, O. V.; Duportail, G.; Mély, Y.; Pivovarenko, V. G. *Tetrahedron Lett.* **2006**, *47*, 905.
(21) Yushchenko, D. A.; Shvadchak, V. V.; Klymchenko, A. S.; Duportail, G.; Mely, Y.; Pivovarenko, V. G. *New J. Chem.* **2006**, *30*, 774.
(22) Yushchenko, D. A.; Shvadchak, V. V.; Bilokin', M. D.; Klymchenko, A. S.; Duportail, G.; Mély, Y.; Pivovarenko, V. G. *Photochem. Photobiol. Sci.* **2006**, *5*, 1038.
(23) Garg, S. K.; Smyth, C. P. *J. Phys. Chem.* **1965**, *69*, 1294.
(24) McMorrow, D.; Kasha, M. *J. Phys. Chem.* **1984**, *88*, 2235.
(25) Gray, D. E. *American Institute of Physics Handbook*, 2nd ed.; McGraw-Hill: New York, 1963.
(26) George, J.; Sastry, N. V. *J. Chem. Eng. Data* **2003**, *48*, 1529.
(27) Eastman, J. W. *Photochem. Photobiol.* **1967**, *6*, 55.
(28) Shynkar, V. V.; Mély, Y.; Duportail, G.; Piémont, E.; Klymchenko, A. S.; Demchenko, A. P. *J. Phys. Chem. A* **2003**, *107*, 9522.
(29) Dharia, J. R.; Johnson, K. F.; Schlenoff, J. B. *Macromolecules* **1994**, *27*, 5167.
(30) Klymchenko, A. S.; Demchenko, A. P. *Phys. Chem. Chem. Phys.* **2003**, *5*, 461.
(31) Forster, Th.; Hoffmann, G. *Z. Phys. Chem.* **1971**, *75*, 63.
(32) Laws, W. R.; Brand, L. *J. Phys. Chem.* **1979**, *83*, 795.

2.1.4. Isotopic effect: Application to water detection

ESIPT reaction in 3HQs is irreversible and the ratio of their two emission bands (N*/T*) is controlled by the proton transfer rate. Any factor that slows down ESIPT increases also the N*/T* ratio.

Substitution of the proton in the 3-OH group of the fluorophore by its heavier isotope (deuterium) decreases the ESIPT reaction rate and thus, deuterated analog 3DMQs shows 3-fold higher N*/T* band ratio than 3HMQs (**Fig. 2.8)**.

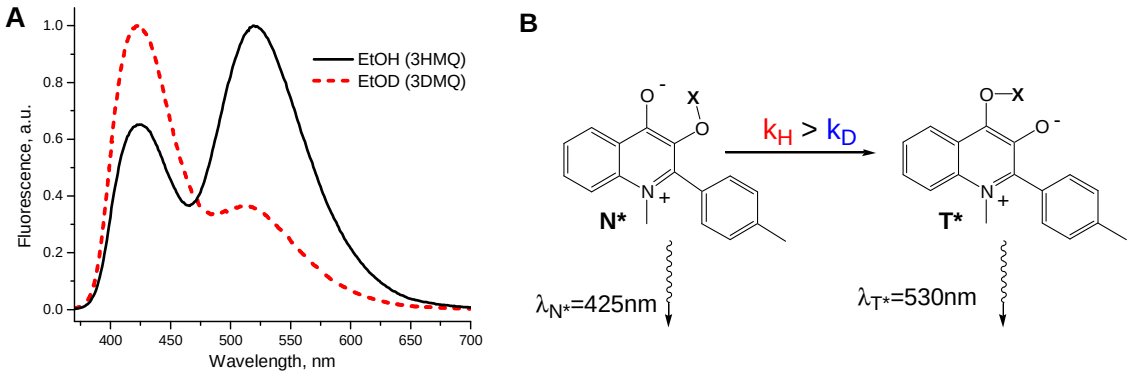

Figure 2.8. (**A**) Normalized fluorescence emission spectra of 3HMQ and 3DMQ in EtOH and EtOD respectively (λ_{ex}= 360 nm) and (**B**) scheme of excited state intramolecular proton (deuterium) transfer.

Isotopic exchange in protic solvents occurs very rapidly and in EtOD/EtOH mixtures ratio of concentration of deuterated (3DMQ) and protonated (3HMQ) dye is equal to the ratio of deuterated and not deuterated solvent (**Fig. 2.9**). Therefore, the recorded fluorescence spectrum of the dye depends on the molar fraction of the deuterated solvent component and on the relative quantum yields of 3DMQ and 3HMQ. Practically the relationship N*/T* ratio *vs*. concentration of the deuterated solvent component is close to linear (**Fig. 2.9 B**). Thus, the N*/T* emission band ratio determines D/H ratio in the system.

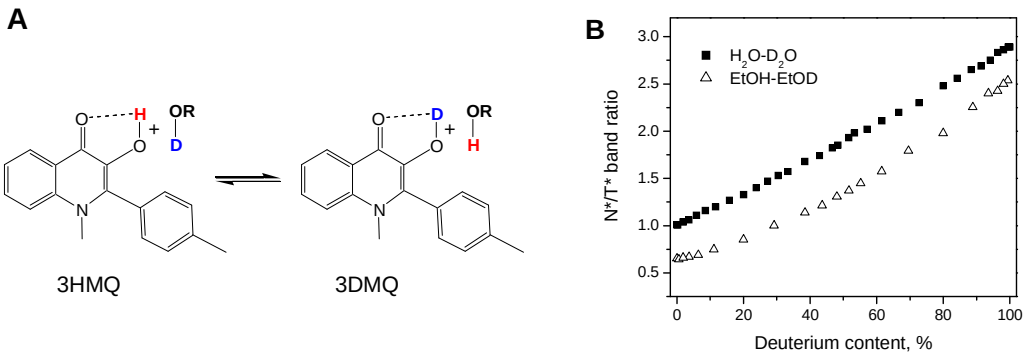

Figure 2.9. (**A**) Isotopic exchange in 3HMQ/3DMQ (**B**) Influence of the deuterium content on the N*/T* band ratio.

In aprotic solvents 3DMQ and 3HMD also show different emission spectra (**Fig. 2.10**). Moreover, the addition of water to 3DMQ solution in DMF switches its fluorescence spectrum to that of 3HMQ due to the fast deuterium-proton exchange. As in the case of protic solvents fluorescence depends on the ratio of OH groups and OD groups in the system. This allows highly sensitive detection of water, because the spectrum of the dye depends practically on the concentration ratio water/deuterated dye. The fluorescence spectrum of the 3HQ dye could be easily measured at 10 nM concentration, which gives about 1 p.p.b. detection limit for water in aprotic solvents. Normally, much higher concentrations of water and other protic impurities are present and signal would be saturated due to negligible concentration of 3DMQ in respect to water. To overcome this problem the sensitivity of the method could be decreased by increasing the deuterium concentration, for example, by addition of higher amount of deuterated dye. Another possibility is addition of known amount of D_2O to the system. In this case H_2O concentration could be easily calculated from H/D ratio (determined from the fluorescence spectrum) and D_2O concentration. It can be seen from **Fig. 2.10**, that the sensitivity range could be easily shifted to higher water concentrations by addition of the deuterated component.

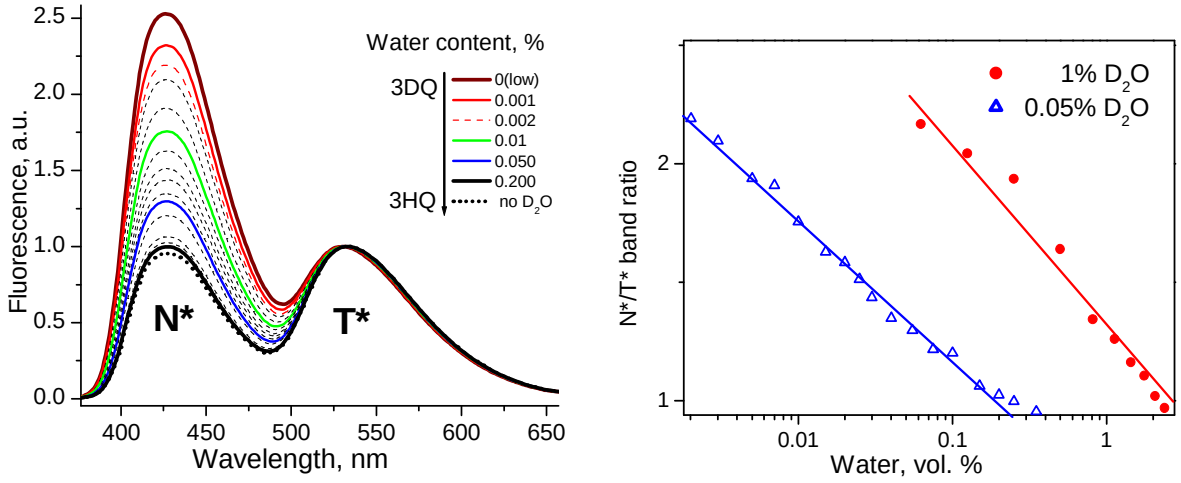

Figure 2.10. (**A**) Fluorescence spectra of 3HMQ in DMF solutions containing 0.005% D_2O and different amounts of H_2O. (λ_{ex}= 360 nm) The spectra were normalised at 520nm.
(**B**) Titration curves of DMF containing 0.05% (blue) and 1% (red) of D_2O. The N*/T* emission band ratio of the dye depend on the H_2O/D_2O ratio.

This approach could be used for detection of any protic impurities in aprotic systems. Up to now many fluorescent dyes were proposed for water detection in organic solvents but all of them sense the presence of water either through changes of bulk media parameters or through specific dye-water interactions. In the case of a 3HQ dye we have realized direct response based on hydrogen/deuterium exchange that provides significantly enhanced sensitivity, which is limited only by the sensitivity of the fluorescence detection technique.

2.2. 3-Hydroxychromones for peptide labeling

Dyes of 3-hydroxychromone family are used as solvatochromic probes for different systems, namely as covalent and non-covalent labels for proteins and membranes. In most cased derivatives of 4'-dialkylamino-3-hydroxyflavone are applied because of theirs strong sensitivity to polarity in aprotic systems. In lipid membranes they show highly efficient dual emission and therefore are suitable for probing their properties. Meantime application of these dyes in the aqueous media is limited due to the absence of the T* emission band and low quantum yields. Fluorescence dyes with environment-sensitive dual emission in polar media are needed for monitoring interactions of small proteins and peptides in aqueous environment. This issue was addressed by introducing 2-fury-3-hydroxychromones that have two-band fluorescence in protic media [103]. Some of them, like 6-bromomethyl derivatives were successfully used for covalent labelling of -SH groups in α-crystallin for investigating its conformational changes [111] and in short peptides [262] for monitoring their interaction with antibodies.

In this study we compared fluorescence properties of 4'-dialkylamino-3-hydroxyflavones with 2-fury/thienyl-3-hydroxychromones in order to be able to select dye with polarity sensitivity range suitable for a particular task.

2.2.1. 2-Furyl and 2-thienyl 3-hydroxychromones

2-Furyl-3-hydroxychromone (**1**), its thienyl analogue (**2**) and 6-acetamido-2-fury-3-hydroxychromone (**3**) were selected for studies of solvent effect on the fluorescence properties of the dyes.

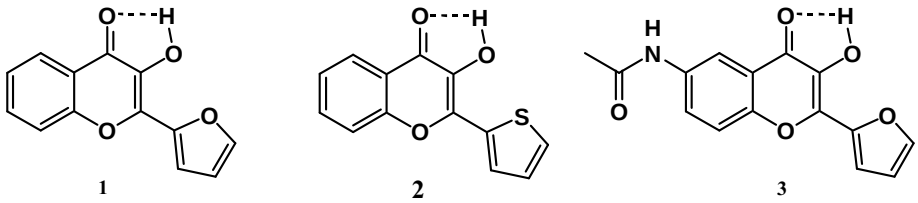

2-Furyl-3-hydroxychromone was previously reported to show good fluorescence quantum yield and dual emission in water [103]. The 2-thienyl-analogue **2** was expected to show similar fluorescence properties, while it is potentially interesting due to its higher chemical stability. Compound **3** is an intermediate compound that can be further derivatized into to an amino-reactive label. Its characterization is required to evaluate the substituent effect.

As expected, all three selected dyes undergo ESIPT and show two-colour fluorescence in protic and aprotic solvents (**Fig. 2.11** and **2.12**). The N* and T* emission bands are well separated (about 120 nm) and of comparable intensities in methanol. Meanwhile in aprotic DMF,

a solvent of similar polarity, the N*/T* band ratio is about 10-fold lower. This strong effect could be explained by inhibition effect of H-bond donor (acidic) solvent on the ESIPT process. In contrary, these dyes show no sensitivity to environment basicity (H-bond acceptor ability). This sensitivity profile is opposite to one observed in the case of 3-hydroxyquinolones (Chapter 2.1).

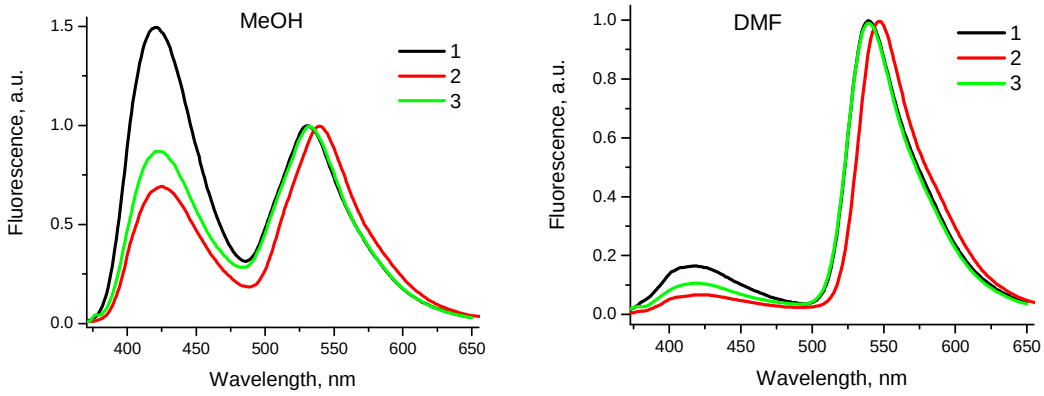

Figure 2.11. Comparison of the fluorescence emission spectra of dyes 1, 2 and 3 in methanol (**A**) and DMF (**B**) (λ_{ex}= 340 nm).

An additional effect of H-bond donor properties of the media is blue shift of the T* band. In water it reaches 35nm in comparison with DMF (**Table 2.1**). Thus, T* band position could be used as an independent information channel that monitors environment hydration.

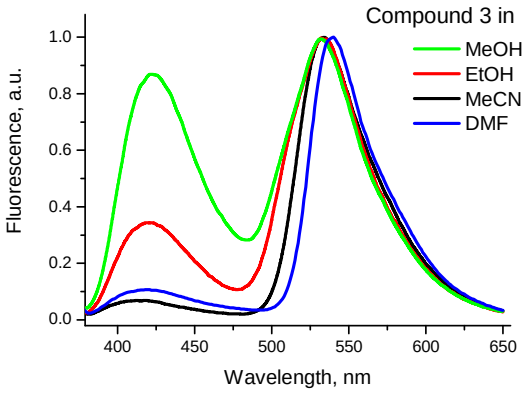

Figure 2.12. Normalized fluorescence spectra of the dye 3 in protic (methanol, ethanol) and aprotic (DMF, acetonitrile) organic solvents (λ_{ex}= 340 nm).

The studied dyes **1-3** provide similar response to changes in the environment. They also exhibit similar positions of the absorption and the emission band maxima. Meantime compounds **2** and **3** show about 2-fold lower N*/T* band ratio compared to compound **1** in the same conditions (**Fig. 2.11**). Thus, the optimal sensitivity range of 2-thienyl-3-hydroxychromone corresponds to higher polarities as compared to its 2-furyl analogue. 6-Acetamido derivative shows intermediate properties, so that the suitable N*/T* band ratio is observed in the range of polarities from water to ethanol.

Table 2.1. Spectral properties of dyes **1**-**3**

Solvent	Dye	λ_{ABS}, nm	λ_{N^*}, nm	λ_{T^*}, nm	N*/T*	φ, %
Water	**1**	358	427	513	(≈3)	4.5
(α=1.17,[b]	**2**	363	432	510	1.53	2.1
ε=78.4)	**3**	357	431	506	1.61	2.3
MeOH	**1**	356	416	527	1.71	8.1
(α=0.43,	**2**	359	425	540	0.70	6
ε=32.6)	**3**	349	422	532	0.88	6.3
EtOH	**1**	357	416	531	0.65	8
(α=0.37,	**2**	361	422	540	0.28	5.5
ε=24.9)	**3**	351	422	532	0.35	6.2
DMF	**1**	354	418	539	0.13	7
(α=0,	**2**	359	420	547	0.07	7.1
ε=37.2)	**3**	344	420	540	0.11	8.1
CH_3CN	**1**	348	409	533	0.10	6
(α=0,	**2**	355	415	539	0.06	6.2
ε=35.7)	**3**	346	413	534	0.07	5.8
EtOAc	**1**					
(α=0,	**2**	355	413	543	0.05	9.7
ε=5.99)	**3**	345	413	535	0.05	12.1

λ_{abs} – position of absorption maxima, λ_{N^*} and λ_{T^*} - position of fluorescence maxima of N* and T* forms respectively. N*/T* - ratio of the intensities of the two emission bands at their peak maxima. φ - fluorescence quantum yield. Excitanion wavelength in all the cases was 340nm.

2.2.2. 4'-Dimethylamino-3-hydroxyflavone

Fluorescence properties of 4'-dimethylamino-3-hydroxyflavone are well described (see literature review). It discriminates clearly protic and aprotic environments showing one-band and two-band fluorescence, respectively [80]. Observed difference could be attributed to the H-bonding of solvent H-bond donors with the 4-carbonyl group [82]. In aprotic environment emission band ratio depends strictly on the solvent polarity due to excited-state equilibrium between N* and T* forms. Similar dyes were used for study properties of lipid membrane [115-117, 121, 122].

Compound **4** bearing acetamide group at position 6 shows fluorescence properties close to the non-substituted fluorophore. It shows good quantum yield in all solvents except water. In aprotic media ratio of N* and T* emission bands correlates with polarity (**Fig. 2.13**). Meanwhile in

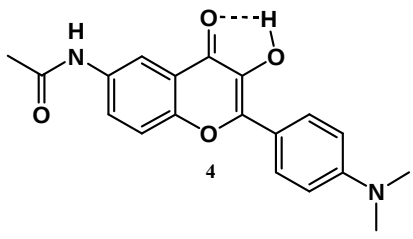

4

alcohols and water only one emission band is observed. Nevertheless its position could be used for rough estimation of polarity (**Table 2.2**).

Table 2.2. Spectral properties dye **4**

	Solvent	λ_{ABS}, nm	λ_{N^*}, nm	λ_{T^*}, nm	N*/T*	φ, %
aprotic	Toluene	403	466	566	0.05	22.6
	EtOAc	396	487	567	0.34	9.5
	THF	398	491	571	0.29	9.2
	CH_2Cl_2	409	493	568	0.62	29.4
	CH_3CN	399	515	566	1.15	15.4
	DMF	399	511	578	0.81	13.8
	DMSO	405	519	579	1.30	18.3
protic	EtOH	408	529	-	-	48.2
	MeOH	406	533	-	-	26.2
	H_2O	394	551	-	-	0.4

[a] λ_{abs} – position of absorption maxima, λ_{N^*} and λ_{T^*} - position of fluorescence maxima of N* and T* forms. N*/T* - ratio of the intensities of the two emission bands at their peak maxima. φ - fluorescence quantum yield. Excitanion wavelength in all the cases was 400nm.

Fluorescence properties of **4** in aprotic solvents allow us to suggest application of this fluorophore for sensing properties of membrane environment. To check this we measured the dye fluorescence in liposomes. Relatively apolar compound **4** is able to bind lipid membranes due to the hydrophobic interactions. It shows two-band fluorescence in liposome suspensions. As the binding is not covalent, location of the dye in the membrane is not fixed and spectra could not be attributed to exact environment. Nevertheless it is clearly seen that dye **4** shows two emission bands of comparable intensity, which indicates that its binding site in membranes is of medium polarity.

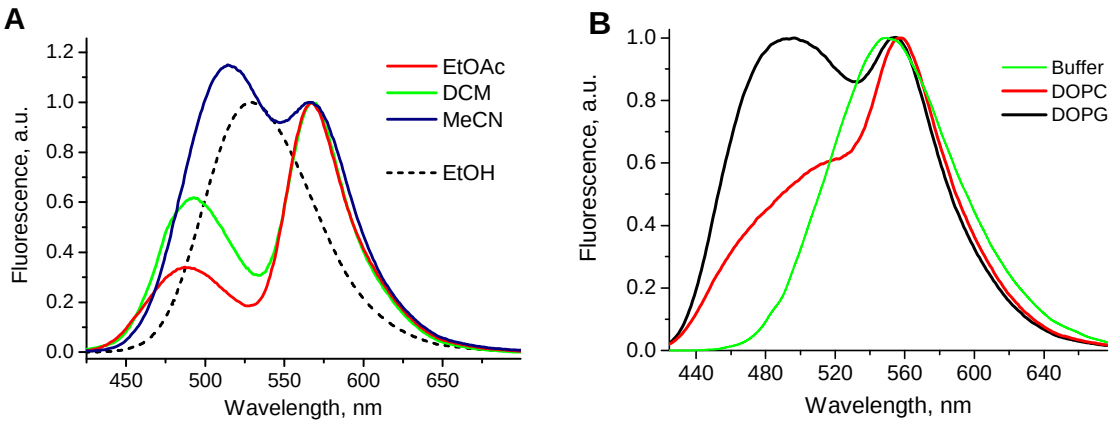

Figure 2.13. Normalized fluorescence spectra of the dye **4** in (**A**) aprotic organic solvents (ethyl acetate, dichloromethane, acetonitrile) compared with ethanol and (**B**) neutral (DOPC) and negatively charged (DOPG) liposome suspension compared with buffer (λ_{ex}= 400 nm). Dye per lipid ratio was 1: 500.

2.3. Comparison of 3HQs and 3HCs

The dual emission of 3HQ dyes is sensitive to solvent polarity, H-bond donor ability, H-bond acceptor ability and viscosity. This poor selectivity of the dye to particular physico-chemical property of the environment makes 3HQs unsuitable for application as sensors of biomolecular interaction. In contrast, the dual emission 3HC dyes is sensitive only to solvent polarity and H-bond donor ability, which correlate directly with the environment hydration.

As it will be shown below biomolecular interactions frequently lead to decrease in the environment polarity and hydration. While for 3HC dyes it leads to clear decrease in the N*/T* ratio, for 3HQ dyes it results in an unclear spectroscopic effects, due to influence of other parameters changing during the interaction. Moreover, none of the studied 3HQs is suitable for sensing interactions with membranes, because of the low N*/T* band ratio in apolar systems. Therefore, we focused our studies mainly on application of 3HC dyes for sensing peptide-oligonucleotide and peptide membrane interactions.

2.4. Synthesis and properties of amino group reactive labels

Since dyes **3** and **4** showed suitable fluorescence properties, we utilized them for construction of fluorescent labels for solid phase peptide synthesis. Formation of amide bond with N-terminal amino group was selected as dye-peptide coupling method due to high stability of the formed bond. Consequently labels should contain non-hindered carboxyl group. It could be easily introduced by chemical modifications of the 6-acetamido group in 3HC dyes.

The complete synthesis of FCL and MFL labels based on dyes **3** and **4** respectively is shown on the **Fig. 2.14**. The key point of the synthesis was coupling of *ortho*-hydroxyacetophenone with aromatic aldehyde followed by oxidization (Algar-Flynn-Oyamada Reaction) to give 3-hydroxychromones **3** and **4**. Hydrolysis of 6-acetamido groups in **3** and **4** followed by acylation by succinic anhydride afforded the desired labels FCL and MFL, respectively. After purification their identity and purity were confirmed by NMR and HPLC. Both labels are greatly soluble in polar organic solvents that are used for the solid phase peptide synthesis, namely DMF and NMP.

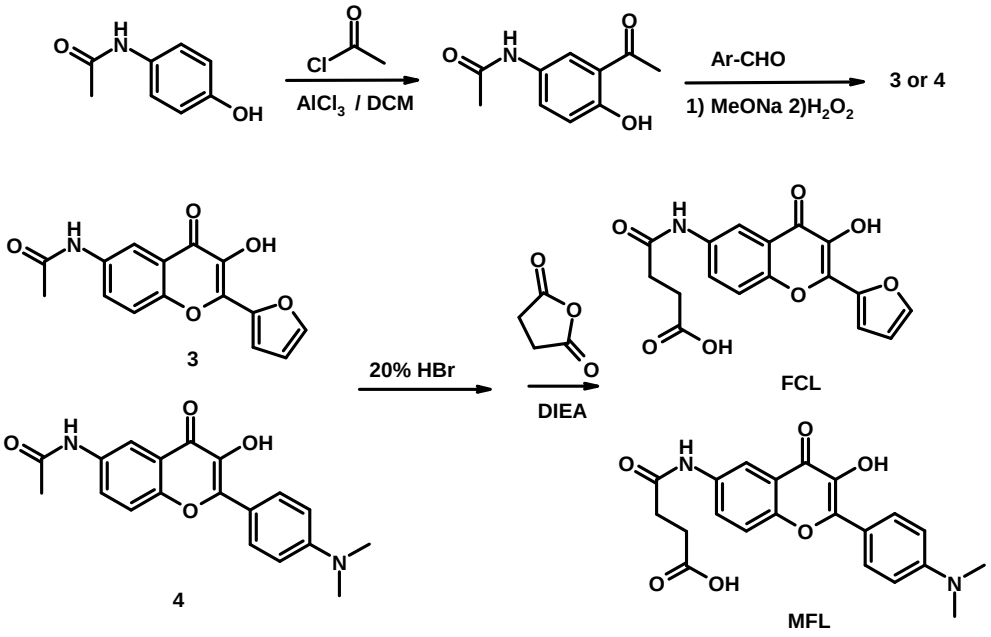

Figure 2.14. Synthesis of the fluorescent labels FCL and MFL.

Spectroscopic properties of the new labels were studied and compared with properties of the parent dyes **3** and **4**. FCL shows absorption maxima about 350 nm and extinction coefficient about 15000 $M^{-1}cm^{-1}$. Meanwhile, MFL exhibited absorption maximum around 400 nm and

more than twice as high extinction coefficient (33000 $M^{-1}cm^{-1}$). Thus, for the both labels the absorption properties are close to the parent fluorophores. According to the fluorescence measurements, in the tested solvents FCL showed the same position of the two emission bands as dye **3**. Moreover, the N*/T* band ratio is almost identical in all solvents except water (**Fig. 2.15**, **Table 2.3**) where aliphatic linker can disturb water solvation shell and provide some apparent decrease in the local polarity. Similarly to the parent dye **4**, MFL show one emission band in protic solvents and two in aprotic ones. Moreover only the slight differences in the N*/T* ratio and the emission band maxima were observed between these two dyes (**Table 2.3**). Thus, both absorption and fluorescence properties of FCL and MFL are also close to the properties of the dyes **3** and **4** respectively (**Table 2.3**, **Fig. 2.15**). Therefore, the extensive experimental data obtained for the parent dyes **3** and **4** in different solvents could be used as a reference for estimating of environment of FCL and MFL labels grafted to the biomolecules.

Table 2.3. Comparison of labels and parent fluorophores

Solvent	Dye	λ_{ABS}, nm	λ_{N^*}, nm	λ_{T^*}, nm	N*/T*	φ, %
DMF	3	344	420	540	0.11	8.1
	FCL	344	421	539	0.10	6.9
H_2O	3	357	431	506	1.61	2.3
	FCL	357	431	508	1.47	2.0
EtOH	3	351	420	535	0.34	6.1
	FCL	351	422	532	0.35	6.2
CH_3CN	4	399	515	566	1.15	15.4
	MFL	400	515	565	1.12	10.2
DMF	4	399	511	578	0.81	13.8
	MFL	399	510	577	0.79	9.0
H_2O	4	394	551	-	-	0.4
	MFL	394	555	-	-	0.5

λ_{abs} – position of absorption maxima, λ_{N^*} and λ_{T^*} - position of fluorescence maxima of N* and T* forms. N*/T* - ratio of the intensities of the two emission bands at their peak maxima. φ - fluorescence quantum yield. Excitanion wavelength was 340 nm (**3** and FCL) or 400 nm (**4** and MFL).

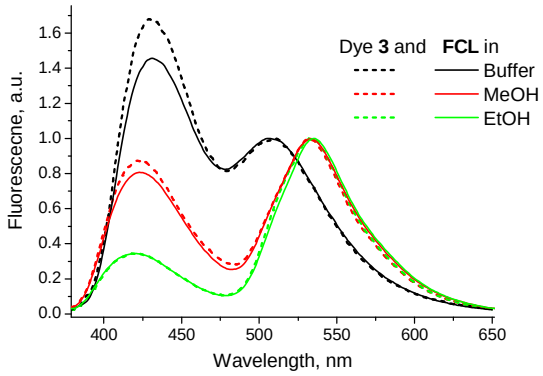

Figure 2.15. Comparison of fluorescence properties of FCL (solid lines) and the dye 3 (dashed lines). Spectra were normalized at T* emission band.

3. Sensing peptide interactions by 3HC labels

Peptides interact with three main types of biological targets: nucleic acids (DNA, RNA), biomembranes and other peptides or proteins. Application of the labeled peptides for sensing peptide-target interactions is efficient only if they meet two criteria:

1) Biological properties of a peptide (protein) are not affected by the labeling.

2) Label provides strong response to an interaction event.

Regarding the first criteria, FCL and MFL are non-charged fluorophores of a relatively small size and should disturb peptide properties much less than widely used fluoresceine or rhodamine. Nevertheless, to minimize possible problems a flexible four-atom linker was introduced between the fluorophore and the reactive carboxylic group of the label.

Strong sensitivity of FCL and MFL to the environment properties was shown above. Moreover, due to their dual emission 3HC-based labels are suitable for precise ratiometric fluorescence detection and they provide additional spectroscopic information channels for analysis of the probe environment.

3.1. Peptide synthesis and characterization

3.1.1. Synthesis of labeled peptides

Solid phase peptide synthesis is the most convenient way to produce modified peptides of up to 70 amino acids. It combines high yields of the products with relatively easy handling. All peptides used in this work were synthesized on solid support using Fmoc chemistry and automatic peptide synthesizer. **Fig. 3.1** shows a representative example of a synthetic procedure.

For coupling of the labels to peptides the N-terminal amino group was selected. This position is preferable to other reactive groups since, commonly, it does not participate in peptide (protein) interactions. Thus biochemical properties of a peptide labeled by its N-terminus should be close to the non-labeled one. Moreover, presence of the N-terminal amino group in all peptides makes such approach universal and allows comparison between different systems. The labeling was done before side-chain deprotection to ensure specific dye introduction at the N-terminus of peptide.

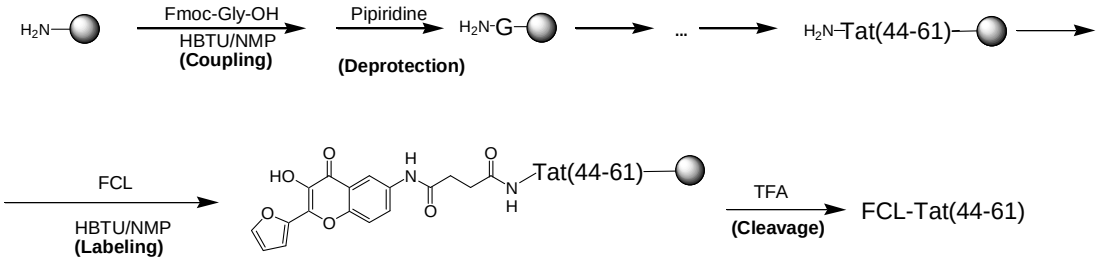

Figure 3.1. Synthesis of FCL-Tat(44-61). Amino acid sequence was built on solid support (represented as grey balls) by repetitive coupling/deprotection cycles. Then it was labeled by FCL and cleaved with parallel side-chain deprotection.

To achieve high peptide synthesis yields, natural Fmoc-protected amino acids were used in a ten-fold excess and an HBTU coupling reagent is applied. For coupling of the label to the peptide only four-fold excess was used, which was compensated by increased coupling time to 4 hours. The HPLC analysis of all obtained peptides shows more than 90% labeling efficiency by this method.

Cleavage of the peptides from solid-phase support and amino acid side chains deprotection were performed in 95% TFA. To protect reactive amino acids in such harsh conditions, so-called "scavengers" were added. Both FCL and MFL labels were found to be stable in standard cleavage conditions applied to peptides (reaction mixture contains ethanedithiol or triisopropylsilane to avoid formation of carbocations).

After the cleavage peptides were precipitated, filtered, purified by the reverse-phase HPLC and characterized by mass-spectroscopy. Since the procedure of the standard solid-phase peptide synthesis was not modified for N-terminal peptide labeling with MFL and FCL, we can conclude that these dyes are convenient for labeling of variety of peptides at their N-terminus.

3.1.2. Fluorescence properties of the labeled peptides

Coupling to peptides could affect spectroscopic properties of labels. To characterize the coupling effect on the FCL fluorescence, a short peptide composed of five glycines (G5) was synthesized and labeled at its N-terminus. This peptide is neutral and has no amino acid side chain groups able to interact specifically with the fluorophore. Nevertheless the labeled peptide (FCL-G5) showed about 10% decrease in the N*/T* band ratio, 3 nm T* red-shift of T* band and 50% increase in fluorescence quantum yield in respect to the free label (**Fig. 3.2**, **Table 3.1**). These changes indicate that interactions of the probe with the flexible backbone of the G5 peptide can reduce the overall accessibility of the probe to water molecules. Coupling of the label to another short peptide A12C leaded to similar effects (**Table 3.1**) For the large peptide FCL-NC(11-55), the differences from the free label fluorescence are more significant. Four-fold increase in the fluorescence quantum yield, 25% N*/T* band ratio

decrease and especially 10 nm red-shift of the T* band indicate decrease of local environment polarity and hydration. These effects are not directly connected with peptide size. Short but highly basic FCL-Tat(44-61) shows approximately the same fluorescence properties as FCL-NC(11-55). Likely, observed label environment changes are due to more efficient screening of the label from bulk water by side chains of the peptide amino acids. In the case of FCL-NC(1-55) this screening is stronger then in others because label emission spectrum is much more modified than in others peptides.

Surprisingly, for two labeled peptides FCL-K15C and FCL-NC(11-55) an 8 nm blue shift of the N* emission band was observed. This effect is not accompanied by the T* band maxima shift or the N*/T* band ratio change that reflect environment polarity and hydration. Meantime, in both cases in contrary to other studied peptides, the label is connected to a positively-charged N-terminal amino acid (Lys), suggesting that the charge of the neighboring amino acid side chain affects the position of the N* band maximum of the label.

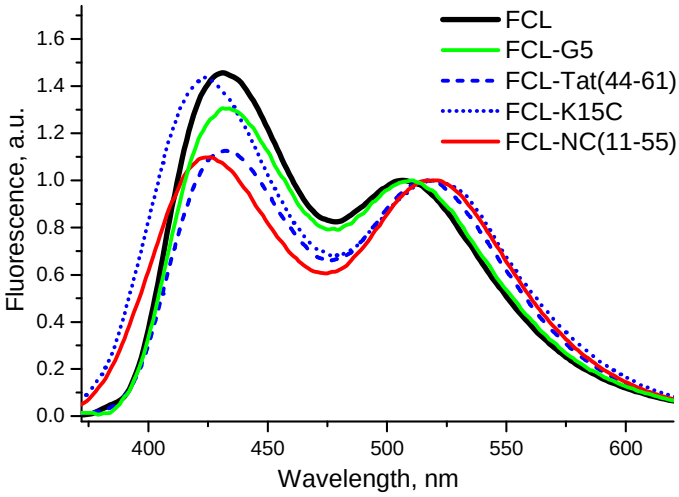

Figure 3.2. Normalized fluorescence spectra of different peptides labelled with FCL compared with free label (black line). Excitation wavelength was set to 340 nm in all the cases. Spectra were recorded in pH 7 phosphate buffer.

Table 3.1. Spectroscopic properties of peptides labeled with FCL

Peptide	λ_{ABS}, nm	λ_{N^*}, nm	λ_{T^*}, nm	N*/T*	φ, %	Sequence near N-term	Peptide length, aa
FCL Label	357	431	507	1.47	2.0		
FCL-G5	360	433	510	1.32	3.3	GGGGG	5
FCL-A12C	360	434	511	1.34	4.3	AMFQD…	12
FCL-K15C	358	423	517	1.43	3.5	**K**RTAM…	15
FCL-Tat(44-61)	359	433	517	1.13	6.0	GISYG…	18
FCL-NC(11-55)	358	425	516	1.12	7.8	**K**NVKC…	45
FCL-NC(1-55)	356	438	517	0.78	5.0	MQRGN…	55

Labels meanings and conditions of the experiments are the same as for Table 2.1.

Peptides labeled by MFL label show only one fluorescence emission band in buffer solution, similarly to the free label. In contrast, the quantum yields of the labeled peptides are more than ten-fold higher then the one of the MFL label in water being closer to results obtained in alcohols (see above). Moreover, the position of the absorption maxima of the labeled peptides is significantly red shifted with respect to the free label in water (**Table 3.2**), while it is closer to that in alcohols. These

observations are in line with expected decrease of the local environment polarity and hydration due to the screening effect of the peptide on the label.

Table 3.2. Spectroscopic properties of peptides labeled with MFL

Peptide	λ_{ABS}, nm	λ_{EM}, nm	φ, %	Sequence near N-term	Peptide length, aa
MFL label	394	551	0.5		
MFL-NC(11-55)	420	547	10.1	**K**NVKC…	45
MFL-NC(1-55)	420	548	7.0	MQRGN…	55
MFL-Vpr(52-96)	419	545	7.2	DTWTG…	45

Labels meanings and conditions of the experiments are the same as for Table 2.2.

In conclusion, the coupling of MFL and FCL to the peptide affects the spectroscopic properties of the labels, probably due to the screening of the label from water by the peptide backbone. Moreover, the spectroscopic effect depends on the nature of amino acid near the labeling position. In all the cases environment of the labels coupled to peptides is closer by polarity to the alcohols than to neat water.

3.2. Peptide-DNA interactions

Most of the processes occurring with DNA and RNA are governed by proteins. Several classes of proteins have DNA as theirs main target (DNA polymerases, proteins for DNA repairing, DNA chaperone proteins, etc.). Frequently binding is enhanced by basic amino acids and/or so-called Zn fingers like in the case of NC peptides (Chapter 1.3.4). As a consequence, peptide-DNA interface shows relatively high environment polarity close to the polarity of alcohols [263, 264]. Classical solvatochromic dyes have low sensitivity in this highly polar media. In contrast, for the proposed 3HC-based FCL label this environment is optimal because of suitable emission band ratio and its strong variation in this polarity range. This allows us to expect that it will show strong response on peptide-DNA binding.

3.2.1. Model systems

Two model systems were selected to characterize FCL sensitivity to peptide-DNA interactions. The simplest model was 3HC fluorophore conjugated with natural polycationic DNA-binding compound – spermine that should bind well DNA fixing dye in close proximity of phosphate backbone and base-pair region. In the second step, a short labeled DNA-binding peptide Tat(44-61) was used as a relevant model.

A) Monitoring oligocation-DNA interaction

3HC was conjugated to an amino group of a natural polyamine, spermine, which is a polycation at neutral pH. In eukaryotic cells, spermine and its shorter analog spermidine form strong complexes with DNA and, thus, stabilize chromatin and prevent DNA damage. Instead of FCL label having four-carbon linker 6-isothiocyano-2-furyl-3-hydroxychromone was used (**Fig. 3.3**) that allowed localizing the dye directly near the DNA-binding centers. Two isomeric conjugates **C1** and **C2** were synthesized and isolated by HPLC. The fluorescence properties of these conjugates are close to FCL label and dye **3** because of very similar behavior of thiourea and acetamido groups (**Fig. 3.4**).

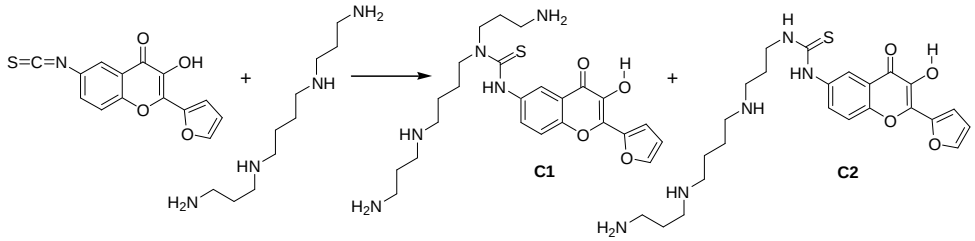

Figure 3.3. Synthesis of 3-hydroxychromone dye conjugates with spermine.

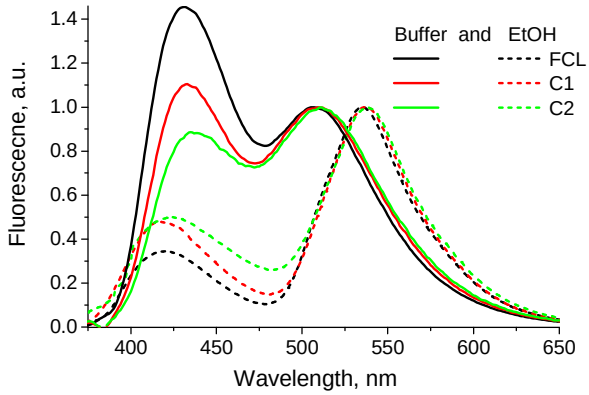

Figure 3.4. Normalized fluorescence spectra of FCL label (black), and conjugates **C1** (red) and **C2** (green) in the buffer (solid lines) and ethanol (dashed lines). Excitation wavelength was 340 nm. 10 mM phosphate buffer (pH 7.0) was used.

Addition of double-stranded DNA (dsDNA) (calf thymus DNA, CT-DNA) to conjugates C**1** and C**2** in buffer changes dramatically their spectroscopic properties (**Fig. 3.5 A**). On DNA binding the increase in the fluorescence quantum yield, the red shift of the T* band from 510 nm to 539 nm and the strong decrease in the N*/T* band ratio were observed.

Comparison of obtained spectra with spectra of the dye **3** in the organic solvents allows us to conclude that environment polarity and hydration are strongly decreased. The poor water exposure of the 3HC fluorophore of our conjugates in dsDNA suggests that the fluorophore is probably intercalated between the DNA bases, where the amount of water molecules is limited (**Fig. 3.5 B**). An additional

proof of the intercalation is the observed red-shift in the absorption maximum with decreasing of extinction coefficient (hypochromic effect) (**Fig. 3.5 A**).

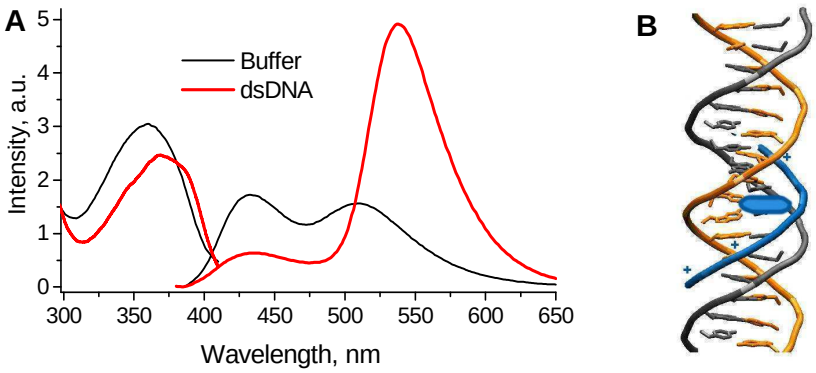

Figure 3.5. (**A**) Absorption (left) and fluorescence (right) spectra of C**1** in buffer (thin black curves) and in the presence of CT-DNA (thick red curves). Concentrations of C**1** and DNA base pairs were 0.1 μM and 1 μM respectively. Long double stranded calf thymus DNA (CT-DNA) and 10 mM phosphate buffer (pH 7.0) were used. (**B**) Schematic representation of the interaction of **C1** and double-strand DNA. Fluorophore (blue ellipse) has possibility to interact with DNA base pairs.

Interaction of conjugates with single-stranded DNA (ssDNA) that has no rigid base-pairs structure shows smaller impact on the dye fluorescence (**Fig. 3.6**). Only minor decrease of the N*/T* band ratio is observed in this case while T* band is red-shifted to 535 nm. Such differences of effects on binding to single- and double-strand DNA are in line with hypothesis of the dye interaction, which can be realized only in the case of dsDNA.

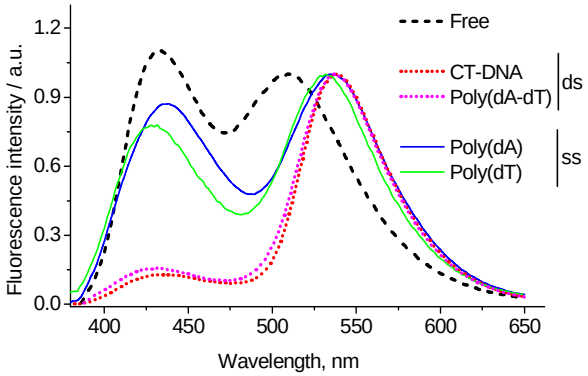

Figure 3.6. Comparison of **C1** fluorescence in free form (dashed line) and bound to ssDNAs (solid lines) or to dsDNAs (dotted lines). Fluorescence spectra recorded in pH 7 phosphate buffer using excitation at 340 nm and normalized by T* band emission.

Strong fluorescence response of conjugates **C1** and **C2** on binding to DNA allows us to conclude that fluorescence of 2-furyl-3-hydroxychromone dyes is highly sensitive to the proximity of the label to DNA. This high sensitivity is probably because the optimal polarity range, where the dye exhibits strong variation of its dual emission, corresponds to relatively polar environment.

Results of this work are presented in Article 6.

Article 6

Excited-state intramolecular proton transfer distinguishes microenvironments in single-and double-stranded DNA

Excited-State Intramolecular Proton Transfer Distinguishes Microenvironments in Single- And Double-Stranded DNA

Andrey S. Klymchenko,* Volodymyr V. Shvadchak, Dmytro A. Yushchenko, Namrata Jain, and Yves Mély

Photophysique des Interactions Biomoléculaires, UMR 7175 du CNRS, Faculté de Pharmacie, Université Louis Pasteur, 67401, Illkirch, France

Received: February 11, 2008

Herein, the efficient interaction of an environment-sensitive fluorophore that undergoes excited-state intramolecular proton transfer (ESIPT) with DNA has been realized by conjugation of a 3-hydroxychromone (3HC) with polycationic spermine. On binding to a double-stranded DNA (dsDNA), the ratio of the two emission bands of the 3HC conjugates changes up to 16-fold, so that emission of the ESIPT product increases dramatically. This suggests an efficient screening of the 3HC fluorophore from the water molecules in the DNA complex, which is probably realized by its intercalation into dsDNA. In sharp contrast, the 3HC conjugates show only moderate changes in the dual emission on binding to a single-stranded DNA (ssDNA), indicating a much higher fluorophore exposure to water at the binding site. Thus, the 3-hydroxychromone fluorophore being conjugated to spermine discriminates the binding of this polycation to dsDNA from that to ssDNA. Consequently, ESIPT-based dyes are promising for monitoring the interaction of polycationic molecules with DNA and probing the microenvironment of their DNA binding sites.

Introduction

Solvatochromic (environment-sensitive) fluorescent dyes are highly useful for obtaining new information about biomolecules and their interactions.[1−3] However, applications of these dyes for DNA research remains a challenge and only few examples are available in the literature. For instance, a dansyl fluorophore has been used to estimate the microenvironment polarity in the major groove of double-stranded DNA (dsDNA).[4,5] Moreover, DNA dynamics has been monitored by the time-resolved solvent relaxation of a coumarin.[6] In recent reports, a PRODAN-based fluorophore was conjugated with DNA bases[7−9] to evidence differences in the microenvironment of the major and minor grooves of A-, B- and Z-DNA. Environment-sensitive fluorophores having cationic groups, can bind DNA and report on the local properties of the DNA binding sites. For instance, the polarity of the minor groove of dsDNA has been estimated using the polycationic bisbenzimide (Hoechst 33258).[10] Similarly, a cationic anthracene derivative[11] and cationic acridizinium salts[12] provide a site-specific fluorescence signal on binding to DNA. Consequently, environment-sensitive fluorophores are highly promising for detecting the interaction of small molecules with DNA and probing the microenvironment of their binding site. In this respect, a prospective approach, which has not been realized so far, is to use a fluorophore undergoing excited-state intramolecular proton transfer (ESIPT) reaction as a building block of a DNA probe. ESIPT results in the formation of a new long-wavelength emission band.[13−16] This reaction is highly sensitive to the environment, so that solvent polarity and H-bonding may strongly modulate the relative intensity of the ESIPT product.[17−19] In this respect, 3-hydroxychromone (3HC) derivatives are probably among the best candidates for DNA applications. They undergo ESIPT between their 3-hydroxyl and 4-carbonyl groups[20] resulting in the emission of both normal excited-state (N*) and phototautomer (T*) species (Scheme 1).

SCHEME 1: 3-Hydroxychromone Derivative and Its Excited State Intramolecular Proton Transfer (ESIPT) Reaction (A) and, for Comparison, the Structure of a Natural Base Pair (dA-dT) (B)

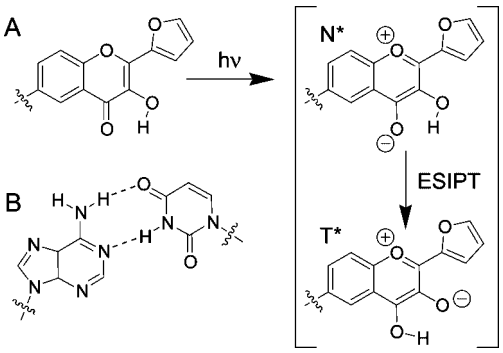

The dual emission of 3HCs is highly sensitive to the environment,[17,18,21−23] since an increase in the polarity and H-bond donor ability of solvents inhibits the ESIPT reaction and thus, decreases the relative intensity of the T* band.[23,24] Moreover, the position of the maximum of the T* band in 3HCs is insensitive to solvent polarity, but exhibits high sensitivity to H-bond donor ability.[24] Thus, 3HCs provide two independent spectroscopic channels allowing a detailed characterization of their environment. These unique properties of 3HCs have already been applied for probing proteins, lipid bilayers and cell membranes.[25−28] However, application of 3HCs for DNA probing has never been shown so far. For this purpose, 2-(2-furanyl)-3-hydroxychromone is probably the most convenient fluorophore among known 3HCs, since it is a flat molecule with a size close to that of a base pair (Scheme 1), and exhibiting dual emission in aqueous media with a satisfactory fluorescence quantum yield.[29] In the present work, we conjugated 2-(2-furanyl)-3HC to an amino group of a natural polyamine, spermine, which is a polycation at neutral pH. In eukaryotic

* Corresponding author. E-mail: aklymchenko@pharma.u-strasbg.fr.

10.1021/jp8058068 CCC: $40.75
Published on Web 09/03/2008

SCHEME 2: Synthesis of Conjugates 1 and 2[a]

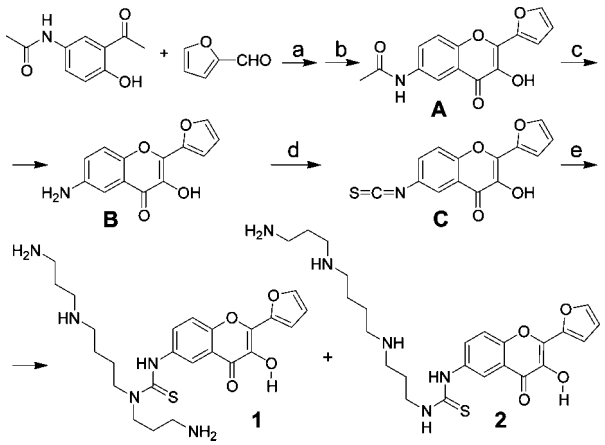

[a] Reagents: (a) DMF, MeONa; (b) H_2O_2, EtOH, NaOMe; (c) 10% HCl; (d) DPT, THF; (e) spermine, DMF.

cells, spermine and its shorter analog spermidine form strong complexes with DNA and, thus, stabilize chromatin and prevent DNA damage.[30−32] Moreover, their lipid conjugates are efficient gene delivery vectors.[33] Our results show that binding of 3HC-spermine conjugates to dsDNA strongly increases the relative intensity of the T* state, indicating a low polar surrounding of the fluorophore inside DNA probably due to an intercalation of the dye between the DNA bases. In contrast, in complex with single-stranded DNA (ssDNA), a different dual emission profile is observed, indicating a significantly higher polarity of the fluorophore surrounding. Thus, our environment-sensitive dye conjugated with spermine can distinguish between ssDNA and dsDNA. Application of environment-sensitive dyes undergoing ESIPT constitutes thus a new approach for DNA probing.

Materials and Methods

Reagents and Solvents. All the reagents were purchased from Aldrich-Sigma Chemical Company. Solvents for synthesis were of reagent quality, they were appropriately dried if necessary. For absorption and fluorescence studies the solvents were of spectroscopic grade. Calf thymus DNA (CT-DNA) and single-stranded polydeoxyadenylic acids poly(dA) and poly(dT) were from Sigma.

Synthesis of 3HC Conjugates with Spermine (See Scheme 2). 5′-Acetamido-2′-hydroxyacetophenone and furfural were condensed into the corresponding chalcone in dry DMF in the presence of sodium methoxide (RT, 24 h). The reaction mixture was diluted with several volumes of ethanol and treated with 10 mol excess of hydrogen peroxide and 12 mol excess of sodium methoxide. Refluxing the mixture for 5 min afforded corresponding 3-hydroxychromone (**A**) with yield 55%. ^{1}H NMR (300 MHz, DMSO-d6) δ 10.25 (s, 1H, OH), 9.95 (br.s, 1H, NH), 8.43 (d, J = 2.5 Hz, 1H, ArH), 8.03 (br.s, 1H, HetH), 7.97 (dd, J = 9 Hz, J = 2.5 Hz,1H, ArH), 7.69 (d, J = 9 Hz, 1H, ArH), 7.29 (d, J = 3.5 Hz, 1H, HetH), 6.8 (dd, J = 3.5 Hz, J = 1.5 Hz, 1H, HetH), 2.09 (s, 3H, $COCH_3$); m/z 286.4 (M++H).

The above-obtained acetamide (**A**) was hydrolyzed in 10% HCl under refluxing during 7 h (100 °C). Then water was added and the mixture was neutralized with base to pH 7. The obtained product was filtrated and dried to give the corresponding amine (**B**) with yield 90%. ^{1}H NMR (300 MHz, DMSO-d_6) δ 9.63 (s, 1H, OH), 7.99 (s, 1H, HetH), 7.44 (d, J = 9 Hz, 1H, ArH), 7,23 (m, 2H, ArH, HetH), 7.08 (dd, J = 9 Hz, J = 2.5 Hz,1H, ArH), 6.77 (dd, J = 3.5 Hz, J = 1.5 Hz, 1H, HetH), 5.47 (br.s, 2H, NH_2); m/z 244.2 (M^+ + H).

A 0.2 g (0.82 mmol) sample of 6-amino-2-furan-2-yl-3-hydroxychromone (**B**) was dissolved in 10 mL of dry THF and 0.35 g (1.5 mmol) of DPT (1,1′-thiocarbonyldi-2(1*H*)pyridone) was added to this solution. The reaction mixture was stirred under Ar at room temperature for 2 h. The solvent was removed in vacuo, and the product was purified by column chromatography (CH_2Cl_2/cyclohexane = 50/50) to give 0.17 g (72%) of pure isothiocyanate (**C**). ^{1}H NMR (300 MHz, DMSO-d_6) δ 10.26 (s, 1H, OH), 8.07 (m, 2H, ArH), 7.82 (s, 2H, HetH), 7.32 (d, J = 4 Hz 1H, ArH), 6.82 (dd, J = 3.5 Hz, J = 1.5 Hz, 1H, HetH); m/z 286.3 (M^+ + H).

A solution of 30 mg of **C** (2-furan-2-yl-3-hydroxy-6-isothiocyanato-chromen-4-one) in 1 mL of DMF was added dropwise to 100 μL of spermine with constant stirring for 2 h at rt. Crude mixture of two isomers (**1** and **2**) was applied to a reversed-phase C8 high-pressure liquid chromatography (HPLC) column (5 μm particle size) eluted with (A) aqueous TFA (0.05%, v/v), and (B) 70% of MeCN, 30% of water, with addition of TFA (0.05%, v/v). Linear gradient from 10 to 30% of B in 30 min was used. Fractions were collected at a flow rate of 4 mL/min and the eluant was monitored by adsorption at 360 nm. Fractions containing compounds **1** and **2** were freeze-dried to give lyophilized powders. For compound **1**, ^{1}H NMR (300 MHz, D_2O + drop of TFA) δ 7.65 (m, 2H, ArH), 7.28 (m, 3H, ArH), 6.64 (dd, J = 3.5 Hz, J = 1.5 Hz, 1H, HetH), 3.65 (m, 2H, C**H**$_2$NC=S), 2.84 (m, 10H, C**H**$_2$N), 1.92 (m, 2H, NCH$_2$C**H**$_2$CH$_2$N), 1.76 (m, 2H, NCH$_2$C**H**$_2$CH$_2$N), 1.54 (m, 4H, CH$_2$C**H**$_2$C**H**$_2$CH$_2$). For Compound **2**, ^{1}H NMR (300 MHz, D_2O + drop of TFA) δ 7.69 (m, 2H, ArH), 7.38 (m, 3H, ArH), 6.66 (dd, J = 3.5 Hz, J = 1.5 Hz, 1H, HetH), 3.8 (m, 2H, C**H**$_2$NHC=S), 3.6 (m, 2H, C**H**$_2$NHC=S), 2.88 (m, 8H, C**H**$_2$N), 1.99 (m, 2H, NCH$_2$C**H**$_2$CH$_2$N), 1.86 (m, 2H, NCH$_2$C**H**$_2$CH$_2$N), 1.65 (m, 4H, CH$_2$C**H**$_2$C**H**$_2$CH$_2$).

Instrumentation. Proton NMR spectra were recorded on a 300 MHz Bruker spectrometer and mass spectra were recorded on a Mariner System 5155 mass spectrometer using the electrospray ionization (ESI) method. All column chromatography experiments were performed on silica gel (Merck, Kieselgel 60H, Art 7736). Purification was carried out on a Shimadzu SPD-20A HPLC using a C8 column (uptisphere 300A, 5 μm; 250 × 10, Interchim, France) with a 10 to 70% linear gradient and monitoring the 3HC dye absorption at 360 nm. Absorption and fluorescence spectra were recorded on a Cary 400 spectrophotometer (Varian) and FluoroMax 3.0 spectrofluorimeter (Jobin Yvon, Horiba), respectively. For fluorescence studies, the dyes were used at 0.1 to 1 μM concentrations. Excitation wavelength was 340 nm. Fluorescence quantum yields were determined using quinine sulfate in 0.5 M sulfuric acid as a reference (quantum yield, φ = 0.577).[34] For the experiments in water, 10 mM phosphate buffer (pH 7.0) was used systematically. Hybridization of poly(dA) with poly(dT) was performed by annealing their equimolar mixture (100 μM, expressed in phosphate groups) in the phosphate buffer containing 100 mM NaCl at 95 °C for 10 min, followed by slow cooling (within *ca* 6 h) to room temperature. For the spectroscopic measurements, the obtained stock solution of the hybridized DNA, poly(dA-dT), was diluted to a final concentration (1 μM) using 10 mM phosphate buffer.

Results and Discussion

Initially, we synthesized a fluorophore building block **A** starting from 2-hydroxyacetonenone and 2-furaldehyde. The **A**

TABLE 1: Spectroscopic Properties of the Parent Dye A, and the Conjugates 1 and 2 in Different Organic Solvents, in Buffer, and as Bound to Different ssDNAs and dsDNAs[a]

media	dye	λ_{N^*}, nm	λ_{T^*}, nm	I_{T^*}/I_{N^*}	Q, %
water ($\alpha = 1.17$,[b] $\epsilon = 78.4$)	**A**	431	506	0.62	2.4
	1	433	510	0.90	0.5
	2	435	510	1.14	0.7
MeOH ($\alpha = 0.43$, $\epsilon = 32.6$)	**A**	421	532	1.14	6.3
	1	423	537	1.01	1.0
	2	425	537	1.32	1.0
EtOH ($\alpha = 0.37$, $\epsilon = 24.9$)	**A**	422	532	2.88	6.2
	1	422	538	2.08	1.0
	2	422	537	2.56	0.94
1-octanol ($\alpha = 0.37$, $\epsilon = 9.86$)	**A**	418	534	4.83	14.6
	1	421	536	5.00	3.0
	2	421	538	5.00	2.8
DMF ($\alpha = 0$, $\epsilon = 37.2$)	**A**	420	540	9.30	8.2
	1	425	543	7.52	1.3
	2	431	543	5.49	2.0
acetone ($\alpha = 0$, $\epsilon = 20.5$)	**A**	411	536	13.9	8.6
	1	419	538	7.4	1.7
	2	420	539	5.8	2.4
EtOAc ($\alpha = 0$, $\epsilon = 5.99$)	**A**	413	535	19.8	12.1
	1	417	537	14.9	3.9
	2	419	537	10.8	5.9
CT-DNA	**1**	435	539	7.70	1.3
	2	439	539	18.2	6.7
poly(dA)	**1**	436	535	1.15	0.7
	2	442	535	1.79	1.2
poly(dT)	**1**	431	532	1.35	0.7
	2	432	535	1.90	0.7
CT-DNA 83 °C	**1**	440	532	0.97	–
	2	444	539	1.88	–
poly (dA-dT)	**1**	430	537	6.35	1.4
	2	433	539	10.4	2.6

[a] Key: Q, fluorescence quantum yield, measured using quinine sulfate in 0.5 M sulfuric acid as a reference; λ_{N^*} and λ_{T^*}, position of the N* and T* emission band maximum, respectively; I_{T^*}/I_{N^*}, intensity ratio of the two emission bands. A 10 mM phosphate buffer was used. α: Abraham's H-bond donor ability (from ref 35). ϵ: dielectric constant. [b] The presented value of α corresponds to the H-bond donor ability introduced by Kamlet−Taft.[36]

compound was further hydrolyzed in hydrochloric acid and the obtained 6-amino derivative was converted into the 6-isothiocyanate derivative of 2-(2-furanyl)-3HC by using DPT (Scheme 2). The resulting derivative was further reacted with spermine giving two products of nearly equal quantities. After isolation with HPLC, we identified compounds **1** and **2**, corresponding to spermine modified with 3HC at the secondary and primary amino groups, respectively. Since the amino group of spermine used for conjugation cannot be protonated, conjugate **2** can be considered as a derivative of spermidine.

Spermine conjugates **1** and **2** as well as compound **A** which corresponds to the fluorophore, were studied in organic solvents of different polarity and H-bond donor ability (Table 1). The compound **A**, similarly to its parent 2-(2-furanyl)-3-hydroxychromone, exhibits dual emission highly sensitive to solvent properties.[24] In aprotic solvents, the I_{T^*}/I_{N^*} ratio is large, so that the emission of the ESIPT product T* dominates. On increase in solvent polarity within aprotic solvents from ethyl acetate to DMF, a decrease in the I_{T^*}/I_{N^*} ratio is observed (Table 1). In protic solvents, the emission of the ESIPT product is strongly decreased, due to the H-bonding perturbation of the ESIPT by the H-bond donor ability of the protic solvents.[17,24] Thus, comparison of protic and aprotic solvents of similar polarity, such as DMF and methanol, shows that in protic solvents, the relative intensity of the ESIPT product T*, the I_{T^*}/I_{N^*} ratio is much lower than in aprotic solvents (where the H-bond donor ability close to 0) (Table 1). Moreover, in protic solvents the dual emission of A varies also as a function of solvent polarity, so that in the polar solvent methanol, the I_{T^*}/I_{N^*} ratio is nearly 5-fold lower than in the less polar 1-octanol. Thus, both the H-bond donor ability and the solvent polarity hamper the ESIPT reaction and thus the emission of the T* form in **A**. As a result, in water, where both parameters are extremely high, the I_{T^*}/I_{N^*} ratio exhibits the lowest values (Table 1). Spectroscopic studies of conjugates **1** and **2** in organic solvents show that the 3HC moiety keeps its dual emission (Figure 1), and thus, undergoes ESIPT. Moreover, the positions of the two bands and the ratio of their intensities, I_{T^*}/I_{N^*} are not strongly modified on conjugation with spermine, as it can be seen by comparison of conjugates **1** and **2** with the parent dye **A** in most of the studied solvents (Table 1, some deviations are observed in water and aprotic solvents, see below). However, **1** and **2** show significantly lower fluorescence quantum yields than **A**, indicating a quenching of 3HC likely by the amine groups of spermine.[37] Similarly to **A**, the nature of the solvent affects strongly the dual emission of **1** and **2**. Indeed, for both conjugates the I_{T^*}/I_{N^*} ratio is much higher in aprotic than in protic solvents. Moreover, an increase in solvent polarity from 1-octanol to methanol also decreases the I_{T^*}/I_{N^*} ratio (Figure 1, Table 1). Noteworthy, the I_{T^*}/I_{N^*} ratio of **1** and **2** varies in a less broad range with solvent properties than that of **A** (its value being higher in water and lower in aprotic solvents, Table 1). This poorer spectroscopic sensitivity of **1** and **2** to solvent could be explained by a screening of the 3HC fluorophore by the spermine backbone. In water, spermine probably decreases the local polarity and H-bond donor ability around the fluorophore, while in aprotic solvents, it may considerably increase the local H-bond donor ability (due to presence of its NH-protons). Thus, similarly to the parent fluorophore A and other 3HC analogs,[17,18,22−24] conjugates **1** and **2** exhibit high sensitivity of their emission to solvent polarity and H-bond donor ability. These two solvent parameters also affect the fluorescence quantum yield of the dyes, so that it is the highest in the apolar aprotic ethyl acetate and the lowest in water.

Since water is a key solvent that modulates the local polarity and H-bond donor ability in biomolecules, we studied the influence of water in the aprotic acetone solvent on the dual emission of conjugates **1** and **2**. The fluorescence spectra of conjugates **1** and **2** exhibit a strong decrease in the I_{T^*}/I_{N^*} ratio on increase in the water content in acetone (Figure 1), so that water hampers the ESIPT process and thus decreases the emission of the ESIPT product. Moreover, the increase in water content shifts considerably the T* band maximum to the blue (Table 1), which according to our previous studies is likely due to the high H-bond donor ability of water.[24,29] Thus, both the ratio of the two emission bands and the position of the tautomer band of 3HC dyes provides information on the water content in their surrounding, so that being bound to biomolecules, 3HC fluorophore can report on its exposure to water.

Addition of dsDNA (calf thymus DNA, CT-DNA) to conjugates **1** and **2** in buffer changes dramatically their fluorescence spectra (Figure 2), while dye **A** does not show any spectroscopic response to dsDNA (data not shown). Thus, conjugation with spermine enables the 3HC fluorophore to bind dsDNA. This binding strongly increases the fluorescence intensity of the T* band and decreases the intensity of the N* band, so that the I_{T^*}/I_{N^*} ratio increases (Table 1). Thus, binding to dsDNA favors the emission of the ESIPT product (T*). Noticeably, the increase in the T* emission on binding to

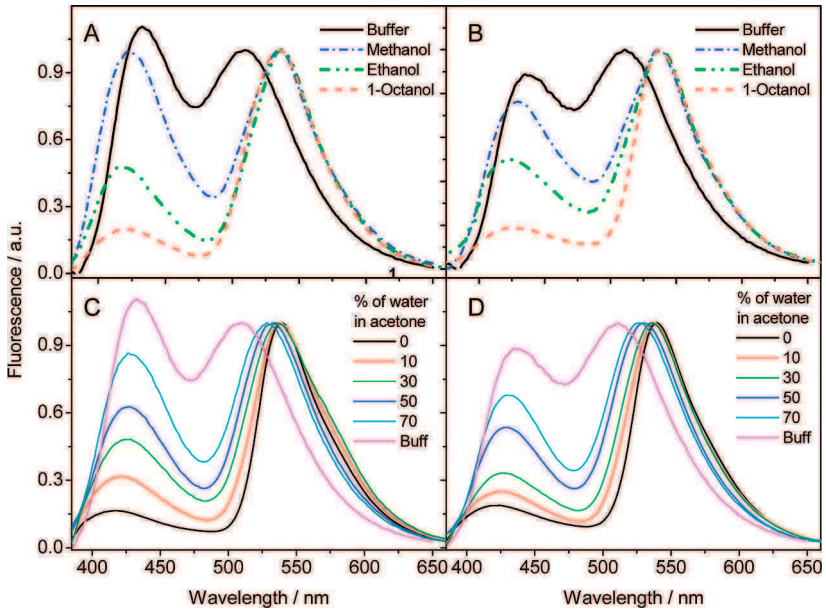

Figure 1. Effect of solvents on the dual emission of conjugates **1** and **2**. A and B: Fluorescence spectra of **1** and **2**, respectively, in different protic solvents. C and D: Fluorescence spectra of **1** and **2**, respectively, in acetone−water mixtures. The spectra were normalized at the maximum of the long wavelength T* band. Excitation wavelength was 340 nm.

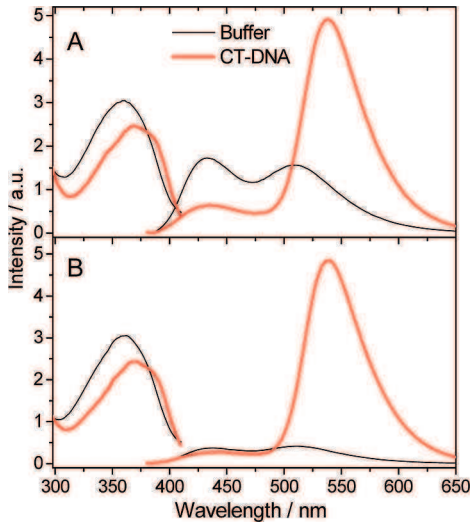

Figure 2. Absorption (left) and fluorescence (right) spectra of **1** (A) and **2** (B) in buffer (thin black curves) and in the presence of CT-DNA (thick red curves). 10 mM phosphate buffer (pH 7.0) was used. Concentration of **1** and **2** was 0.1 μM. The concentration of CT-DNA base pairs was 1 μM. Excitation wavelength was 340 nm.

dsDNA is more pronounced for **2** than for **1** (Figure 2). Moreover, both **1** and **2** exhibit shifts of their T* band to the red (Figure 2, Table 1). According to the data in solvents, the observed spectroscopic effects suggest that on binding to dsDNA, the environment of the 3HC fluorophore changes from a highly polar aqueous one with high H-bond donor ability (high exposure to water) to a less polar one with low H-bond donor ability (low exposure to water). On binding to dsDNA, the absorbance of **1** and **2** decreases by 20−25% (hypochromic effect), and the absorption maximum shifts to the red (from 361 to 369 nm) (Figure 2), strongly suggesting an intercalation of the 3HC fluorophore between the DNA bases. Remarkably, an increase in the fluorescence quantum yield accompanies the binding of **1** and **2** to dsDNA (Table 1), while many fluorescent dyes are quenched by DNA bases.[11,38] This increase in the quantum yield on intercalation of 3HC between the DNA bases can be explained by a screening of the 3HC fluorophore from the bulk aqueous environment and a decreased quenching by the amino groups of spermine. Remarkably, the I_{T^*}/I_{N^*} ratio in dsDNA for both conjugates is significantly lower than in any protic solvent including the low polar 1-octanol (Table 1), confirming the absence in the probe vicinity of water molecules, which are the major H-bond donors in the DNA surrounding. According to previous studies using other environment sensitive dyes, the polarity of the minor and major grooves of dsDNA is rather high, namely $\varepsilon \approx 20$[10] and 40−60[4] respectively, indicating a significant amount of water molecules in the grooves. The poor water exposure of the 3HC fluorophore of our conjugates in dsDNA declines its possible localization in the DNA grooves, but confirms that the fluorophore is probably intercalated between the DNA bases, where the amount of water molecules is limited. Interestingly, a highly efficient ESIPT was also observed for a 2-(2′-hydroxyphenyl)benzoxazole derivative incorporated in dsDNA opposite an abasic site, in line with a low-polar and aprotic environment between the base pairs.[39]

What should happen then on binding of **1** and **2** to ssDNA, where intercalation is not expected? Addition of the poly(dA) ssDNA also modifies the fluorescence spectra of both conjugates (Figure 3), but the resulting spectra are strongly different from those with dsDNA. Indeed, the I_{T^*}/I_{N^*} ratio with poly(dA) is 7−10 fold lower than with dsDNA, while the T* band position with ssDNA is slightly shifted to the blue (Table 1). Importantly, on binding to another ssDNA, poly(dT), the conjugates **1** and **2** exhibit very close fluorescence spectra to those in poly(dA) (Figure 3). Similar fluorescence spectra were also obtained when CT-DNA was melted at 83 °C (Table 1).[40] Finally, annealing of poly(dA) with poly(dT) changes dramatically the spectra of **1** and **2**, so that they become very close to the spectrum with double-stranded CT-DNA (Figure 3, Table 1). Thus, irrespective to the DNA sequence, the spectra with ssDNA are strongly different from those with dsDNA, the relative intensity of the ESIPT product (i.e., I_{T^*}/I_{N^*} ratio) being strongly decreased in ssDNA (Table 1). Moreover, the fluorescence quantum yields of **1** and **2** bound to ssDNA are systematically lower compared to dsDNA (Table 1). Finally, ssDNAs modify the absorption spectra of **1** and **2** to a much lower extent than dsDNAs,

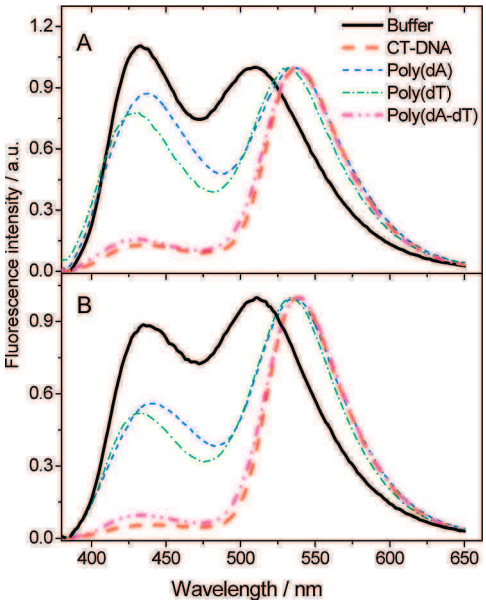

Figure 3. Fluorescence spectra of 0.1 μM of conjugates **1** (A) and **2** (B) in 10 mM phosphate buffer (pH 7) in the absence and in the presence of an excess of dsDNA (CT-DNA and poly(dA-dT) at 20 °C) or ssDNA (poly(dA) and poly(dT)). Concentration of dsDNA (base pairs) and ssDNA (bases) was 1 μM. The spectra were normalized at the T* band maximum. Excitation wavelength was 340 nm.

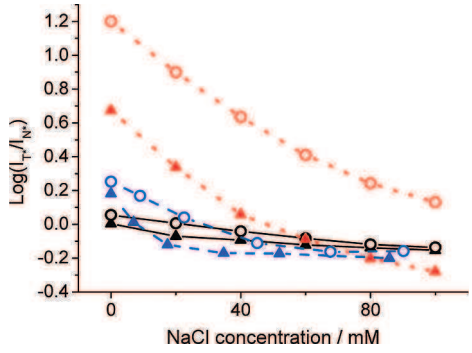

Figure 4. Salt effect on log(I_{T*}/I_{N*}) of conjugates **1** (▲) and **2** (○) in free form (solid curve and symbols in black), bound to CT-DNA (dotted curve and symbols in red) or to poly(dA) (dashed curve and symbols in blue). Conditions were as in Figure 3.

providing only a 5−7% hypochromism and *ca* 5 nm red shift. These data suggest that the 3HC fluorophore of the spermine conjugates is much more exposed to water in ssDNA than in dsDNA, probably because an efficient screening of the fluorophore from the bulk water due to intercalation between the base pairs can only be realized in dsDNAs. Thus, the ESIPT-based fluorophore allows us to clearly distinguish between ssDNAs and dsDNAs, simply by the ratio of the two emission bands.

Due to the polycationic nature of conjugates **1** and **2**, their interaction with DNA should be mainly electrostatic, and therefore, it should strongly depend on salt concentration. In line with our expectations, log(I_{T*}/I_{N*}), which is a function of the I_{T*}/I_{N*} ratio exhibiting a linear correlation with solvent parameters,[23,41] strongly decreases with increasing salt concentrations for **1** and **2** complexed with dsDNA (CT-DNA), while in DNA-free buffer the salt effect is negligible (Figure 4). For both conjugates, the log(I_{T*}/I_{N*}) values at high salt concentrations approach the values in DNA-free buffer, indicating that the complexes of **1** and **2** with dsDNA are probably dissociated. Noticeably, the salt effect is stronger for conjugate **1,** suggesting that it forms weaker complexes with DNA than conjugate **2**. Relatively weak complexes are formed with poly(dA), since the log(I_{T*}/I_{N*}) values of their complexes with **1** and **2** decrease very rapidly with increasing salt concentrations (Figure 4). Titrations in 30 mM NaCl confirm that both conjugates bind dsDNA much stronger than ssDNA, since the binding constants for **1** and **2** with dsDNA are $(2.5 \pm 0.5) \times 10^7$ M^{-1} and $(9.1 \pm 1.4) \times 10^7$ M^{-1}, respectively, while for ssDNA, the corresponding values are $(1.0 \pm 0.5) \times 10^6$ M^{-1} and $(2 \pm 1) \times 10^6$ M^{-1}. The binding constants for dsDNA correspond well to the literature values for spermidine in low-salt buffer.[42] Moreover, the higher affinity of both conjugates to dsDNA as compared to ssDNA is in line with the reported preference of spermine and spermidine for dsDNA.[42] Finally, the higher affinity of **2** compared to **1** can be understood considering that the modification of a primary amino group of spermine (in **2**) perturbs less the binding to DNA than modification of its secondary amino group (in **1**). In case of **2**, the cationic spermidine residue likely binds to the dsDNA minor or major grooves,[43,44] while the long and flexible fluorophore spacer (Figure 1) enables the fluorophore to intercalate between the bases. The appropriate size, the flat aromatic structure (Scheme 1) and the hydrophilicity of the 3HC fluorophore are likely the key factors that favor its intercalation into dsDNA. In case of **1** bound to dsDNA, the 3HC fluorophore is probably locked between the cationic groups, and, therefore, due to insufficient freedom intercalates less efficiently. This reduced intercalation is evidenced by the significantly lower I_{T*}/I_{N*} ratio and thus, the higher water accessibility of **1** compared to **2** in complex with dsDNA. This poorer intercalation could be an additional factor of the lower affinity of **1** compared to **2** for dsDNA.

In conclusion, we have conjugated an environment-sensitive 3HC fluorophore undergoing ESIPT to spermine. On binding to dsDNA and ssDNA, the conjugates show dramatic change in their dual emission. This enables to directly monitor their interaction with DNA by recording the ratio of the two emission bands. In complex with dsDNA, the enhanced emission of the ESIPT product indicates an efficient screening of the 3HC fluorophore from the bulk water, probably due to its intercalation in dsDNA. A very different spectral profile is observed on binding to ssDNA, suggesting that in ssDNA the fluorophore is much less screened from water molecules. Thus, our dyes can clearly distinguish between ssDNA and dsDNA. Consequently, this study shows that labeling of a polycationic molecule (like spermine) with 3HC allows monitoring its interaction with nucleic acids as well as probing the microenvironment of local binding sites.

Acknowledgment. This work was supported by FRM, TRIoH, and ANR research grants, as well as by ARCUS. V.V.S. and D.A.Y. acknowledge the financial support of the Eiffel Fellowship Program. We thank Alain Burger and Rachid Benhida for fruitful discussions.

References and Notes

(1) Cohen, B. E.; McAnaney, T. B.; Park, E. S.; Jan, Y. N.; Boxer, S. G.; Jan, L. Y. *Science* **2002**, *296*, 1700.
(2) Sloan, D. J.; Hellinga, H. W. *Protein Eng.* **1998**, *11*, 819.
(3) Altschuh, D.; Oncul, S.; Demchenko, A. P. *J. Molecular Recognition* **2006**, *19*, 459.
(4) Jadhav, V. R.; Barawkar, D. A.; Ganesh, K. N. *J. Phys. Chem. B* **1999**, *103*, 7383.
(5) Barawkar, D. A.; Ganesh, K. N. *Nucleic Acids Res.* **1995**, *23*, 159.
(6) Somoza, M. M.; Andreatta, D.; Murphy, C. J.; Coleman, R. S.; Berg, M. A. *Nucleic Acids Res.* **2004**, *32*, 2494.
(7) Kimura, T.; Kawai, K.; Majima, T. *Org. Lett.* **2005**, *7*, 5829.
(8) Kimura, T.; Kawai, K.; Majima, T. *Chem. Commun.* **2006**, 1542.

(9) Tainaka, K.; Tanaka, K.; Ikeda, S.; Nishiza, K.; Unzai, T.; Fujiwara, Y.; Saito, I.; Okamoto, A. *J. Am. Chem. Soc.* **2007**, *129*, 4776.
(10) Jin, R; Breslauer, K. J. *Proc. Natl. Acad. Sci. U.S.A.* **1988**, *85*, 8939.
(11) Kumar, C. V.; Asuncion, E. H. *J. Am. Chem. Soc.* **1993**, *115*, 8547.
(12) Granzhan, A.; Ihmels, H.; Viola, G. *J. Am. Chem. Soc.* **2007**, *129*, 1254.
(13) Formosinho, S. J.; Arnaut, L. G. *J. Photochem. Photobiol. A: Chem.* **1993**, *75*, 21.
(14) Douhal, A.; Lahmani, F.; Zewail, A. H. *Chem. Phys.* **1996**, *207*, 477.
(15) Henary, M.; Fahrni, C. *J. Phys. Chem. A* **2002**, *106*, 5210.
(16) Santra, S.; Krishnamoorthy, G.; Dogra, S. K. *Chem. Phys. Lett.* **1999**, *311*, 55.
(17) McMorrow, D.; Kasha, M. *J. Phys. Chem.* **1984**, *88*, 2235.
(18) Chou, P. T.; Martinez, M. L.; Clements, J. H. *J. Phys. Chem.* **1993**, *97*, 2618.
(19) Chou, P.; Yu, W.; Cheng, Y.; Pu, S.; Yu, Y.; Lin, Y.; Huang, C.; Chen, C. *J. Phys. Chem. A* **2004**, *108*, 6487.
(20) Sengupta, P. K.; Kasha, M. *Chem. Phys. Lett.* **1979**, *68*, 382.
(21) Ormson, S. M.; Brown, R. G; Vollmer, F.; Rettig, W. *J. Photochem. Photobiol. A: Chem.* **1994**, *81*, 65.
(22) Swinney, T. C.; Kelley, D. F. *J. Chem. Phys.* **1993**, *99*, 211.
(23) Klymchenko, A. S.; Demchenko, A. P. *Phys. Chem. Chem. Phys.* **2003**, *5*, 461.
(24) Klymchenko, A. S.; Kenfack, C.; Duportail, G.; Mely, Y. *J. Chem. Sci.* **2007**, *119*, 83.
(25) Klymchenko, A. S.; Avilov, S. V.; Demchenko, A. P. *Analyt. Biochem.* **2004**, *329*, 43.
(26) Klymchenko, A. S.; Duportail, G.; Mely, Y.; Demchenko, A P *Proc. Natl. Acad. Sci. U.S.A.* **2003**, *100*, 11219.
(27) Shynkar, V. V.; Klymchenko, A. S.; Duportail, G.; Demchenko, A. P.; Mely, Y. *Biochim. Biophys. Acta* **2005**, *1712*, 128.
(28) Shynkar, V. V.; Klymchenko, A. S.; Kunzelmann, C.; Duportail, G.; Muller, C. D.; Demchenko, A. P.; Freyssinet, J. M.; Mely, Y. *J. Am. Chem. Soc.* **2007**, *129*, 2187.
(29) Klymchenko, A. S.; Demchenko, A. P. *New J. Chem.* **2004**, *28*, 687.
(30) Feuerstein, B. G.; Pattabiraman, N.; Marton, L. J. *Proc. Natl. Acad. Sci. U.S.A.* **1986**, *83*, 5948.
(31) Feuerstein, B. G.; Pattabiraman, N.; Marton, L. J. *Nucleic Acids Res.* **1990**, *18*, 1271.
(32) Khan, A. U.; Mei, Y. H.; Wilson, T. *Proc. Natl. Acad. Sci. U.S.A.* **1992**, *89*, 11426.
(33) Behr, J. P.; Demeneix, B.; Loeffler, J. P.; Perez-Mutul, J. *Proc. Natl. Acad. Sci. U.S.A.* **1989**, *86*, 6982.
(34) Eastman, J. W. *Photochem. Photobiol.* **1967**, *6*, 55–72.
(35) Abraham, M. H. *J. Phys. Org. Chem.* **1993**, *6*, 660–684.
(36) Kamlet, M. J.; Abboud, J. L. M.; Abraham, M. H.; Taft, R. W. *J. Org. Chem.* **1983**, *48*, 2877–2887.
(37) Gordon, M., Ware, W. R., Eds. *The Exiplex*; Academic Press: New York, 1975.
(38) Yang, X.; Liu, W.-H.; Jin, W.-J.; Shen, G.-L.; Yu, R.-Q. *Spectrochim. Acta A* **1999**, *55*, 2719.
(39) Ogawa, A. K.; Abou-Zied, O. K.; Tsui, V.; Jimenez, R.; Case, D. A.; Romesberg, F. E. *J. Am. Chem. Soc.* **2000**, *122*, 9917–9920.
(40) At the molar ratio dye/base pairs = 1/10, **1** and **2** do not modify considerably the melting point of CT-DNA, according to measurements of absorbance at 260 nm vs temperature (data not shown).
(41) Klymchenko, A. S.; Pivovarenko, V. G.; Ozturk, T.; Demchenko, A. P. *New. J. Chem.* **2003**, *27*, 1336.
(42) Morgan, J. E.; Blankenship, J. W.; Matthews, H. R. *Arch. Biochem. Biophys.* **1986**, *246*, 225.
(43) Schmid, N.; Behr, J. P. *Biochemistry* **1991**, *30*, 4357–4361.
(44) Yuki, M.; Grukhin, V.; Lee, C.-S.; Haworth, I. S. *Arch. Biochem. Biophys.* **1996**, *325*, 39–46.

JP8058068

Response of model peptides on binding to DNA

To further validate FCL label for sensing peptide-DNA interactions we have selected 18 amino acids basic peptide from HIV-1 Tat protein. Selected peptide, Tat(44-61), is a linear basic fragment that is responsible for the binding to the TAR RNA sequence.

To characterize an effect of binding to oligonucleotides on the fluorescence we have selected the DNA analog of TAR RNA (dTAR) that forms complex with Tat(44-61) peptide. Addition of the oligonucleotide to FCL-Tat(44-61) leads to the strong changes in the fluorescence spectrum (**Fig. 3.7**). Formation of the complex is accompanied by about 4-fold decrease in the N*/T* band ratio and about 20 nm red shift in T* emission band maximum. Comparing this result with data in model solvent systems (see chapter 2.2.1) we could conclude that binding of the labeled peptide to DNA leads to strong decrease of the polarity and hydration of the environment. Meanwhile the effects are significantly smaller than ones observed for conjugates **C1** and **C2** (see above). Likely distance from the label to DNA in this case is longer due to much larger size of the Tat(44-61) peptide as compared with spermine polycation. Binding of FCL-Tat(44-61) to another oligonucleotides leads to similar but not identical changes in its emission spectrum (**Fig. 3.7**). The N*/T* band ratio of the peptide-DNA complex depends on the structure of oligonucleotide probably due to not equal peptide conformation and label-DNA distance in these complexes.

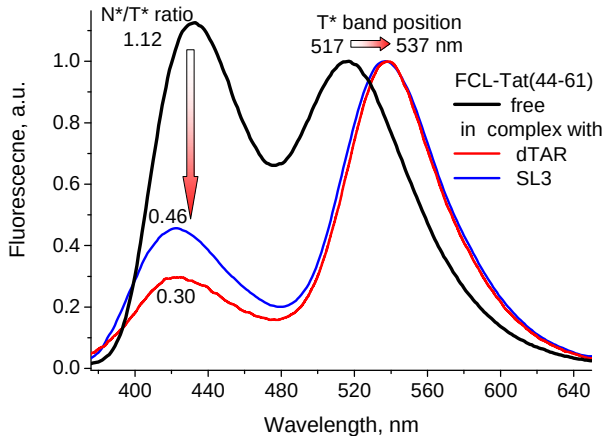

Figure 3.7. Comparison of FCL-Tat(44-61) fluorescence in free form (black line) and bound to oligonucleotides (blue and red lines). Fluorescence spectra recorded in pH 7 phosphate buffer using excitation at 340 nm and normalized by T* band emission.

Tests of the FCL label on model systems showed that the label can clearly detect interaction of labeled molecules (oligocations and peptides) with DNA. Moreover it can discriminate difference in the environment in complexes of the peptide with different oligonucleotides, which could be used for monitoring fine structural differences in the peptide-DNA complexes and for studies of interactions of a peptide with multiple sites of DNA.

3.2.2. Monitoring NC – oligonucleotide interactions

The nucleocapsid protein of HIV-1 (NC) is a 55 amino acid basic protein. Most of its functions are connected with its DNA and RNA binding properties (reviewed in the Chapter 1.3.4). In the present work, we applied the FCL label to study the interactions of the NC protein with oligonucleotides. A large part of NC-oligonucleotide interaction studies in the literature have been performed using a truncated peptide lacking the non-folded N-terminus that promotes nucleic acid aggregation but is not critical for the protein activity. In our studies, we synthesized and labeled both the full-length protein NC(1-55) and its truncated version NC(11-55) (**Fig. 3.8**).

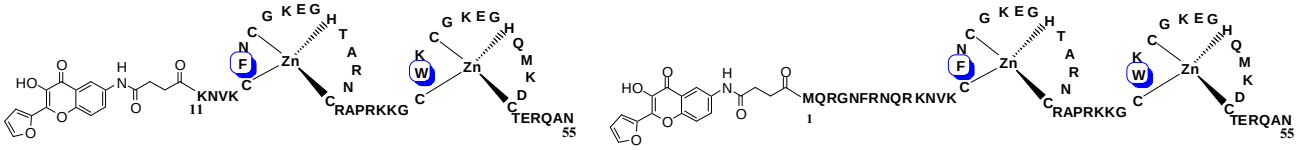

Figure 3.8. Structures of FCL-NC(1-55) and FCL-NC(11-55). The aromatic amino acids of NC are marked in blue.

Both labeled peptides show two-band fluorescence spectra in aqueous solutions. The N*/T* band ratio of FCL-NC(1-55) is significantly lower than those of FCL-NC(11-55) and the free label (see **Table 3.1** for the comparison), which suggests a specific interaction of the fluorophore with the hydrophobic amino acids at the N-terminus of the full-length NC. Interaction of the peptides with the SL3 stem-loop of the HIV-1 encapsidation sequence and to oligonucleotides in general, leads to decrease in the N*/T* ratio and a red shift of the T* band (**Fig. 3.9**). The truncated peptide shows larger spectroscopic effects on binding to oligonucleotides, in line with the closer position of the label to the amino acids participating in the interaction. Therefore, our further studies were focused on the interactions of FCL-NC(11-55) with the oligonucleotides.

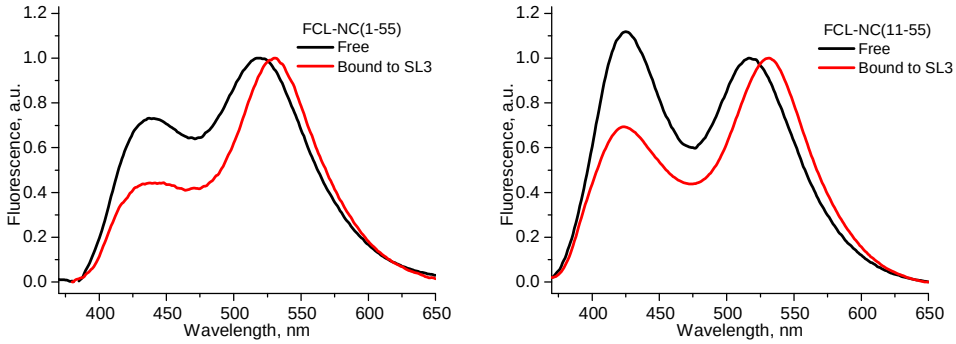

Figure 3.9. Effect of SL3 RNA interaction on the fluorescence spectra of FCL-NC(1-55) and FCL-NC(11-55).

Prior to the next steps, the activities of FCL-NC(11-55) and non-labeled peptide were compared to check the effect of the label on the peptide properties. One of the NC functions is to promote the annealing between complementary DNA sequences. Activities of the labeled and non-labeled peptides were assayed using doubly-labeled oligonucleotides [200, 201]. FCL-NC(11-55) was found to promote the annealing reaction, approximately with the same efficiency as the non-labeled peptide, while in the absence of protein the reaction is about 100 times slower (**Fig. 3.10**). These results indicate that the FCL label does not affect the peptide activity, probably due to its small size and its N-terminal position.

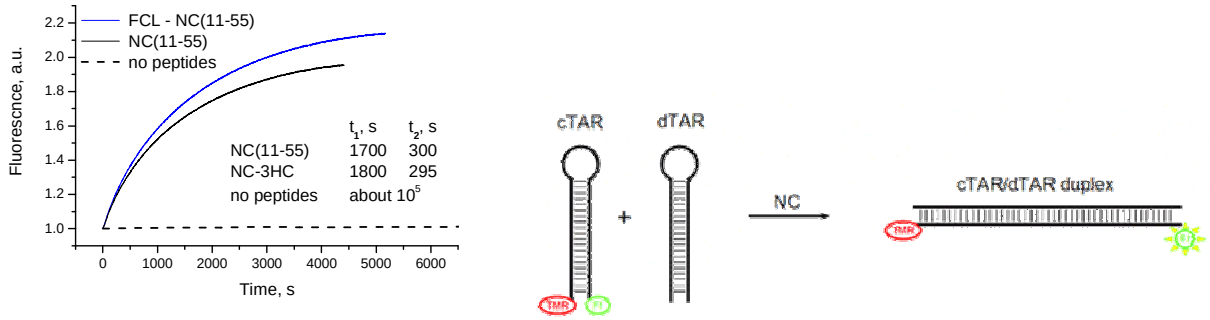

Figure 3.10. Activation by NC(11-55) and FCL-NC(11-55) of the annealing of cTAR with dTAR. The doubly labeled TMR-5'-cTAR-3'-Fl (10 nM) was mixed with 100 nM of unlabeled dTAR, either in the absence (dotted line) or in the presence of 330 nM FCL-NC(11-55) (dark solid line) or NC(11-55) (blue solid line), respectively.

Titration of FCL-NC(11-55) with oligonucleotides leads to a gradual decrease in the N*/T* band ratio, in proportion to the fraction of bound peptide. This titration could be used for calculation of the FCL-NC(11-55)/oligonucleotide binding constants using the N*/T* band ratio as an analytical signal. Values obtained by this method were found to be close to those obtained for the non-labeled peptide by monitoring the tryptophan fluorescence. For example, for the short oligonucleotide d(AACGCC) we found a binding constant of 1.5(±0.3) $\times 10^5$ M^{-1}, close to the 1.1(±0.2) $\times 10^5$ M^{-1} value reported for the non-labelled peptide [182].

The values of the N*/T* band ratios for the complexes between FCL-NC(11-55) and different oligonucleotides varied from about 0.4 for SL2 RNA to 0.85 for (-)PBS DNA. No correlation of these values with the binding affinity or the size of the oligonucleotide was found. In contrast, the values of the N*/T* band ratio correlated well with the 3D structure of the complexes [180, 188, 189, 211]. The lowest values were found with complexes where the peptide N-terminus is close to the nucleotide bases and the label can stack with them. To check our hypothesis, we synthesized NC(11-55) N-terminally labeled by a fluorescein and studied its rotational motions by time-resolved fluorescence anisotropy. A good correlation between the N*/T* band ratio of the FCL label and the contribution of the local motion of fluorescein in the anisotropy decay was observed (**Fig. 3.11**). This confirms that the response of the FCL label depends on the proximity with the oligonucleotide, allowing the label to stack with the bases or to contact with the phosphoribose backbone.

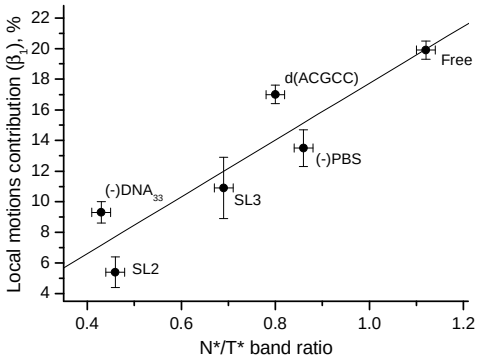

Figure 3.11. Correlation of the N*/T* ratio of FCL-NC(11-55) with the contribution of the local motion of the fluorescein dye in the time-resolved anisotropy decay of fluorescein-labeled-NC(11-55) for complexes with different oligonucleotides. Bars are corresponding to the experimental errors.

Discrimination of the different oligonucleotides by the label could be used for the identification of the NC preferential binding sites on longer oligonucleotides. This was shown on the example of the (-)DNA_{33} sequence (**Fig. 3.12**) corresponding to the 3′ terminal 33 nucleotides of the (-)DNA copy of the HIV-1 genome. (-)DNA_{33} consists of two stem-loops (SL_{14} and (-)PBS) and likely contains multiple binding sites for the NC. The fluorescence spectra of FCL-NC(11-55) bound to (-)DNA_{33} and to its SL_{14} fragment are similar, but differed markedly from that of the complex with (-)PBS (**Fig. 3.12**). This suggests that the SL_{14} loop is the preferential NC binding site in (-)DNA_{33}. Experiments with a mixture of SL_{14} and (-)PBS as well as the comparison of the binding constants of NC to the corresponding sequences confirmed this conclusion.

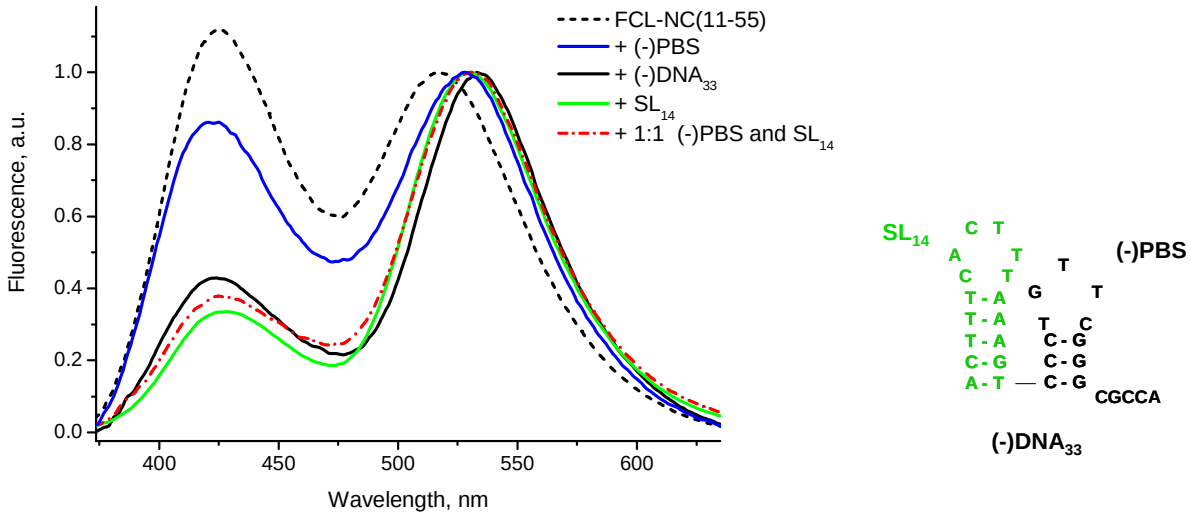

Figure 3.12. Normalized fluorescence spectra of FCL-NC(11-55) in interaction with (-)PBS (blue), SL_{14} (green), (-)DNA_{33} (black) and an equimolar mixture of (-)PBS and SL_{14} (red). FCL-NC(11-55) and oligonucleotide concentration were 0.4 μM and 0.8 μM, respectively. The spectrum of free FCL-NC(11-55) (black dashed curve) is shown for comparison. Measurements were performed in 10 mM phosphate buffer, 100 mM NaCl, pH 7.0 using an excitation wavelength of 340 nm.

Being attached to the N-terminus of the NC(11-55) peptide, the FCL label reports on the interaction with oligonucleotides by a change in the ratio of its two emission bands. This change in the ratiometric response results from a decrease in the exposure of the labeling site to bulk water induced by the proximity to nucleic bases and could be used for site-selective characterization of the peptide/oligonucleotide structures. Moreover, the dependence of the label response on the oligonucleotide sequence allows the identification of the preferential binding site(s) on oligonucleotides with multiple binding sites.

Application of the FCL label to the studies of NC-oligonucleotide interactions are presented in Article (7)

Article 7

Sensing peptide-oligonucleotide interactions by a two-color fluorescence label: application to the HIV-1 nucleocapsid protein

Nucleic Acids Research Advance Access published January 16, 2009

*Nucleic Acids Research, 2009, **1–12***
doi:10.1093/nar/gkn1083

Sensing peptide–oligonucleotide interactions by a two-color fluorescence label: application to the HIV-1 nucleocapsid protein

Volodymyr V. Shvadchak, Andrey S. Klymchenko*, Hugues de Rocquigny and Yves Mély*

Laboratoire de Biophotonique et Pharmacologie, Faculté de Pharmacie, UMR 7213 du CNRS, Université de Strasbourg, 67401 Illkirch, France

Received October 10, 2008; Revised December 22, 2008; Accepted December 23, 2008

ABSTRACT

We present a new methodology for site-specific sensing of peptide–oligonucleotide (ODN) interactions using a solvatochromic fluorescent label based on 3-hydroxychromone (3HC). This label was covalently attached to the N-terminus of a peptide corresponding to the zinc finger domain of the HIV-1 nucleocapsid protein (NC). On interaction with target ODNs, the labeled peptide shows strong changes in the ratio of its two emission bands, indicating an enhanced screening of the 3HC fluorophore from the bulk water by the ODN bases. Remarkably, this two-color response depends on the ODN sequence and correlates with the 3D structure of the corresponding complexes, suggesting that the 3HC label monitors the peptide–ODN interactions site-specifically. By measuring the two-color ratio, we were also able to determine the peptide–ODN-binding parameters and distinguish multiple binding sites in ODNs, which is rather difficult using other fluorescence methods. Moreover, this method was found to be more sensitive than the commonly used steady-state fluorescence anisotropy, especially in the case of small ODNs. The described methodology could become a new universal tool for investigating peptide–ODN interactions.

INTRODUCTION

Fluorescence is a powerful tool for investigating biomolecular interactions. The most widely used technique in this respect is FRET that allows measuring the distance between two fluorophores (1–5). However, FRET shows limitations since it requires double labeling. A single-labeling technique commonly used for the same purpose is steady-state fluorescence anisotropy (6,7), which senses changes in the fluorophore mobility upon interactions. Despite its wide use in bio-sensing technologies, fluorescence anisotropy gives frequently limited response on binding, since it depends on the fluorescence lifetime of the probe and different types of molecular motions such as the local motion of the probe and both segmental and overall motions of the labeled biomolecule.

Environment-sensitive (or solvatochromic) fluorescent dyes, which monitor biomolecular interactions by sensing environment changes at the labeled site, become an attractive alternative to fluorescence anisotropy in the recent years. A series of environment-sensitive fluorescent labels, such as Prodan derivatives (8–10), dimethylaminophtalimide (11), dimethylaminonaphtamides (12,13) and others (14) have recently been applied to study protein–protein interactions and protein conformational transitions (8,9,11,12,14). Short peptides labeled by these dyes were successfully used to study phosphorylation-dependent peptide–protein interactions (10), δ-opioid antagonist binding (15) and peptide binding to proteins of a major histocompatibility complex (MHC) at the cell surface (16). Biomolecular interactions commonly decrease the polarity at the labeling site due to screening from water by the binding of the protein partner (16). This change in the polarity can be readily detected by environment-sensitive labels through shifts in their emission maximum or changes in their fluorescence intensity. However, applications of these dyes for sensing interactions of peptides with oligonucleotides (ODNs) have not been described so far, likely because the ODN environment is relatively polar (17,18) so that polarity may not be dramatically affected by the interaction. In addition, most of the mentioned environment-sensitive dyes show relatively low quantum yields in polar protic media (12), and ODN bases frequently play a role of a fluorescence quencher (19,20). Therefore, for studying peptide–ODN interactions we have selected a 3-hydroxychromone (3HC) derivative, 2-(2-furyl)-3HC, which having a satisfactory

*To whom correspondence should be addressed. Tel: +33 3 90 24 42 63; Fax: +33 3 90 24 43 13; Email: yves.mely@pharma.u-strasbg.fr
Correspondence may also be addressed to Andrey Klymchenko. Tel: +33 3 90 24 42 55; Fax: +33 3 90 24 43 13;
Email: aklymchenko@pharma.u-strasbg.fr

quantum yield in polar protic solvents, shows a high sensitivity of its dual emission to environment changes in polar media (21,22). 3HC dyes undergo excited-state intramolecular proton transfer (ESIPT) (23) (Figure 1) resulting in the emission of both the normal (N*) excited state and the ESIPT product photo-tautomer (T*). The dual emission of 3HC dyes is highly sensitive to polarity and H-bonding interactions (21,24–29). Increase in the polarity and H-bond donor ability of solvents inhibits the ESIPT reaction and thus decreases the relative intensity of the ESIPT product (T*) (27). Moreover, the position of the maximum of the T* band, being insensitive to solvent polarity, exhibits high sensitivity to H-bond donor ability (21). Thus, the present class of fluorophores provides two independent information channels allowing a thorough characterization of the environment. These unique properties of 3HCs have already been applied for probing proteins, lipid bilayers and cell membranes as well as for monitoring protein–protein and polycation–DNA interactions (30–37).

As a target protein for labeling with our dye, we selected the nucleocapsid protein (NC) of the human immunodeficiency virus, type 1 (HIV-1). NC is a small (55 amino acids) basic protein, characterized by two rigid retroviral-type zinc fingers connected by a flexible basic linker and flanked by poorly folded N- and C-terminal basic domains (Figure 2) (38–40). NC is thought to be critically involved in the reverse transcription, integration and encapsidation steps of the viral life cycle, mainly through interaction with nucleic acids (41). NC binds both specifically (42–45) and non-specifically (46,47), to a large range of nucleic-acid sequences. Specific binding to the ψ encapsidation sequence is required for the selective recognition of viral RNA among the large excess of cellular RNAs (48,49). Selectivity is supported by the interaction of the hydrophobic platform at the top of NC folded fingers with the GXG- containing loops of the SL2 and SL3 stem loop sequences of ψ RNA (50–53). In contrast, the coating of the viral RNA by about 2000 copies of NC relies largely on NC ability to bind to nearly any sequence of five to seven nucleotides length (44,47,50,54,55). NC also exhibits nucleic-acid chaperone properties (56,57), which rely on its ability to transiently melt the secondary structure and to activate the annealing of complementary ODNs (58–70). These properties are thought to be essential during reverse transcription, to anneal the primer $tRNA^{Lys,3}$ to the RNA primer-binding site (PBS) and to promote the two obligatory strand transfers (71,72) which are required for copying the HIV-1 RNA genome into double-stranded DNA.

In the present work, to explore the potency of the environment sensitive 3HC dyes for sensing peptide–ODN interactions, we coupled a newly designed 3HC label selectively to the N-terminus of the NC (11–55) peptide using solid phase peptide synthesis. This peptide corresponding to the domain of NC fingers was preferred to the native NC since it preserves the nucleic-acid binding and chaperone properties of the protein (65–67,73) but does not aggregate the ODNs (74). The response of the labeled peptide on interaction with SL2 RNA, SL3 RNA, (−)PBS DNA and d(ACGCC) (Figure 2) was investigated

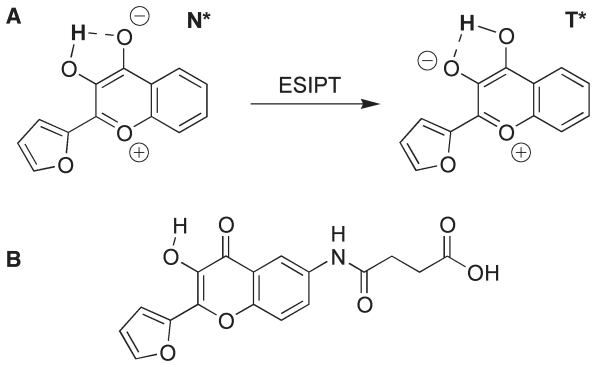

Figure 1. Proton transfer reaction of a 3HC dye in the excited state (**A**) and chemical structure of the used 3HC label (**B**).

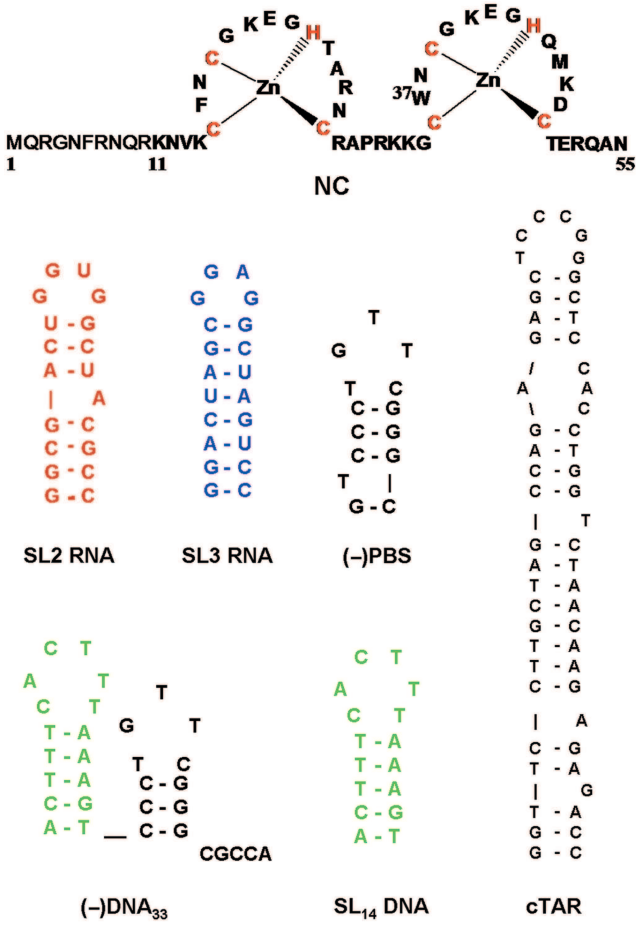

Figure 2. Sequences of the NC protein and the ODNs used in this study. Secondary structures are based on ref. (52,62,66,75,78,79) and *m*-fold predictions.

and correlated with the known 3D structure of these complexes (52,53,76,77) as well as with the fluorescence anisotropy response of fluorescein-labeled NC(11–55) in the same complexes. Finally, the probe was applied to demonstrate the existence of preferential binding sites on ODNs with multiple NC-binding sites.

MATERIALS AND METHODS

Materials

Reagents were from Merck, Sigma-Aldrich or Applied Bio Systems (Foster City, USA). ODNs were synthesized and HPLC-purified by IBA GmbH (Germany). Their sequences are given in Figure 2. ODN concentrations were determined using the following extinction coefficients at 260 nm (ε_{260}, $M^{-1} \times cm^{-1}$): 48 360, 58 050, 231 000, 246 000, 168 000, 178 000, 325 000 and 521 900 $M^{-1} \times cm^{-1}$ for d(ACGCC), d(AACGCC), SL2 RNA, SL3 RNA, SL_{14} DNA, (−)PBS DNA, (−)DNA_{33} and cTAR DNA, respectively.

Synthesis of *N*-(2-furan-2-yl-3-hydroxychromon-6-yl)-succinamic acid

Total 0.2 g (0.82 mmol) of 6-amino-2-furan-2-yl-3HC (37) was dissolved in 10 ml dry DMF and 0.09 g (0.9 mmol) of succinic anhydride was added to this solution. The mixture was left for stirring overnight. Then, it was poured into water and filtrated to give 0.235 g (84%) of the final acid. ^{1}H NMR (300 MHz, DMSO-d6) δ 10.27 (s, 1H, NH), 8.44 (d, $J = 3.5$ Hz, 1H, ArH), 8.01 (s, 1H, ArH), 7.89 (d, $J = 9$ Hz, 1H, ArH), 7,67 (d, $J = 9$ Hz, 1H, ArH), 7.28 (d, $J = 2.5$ Hz, 1H, ArH), 6.78 (s, 1H, ArH), 2.59–2.50 (m, 4H, CH_2CH_2).

3HC-NC(11–55). The NC(11–55) peptide (Figure 2) was synthesized by solid phase peptide synthesis on a 433A synthesizer (ABI, Foster City, CA) as previously described (80). The synthesis was performed at a 0.1 mmol scale using the standard fluorenylmethoxycarbonyl (Fmoc)-amino-acid-coupling protocol starting from 0.54 mmol/g HMP Asn-preloaded resin (ABI). At the end of the synthesis, 100 mg of Fmoc-deprotected peptidylresin was isolated, and washed twice by NMP. Four equivalents of the label [*N*-(2-furan-2-yl-3-hydroxychromon-6-yl)-succinamic acid] were mixed with 4 eq. of HBTU/HOBt coupling solution (in DMF) and 5 eq. of DIEA. This mixture was immediately added to the peptidylresin and stirred at 40°C for 40 min. Resin was filtrated and washed by NMP and methanol.

Cleavage of the peptidylresin and deprotection was performed for 2 h using a 10 ml trifluoroacetic acid (TFA) solution containing water (5%, v/v), phenol (2%, w/v), thioanisole (5%, v/v) and ethanedithiol (2.5%, v/v). Solution was concentrated *in vacuo* and the peptide was precipitated using ice-cold diethyl ether and pelleted by centrifugation. The pellet was then washed with diethyl ether and dried before solubilization with aqueous TFA (0.05%, v/v). Purification by HPLC was carried out on a C8 column (uptisphere 300A, 5 μm; 250 × 10, Interchim, France) in water/acetonitrile mixture containing 0.05% TFA with a linear gradient 10–70% of acetonitrile for 30 min and monitored at 360 nm (3HC dye absorption). Molecular mass found by ion spray mass spectrometry (5463) corresponds to the calculated value.

Fl-NC(11–55). Peptide synthesis was performed as for 3HC-NC(11–55), except that labeling was done with 4 eq. of 5(6)-carboxyfluorescein (Fl) overnight. In the crude mixture, two fluorescein-containing peptides in the ratio 10:1 were found. The main product was isolated by HPLC using the same conditions as for 3HC-NC(11–55). Molecular mass found by ion spray mass spectrometry (5496) corresponds to the calculated value.

Preparation of Zn-bound peptides. Lyophilized peptides were dissolved in water (~0.5 mg in 500 μl). Then, the peptide concentration was determined using an extinction coefficient of 15 000 $M^{-1} \times cm^{-1}$ at 350 nm for 3HC-NC(11–55) and 86 000 $M^{-1} \times cm^{-1}$ at 500 nm for Fl-NC(11–55). Next, 2.2 molar equivalents of $ZnSO_4$ were added to the peptide and pH was raised to its final value, by adding buffer. The increase of pH was done only after zinc addition to avoid oxidization of the zinc-free peptide. Noticeably, addition of a large excess of Zn^{2+} ions should be avoided since it can affect the 3HC fluorescence properties.

3HC-G5. The pentaglycine peptide was synthesized as described above. N-terminal labeling by *N*-(2-Furan-2-yl-3-hydroxychromon-6-yl)-succinamic acid was performed with 1.5 eq of the label, 1.5 eq of HBTU/HOBt coupling solution (in DMF) and 3 eq of DIEA overnight. Cleavage was done using 10 ml TFA containing water (10% v/v) and triisopropilsilane (2.5%, v/v). The product was purified by HPLC using the same conditions as for 3HC-NC(11–55) but with a linear gradient 10–50% of acetonitrile for 20 min.

Spectroscopic measurements

Unless otherwise indicated, the experiments were performed in 10 mM phosphate buffer, pH 7.0, 100 mM NaCl, at 20°C.

Absorption spectra were recorded with a Cary 4000 UV-visible spectrophotometer (Varian). Fluorescence spectra were recorded on FluoroMax3 and FluoroLog spectrofluorimeters (Jobin Yvon) equipped with thermostated cell compartments. Steady-state anisotropy was measured on SLM 8000 spectrofluorometer (Aminco, Urbana, IL). Fluorescence spectra were corrected for Raman scattering. Quantum yields were calculated using quinine sulphate in 0.5 M sulphuric acid (quantum yield, $\phi = 0.577$) as a ref. (81). Excitation wavelength was 340 nm for the 3HC-label and 480 nm for the fluorescein label. To determine the affinity of 3HC-NC(11–55) for the ODNs, fixed amounts of the peptide were titrated with ODNs by monitoring the 3HC two-band fluorescence. Affinity constants were determined from direct fitting of the experimental signal to the rewritten Scatchard equation:

$$I = I_0 - \frac{(I_0 - I_t)}{P_t} \times \frac{(1 + (P_t + nN_t)K_a) - \sqrt{(1 + (P_t + nN_t)K_a)^2 - 4P_t nN_t K_a^2}}{2K_a} \quad \mathbf{1}$$

where I and I_t are the signal (the N^*:T^* intensity ratio) at a given and a saturating ODN concentration, respectively, I_0 is the signal in the absence of ODN, N_t is the

total ODN concentration, P_t is the total concentration of peptide, K_a is the apparent affinity constant, n is the number of binding sites. The parameters were recovered from non-linear fits of Equation (1) to experimental datasets by the Microcal Origin^{TM} 6.0 program.

Time-resolved fluorescence measurements were performed with the time-correlated, single-photon counting technique using the excitation pulses at 480 nm provided by a pulse-picked frequency doubled Ti-sapphire laser (Tsunami, Spectra Physics) pumped by a Millenia X laser (Spectra Physics). The emission was collected through a polarizer set at the magic angle and an 8 nm band-pass monochromator (Jobin-Yvon H10) at 520 nm. The instrumental response function was recorded with a polished aluminium reflector, and its full-width at half-maximum was 40 ps.

For time-resolved anisotropy measurements, the fluorescence decay curves were recorded at the vertical and horizontal positions of the polarizer as described (82) and analyzed by the following equation:

$$r(t) = \frac{I_{\parallel}(t) - GI_{\perp}(t)}{I_{\parallel}(t) + 2GI_{\perp}(t)} = r_0 \sum \beta_i \exp\left(\frac{-t}{\theta_i}\right) \qquad 2$$

where β_i are the amplitudes of the rotational correlation times θ_i; $I_{||}$ and $I_{\perp}$ are the intensities collected at emission polarizations parallel and perpendicular, respectively, to the polarization axis of the excitation beam, and G is the geometry factor at the emission wavelength, determined in independent experiments.

Time-resolved intensity and anisotropy data were treated with a non-linear least-square analysis using a home-made software (kindly provided by G. Krishnamoorthy) and the Maximum Entropy Method (MEM) (83). In all cases, the χ^2 values were close to 1, and the weighted residuals as well as the autocorrelation of the residuals were distributed randomly around 0, indicating an optimal fit.

RESULTS AND DISCUSSION

Spectroscopic characteristics of the free 3HC label

For labeling the N-terminus of NC(11–55), we have synthesized a 3HC derivative bearing a carboxyl functionality. First, we characterized the spectroscopic properties of this label in different organic solvents. The fluorescence spectra of the label are composed of two bands (Figure 3A), where the short- and long-wavelength bands can be unambiguously attributed to the emission of the N* and T* forms of the fluorophore, respectively (Figure 1).

The nature of the solvent affects strongly the dual emission of the label. In a non-polar aprotic solvent ethyl acetate, the label shows a very low ratio of the N* to T* fluorescence intensities. More polar aprotic solvent DMF induces an increase of the N*:T* band ratio. In protic solvents, the N*:T* intensity ratio is much higher than in aprotic solvents, indicating that the H-bond donor ability of the former inhibits the ESIPT reaction, and thus

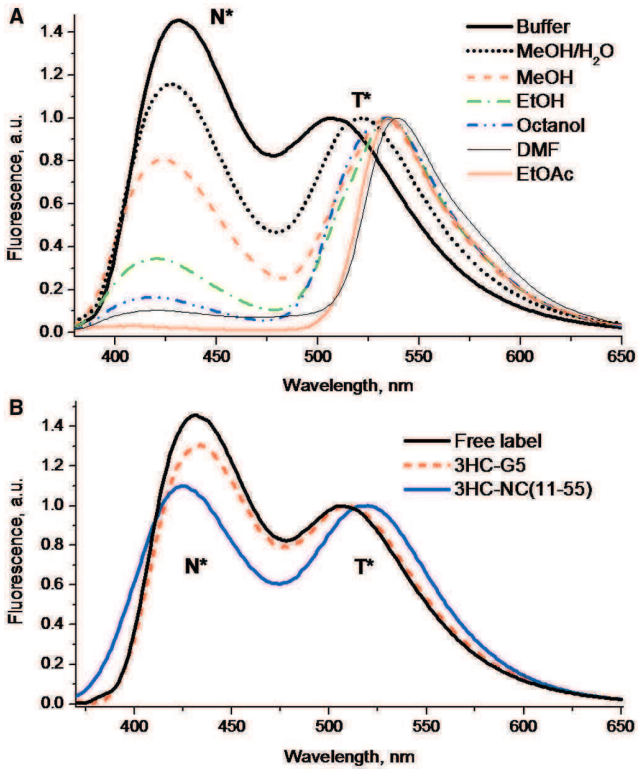

Figure 3. Fluorescence spectra of the free 3HC label in different solvents (**A**) and the labeled peptide 3HC-NC(11–55) in buffer (**B**). The spectra of the free label and the labeled model peptide (3HC-G5) in buffer are presented for comparison. All the spectra were normalized at the T* band. Excitation wavelength was 340 nm. Buffer was 10 mM phosphate buffer, 100 mM NaCl, pH 7.0.

Table 1. Spectroscopic properties of the free label and the labeled peptides[a]

	Solvent	λ_{Abs} (nm)	λ_{N^*} (nm)	λ_{T^*} (nm)	N*:T*	QY (%)
Label	Buffer	357	431	508	1.47	2.0
	MeOH/H_2O	354	427	521	1.16	3.2
	MeOH	349	423	533	0.81	5.6
	EtOH	351	420	535	0.34	6.1
	Octanol	356	419	534	0.16	13.0
	DMF	344	421	539	0.10	6.9
	EtOAc	345	410	535	0.03	13.0
3HC-G5	Buffer	360	432	510	1.33	3.3
3HC-NC(11–55)	Buffer	358	426	517	1.12	7.8

[a]λ_{Abs}, λ_{N^*} and λ_{T^*} are the maxima of absorption, N* and T* emission bands respectively. N*:T* is the intensity ratio of the two emission bands measured at the peak maxima; QY is the fluorescence quantum yield. MeOH/H_2O is 1/1 methanol–water mixture. EtOAc is ethyl acetate. Excitation wavelength was 340 nm. The peptides were in 10 mM phosphate buffer, 100 mM NaCl, pH 7.0.

decreases the emission of the ESIPT product T* (21,84). Moreover, the band ratio increases with polarity in alcohols and reaches its highest value in buffer (Figure 3A, Table 1). The high value of the N*:T* ratio in buffer was independent on NaCl concentration (data not shown), indicating that it is due to water. In addition, due to its strong H-bond donating properties, water induces an

outstanding blue shift of the T* band in comparison with alcohols or aprotic solvents. The observed increase of the N*:T* intensity ratio with the polarity and H-bond donor ability of the solvents is fully in line with that reported for the parent non-substituted 2-(2-furyl)-3-HC (21,84). Therefore, being attached to a peptide, the present label is expected to report on the accessibility of the site of labeling to bulk water (which is characterized by high polarity and H-bond donor ability) by its N*:T* ratio and the position of the T* band.

Synthesis and characterization of the labeled NC(11–55) peptide

To achieve selective labeling, NC(11–55) peptide was prepared by solid phase synthesis (80) and being attached to the resin was further labeled at its N-terminus with the carboxylic-acid derivative of 3HC. The HPLC-purified labeled peptide was checked by mass spectrometry, confirming that the expected labeled peptide was obtained. The chaperone properties of the labeled peptide were tested using previously described protocols (62,64,67) and were found comparable to those of the native peptide (Figures S1 and S2 in Supplementary Data), indicating that the 3HC label does not interfere with the peptide activity. Moreover, since these chaperone properties are exquisitely sensitive on the proper folding of NC(11–55) (73), it can be further concluded that the 3HC label does not alter the folding of the peptide. Thus, as was expected from its relatively small size and N-terminal location with a four amino-acid separation from the proximal Zn finger, the probe does not perturb the activity and the folding of the peptide.

The emission spectrum of 3HC-NC(11–55) exhibited significant differences with the spectrum of the free label in water, with a decrease of the N*:T* ratio from 1.47 to 1.12 and a 9 nm red-shift of the T* band (Figure 3B, Table 1). Moreover, its fluorescence quantum yield was nearly 4-fold higher than that of the free label in water. According to the data of the probe in model solvents (Table 1) and our previous data (21,84), these changes indicate a decrease in the polarity and/or H-bond donor ability in the probe environment. This decrease was independent of the peptide concentration in the 50–1000 nM range (data not shown) and was thus interpreted as an intramolecular screening of the label from the bulk water in conformations where the probe is in proximity to the KNVK(11–14) sequence and to the zinc finger domain (Figure 4) of the labeled peptide. Indeed, a large collection of conformations is probably explored by the N-terminal domain of NC(11–55) as a consequence of the flexibility of the spacer connecting the label to the peptide and the flexibility of the KNVK(11–14) sequence to which the label is linked (39,40). Noticeably, both the N*:T* band ratio and the T* band position of 3HC-NC were marginally dependent on the NaCl concentration (data not shown), indicating that the intramolecular screening of the dye from water was poorly affected by the ionic strength.

To further assess the effect of the peptide backbone on the fluorescence properties of the 3HC label, we coupled it

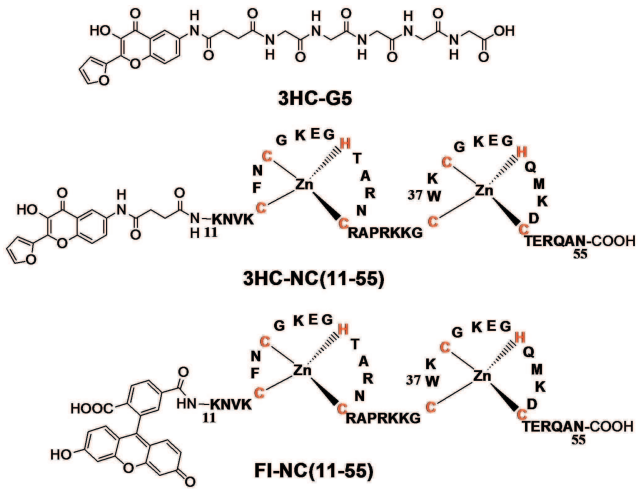

Figure 4. Labeled peptides.

to a pentaglycine peptide (3HC-G5) using the same solid phase-based method (Figure 4). As with NC(11–55), labeling of G5 induced a decrease of the N*:T* ratio (from 1.47 to 1.33) and a red-shift (2 nm) of the T* band in respect with the spectrum of the free label in water (Figure 3B, Table 1), as well as a significant fluorescence quantum yield increase. Though less pronounced than with NC(11–55), these changes indicate that interactions of the probe with the flexible backbone of the G5 peptide can reduce the overall accessibility of the probe for water molecules. The more efficient screening from the bulk water seen with NC(11–55) as compared to G5, is likely due to the amino-acid side chains of NC(11–55), which are absent in the G5 peptide.

Interactions of 3HC-NC(11–55) with single binding site ODNs

To explore the applicability of the 3HC label to probe peptide–ODN interactions, we first characterized the interaction of the labeled peptide with d(ACGCC), SL2 RNA, SL3 RNA and (−)PBS DNA (Figure 2). These sequences were selected since they preferentially bind one NC molecule per ODN and the 3D structures of their complexes with NC have been solved (52,53,76,77).

All ODNs induced a substantial decrease of the N*:T* ratio and a red-shift of the T* band in respect with the free 3HC-NC(11–55) peptide (Table 2), indicating an increased screening of the probe from the bulk water. Competition experiments using the SL3 sequence showed that the labeled and the non-labeled peptides bind to the same binding site (Figure S3 in Supplementary Data), suggesting that the 3HC label does not change the binding specificity. Remarkably, large spectroscopic differences were observed among the tested ODNs, underlining differences in the interaction of the N-terminal part of the peptide with these ODNs. The strongest changes were observed with the SL2 stem-loop, which binds strongly NC at the level of its loop (52). With SL2, the N*:T* intensity ratio dropped to 0.46 and the T* band shifted 16 nm to the red (Figure 5, Table 2). The resulting spectrum and quantum

Table 2. Spectroscopic properties of 3HC-NC(11–55) complexes with ODNs[a]

Complex with	λ_{Abs} (nm)	λ_{N^*} (nm)	λ_{T^*} (nm)	$N^*:T^*$	QY (%)
Free	358	426	517	1.12	7.8
SL2 (RNA)	360	425	533	0.46	7.0
SL3 (RNA)	362	424	532	0.69	4.4
(−)PBS	361	423	528	0.86	4.3
d(ACGCC)b	359	424	519	0.77	6.7
d(AACGCC)b	359	426	526	0.63	4.1

[a]λ_{Abs}, λ_{N^*} and λ_{T^*} are the maxima of absorption, N^* and T^* emission bands respectively. $N^*:T^*$ is the intensity ratio of the two emission bands measured at the peak maxima; QY is the fluorescence quantum yield. Excitation wavelength was 340 nm. Measurements were done in 10 mM phosphate buffer, 100 mM NaCl, pH 7.0. [b]For measurements with d(ACGCC) and d(AACGCC), NaCl concentration was 30 mM due to their lower binding affinity.

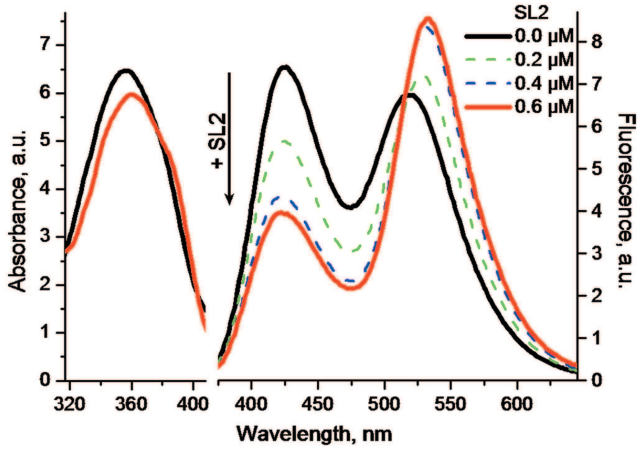

Figure 5. Changes in the absorption (left) and emission (right) spectra of 3HC-NC(11–55) on binding to SL2 RNA. The spectra of 0.4 μM 3HC-NC(11–55) was recorded in the absence (black) and in the presence of 0.2 (green) 0.4 (blue) and 0.6 μM (red) SL2 RNA in 10 mM phosphate buffer, 100 mM NaCl, pH 7.0. Excitation wavelength was 340 nm.

yield were close to that of the free probe in ethanol, indicating a strong screening of the label from water in the NC(11–55)/SL2 complex, with marginal quenching of the probe by SL2. Moreover, binding of the peptide to SL2 resulted in a significant absorbance decrease (8% hypochromicity) and a 3 nm red shift of the absorption maximum (Table 1, Figure 5), suggesting a stacking of the label with the SL2 bases. Thus, the 3HC label senses the formation of the 3HC-NC(11–55)/SL2 complex as a decrease in its exposure to water, likely due to its stacking with the ODN bases (37). To strengthen this conclusion, these spectral changes were further related to the known structure of the full-length NC protein bound to SL2. Since NC binds with the SL2 loop mainly through its zinc fingers, and since NC and NC(11–55) exhibit similar binding constants to ODNs (50,73), we reasonably assume that the two proteins bind similarly to SL2. According to the NMR data, the distance of the α-amino group of Lys11 to the SL2 stem in the complex is sufficiently short to allow stacking of the 3HC probe with the ODN bases (Figure 6A).

With SL3, the spectral changes of 3HC-NC(11–55) were slightly less pronounced than with SL2, showing a $N^*:T^*$ ratio value of 0.69 and a 15 nm red-shift of the T^* band (Figure 7). These changes were also associated with a significant decrease of the absorbance (8% hypochromicity) and a 4 nm red-shift of the absorption maximum, indicating that the decreased exposure of the probe to water may also be due to its stacking with the bases. As for SL2, the structural model of the NC/SL3 complex (52) suggests that the distance of the N-terminal amino group of NC(11–55) to the SL3 stem allows the stacking of 3HC with one of the bases of the stem (data not shown).

In contrast to SL2 and SL3, only limited spectroscopic changes were observed with d(ACGCC) since its binding to 3HC-NC(11–55) decreased the $N^*:T^*$ ratio only to a 0.77 value and shifted the T^* band by only 2 nm. Moreover, no significant change in the absorption spectrum could be observed, indicating that the stacking of the 3HC probe with the d(ACGCC) bases is negligible. Our data are in line with the NMR-derived structure of the NC(12–53)/d(ACGCC) complex showing that the N-terminus of the peptide does not directly interact with the ODN (Figure 6B) (77). Furthermore, as compared to the NC(12–53) peptide, the additional Lys11 residue of the NC(11–55) peptide is expected to further increase the distance between the peptide N-terminus and the 5′-end of the ODN. Consequently, the limited spectroscopic changes observed with d(ACGCC) are likely due to the poor screening of the 3HC probe from water in conformations where the flexible extremities of the peptide and the ODN contact each other. To check our interpretation, we extended the d(ACGCC) sequence by an additional A residue at its 5′-end. Since the determinant binding region is the central CGC sequence (77), NC(11–55) binds similarly to d(ACGCC) and d(AACGCC) (82). Interaction of 3HC-NC(11–55) with d(AACGCC) resulted in a larger red shift of the T^* band (9 nm) than with d(ACGCC) (2 nm), as well as a larger decrease in the $N^*:T^*$ ratio (Figure 7). According to the NMR-derived NC(12–53)/d(ACGCC) structure (Figure 6B), the additional A nucleotide should come closer to the peptide N-terminus and additionally screen the label from water.

Finally, the smallest decrease in the $N^*:T^*$ ratio was observed with (−)PBS. However, the shift in the T^* band appears rather large, being of 11 nm. As for d(AC GCC), no decrease in the 3HC absorbance and thus, only marginal stacking of the 3HC probe with the bases occurs on binding of (−)PBS. As a consequence, the observed decrease in the $N^*:T^*$ ratio and the red-shift of the T^* band are likely due to transient contacts of the probe with the backbone of the (−)PBS stem (Figure 6C). Since the phosphoribose backbone of the stem is more hydrated than the internal base pair region, only limited shielding of the 3HC label from water can be achieved through this interaction.

Taken together, our data show that the 3HC probe can sensitively differentiate the tested ODNs, both by its

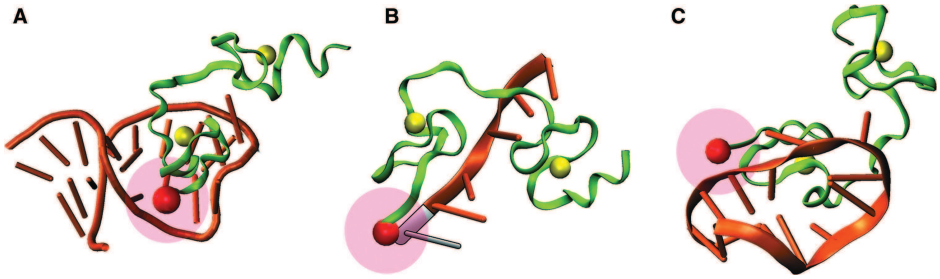

Figure 6. 3D structure of NC complexes with SL2 (**A**); d(ACGCC) (**B**) and (−)PBS (**C**). Structures are drawn based on NMR data [ref. (53,77,76) corresponding to PDB structures: 1A1T, 1BJ6, 2EXF, respectively]. The red sphere represents the position of the α-amino group of Lys11 (A) and Asn12 (B, C), respectively. The pink sphere corresponds to all possible positions of the 3HC probe, taking into account the length of the linker. Zn atoms are presented as yellow spheres. The nucleotide in gray (B) shows the assumed position of the additional 5′ end A-residue in d(AACGCC).

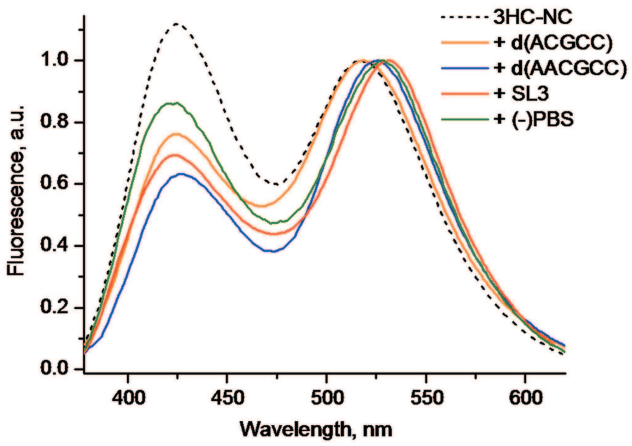

Figure 7. Normalized fluorescence spectra of 3HC-NC(11–55) complexes with SL3 (red), (−)PBS (green), d(ACGCC) (orange) and d(AACGCC) (blue). The spectrum of the free 3HC-NC(11–55) peptide is given for comparison (dashed black curve). Peptide concentration was 0.2 μM with a 3HC-NC(11–55)/ODN ratio of 1:2 for SL2 and (−)PBS. The buffer was 10 mM phosphate, 100 mM NaCl, pH 7.0. To ensure complete peptide binding with d(ACGCC) and d(AACGCC), the salt concentration was decreased to 30 mM, while the peptide and ODN concentrations were raised to 1 μM and 10 μM, respectively. In these conditions, about 95% of the peptide was saturated by the ODNs (50).

N^*:T^* ratio and the position of its T^* band. The response of the probe likely depends on the proximity of the peptide N-terminus with the ODN and the possibility for the probe to stack with the ODN bases or to contact with the phosphoribose backbone.

To further characterize the environment changes affecting the N-terminus of NC(11–55) on its interaction with ODNs, we investigated by time-resolved fluorescence anisotropy, the interaction of the same ODNs with NC(11–55) labeled at its N-terminus with fluorescein, Fl-NC(11–55). This technique allows characterizing the changes in the local motion of the probe and the tumbling of the labeled protein, resulting from the ODN binding. Similar to 3HC, the Fl probe did not significantly modify the folding and the chaperone properties of NC(11–55) (data not shown). The time-resolved anisotropy decay of the fluorescein-labeled NC(11–55) was characterized by two correlation times (Table 3). The 2.6 ns correlation time is in excellent agreement with the 2.3 ns correlation time previously reported for the tumbling motion of the NC(12–53) peptide, as measured from the time-resolved anisotropy of the intrinsic Trp37 residue (85). The 0.23 ns component is typical of the probe local motion (85,86). The moderate amplitude ($\beta_1 = 0.20$) associated with this short component suggests that Fl rotation is restricted, likely by the proximal finger and the KNVK(11–14) sequence. The restriction of Fl local motion is fully consistent with the partial screening from water observed for 3HC when it is coupled to NC(11–55). Addition of ODNs increased the long correlation time, as expected from the dependence of the tumbling motion on the size and thus, on the molecular weight of the complex. A new intermediate correlation time (1–1.6 ns) appeared in the presence of ODNs, likely due to a segmental motion independent of the overall peptide motion. More interestingly, a sequence-dependent decrease in the amplitude β_1 of the short-lived correlation time was observed. This decrease in the β_1 value indicates that the bound ODN further restricts the accessible volume in which Fl can rotate. Remarkably, the amplitude associated with the Fl local motion linearly correlates with the N^*:T^* ratios observed with 3HC-NC(11–55) (Figure 8), further substantiating the established dependence of the 3HC response on the proximity of the probe with the ODN. Moreover, this correlation also suggests that the two dyes behave similarly, so that no specific interaction of 3HC with the ODNs biases its spectroscopic response.

As a consequence, the N^*:T^* ratio of the 3HC label provides through simple fluorescence intensity measurements, information on the proximity of the labelling site with the ODN, comparable to that obtained from time-resolved measurements with the Fl label. To further show the potency of the proposed 3HC-based methodology, we compared it with steady-state fluorescence anisotropy, which is commonly used as another single-labeling technique for sensing biomolecular interactions. The steady-state fluorescence anisotropy data of the Fl-labeled protein free and bound to the various ODNs are reported in Table 3. No significant change in the Fl-NC(11–55) steady-state anisotropy could be observed with addition of relatively small ODNs, d(ACGCC) or (−)PBS, while with larger ODNs, SL2 and SL3, the Fl anisotropy showed a significant increase. In sharp contrast, significant changes in the N^*:T^* ratios accompanied the binding of all

Table 3. Time-resolved and steady-state fluorescence anisotropy of fluorescein-labeled NC(11–55) in complexes with different ODNs[a]

	θ_1 (ns)	β_1	θ_2 (ns)	β_2	θ_3, (ns)	β_3	r	N*:T*
Free	0.23 ± 0.01	0.20 ± 0.01	–	–	2.6 ± 0.2	0.80 ± 0.01	0.102 ± 0.004	1.12
d(ACGCC)	0.12 ± 0.01	0.18 ± 0.01	1.0 ± 0.3	0.36 ± 0.09	3.2 ± 1	0.46 ± 0.09	0.105 ± 0.004	0.80
(−)PBS	0.12 ± 0.01	0.14 ± 0.01	1.0 ± 0.3	0.39 ± 0.08	3.6 ± 1	0.47 ± 0.09	0.106 ± 0.004	0.86
SL3	0.12 ± 0.01	0.14 ± 0.02	1.6 ± 0.2	0.46 ± 0.06	7.1 ± 1	0.40 ± 0.05	0.132 ± 0.004	0.69
SL2	0.13 ± 0.01	0.05 ± 0.01	1.3 ± 0.2	0.43 ± 0.08	6.4 ± 0.9	0.52 ± 0.08	0.141 ± 0.004	0.46

[a]Results of at least two independent measurements. θ_1 is the correlation time describing the local probe motion and β_1 is the contribution of this motion to the fluorescence depolarization. θ_2/β_2 and θ_3/β_3 describe segmental and overall motions, respectively. r corresponds to the steady-state fluorescence anisotropy. N*:T* is the band intensity ratio of the 3HC label shown for the comparison.

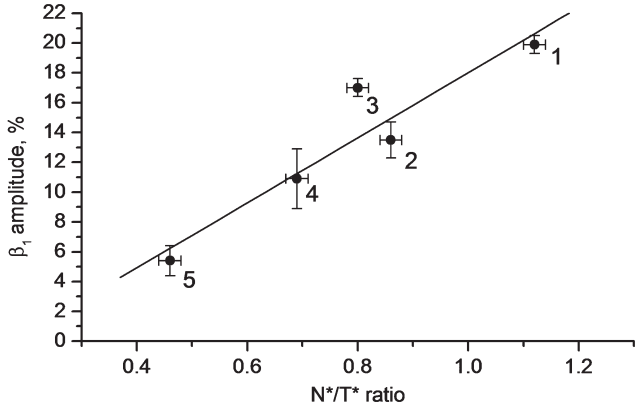

Figure 8. Correlation of the N*:T* ratio of 3HC-NC(11–55) with the time-resolved amplitude β_1 associated with the fluorescein local motion in Fl-NC(11–55) for their complexes with different ODNs. Bars are corresponding to the experimental errors. Points correspond to free NC(11–55) ('1') and complexes with (−)PBS ('2'), d(ACGCC) ('3'), SL3 ('4') and SL2 ('5').

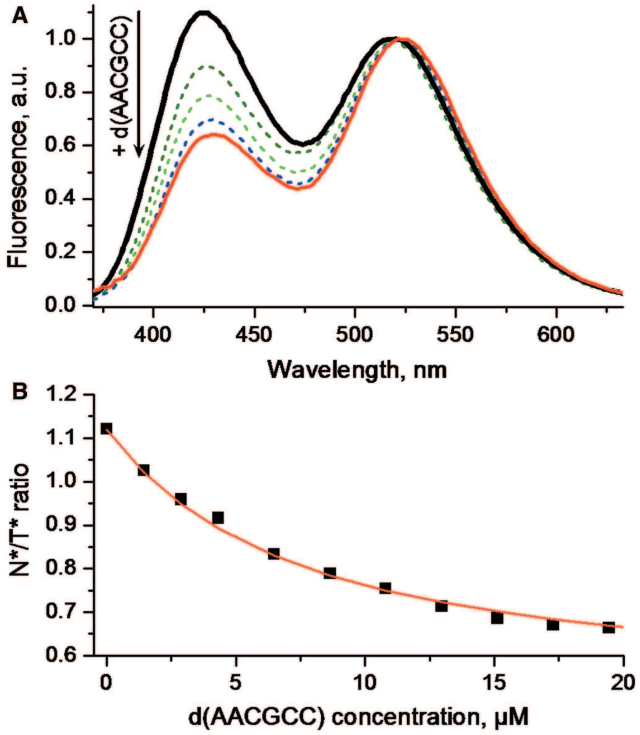

Figure 9. Titration of 3HC-NC(11–55) with d(AACGCC) monitored by 3HC fluorescence. (**A**) Normalized fluorescence spectra. (**B**) Titration curve. The solid red line corresponds to the fit of the data points (squares) by a one binding site model. The calculated binding constant was $1.5(\pm 0.3) \times 10^5\,M^{-1}$. Peptide concentration was 1 μM. Experimental conditions were as for Figure 5.

the studied ODNs to 3HC-NC(11–55), including the small ones, indicating that the 3HC-based approach is not limited by the ODN size. In fact, the environment-sensitive label 3HC reports exclusively on the local properties of the interaction site, so that its signal is not directly affected by variation in the molecular weight of the complex. Thus, labeling peptides with 3HC and monitoring the changes in the N*:T* ratio appears as an interesting and simple methodology for sensing interactions based on the proximity of the labeled site with the ODN, instead of sensing changes in the molecular weight as with anisotropy-based methods. Thus, the methods of anisotropy and the ratiometric measurements with the 3HC label appear complementary.

Since large changes in the N*:T* ratio accompanied the binding of the various ODNs to 3HC-NC(11–55), we next explored the possibility to use these changes to determine the binding constants of the NC(11–55)/ODN complexes. The d(AACGCC) and the SL3 RNA were taken as representative examples. Addition of increasing concentrations of d(AACGCC) gradually decreased the N*:T* ratio (Figure 9). Plotting the N*:T* ratio as a function of the 3HC-NC(11–55) concentration and assuming a 1/1 stoichiometry, we could adequately fit the binding curve (Figure 9B) with a binding constant of $1.5(\pm 0.3) \times 10^5\,M^{-1}$, close to the $1.1(\pm 0.2) \times 10^5\,M^{-1}$ value reported in the literature for non-labeled NC(12–53) (50). Similarly, titrations of 3HC-NC(11–55) with SL3 (data not shown) provided a binding constant of $2.7(\pm 0.6) \times 10^6\,M^{-1}$, again in reasonable agreement with the $1.0(\pm 0.2) \times 10^6\,M^{-1}$ value obtained with the slightly shorter NC(12–53) peptide (50). Both examples showed that the 3HC label does not strongly affect the peptide–ODN interaction and could thus, be used to determine the corresponding binding constants.

Interactions of 3HC-NC(11–55) with multiple binding site ODNs

To further characterize the potential use of the 3HC label in peptide–ODN interactions, we next investigated the interaction of 3HC-NC(11–55) with the (−)DNA_{33}

sequence (Figure 2) corresponding to the 3′-terminal 33 nucleotides of the (−)DNA copy of the HIV-1 genome, generated during reverse transcription (65,66).

This sequence is involved in the second strand transfer and contains the (−)PBS stem-loop as well as a second stem-loop of 14 bases, that we call SL_{14} (Figure 2). Due to its length, (−)DNA_{33} likely contains multiple binding sites. In this respect, knowing the spectroscopic response associated with the binding of 3HC-NC(11–55) to the (−)PBS loop, we determined whether the peptide preferentially binds to (−)PBS in the (−)DNA_{33} sequence. Addition of 3HC-NC(11–55) at a 1:1 ratio to (−)DNA_{33} gives a much lower N^*:T^* ratio (0.43) than with (−)PBS (0.86), suggesting that the (−)PBS loop does not constitute a preferential binding site. This conclusion was further strengthened by the much higher red-shift of the T^* band observed with (−)DNA_{33} (16 nm) as compared with (−)PBS (11 nm). It thus follows that the peptide may preferentially bind to a different binding site, where the peptide N-terminus is closer to the ODN bases. To determine whether this site is localized in the SL_{14} stem loop, we characterized the spectroscopic changes of 3HC-NC(11–55) resulting from its binding to the isolated SL_{14} sequence. Adding the protein at a 1:1 molar ratio, we observed a N^*:T^* ratio (0.36) and a 13-nm red-shift of the T^* band, close to the values obtained with (−)DNA_{33} (Figure S4 in Supplementary Data), suggesting that the preferential binding site for 3HC-NC(11–55) in (−)DNA_{33} is located on the SL_{14} sequence. Nevertheless, a limited binding to the (−)PBS loop is also likely, since the N^*:T^* ratio for (−)DNA_{33} is somewhat higher than for SL_{14}. These conclusions on the preferential binding to SL_{14} and the limited binding to (−)PBS were further supported by titration experiments, revealing that 3HC-NC(11–55) binds with 4-fold higher affinity to SL_{14} [$1.0(\pm0.3) \times 10^6\,M^{-1}$] as compared to (−)PBS [$2.7(\pm0.6) \times 10^5\,M^{-1}$]. The preferential binding of 3HC-NC(11–55) to SL_{14} was further assessed by the spectrum obtained in the presence of an equimolar mixture of (−)PBS and SL_{14}, which shows a N^*:T^* ratio of 0.38 very close to that of SL_{14} alone (0.36) (Figure S4 Supplementary Data). Thus, the proposed environment-sensitive label attached to a peptide can help to localize its preferential binding sites on ODNs, provided the probe responses associated with peptide binding to the individual sites are known from independent measurements.

Finally, we characterized the interaction of 3HC-NC(11–55) with cTAR DNA, a stem-loop of 55 nucleotides involved in the NC-promoted first strand transfer, during reverse transcription (61,62,71). This sequence was previously shown to bind eight NC(12–55) molecules with an affinity of $1.7 \times 10^7\,M^{-1}$ at 30 mM NaCl (73), assuming identical and non-interacting binding sites. Though this assumption was adequate for obtaining good fits of the binding curves and comparing various NC mutants (65,73), it was recognized by the authors to be rather unrealistic, since NC binding is known to depend on the ODN sequence (44,50). To check the hypothesis of identical and non-interacting binding sites, we added increasing concentrations of 3HC-NC(11–55) to 1 μM cTAR up to a molar ratio of five peptides per cTAR molecule in a buffer with 30 mM NaCl. Due to the high affinity of NC(11–55) for cTAR and the high concentrations of cTAR and peptide used, the concentration of free 3HC-NC(11–55) is negligible in these conditions. As a consequence, if 3HC-NC(11–55) binds with identical affinity to all cTAR binding sites, the latter should be populated in parallel with increasing peptide concentration and thus, no change in the N^*:T^* ratio should appear. In contrast to this expectation, the N^*:T^* ratio regularly increases from a 0.34 value at a 1:1 molar ratio up to a 0.44 value at a 5:1 molar ratio (Figure 10). This indicates that 3HC-NC(11–55) first binds to sites giving a low N^*:T^* ratio while sites associated with higher N^*:T^* ratios are less affine, highlighting differences in the binding constants of the different sites. In contrast to the N^*:T^* ratio, the position of the T^* band remains nearly constant during the titration, being red-shifted by about 16 nm in respect with the free 3HC-NC(11–55) protein. This absence of change of the T^* band confirmed that the concentration of free protein remains negligible.

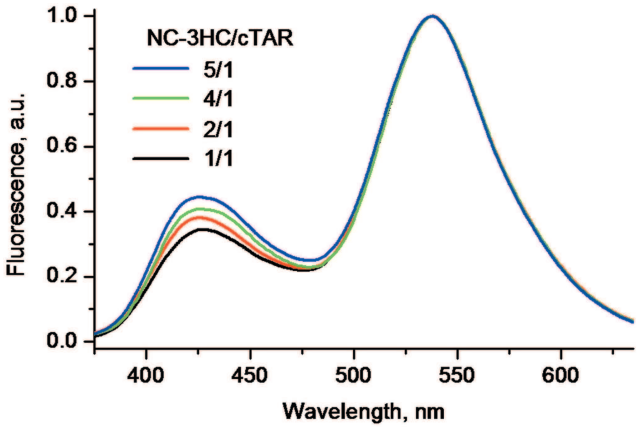

Figure 10. Normalized fluorescence spectra of 3HC-NC(11–55) added to cTAR at different molar ratios: 1:1 (black), 2:1 (red), 4:1 (green) and 5:1 (blue). cTAR concentration was 1 μM. Experiment was performed at 30 mM NaCl concentration to ensure complete binding (73).

CONCLUSIONS

Herein, we presented a new environment-sensitive ratiometric fluorescent label for sensing peptide–ODN interactions. Being attached to the N-terminus of the NC(11–55) peptide, the label reports on the interaction with ODNs by a change in the ratio of its two emission bands. The response of the label is connected with a decrease in the exposure of the labeling site to bulk water induced by the interaction of the peptide with ODN. Using this ratiometric approach, we were able to distinguish different peptide–ODN complexes by monitoring the local properties of the peptide labeling site. This property was successfully used to evaluate quantitatively peptide–ODN interactions, to localize preferential binding sites on ODNs and to show the presence of binding sites with different affinities. This approach provided us new insights on the binding of NC to two target sequences of the (−)DNA copy of the HIV-1

genome, which are critically involved in the two obligatory strand transfers during reverse transcription. Since the N^*:T^* ratio of the label is sensitive to its close environment and not to the molecular weight of the peptide–ODN complex, the proposed methodology appears as a simple and complementary alternative to steady-state anisotropy for monitoring protein–ODN interactions.

SUPPLEMENTARY DATA

Supplementary Data are available at NAR Online.

FUNDING

This work was supported by a grant from the Agence Nationale de la Recherche, Agence Nationale de la Recherche sur le SIDA, and ARCUS program. V.V.S. was supported by an Eiffel fellowship. Funding for open access charge: Agence Nationale de la Recherche.

Conflict of interest statement. None declared.

REFERENCES

1. Heyduk,T. (2002) Measuring protein conformational changes by FRET/LRET. *Curr. Opin. Biotechnol.*, **13**, 292–296.
2. Selvin,P.R. (2000) The renaissance of fluorescence resonance energy transfer. *Nat. Struct. Biol.*, **7**, 730–734.
3. Schuler,B. (2005) Single-molecule fluorescence spectroscopy of protein folding. *Chem. Phys. Chem.*, **6**, 1206–1220.
4. Kajihara,D., Abe,R., Iijima,I., Komiyama,C., Sisido,M. and Hohsaka,T. (2006) FRET analysis of protein conformational change through position-specific incorporation of fluorescent amino acids. *Nat. Methods*, **3**, 923–929.
5. Cao,H., Tamilarasu,N. and Rana,T.M. (2006) Orientation and affinity of HIV-1 Tat fragments in Tat-TAR complex determined by fluorescence resonance energy transfer. *Bioconjug. Chem.*, **17**, 352–358.
6. Jameson,D.M. and Sawyer,W.H. (1995) Fluorescence anisotropy applied to biomolecular interactions. *Methods Enzymol.*, **246**, 283–300.
7. Lakowicz,J.R., Gryczynski,I., Piszczek,G., Tolosa,L., Nair,R., Johnson,M.L. and Nowaczyk,K. (2000) Microsecond dynamics of biological macromolecules. *Methods Enzymol.*, **323**, 473–509.
8. Cohen,B.E., McAnaney,T.B., Park,E.S., Jan,Y.N., Boxer,S.G. and Jan,L.Y. (2002) Probing protein electrostatics with a synthetic fluorescent amino acid. *Science*, **296**, 1700–1703.
9. Nitz,M., Mezo,A.R., Ali,M.H. and Imperiali,B. (2002) Enantioselective synthesis and application of the highly fluorescent and environment-sensitive amino acid 6-(2-dimethylamino-naphthoyl) alanine (DANA). *Chem. Commun.*, **8**, 1912–1913.
10. Vazquez,M.E., Nitz,M., Stehn,J., Yaffe,M.B. and Imperiali,B. (2003) Fluorescent caged phosphoserine peptides as probes to investigate phosphorylation-dependent protein associations. *J. Am. Chem. Soc.*, **125**, 10150–10151.
11. Vazquez,M.E., Rothman,D.M. and Imperiali,B. (2004) A new environment-sensitive fluorescent amino acid for Fmoc-based solid phase peptide synthesis. *Org. Biomol. Chem.*, **2**, 1965–1966.
12. Vazquez,M.E., Blanco,J.B. and Imperiali,B. (2005) Photophysics and biological applications of the environment-sensitive fluorophore 6-N,N-dimethylamino-2,3-naphthalimide. *J. Am. Chem. Soc.*, **127**, 1300–1306.
13. Loving,G. and Imperiali,B. (2008) A versatile amino acid analogue of the solvatochromic fluorophore 4-N,N-dimethylamino-1,8-naphthalimide: a powerful tool for the study of dynamic protein interactions. *J. Am. Chem. Soc.*, **130**, 13630–13638.
14. Cohen,B.E., Pralle,A., Yao,X., Swaminath,G., Gandhi,C.S., Jan,Y.N., Kobilka,B.K., Isacoff,E.Y. and Jan,L.Y. (2005) A fluorescent probe designed for studying protein conformational change. *Proc. Natl Acad. Sci. USA*, **102**, 965–970.
15. Chen,H., Chung,N.N., Lemieux,C., Zelent,B., Vanderkooi,J.M., Gryczynski,I., Wilkes,B.C. and Schiller,P.W. (2005) [Aladan3]TIPP: a fluorescent delta-opioid antagonist with high delta-receptor binding affinity and delta selectivity. *Biopolymers*, **80**, 325–331.
16. Venkatraman,P., Nguyen,T.T., Sainlos,M., Bilsel,O., Chitta,S., Imperiali,B. and Stern,L.J. (2007) Fluorogenic probes for monitoring peptide binding to class II MHC proteins in living cells. *Nat. Chem. Biol.*, **3**, 222–228.
17. Sen,S., Paraggio,N.A., Gearheart,L.A., Connor,E.E., Issa,A., Coleman,R.S., Wilson,D.M. 3rd, Wyatt,M.D. and Berg,M.A. (2005) Effect of protein binding on ultrafast DNA dynamics: characterization of a DNA:APE1 complex. *Biophys. J.*, **89**, 4129–4138.
18. Okamoto,A., Tainaka,K. and Saito,I. (2005) A dielectric-sensitive fluorescent DNA probe for monitoring polarities on the interior of a DNA-binding protein. *Bioconjug. Chem.*, **16**, 1105–1111.
19. Yang,X., Liu,W.H., Jin,W.J., Shen,G.L. and Yu,R.Q. (1999) DNA binding studies of a solvatochromic fluorescence probe 3-methoxybenzanthrone. *Spectrochim. Acta A. Mol. Biomol. Spectrosc.*, **55A**, 2719–2727.
20. Kumar,C.V. and Asuncion,E.H. (1993) DNA binding studies and site selective fluorescence sensitization of an anthryl probe. *J. Am. Chem. Soc.*, **115**, 8547–8553.
21. Klymchenko,A.S., Kenfack,C., Duportail,G. and Mely,Y. (2007) Effects of polar protic solvents on dual emissions of 3-hydroxychromones. *J. Chem. Sci.*, **119**, 83–89.
22. Avilov,S.V., Bode,C., Tolgyesi,F., Klymchenko,A.S., Fidy,J. and Demchenko,A.P. (2005) Temperature effects on alpha-crystallin structure probed by 6-bromomethyl-2-(2-furanyl)-3-hydroxychromone, an environmentally sensitive two-wavelength fluorescent dye covalently attached to the single Cys residue. *Int. J. Biol. Macromol.*, **36**, 290–298.
23. Sengupta,P.K. and Kasha,M. (1979) Excited state proton-transfer spectroscopy of 3-hydroxyflavone and quercetin. *Chem. Phys. Lett.*, **68**, 382–385.
24. Chou,P.T., Martinez,M.L. and Clements,J.H. (1993) Reversal of excitation behavior of proton-transfer vs. charge-transfer by dielectric perturbation of electronic manifolds. *J. Phys. Chem.*, **97**, 2618–2622.
25. Ormson,S.M., Brown,R.G., Vollmer,F. and Rettig,W. (1994) Switching between charge- and proton-transfer emission in the excited state of a substituted 3-hydroxyflavone. *J. Photochem. Photobiol. A: Chem.*, **81**, 65–72.
26. Swinney,T.C. and Kelley,D.F. (1993) Proton transfer dynamics in substituted 3-hydroxyflavones: Solvent polarization effects. *J. Chem. Phys.*, **99**, 211–221.
27. Klymchenko,A.S. and Demchenko,A.P. (2003) Multiparametric probing of intermolecular interactions with fluorescent dye exhibiting excited state intramolecular proton transfer. *Phys. Chem. Chem. Phys.*, **5**, 461–468.
28. Strandjord,A.J.G. and Barbara,P.F. (1985) Proton-transfer kinetics of 3-hydroxyflavone: solvent effects. *J. Chem. Phys.*, **89**, 2355–2361.
29. McMorrow,D. and Kasha,M. (1984) Intramolecular excited-state proton transfer in 3-hydroxyflavone. Hydrogen-bonding solvent perturbations. *J. Phys. Chem.*, **88**, 2235–2243.
30. Avilov,S.V., Bode,C., Tolgyesi,F.G., Klymchenko,A.S., Fidy,J. and Demchenko,A.P. (2005) Heat perturbation of bovine eye lens alpha-crystallin probed by covalently attached ratiometric fluorescent dye 4′-diethylamino-3-hydroxyflavone. *Biopolymers*, **78**, 340–348.
31. Klymchenko,A.S., Avilov,S.V. and Demchenko,A.P. (2004) Resolution of Cys and Lys labeling of alpha-crystallin with site-sensitive fluorescent 3-hydroxyflavone dye. *Anal. Biochem.*, **329**, 43–57.
32. Enander,K., Choulier,L., Olsson,A.L., Yushchenko,D.A., Kanmert,D., Klymchenko,A.S., Demchenko,A.P., Mely,Y. and Altschuh,D. (2008) A peptide-based, ratiometric biosensor construct for direct fluorescence detection of a protein analyte. *Bioconjug. Chem.*, **19**, 1864–1870.
33. Klymchenko,A.S., Duportail,G., Mely,Y. and Demchenko,A.P. (2003) Ultrasensitive two-color fluorescence probes for dipole potential in phospholipid membranes. *Proc. Natl Acad. Sci. USA*, **100**, 11219–11224.

34. Klymchenko,A.S., Duportail,G., Ozturk,T., Pivovarenko,V.G., Mely,Y. and Demchenko,A.P. (2002) Novel two-band ratiometric fluorescence probes with different location and orientation in phospholipid membranes. *Chem. Biol.*, **9**, 1199–1208.
35. Shynkar,V.V., Klymchenko,A.S., Duportail,G., Demchenko,A.P. and Mely,Y. (2005) Two-color fluorescent probes for imaging the dipole potential of cell plasma membranes. *Biochim. Biophys. Acta*, **1712**, 128–136.
36. Shynkar,V.V., Klymchenko,A.S., Kunzelmann,C., Duportail,G., Muller,C.D., Demchenko,A.P., Freyssinet,J.M. and Mely,Y. (2007) Fluorescent biomembrane probe for ratiometric detection of apoptosis. *J. Am. Chem. Soc.*, **129**, 2187–2193.
37. Klymchenko,A.S., Shvadchak,V.V., Yushchenko,D.A., Jain,N. and Mely,Y. (2008) Excited-state intramolecular proton transfer distinguishes microenvironments in single- and double-stranded DNA. *J. Phys. Chem. B*, **112**, 12050–12055.
38. Lee,B.M., De Guzman,R.N., Turner,B.G., Tjandra,N. and Summers,M.F. (1998) Dynamical behavior of the HIV-1 nucleocapsid protein. *J. Mol. Biol.*, **279**, 633–649.
39. Summers,M.F., Henderson,L.E., Chance,M.R., Bess,J.W. Jr, South,T.L., Blake,P.R., Sagi,I., Perez-Alvarado,G., Sowder,R.C. III, Hare,D.R. *et al.* (1992) Nucleocapsid zinc fingers detected in retroviruses: EXAFS studies of intact viruses and the solution-state structure of the nucleocapsid protein from HIV-1. *Protein Sci.*, **1**, 563–574.
40. Morellet,N., Jullian,N., De Rocquigny,H., Maigret,B., Darlix,J.L. and Roques,B.P. (1992) Determination of the structure of the nucleocapsid protein NCp7 from the human immunodeficiency virus type 1 by 1H NMR. *EMBO J.*, **11**, 3059–3065.
41. Thomas,J.A. and Gorelick,R.J. (2008) Nucleocapsid protein function in early infection processes. *Virus Res.*, **134**, 39–63.
42. Berkowitz,R.D., Luban,J. and Goff,S.P. (1993) Specific binding of human immunodeficiency virus type 1 gag polyprotein and nucleocapsid protein to viral RNAs detected by RNA mobility shift assays. *J. Virol.*, **67**, 7190–7200.
43. Clever,J., Sassetti,C. and Parslow,T.G. (1995) RNA secondary structure and binding sites for gag gene products in the 5' packaging signal of human immunodeficiency virus type 1. *J. Virol.*, **69**, 2101–2109.
44. Fisher,R.J., Rein,A., Fivash,M., Urbaneja,M.A., Casas-Finet,J.R., Medaglia,M. and Henderson,L.E. (1998) Sequence-specific binding of human immunodeficiency virus type 1 nucleocapsid protein to short oligonucleotides. *J. Virol.*, **72**, 1902–1909.
45. Darlix,J.-L., Gabus,C., Nugeyre,M.-T., Clavel,F. and Barré-Sinoussi,F. (1990) Cis elements and trans-acting factors involved in the RNA dimerization of the human immunodeficiency virus HIV-1. *J. Virol.*, **216**, 689.
46. Tsuchihashi,Z. and Brown,P.O. (1994) DNA strand exchange and selective DNA annealing promoted by the human immunodeficiency virus type 1 nucleocapsid protein. *J. Virol.*, **68**, 5863–5870.
47. Mely,Y., de Rocquigny,H., Sorinas-Jimeno,M., Keith,G., Roques,B.P., Marquet,R. and Gerard,D. (1995) Binding of the HIV-1 nucleocapsid protein to the primer tRNA(3Lys), in vitro, is essentially not specific. *J. Biol. Chem.*, **270**, 1650–1656.
48. Cimarelli,A. and Darlix,J.L. (2002) Assembling the human immunodeficiency virus type 1. *Cell Mol. Life Sci.*, **59**, 1166–1184.
49. Muriaux,D., Darlix,J.L. and Cimarelli,A. (2004) Targeting the assembly of the human immunodeficiency virus type I. *Curr. Pharm. Des.*, **10**, 3725–3739.
50. Vuilleumier,C., Bombarda,E., Morellet,N., Gerard,D., Roques,B.P. and Mely,Y. (1999) Nucleic acid sequence discrimination by the HIV-1 nucleocapsid protein NCp7: a fluorescence study. *Biochemistry*, **38**, 16816–16825.
51. Shubsda,M.F., Paoletti,A.C., Hudson,B.S. and Borer,P.N. (2002) Affinities of packaging domain loops in HIV-1 RNA for the nucleocapsid protein. *Biochemistry*, **41**, 5276–5282.
52. De Guzman,R.N., Wu,Z.R., Stalling,C.C., Pappalardo,L., Borer,P.N. and Summers,M.F. (1998) Structure of the HIV-1 nucleocapsid protein bound to the SL3 psi-RNA recognition element. *Science*, **279**, 384–388.
53. Amarasinghe,G.K., De Guzman,R.N., Turner,R.B., Chancellor,K.J., Wu,Z.R. and Summers,M.F. (2000) NMR structure of the HIV-1 nucleocapsid protein bound to stem-loop SL2 of the psi-RNA packaging signal. Implications for genome recognition. *J. Mol. Biol.*, **301**, 491–511.
54. You,J.C. and McHenry,C.S. (1993) HIV nucleocapsid protein. Expression in Escherichia coli, purification, and characterization. *J. Biol. Chem.*, **268**, 16519–16527.
55. Urbaneja,M.A., Kane,B.P., Johnson,D.G., Gorelick,R.J., Henderson,L.E. and Casas-Finet,J.R. (1999) Binding properties of the human immunodeficiency virus type 1 nucleocapsid protein p7 to a model RNA: elucidation of the structural determinants for function. *J. Mol. Biol.*, **287**, 59–75.
56. Herschlag,D. (1995) RNA chaperones and the RNA folding problem. *J. Biol. Chem.*, **270**, 20871–20874.
57. Rein,A., Henderson,L.E. and Levin,J.G. (1998) Nucleic-acid-chaperone activity of retroviral nucleocapsid proteins: significance for viral replication. *Trends Biochem. Sci.*, **23**, 297–301.
58. You,J.C. and McHenry,C.S. (1994) Human immunodeficiency virus nucleocapsid protein accelerates strand transfer of the terminally redundant sequences involved in reverse transcription. *J. Biol. Chem.*, **269**, 31491–31495.
59. Guo,J., Wu,T., Anderson,J., Kane,B.F., Johnson,D.G., Gorelick,R.J., Henderson,L.E. and Levin,J.G. (2000) Zinc finger structures in the human immunodeficiency virus type 1 nucleocapsid protein facilitate efficient minus- and plus-strand transfer. *J. Virol.*, **74**, 8980–8988.
60. Lapadat-Tapolsky,M., De Rocquigny,H., Van Gent,D., Roques,B., Plasterk,R. and Darlix,J.L. (1993) Interactions between HIV-1 nucleocapsid protein and viral DNA may have important functions in the viral life cycle. *Nucleic Acids Res.*, **21**, 831–839.
61. Lapadat-Tapolsky,M., Pernelle,C., Borie,C. and Darlix,J.L. (1995) Analysis of the nucleic acid annealing activities of nucleocapsid protein from HIV-1. *Nucleic Acids Res.*, **23**, 2434–2441.
62. Bernacchi,S., Stoylov,S., Piemont,E., Ficheux,D., Roques,B.P., Darlix,J.L. and Mely,Y. (2002) HIV-1 nucleocapsid protein activates transient melting of least stable parts of the secondary structure of TAR and its complementary sequence. *J. Mol. Biol.*, **317**, 385–399.
63. Azoulay,J., Clamme,J.P., Darlix,J.L., Roques,B.P. and Mely,Y. (2003) Destabilization of the HIV-1 complementary sequence of TAR by the nucleocapsid protein through activation of conformational fluctuations. *J. Mol. Biol.*, **326**, 691–700.
64. Beltz,H., Azoulay,J., Bernacchi,S., Clamme,J.P., Ficheux,D., Roques,B., Darlix,J.L. and Mely,Y. (2003) Impact of the terminal bulges of HIV-1 cTAR DNA on its stability and the destabilizing activity of the nucleocapsid protein NCp7. *J. Mol. Biol.*, **328**, 95–108.
65. Egele,C., Schaub,E., Ramalanjaona,N., Piemont,E., Ficheux,D., Roques,B., Darlix,J.L. and Mely,Y. (2004) HIV-1 nucleocapsid protein binds to the viral DNA initiation sequences and chaperones their kissing interactions. *J. Mol. Biol.*, **342**, 453–466.
66. Ramalanjaona,N., de Rocquigny,H., Millet,A., Ficheux,D., Darlix,J.L. and Mely,Y. (2007) Investigating the mechanism of the nucleocapsid protein chaperoning of the second strand transfer during HIV-1 DNA synthesis. *J. Mol. Biol.*, **374**, 1041–1053.
67. Godet,J., de Rocquigny,H., Raja,C., Glasser,N., Ficheux,D., Darlix,J.L. and Mely,Y. (2006) During the early phase of HIV-1 DNA synthesis, nucleocapsid protein directs hybridization of the TAR complementary sequences via the ends of their double-stranded stem. *J. Mol. Biol.*, **356**, 1180–1192.
68. Liu,H.W., Cosa,G., Landes,C.F., Zeng,Y., Kovaleski,B.J., Mullen,D.G., Barany,G., Musier-Forsyth,K. and Barbara,P.F. (2005) Single-molecule FRET studies of important intermediates in the nucleocapsid-protein-chaperoned minus-strand transfer step in HIV-1 reverse transcription. *Biophys. J.*, **89**, 3470–3479.
69. Liu,H.W., Zeng,Y., Landes,C.F., Kim,Y.J., Zhu,Y., Ma,X., Vo,M.N., Musier-Forsyth,K. and Barbara,P.F. (2007) Insights on the role of nucleic acid/protein interactions in chaperoned nucleic acid rearrangements of HIV-1 reverse transcription. *Proc. Natl Acad. Sci. USA*, **104**, 5261–5267.
70. Cosa,G., Zeng,Y., Liu,H.W., Landes,C.F., Makarov,D.E., Musier-Forsyth,K. and Barbara,P.F. (2006) Evidence for non-two-state kinetics in the nucleocapsid protein chaperoned opening of DNA hairpins. *J. Phys. Chem. B*, **110**, 2419–2426.
71. Levin,J.G., Guo,J., Rouzina,I. and Musier-Forsyth,K. (2005) Nucleic acid chaperone activity of HIV-1 nucleocapsid protein:

critical role in reverse transcription and molecular mechanism. *Prog. Nucleic Acid Res. Mol. Biol.*, **80**, 217–286.
72. Darlix,J.L., Garrido,J.L., Morellet,N., Mely,Y. and de Rocquigny,H. (2007) Properties, functions, and drug targeting of the multifunctional nucleocapsid protein of the human immunodeficiency virus. *Adv. Pharmacol.*, **55**, 299–346.
73. Beltz,H., Clauss,C., Piemont,E., Ficheux,D., Gorelick,R.J., Roques,B., Gabus,C., Darlix,J.L., de Rocquigny,H. and Mely,Y. (2005) Structural determinants of HIV-1 nucleocapsid protein for cTAR DNA binding and destabilization, and correlation with inhibition of self-primed DNA synthesis. *J. Mol. Biol.*, **348**, 1113–1126.
74. Stoylov,S.P., Vuilleumier,C., Stoylova,E., De Rocquigny,H., Roques,B.P., Gerard,D. and Mely,Y. (1997) Ordered aggregation of ribonucleic acids by the human immunodeficiency virus type 1 nucleocapsid protein. *Biopolymers*, **41**, 301–312.
75. Amarasinghe,G.K., De Guzman,R.N., Turner,R.B. and Summers,M.F. (2000) NMR structure of stem-loop SL2 of the HIV-1 psi RNA packaging signal reveals a novel A-U-A base-triple platform. *J. Mol. Biol.*, **299**, 145–156.
76. Bourbigot,S., Ramalanjaona,N., Boudier,C., Salgado,G.F., Roques,B.P., Mely,Y., Bouaziz,S. and Morellet,N. (2008) How the HIV-1 Nucleocapsid Protein Binds and Destabilises the (-)Primer Binding Site During Reverse Transcription. *J. Mol. Biol.*, **383**, 1112–1128.
77. Morellet,N., Demene,H., Teilleux,V., Huynh-Dinh,T., de Rocquigny,H., Fournie-Zaluski,M.C. and Roques,B.P. (1998) Structure of the complex between the HIV-1 nucleocapsid protein NCp7 and the single-stranded pentanucleotide d(ACGCC). *J. Mol. Biol.*, **283**, 419–434.
78. Baudin,F., Marquet,R., Isel,C., Darlix,J.L., Ehresmann,B. and Ehresmann,C. (1993) Functional sites in the 5′ region of human immunodeficiency virus type 1 RNA form defined structural domains. *J. Mol. Biol.*, **229**, 382–397.
79. Johnson,P.E., Turner,R.B., Wu,Z.R., Hairston,L., Guo,J., Levin,J.G. and Summers,M. F. (2000) A mechanism for plus-strand transfer enhancement by the HIV-1 nucleocapsid protein during reverse transcription. *Biochemistry*, **39**, 9084–9091.
80. de Rocquigny,H., Ficheux,D., Gabus,C., Fournie-Zaluski,M.C., Darlix,J.L. and Roques,B.P. (1991) First large scale chemical synthesis of the 72 amino acid HIV-1 nucleocapsid protein NCp7 in an active form. *Biochem. Biophys. Res. Commun.*, **180**, 1010–1018.
81. Eastman,J.W. (1967) Quantitative spectrofluorimetry-the fluorescence quantum yield of quinine sulfate. *Photochem. Photobiol.*, **6**, 55–72.
82. Avilov,S.V., Piemont,E., Shvadchak,V., de Rocquigny,H. and Mely,Y. (2008) Probing dynamics of HIV-1 nucleocapsid protein/target hexanucleotide complexes by 2-aminopurine. *Nucleic Acids Res.*, **36**, 885–896.
83. Livesey,A.K. and Brochon,J.-C. (1987) Analyzing the distribution of decay constants in pulse-fluorimetry using the maximum entropy method. *Biophys. J.*, **52**, 693–706.
84. Klymchenko,A.S. and Demchenko,A.P. (2004) 3-Hydroxychromone dyes exhibiting excited-state intramolecular proton transfer in water with efficient two-band fluorescence. *New J. Chem.*, **28**, 687–692.
85. Ramboarina,S., Srividya,N., Atkinson,R.A., Morellet,N., Roques,B.P., Lefevre,J.F., Mely,Y. and Kieffer,B. (2002) Effects of temperature on the dynamic behaviour of the HIV-1 nucleocapsid NCp7 and its DNA complex. *J. Mol. Biol.*, **316**, 611–627.
86. Lakowicz,J.R. (1999) *Principles of Fluorescence Spectroscopy*. 2nd edn. Kluwer Academic/Plenum Publishers, New York.
87. Bernacchi,S., Piemont,E., Potier,N., Dorsselaer,A. and Mely,Y. (2003) Excitonic heterodimer formation in an HIV-1 oligonucleotide labeled with a donor-acceptor pair used for fluorescence resonance energy transfer. *Biophys. J.*, **84**, 643–654.

3.3. Protein-protein interactions

Protein-protein interactions govern almost any aspect of cellular life. Proteins differ by size and polarity according to their functions. Interaction between them is accomplished by changes in environment properties. Classical solvatochromic probes as well as 3HC dyes have been efficiently applied for the detection of such interactions. Environment-sensitive dyes working on the principle of the emission band shift and fluorescence quantum yield changes are purely sensitive in polar media. Thus, in the case of relatively small peptides and proteins application of ESIPT-based 3HC labels have wide perspectives. We decided to apply FCL label adopted for the polar environment for studies of the interactions of relatively small peptides accessible by SPPS.

3.3.1. Peptide-antibody interactions

To check the applicability of the FCL label to peptide-protein interaction sensing we have used a model system of antibody against HPV E6 protein (AB) and the labeled synthetic peptide containing the recognized part of E6. Such peptide could potentially serve as convenient sensor for antibody.

The detection would be effective when peptide is labeled close enough to active binding site. Meantime too close position of the label could disturb the interaction. To optimize labeling position we have synthesized three peptides with different label-binding site distance. All peptides were labeled at N-terminus by FCL that have a good sensitivity to the environment changes in polar hydrated media.

FCL-K15C = FCL-KRTAMF**QDP**QERPRC
FCL-A12C = FCL-AMF**QDP**QERPRC
FCL-F10C = FCL-F**QDP**QERPRC

In the first peptide (FCL-K15C) label is located 6 amino acids from binding region. FCL-K15C shows only slight response on binding to antibody (AB) likely because of too far label location (**Fig. 3.13**). This peptide could not be used as detecting system.

FCL-A12C peptide with three amino acid distance between binding site and label shows more than 50% change in the N*/T* fluorescence emission band ratio upon binding to the antibody (**Fig. 3.13**). Observed spectral effect is sufficient for clear detection of the interaction.

Finally, the third tested peptide FCL-F10C with the minimal one amino acid distance between label and binding site shows only pure fluorescence changes in the presence of the antibody. This could be explained by interaction perturbation due to the too close label position.

So FCL-A12C, peptide with three amino acid distance between label and binding site was considered as an optimal for sensing an interactions.

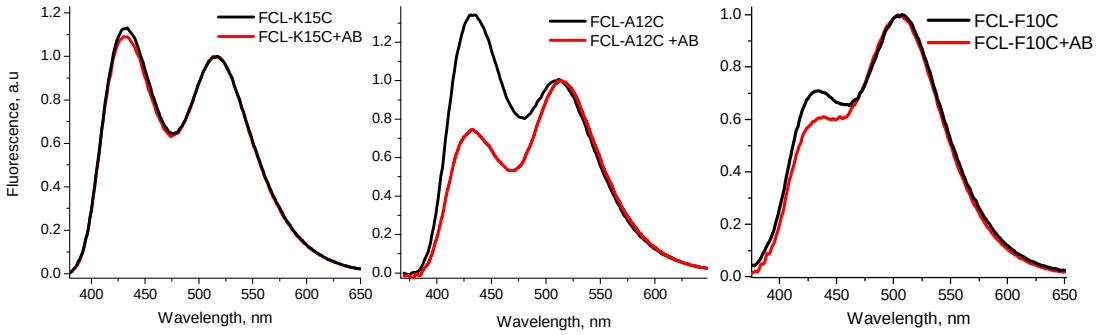

Figure 3.13. Response labeled peptides on binding to antibody. Fluorescence emission spectra were normalized after baseline correction. Concentrations of peptide and antibody were 100 nM and 110 nM respectively. Measurements were performed in pH 7 10 mM HEPES buffer containing 150 mM NaCl and 3.4 mM EDTA. Excitation wavelength was 340 nm.

In the free form FCL-A12C shows fluorescence similar to one of the free label indicating that the environment of the chromophore is close to the water by polarity. Addition of the antibody solution leads to the decrease of the N*/T* band ratio from 1.34 to 0.74 and slight shift of the T* band (from 510 to 513 nm). Comparison with model systems allows to conclude that observed effects correspond to the decreasing of environment polarity without strong modification of the hydration. Observed changes are in line with much apolar properties of big antibody in respect with relatively small peptide.

Titration of FCL-A12C by the antibody shows the linear increase of the N*/T* signal till 1:1 antibody:peptide ratio indicating a high binding efficiency. This allows quantitative determination of the antibody concentration by measuring the N*/T* band ration in FCL-A12C solution of known concentration.

The labeled peptide could be also used for the detection of other proteins and peptides binding this antibody. As an example non-labeled A12C peptide that have similar binding constant to AB was used. Addition of A12C to the FCL-A12C/AB complex leads to release of the labeled peptide due to the competitive binding. The resulted fluorescence spectrum directly depends on the concentration of added A12C (concurrent

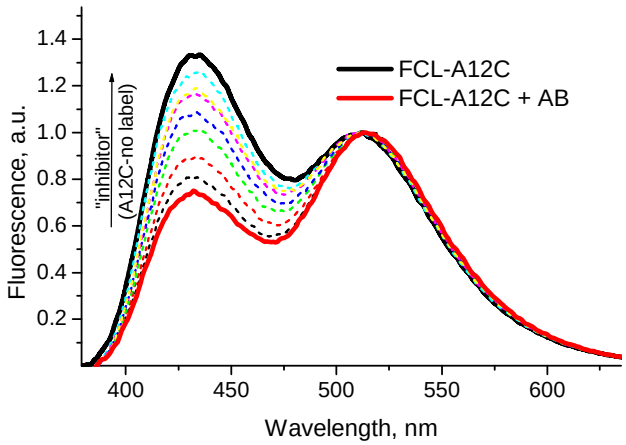

Figure 3.14. Competition experiment. FCL-A12C/AB complex (red line) in presence of increasing amounts of non labeled A12C peptide (dashed lines). Spectrum of free FCL-A12C is shown for comparison.
Experimental conditions the same as for Fig. 3.13. Non labeled peptide concentration varied from 0 nm to 700 nm.

antibody target) in respect to the initial concentration of FCL-A12C/AB complex and could be used for quantitative determination (**Fig. 3.14**).

So, easily accessible FCL-labeled peptides are efficient tool for antigen and antibody detection in vitro.

3.3.2. Vpr oligomerization

Oligomerization is an important case of protein-protein interactions. Most of the known techniques have difficulties to quantify small peptide oligomerization process and discriminate different oligomeric/aggregated forms. We have tried to apply FCL label to studying of HIV-1 Vpr protein oligomerization. C-terminal fragment of the protein (Vpr(52-96)) contains a leucine-zipper motif and was selected for studies. According to the NMR data [222] this peptide except the C-terminal part is in the form of α-helix and the label graved at the N-terminus was expected to be strongly affected by peptide-peptide interactions.

In the neutral pH the fluorescence spectrum of the labeled peptide shows abnormally low N* form intensity (**Fig. 3.15**) indicating apolar environment or specific quenching. The both effects could be explained by aggregate formation. Indeed performed DLS measurements showed that most of the peptide at these conditions is in the form of μm scale aggregates. Decreasing of the pH leads to a partial dissociation of such aggregates that is reflected in the fluorescence spectra by increasing of the N*/T* band ratio. At low pH the fluorescence spectra of FCL-Vpr(52-96) show quite apolar environment (**Fig. 3.15**), which could be explained by a oligomeric/aggregated form of the peptide observed by DLS. Finally, in the acidic (pH 3) solutions with addition of less polar solvent, TFE (30%), the N*/T* ratio reaches the values common for non-aggregating peptides. Taking into account DLS data that shows absence of aggregates we could assume that such conditions correspond to the monomeric form of Vpr(52-96).

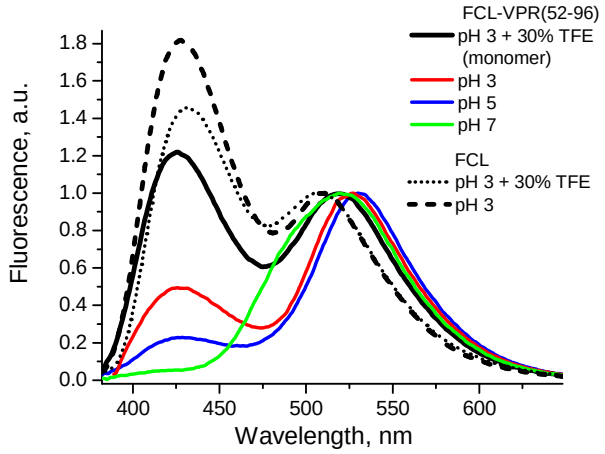

Figure 3.15. Normalized fluorescnce spectra of FCL-Vpr(52-96) in monomeric (black curve), highly aggregated (green curve) and intermediate conditions. Spectra of FCL label are shown for comparison as dashed and dotted lines.

Proposed label report on peptide aggregation/oligomerization by changing of the N*/T* emission band ratio. This signal could be correlated with DLS data but quantitative analysis of multicomponent systems is difficult. Application of the FCL label for studying of formation of the oligomers of exact composition would be more appropriate.

3.4. Protein-membrane interactions

Numerous non-covalent solvatochromic membrane probes were proposed to monitor membrane properties and their changes upon interaction with proteins. Meantime, labeling of proteins (or peptides) with environment-sensitive dye for detection of their incteraction with membranes has not been well explored. Successful applications of two-band ratiometric probes based on 3HC dyes for studies of membrane properties [117, 122] allow us to expect that 3HC dyes grafted to the proteins could efficiently report on their interactions with membranes.

However, FCL label is adapted to the high polarity range and show very low N*/T* band ratio already in solvents in medium polarity (**Fig. 3.16**). Taking into account that the polarity inside the membrane is relatively low, FCL is probably not appropriate for detection of peptide-membrane interactions and probing proberties of the membrane binding site. Indeed, the expected low intense N* band fluorescence of FCL will be difficult to measure and correct from the strong light scattering of the solutions containing liposomes or other membrane systems.

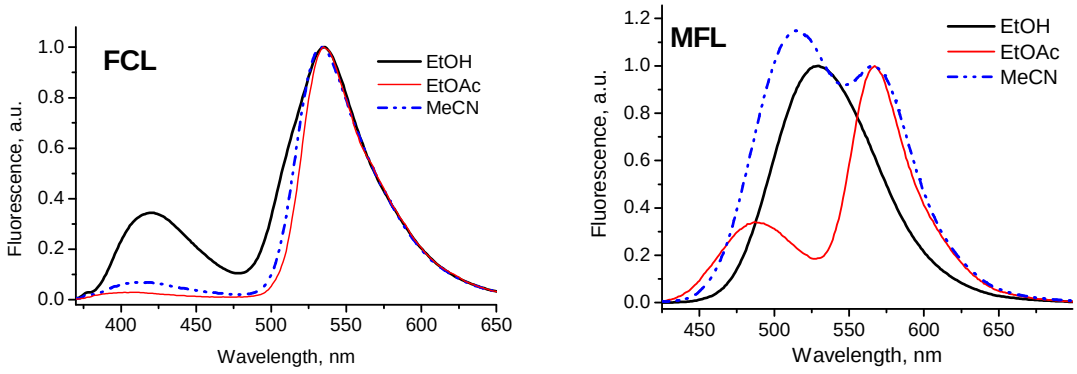

Figure 3.16. Comparison of FCL and MFL labels. Normalized fluorescence spectra in protic ethanol and two aprotic solvents of different polarity (acetonitrile and ethyl acetate) are shown in black, red and blue, respectively. Excitation wavelengths were 340 nm and 400 nm for FCL and MFL, respectively.

To overcome these problems we selected for the present work label MFL label, based on 4'-dimethylamino-3-hydroxyflavone. It shows an optimal polarity sensitivity range for membrane studies and clear difference of the fluorescence properties in protic and aprotic environment (**Fig. 3.16**). Moreover MFL shows about 50 nm red-shifted absorption and emission in respect to FCL label, which should minimize problems related to the light scattering and make it attractive for cellular studies, particularly cell imaging.

3.4.1. Binding of NC to membranes

To test applicability of MFL for studies of protein-membrane interactions we have synthesized HIV-1 nucleocapsid protein (NC) labeled with MFL at its N-terminus. This small protein is relatively basic but contains a hydrophobic plateau that allows its DNA binding and may enforce interactions with membranes. As a model system we used unilaminar vesicles (LUV) that could be prepared from synthetical or natural lipids and allows modeling of membranes with different properties. They are thermodynamically stable and uniform in size that allows obtaining highly reproducible results.

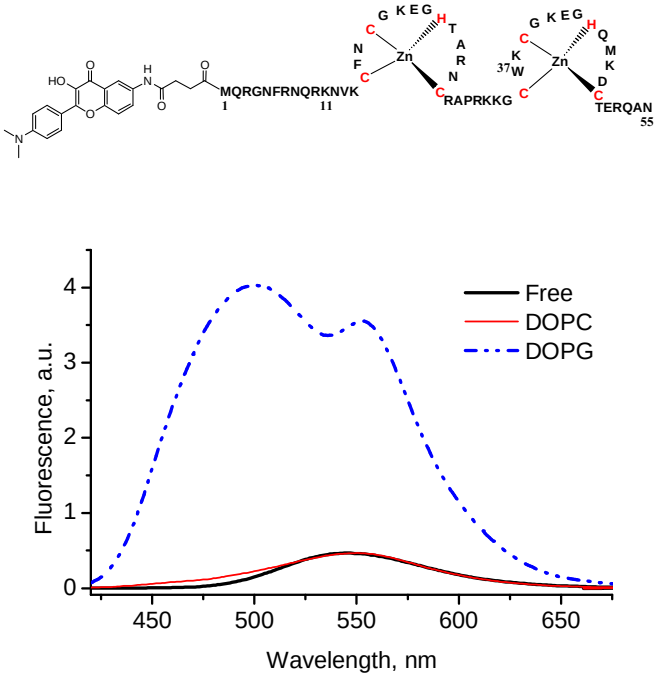

Figure 3.17. Fluorescence of MFL-NC in the pH 7 phosphate buffer solution in the absence (black) and in the presence of LUVs composed of neutral DOPC (red) and negatively charged DOPG (blue) lipids. Peptide was added to the solution containing large excess of LUVs (about 400 lipids per protein). To minimize impact of the electrostatic interactions, the measurements were performed in the buffer containing 150 mM of NaCl.

Labeled protein (MFL-NC) in the buffer solution shows only one low-intensive band, which could be assigned to emission of the N* species of 3HC fluorophore. In the presence of negatively charged LUVs (composed of DOPG) the fluorescence intensity strongly increases and two separated bands appear in the emission spectra (**Fig. 3.17**, **Table 3.3**). Observed effects clearly show that the dye is in aprotic environment that could be explained only by NC-membrane interaction. Fluorescence emission profile is close to that of the dye **4** in LUVs or acetonitrile (**Table 2.3**, **Fig 2.13**). Separation of the two emission bands is more than 50 nm that allows independent measurement of their intensity and positions. Relatively high N*/T* band ratio points that label is located in an environment of medium polarity and could not be deeply immersed into the membrane being likely in the region of lipid ester groups. Additional proof of the membrane localization of the label is a high fluorescence quantum yield (> 50%) indicating relatively rigid environment of the dye, which is typical for lipid membranes.

In contrary to the negatively charged LUVs, the neutral ones do not significantly affect fluorescence properties of MFL-NC (**Fig. 3.17**, **Table 3.3**). In the presence of LUVs, composed of neutral lipid DOPC, the labeled protein shows only one emission band position of low quantum yield, similar to that observed in the buffer. In this case, most of the protein is probably in the free form because of the absence of the sufficient interaction.

Table 3.3. Spectroscopic properties of MFL-NC

Media	λ_{ABS}, nm	λ_{N^*}, nm	λ_{T^*}, nm	N*/T*	φ, %
Buffer	419	545	-	-	7.2
DOPC	420	547	-	-	8.2
SM/Ch	419	547	-	-	6.8
DOPG	410	502	552	1.12	62.0
DOPS	404	495	553	1.18	56.3

λ_{abs} – position of absorption maxima, λ_{N^*} and λ_{T^*} - position of fluorescence maxima of N* and T* forms respectively. N*/T* - ratio of the intensities of the two emission bands at their peak maxima. φ - fluorescence quantum yield.
SM/Ch is 65/35 mixture of sphingomyelin and cholesterol.
Buffer is pH=7 phosphate containing 150 mM of NaCl.
Excitanion wavelength was 400nm .

We can conclude that MFL label can detect binding of NC to the membranes composed of negatively charged lipids. In the peptide-membranes complex, the label shows high fluorescence quantum yields and comparable intensities of the emission bands, which make it prospective for studying protein-membrane interactions. Moreover, the low quantum yield and one emission band observed in aqueous media allows clear discrimination between bound and non-bound proteins.

3.4.2. Binding of Vpr(52-96) to membranes

Vpr interacts with membrane and perturbs the membrane integrity. This phenomenon is attributed to the Vpr potency to induce channels, membrane depolarization or membrane herniation [265]. This property could explain Vpr features required for HIV replication and HIV neurodisorders. For instance, at the level of the nucleus, the presence of Vpr in the PIC (preintegration complex) [266] could be required for its translocation since the PIC's diameter of 56 nm exceeds the 25-nm diameter of the nuclear pore channel [267]. Moreover, membrane herniations in the nuclear envelop and membrane permeabilization of the mitochondria probably contributes to the induction of cell cycle arrest [268]. At least, Vpr-membrane interaction of extracellular Vpr diffusing in the serum may have important implications for Vpr neuropathology's in AIDS [269].

Thus, Vpr-membrane interaction merits further evaluation to decipher the mechanism of interaction and to understand both Vpr and membrane perturbation along the interaction. We applied the MFL label to investigate the interaction of the C-terminal domain of Vpr (Vpr(52-96)) with membranes. Vpr is highly structured amphipathic protein consisting of three α-helixes mutually oriented to form a hydrophobic central plateau. The C-terminal fragment contains the longest helix followed by a flexible and non structured positively charged part. The label was attached to the relatively rigid N-terminus of the peptide (**Fig. 3.18**) using solid phase peptide synthesis. Interestingly, the selected peptide contains one tryptophan residue in close proximity of the labeling position that allows to correlate results obtained by our label with those obtained from Trp fluorescence.

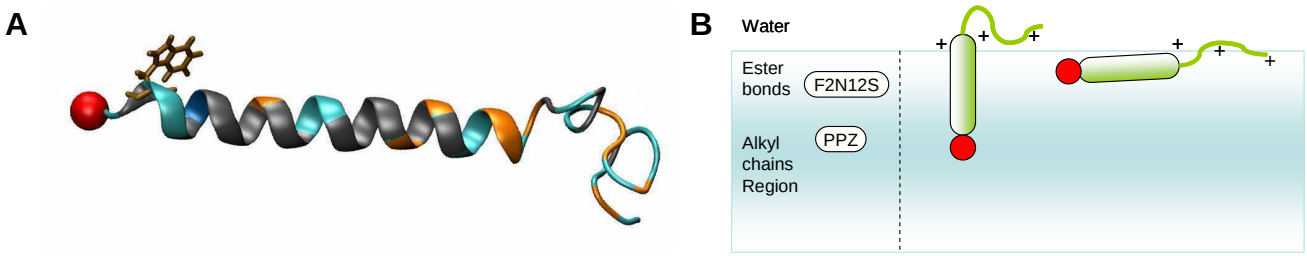

Figure 3.18. (**A**) Structure of Vpr(52-96) based on NMR data [222]. Positively charged amino acids are in orange, negatively in blue, lipophilic in grey. Trp54 is shown in brown. The labeling position is marked by a red sphere.
(**B**) Possible conformations of Vpr(52-96) in membrane and positions of the two described 3HC membrane probes [115, 122].

The fluorescence spectrum of MFL-Vpr(52-96) in pH 6 buffer is composed of one band (N* form), which is significantly blue shifted compared to that of the MFL label or MFL-NC in buffer, being close to that of the MFL label in the less polar ethanol (**Table 3.4**). This could be explained by the aggregation of Vpr in the buffer, which results in a significant screening of the label from the bulk water. This observation is in line with our previous data presented in Chapter 2.3.2.

Addition of LUVs leads to a strong increase in the fluorescence intensity (> ten- fold) and to the appearance of the two separated bands in the emission spectra (**Fig. 3.19**). The N*/T* ratio of the fluorescence emission bands is close to the ratio obtained for the free label in polar aprotic solvents and for MFL-NC in LUVs composed of negatively charged lipids.

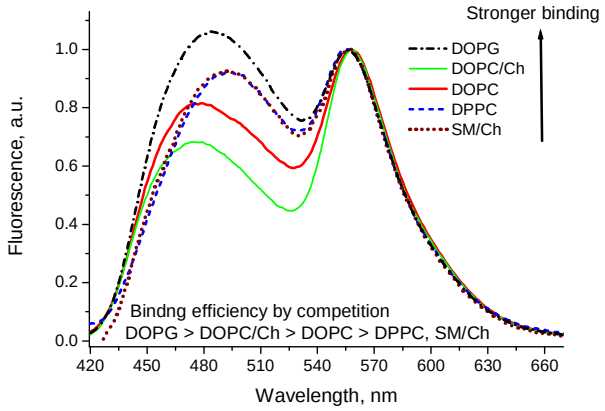

Figure 3.19. Normalized fluorescence spectra of MFL-Vpr(52-96) in different LUVs. Peptide was added to a big excess of LUVs (about 400 lipids per protein). Experiments were performed in 10mM phosphate buffer pH 6.2, using an excitation wavelength of 400 nm.

Table 3.4 Spectral properties of MFL-Vpr(52-96)

	Media	λ_{N^*}, nm	λ_{T^*}, nm	N*/T*	φ, %
MFL label	buffer	555	-	-	0.5
	Ethanol	529	-	-	48.2
MFL-Vpr (52-96)	buffer	529	-	-	2.1
	DOPC	475	558	0.81	19.7
	DOPC/Ch	476	558	0.68	24.4
	SM/Ch	492	557	0.93	20
	DPPC	491	557	0.92	21
	DOPS	498	552	1.06	33.3
	DOPG	483	556	1.07	41.6
F2N12S	DOPC	514	570	1.01	
	EYPG	509	570	1.24	
PPZ	DOPC	518	570	0.63	25
	DOPG	520	569	0.55	33

λ_{abs} – position of absorption maxima, λ_{N^*} and λ_{T^*} - position of fluorescence maxima of N* and T* forms respectively. N*/T* - ratio of the intensities of the two emission bands at their peak maxima. φ - fluorescence quantum yield. Experiments were performed in 10mM phosphate buffer, pH 6.2. Excitation was at 400 nm. DOPC/Ch and SM/Ch are (75% DPPC / 25% Ch) and (67% SM / 33% Ch) mixtures, respectively. Data for PPZ and F2N12S are from [115, 122].

The ratiometric response of the label not only monitors the Vpr-lipid interaction but also provides some information on the local environment of the probe in the membranes (**Fig. 3.19**, **Table 3.4**).

The differences in the fluorescence emission of MFL-Vpr(52-96) bound to different membranes could be used for the determination of the peptide binding preferences. For example, the spectrum of MFL-Vpr(52-96) with a 1:1 mixture of DOPC and DOPG liposomes is similar to the spectrum with DOPG liposomes (**Fig. 3.20**). Thus, in the presence of equimolar concentrations of both LUVs, most of the peptide is bound to DOPG LUVs, which reflects a tighter binding affinity of the peptide to the negatively charged DOPG than to neutral DOPC. This approach could be used when the N*/T* ratio is significantly different for two systems and the binding constant to one type of LUVs is at least 5-fold higher than to the other. Using this competition assay for different pairs of LUVs (**Fig. 3.20**), we found the following ranking of Vpr(52-96) preferential binding : DOPG > DOPC/Ch > DOPC > DPPC, SM/Ch. Comparison of the binding preference to DPPC and SM/Ch was impossible because of the

very close fluorescence emission profiles with the two lipid compositions. The strong binding observed with the charged membranes (DOPG) could be explained by additional electrostatic interactions between the positively charged peptide and the negatively charged membrane surface. For the neutral membranes in the fluid phase, the binding of Vpr(52-96) is stronger in the presence of cholesterol. Finally, Vpr(52-96) shows the smallest affinity to membranes in the gel and liquid ordered phase (DPPC and SM/Ch, respectively). Remarkably, for the neutral membranes, a correlation could be observed between the N*/T* band ratio and the binding affinity. Indeed, in the membranes of higher affinity for the peptide, MFL-Vpr(52-96) shows a lower N*/T* ratio and a more blue-shifted N* band position, suggesting poor exposure of the label to the bulk water. Thus, the stronger binding to membranes with the less tightly packed lipids (fluid phase) is probably associated with the deeper embedding of the peptide in the membrane, resulting in a better screening from the bulk water of the N-terminal domain of Vpr(52-96) and the MFL label.

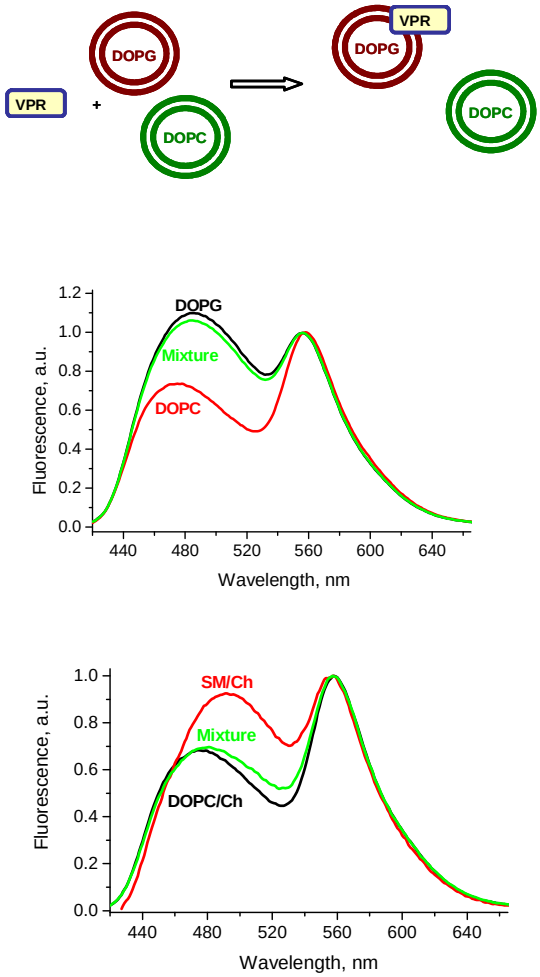

Figure 3.20. (**A**) Schematic representation of the competition system. (**B**) Normalized fluorescence spectra of MFL-Vpr(52-96) in the presence of DOPG (black), DOPC (red) and their 1:1 mixture (green) (**C**) the same for LUVs composed of DOPC/Cholesterol and Sphingomielin/Cholesterol.

Vpr(52-96)-membrane interactions are mostly governed by hydrophobic forces. Thus, the location of the peptide bound to the membrane is determined by the positions of the hydrophobic and charged amino acids. The α-helix of Vpr(52-96) is mostly composed of neutral apolar amino acids, meanwhile positively charged residues are located in the more flexible C-terminal part (**Fig. 3.18**). Possible locations of the peptide interacting with the membrane are schematically presented on **Fig. 3.18 B** (1) "vertical" with deeply immersed N-terminus; (2) "horizontal" with all the peptide located near the membrane interface. These possible positions differ significantly by the N-terminus environment that could be reported by the MFL label.

For several 3HC-based membrane probes, the fluorescence spectrum was correlated with the position of their fluorophore in the membrane [270]. The F2N12S label locates at the level of the ester groups of lipids (**Fig 3.18 B**) and shows N*/T* band ratios close to 1.1 (**Table 3.4**) while PPZ is

deeply immersed and reports twice lower values (**Table 3.4**) [115, 122]. In negatively charged membranes, MFL-Vpr(52-96) shows N*/T* band ratios close to 1.05 (**Table 3.4**, **Fig. 3.19**), suggesting that the label is close to the membrane/water interface with a "horizontal" orientation of the peptide.

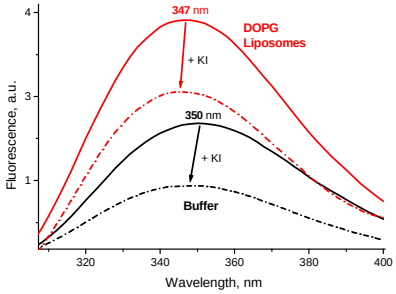

Figure 3.21. Fluorescence of Trp54 of Vpr(52-96) in buffer (black) and in DOPG liposomes (red). Quenching of the fluorescence by 50 mM KI (dash-dot lines) is about 50% and 30%, respectively.

To confirm the orientation of the peptide bound to the membrane, we studied the fluorescence of Trp54 located in close proximity to the label. (**Fig. 3.18 A**) Interaction of the peptide with DOPG LUVs leads to a two-fold Trp fluorescence increase and a 4 nm blue shift of its fluorescence emission maximum (**Fig. 3.21**). This corresponds to a moderate decrease in the Trp environment polarity. A more precise location of this amino acid could be defined by its accessibility to the water soluble iodide quencher. After Vpr(52-96) binding to DOPG LUVs, Trp is still accessible to iodide (**Fig. 3.21**). This excludes a "vertical" binding of the peptide, where Trp should be efficiently screened from the quencher. These results are in line with the data on the MFL label.

Our work on LUVs was extended to biological membranes. The red-shifted absorption of the MFL label (about 400 nm) is convenient for spectroscopic and microscopic studies in a cellular environment. In our laboratory, we recently demonstrated by confocal microscopy and two photon fluorescence lifetime imaging that Vpr(52-96) was able to enter and to accumulate in the cells. This entry occurs in a time-dependant manner through active clathrin-caveolae mediated endocytosis and the peptide accumulates in acidic endosomes remaining stable over 48h (data to be published). To further understand whether the incorporation of Vpr(52-96) is associated with membrane binding, we incubated MFL-Vpr(52-96) with HeLa cells. The fluorescence was recorded in a cell suspension of detached HeLa cells after trypsinization. Resulting spectra contain two emission bands characteristic for the membrane environment and are similar to the spectrum observed in neutral LUVs (**Fig. 3.22** and **3.19**). Moreover, this spectrum is dramatically different from that of the peptide in buffer, where only one N* emission band is observed (**Fig. 3.22**). These results suggest that most of the peptide is bound to the cell membranes, in line with literature data [229]. Nevertheless,

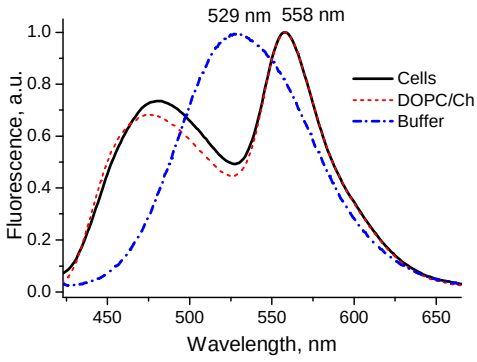

Figure 3.22. Fluorescence of MFL-Vpr(52-96) in cells (black line) compared with liposomes (red dots) and buffer (blue dash dot line). Normalized spectra were recorded using an excitation wavelength of 400 nm.

some amount of free protein could be present in cells being not detected due to the ten-fold lower quantum yield compared to the membrane-bound form.

In conclusion, application of the MFL label for studying interaction of the C-terminal Vpr fragment allowed us to determine the location of this peptide bound to the membrane and the relationship between the membrane composition and its binding affinity. Moreover, the dye could provide information about the peptide-membrane interactions in cells.

4. CONCLUSIONS

The aim of this work was to develop new environment sensitive fluorescent labels for monitoring protein interactions with various biological targets. In this respect, we were taking benefit of dyes undergoing an ESIPT reaction to develop two-color ratiometric labels that offer advantages over the common "intensiometric" or solvatochromic probes. Our main efforts were focused on the development of environment-sensitive fluorescent labels based on 3-hydroxychomone and its analogues and their application for monitoring interactions of proteins with nucleic acids, biomembranes or other proteins.

The first part of the work was focused on the development of two-color labels that can sense the environment properties through perturbations of the ESIPT reaction. Namely, the sensitivity to the environment of 3-hydroxychromones (3HCs) and their recently described analogues 3-hydroxyquinolones (3HQs) were studied and compared. The rate of ESIPT reaction in these dyes depends strongly on the chemical substituents at 2-position. In 3HQ, this rate strongly depends on the spatial hindrance between the 3-hydroxy group and the substituent at 2-position.The introduced 2-methyl-3-hydroxyquinolones are the smallest two-band environment sensitive dyes described up to now.

The two-band fluorescence of 3HCs and 3HQs display strong dependence on on the environment polarity. In contrast to 3HCs, the 3HQ dyes are sensitive to the basicity of the medium. Hydrogen-bond acceptors disrupt the intramolecular H-bond and slow down the ESIPT reaction. 3HQs exhibit an irreversible ESIPT that leads to a kinetic control of the emission band intensity ratio. To apply 3HQs for the selective sensing of the environment H-bonding basicity, the effects of polarity and basicity should be separated. To this end, a new dye with lower sensitivity to polarity was designed and characterized.

Another important property of 3HQs resulting from the irreversibility of their ESIPT reaction is their sensitivity to the viscosity of their environment. Their intramolecular H-bond is partially disrupted by protic solvents. Therefore, the ESIPT reaction requires a reorganization of the solvation shell of these dyes that is rate-limiting in viscous media. Consequently, the N*/T* intensity ratio of the emission bands increases with viscosity. Application of these dyes for monitoring local and global viscosity changes can be foreseen.

The kinetic control of the emission bands ratio in 3HQs leads to an about 3-fold increase of this ratio when the hydrogen in the 3-hydroxy group is substituted by deuterium that undergoes a slower

ESIPT. This property was applied for the detection of small amounts of water in aprotic solvents by monitoring the isotopic exchange.

Together with this study of 3HQs dyes, the fluorescence properties of several 3HC dyes were also studied. Acetamido derivatives of 2-fury-3-hydroxychromone and 4'-dimethylamino-3-hydroxyflavone show an increase of their N*/T* emission band intensity ratio with an increase of polarity or H-bond donor ability (hydration) of their environment.

A high hydration level of the environment leads to an increase of the N*/T* ratio in the case of 3HCs while for 3HQs, the effect is opposite. In most biological systems, the environment polarity and hydration level are strongly related. Their simultaneous decrease leads to a clear decrease in the N*/T* ratio of the 3HC dyes, while for the 3HQ dyes it gives less clear spectroscopic changes, since the effects induced by polarity and hydration compensate each other. Therefore, for design of our protein labels, we have selected 3HC dyes.

Based on our spectroscopic studies, we proposed two different fluorescent labels, working in two different polarity range. First, the FCL label, which is based on 2-furyl-3-hydroxychromone shows a two-band fluorescence with a suitable N*/T* band ratio in water and thus could be used for environment sensing in polar protic media. Second, the MFL label which is based on the 4'-(dimethylamino)-3-hydroxyflavone fluorophore is more adapted for applications in apolar media, as it shows only a single emission band of low intensity in water and alcohols. Thus, these two labels are complementary and could be used in parallel for sensing environment changes sensing in a wide polarity range. Both labels contain a non-hindered carboxylic group well suited for amino group labelling during solid phase peptide synthesis.

The second part of the work was devoted to the application of the synthesized fluorescent labels for sensing peptide interactions.

Peptides were labeled with the new 3HC dyes at their N-terminal amino group, which did not modify their biological activity. Since nuclec acid-binding peptides and their nucleic acid targets are are relatively polar molecules, the FCL label was selected to study their interactions. Its applicability to this purpose was tested on two model systems, which are well interacting with DNA: 1) the natural polycationic compound spermine conjugated with the 3HC fluorophore and 2) the short cationic peptide Tat(44-61) labeled with FCL. In both cases, the fluorophore reports on DNA binding by a several-fold decrease of the N*/T* ratio as well as by a significant red shift of the T* band maximum. This spectroscopic response results from a decrease in the exposure to bulk water of the labeling site due to its proximity to the nucleic bases.

The label was then applied to study the HIV-1 nucleocapsid protein (NC) interactions with oligonucleotides. Different fluorescence ratiometric response was obtained for different DNA/RNA targets, which was correlated with the 3D structure of NC/oligonucleotide complexes known from the NMR spectroscopy. This approach was also successfully used to measure the binding parameters and to localize preferential binding sites on oligonucleotides.

The FCL label was also applied to study peptide-protein interactions. The used system consisted of the antibody against the HPV E6 protein and a FCL-labeled peptide containing the recognized part of the E6 protein. The labeled peptide showed more than 50% decrease of its N*/T* emission band ratio on binding with the antibody. Moreover, in the presence of other antigens, the labeled peptide was removed from the complex and the fluorescence profile of the free peptide was restored. Thus, this labeling approach appears useful for monitoring and quantifying antigen-antibody interactions.

To study protein-membrane interactions, the MFL label adapted to aprotic apolar media was found to be more appropriate. This label was coupled to the C-terminal Vpr fragment to study its interaction with membranes. Binding of the labeled peptide to large unilaminar vesicles serving as model membranes leads to a switch from a single band emission of low intensity observed in water to a bright two band emission, as observed in apolar media. The dual emission of the labeled Vpr peptide showed dependece on the properties of the membrane, which was used to determine the binding preference of the peptide to vesicles of different lipid composition. The studied Vpr fragment interacts also with cells and is able to cross cellular membrane. Incubation of the cells with the MFL-labeled peptide allowed us to record its emission spectrum in the cellular environment. This spectrum was found to be similar to spectra observed in model membranes, which indicate that most of the peptide was bound to membranes.

Thus, our results suggest FCL and MFL labels as powerful tools for studying protein-protein, protein-DNA and protein-biomembrane interactions.

5. PERSPECTIVES

The present work could be extended in two main directions, either for applications or for development, in order:

- to study in further detail, the biological systems presented in this work or to apply our labels to new biological systems
- to improve the labels or/and the labeling techniques .

To further investigate the Vpr-membrane interactions, the synthesis of the labeled full-length protein is required. Its binding to different types of membranes could be analyzed by using the same approaches as with the fragment MFL-Vpr(52-96). Moreover, comparison of the properties of the full-length protein with those of its C-terminal domain, will inform about the respective roles of the N- and C-terminal domains in the membrane binding. These studies should be combined with other methods, namely the atomic force microscopy, in order to explore the influence of the protein on the membrane properties. The labeled proteins could also be used for two-photon imaging in cells.

Improvement on the level of the labels could be achieved through the synthesis of non-natural amino acids based on the 3HC moiety. This will provide the possibility to incorporate the fluorophore in any position of a synthetic peptide. The 3HC dyes are less than twice larger than tryptophan and thus could be introduced into peptides without strong perturbation of their structure. Their high chemical stability is compatible with solid phase peptide synthesis.

Introduction of such fluorescent amino acid analogues in Vpr protein will provide additional information about its interaction with the membranes. Introduction of the probe at different locations within the different protein domains will give site-selective information on the protein conformation and its position in the membrane. 3HC-based amino acids will also help to characterize NC binding to DNAs or RNAs. Introduction of the fluorophore close to a putative interaction site should induce a strong change in its signal, allowing a site-selective characterization of its environment within the binding site. In addition, synthesis of peptides with different label localization could be envisioned for mapping the binding sites.

A perspective field of the two-color ratiometric label application is the construction of fluorescence-based biosensors. As it was shown in this work, peptides labeled with such fluorophores could be used for sensing specific antibodies in vitro. The application field could be expanded to *in vivo* systems by developing fluorophores of the same family presenting a red-shifted absorption. One prospective direction could be the 7-methoxy analogue of the MFL label, which is expected to combine a strong environment sensitivity in polar media with a wavelength excitation range compatible with biological media.

Environment-sensitive labels could also be used in high throughput screening of small molecules expected to bind the protein. For this aim, two approaches could be applied 1) to introduce the ratiometric label in close proximity of potential binding sites and to monitor the interaction through the environment changes induced by the binding process and, 2) to label natural effectors of the protein and to monitor their displacement by competitive inhibitors.

6. MATERIALS AND METHODS

6.1. Fluorophore Synthesis

All the solvents and chemicals were purchased from Aldrich. The solvents were of analytical grade. Melting points were determined using a Gallenkamp Melting Point Apparatus. Mass spectra were measured using a Mass Spectrometer Mariner System 5155. 1H-NMR spectra were recorded on a Bruker 300 MHz spectrometer.

6.1.1. 3-Hydroxyquinolones (3HQs)

The synthesis of 3HQs was described in Article 1.

A typical synthetic procedure consists in two steps (as given for the following example concerning 2-phenyl-3-hydroxyquinolone):

1) Preparation of phenacylantranilate. To a solution of anthranilic acid (3 g, 22 mmol) in 10 ml of DMF, 6 g (44 mmol) of potassium carbonate were added. The mixture was heated to 70^{o}C and stirred during 1h. After cooling to room temperature, phenacyl bromide (4.1 g, 20 mmol) was added. Then, the mixture was heated to 50^{o}C and stirred during 1h. After that, the mixture was poured into 100 ml of cold water. The filtered precipitate after washing by water and drying was fenacylantranilate (4.9 g, 87%), pure enough for the next usage.

2) Cyclization to 3HQ. Phenacylantranilate (0.5 g, 1.9 mmol) was dissolved in polyphosphoric acid (3.3 g of 1:1 H_3PO_4:P_2O_5 mixture by weight) and heated to 120^{o}C for 2 h. Then, mixture was poured into 20 g of ice and neutralized by 10% aqueous sodium carbonate. Filtered precipitate after washing, drying and recrystallizing from DMF. ^{1}H NMR (300 MHz, $CDCl_3$) δ_H: 11.59 (br. s, 1H, NH), 8.15 (d, J = 8.5 Hz, 2H, ArH), 7.81 (d, J = 7 Hz, 2H, Ar'H), 7.72 (d, J = 8 Hz, 1H, ArH), 7.57 (m, 4H, ArH, Ar'H), 7.27 (t, J = 7 Hz, 1H, Ar'H) ; m/z 238.24 (M^++H); mp 276°C.

6.1.2. 3-hydroxychromones (3HCs)

Dyes **1** and **2** were prepared by the protocol described earlier for **1** [78].

Synthesis of the dye **3** and 3HC conjugates with spermine (**C1** and **C2**) were described in Article 6.

Dye **4** was synthesized by a similar protocol.

5'-acetamido-2'-hydroxyacetophenone and 4'-dimethylaminobenzalde were condensed into the corresponding chalcone in dry DMF in the presence of sodium methoxide (RT, 24 h). The reaction mixture was diluted with several volumes of ethanol and treated with 10 mol excess of hydrogen peroxide and 12 mol excess of sodium methoxide. Refluxing the mixture for 5 min was leading to the corresponding 3-hydroxychromone (**4**) with yield 50%. ^{1}H NMR (300 MHz, DMSO-d6) δ 10.25 (s, 1H, OH), 9.95 (br.s, 1H, NH), 8.43 (d, J = 2.5 Hz, 1H, ArH), 7.75 (d, J = 7.5 Hz 2H, 2' and 6'), 7.69 (d, J = 9 Hz, 1H, ArH), 6.97 (dd, J = 9 Hz, J = 2.5 Hz,1H, ArH), 6.82 (d, J = 7.5 Hz 2H, 3' and 5'), 3.01 (s, 6H, NMe_2), 2.09 (s, 3H, $COCH_3$).

FCL and **MFL** labels were prepared from dyes **3** and **4** respectively. In both cases, the acetamide group was hydrolyzed and the obtained amide was acylated by succinic anhydride.

1) Acetamide hydrolysis. Compound **3** (or **4**) was refluxed in 10% HCl during 7h (100°C). Then, the solution was evaporated and a small amount of alkaline water was added up to pH = 7. The obtained product was filtrated and dried to give the corresponding amine (yield 90%).

1) Acylation by succinic anhydride. The obtained amine (0.82 mmol, about 0.2 g) was dissolved in 10 ml a dry DMF and 0.09 g (0.9 mmol) of succinic anhydride was added to this solution. The mixture was left for stirring overnight. Then, it was poured into water to give a precipitate of the final acid which was filtrated. The product was recrystallized from propanol-2. The overall yields were 55% and 65% for **FCL** and **MFL** respectively.

^{1}H NMR (300 MHz, DMSO-d6) **FCL:** δ 10.27 (s, 1H, NH), 8.44 (d, J = 3.5 Hz, 1H, ArH), 8.01 (s, 1H, ArH), 7.89 (d, J = 9 Hz, 1H, ArH), 7,67 (d, J = 9 Hz, 1H, ArH), 7.28 (d, J = 2.5 Hz, 1H, HetH), 6.78 (s, 1H, HetH), 2.59-2.50 (m, 4H, CH_2CH_2).

MFL: δ 10.27 (s, 1H, NH), 8.43 (d, J = 3 Hz, 1H, ArH), 7.89 (d, J = 9 Hz, 1H, ArH), 7.75 (d, J = 7.5 Hz 2H, 2' and 6'), 7,67 (d, J = 9 Hz, 1H, ArH), 6.97 (dd, J = 9 Hz, J = 2.5 Hz,1H, ArH), 6.82 (d, J = 7.5 Hz 2H, 3' and 5'), 3.01 (s, 6H, NMe_2) , 2.55 (m, 4H, CH_2CH_2).

The synthesis of **FCL** was described in Article 7.

6.2. Peptide synthesis

6.2.1. General methods

A) Synthesis

Peptides were synthesized by solid phase peptide synthesis on a 433A synthesizer (ABI, Foster City, CA). The synthesis was performed at a 0.1 mmole scale using the standard side-chain protected fluorenylmethoxycarbonyl (Fmoc)-amino acids and HBTU/HOBt coupling protocol. HMP resin (ABI, 0.44 mmol/g reactive group concentrations) was used as solid support. Deprotection steps were performed by piperidine and automatically controlled by UV absorbance. At the end of the synthesis peptidylresin was isolated, and twice washed by NMP.

B) Labeling

Labeling procedures were performed in flasks. Four equivalents (0.4 mmole) of the label (FCL or MFL) were dissolved in 1 ml of NMP mixed with four eq. of HBTU/HOBt coupling solution (in DMF) and added to Fmoc-deprotected peptidylresin (0.1 mmole) swelled in 1 mL of NMP. After a few minutes of shaking five eq. of DIEA solution was added. Then the reaction mixture was stirred at 40°C for 4 hours. Resin was filtrated and washed by NMP. In the case of lipophilic peptides, this procedure was repeated, if not the resin was washed by methanol and DCM was dried and weighted.

C) Cleavage and deprotection

Cleavage of the peptidylresin and its deprotection was performed for 2 h using a 10 ml trifluoroacetic acid (TFA) solution containing water (5%, v/v), phenol (2%, w/v), thioanisole (5%, v/v) and ethanedithiol (2.5%, v/v). The solution was concentrated *in vacuo* and the peptide was precipitated by using ice-cold diethyl ether and then pelleted by centrifugation. The pellet was washed with diethyl ether and dried.

D) Purification

Before purification, the peptides were solubilized with aqueous TFA (0.05 %, v/v). In the case of lipophilic peptides, the necessary amount of acetonitrile was added. HPLC purification was carried out on a C8 column (uptisphere 300A, 5µm; 250X10, Interchim, France) in water/acetonitrile mixture containing 0.05% TFA with linear gradients depending on the peptide (typically 20 to 50% of acetonitrile for 30 min) and monitored at 210 nm (detection of all peptides including non-labeled) and 370 nm (detection of labeled peptides only). After purification, the fractions containing pure peptide were combined and lyophilized.

All peptides were characterized by ion spray mass spectrometry and the expected molecular masses were found. Prior to use, the peptides were dissolved in distilled water, to be aliquoted and stored at -20°C.

6.2.2. Vpr (52-96)

Sequence: DTWTGVEALIRILQQLLFIHFRIGCRHSRIGIIQQRRTRNGASKS

Purification: a linear gradient 20 to 70% of acetonitrile for 30 min, then 90% of acetonitrile for 10 min. The oligomerization of the peptide complicates its purification but the oligomer could be eluted at high acetonitrile concentration (about 90%).

MS FCL-Vpr(52-96) Found: 5572 Calculated: 5572

MFL-Vpr(52-96) Found: 5634 Calculated: 5633

Vpr(52-96) Found: 5247 Calculated: 5246

6.2.3. NC

NC(11-55)

Sequence: KNVKCFNCGKEGHTARNCRAPRKKGCWKCGKEGHQMKDCTERQAN

MS FCL-NC(11-55) Found: 5464 Calculated: 5463

NC(1-55)

Sequence: MQRGNFRNQRKNVKCFNCGKEGHTARNCRAPRKKGCWKCGKEGHQMKDCTERQAN

MS FCL-NC(1-55) Found: 6752 Calculated: 6752

MFL-NC(1-55) Found: 6805 Calculated: 6805

Purification: Linear gradient 10 to 40% of acetonitrile for 30 min

Preparation of Zn-bound peptides. The lyophilized peptides were dissolved in water (≈ 0.5mg in 500µL). Then, about 10 µL of this solution was used to determine the peptide concentration using an extinction coefficient of 15,000 $M^{-1}\times cm^{-1}$ at 350 nm for 3HC-NC(11-55). Next, 2.2 molar equivalents of $ZnSO_4$ were added to the peptide and pH was raised to its final value by adding buffer. This last step was done only at the end of the preparation to prevent peptide oxidization. Noticeably, a large excess of Zn^{2+} ions should be avoided since this ion could affect 3HC fluorescence.

6.2.4. Tat (44-61)

Sequence: GISYGRKKRRQRRRPPQG

MS FCL-Tat(44-61) Found: 2522 Calculated: 2523

Purification: Linear gradient 10 to 40% of acetonitrile for 30 min

6.2.5. F10C, A12C and K15C

Sequence: K15C KRTAMFQDPQERPRC

A12C AMFQDPQERPRC

F10C FQDPQERPRC

The peptides were synthesized in one run by splitting the resin at corresponding steps of the synthesis (30% part of Fmoc-deprotected resin was used for labeling, the remainig 70%r for peptide prolongation).

Purification: Linear gradient 10 to 40% of acetonitrile for 30 min

MS FCL-K15C Found: 2188; Calculated: 2188

6.2.6. G5

Sequence: GGGGG

Labeling: 1.5 equivalents of the FCL, 1.5eq of the coupling solution and 3eq of DIEA overnight. Labeling efficiency by HPLC >90%.

Cleavage: 10 ml TFA containing water (10% v/v) and triisopropilsilane (2.5%, v/v).

Purification: Linear gradient 10 to 50% of acetonitrile for 20 min

6.3. Oligonucleotides

All oligonucleotides were synthesized and HPLC-purified by IBA GmbH (Germany). Their concentrations were determined using extinction coefficients at 260 nm provided by the manufacturer or calculated according to their nucleotide composition.

6.4. Lipids and liposome preparation

All phospholipids and sterols were from Sigma-Aldrich or Avanti and used without further purification. The synthetic lipids correspond to well-defined molecular species (**Table 4.1**, **Fig. 4.1**).

Table 4.1. Used membrane lipids:

Abbreviation	Name	Charge
DOPC	1,2-dioleoyl-*sn*-glycero-3-phosphocholine	0
DOPG	1,2-dioleoyl-*sn*-glycero-3-phosphoglycerol	-1
DOPS	1,2-dioleoyl-*sn*-glycero-3-phosphoserine	-1
DPPC	1,2-dipalmitoyl-*sn*-glycero-3-phosphocholine	0
SM	Sphingomyelin	0
Ch	Cholesterol	0

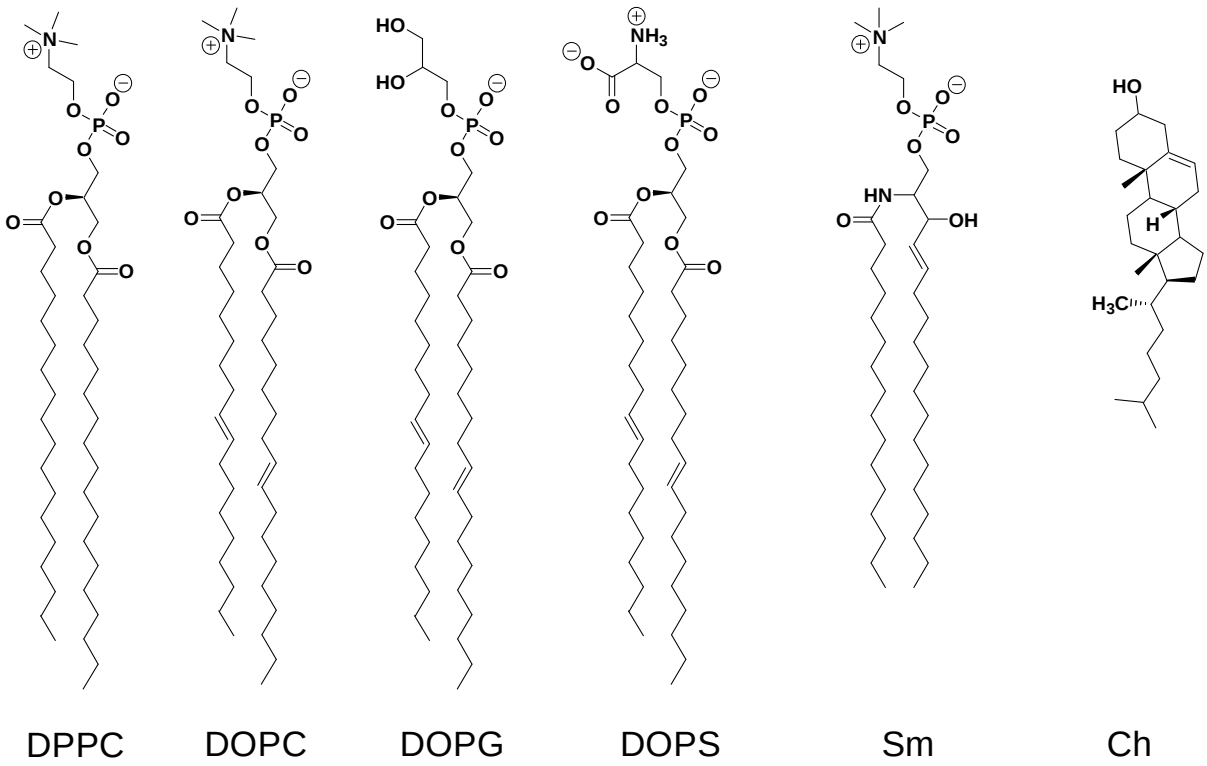

Figure. 4.1. Structures of used phospholipids and sterols

A) Preparation of multilamellar lipids vesicles

Properties of liposomes can vary depending on their composition (cationic, anionic, neutral lipid species). However, the same preparation method can be used for all lipid vesicles regardless of their composition. The general elements of the procedure involve preparation of the lipids for hydration, hydration with agitation, and sizing to a homogeneous distribution of vesicles.

When preparing liposomes with single or mixed lipid compositions, the lipids must first be dissolved and mixed in an organic solvent to ensure a homogeneous distribution of lipids. Usually, this process is carried out using chloroform or chloroform/methanol mixtures. The organic solvent should then be removed by rotary evaporation yielding a thin lipid film on the wall of a round bottom flask. The lipid film is thoroughly dried to remove residual organic solvent by continuing evaporation with additional heating during 30 minutes. Hydration of the dry lipid film is accomplished simply by adding corresponding buffer to the flask. This step of hydration should be maintained approximately 30 minutes. Typically lipid solutions are prepared in order to obtain a 0.2 mM final concentration, although higher concentrations may be used. After hydration, the solution is thoroughly vortexed during 2 minutes, giving rise to a suspension of multilamellar vesicles (MLV) with a heterogeneous size distribution. Once a stable, hydrated MLV suspension has been produced, the particles can be downsized by extrusion.

B) Preparation of large unilamellar vesicles by extrusion

Lipid extrusion is a technique in which a lipid suspension is forced through a polycarbonate filter with a defined pore size to yield particles having a diameter near the pore size. An extruder (Lipex Biomembranes Inc) with polycarbonate filters of calibrated pores (Nucleopore) was used. Prior to extrusion through the final pore size, the MLV suspension was first downsized by passing through a large pore size (0.2μm) filter seven times. Then, the suspension is passed through the filter with the final pore size (0.1 μm) ten times. This final extrusion through filters with 0.1 μm pores yields to large unilamellar vesicles (LUV) with a mean diameter of 110-120 nm. Mean particle size depends slightly on lipid composition and is reproducible from batch to batch. The extrusion method ensures an homogeneous size distribution of the final suspension. As previous procedures, like hydration and vortexing, the extrusion should be done at a temperature that is higher than the temperature of the gel-liquid crystal transition of the lipid.

6.5. Physical measurements

6.5.1. Absorption spectroscopy

Absorption spectra were recorded on a double-beam spectrophotometer Cary 400 (Varian). The absorbance is characterized by:

$$A = \log(I_0/I)$$

where I_0 and I are the incident and transmitted intensities, respectively [271].

A correction for the cuvettes also should be done, because the two cuvettes are never perfectly identical. To this end, the baseline of the instrument is first recorded (with both cuvettes filled with the solvents). Then, the dye is added into the solvent of the sample cuvette and the true absorption spectrum is recorded.

6.5.2. Steady-state fluorescence spectroscopy

Steady-state fluorescence measurements were performed on spectrofluorometers FluoroMax-3 (Jobin Yvon) and Fluorolog (Jobin Yvon), equipped with a thermostatic cuvette holder.

The FluoroMax-3 and Fluorolog are the photon counting devices with a linear response in the range of measurements (<3 Mcps). The source of light is a xenon lamp. The signals are measured with a photomultiplier. The correction of the excitation beam is performed with a calibrated photodiode. The wavelength-dependent correction functions for the excitation and emission monochromators and for the photomultiplier are provided by the manufacturer and are incorporated into the FluoroMax-3 and Fluorolog softwares. The fluorescent spectra are automatically corrected by these calibration functions.

A) Quantum yield determination

Absorption and emission spectroscopic measurements were also used for quantum yield determination. Usually, to measure the quantum yield of a dye (x), we need to know the quantum yield of a reference dye (r) for which both absorption and emission spectra are overlapping with the corresponding spectra of the investigated dye. The next formula has to be applied:

$$\Phi_x = \frac{I_x(1-10^{-OD_r})}{I_r(1-10^{-OD_x})}\Phi_r \frac{n_x^2}{n_r^2}$$

where, Φ_x is the quantum yield of the dye; Φ_r is the known quantum yield of the reference dye; OD_x and OD_r are respectively the absorbance of x and r at an appropriate excitation wavelength; I_x and I_r are their respective fluorescence intensities as measured by integration of the

surface under the emission spectrum corrected for the photomultiplier response; n_x and n_r are the refractive indexes of their respective solvents.

Quinine sulphate in 0.5 M sulphuric acid (quantum yield, φ = 0.577 [272]) and 4'-(dialkylamino)-3-hydroxyflavone in ethanol (φ = 0.52 [273]) were used as references for the dyes absorbing below and above 370 nm respectively.

6.5.3. Time-resolved fluorescence spectroscopy

Time-resolved fluorescence measurements were performed with the time-correlated, single-photon counting technique using excitation pulses at 320 (or 480) nm provided by a pulse-picked frequency tripled (or doubled) Ti-sapphire laser (Tsunami, Spectra Physics) pumped by a Millenia X laser (Spectra Physics) [201]. The emission was collected through a polarizer set at magic angle and an 8 nm band-pass monochromator (Jobin-Yvon H10) at 470 nm. The instrumental response function was recorded with a polished aluminum reflector, and its full-width at half-maximum was 40 ps. Time resolution was 25.5 ps/channel.

For time-resolved anisotropy measurements, the fluorescence decay curves were recorded at vertical and horizontal positions of the polarizer and analyzed by the following equation:

$$r(t) = \frac{I_{\parallel}(t) - GI_{\perp}(t)}{I_{\parallel}(t) + 2GI_{\perp}(t)} = r_0 \sum \beta_i \, exp(-t/\theta_i)$$

where β_i are the amplitudes of the rotational correlation times θ_i; $I_{\parallel}$ and $I_{\perp}$ are the intensities collected at emission polarizations parallel and perpendicular, respectively, to the polarization axis of the excitation beam, and G is the geometry factor at the emission wavelength, determined in independent experiments.

Time-resolved intensity and anisotropy data were treated with a nonlinear least-square analysis using a home-made software (kindly provided by G. Krishnamoorthy)and with the Maximum Entropy Method (MEM) [274]. In all cases, the χ^2 values were close to 1, and the weighted residuals as well as the autocorrelation of the residuals were distributed randomly around zero, indicating an optimal fit.

6.5.4. Dynamic light scattering

Dynamic Light Scattering (DLS) (sometimes referred to as Photon Correlation Spectroscopy or Quasi-Elastic Light Scattering) is a technique for measuring the size of particles typically in the sub micron region. DLS measures the Brownian motion and relates this to the size of the particles. The larger the particle, the slower the Brownian motion will be. Smaller particles are "kicked" further

by the solvent molecules and move more rapidly. An accurately known temperature and solvent compositions are necessary for DLS because it depends on the viscosity.

The diameter that is measured in DLS is a value that refers to how a particle diffuses within a fluid so it is referred to as a hydrodynamic diameter. The diameter that is obtained by this technique is the diameter of a sphere that has the same translational diffusion coefficient as the particles. The size of the spherical particle is calculated from the translational diffusion coefficient by using the Stokes-Einstein equation:

$$d(H) = \frac{kT}{3\pi\eta D}$$

Where: ***d (H)*** = hydrodynamic diameter; ***D*** = translational diffusion coefficient; ***k*** = Boltzmann's constant; ***T*** = absolute temperature; ***η*** = viscosity

In a dynamic light scattering instrument, a laser is used as the light source to illuminate the sample cells. For dilute concentrations, most of the laser beam passes through the sample, but some is scattered by the particles within the sample at all angles. The detector in our device measures the scattered light at 173°. The scattering intensity signal from the detector is processed by a correlator and then analyzed by the manufacturer software to obtain the size information. All our measurements were done on Zetasizer Nano-ZS (Malvern Instruments, Paris, France). The peptide (Vpr (52-96)) concentration was set at 30μM to ensure good signal reproducibility.

7. APPENDIX

In addition to my dissertation work, I had the opportunity to collaborate on other projects that are presented in papers shortly introduced below:

1) Article "Fluorescent dyes undergoing intramolecular proton transfer with improved sensitivity to surface charge in lipid bilayers"

The development of dyes for sensing biomembrane properties is one of the main topics of research of our research team. Fluorophores sensitive to the surface charge in lipid bilayers are useful in many ways, and notably for apoptosis detection. The dialkylaminoaryl-3HC dyes studied presently, are sensitive to the membrane surface charge and are similar to the dyes used for sensing the protein-membrane interactions. The designed fluorophores exhibit two-band emission spectra highly sensitive to the polarity and H-bond donor basicity of their environment, together with a suitable ratio of their emission band intensities in apolar media. Thus, these dyes appear as prospective biomembrane probes.

2) Article "Probing dynamics of HIV-1 nucleocapsid protein/target hexanucleotide complexes by 2-aminopurine"

Many projects of our team are focused on the HIV-1 nucleocapsid protein (NC) and its interactions with nucleic acids. In parallel to the synthesis of the labeled protein, NC-oligonucleotide interactions were studied also by using oligonucleotides with a fluorescent adenine analog: 2-aminopurine. This residue exhibits a red-shifted absorption spectrum as compared to the natural nucleic bases and can be used to study the oligonucleotide dynamics within their complexes with proteins. Time-resolved fluorescence measurements of 2-aminopurine provide site specific information on the NC-induced changes in the local dynamics of the bases and the oligonucleotide backbone. Several mutants of NC were synthesized and compared with the native protein to determine the role of the different protein domains in the modulation by NC of the oligonucleotide dynamics. By this approach, the NC hydrophobic platform in the correctly folded zinc fingers, was shown to be critical for NC to restrict the local dynamics of the oligonucleotide bases and limit the flexibility of the oligonucleotide backbone.

3) Review Article "Targeting the Viral Nucleocapsid Protein in Anti-HIV-1 Therapy".

NC is one of the most conserved proteins of the HIV virus, and it plays a critical role in the virus assembly and replication due to its DNA chaperone properties. Accordingly, NC constitutes

an interesting target for antiviral therapy. Different strategies have been developed to inhibit the NC activities, but up to now, no clinical-ready compound was found.

4) Manuscript **"**Identification by high throughput screening of small compounds inhibiting the chaperone activity of the HIV-1 nucleocapsid protein".

A high throughput screening assay based on NC ability to transiently melt fluorescently-labeled hairpin oligonucleotides was developed in our laboratory and tested on an "in-house" chemical library of 4800 molecules. Five compounds with IC_{50} values in the low micromolar range have been selected. The hits were shown, by mass spectrometry and fluorescence anisotropy titration, to prevent binding of NC to cTAR through direct interaction with the NC folded fingers, but without promoting zinc ejection. These non zinc ejecting NC binders are a new series of anti NC molecules that could be used as a starting point to rationally design molecules with potential antiviral activity.

Fluorescent dyes undergoing intramolecular proton transfer with improved sensitivity to surface charge in lipid bilayers

Gora M'Baye,[a] Andrey S. Klymchenko,*[a] Dmytro A. Yushchenko,[a] Volodymyr V. Shvadchak,[a] Turan Ozturk,[b] Yves Mély[a] and Guy Duportail[a]

Received 14th August 2006, Accepted 27th October 2006
First published as an Advance Article on the web 23rd November 2006
DOI: 10.1039/b611699j

4′-(Dialkylamino)-3-hydroxyflavones are characterized by an excited-state proton transfer reaction between two tautomeric excited states, which results in two emission bands well separated on the wavelength scale. Due to the high sensitivity of the relative intensities of the two emission bands to solvent polarity, hydrogen bonding and local electric fields, these dyes found numerous applications in biomembrane studies. In order to further improve their fluorescence characteristics, we have synthesized new dyes where the 2-phenyl group is substituted with a 2-thienyl group. In organic solvents, the new dyes exhibit red shifted absorption and dual fluorescence. Although they show lower sensitivity to solvent polarity and H-bond donor ability (acidicity) than their parent 3-hydroxyflavone dyes, they exhibit a much higher sensitivity to solvent H-bond acceptor ability (basicity). Moreover, when tested in lipid vesicles of different surface charge, the new dyes show much better resolved dual emission and higher sensitivity to the surface charge of lipid bilayers than the parent dyes. The response of the new dyes to surface charge is probably connected with the H-bond basicity of the membrane surface, which is the highest for negatively charged surfaces. As a consequence, the new dyes appear as prospective fluorophores for the development of new fluorescent probes for biomembranes.

Introduction

3-Hydroxychromone dyes are dual emission fluorophores due to an excited state intramolecular proton transfer (ESIPT) that results in two excited state forms: a normal (N*) and a tautomer (ESIPT product, T*) forms.[1] Both N* and T* forms are highly emissive exhibiting well separated bands in the emission spectra. Importantly, these dyes can report the physicochemical properties of their microenvironment both by the positions and the relative intensities of their two emission bands.[2] Due to these unique features, numerous 3-hydroxychromone dyes have been synthesized and studied during the recent years, resulting in the development of new fluorescence probes to study solvent polarity,[2–4] ion binding[5] and electric fields,[6,7] with applications in the field of polymers,[8] reverse micelles,[9,10] lipid vesicles,[7,11–14] cellular membranes[15] and proteins.[16–18] The most prospective biochemical targets for these dyes are biomembranes, which are characterized by relatively low fluidity and polarity. In this respect, the most suitable dyes are 4′-(dialkylamino)-3-hydroxyflavone derivatives (see the typical representative dye **1** in Fig. 1), since the polarity range of their dual emission corresponds well to that of the lipid membranes. However, the main disadvantage of these dyes is their absorption close to 400 nm, which is inconvenient for cellular studies due to the high phototoxicity of short wavelength excitation. In order to improve their absorption and fluorescence properties, several modifications of the basic fluorophore were considered.

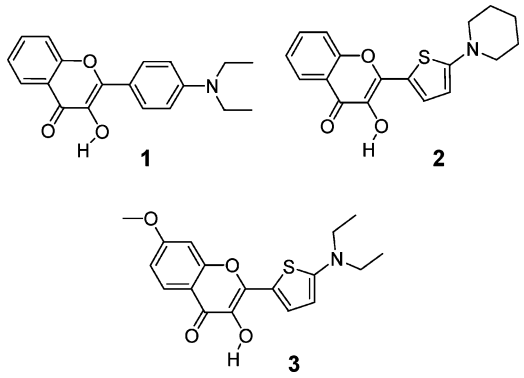

Fig. 1 Chemical structures of the 4′-(dialkylamino)-3-hydroxyflavone reference dye **1** and the new 2-(2-thienyl)-3-hydroxychromone dyes **2** and **3**.

For instance, an increase in the electron donor ability at the 2-aryl group and an extension of the fluorophore shifted the absorption and emission spectra of the dyes to the red and increased their fluorescence quantum yield.[19] Additional red shifts were achieved by the introduction of an electron acceptor group from the opposite side of the fluorophore.[20] However, in all cases the shifts to the red were accompanied by strong variations in the intensity ratios. As a consequence, the polarity range where the dual emission can be observed was shifted to lower polarities. For instance, recently developed 3-hydroxychromone dyes absorbing around 440–450 nm show a dual emission only in highly apolar media (dielectric constant, $\varepsilon = 2$–6),[19] which are uncommon in biological systems. The most apolar sites in living cells are in biomembranes, where the probes are exposed to an environment that corresponds to $\varepsilon = 3$–20. Therefore, an improved fluorophore

[a]*Département de Pharmacologie et Physicochimie, Photophysique des Interactions Biomoléculaires, UMR 7175, Institut Gilbert Laustriat, 74 Route du Rhin, Université Louis Pasteur (Strasbourg I), BP 60024, 67401, Illkirch, France. E-mail: aklymchenko@pharma.u-strasbg.fr*
[b]*Istanbul Technical University, Science Faculty, Chemistry Department, Organic Chemistry, Maslak 34469, Istanbul, Turkey*

for biomembranes should exhibit a dual emission in a more extended polarity range.

The other important issue of 3-hydroxychromone (3HC) dyes, which determines their applicability to biological systems, is their sensitivity to specific interactions. Previously, it was shown that H-bonds with water and alcohols strongly modify the ESIPT reaction in a non-substituted 3-hydroxyflavone.[21] Moreover, we showed that protic solvents form a H-bond with the 4-carbonyl group of dialkylamino-substituted flavones, inhibiting the ESIPT reaction and favoring the emission of the N* excited state.[2,22] However, in these studies the dyes did not show any sensitivity to the H-bond basicity, probably because the complexes of the dyes with H-bond acceptor solvents are not emissive.[23]

In the present work, we show that substitution of the phenyl ring by thiophene (3-hydroxy-2-(5-(1-dialkylamino)-2-thienyl)chromones, compounds **2** and **3**, Fig. 1) strongly red-shifts the absorption and emission spectra. Moreover, the polarity range where the dual emission of this new dye is observed is broader than that of the parent molecule **1**. In addition, we found that the new dyes, unlike other studied 3-hydroxychromones, are sensitive to solvent basicity. Furthermore, being bound to lipid vesicles, the new dyes demonstrate improved fluorescence properties as well as higher sensitivity to the vesicle surface charge as compared to the parent 4′-(dialkylamino)-3-hydroxyflavones. This high sensitivity of the new dyes is probably connected to their sensitivity to solvent basicity, suggesting that the dye responds to the basicity differences of lipid bilayers with different surface charge. The improved fluorescence properties as well as the new solvent sensitivity profile make these new fluorophores highly prospective for further applications in biological research, particularly for the development of new biomembrane probes.

Materials and methods

All reagents were purchased from Sigma-Aldrich. Solvents for synthesis were of reagent quality and were appropriately dried if necessary. For absorption and fluorescence studies, solvents were of spectroscopic grade.

Absorption and fluorescence spectra were recorded on a Cary 400 spectrophotometer (Varian) and FluoroMax 3.0 spectrofluorimeter (Jobin Yvon, Horiba), respectively. For fluorescence studies, the dyes were used at an absorbance of 0.1 at the 420 nm excitation wavelength. Quantum yields of the dyes were determined with respect to a solution of dye **1** in ethanol as a reference ($\Phi = 0.52$).[24] Deconvolution of fluorescence spectra with two overlapping bands was performed with the program Siano, kindly provided by the author (Dr A. O. Doroshenko from the Karazin University, Kharkov, Ukraine).[25] The program uses an iterative non-linear least-square method based on the Fletcher–Powell algorithm.[25] The shapes of the individual emission bands were approximated by a log-normal function, which accounts for the asymmetry of the spectral bands.

Proton NMR spectra were recorded on a 300 MHz Bruker spectrometer and mass spectra were recorded on a Mariner System 5155 mass spectrometer using the electro-spray ionization (ESI) method. All column chromatography experiments were performed on silica gel (Merck, Kieselgel 60H, Art 7736).

Large unilamellar vesicles (0.11–0.12 μm in diameter) were obtained by extrusion as previously described.[26] They were made either of egg yolk phosphatidylcholine (EYPC) and/or phosphatidylglycerol (EYPG), of bovine brain phosphatidylserine (BBPS) and of the synthetic cationic lipid *N*-[1-(2,3-dimyristoyloxy)-propyl]-*N*,*N*,*N*-trimethylammonium tosylate salt (DMTAP). Natural phospholipids were from Sigma and DMTAP was a gift from Dr Heissler (Institut de Chimie, Strasbourg). Experiments with vesicles were performed in phosphate–citrate buffer at 15 mM ionic strength, pH 7. Vesicles, at a concentration of 200 μM of lipids, were labeled at a lipid : dye ratio of 100 by adding small aliquots (~2 μl) of DMSO stock solution of dye **2** in 1 ml solutions of vesicles, under vigorous vortexing.

Synthesis of 3-hydroxy-2-(5-(1-piperidinyl)-2-thienyl)chromone (2)

5-(1-Piperidinyl)-2-thiophenecarbaldehyde[27] (1 mol) and 2′-hydroxyacetophenone (1 mol) were dissolved in a minimum volume of DMF followed by 3 mol of NaOMe. After the mixture was stirred overnight, it was diluted with ethanol and then, subsequently, 15 mol of sodium methoxide and 12 mol of 30% hydrogen peroxide were added. The mixture was refluxed for 3 min, cooled to room temperature and poured into water. After neutralization with diluted HCl, the resultant precipitate was filtered and the product was purified by column chromatography using as eluent a ethyl acetate–heptane mixture (EtOAc–Hept = 20 : 80). Yield 32%. ^{1}H NMR (300 MHz, $CDCl_3$) δ 8.20 (d, J = 8 Hz, 1H), 7.79 (d, J = 4 Hz, 1H), 7.60 (t, J = 7 Hz, 1H), 7.45 (d, J = 7 Hz, 1H), 7.35 (t, J = 8 Hz, 1H), 6.15 (d, J = 4 Hz, 1H), 3.30 (m, 4H), 1.70 (m, 6H). MS (EI): m/z 328.2 (M^+). Elemental analysis: $C_{18}H_{17}NO_3S$; Calcd. C 66.03, H 5.23, N 4.28; Found C 66.2, H 5.1, N 4.2%.

3-Hydroxy-7-methoxy-2-(5-(1-(*N*,*N*-dimethylamino))-2-thienyl)chromone (3)

This was synthesized using the same procedure as dye **2**starting from 5-(1-(*N*,*N*-diethylamino))-2-thiophenecarbaldehyde and 2′-hydroxy-4′-methoxyacetophenone. It was purified by column chromatography on silica gel (eluent was ethyl acetate–heptane = 40 : 60). Yield 37%. ^{1}H NMR (300 MHz, $CDCl_3$) δ 8.08 (d, J = 8 Hz, 1H), 7.72 (d, J = 4 Hz, 1H), 6.9 (d, J = 8 Hz, 1H), 6.86 (s, 1H), 5.95 (d, J = 4 Hz, 1H), 3.89 (s, 1H), 3.40 (q, J = 7 Hz, 4H), 1.25 (t, J = 7 Hz, 6H). MS (EI): m/z 346.2 (M^+). Elemental analysis: $C_{18}H_{17}NO_3S$; Calcd. C 62.59, H 5.54, N 4.05; Found C 62.7, H 5.6, N 4.1%.

Results and discussion

Absorption and fluorescence properties of dyes **2** and **3** were studied in different organic solvents and compared with those of dye **1**. The solvents were chosen to provide maximal variation of the physicochemical properties and were classified into three groups: protic (high H-bonding donor ability, α, Table 1), H-bonding acceptor (large β value) and neutral (low α and β values).[28,29]

The absorption spectra of **2** and **3** exhibit significant red shifts with respect to the parent compound **1** in all studied solvents (Fig. 2, Table 1). With a few exceptions, similar red shifts are also observed in the fluorescence spectra (Fig. 2, Table 1). These red shifts can be related to the substitution of the phenyl ring by the highly polarisable and stronger electron donating thienyl ring,

Table 1 Spectroscopic properties of dyes **1**, **2** and **3** in different solvents[a]

Solvents	f(ε)	β	λ_{abs}/nm			λ_{N^*}/nm			λ_{T^*}/nm			I_{N^*}/I_{T^*}			φ (%)		
			1	**2**	**3**	**1**	**2**	**3**	**1**	**2**	**3**	**1**	**2**	**3**	**1**	**2**	**3**
Heptane	0.1889	0.00	396	425	432	423	465	453	554	595	600	0.011	0.092	0.069	14	14	14
Toluene	0.2390	0.14	409	435	442	456	495	482	566	605	609	0.044	0.18	0.132	14	15	14
Trichloroethylene	0.3087	0.00	412	438	446	462	499	489	563	596	603	0.119	0.42	0.293	19	34	28
Fluorobenzene	0.3733	0.10	—	437	444	—	509	495	—	603	608	—	0.50	0.24	—	24	45
Ethyl acetate	0.3843	0.45	401	429	437	475	509	493	570	606	610	0.253	0.78	0.350	5.0	14	14
Tributylphosphate	0.414	1.21	404	430	438	482	509	492	576	610	612	0.594	1.79	0.90	13	22	23
Dichloromethane	0.4204	0.05	411	442	450	492	519	508	568	600	605	0.621	0.81	0.471	17	31	30
HMPA	0.475	1.0	403	429	435	506	521	501	583	618	618	1.45	3.20	1.57	14	21	18
Acetonitrile	0.4792	0.32	404	435	441	509	530	514	574	600	608	1.72	1.20	0.67	9.0	18	18
Dimethylformamide	0.4801	0.74	407	440	443	509	530	512	583	600	618	1.78	2.67	1.44	7.7	26	18
Dimethyl sulfoxide	0.4841	0.88	411	442	448	514	534	518	584	610	620	2.83	4.97	3.76	13	39	15
2-Methyl-2-Butanol	0.3805	—	410	440	448	487	512	507	558	588	592	2.38	1.55	0.90	22	28	28
1-Butanol	0.4579	0.48	415	444	454	517	535	525	567	586	588	6.57	2.44	1.38	58	34	46
Ethanol	0.4704	0.48	413	444	453	521	539	528	570	588	587	10.0	3.21	1.49	52	20	41

[a] f(ε)—Polarity of a solvent as a function of the dielectric constant $f(\varepsilon) = (\varepsilon + 1)/(2\varepsilon - 1)$; β—Abraham's H-bond basicity introduced in ref. 28 and 29; λ_{abs}—position of absorption maxima; λ_{N^*} and λ_{T^*}—positions of fluorescence maxima of the N* and T* states; φ is the fluorescence quantum yield; I_{N^*}/I_{T^*} is the intensity ratio of the two emission bands measured at the peak maxima; HMPA is hexamethylphosphoramide. Data on dye **1** are from ref. 2.

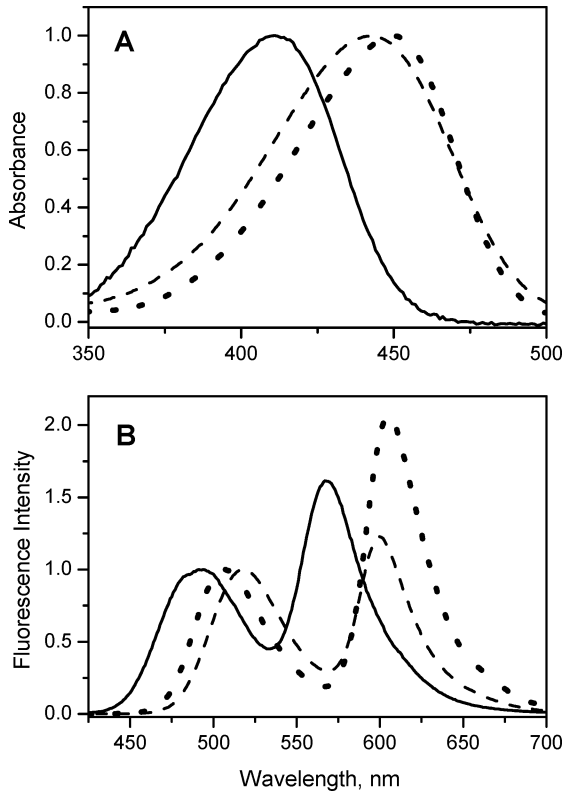

Fig. 2 Normalised absorption (A) and fluorescence (at the N* band maximum) (B) spectra of dyes **1** (solid lines), **2** (dashed lines) and **3** (dotted lines) in dichloromethane.

which increases the charge transfer character of the excited state of the dye. Moreover, the thiophene group, being a five-member ring, is probably smaller than the phenyl group and thus, by analogy with furyl-substituted 3HC, may be more planar.[18,30] Similarly to **1**, the new dyes show dual emission (Fig. 2, Table 1), which could be unambiguously assigned to the emission of the normal (N*) and the tautomer (T*) states in the short-wavelength and long-wavelength spectral regions, respectively. Excitation spectra recorded at the emission maxima are nearly identical (not shown), confirming that both states originate from the same ground state species. The red shifts in the fluorescence spectra of **2** with respect to **1** are generally accompanied by an increase in the ratio of the two emission bands, I_{N^*}/I_{T^*} (Fig. 2, Table 1). According to our previous studies, this effect is an additional indication of an increased charge transfer of the N* excited state of dye **2**, which decreases the energy of this state with respect to that of the T* state and thus increases its relative intensity (*i.e.* increases the I_{N^*}/I_{T^*} ratio).[18] Meantime, the electron donor methoxy group at the 7-position of dye **3** decreases the I_{N^*}/I_{T^*} ratio, in line with the previously observed effect of this group in 3HF.[19] The red-shifted absorption and emission spectra of the new dyes make them more suitable for biological applications. Noticeably, the absorption of the new dyes around 440 nm makes them suitable for excitation with an He–Cd laser (442 nm). Another important property of the new dyes is their higher fluorescence quantum yield in most of studied solvents as compared to **1**. The most notable exceptions are in highly polar protic solvents for which the quantum yields are lower. This last effect was previously observed with other dyes showing higher charge transfer character of their excited state[19] and was attributed to solvent quenching effects.

Similarly to the parent dye **1**,[2,31] the fluorescence spectra of **2** and **3** show a strong sensitivity to the solvent properties. Indeed, an increase of solvent polarity (a function of the dielectric constant ε)[32,33] shifts the N* band to the red and increases the I_{N^*}/I_{T^*} ratio (Table 1). The logarithm of the I_{N^*}/I_{T^*} ratio of **2** and **3** increases linearly with the solvent polarity function of neutral solvents (Fig. 3). However, the slope of the linear fit for both dyes is lower than that observed for dye **1**, indicating a lower sensitivity to solvent polarity. This implies that the polarity-dependent dual emission of the new dyes can be observed in a broader polarity range.

In H-bond donor (protic) solvents, the $\log(I_{N^*}/I_{T^*})$ of dye **2** and **3** deviates upwards from the linear function in neutral solvents (Fig. 3), indicating that as in the case of **1**, protic solvents inhibit the ESIPT reaction in these dyes. However, when protic and

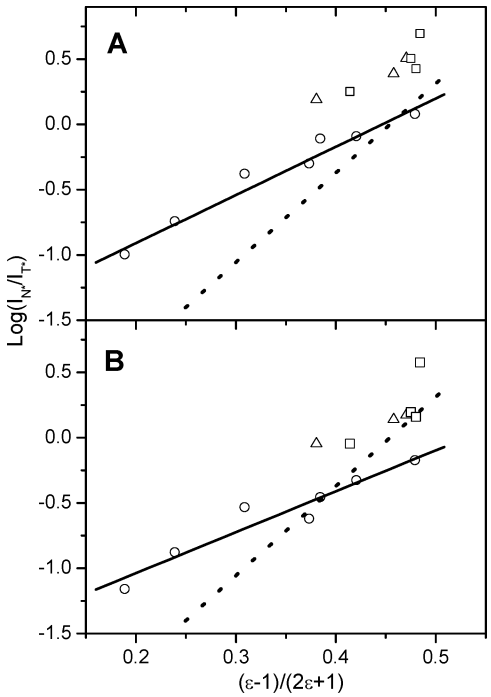

Fig. 3 Logarithm of I_{N^*}/I_{T^*} of dyes **2** (A) and **3** (B) *vs.* the solvent polarity function f(ε) for neutral (○), H-bond donor (protic, (△) and H-bond acceptor (□) solvents. Solid lines correspond to the linear fits for neutral solvents. Dotted lines correspond to the linear fit for dye **1** in neutral and basic solvents based on data from ref. 2.

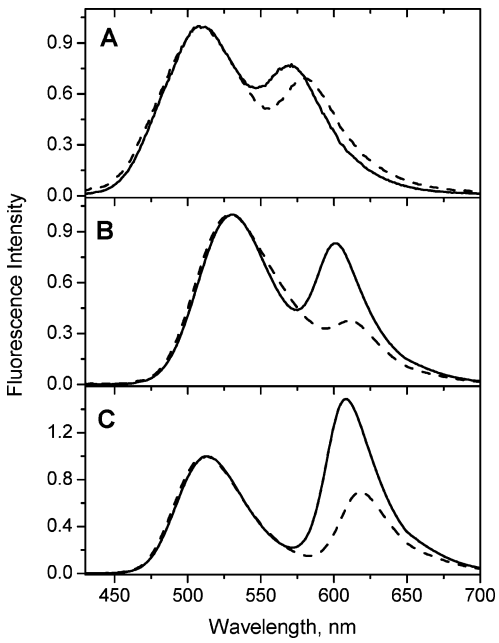

Fig. 4 Effect of solvent basicity on the dual emission of the dyes. Fluorescence spectra of **1** (A), **2** (B) and **3** (C) in acetonitrile (solid line) and dimethylformamide (dashed line).

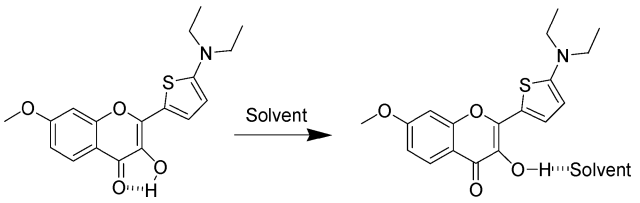

Fig. 5 Proposed scheme of interaction of dye **3** with solvents of high basicity.

aprotic solvents of close polarity are compared (ethyl acetate and 2-methyl-2-butanol, see Table 1), we observe that the I_{N^*}/I_{T^*} ratio (8.3-fold) of dye **1** exhibits a dramatic increase in protic solvent, while for dyes **2** and **3** this increase is less pronounced (1.8 and 2.4-fold respectively). This indicates that the dual emission of dyes **2** and **3** is less sensitive to solvent acidicity. For dyes **2** and **3** in basic solvents, an upward deviation of log(I_{N^*}/I_{T^*}) from the linear function in neutral solvents is also observed (Fig. 3A). Remarkably, this deviation was not detected for dye **1**.[2] This differential sensitivity of the dyes to solvent basicity can be illustrated from the comparison of the dyes in a pair of solvents of similar polarity but different basicity (acetonitrile and DMF). While the ratio of the two emission bands of dye **1** is similar in these two solvents, we observe a strong increase in the I_{N^*}/I_{T^*} ratio for dyes **2** and **3** in the more basic DMF (Fig. 4). Therefore, we conclude that unlike **1**, the dual emission of dyes **2** and **3** is sensitive to solvent basicity. Basic solvents probably inhibit the ESIPT reaction in **2** and **3**, resulting in an increase of the intensity ratio of the N* state with respect to the T* state.

The inhibition of the ESIPT reaction with basic solvents can be explained by the formation of an intermolecular H-bond between the dye and a molecule of solvent (Fig. 5). This H-bond likely disrupts the intramolecular H-bond in the dye and thus uncouples the ESIPT reaction. In this case, the complexes of dyes **2** and **3** with basic solvents are emissive and contribute to the observed increase in the relative intensity of the N* band (*i.e.* the I_{N^*}/I_{T^*} ratio). In contrast, the solvent basicity does not affect the I_{N^*}/I_{T^*} ratio of the parent compound **1**,[2] probably because the corresponding H-bonded complex is not emissive.[23] In summary, the new dyes **2** and **3** exhibit lower sensitivity to solvent polarity and acidicity than **1**, but show a strong sensitivity to solvent basicity, which constitutes a new feature of these dyes.

Having improved the spectroscopic properties and different sensitivity to the environment, the new dyes are attractive for studying lipid bilayers. Previously, we reported that analogs of dye **1** exhibit a high sensitivity to the surface charge in lipid vesicles.[12,34] However, the mechanism of this response is still unclear. Initially, it was proposed that the increased I_{N^*}/I_{T^*} ratio in negatively charged lipid bilayers is due to their higher hydration. In later studies, when we succeeded to separate the "hydrated" and "non-hydrated" states of the dye, we found that the negative surface charge of the bilayers does not affect the hydration of the dye, but influences the I_{N^*}/I_{T^*} ratio of its non-hydrated form.[13] In this respect, examination of dyes **2** and **3** in lipid vesicles of different surface charge may contribute to understand the observed phenomenon.

Binding of dyes **2** and **3** to large unilamellar phospholipid vesicles results in a more than 5000-fold increase of the fluorescence intensity, as it can be seen from the comparison of the quantum yields in lipid vesicles and buffer (Table 2). In vesicles composed of neutral lipid EYPC, the dyes show dual emission (Fig. 6), which could be assigned to N* (short-wavelength) and T* (long-wavelength) bands. Excitation spectra recorded at the two emission bands are the same, confirming the presence of only one ground state species. The resolution between the N* and T*

Table 2 Spectroscopic properties of dyes **2** and **3** in lipid vesicles[a]

		λ_{abs}/nm		λ_{N^*}/nm		λ_{T^*}/nm		I_{N^*}/I_{T^*}		ϕ (%)	
Lipid vesicles	Surface charge	**2**	**3**	**2**	**3**	**2**	**3**	**2**	**3**	**2**	**3**
DMTAP + EYPC	+0.5	446	455	525	529	600	605	0.957	0.56	17	16
EYPC	0	441	450	526	525	598	603	1.29	0.75	35	52
EYPG + EYPC	−0.5	444	450	526	527	596	601	1.58	0.94	45	35
EYPG	−1	445	455	525	522	591	598	2.20	1.61	36	34
BBPS	−1	445	454	529	524	592	599	2.28	1.80	34	40
Buffer	—	444	465	576	552	—	—	—	—	0.008	0.006

[a] Symbols are as in Table 1.

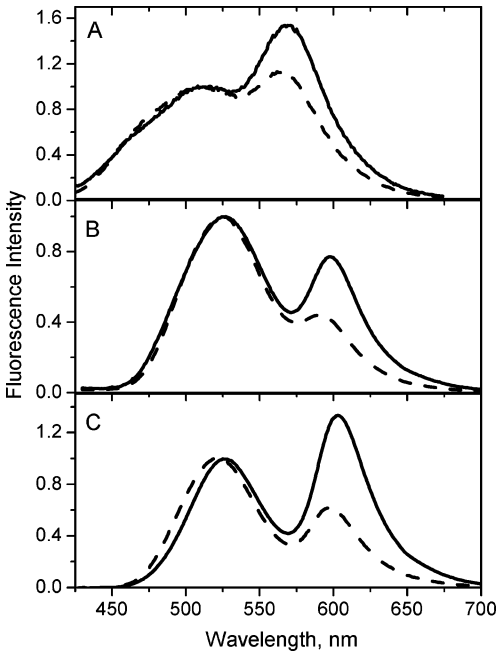

Fig. 6 Fluorescence spectra of an analog of dye **1**, 4′-(dimethylamino)-3-hydroxyflavone (A), **2** (B) and **3** (C) in lipid vesicles of neutral, EYPC (solid curve) and anionic, EYPG (dashed curve) lipids.

emission bands of dye **2** and especially dye **3** is much better than that observed previously for analogs of dye **1** (Fig. 6),[12,34] showing a significant improvement for their further applications as two-band ratiometric probes.

To test the sensitivity of the dyes to the surface charge, we performed a series of experiments with vesicles composed of lipids (either pure lipids or equimolar binary mixtures) with differently charged polar heads. As shown in Fig. 6, the decrease of the surface charge (or surface potential) from neutral (EYPC vesicles) to negative value (−1, EYPG or BBPS vesicles) results in a pronounced decrease of the relative intensity of the T* emission (*i.e.* increase in the I_{N^*}/I_{T^*} ratio, Table 2). Meantime, the positions of the absorption and emission bands do not show significant changes (Table 2). These effects are in line with those previously observed for analogs of dye **1**.[12,34] However, the changes in the ratio of the two bands are larger in the case of the new dyes, indicating their higher sensitivity to the surface charge of lipid bilayers. For instance, in the case of dye **3**, the intensity ratio at the peak maxima changes 2.4-fold from PC to PS, while this ratio changes only 1.35-fold for the analog of dye **1**.[12] Several factors could be responsible for the higher sensitivity of the new dyes to the surface charge. First, the improved resolution of the two emission bands evidently decreases the effects of band overlap and can thus increase to some extent the variation in the I_{N^*}/I_{T^*} ratio as a function of the surface charge. Second, as it was shown above, the new dyes exhibit higher sensitivity to the environment basicity but lower sensitivity to polarity and H-bond donor ability. Therefore, the observed increase in the sensitivity to the surface charge may be related to the H-bond basicity differences between negatively charged bilayers (high basicity) and neutral bilayers (low basicity). This conclusion is in line with previous reports showing that lipid bilayers of higher negative charge deprotonate a 7-hydroxycoumarin derivative.[35] Thus, the present results suggest that the changes in the environment basicity could be a general mechanism for the response to the surface charge of the 3-hydroxychromone dyes studied so far.[12,34] However, as we already showed, analogs of dye **1** are nearly insensitive to solvent basicity. In lipid vesicles, the situation can be different. Indeed, in a highly rigid environment containing H-bond acceptor groups, complexes with broken intramolecular H-bond can become emissive[2,10,21,36] and thus increase the relative intensity of the N* emission. In the case of **2** and **3**, the form with broken intramolecular H-bond (Fig. 5) is emissive already in solvents and contributes to the high sensitivity of these dyes to the surface charge of the vesicles.

Conclusions

The aim of the present work was to improve the spectroscopic properties of 3-hydroxychromone dyes by increasing their fluorescence quantum yields and shifting their absorption to longer wavelengths. This was realized by substitution of the phenyl ring of 3-hydroxychromones with a thiophene moiety. In comparison with their 3-hydroxyflavone analogs, the dual emission of the new dyes is highly sensitive to solvent basicity, while their sensitivity to solvent polarity and H-bond donor ability is significantly lower. The new dyes show strong response to the surface charge in lipid vesicles, probably in response to the differences in the H-bond basicity of the membrane surface. These new properties make these dyes prospective candidates for the study of lipid vesicles. In comparison to commonly used membrane dyes such as Prodan, Laurdan and Nile red,[35,37–39] the new probes exhibit ESIPT-generated dual emission, which provides an additional information channel[2] to study the membrane environment. Finally, substituting dyes **2** and **3** with amphiphilic groups, as it was done with dye **1**,[12,15] will allow the development of a new generation of membrane probes for surface potential in cellular membranes.

Acknowledgements

This work was supported by CNRS and Université Louis Pasteur. The laboratory of André Mann and Jean Suffert is acknowledged for providing support for the organic syntheses. GM is a fellow from the Agence Universitaire de la Francophonie and DAY from the Ministère des Affaires Etrangères (Bourse d'excellence Eiffel). AK and VVS were fellows from the European Project TriOH.

References

1 P. K. Sengupta and M. Kasha, Excited state proton-transfer spectroscopy of 3-hydroxyflavone and quercetin, *Chem. Phys. Lett.*, 1979, **68**, 382–391.
2 A. S. Klymchenko and A. P. Demchenko, Multiparametric probing of intermolecular interactions with fluorescent dye exhibiting excited state intramolecular proton transfer, *Phys. Chem. Chem. Phys.*, 2003, **5**, 461–468.
3 S. Ercelen, A. S. Klymchenko and A. P. Demchenko, Ultrasensitive fluorescent probe for the hydrophobic range of solvent polarities, *Anal. Chim. Acta*, 2002, **464**, 273–287.
4 W. Liu, Y. Wang, W. Jin, G. Shen and R. Yu, Solvatochromogenic flavone dyes for the detection of water in acetone, *Anal. Chim. Acta*, 1999, **383**, 299–307.
5 A. D. Roshal, A. V. Grigorovich, A. O. Doroshenko, V. G. Pivovarenko and A. P. Demchenko, Flavonols and crown-flavonols as metal cation chelators. The different nature of Ba^{2+} and Mg^{2+} complexes, *J. Phys. Chem. A*, 1998, **102**, 5907–5914.
6 A. S. Klymchenko and A. P. Demchenko, Electrochromic modulation of excited-state intramolecular proton transfer: The new principle in design of fluorescence sensors, *J. Am. Chem. Soc.*, 2002, **124**, 12372–12379.
7 A. S. Klymchenko, G. Duportail, Y. Mély and A. P. Demchenko, Ultrasensitive two-color fluorescence probes for dipole potential in phospholipid membranes, *Proc. Natl. Acad. Sci. U. S. A.*, 2003, **100**, 11219–11224.
8 J. R. Dharia, K. F. Johnson and J. B. Schlenoff, Synthesis and characterization of wavelength-shifting monomers and polymers based on 3-hydroxyflavone, *Macromolecules*, 1994, **27**, 5167–5172.
9 S. M. Dennison, J. Guharay and P. K. Sengupta, Excited-state intramolecular proton transfer (ESIPT) and charge transfer (CT) fluorescence probe for model membranes, *Spectrochim. Acta, Part A*, 1999, **55**, 1127–1132.
10 A. S. Klymchenko and A. P. Demchenko, Probing AOT reverse micelles with two-color fluorescence dyes based on 3-hydroxychromone, *Langmuir*, 2002, **18**, 5637–5639.
11 O. P. Bondar, V. G. Pivovarenko and E. S. Rowe, Flavonols-new fluorescent membrane probes for studying the interdigitation of lipid bilayers, *Biochim. Biophys. Acta*, 1998, **1369**, 119–130.
12 A. S. Klymchenko, G. Duportail, T. Oztürk, V. G. Pivovarenko, Y. Mély and A. P. Demchenko, Novel two-band ratiometric fluorescence probes with different location and orientation in phospholipid membranes, *Chem. Biol.*, 2002, **9**, 1199–1208.
13 A. S. Klymchenko, G. Duportail, A. P. Demchenko and Y. Mély, Bimodal distribution and fluorescence response of environment-sensitive probes in lipid bilayers, *Biophys. J.*, 2004, **86**, 2929–2941.
14 A. S. Klymchenko, Y. Mély, A. P. Demchenko and G. Duportail, Simultaneous probing of hydration and polarity of lipid bilayers with 3-hydroxyflavone fluorescent dyes, *Biochim. Biophys. Acta*, 2004, **1665**, 6–19.
15 V. V. Shynkar, A. S. Klymchenko, G. Duportail, A. P. Demchenko and Y. Mély, Two-color fluorescent probes for imaging the dipole potential of cell plasma membranes, *Biochim. Biophys. Acta*, 2005, **1712**, 128–136.
16 S. Ercelen, A. S. Klymchenko and A. P. Demchenko, Novel two-color fluorescence probe with extreme specificity to bovine serum albumin, *FEBS Lett.*, 2003, **538**, 25–28.
17 A. S. Klymchenko, S. V. Avilov and A. P. Demchenko, Resolution of Cys and Lys labeling of alpha-crystallin with site-sensitive fluorescent 3-hydroxyflavone dye, *Anal. Biochem.*, 2004, **329**, 43–57.
18 S. V. Avilov, C. Bode, F. G. Tolgyesi, A. S. Klymchenko, J. Fidy and A. P. Demchenko, Temperature effects on alpha-crystallin structure probed by 6-bromomethyl-2-(2-furanyl)-3-hydroxychromone, an environmentally sensitive two-wavelength fluorescent dye covalently attached to the single Cys residue, *Int. J. Biol. Macromol.*, 2005, **36**, 290–298.
19 A. S. Klymchenko, V. G. Pivovarenko, T. Oztürk and A. P. Demchenko, Modulation of the solvent-dependent dual emission in 3-hydroxychromones by substituents, *New J. Chem.*, 2003, **27**, 1336–1343.
20 A. S. Klymchenko and Y. Mély, 7-(2-Methoxycarbonylvinyl)-3-hydroxychromones: new dyes with red shifted dual emission, *Tetrahedron Lett.*, 2004, **45**, 8391–8394.
21 D. McMorrow and M. Kasha, Intramolecular excited-state proton transfer in 3-hydroxyflavone. Hydrogen-bonding solvent perturbations, *J. Phys. Chem.*, 1984, **88**, 2235–2243.
22 A. S. Klymchenko, V. G. Pivovarenko and A. P. Demchenko, Elimination of the hydrogen bonding effect on the solvatochromism of 3-hydroxyflavones, *J. Phys. Chem. A*, 2003, **107**, 4211–4216.
23 A. S. Klymchenko, V. G. Pivovarenko and A. P. Demchenko, Perturbation of planarity as the possible mechanism of solvent-dependent variations of fluorescence quantum yield in 2-aryl-3-hydroxychromones, *Spectrochim. Acta, Part A*, 2003, **59**, 787–792.
24 P.-T. Chou, M. L. Martinez and J. H. Clements, Reversal of excitation behavior of proton-transfer *vs.* charge-transfer by dielectric perturbation of electronic manifolds, *J. Phys. Chem.*, 1993, **97**, 2618–2622.
25 D. B. Siano and D. E. Metzler, Band shapes of the electronic spectra of complex molecules, *J. Chem. Phys.*, 1969, **51**, 1856–1861.
26 M. J. Hope, M. B. Bally, G. Webb and P. R. Cullis, Production of large unilamellar vesicles by a rapid extrusion procedure. Characterization of size distribution, trapped volume and ability to maintain a membrane potential, *Biochim. Biophys. Acta*, 1985, **812**, 55–65.
27 D. Prim, G. Kirsch and J. F. Nicoud, Efficient synthesis of *N*,*N*-disubstituted 5-aminothiophene-2-carboxaldehydes by nucleophilic aromatic substitution in water, *Synlett.*, 1998, 383–384.
28 M. H. Abraham, Hydrogen bonding. 31. Construction of a scale of solute effective or summation hydrogen-bond basicity, *J. Phys. Org. Chem.*, 1993, **6**, 660–684.
29 M. H. Abraham, H. S. Chadha, G. S. Whiting and R. C. Mitchell, Hydrogen bonding. 32. An analysis of water–octanol and water–alkane partitioning and the delta log *P* parameter of Seiler, *J. Pharm. Sci.*, 1994, **83**, 1085–1100.
30 S. O. Yesylevskyy, A. S. Klymchenko and A. P. Demchenko, Semi-empirical study of two-color fluorescent dyes based on 3-hydroxychromone, *J. Mol. Struct. (THEOCHEM)*, 2005, **755**, 229–239.
31 T. C. Swiney and F. D. Kelley, Proton transfer dynamics in substituted 3-hydroxyflavones: Solvent polarization effects, *J. Chem. Phys.*, 1993, **99**, 211–221.
32 E. L. Lippert, in *Organic Molecular Photophysics*, ed. J. B. Birks, Wiley, New York, 1975, vol. 2, p. 1.
33 N. Mataga and T. Kubota, in *Molecular interactions and electronic spectra*, M. Dekker, New York, 1970.
34 G. Duportail, A. S. Klymchenko, Y. Mély and A. P. Demchenko, Neutral fluorescence probe with strong ratiometric response to surface charge of phospholipid membranes, *FEBS Lett.*, 2001, **508**, 196–200.
35 J. B. Massey, Effect of cholesteryl hemisuccinate on the interfacial properties of phosphatidylcholine bilayers, *Biochim. Biophys. Acta*, 1998, **1415**, 193–204.
36 A. Sytnik, D. Gormin and M. Kasha, Interplay between excited-state intramolecular proton transfer and charge transfer in flavonols and their use as protein-binding-site fluorescence probes, *Proc. Natl. Acad. Sci. U. S. A.*, 1994, **91**, 11968–11972.
37 T. M. Parasassi, M. Di Stefano, M. Loiero, G. Ravagnan and E. Gratton, Cholesterol modifies water concentration and dynamics in phospholipid bilayers: a fluorescence study using Laurdan probe, *Biophys. J.*, 1994, **66**, 763–768.
38 P. Jurkiewicz, J. Sýkora, A. Olżyńska, J. Humpolickova and M. Hof, Solvent relaxation in phospholipid bilayers: Principles and recent applications, *J. Fluoresc.*, 2005, **15**, 883–894.
39 Ira and G. Krishnamoorthy, Probing the dynamics of planar supported membranes by Nile red fluorescence lifetime distribution, *Biochim. Biophys. Acta*, 1998, **1414**, 255–259.

Nucleic Acids Research Advance Access published December 17, 2007

*Nucleic Acids Research, 2007, **1–12***
doi:10.1093/nar/gkm1109

Probing dynamics of HIV-1 nucleocapsid protein/target hexanucleotide complexes by 2-aminopurine

S. V. Avilov[1,2], E. Piemont[1], V. Shvadchak[1], H. de Rocquigny[1] and Y. Mély[1,*]

[1]Institut Gilbert-Laustriat, UMR 7175 CNRS/Université Louis Pasteur (Strasbourg I), Dépt. Pharmacologie et Physicochimie, Faculté de Pharmacie, 74 route du Rhin, 67401 Illkirch, France and [2]Palladin Institute of Biochemistry, 9, Leontovich str., 01030 Kiev, Ukraine

Received August 24, 2007; Revised November 23, 2007; Accepted November 28, 2007

ABSTRACT

The nucleocapsid protein (NC) plays an important role in HIV-1, mainly through interactions with the genomic RNA and its DNA copies. Though the structures of several complexes of NC with oligonucleotides (ODNs) are known, detailed information on the ODN dynamics in the complexes is missing. To address this, we investigated the steady state and time-resolved fluorescence properties of 2-aminopurine (2Ap), a fluorescent adenine analog introduced at positions 2 and 5 of AACGCC and AATGCC sequences. In the absence of NC, 2Ap fluorescence was strongly quenched in the flexible ODNs, mainly through picosecond to nanosecond dynamic quenching by its neighboring bases. NC strongly restricted the ODN flexibility and 2Ap local mobility, impeding the collisions of 2Ap with its neighbors and thus, reducing its dynamic quenching. Phe^{16}→Ala and Trp^{37}→Leu mutations largely decreased the ability of NC to affect the local dynamics of 2Ap at positions 2 and 5, respectively, while a fingerless NC was totally ineffective. The restriction of 2Ap local mobility was thus associated with the NC hydrophobic platform at the top of the folded fingers. Since this platform supports the NC chaperone properties, the restriction of the local mobility of the bases is likely a mechanistic component of these properties.

INTRODUCTION

Nucleocapsid protein (NC), either as a domain of the Gag polyprotein precursor or as the mature protein, is essential for several important steps of the virus life cycle (1). For instance, selection of viral genomic RNA for packaging into virions is mediated by NC binding to the ψ encapsidation sequence within the untranslated region of the HIV-1 genome (2). Furthermore, NC chaperones the annealing of the primer tRNA to the primer binding site (PBS), and the two obligatory strand transfers necessary for the synthesis of a complete proviral DNA by reverse transcriptase (3,4). Mature NC is a basic protein of 55 amino acids (Figure 1) containing two highly conserved $CX_2CX_4HX_4C$ zinc fingers (5). Mutations of the zinc coordinating residues and the two aromatic residues of the zinc fingers lead to completely noninfectious viruses (6–9).

Most NC functions rely on interactions with nucleic acid targets. The structure of NC complexed to the SL2 and SL3 stem-loops as well as to the ACGCC sequence of the ψ encapsidation sequence have been solved by NMR (10–12). In all these complexes, the hydrophobic platform formed by the Val^{13}, Phe^{16}, Thr^{24}, Ala^{25}, Trp^{37} and Met^{46} residues at the surface of the two folded zinc fingers has been shown to be critical for binding. A particularly important role was notably demonstrated for Trp^{37} that stacks with G residues in all these complexes.

Though 3D structures of NC complexes with several oligonucleotides (ODNs) are available, the dynamics of the ODNs in the complexes is still not well characterized. Dynamics of either single- and double-stranded nucleic acids plays an important role in their interaction with various ligands (13,14). For instance, in the HIV-1 RNA TAR stem-loop, the magnitude of the adaptive structure change due to ligand binding at a given site correlates with the degree of spontaneous internal motions at this site (15). It is likely that the local dynamics of ODNs are important for NC binding and activities as well.

Site-specific information on ODN dynamics can be provided by environmentally sensitive fluorescent probes, such as 2-aminopurine (2Ap), a fluorescent analog of adenine that can be selectively excited at 315–320 nm, where Trp does not absorb (16). The quantum yield of free 2Ap at pH 7.0 is 0.68 (17) but within ODNs it is significantly quenched due to interactions with its neighbor bases (18–22). Free 2Ap in water exhibits a single lifetime

*To whom correspondence should be addressed. Tel: +33 3 90 24 42 63; Fax: +33 3 90 24 43 13; Email: mely@pharma.u-strasbg.fr

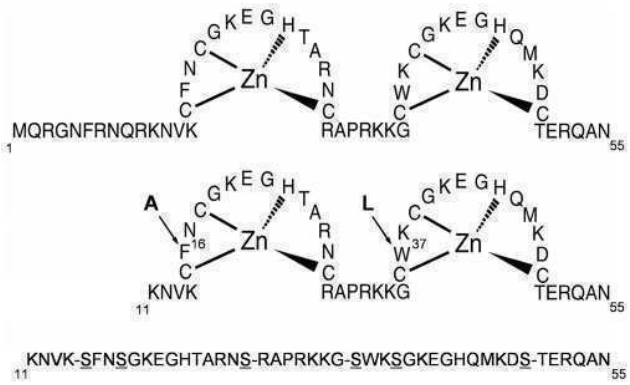

Figure 1. Structures of the native and mutated HIV-1 NC peptides used in this study: NC(1-55), NC(11-55), A^{16}NC(11-55), L^{37}NC(11-55) and $(SSHS)_2$NC(11-55).

of about 10–11 ns, while multiple shorter lifetimes appear when 2Ap is incorporated into ODNs, indicating a highly heterogeneous environment of the probe. As a consequence, time-resolved fluorescence of 2Ap has been largely used to site-specifically characterize the interactions of ODNs with various ligands, including complementary nucleic acids strands and proteins (23–27).

To site-specifically investigate the changes in the dynamics of ACGCC during NC binding and correlate them with the known 3D structure of the NC/ACGCC complex (11), 2Ap was introduced either downstream or upstream to the CG motif. Moreover, since the environment of 2Ap at the 3′ or 5′ terminus of an ODN differs significantly from that at an internal position (18,28), complicating the data interpretation, an extra adenine was added at the 5′-terminus of ACGCC. This extra adenine was shown to not affect the binding of the ODN to NC (29). Moreover, substitutions of A2 and C5 with 2Ap within ^{1}AACGCC^6 were also expected to not affect NC binding, since the corresponding residues of ACGCC only marginally interact with NC (11). Furthermore, since NC binds with strong affinity to TG motifs (29,30), we studied the interaction of NC with 2Ap-labeled AATGCC sequences. Finally, the native NC was substituted with several NC mutants (Figure 1) to investigate the role of the N-terminal basic domain and the folded finger domain as well as the hydrophobic platform on the top of the fingers on the dynamics of the labeled ODNs.

MATERIALS AND METHODS

Materials

NC(1-55) (further referred as NC), NC(11-55), $(SSHS)_2$NC(11-55), L^{37}NC(11-55) and A^{16}NC(11-55) (Figure 1) were synthesized on a Applied Biosystems A433 peptide synthesizer as described (31). 2Ap-substituted DNA ODNs were synthesized and HPLC-purified by IBA GmbH (Germany). Absorbance spectra were recorded with a Cary 400 UV-visible spectrophotometer (Varian). ODN concentrations were calculated using the extinction coefficients (ε_{260}, $M^{-1} \times cm^{-1}$) of 58 050, 44 190, 51 390, 59 220, 45 360 and 52 560 for AACGCC, AApCGCC, AACGApC, AATGCC, AApTGCC and AATGApC, respectively. All experiments were performed in 50 mM HEPES, pH 7.5, at 20°C. 'Fluorescence microscopy' grade glycerol (Merck, Germany) was used. All other chemicals were purchased from Sigma, USA.

Steady-state fluorescence spectroscopy

Fluorescence spectra were recorded on FluoroMax3 and FluoroLog spectrofluorimeters (Jobin Yvon) equipped with thermostated cell compartments. Spectra were corrected for screening effects and buffer fluorescence. Quantum yield was calculated using free 2Ap as a reference [0.68 (17)]. 2Ap was excited at 315 nm. To determine the affinity of NC for the 2Ap-labeled ODNs, fixed amounts of NC were titrated with ODNs by monitoring the intrinsic Trp fluorescence of NC at 320-nm emission wavelength (to exclude 2Ap fluorescence). Affinity constants were determined from direct fitting of the experimental signal to the rewritten Scatchard equation:

$$I = I_0 - \frac{(I_0 - I_t)}{P_t} x \frac{\left[\begin{array}{c} (1 + (P_t + nN_t)K_{app}) \\ -\sqrt{(1 + (P_t + nN_t)K_{app})^2 - 4P_t nN_t K_{app}^2} \end{array} \right]}{2K_{app}} \quad \mathbf{1}$$

where I and I_t are the intensities at a given and a saturating ODN concentration, respectively, I_0 is the intensity in the absence of ODN, N_t is the total ODN concentration, P_t is the total concentration of peptide, K_{app} is the apparent affinity constant, n is the number of binding sites. Alternatively, the K_{app} values were also obtained by titrating fixed amounts of 2Ap-labeled ODNs with the peptides and monitoring the 2Ap fluorescence at 370 nm. The data were fitted with a slightly modified version of Equation (1). The parameters were recovered from nonlinear fits of Equation (1) to experimental datasets by the Microcal Origin^{TM} 6.0 program.

Time-resolved fluorescence measurements

Time-resolved fluorescence measurements were performed with the time-correlated, single-photon counting technique using the excitation pulses at 315 nm provided by a pulse-picked frequency tripled Ti-sapphire laser (Tsunami, Spectra Physics) pumped by a Millenia X laser (Spectra Physics) (32). The emission was collected through a polarizer set at magic angle and an 8-nm band-pass monochromator (Jobin-Yvon H10) at 370 nm. The instrumental response function was recorded with a polished aluminum reflector, and its full width at half-maximum was 40 ps. The mean lifetime $<\tau>$ was calculated from the individual fluorescence lifetimes, τ_i, and their relative amplitudes, α_i, according to $<\tau> = \Sigma\alpha_i\tau_i$. The population, α_0, of dark species of 2Ap within the ODNs was calculated by: $\alpha_0 = 1 - \tau_{free}/(\tau_{sample} \times R_m)$, where τ_{free} is the lifetime of free 2Ap, τ_{sample} is the measured lifetime of 2Ap within the ODN (either free or bound to NC) and R_m is the ratio of the corresponding

steady-state fluorescence intensities. The remaining amplitudes, α_{ic}, were recalculated from the measured amplitudes, α_i, according to: $\alpha_{ic} = \alpha_i \times (1 - \alpha_0)$.

For time-resolved anisotropy measurements, the fluorescence decay curves were recorded at vertical and horizontal positions of the polarizer and analyzed by the following equations:

$$I_{\parallel}(t) = \frac{I(t)[1 + 2r(t)]}{3}$$

$$I_{\perp}(t) = \frac{I(t)[1 - r(t)]}{3}$$

$$r(t) = \frac{I_{\parallel}(t) - GI_{\perp}(t)}{I_{\parallel}(t) + 2GI_{\perp}(t)} = r_0 \sum \beta_i \exp\left(\frac{-t}{\varphi_i}\right) \quad \mathbf{2}$$

where β_i are the amplitudes of the rotational correlation times φ_i; $I_{\parallel}$ and $I_{\perp}$ are the intensities collected at emission polarizations parallel and perpendicular, respectively, to the polarization axis of the excitation beam, and G is the geometry factor at the emission wavelength, determined in independent experiments. The initial anisotropy value (0.33) was determined independently for 2Ap in 77% glycerol (v/v) from the extrapolation of the anisotropy decay curves to zero time. The theoretical values of the rotational correlation times were calculated from the molecular masses (M) of the molecules and their complexes, assuming spherical shapes, by:

$$\varphi = \frac{\eta M(\upsilon + h)}{RT} \quad \mathbf{3}$$

where η is the viscosity (assumed to be 0.01 P), T is the temperature (maintained at 293 K), υ is the specific volume of the particle [assumed to be 0.83 ml/g, (33)], h is the hydration degree (assumed to be 0.2 ml/g for proteins) and R is the molar gas constant.

The cone semiangle (θ_0) providing an estimate for the local motions of 2Ap modeled as diffusion within a cone (34,35) was calculated as:

$$\theta_0 = \cos^{-1}(0.5 \times (\sqrt{1 + 8S} - 1)) \quad \mathbf{4}$$

where S is the generalized order parameter: $S = (\beta'_2/(\beta'_1 + \beta'_2))^{1/2}$, β'_1 and β'_2 are the amplitudes of the rotational correlation times, recalculated such that $\Sigma\, \beta'_i = r_0$.

Time-resolved intensity and anisotropy data were treated with a nonlinear least-square analysis (39) using a homemade software (kindly provided by G. Krishnamoorthy). In all cases, the χ^2 values were close to 1, and the weighted residuals as well as the autocorrelation of the residuals were distributed randomly around zero, indicating an optimal fit.

RESULTS

2Ap fluorescence within free hexanucleotides

Fluorescence spectra of the AACGCC and AATGCC sequences labeled by 2Ap at position 2 or 5 showed a maximum emission wavelength at around 370 nm, similarly to free 2Ap (Figure 2). In contrast, the quantum yield

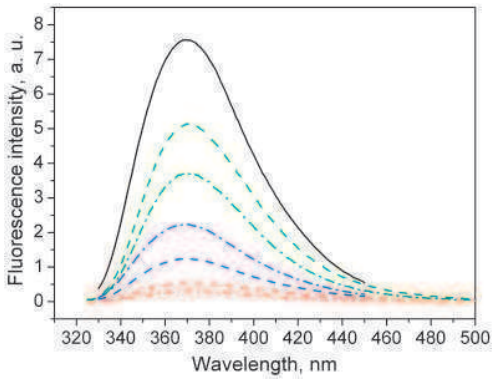

Figure 2. Effect of NC and glycerol on the fluorescence spectra of AApCGCC and AACGApC. The fluorescence spectra of AApCGCC (dashed lines) and AACGApC (dash-dotted lines) sequences were recorded in the absence of NC either in buffer (red), in 77% glycerol (green) or in the presence of a 7.5-fold molar excess of NC (blue). Solid line is free 2Ap. Excitation at 315 nm, excitation and emission slits: 2 and 5 nm, respectively.

of 2Ap within ODNs is much lower than that of the free fluorophore (Figure 2), in agreement with the literature (36). The quenching in respect with free 2Ap is more pronounced for 2Ap in the position 5 (38-fold intensity decrease) than in the position 2 (about 19-fold decrease) (Table 1), probably due to the flanking G4 residue, since guanine is the best quencher of 2Ap fluorescence among the bases (37). Moreover, the identical quantum yield of AApCGCC and AApTGCC suggests that 2Ap fluorescence does not depend on the nature of the pyrimidine base in position 3.

Since steady-state fluorescence is unable to report on the dynamics and heterogeneity of the fluorophore microenvironment, time-resolved fluorescence measurements were performed. Four components ranging from ≈100 ps to 5 ns were required for good fitting ($\chi^2 < 1.4$) of the intensity decay curves (Table 1), demonstrating a large conformational heterogeneity of 2Ap in the studied ODNs. Multiple lifetimes are frequently observed in 2Ap-labeled ODNs and are usually associated with partially stacked structures with the shortest component reflecting decay from stacked conformations and the 8–10 ns components assigned to conformations where the 2Ap is extrahelical (37,38). In the studied ODNs, the longest lifetime (4–5 ns) was substantially lower than the lifetime of free 2Ap in water but comparable to that of 2Ap-labeled trinucleotides (19) and single-stranded ODNs (28). By analogy to the latter sequences, nanosecond conformational fluctuations of the 2Ap-labeled hexanucleotides in their excited state can drive 2Ap from an unstacked to a stacked conformation, leading to a fluorescence quenching and thus, a lifetime shortening.

The mean lifetime of 2Ap in the four ODNs (0.91–1.33 ns) was found to be 7.7- to 11.2-fold shorter than that of the free probe (10.2 ns) (Table 1). However, this difference in lifetimes was far less than the 19- to 38-fold difference in the corresponding quantum yields, suggesting the presence of a significant subpopulation of 'dark' species (α_0), i.e. species with a lifetime shorter than

Table 1. Steady-state and time-resolved fluorescence parameters for 2Ap-substituted hexanucleotides[a]

	Quantum yield	R_m ($I_{free2Ap}/I$)	α_0	τ_1 (ns)	α_1	τ_2 (ns)	α_2	τ_3 (ns)	α_3	τ_4 (ns)	α_4	$<\tau>$ (ns)
Free 2Ap	0.680[b]									10.2	1.00	10.2
AApCGCC	0.036	19.0	0.41	0.19	0.20	0.60	0.27	1.94	0.08	4.99	0.04	0.91
AApCGCC, glycerol 77%	0.289	2.35	0.11	0.39	0.21			3.78	0.30	8.17	0.38	4.86
AApCGCC + NC	0.090	7.57	0.36	0.17	0.15	0.69	0.24	2.01	0.11	6.58	0.14	2.09
AApCGCC + NC(11-55)	0.070	9.74	0.33	0.14	0.17	0.81	0.33	3.05	0.11	6.91	0.06	1.57
AApCGCC + $(SSHS)_2$NC(11-55)	0.039	17.6	0.41	0.14	0.22	0.64	0.24	2.28	0.09	5.62	0.04	0.99
AApCGCC + A^{16}NC(11-55)	0.047	14.6	0.33	0.11	0.29	0.59	0.23	2.28	0.10	6.55	0.05	1.05
AACGApC	0.018	37.4	0.79	0.08	0.10	0.55	0.04	2.20	0.04	4.93	0.03	1.27
AACGApC, glycerol 77%	0.176	3.86	0.38	0.24	0.24			2.60	0.10	8.18	0.28	4.25
AACGApC + NC	0.134	5.06	0.21	0.12	0.19	0.75	0.19	3.77	0.32	7.85	0.09	2.56
AACGApC + NC(11-55))	0.105	6.49	0.33	0.10	0.19	0.91	0.18	3.52	0.18	6.36	0.12	2.35
AACGApC + $(SSHS)_2$NC(11-55)	0.020	34.0	0.80	0.08	0.09	0.72	0.04	2.79	0.05	6.01	0.02	1.49
AACGApC + A^{16}NC(11-55)	0.108	6.28	0.25	0.15	0.24	0.85	0.17	3.03	0.20	5.98	0.14	2.15
AApTGCC	0.036	18.9	0.51	0.14	0.22	0.85	0.18	2.16	0.04	5.26	0.05	1.11
AApTGCC, glycerol 77%	0.287	2.37	0.0	0.12	0.27			2.03	0.23	7.60	0.50	4.30
AApTGCC + NC	0.147	4.62	0.20	0.20	0.17	1.04	0.30	3.49	0.15	7.54	0.18	2.77
AApTGCC + NC(11-55)	0.085	7.97	0.28	0.44	0.41	1.48	0.14	3.66	0.08	6.55	0.09	1.77
AApTGCC + $(SSHS)_2$NC(11-55)	0.034	19.8	0.54	0.08	0.18	0.66	0.17	2.47	0.07	6.13	0.04	1.12
AApTGCC + A^{16}NC(11-55)	0.045	15.1	0.49	0.10	0.19	0.65	0.20	2.55	0.08	6.56	0.04	1.30
AApTGCC + L^{37}NC(11-55)	0.107	6.39	0.16	0.12	0.29	0.75	0.28	2.98	0.16	7.84	0.11	1.90
AATGApC	0.018	38.4	0.80	0.10	0.10	1.10	0.03	2.28	0.03	4.75	0.04	1.33
AATGApC, glycerol 77%	0.227	3.00	0.16	0.12	0.29			1.55	0.15	7.83	0.40	4.06
AATGApC + NC	0.125	5.45	0.25	0.12	0.22	1.02	0.18	3.81	0.30	6.58	0.05	2.50
AATGApC + NC(11-55)	0.126	5.39	0.22	0.19	0.28	1.25	0.13	3.95	0.28	6.58	0.09	2.43
AATGApC + $(SSHS)_2$NC(11-55)	0.018	37.7	0.81	0.09	0.09	0.80	0.04	2.83	0.04	5.97	0.02	1.39
AATGApC + A^{16}NC(11-55)	0.106	6.40	0.27	0.19	0.26	1.09	0.16	3.59	0.22	6.86	0.09	2.17
AATGApC + L^{37}NC(11-55)	0.073	9.28	0.43	0.09	0.24	0.72	0.10	2.70	0.12	6.28	0.11	1.95

[a]Experiments were performed with 1–8 μM 2Ap-labeled ODN in 50 mM HEPES, pH 7.5. The concentrations of NC derivatives were at least seven times higher. The amplitude values are corrected for the dark species, as described in Materials and Methods section. Standard deviations are lower than 15% for the quantum yield, 20% for lifetimes (except for τ_1, where they are below 45%), 20% for amplitudes and 15% for the mean lifetimes, respectively.
[b]Data from Ref. (17).

the detection limit of our equipment (≈30 ps) (Table 1). Generally, such apparently 'null' lifetime may appear as a result of either static quenching or very fast dynamic quenching. To discriminate between 'true' static and fast dynamic quenching, we studied the effect of viscosity on 2Ap fluorescence since only dynamic quenching is affected by viscosity. We observed that in 77% glycerol (v/v), both the quantum yield and the mean lifetime strongly increased (Table 1). Moreover, the number of components needed for good fitting of the decay curves dropped to 3, suggesting a less heterogeneous 2Ap microenvironment. All the observed lifetimes were substantially longer than in the absence of glycerol. The longest component became close to the lifetime of free 2Ap and its amplitude grew to 28–50%, indicating that a large subpopulation of 2Ap does not interact with its neighbors during the excited state lifetime in this case. Moreover, α_0 dramatically decreased at high viscosity (Table 1), demonstrating that the 'null' lifetime mostly represents ultra-fast dynamic quenching. The corresponding ultra-short lifetime that cannot be measured with our device likely corresponds to the 10-ps lifetime measured with a streak camera for 2Ap within single-stranded DNAs (39). Interestingly, α_0 values for ODNs labeled at position 5 were much higher than for ODNs labeled at position 2, probably due to the flanking G4 residue which causes a more efficient quenching than other bases (21,24,39).

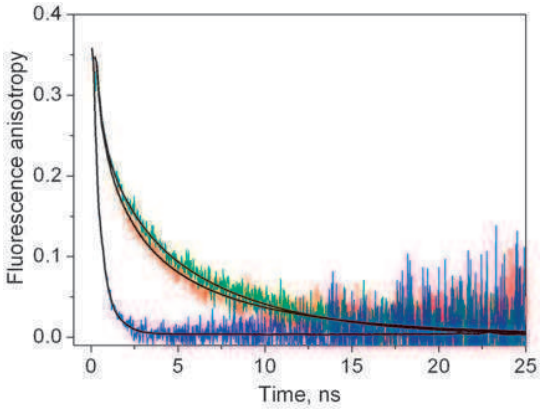

Figure 3. Experimental anisotropy decay curves of the 2Ap-labeled ODNs and their complexes. AApCGCC alone (blue), AApCGCC/NC (green) and AACGApC/NC (red). The corresponding fitted curves, using the parameters in Table 2 are in black.

Fluorescence anisotropy decay curves (Figure 3) of the 2Ap-labeled ODNs were fitted adequately with a two-exponential model (Table 2). Since the slower component φ_2 (0.68–0.83 ns) is slightly shorter than the 1 ns theoretical correlation time for the tumbling of a sphere with the same molecular mass than the ODN (33),

Table 2. Fluorescence anisotropy decay parameters for 2Ap-substituted hexanucleotides[a]

	φ_1 (ns)	β_1	φ_2 (ns)	β_2	S	θ_0 (degree)
2Ap	0.08	1.00			0	90.0
AApCGCC	0.28	0.59	0.83	0.41	0.633	42.9
AApCGCC + NC	0.30	0.38	4.31	0.62	0.787	31.8
AApCGCC + NC(11-55)	0.34	0.43	3.10	0.57	0.755	34.2
AApCGCC + $(SSHS)_2$NC(11-55)	0.24	0.61	2.21	0.39	0.625	43.4
AApCGCC + A^{16}NC(11-55)	0.36	0.44	3.11	0.56	0.755	34.2
AACGApC	0.18	0.57	0.76	0.43	0.656	41.7
AACGApC + NC	0.46	0.42	4.08	0.58	0.762	33.9
AACGApC + NC(11-55)	0.35	0.41	3.17	0.59	0.768	32.9
AACGApC + $(SSHS)_2$NC(11-55)	0.30	0.61	2.21	0.39	0.625	43.8
AACGApC + A^{16}NC(11-55)	0.43	0.41	3.52	0.59	0.768	33.2
AApTGCC	0.23	0.56	0.74	0.44	0.663	40.8
AApTGCC + NC	0.26	0.39	4.13	0.61	0.781	32.2
AApTGCC + NC(11-55)	0.33	0.40	3.04	0.60	0.775	32.7
AApTGCC + $(SSHS)_2$NC(11-55)	0.32	0.67	1.99	0.33	0.575	47.1
AApTGCC + A^{16}NC(11-55)	0.38	0.37	3.00	0.63	0.794	31.2
AApTGCC + L^{37}NC(11-55)	0.42	0.36	3.86	0.64	0.802	30.6
AATGApC	0.14	0.54	0.68	0.46	0.678	39.7
AATGApC + NC	0.50	0.45	4.33	0.55	0.742	34.2
AATGApC + NC(11-55)	0.52	0.41	3.45	0.59	0.768	33.2
AATGApC + $(SSHS)_2$NC(11-55)	0.31	0.69	2.27	0.31	0.554	48.3
AATGApC + A^{16}NC(11-55)	0.44	0.41	3.23	0.59	0.768	33.2
AATGApC + L^{37}NC(11-55)	0.28	0.44	3.03	0.56	0.751	34.0

[a]β_1 and β_2, the amplitudes of the components; S, generalized order parameter; θ_0, cone semi-angle for 2Ap local motion (calculated as described in Materials and Methods section). Standard deviations are <10% for the amplitudes, <30% for φ_1 and <20% for φ_2.

the φ_2 component likely represents a combination of both tumbling and segmental motions, in line with the high flexibility expected for single-stranded ODNs. Moreover, the faster component φ_1 (0.14–0.28 ns) can be attributed to the local motion of 2Ap in the ODNs (37). The relative amplitude (β_1) of this faster component allowed to estimate the angular range of the local motion of 2Ap modeled as the diffusion in a cone semi-angle (θ_0) [Equation (4)] (34,37). In further keeping with the high flexibility of the ODNs, rather large θ_0 values were obtained (40–43°) indicating an important rotational freedom for 2Ap (Table 2). Noticeably, since the most quenched conformations (with lifetimes below 0.3 ns) contribute very little (<10%) to the total fluorescence intensity, the calculated diffusion angle likely describes mainly the local motion of the less quenched conformations.

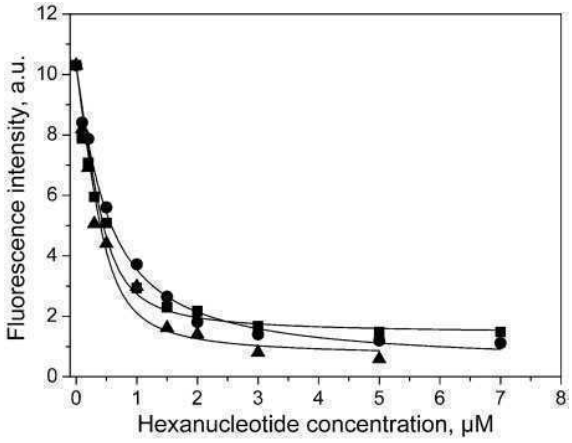

Figure 4. Effect of 2Ap substitution on the binding of NC(11-55) to AACGCC. The concentration of NC(11-55) was 1 μM in 50 mM HEPES, pH 7.5. The concentration of AApCGCC (filled circles), AACGApC (filled triangles) and AACGCC (filled squares) is expressed in strands. Solid lines correspond to the fit of the experimental points with Equation (1) and the parameters are given in the text.

Effects of NC on the dynamics of the 2Ap-labeled hexanucleotides

Our objective was to characterize site-selectively the interaction of NC with the AACGCC and AATGCC sequences, by using 2Ap-labeled ODNs. However, this approach is only valid if the substitution of a natural base by 2Ap does not modify the interaction of NC with the ODNs. To check this, we compared the binding of the 2Ap-labeled sequences with the corresponding unlabeled sequences. The binding parameters were determined by monitoring the Trp emission at 320 nm (where 2Ap does not fluoresce) in the presence of increasing ODN concentrations in 50 mM HEPES, pH 7.5 (Figure 4). Due to the limited sensitivity of Trp fluorescence that does not permit to work at very low protein concentrations, binding experiments were performed with the NC(11-55) peptide that binds in the same way than the native NC, but with a lower affinity (29,40). K_{app} values of $4(\pm1)\times10^6\,M^{-1}$, $9(\pm4)\times10^6\,M^{-1}$ and $9(\pm3)\times10^6\,M^{-1}$ were found for AApCGCC, AACGApC and AACGCC, respectively. For the two last sequences, similar affinities were obtained by monitoring the changes in the 2Ap fluorescence when adding increasing peptide concentrations (data not shown). Accordingly, no change in affinity accompanied the C→2Ap substitution at position 5. This result may be rationalized from the NMR data of the ACGCC/NC

complex showing that NC binds the corresponding C residue only through a single H-bond with its N4 atom (11). It is thus likely that the N7 atom of 2Ap forms the same H-bond with NC since it is located virtually at the same place than the N4 atom in cytosine relatively to the sugar-phosphate axis (11). For AApCGCC, a limited affinity decrease was observed in respect with the native ODN. Since NMR showed no direct interaction between the corresponding A residue with NC, 2Ap may indirectly decrease the binding constant, by decreasing for instance the interaction of the neighbor C residue with NC. Since AATGCC was shown to bind NC much stronger than AACGCC (29), we used a buffer containing 0.1 M NaCl to get reliable binding constants with this ODN. No decrease of NC affinity for AATGApC appeared ($K_{app} = 5(\pm3) \times 10^6\,M^{-1}$) as compared to AATGCC ($K_{app} = 4(\pm1) \times 10^6\,M^{-1}$) whereas the affinity for AAp TGCC ($K_{app} = 8(\pm2) \times 10^6\,M^{-1}$) was slightly higher. As a consequence, 2Ap does not perturb significantly the interaction of the studied ODNs with NC and thus can be reliably used to probe the NC/ODN complexes.

Binding of NC was found to strongly increase the quantum yield of 2Ap within all species, although to different extents: from 2.5-fold for AApCGCC to more than 7-fold for AACGApC (Figure 2 and Table 1). Meanwhile, the position of the emission maximum did not change (Figure 2). Thus, NC binding significantly reduces the quenching of 2Ap fluorescence by its neighbor bases but does not change the polarity of its surrounding. As in the absence of NC, the time-resolved intensity decay of 2Ap within the ODN/NC complexes needed four lifetimes for good fitting. In the complexes, the 2Ap fluorescence decayed slower than in the absence of NC, with an increase in the mean lifetime by a factor of about two (Table 1). Significant differences appear as a function of the labeled position and the ODN nature. For AApCGCC, the increase in the mean lifetime is fully consistent with the quantum yield increase, indicating that NC negligibly affects α_0 in this case. In fact, the NC-induced increase in both the quantum yield and mean lifetime of this ODN is essentially due to an increase of the α_4 and τ_4 values. Since the τ_4 value approaches the lifetime of free 2Ap, unstacked conformers are probably driven less rapidly than in the free ODN to quenched conformers by conformational fluctuations. For AACGApC and the 2Ap-labeled TG-containing sequences, the NC-induced increase in quantum yield was found to be much higher than the increase in the mean lifetime, suggesting that NC dramatically decreases the α_0 value and thus, the ultra-fast dynamic quenching of 2Ap in these ODNs. This decrease in α_0 is accompanied by a large increase of the α_2 to α_4 values as well as an increase of the τ_3 and τ_4 values. Consequently, NC shifts the equilibrium of the 2Ap sub-populations to the less quenched ones and decreases the quenching efficiency in the latter. Interestingly, the effect of NC appears quite homogeneous since NC increases the summed populations ($\alpha_3 + \alpha_4$) of the two less quenched 2Ap conformers from about 10% to 35–40% in all three ODNs.

The effect of NC was found to be quite similar on the time-resolved anisotropy decays of the various 2Ap-labeled ODNs (Figure 3 and Table 2). In all cases, NC induces a striking increase of the φ_2 component, in line with the formation of NC/ODN complexes. The measured φ_2 values are significantly higher than the theoretical 3.3 ns value calculated for the tumbling of a 1:1 complex with a spherical shape. Thus, the shape of the complexes likely deviates from a sphere and, in contrast to the free ODNs, the φ_2 component only describes the tumbling motion of the complex, with no contribution of segmental motions. As a consequence, the binding of NC reduces the degrees of freedom of the ODNs. This conclusion is further substantiated by the decrease of the amplitude associated with the local motion. This decrease corresponds to a reduction by 6° to 11° of the cone semi-angle in which 2Ap rotates. Moreover, NC was found to also increase the value of the φ_1 component for 2Ap at position 5, but not in position 2, indicating that the binding of NC directly altered the flexibility of the 2Ap base at position 5. As in the free ODNs, the conclusions on the local mobility of 2Ap in the complexes probably concern mainly the less quenched subpopulations that contribute strongly to the total fluorescence intensity.

Effects of NC variants on the local dynamics of the 2Ap-labeled hexanucleotides

To determine the contributions of the N-terminal basic domain, the folded zinc fingers and the conserved aromatic residues (Phe^{16} and Trp^{37}) to the effects of NC on the dynamics of the 2Ap-labeled ODNs, we analyzed the fluorescence properties of these ODNs complexed with various NC mutants (Figure 1). The contribution of the N-terminal domain was investigated with the NC(11-55) mutant which includes the zinc finger domain but lacks the N-terminal domain. The contribution of the folded fingers was analyzed with the $(SSHS)_2$NC(11-55) mutant where all cysteines are substituted for serines, which prevents the binding of zinc and therefore the folding of the peptide (8). The contributions of the conserved Phe^{16} residue in the proximal finger and the conserved Trp^{37} residue in the distal finger were investigated by using the A^{16}NC(11-55) mutant with Phe^{16} replaced by Ala and L^{37}NC(11-55) with Trp^{37} replaced by Leu, respectively. Since both Phe^{16} and Trp^{37} residues do not participate to zinc binding (41), their substitution is expected to not alter the zinc-driven folding of the A^{16}NC(11-55) and L^{37}NC(11-55) mutants. In contrast, since both residues participate to the hydrophobic plateau at the top of the folded zinc fingers, substantial alterations in this plateau should occur, likely explaining the significant alterations of the binding of the corresponding NC mutants to their ODN targets (7,40,42).

Both the steady-state and time-resolved fluorescence parameters of the complexes of NC(11-55) with AApCGCC, AACGApC and AATGApC were similar to those of the corresponding complexes with the native NC, suggesting that the NC-induced changes in the dynamics of these 2Ap-labeled ODNs are mediated by the zinc finger domain. In contrast to the aforementioned ODNs, an ~2-fold decrease in the quantum yield and the amplitudes associated with the τ_3 and τ_4 lifetimes was

observed when NC was substituted with NC(11-55) in its complex with AApTGCC. Thus, the N-terminal basic domain of NC likely contributes to the NC-induced changes of the local dynamics of 2Ap in this ODN (Table 1). Noticeably, the φ_2 correlation time of all tested ODNs was substantially lower in their complexes with the truncated mutant than with the native NC. This may be rationalized by the smaller molecular weight of the truncated peptide and probably, the more spherical shape of its complexes with the ODNs (Table 2).

In sharp contrast to NC and NC(11-55), the unfolded $(SSHS)_2$NC(11-55) mutant induced only limited changes in the steady-state and time-resolved parameters of the 2Ap-labeled ODNs. For instance, neither the quantum yield nor the α_0, α_1 and τ_1 values were significantly affected by $(SSHS)_2$NC(11-55), indicating that the peptide does not affect 2Ap in the most quenched conformers. In contrast, slight increases of about 0.3–0.6 ns and 1 ns were observed for the τ_3 and τ_4 values, respectively, indicating that $(SSHS)_2$NC(11-55) interacts with 2Ap in the less quenched conformers. The limited changes in the time-resolved intensity parameters were not due to poor binding, since this peptide was found to bind even stronger than NC(11-55) to the various target ODNs (data not shown), in line with previous data on other ODNs (43). Moreover, $(SSHS)_2$NC(11-55) increased the φ_2 correlation time of all 2Ap-labeled ODNs from 0.68–0.83 ns to 2–2.2 ns, confirming that this peptide binds to the ODNs. The correlation time of the complex is substantially lower than the 2.8 ns correlation time expected for the tumbling of a spherical 1:1 complex, indicating that the φ_2 component describes a combination of tumbling and segmental motions. Thus, $(SSHS)_2$NC(11-55) decreases the overall flexibility of the ODNs to a lesser extent than NC and NC(11-55).

Substitution of the Phe^{16} residue by Ala in the A^{16}NC(11-55) mutant was found to decrease the affinity for the various ODNs by about 20-fold (data not shown), in line with a significant contribution of Phe^{16} in the binding process (42). Nevertheless, at the high concentrations needed for the time-resolved experiments, we calculated that more than 80% of the 2Ap labeled ODNs were bound to A^{16}NC(11-55). Substitution of NC(11-55) by A^{16}NC(11-55) only marginally altered the amplitudes associated with the different fluorescence lifetimes as well as the time-resolved anisotropy parameters of the ODNs labeled by 2Ap at the 5 position (Tables 1 and 2). The only significant change was the decrease of the τ_3 to τ_4 values, suggesting that A^{16}NC(11-55) reduces less efficiently than NC(11-55) the quenching of 2Ap fluorescence by its neighbor bases in these conformations. As a consequence, the $Phe^{16}\rightarrow$Ala mutation induces only subtle changes in the interaction of NC with 2Ap at position 5. In sharp contrast, strong differences between NC(11-55) and A^{16}NC(11-55) were observed when the two peptides interact with ODNs labeled at position 2. Indeed, the quantum yield and time-resolved intensity values of both AApCGCC and AApTGCC derivatives were much lower in the presence of A^{16}NC(11-55) than in the presence of NC(11-55) and approached the values of the free ODNs, indicating that substitution of Phe^{16} with Ala prevented modifications of the local dynamics of 2Ap at position 2. However, the values of the longer correlation time of AApCGCC and AApTGCC bound with A^{16}NC(11-55) and NC(11-55) were indistinguishable, indicating that both peptides decrease the overall flexibility of the ODNs to the same extent. Moreover, the two peptides provide similar β_1 values, suggesting that they similarly restrict the amplitude of the 2Ap motion.

Substitution of Trp^{37} by Leu dramatically decreased (by two orders of magnitude) the binding constants of NC to the various ODNs, in line with the critical role of Trp^{37} in nucleic acid recognition (6,10,11,29,44–48). As a consequence, only the more affine TG-containing ODNs could be used to obtain a sufficient level of binding (> 80%) in the time-resolved experiments. NC(11-55) and L^{37}NC(11-55) were found to substantially differ in their ability to alter the time-resolved fluorescence intensity parameters of the AATGApC sequence (Table 1). Indeed, the L^{37}NC(11-55) mutant induced about two times lower increase than NC(11-55) in the quantum yield of AATGApC, due to its lower efficiency in shifting the populations of the more quenched species toward the less quenched ones. Nevertheless, the L^{37}NC(11-55) mutant significantly increased the τ_3 and τ_4 values of AATGApC as well as their associated amplitudes, indicating that the mutated peptide was able to interact with the less stacked conformers, though less efficiently than the unmodified NC(11-55) peptide. In contrast to AATGApC, only limited differences in the fluorescence parameters of AApTGCC were observed in its complexes with NC(11-55) and L^{37}NC(11-55) (Table 1), suggesting that the $Trp^{37}\rightarrow$Leu mutation affects essentially the ability of NC to perturb the local kinetics of 2Ap at position 5. This conclusion was further substantiated by the different effects of L^{37}NC(11-55) and NC(11-55) on the value of the short rotational correlation time of 2Ap at position 5, but not at position 2 (Table 2). In contrast to NC(11-55), the L^{37} mutant only moderately slowed down the local motion of 2Ap at position 5.

DISCUSSION

In this study, we investigated the steady state and time resolved fluorescence properties of 2Ap-substituted AACGCC and AATGCC sequences and their complexes with native and mutated NC proteins. In the absence of NC, the complex intensity decays with four resolved lifetimes and one nonmeasurable 'null' lifetime suggest that 2Ap adopts at least five different conformations in these ODNs (18,49). Probably, even more geometries are explored but cannot be experimentally observed due to the limited resolution of the time-resolved measurements. The very low quantum yield as well as the time-resolved fluorescence parameters (and notably the absence of a free 2Ap-like component) of the 2Ap-labeled hexanucleotides are reminiscent of those previously observed with 2Ap-labeled trinucleotides (19). In further analogy with the latter sequences, a dramatic fluorescence increase of the 2Ap-labeled hexanucleotides was observed in a viscous

medium, due to a strong decrease of the population of the most quenched conformers and a corresponding increase of the population of the less quenched conformers (Table 1). The fluorescence quenching of 2Ap appears thus highly dynamic and results probably from a charge transfer mechanism occurring during its collisions with its neighbors (19,20). This mechanism is in line with the strong quenching observed when 2Ap is next to a guanine, since this last residue shows the lowest redox potential among the bases (21,22,39). These fluorescence properties of the labeled hexanucleotides largely rely on their highly flexible structure, which allows conformational fluctuations in the picosecond–nanosecond (ps–ns) range. The high flexibility of the ODNs is substantiated by the large amplitude associated with their short correlation time as well as by the low value of their long rotational correlation time, showing strong contributions of both local and segmental motions that prevent observation of the tumbling motion. In this respect, even if unstacked 2Ap conformations are excited, rapid conformational changes will bring 2Ap close to one of its neighbor, allowing charge transfer and thus, fluorescence quenching. Moreover, the 'null' lifetime likely corresponds to a conformation where 2Ap stacks with one of its neighbors, leading to an almost immediate quenching.

Binding of NC induces a strong decrease of the ODN flexibility, with notably a disappearance of the segmental motions, as shown by the values of the long rotational correlation times (Table 2). This decrease in ODN flexibility is consistent with the well-resolved structure of ACGCC in its complex with NC(12-53) (11) as well as with the 'freezing' by NC of the nanosecond dynamics of a dsDNA (50). The effect of NC on ODN flexibility is in line with an 'adaptive binding' mechanism where a flexible nucleic acid sequence becomes more ordered upon binding of a protein (51,52). As a consequence of this decreased flexibility, collisions of 2Ap with its neighbors needed for fluorescence quenching are restricted, explaining the increased quantum yields and the shift toward the less quenched populations (associated with the longer lifetimes) in the presence of NC. In addition, NC also affects the local motion of 2Ap at positions 2 and 5 by decreasing its excursion angle, in full line with the NMR structure of the ACGCC/NC(12-53) complex showing that the local motion of the corresponding bases in ACGCC is constrained by the Asn^{12} and Gln^{45} residues, respectively (Figure 5). Though the effect of NC on the fluorescence properties of the 2Ap-labeled ODNs is qualitatively similar to that of glycerol, it differs by an important aspect. Indeed, glycerol induces similar increases of the 2Ap quantum yield in the four ODNs due to a mechanical decrease of the number of collisions of 2Ap with its neighbors by viscosity. In contrast, NC differently affects the dynamics of the bases at positions 2 and 5, since the quantum yield of 2Ap in AApCGCC increases by only 2.5-fold while it increases by about 7-fold in AACGApC. Moreover, NC does not affect the local motion rate of 2Ap at position 2 while it slows down the local motion of the probe at position 5. This slowing down may be due to an interaction of 2Ap at position 5 with the side chain of Gln^{45} (Figure 5) since a H-bond was reported between this

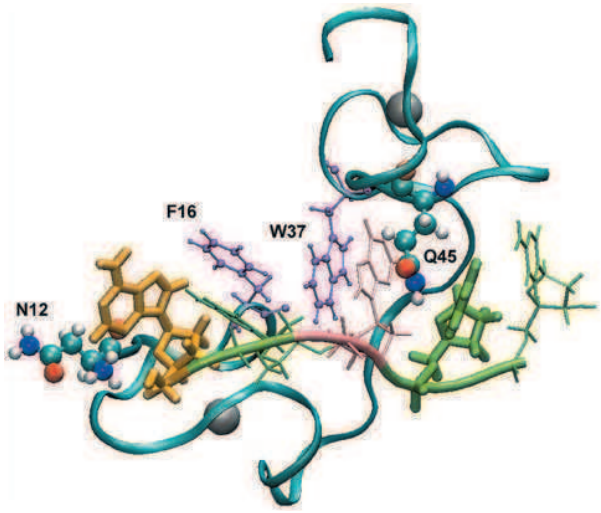

Figure 5. Structure of the NC(12-53)/ACGCC complex. NC protein backbone, blue ribbon; Phe^{16} and Trp^{37} residues, magenta. Zinc atoms are as gray spheres. The side chains of Asn^{12} and Gln^{45} are represented in CPK color code. The A (yellow) and C (green) residues of the ODN which have been substituted by 2Ap in our study are in bold. The G residue that interacts with Trp^{37} is in pink.

Gln^{45} side chain and the corresponding C residue in the ACGCC/NC(12-53) complex (11). Alternatively, the effect on the local motion of 2Ap may also be an indirect consequence of the interaction of its neighbors with NC. In this respect, the strong fluorescence increase of 2Ap at position 5 (giving a fluorescence quantum yield that is only five times lower than that of the free ODN) is likely a consequence of the strong stacking of G4 with the Trp^{37} residue that freezes the mobility of G4 and thus restricts its collisions with 2Ap (11,29). Moreover, this stacking also rotates the guanine residue in respect to the phosphate ribose axis, further preventing its collisions with 2Ap. In contrast, the stacking of C3 with Phe^{16} appears less stable and constrained since two orientations of this couple were found in the complex. Moreover, the A1 residue likely protrudes out of the complex and is thus quite mobile. Thus, both C3 and A1 residues are still able to collide with 2Ap in this complex, explaining its efficient quenching.

The fluorescence signal of 2Ap can also be used to characterize the complex of AATGCC with NC. From the strong similarities of the steady state and time-resolved fluorescence parameters of AACGApC and AATGApC complexed with NC, it can be inferred that G4 stacks similarly with the Trp^{37} residue in both complexes. More generally, since the 3′ half of the ODNs interacts mainly with the distal finger of NC, this interaction is likely similar in both complexes. In contrast, the stronger NC-induced increase of 2Ap fluorescence in AApTGCC as compared to AApCGCC suggests that the flexibility of the 5′ half of the ODN is more strongly decreased by NC in the former sequence. This observation may be related to a stronger interaction of T3 as compared to C3 with NC, due to a stable interaction of the methyl group of T3 with the aromatic protons of Phe^{16} as well as with the methyl

groups of Val^{13} as Thr^{24} (N. Morellet, personal communication). This stable interaction with T3 may strongly hinder its collisions with 2Ap. Alternatively, the binding of T3 to NC may favor a direct interaction of NC with 2Ap, preventing its collisions with neighbor bases. However, the absence of change in the rate of the 2Ap local motion does not favor this hypothesis. The more 'frozen' complex obtained with the TG-containing sequence is in line with its stronger binding constant as compared to the CG-containing sequence (29).

Comparison of the native NC with the truncated NC(11-55) derivative indicated that the finger domain plays a central role in restricting the ODN flexibility and local dynamics of 2Ap at positions 2 and 5. In AApTGCC, both the ODN flexibility and 2Ap local dynamics are further restricted by the terminal basic domain of NC (Table 1). The stronger dependence of the fluorescence parameters of AApTGCC as compared to AApCGCC on the N-terminal domain suggests that this domain interacts tighter with 2Ap at position 2 in the former ODN. This tight interaction is likely a consequence of a different binding mode of the proximal NC finger to AApTGCC that orientates differently the N-terminal domain.

In sharp contrast to NC(11-55), $(SSHS)_2$NC(11-55) minimally affects the fluorescence parameters of the four tested 2Ap-labeled ODNs. This does not result from a decreased binding level since this mutant was shown to bind to various ODNs with high affinity (40,46). The poor effect of $(SSHS)_2$NC(11-55) is likely a consequence of its inability to restrict the ODN flexibility and 2Ap local dynamics. As a result, the distribution of the 2Ap conformers and the quenching of 2Ap by its neighbors are similar to those in the free ODN. Thus, the folding of the finger domain appears critical for restricting the ODN flexibility and 2Ap local dynamics. This crucial role of folding is likely related to the hydrophobic platform (formed by the Val^{13}, Phe^{16}, Thr^{24}, Ala^{25}, Trp^{37} and Met^{46} residues) at the folded finger surface that plays a key role in ODN binding (10,11,40,53) and specific structural changes (10–12). In line with this hypothesis, only a limited stacking of Trp^{37} with the ODN bases was observed in the complexes with $(SSHS)_2$NC(11-55), as shown by the limited decrease of Trp^{37} fluorescence (data not shown). This explains that the G4 residue is not 'frozen' by stacking with Trp^{37} and can thus efficiently quench 2Ap at the position 5 in the complex. Stacking interactions with Phe^{16} may be prevented as well in the complexes with $(SSHS)_2$NC(11-55) since the interaction of Phe^{16} with ACGCC has been shown to be largely altered with a NC mutant exhibiting a distorted proximal finger (11). The limited restriction of the mobility of the ODN bases in the complexes with $(SSHS)_2$NC(11-55) is in line with a binding of the unfolded peptide mainly to the phosphate backbone. This binding is likely mediated mainly through electrostatic interactions that compensate for the loss of hydrophobic interactions with the bases (40,46). Since unfolded NC peptides are unable to destabilize the secondary structure of cTAR (40) and alter the cooperativity of the helix–coil transition of λ DNA molecules (54), the restriction of the ODN flexibility and local dynamics of the bases is certainly essential for the destabilizing component of NC chaperone activity. In addition, since mutations that prevent the folding of the finger domain lead to completely noninfectious viruses (6–9), 'freezing' of the ODN dynamics may be a key feature of NC during the viral life cycle.

The relationship between the restriction of the ODN dynamics and the biological activities of NC was further substantiated with the A^{16}NC(11-55) and L^{37}NC(11-55) mutants. Both mutations led to fully noninfectious viruses (6), likely by altering the nucleic acid binding and chaperone properties of NC (40,42,46,48). With A^{16}NC(11-55), the local dynamics of 2Ap at position 5 and its close neighbors was restricted to the same level than with NC(11-55) while in contrast, the local dynamics of 2Ap at position 2 in the presence of A^{16}NC(11-55) was comparable to that in the free ODNs. Accordingly, the distal finger of A^{16}NC(11-55) likely interacts with the 3′ half of the ODN sequences in the same way than the unmodified NC(11-55). In contrast, the $Phe^{16}\rightarrow$Ala mutation deeply modified the interaction of the proximal finger with the 5′ half of the ODN sequences, probably due to the inability of Ala^{16} to interact with C3 and prevent its rapid collisions with 2Ap at position 2. Symmetric effects were observed with the L^{37}NC(11-55) mutant, which showed a strongly reduced ability to prevent quenching of 2Ap at position 5. This indicates that Leu^{37} is probably unable to interact with the G4 base and thus cannot prevent the fast collisions of this residue with 2Ap at position 5. In addition, the change induced by L^{37}NC(11-55) in the rate of the 2Ap local motion further suggests that in contrast to the unmodified peptide, the Gln^{45} residue of L^{37}NC(11-55) does probably not interact with 2Ap at position 5 in the complex. Nevertheless, in contrast to $(SSHS)_2$NC(11-55), both A^{16}NC(11-55) and L^{37}NC(11-55) mutants restrict the overall ODN flexibility, as shown by the absence of any contribution from segmental motions in the long rotational correlation time of their complexes with the 2Ap-labeled ODNs (Table 2). Accordingly, the complexes with these two mutants are probably stabilized through hydrophobic interactions between the correctly folded fingers of the mutants and the ODN bases. Taken together, the data with the A^{16}NC(11-55) and L^{37}NC(11-55) mutants unambiguously confirmed that the aromatic residues of the hydrophobic plateau at the top of the folded fingers play a key role in the nucleic acid recognition and the restriction of the ps–ns local dynamics of the nucleotide subdomains to which they bind.

In conclusion, 2Ap fluorescence allowed us to characterize sub-nanosecond and nanosecond dynamics of NC target hexanucleotides and their complexes with NC. The effects of NC binding on 2Ap fluorescence are explained by restriction of the ODN flexibility and 2Ap local mobility that impedes collisions of 2Ap with neighbor bases and thus, largely decreases its dynamic quenching. This is consistent with the 'adaptive binding' model of protein–nucleic acid interaction where the conformational freedom of single-stranded ODNs becomes restricted due to protein binding. The 'freezing' of the ODN flexibility seemed to be mainly supported by the folded

zinc finger domain. The restriction of the local dynamics of the bases was more specifically attributed to the hydrophobic platform at the top of the folded fingers and notably, to the stacking of Trp^{37} with the G base and the interaction of Phe^{16} with the preceding C base. Since this hydrophobic plateau also supports the NC chaperone properties and notably the ability of NC to destabilize the stem of various stem-loops (40), the restriction of the ps–ns ODN dynamics is likely a mechanistic component of these properties. In this respect, together with the increase in the distance and the rotation of the consecutive bases which interact with Phe^{16} and Trp^{37} (10,11), the restriction of the local motion of these bases and their close neighbors may induce the disruption of base pairs in the double strand segments destabilized by NC (32,55–59). Thus, the NC-induced distortion of the ODN structure and local 'freezing' of the bases likely constitute the initial events responsible notably for the NC-chaperoned opening/closing of the cTAR DNA stem (56,60–62). Moreover, the NC-induced conformational changes and restriction of the local base motion probably favor the interaction of the loops of stem-loop sequences with their complementary sequences, explaining the loop–loop promoted annealing of (–)PBS/(+)PBS (63) and mini-TAR sequences (64) as well as the NC-promoted formation of PBS (65,66) and DIS (67) kissing loop homodimers. These hypotheses on the dependence of NC chaperone properties on the NC-promoted changes in the local dynamics of various 2Ap-labeled stem-loop sequences are currently investigated. Finally, since the NC-induced changes in the 2Ap fluorescence parameters were shown to depend on the position and the context of the probe, 2Ap can be used to site-specifically report on the binding of NC to more complex sequences.

ACKNOWLEDGEMENTS

We acknowledge N. Morellet for providing the NMR data on the AATGCC/NC complex and fruitful discussion. This work was funded by Agence Nationale de Recherches sur le SIDA (peptide synthesizer); the European Commission Consortium 'Targeting Replication and Integration of HIV'; Fondation pour la Recherche Medicale, France (ACE2005120624 to S.V.A.). Funding to pay the Open Access publication charges for this article was provided by Agence Nationale de Recherches sur le SIDA.

Conflict of interest statement. None declared.

REFERENCES

1. Darlix,J.L., Cristofari,G., Rau,M., Pechoux,C., Berthoux,L. and Roques,B. (2000) Nucleocapsid protein of human immunodeficiency virus as a model protein with chaperoning functions and as a target for antiviral drugs. *Adv. Pharmacol.*, **48**, 345–372.
2. Clever,J., Sassetti,C. and Parslow,T.G. (1995) RNA secondary structure and binding sites for gag gene products in the 5′ packaging signal of human immunodeficiency virus type 1. *J. Virol.*, **69**, 2101–2109.
3. De Rocquigny,H., Gabus,C., Vincent,A., Fournie-Zaluski,M.C., Roques,B. and Darlix,J.L. (1992) Viral RNA annealing activities of human immunodeficiency virus type 1 nucleocapsid protein require only peptide domains outside the zinc fingers. *Proc. Natl Acad. Sci. USA*, **89**, 6472–6476.
4. Bampi,C., Jacquenet,S., Lener,D., Decimo,D. and Darlix,J.L. (2004) The chaperoning and assistance roles of the HIV-1 nucleocapsid protein in proviral DNA synthesis and maintenance. *Int. J. Biochem. Cell Biol.*, **36**, 1668–1686.
5. D'Souza,V. and Summers,M.F. (2005) How retroviruses select their genomes. *Nat. Rev. Microbiol.*, **3**, 643–655.
6. Dorfman,T., Luban,J., Goff,S.P., Haseltine,W.A. and Gottlinger,H.G. (1993) Mapping of functionally important residues of a cysteine-histidine box in the human immunodeficiency virus type 1 nucleocapsid protein. *J. Virol.*, **67**, 6159–6169.
7. Gorelick,R.J., Gagliardi,T.D., Bosche,W.J., Wiltrout,T.A., Coren,L.V., Chabot,D.J., Lifson,J.D., Henderson,L.E. and Arthur,L.O. (1999) Strict conservation of the retroviral nucleocapsid protein zinc finger is strongly influenced by its role in viral infection processes: characterization of HIV-1 particles containing mutant nucleocapsid zinc-coordinating sequences. *Virology*, **256**, 92–104.
8. Guo,J., Wu,T., Anderson,J., Kane,B.F., Johnson,D.G., Gorelick,R.J., Henderson,L.E. and Levin,J.G. (2000) Zinc finger structures in the human immunodeficiency virus type 1 nucleocapsid protein facilitate efficient minus- and plus-strand transfer. *J. Virol.*, **74**, 8980–8988.
9. Ottmann,M., Gabus,C. and Darlix,J.L. (1995) The central globular domain of the nucleocapsid protein of human immunodeficiency virus type 1 is critical for virion structure and infectivity. *J. Virol.*, **69**, 1778–1784.
10. De Guzman,R.N., Wu,Z.R., Stalling,C.C., Pappalardo,L., Borer,P.N. and Summers,M.F. (1998) Structure of the HIV-1 nucleocapsid protein bound to the SL3 psi-RNA recognition element. *Science*, **279**, 384–388.
11. Morellet,N., Demene,H., Teilleux,V., Huynh-Dinh,T., de Rocquigny,H., Fournie-Zaluski,M.C. and Roques,B.P. (1998) Structure of the complex between the HIV-1 nucleocapsid protein NCp7 and the single-stranded pentanucleotide d(ACGCC). *J. Mol. Biol.*, **283**, 419–434.
12. Amarasinghe,G.K., De Guzman,R.N., Turner,R.B. and Summers,M.F. (2000) NMR structure of stem-loop SL2 of the HIV-1 psi RNA packaging signal reveals a novel A-U-A base-triple platform. *J. Mol. Biol.*, **299**, 145–156.
13. Walker,J.R., Corpina,R.A. and Goldberg,J. (2001) Structure of the Ku heterodimer bound to DNA and its implications for double-strand break repair. *Nature*, **412**, 607–614.
14. Mazin,A.V., Zaitseva,E., Sung,P. and Kowalczykowski,S.C. (2000) Tailed duplex DNA is the preferred substrate for Rad51 protein-mediated homologous pairing. *EMBO J.*, **19**, 1148–1156.
15. Zhang,Q., Sun,X., Watt,E.D. and Al-Hashimi,H.M. (2006) Resolving the motional modes that code for RNA adaptation. *Science*, **311**, 653–656.
16. Mollova,E.T. (2002) Single-molecule fluorescence of nucleic acids. *Curr. Opin. Chem. Biol.*, **6**, 823–828.
17. Ward,D.C., Reich,E. and Stryer,L. (1969) Fluorescence studies of nucleotides and polynucleotides. I. Formycin, 2-aminopurine riboside, 2,6-diaminopurine riboside, and their derivatives. *J. Biol. Chem.*, **244**, 1228–1237.
18. Jean,J.M. and Hall,K.B. (2001) 2-Aminopurine fluorescence quenching and lifetimes: role of base stacking. *Proc. Natl Acad. Sci. USA*, **98**, 37–41.
19. Jean,J.M. and Hall,K.B. (2004) Stacking-unstacking dynamics of oligodeoxynucleotide trimers. *Biochemistry*, **43**, 10277–10284.
20. O'Neill,M.A. and Barton,J.K. (2002) 2-Aminopurine: a probe of structural dynamics and charge transfer in DNA and DNA:RNA hybrids. *J. Am. Chem. Soc.*, **124**, 13053–13066.
21. Fiebig,T., Wan,C. and Zewail,A.H. (2002) Femtosecond charge transfer dynamics of a modified DNA base: 2-aminopurine in complexes with nucleotides. *Chem. Phys. Chem.*, **3**, 781–788.
22. Wan,C., Fiebig,T., Schiemann,O., Barton,J.K. and Zewail,A.H. (2000) Femtosecond direct observation of charge transfer between bases in DNA. *Proc. Natl Acad. Sci. USA*, **97**, 14052–14055.
23. Bradrick,T.D. and Marino,J.P. (2004) Ligand-induced changes in 2-aminopurine fluorescence as a probe for small molecule binding to HIV-1 TAR RNA. *RNA*, **10**, 1459–1468.

24. Somsen,O.J., Keukens,L.B., de Keijzer,M.N., van Hoek,A. and van Amerongen,H. (2005) Structural heterogeneity in DNA: temperature dependence of 2-aminopurine fluorescence in dinucleotides. *Chem. Phys. Chem.*, **6**, 1622–1627.
25. Rachofsky,E.L., Osman,R. and Ross,J.B. (2001) Probing structure and dynamics of DNA with 2-aminopurine: effects of local environment on fluorescence. *Biochemistry*, **40**, 946–956.
26. Kaul,M., Barbieri,C.M. and Pilch,D.S. (2004) Fluorescence-based approach for detecting and characterizing antibiotic-induced conformational changes in ribosomal RNA: comparing aminoglycoside binding to prokaryotic and eukaryotic ribosomal RNA sequences. *J. Am. Chem. Soc.*, **126**, 3447–3453.
27. Hariharan,C. and Reha-Krantz,L.J. (2005) Using 2-aminopurine fluorescence to detect bacteriophage T4 DNA polymerase-DNA complexes that are important for primer extension and proofreading reactions. *Biochemistry*, **44**, 15674–15684.
28. Ramreddy,T., Rao,B.J. and Krishnamoorthy,G. (2007) Site-specific dynamics of strands in ss- and dsDNA as revealed by time-domain fluorescence of 2-aminopurine. *J. Phys. Chem. B*, **111**, 5757–5766.
29. Vuilleumier,C., Bombarda,E., Morellet,N., Gerard,D., Roques,B.P. and Mely,Y. (1999) Nucleic acid sequence discrimination by the HIV-1 nucleocapsid protein NCp7: a fluorescence study. *Biochemistry*, **38**, 16816–16825.
30. Fisher,R.J., Rein,A., Fivash,M., Urbaneja,M.A., Casas-Finet,J.R., Medaglia,M. and Henderson,L.E. (1998) Sequence-specific binding of human immunodeficiency virus type 1 nucleocapsid protein to short oligonucleotides. *J. Virol.*, **72**, 1902–1909.
31. de Rocquigny,H., Ficheux,D., Gabus,C., Fournie-Zaluski,M.C., Darlix,J.L. and Roques,B.P. (1991) First large scale chemical synthesis of the 72 amino acid HIV-1 nucleocapsid protein NCp7 in an active form. *Biochem. Biophys. Res. Commun.*, **180**, 1010–1018.
32. Bernacchi,S., Stoylov,S., Piemont,E., Ficheux,D., Roques,B.P., Darlix,J.L. and Mely,Y. (2002) HIV-1 nucleocapsid protein activates transient melting of least stable parts of the secondary structure of TAR and its complementary sequence. *J. Mol. Biol.*, **317**, 385–399.
33. Lakowicz,J.R. (1999) *Principles of Fluorescence Spectroscopy*, 2nd edn. Kluwer Academic/Plenum Publishers, New York, p.304.
34. Lipari,G. and Szabo,A. (1980) Effect of librational motion on fluorescence depolarization and nuclear magnetic resonance relaxation in macromolecules and membranes. *Biophys. J.*, **30**, 489–506.
35. Rai,P., Cole,T.D., Thompson,E., Millar,D.P. and Linn,S. (2003) Steady-state and time-resolved fluorescence studies indicate an unusual conformation of 2-aminopurine within ATAT and TATA duplex DNA sequences. *Nucleic Acids Res.*, **31**, 2323–2332.
36. Nag,N., Ramreddy,T., Kombrabail,M., Krishna Mohan,P.M., D'Souza,J., Rao,B.J., Duportail,G., Mely,Y. and Krishnamoorthy,G. (2006) Dynamics of DNA and protein-DNA complexes viewed through time-domain fluorescence. In Geddes,C. and Lakowicz,J.R. (eds), *Reviews in Fluorescence*, Springer Science, New York, Vol. 3, pp. 311–340.
37. Guest,C.R., Hochstrasser,R.A., Sowers,L.C. and Millar,D.P. (1991) Dynamics of mismatched base pairs in DNA. *Biochemistry*, **30**, 3271–3279.
38. Xu,D., Evans,K.O. and Nordlund,T.M. (1994) Melting and premelting transitions of an oligomer measured by DNA base fluorescence and absorption. *Biochemistry*, **33**, 9592–9599.
39. Larsen,O.F., van Stokkum,I.H., Gobets,B., van Grondelle,R. and van Amerongen,H. (2001) Probing the structure and dynamics of a DNA hairpin by ultrafast quenching and fluorescence depolarization. *Biophys. J.*, **81**, 1115–1126.
40. Beltz,H., Clauss,C., Piemont,E., Ficheux,D., Gorelick,R.J., Roques,B., Gabus,C., Darlix,J.L., de Rocquigny,H. *et al.* (2005) Structural determinants of HIV-1 nucleocapsid protein for cTAR DNA binding and destabilization, and correlation with inhibition of self-primed DNA synthesis. *J. Mol. Biol.*, **348**, 1113–1126.
41. Mely,Y., De Rocquigny,H., Morellet,N., Roques,B.P. and Gerad,D. (1996) Zinc binding to the HIV-1 nucleocapsid protein: a thermodynamic investigation by fluorescence spectroscopy. *Biochemistry*, **35**, 5175–5182.
42. Fisher,R.J., Fivash,M.J., Stephen,A.G., Hagan,N.A., Shenoy,S.R., Medaglia,M.V., Smith,L.R., Worthy,K.M., Simpson,J.T. *et al.* (2006) Complex interactions of HIV-1 nucleocapsid protein with oligonucleotides. *Nucleic Acids Res.*, **34**, 472–484.
43. Cruceanu,M., Gorelick,R.J., Musier-Forsyth,K., Rouzina,I. and Williams,M.C. (2006) Rapid kinetics of protein-nucleic acid interaction is a major component of HIV-1 nucleocapsid protein's nucleic acid chaperone function. *J. Mol. Biol.*, **363**, 867–877.
44. Maki,A.H., Ozarowski,A., Misra,A., Urbaneja,M.A. and Casas-Finet,J.R. (2001) Phosphorescence and optically detected magnetic resonance of HIV-1 nucleocapsid protein complexes with stem-loop sequences of the genomic Psi-recognition element. *Biochemistry*, **40**, 1403–1412.
45. Amarasinghe,G.K., Zhou,J., Miskimon,M., Chancellor,K.J., McDonald,J.A., Matthews,A.G., Miller,R.R., Rouse,M.D. and Summers,M.F. (2001) Stem-loop SL4 of the HIV-1 psi RNA packaging signal exhibits weak affinity for the nucleocapsid protein. structural studies and implications for genome recognition. *J. Mol. Biol.*, **314**, 961–970.
46. Urbaneja,M.A., Kane,B.P., Johnson,D.G., Gorelick,R.J., Henderson,L.E. and Casas-Finet,J.R. (1999) Binding properties of the human immunodeficiency virus type 1 nucleocapsid protein p7 to a model RNA: elucidation of the structural determinants for function. *J. Mol. Biol.*, **287**, 59–75.
47. Bombarda,E., Ababou,A., Vuilleumier,C., Gerard,D., Roques,B.P., Piemont,E. and Mely,Y. (1999) Time-resolved fluorescence investigation of the human immunodeficiency virus type 1 nucleocapsid protein: influence of the binding of nucleic acids. *Biophys. J.*, **76**, 1561–1570.
48. Remy,E., de Rocquigny,H., Petitjean,P., Muriaux,D., Theilleux,V., Paoletti,J. and Roques,B.P. (1998) The annealing of tRNA3Lys to human immunodeficiency virus type 1 primer binding site is critically dependent on the NCp7 zinc fingers structure. *J. Biol. Chem.*, **273**, 4819–4822.
49. Jean,J.M. and Hall,K.B. (2002) 2-Aminopurine electronic structure and fluorescence properties in DNA. *Biochemistry*, **41**, 13152–13161.
50. Krishnamoorthy,G., Roques,B., Darlix,J.L. and Mely,Y. (2003) DNA condensation by the nucleocapsid protein of HIV-1: a mechanism ensuring DNA protection. *Nucleic Acids Res.*, **31**, 5425–5432.
51. Ramos,A., Gubser,C.C. and Varani,G. (1997) Recent solution structures of RNA and its complexes with drugs, peptides and proteins. *Curr. Opin. Struct. Biol.*, **7**, 317–323.
52. Leulliot,N. and Varani,G. (2001) Current topics in RNA-protein recognition: control of specificity and biological function through induced fit and conformational capture. *Biochemistry*, **40**, 7947–7956.
53. Stote,R.H., Kellenberger,E., Muller,H., Bombarda,E., Roques,B.P., Kieffer,B. and Mely,Y. (2004) Structure of the His44 –> Ala single point mutant of the distal finger motif of HIV-1 nucleocapsid protein: a combined NMR, molecular dynamics simulation, and fluorescence study. *Biochemistry*, **43**, 7687–7697.
54. Williams,M.C., Rouzina,I., Wenner,J.R., Gorelick,R.J., Musier-Forsyth,K. and Bloomfield,V.A. (2001) Mechanism for nucleic acid chaperone activity of HIV-1 nucleocapsid protein revealed by single molecule stretching. *Proc. Natl Acad. Sci. USA*, **98**, 6121–6126.
55. Beltz,H., Azoulay,J., Bernacchi,S., Clamme,J.P., Ficheux,D., Roques,B., Darlix,J.L. and Mely,Y. (2003) Impact of the terminal bulges of HIV-1 cTAR DNA on its stability and the destabilizing activity of the nucleocapsid protein NCp7. *J. Mol. Biol.*, **328**, 95–108.
56. Azoulay,J., Clamme,J.P., Darlix,J.L., Roques,B.P. and Mely,Y. (2003) Destabilization of the HIV-1 complementary sequence of TAR by the nucleocapsid protein through activation of conformational fluctuations. *J. Mol. Biol.*, **326**, 691–700.
57. Liu,H.W., Cosa,G., Landes,C.F., Zeng,Y., Kovaleski,B.J., Mullen,D.G., Barany,G., Musier-Forsyth,K. and Barbara,P.F. (2005) Single-molecule FRET studies of important intermediates in the nucleocapsid-protein-chaperoned minus-strand transfer step in HIV-1 reverse transcription. *Biophys. J.*, **89**, 3470–3479.
58. Liu,H.W., Zeng,Y., Landes,C.F., Kim,Y.J., Zhu,Y., Ma,X., Vo,M.N., Musier-Forsyth,K. and Barbara,P.F. (2007) Insights on the role of nucleic acid/protein interactions in chaperoned nucleic acid rearrangements of HIV-1 reverse transcription. *Proc. Natl Acad. Sci. USA*, **104**, 5261–5267.

59. Hong,M.K., Harbron,E.J., O'Connor,D.B., Guo,J., Barbara,P.F., Levin,J.G. and Musier-Forsyth,K. (2003) Nucleic acid conformational changes essential for HIV-1 nucleocapsid protein-mediated inhibition of self-priming in minus-strand transfer. *J. Mol. Biol.*, **325**, 1–10.
60. Beltz,H., Piemont,E., Schaub,E., Ficheux,D., Roques,B., Darlix,J.L. and Mely,Y. (2004) Role of the structure of the top half of HIV-1 cTAR DNA on the nucleic acid destabilizing activity of the nucleocapsid protein NCp7. *J. Mol. Biol.*, **338**, 711–723.
61. Cosa,G., Harbron,E.J., Zeng,Y., Liu,H.W., O'Connor,D.B., Eta-Hosokawa,C., Musier-Forsyth,K. and Barbara,P.F. (2004) Secondary structure and secondary structure dynamics of DNA hairpins complexed with HIV-1 NC protein. *Biophys. J.*, **87**, 2759–2767.
62. Cosa,G., Zeng,Y., Liu,H.W., Landes,C.F., Makarov,D.E., Musier-Forsyth,K. and Barbara,P.F. (2006) Evidence for non-two-state kinetics in the nucleocapsid protein chaperoned opening of DNA hairpins. *J. Phys. Chem. B*, **110**, 2419–2426.
63. Ramalanjaona,N., Rocquigny,H.D., Millet,A., Ficheux,D., Darlix,J.L. and Mely,Y. (2007) Investigating the mechanism of the nucleocapsid protein chaperoning of the second strand transfer during HIV-1 DNA synthesis. *J. Mol. Biol.*, **374**, 1074–1053.
64. Vo,M.N., Barany,G., Rouzina,I. and Musier-Forsyth,K. (2006) Mechanistic studies of mini-TAR RNA/DNA annealing in the absence and presence of HIV-1 nucleocapsid protein. *J. Mol. Biol.*, **363**, 244–261.
65. Egele,C., Schaub,E., Ramalanjaona,N., Piemont,E., Ficheux,D., Roques,B., Darlix,J.L. and Mely,Y. (2004) HIV-1 nucleocapsid protein binds to the viral DNA initiation sequences and chaperones their kissing interactions. *J. Mol. Biol.*, **342**, 453–466.
66. Egele,C., Schaub,E., Piemont,E., de Rocquigny,H. and Mely,Y. (2005) Investigation by fluorescence correlation spectroscopy of the chaperoning interactions of HIV-1 nucleocapsid protein with the viral DNA initiation sequences. *C. R. Biol.*, **328**, 1041–1051.
67. Rist,M.J. and Marino,J.P. (2002) Mechanism of nucleocapsid protein catalyzed structural isomerization of the dimerization initiation site of HIV-1. *Biochemistry*, **41**, 14762–14770.

Targeting the Viral Nucleocapsid Protein in Anti-HIV-1 Therapy

Hugues de Rocquigny[1], Volodymyr Shvadchak[1], Sergiy Avilov[1], Chang Zhi Dong[2], Ursula Dietrich[3], Jean-Luc Darlix[4] and Yves Mély[1,*]

[1]*Institut Gilbert Laustriat, Photophysique des interactions moléculaires, UMR 7175 CNRS, Faculté de Pharmacie, Université Louis Pasteur, Strasbourg 1, 74, Route du Rhin, 67401 ILLKIRCH Cedex, France;* [2]*Laboratoire de Pharmacochimie Moléculaire, Université Paris 7, Case 7066, 2, Place Jussieu, 75251 Paris Cedex 05, France;* [3]*Georg Speyer Haus, Institute for Biomedical Research, Paul Ehrlich Strasse 42-44, 60596 Frankfurt, Germany;* [4]*LaboRetro, Unité INSERM de Virologie Humaine, IFR128, ENS de Lyon, 46 allée d'Italie, 69364 Lyon, France*

Abstract: The nucleocapsid protein (NC) plays seminal roles in HIV replication, thus representing a major drug target. NC functions rely on its two zinc-fingers and flanking basic residues. Zinc ejectors inhibit NC functions, but with limited specificity. New classes of molecules competing with NC or its viral nucleic acid and enzyme partners are reviewed here.

Key Words: NCp7, zinc ejector, library, HIV, structure, peptidomimetic, aptamer, intercalator.

I. INTRODUCTION

The human immunodefiency virus type-1 (HIV-1) belongs to the widespread family of Retroviruses. The viral particle is about 110 nm in diameter and is composed of an inner core with an outer envelope formed of a lipid bilayer derived from the infected cell, in which the viral surface (SU) and transmembrane (TM) glycoproteins are anchored. The inner core corresponds to a shell of capsid protein molecules (CA) surrounding the dimeric single stranded RNA genome coated by about 1500 molecules of the nucleocapsid protein NCp7 [1,2]. The core also contains molecules of the viral enzymes protease (PR), reverse transcriptase (RT) and integrase (IN) [3-5]. The HIV-1 replication cycle, as illustrated in Fig. (**1**), is divided into early and late phases, corresponding to virus entry and genome replication by RT, and virus biogenesis, production and maturation by PR, respectively [6-9] during which the nucleocapsid protein (NC) plays seminal roles (Fig. (**1**), steps 3, 4, 5 and 7). After virus entry, the genomic plus strand RNA is converted by RT into a double-stranded proviral DNA flanked by two long terminal repeats (LTR) (step 3) [10]. This process known as reverse transcription takes place in the incoming viral nucleocapsid substructure, where NC chaperones viral DNA synthesis by RT , that necessitates two NC-mediated obligatory strand transfers to generate the complete LTRs [3,11,12]. The proviral DNA is then integrated by IN into the cellular genome, in a reaction also assisted by NC [13] (step 5). During the late phase of virus replication in the infected cell, NC pilots genomic RNA selection and dimerization, and Gag oligomerization, and thus is considered to be an essential determinant of virus assembly (step 7). At the molecular level, the early and late functions of the viral NC protein appear to be mediated by its propensity to specifically bind the viral nucleic acids [14-16] and to chaperone their obligatory transconformation during the process of reverse transcription and virus assembly (for a recent review [17]).

HIV-1 NC is characterized by two highly conserved zinc finger motifs (ZF) flanked by basic residues. Point mutations in these fingers result in the production of totally defective virions [3,18-21] further underlining the importance of NC in the viral life cycle. This highlights the notion that HIV-1 NC represents a major target for the development of new anti-HIV-1 agents that could impair both early and late steps of HIV-1 replication. Anti-NC molecules could thus complement the so-called 'highly active anti-retroviral therapies' (HAART) based on drugs targeting the viral RT and PR. Due to the fact that NCp7 is highly conserved in all HIV-1 subtypes [17], a major benefit of anti-NC drugs should be to provide a sustained replication inhibition of a large panel of HIV-1 strains including those species that are resistant to anti-RT and anti-PR drugs. Different classes of anti-NC molecules have been developed or selected by means of a high throughput screening strategy (HTS). The most important ones are the zinc ejector agents, peptidomimetics, RNA aptamers and non zinc ejecting NC binders. These different classes of anti NC agents will be reviewed here.

II. ZINC EJECTORS

A common feature of a large number of DNA and RNA binding proteins in viruses and host cells is the presence of zinc finger motifs (ZF) [22-25] . Many classes of ZFs differing in their length and zinc ligands have been identified. ZFs of retroviral nucleocapsid proteins are the smallest fingers (or knuckle) yet reported. They coordinate zinc atoms through three Cys and one His residues in a Cys-X_2-Cys-X_4-His-X_4-Cys arrangement (also called CCHC motif). With the exception of spumaretroviruses, all retroviral nucleocapsid proteins are characterized by one or two copies of the CCHC motif. The nucleocapsid protein (NC) of HIV-1 contains two CCHC motifs separated by a short basic linker. The unusual high zinc binding affinity of 10^{13} to 10^{14} M^{-1} (several orders of magnitude higher than that of cellular zinc finger proteins)

*Address correspondence to this author at Institut Gilbert Laustriat, Photophysique des interactions moléculaires, UMR 7175 CNRS, Faculté de Pharmacie, Université Louis Pasteur, Strasbourg 1, 74, Route du Rhin, 67401 ILLKIRCH Cedex, France; Tel: 33.3.90.24.42.63; Fax: 33.3.90.24. 43.12; E-mail: yves.mely@pharma.u-strasbg.fr,

1389-5575/08 $55.00+.00

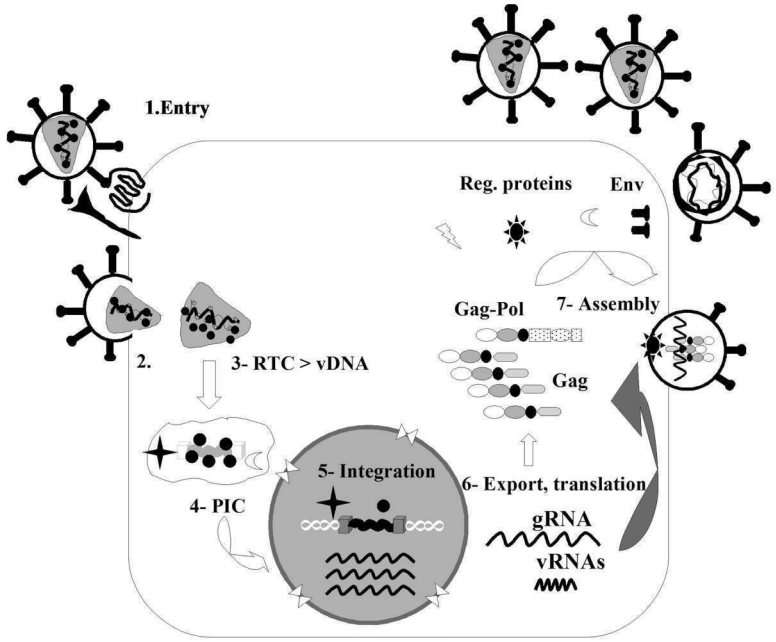

Fig. (1). Schematic illustration of HIV-1 replication in a human target cell.

The mutifunctional nature of the viral nucleocapsid protein NC (black dots) is highlighted at the early and late steps, namely 1, 2, 3, 5 and 7 for its role in the viral core structure, viral DNA synthesis by RT and integration by IN, and lately in virus assembly. Therefore, drugs targeting NC should in principle inhibit early and late steps of HIV-1 replication. Step1-Virus Entry is mediated firstly by interactions between Sugp120 and the cellular receptor CD4 and co-receptor CCR5 and followed by TMgp41-mediated membrane fusion; Step 2- core entry into the cytoplasm followed by virus uncoating ; Step 3- viral DNA synthesis takes place in the reverse transcription complex (RTC) and is chaperoned by NC; Step 4- viral DNA enters the nucleus in the form of a pre-integration complex (PIC) ; Step 5- the vDNA is integrated into the host genome by IN assisted by NC ; Step 6: the genomic RNA (gRNA) is synthesized by transcription of the integrated vDNA and undergoes balanced splicing to generate the 4 kb and 2 kb vRNAs and the gRNA found in the cytoplasm. Note that the roles of the viral factors TAT and REV are not shown here. The gRNA and vRNAs are translated by the host ribosome machinery to generate the virion polyproteins Gag, Gag-Pol, and Env and the regulatory proteins (large arrow). Step 7: selection of the gRNA by the NC domain of Gag is thought to start co-assembly of the gRNA with Gag and Gag-Pol (upper arrow); ultimately newly formed virions accumulate at the plasma membrane and undergo maturation by the viral protease. Viral particles are released by budding (top).

has foreseen the importance of this binding for the bona fide structure of the NC central domain and its implications in HIV replication [24,26-30]. . Indeed, mutations that prevent zinc binding or cause a conformational disorder in the ZF result in the production of defective viral particles [18,19, 31,32] reviewed in [11,12,33] . Thus, in the search for new anti-HIV drugs, many efforts were performed to develop molecules able to specifically remove zinc from the NC ZF.

Structure of Zinc Ejectors

The proof of concept of zinc ejectors as anti-NC drugs was demonstrated in the early 90's with the 3-nitrobenzamides (NOBA) (Fig. (**2**)) [34]. These C-nitroso derivatives were first identified as inhibitors of a cellular enzyme, the poly(ADP ribose) polymerase which possesses a large zinc finger sub-domain. Derivatives such as the 3-nitrosobenzamide or 6-nitroso-1,2-benzopyrone were found to eject zinc from NC in solution and in the virus (either HIV-1 or SIV [35]) through oxidation of the cystein residues [36,37]. Surprisingly, these compounds elicit only small side effects though they are possibly targeting cellular proteins binding zinc. Later, disulfide-substituted benzamides (DIBA) were identified as zinc ejectors with a broad anti-viral activity towards laboratory and clinical HIV-1 isolates [38-40]. The finding that NC ZFs were the target of the DIBA compounds was definitively assessed by showing that DIBA did not modify the infectivity of the human foamy virus, a spumaretrovirus without a canonical NC domain [41]. In the DIBA family, the two benzamide moieties are linked through a disulfide bridge. Nevertheless, the monomeric form of DIBA (with free -SH) exhibits an antiviral activity similar to the parental molecule but does not eject zinc. In contrast, molecules where the disulfide bond or the -SH group are changed to -OH or -SO_2 group or alkylated do not eject zinc or show an antiviral activity [42]. Since in the intracellular reducing environment both reduced and oxidized species may exist [43], the anti-viral activity of the DIBA compounds is likely mediated by both species.

To avoid the S-S bond reduction observed with the DIBA family, substitution for a thioester link was developed leading to the generation of the pyrimidinioalkanoyl thioester (PATE) family [44]. The PATEs were found to exhibit an increased antiviral activity, water solubility, a lack of susceptibility to glutathione reductase and a reduced cell toxicity [44,45]. In an attempt to develop new anti-NC's, a combinatorial chemistry was performed using the PATE skeleton as a scaffold. Series of uncharged S-acyl-2-mercaptobenzamide thioester (SAMT) were generated, some of them showing virucidal activity [46]. Interestingly, no correlation was evi-

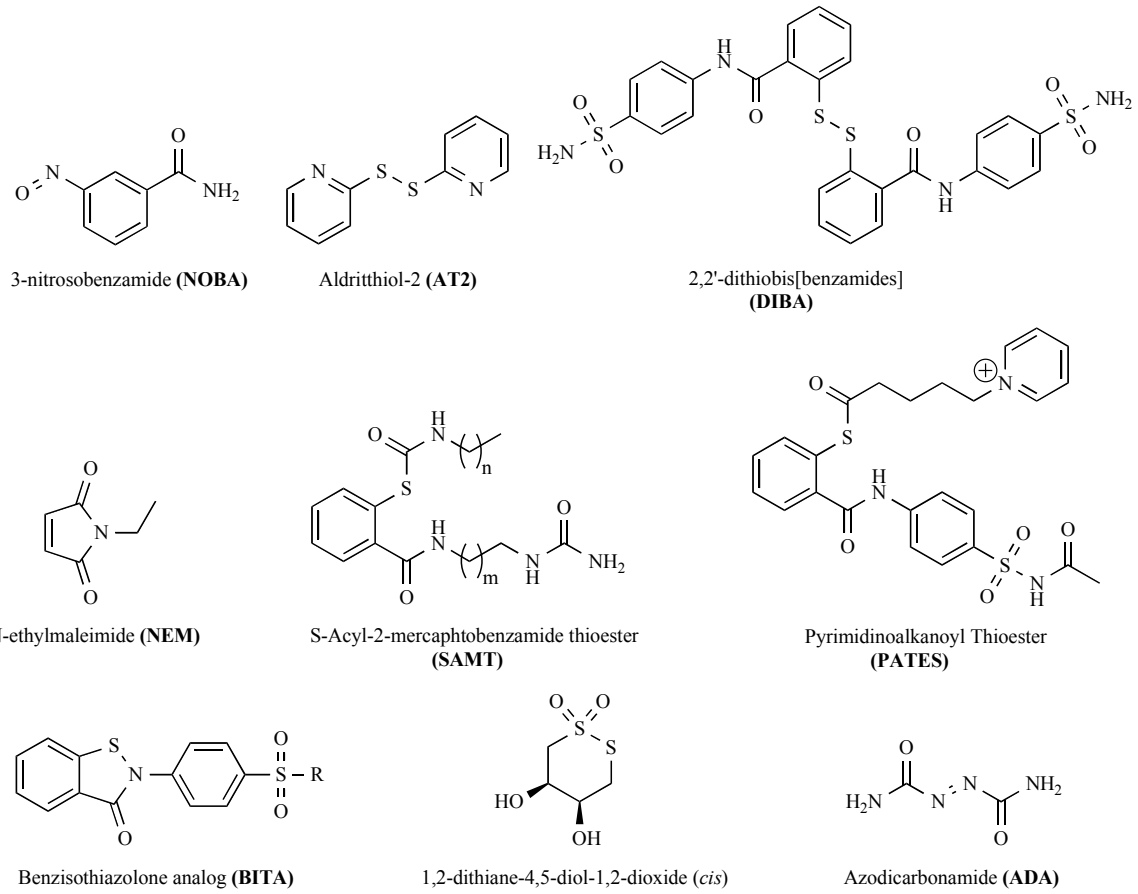

Fig. (2). Zinc ejector structures.

denced between the chemical stability of the thioesters in serum and their antiviral activity. Thus, the rapid release of free –SH groups in the serum does not appear as a solid criteria to discard a SAMT derivative for an *in vivo* study [47]. In fact, the released thiol groups of these compounds are likely re-acylated by acyl CoA, then available for a second round of reaction [48].

Another strategy to prevent disulfide reduction was based on the use of dithiane compounds [49]. The S-S bond in this series is tethered to a ring structure which confers an antiviral activity to the compound even in the presence of a high concentration of glutation reductase. Synthesis of the enantiomers of the first published molecule did not significantly improved the antiviral activity [50]. Last, Vandevelde *et al.* described azodicarbonamide (ADA) derivatives (Fig. (**1**)) as being potent anti-HIV drugs. These compounds were put in clinical trials phases I and II although their mechanism of action was not fully understood [51]. Interestingly, there is no disulfide bond in ADA which could lead to a loss of activity after reduction. The target of ADA was disclosed by Rice and collaborators as being the NC protein [52] even though these results were not confirmed in cell culture experiments (Berthoux L and Darlix JL, personal communication).

Mechanism of Zinc Ejection

Zinc ejectors, such as DIBA, were shown to penetrate into cells and virions [53]. The mechanism of zinc ejection was mainly studied using DIBAs, PATEs, N-ethylmaleimide (NEM) and SAMTs. As mentioned above, NCp7 zinc depletion begins at the level of the C-terminal ZF, which is consistent with its lower thermal stability and lower zinc affinity in comparison with the N-terminal ZF [27,32,54,55]. The nucleophilic attack of the cysteins (Cys39 and Cys 49) of the second ZF leads to a covalent modification of NCp7 (Fig. (**3**)) with the formation of either a disulfide bridge with DIBAs [43] or a thioester bond with SAMTs [48] or a thioether link with NEM [56]. This initial covalent link promotes the reaction of additional reactants with the other Cys residues of the same motif, and finally leads to zinc ejection and the loss of NCp7 folding. The Cys49 thiolate appears to be the major reaction site with DIBAs [40,43], PATES [57] and NEM [56] while Cys 39 seems to be the primary target of the SAMT analogues [58]. The reactivity of various electrophilic agents was found to depend on the ability of these agents to function as soft electrophiles [59]. Steric factors are also important since selective ligand binding regions within the conserved ZF are thought to promote the reaction. The presence of such regions in the ZFs is substantiated by the strong differences in the reactivity patterns to NEM between the native NCp7 and its isolated fingers [56]. In addition, several benzamides structurally related to DIBA failed to extrude the zinc from the ZFs [40,42,56] since they probably do not adopt the right conformation to fit the specific conformation of the putative binding pocket. Differences in the binding pockets may also explain the low sensitivity of large nonviral

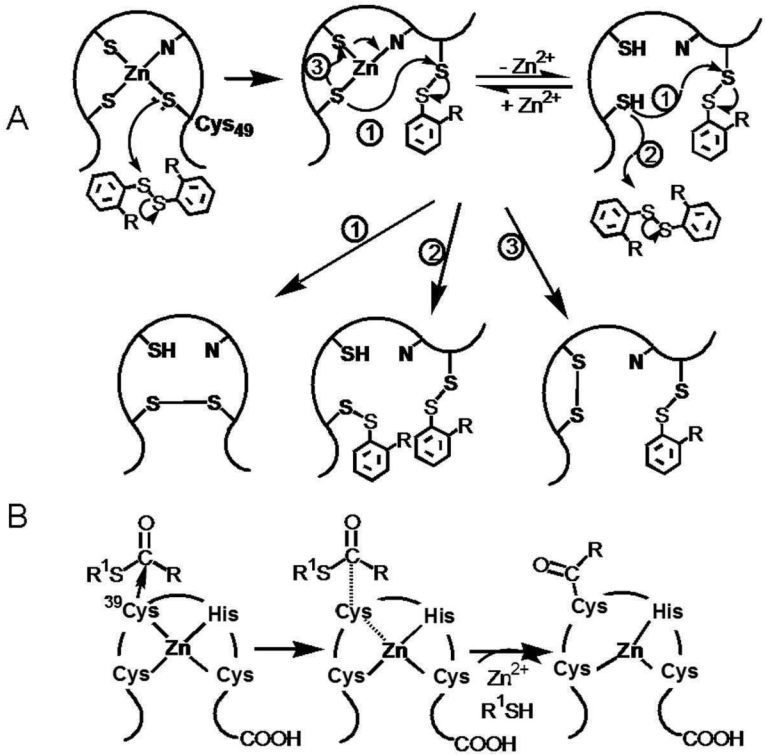

Fig. (3). Proposed mechanism of zinc ejection by DIBA (A) and SAMT (B).

Both zinc ejectors react with the Cys residues of the distal ZF of NC. Cys 49 and Cys 39 residues are the preferential targets for DIBA[43] and SAMT [48], respectively. Covalent reaction of both zinc ejectors with these Cys residues favors the reaction of additional zinc ejector molecules with the remaining Cys. These reactions decrease the zinc binding constant of the ZFs, leading to a release of zinc and NC unfolding.

zinc fingers to DIBAs [44,60]. However, the NC binding pockets have never been characterized due to the rapid structural changes undergone by the ZFs during the zinc removal process that follows binding of the zinc ejectors.

Are Zinc Ejectors Specific for Retroviral Zinc Fingers?

DIBA as well as dithiane ejectors were suggested to be unable to alter cellular ZF proteins [44,49,52,60]. However, this claim contrasts with the sensitivity of the ZFs of cellular transcription factors such as Sp1 and the steroid-binding glucocorticoid receptor (GR) to thiol-reducing agents [61,62]. This sensitivity towards reducing agents has prompted Wang *et al.* [63] to test DIBA derivatives on oestrogen-receptors in a breast cancer model. Interestingly, DIBA derivatives were found to inhibit the oestrogen receptor-mediated growth of breast cancer cells in a dose dependent manner and to decrease the binding of other nuclear receptors to their responsive elements [63]. Recently, various viral and cellular proteins have been challenged with thioesters [58]. The ZFs of GAGA and protein kinase C-delta as well as the C-terminal finger of mouse mammary tumor virus (MMTV) NCp9 were not sensitive to thioesters. In contrast, thioesters were able to efficiently eject zinc from the N-terminal ZF of NCp9, the CCHC motif of FOG-1 and both CCCC motifs of GATA-1. Taken together, these results indicate that the drug response does not depend on the origin of the ZF protein but more probably on the zinc accessibility and the ZF structure [34,58,64].

How do the Zinc Ejectors Block Virus Replication?

In vitro, zinc ejectors were tested on the complex formed between NCp7 and the genomic RNA packaging signal ψ. This specific signal is located in the 5' leader of the HIV-1 genome and composed of four stem-loops (SL1 to SL4). Specific interactions between NCp7 and the SLs govern genomic RNA selection, dimerization and packaging during virus assembly (Fig. (**1**)) [3,12,14,16,65-67]. Interestingly, DIBA, NOBA, SAMTs and ADA (Fig. (**1**)) can impair the binding of NCp7 to its nucleic acid targets [48]. When NCp7 was pre-incubated with various zinc ejectors, a reduction of NCp7 binding to the ψ RNA was observed [40,60]. In contrast, zinc ejection was reduced when zinc ejectors were incubated with a preformed NCp7-SL3 complex [48]. This protection likely results from the involvement of the distal ZF (which is the most susceptible to zinc ejection) in viral RNA recognition notably through the stacking of its Trp37 residue with the G residues of the RNA target [68-70]. Nevertheless, this protection depends on the nucleic acid sequence, probably reflecting different affinities of NCp7 for its targets and varying accessibilities of the reactive Cys in the nucleoprotein complexes [68-70].

The protection of NCp7 ZFs by RNA was also investigated with Acr37 NCp7, a derivative where Trp37 was substituted by an acridine (Acr) moiety. This derivative exhibits the same structure and biological activities as the wild type protein *in vitro* [71]. Addition of zinc to the apoform of Acr37 NCp7 induces a three fold decrease of the Acr fluo-

rescence [71]. In contrast, addition of 5 equivalents of DIBA-1 causes a time-dependent increase of Acr fluorescence (Fig. (**3**), curve A), which is fully consistent with a progressive oxidation of the distal ZF and zinc ejection [39]. Addition of the genomic RNA(1-415) region to the holoprotein in the absence of DIBA-1 results in a fluorescence decrease (Fig (**4**), curve B at t= 0), most probably due to the intercalation of the Acr moiety into the RNA chain. Interestingly, no significant fluorescence change was observed when DIBA-1 was added to the NCp7/RNA complex, indicating that NCp7 was protected by the RNA from oxidation by DIBA-1. To confirm this, sodium dodecylsulfate (SDS), a detergent which disrupts macromolecular complexes, was added. As expected, this restored the fluorescence level of the holoprotein. Thereafter, the fluorescence intensity increased smoothly, as in curve A. It thus appears that the effect of the zinc ejectors on viruses and infected cells is probably due to their interaction with free NC protein or Gag polyprotein, but does not target those molecules bound to their RNA or DNA partners.

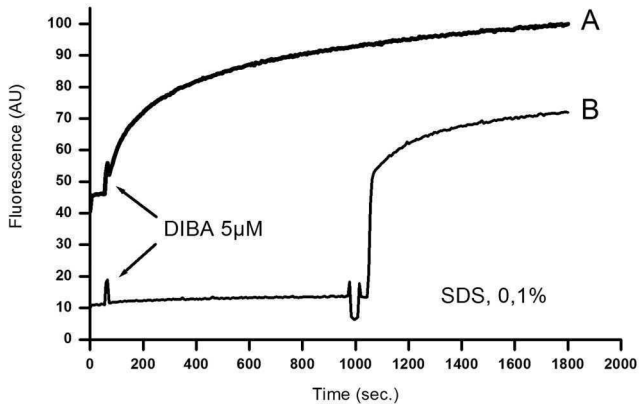

Fig. (4). Protection of NCp7 from DIBA-1 attack by HIV-1 RNA (1-415).

The protective effect of the RNA was evaluated by comparing the effect of DIBA on 1µM of Acr37-NCp7 alone (trace A) or complexed to HIV-1 RNA(1-415) (trace B). Addition of DIBA-1 (5 µM) to NC is indicated by the arrows. Addition of 0.1% SDS (final concentration) in trace B was carried out after 15 min. The SDS-induced dissociation of the protein/RNA complex leads to a sharp increase of the fluorescence due to the DIBA-induced zinc ejection.

In cellular assays, all zinc ejectors inhibit a wide range of HIV-1 isolates [53]. Since NCp7 as a free protein or in the context of Gag is required all along the virus replication cycle, it was interesting to evaluate which steps are affected by the zinc ejectors. Given the importance of the NC ZF structure for the specific packaging of genomic RNA, the effect of the zinc ejector on this recognition should have resulted in low amounts of genomic RNA packaged into newly formed particles [18,21,33]. Surprisingly, a significant amount of genomic RNA was found in the treated viruses [72]. This rather high encapsidation level of genomic RNA could be due to the role of the basic residues surrounding the zinc fingers in RNA recognition or to the protection afforded by the RNA from the attack by the zinc ejectors, as mentioned above [44,48,56,58,72]. This high level of genomic RNA in viruses could also be due to the stability of the first ZF apparently less sensitive than the second one to the attack by zinc ejectors, and which plays a more critical role than the distal ZF in genome packaging [11,16,21,31,43,48,56]. Interestingly, DIBA-1 also causes formation of heterogeneous populations of immature viral particles [72]. This likely results from a DIBA-induced alteration of the viral assembly pathway, in line with recent data showing that the C-terminus of Gag is essential for Gag assembly[73]. Despite a frozen-like core morphology, the surface of the virion keeps the wild type conformation with fusion properties similar to the wild-type virus [56,74,75] but proviral DNA synthesis was strongly impaired. This may result from the inability of oxidized NCp7 to chaperone initiation and elongation of cDNA synthesis [11,76]. Moreover, the oxidized NCp7 is probably unable to interact with RT, which should impair completion of a bona fide proviral DNA [77-79]. NCp7 is not the only protein targeted by DIBA, NEM or Aldrithiol-2 (2-AT) since the free sulfhydryl groups of the capsid protein can also be modified [80]. In contrast, the cysteins of the envelope glycoproteins form disulfide bridges, explaining their poor susceptibility to zinc ejectors. The complete inactivation of virus infectivity together with the preservation of the structure and functions of the viral envelope make these particles a potential attractive vaccine [56,81,82]. This approach was tested with the simian immunodeficiency virus (SIV), which is closely related to HIV-2 and infects monkeys. The AT-2-inactivated SIV was not infectious and elicited both humoral and cellular immune responses [83]. The resulting immunization facilitated effective containment of pathogenic homologous challenge viruses but failed to protect against heterologous SIV isolates.

In Vivo Activity of the Zinc Ejectors

In a chemotherapeutic approach, SAMT derivatives were shown to reduce the levels of infectious viruses in a murine transgenic model, where an integrated provirus was reactivated [47]. More recently, a SAMT derivative was used to treat SIV infected monkeys [84]. This derivative was well tolerated by all monkeys and did not alter the liver, kidney and immunological functions. It showed no clear effect on the virus load but significantly reduced the levels of infectious viruses in peripheral blood mononuclear cells. Thus, the antiviral potency of these zinc ejectors is mainly due to the production of non infectious particles rather than to a decrease in the viral production per se.

In the case of ADA, administration into mice was found to blunt their response to polyclonal T-cell activation induced by the injection of monoclonal antibody against CD3 and to delay rejection of skin allografts. These effects were related to the strong inhibition by ADA of the calcium mobilization machinery in T lymphocytes [85,86] and indicated that, due to its immunosuppressive properties, ADA could be used as a therapeutic agent in allograft rejection, autoimmune diseases and allergic disorders. ADA has also been used for the first, and to our knowledge unique, clinical trial using zinc ejectors. This clinical investigation mainly focused on the safety and tolerability of ADA in patients with advanced AIDS [86]. Preliminary results showed an increase in the number of CD4 cells similar to that obtained with other antiretroviral agents and a decrease in the viral load, but only in 1/3 of the treated patients. Unfortunately, the

ratio of infectious to non infectious particles was not determined in this assay. A combination with other antiretrovirals could be possible, but the renal toxicity of the biurea metabolite of ADA would prevent a combination with PR inhibitors that are nephrotoxic [87].

III. NON ZINC EJECTING NC BINDERS

The work carried out on zinc ejectors demonstrated a straightforward link between the loss of NCp7 activity and the virucidal effect. However, their limited specificity for HIV NC hampered their use in therapy. These results prompted the scientific community to identify compounds able to bind NCp7 but with no zinc ejecting property. To reach this aim, a first medium throughput screening [88] was developed to identify antagonists of the strong binding of NCp7 to oligonucleotides containing TG repeats [89,90]. To that end, a chemical library of approximately 2000 small molecules (the NCI Diversity Set) was screened.

From the 26 active inhibitors that were identified, five contained a xanthenyl ring structure (Table **1**). Further analysis of structurally related compounds led to the identification of tetrachlorogallein, which stoichiometrically binds NCp7 and exhibits a significant anti-HIV activity *in vitro* with an IC50 of about 20 μM. Nevertheless, the correlation was not absolute since several compounds were poor competitors for NC binding to the TG-rich oligonucleotide but exhibited good anti-HIV activity. All the active compounds contain a xanthene ring substituted by two hydroxyls in positions 4' and 5'. These two hydroxyls were found critical for binding to NCp7 and to provide protection against HIV infection. Molecular modelling predicted that these hydroxyl groups bind to the amide nitrogen of Gly35 with additional contacts at the carbonyl oxygens of Gly40 and Lys33 of NC (Fig. (**5**)). The same compounds were then tested for their ability to inhibit NCp7 chaperone properties on λ-DNA, taken as model sequences [91]. The more active compounds such as gallein were found to be active in the low nanomolar range. However, these compounds did not show any activity when added after DNA titration with NCp7, suggesting that they did not compete for NC binding with the large λ-DNA molecule and thus exhibited an antagonist effect against free NC only. It is thought that these compounds might interfere with NC's ability to stack its aromatic residues with the bases of its target nucleic acids. The proposed method based on λ-DNA molecules can be used to further refine the positive hits but, due to its limited speed, it cannot substitute for initial HTS assays.

A new screening assay has recently been developed based on NCp7 ability to destabilize the HIV-1 transactivation response element in the form of cTAR, through an activation of end fraying [92-94]. This assay is thought to be highly specific since the NCp7-promoted destabilization is entirely mediated by the properly folded ZF domain [76]. As a consequence, a HTS based on this NCp7–promoted fraying should select compounds able to block specific interactions between the ZF domain and cTAR. The assay uses a cTAR molecule labeled at its 5' and 3' ends by a fluorophore and a quencher, respectively. In the closed form of cTAR, the emission of the fluorophore is quenched. Addition of NCp7 partly melts the stem, increasing the distance between the two dyes, thus causing a large fluorescence increase. Positive hits in this HTS are detected through the decrease of the fluorophore emission. This assay was used to screen an "in-house" chemical library of 5000 molecules [95] . About ten compounds with IC50 values in the low micromolar range have been selected (Mély *et al.*, unpublished). These compounds were shown to interact with NC but did not eject zinc. Interestingly, this HTS confirmed the importance of the hydroxyl groups in the positive hits. Though non zinc ejecting NC binders are potentially interesting, it is necessary to further understand their mechanism of action, improve their binding to NC and demonstrate their antiviral activity.

IV. NUCLEIC ACID INTERCALATORS AND BINDERS

Targeting the proper nucleic acids of pathogens is a classical way to fight bacterial infections. In fact, most antibiotics interact with bacterial ribosomal RNA rather than with proteins [96]. Through their binding to the bacterial rRNAs, antibiotics impede the interaction of the rRNAs with their cognate partners and facilitate miscoding during protein synthesis. The 5' untranslated leader of HIV-1 RNA is a multifunctional region composed of several SLs required for cDNA synthesis, viral translation and virus assembly (Fig. (**1**)) [66,67]. These SLs being unique to the virus and being engaged in interactions with NC represent targets in order to block NC functions [11,12,33]. In this context, actinomycin D was first identified [97-99]. Actinomycin D is a widely used anti-cancer drug that inhibits the DNA-dependent DNA/RNA synthesis through DNA intercalation and binding to the minor groove. Early reports showed that the replication of both RSV and MLV retroviruses was sensitive to this drug [100-102]. Actinomycin D was found to inhibit the DNA-dependent DNA synthesis catalyzed by RT, only at very high concentrations. In contrast, actinomycin D inhibits efficiently HIV-1 minus strand transfer during reverse transcription. In spite of its strong ability to promote minus-strand transfer NC cannot overcome the inhibitory effect of actinomycin D on the annealing of (-) SSDNA to the acceptor RNA. Since NC (but not RT) is required for efficient annealing, actinomycin D likely inhibits the minus-strand transfer by blocking the nucleic acid chaperone activity of NC. Nevertheless, the main problem of actinomycin D is that it interacts with a large range of nucleic acids, giving a poor specificity. As a consequence, a clinical use of such a molecule will likely generate critical side effects and the emergence of resistant strains as for bacteria [103].

More recently, mass spectroscopy was used to investigate the effects of a small library of nucleic acid binders on the interaction of NCp7 with the SL2, SL3 and SL4 structures of the specific ψ packaging signal [104]. This library included intercalators, minor groove-binders, mixed-mode intercalator/minor groove-binders, and multifunctional polycationic aminoglycosides. Only aminoglycosides were capable of dissociating preformed NC/SL3 and NC/SL4 complexes, but not NC/SL2 complexes. Among the aminoglycosides, a correlation was found between their binding constants to SL3 and SL4 and their ability to dissociate the NC/RNA complexes. Further studies revealed that the competition mechanism on SL3 and SL4 resulted from an extensive overlap of the aminoglycoside and NC binding sites [105]. Indeed, both

Table 1. Structure Activity Relationship of Xanthenyl Derivatives on the Inhibition of NCp7 Chaperone Properties

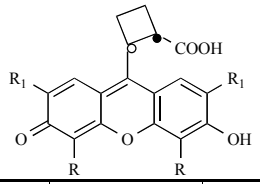

name		R	R1	K_d (M) (SPR)	K_d (M) (Fl)	Antiviral Activity
Gallein		OH	H	ND	8×10^{-8}	A
119911/158917		OH	H	3.5×10^{-7}	5×10^{-8}	A
157411		OH	H	1.5×10^{-5}	I	A
122391	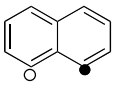	OH	H	1.1×10^{-5}	5×10^{-7}	A
119913		OH	H	3.8×10^{-5}	1×10^{-7}	A
378139	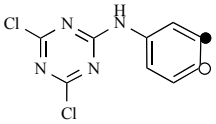	H	H	1.45×10^{-4}	5×10^{-8}	A
Tetrachlorogallein 723402	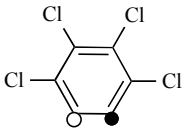	OH	H	ND	$>2.5\times10^{-6}$	A
Tetrabromogallein 119889	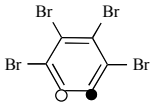	OH	H	2.5×10^{-7}	1×10^{-8}	A
tetrachlorofluorescein	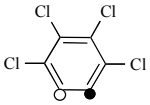	H	H	ND	$>8.5\times10^{-6}$	I
119910 fluorescein		H	H	4.1×10^{-7}	1.5×10^{-6}	M
Eosin Y		Br	Br	ND	$>3.2\times10^{-6}$	I
Erytrosine B		I	I	ND	1×10^{-6}	I

K_d values have been measured by surface plasmon resonance (SPR) and fluorescence (Fl) measurements. In the first row are presented the names and/or the NSC numbers (http://dtp.nci.nih.gov) of the tested compounds. In the structure of the common scaffold (top of the table), X represents the connecting moiety between the xanthenyl ring and the carboxylic group. X maintains the carboxylic group over the xanthenyl cycle. The A, M, I abbreviations refer to the anti-HIV-1 activity, defined as the percentage of cells from the human T-cell line CEM-SS that survived after incubation with HIV-1_{RF} virus. The antiviral activity of these compounds was tested for protection against the HIV-1 induced cytopathic effects. Active (A) compounds provide more than 80% protection, moderate active compounds provide 50-80% protection, while inactive (I) compounds provide less than 50% protection. Data are from [88,91].

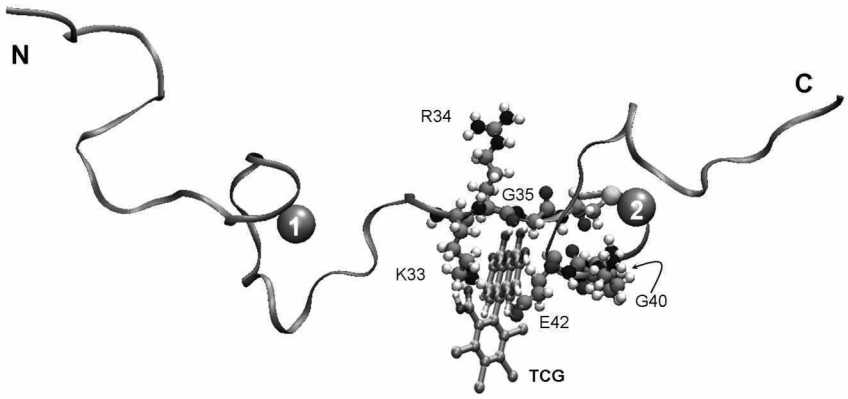

Fig. (5). Molecular modeling of the binding of tetracholorogallein to NCp7.

Tetrachlorogallein (TCG) is thought to bind to a putative binding pocket located between the basic ^{29}RAPRKK^{34} linker and the C-terminal ZF (2) of the native NC. Amino acids thought to interact with the tetrachlorogallein molecule are indicated [88].

the antibiotic and the protein were found to preferentially bind the upper stem and the loop of SL3 and SL4 [30,69, 106,107]. In contrast, the inability of the aminoglycosides to dissociate the NC/SL2 complexes resulted from the minimal overlap between the aminoglycoside binding site (in the middle of SL2 stem) with the NC binding site (at the SL2 loop) 71. Importantly, aminoglycosides inhibit also the TAT-TAR complex [108], highlighting common features between HIV-1 NCp7 and TAT proteins [109]. This observation paves the way for the search of molecules targeting simultaneously these two essential proteins of HIV-1.

V. PEPTIDOMIMETICS

An alternate strategy to inhibit NCp7 functions is to design peptides that can directly compete with NCp7 for the binding to its RNA and DNA substrates. In this context, one approach is to design peptides mimicking part of the NC structure. NCp7 contains two ZFs held in close proximity by a short basic linker containing a Pro residue. The globular conformation of the ZF domain (Fig. (**6**)) is stabilised by hydrophobic and aromatic interactions between the two ZFs.

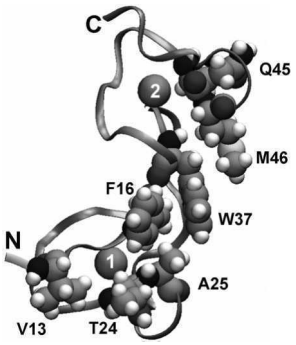

Fig. (6). Structure of the hydrophobic plateau of the NC zinc finger domain.

The polypeptide backbone of the ZF domain of NC adopts a globular structure in which the two ZFs are in close proximity (1 and 2). The peptide backbone is represented as a ribbon. The hydrophobic residues from the two fingers that form the hydrophobic plateau are indicated. This plateau is thought to be involved in the interaction with the DNA and RNA substrates of NC.

Residues Val13, Phe16, Thr24 and Ala25 of the proximal finger and residues Trp37, Gln45 and Met46 of the distal finger form a hydrophobic plateau on the top of the folded fingers [32,110,111]. Interestingly, a similar hydrophobic plateau was also found for SIV NCp8 and MLV NCp10 [112,113]. As illustrated in the NC/SL3 complex (Fig. (**7**)), the role of this plateau is to provide specific hydrophobic and H-bonding interactions with the RNA or DNA bases and notably, to promote the stacking of Trp37 with a guanine residue [69,70,111,114,115]. This complex is further stabilised by electrostatic interactions with the flanking basic amino acids.

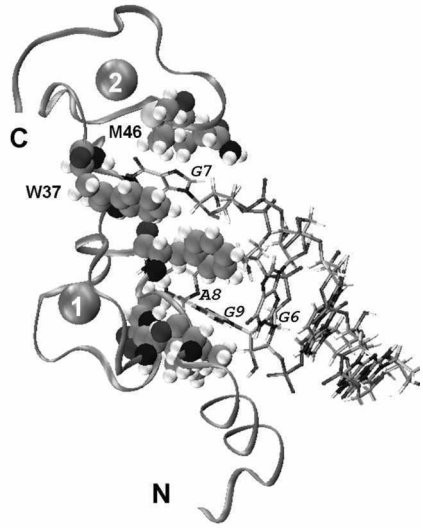

Fig. (7). NMR structure of the NCp7/SL3 complex.

The ZFs of the native NC protein bind the exposed G^6-G^7-A^8-G^9 residues of the SL3 loop. The complex is stabilized by interactions between the side chains of the hydrophobic plateau and the G^7 and G^9 residues of the loop. As illustrated here, the N-terminal region of NC adopts a 3_{10} helix [69]. Only the loop of SL3 and the top of its stem are indicated on the graph. The bases are indicated in italics. The peptide backbone is represented as a ribbon.

NC structure and hydrophobic plateau are remarkably conserved in all 3D structures of NCp7/oligonucleotide complexes that have been solved [69,70,111,114,115]. Moreover,

modification or loss of the hydrophobic plateau through mutations of the two zinc fingers resulted in NC proteins with reduced binding specificity and chaperone properties [76, 89]. Interestingly, the same mutations resulted in a total loss of viral infectivity [18-20,32,97,116], indicating that the NC hydrophobic plateau plays a key role in HIV-1 replication and can thus be used as a structural basis for the design of specific NCp7 inhibitors without zinc ejection. Based on this concept, cyclic peptides mimicking the spatial orientation of Phe16 and Trp37 residues in the hydrophobic plateau have been designed [117]. To further strengthen the interaction of this peptide with the RNA and DNA substrates of NCp7, two basic residues thought to mimic Arg 26 and Arg 32 have been introduced into the cyclic peptide. The leader of this series of peptides was referred to as RB2121. An excellent overlap was found between the structure of RB2121 and the corresponding residues in the folded zinc fingers. In spite of its two Cys residues, RB2121 does not directly interact with NCp7 nor eject zinc. In contrast, RB2121 competes with NCp7 for its RNA and DNA substrates. This competition results in the inhibition of the NCp7-dependent annealing of the primer $tRNA_3^{Lys}$ to the HIV-1 PBS. Moreover, RB2121 also inhibits the interaction between NCp7 and RT while peptides without Trp are inactive [77,78]. Both inhibitory activities lead to a dose-dependent reduction in cDNA levels that may explain the observed inhibition of HIV-1 replication in infected CEM-4 cells. These results clearly indicate that small molecules mimicking structural determinants of NC can impair virus replication [118]. However, though RB2121 shows no cytotoxicity up to 150 μM, its IC50 is still high (about 30 μM), showing that its structure should be improved to augment its antiviral potential. Attempts are actually done to better mimic the NC hydrophobic plateau, in order to increase the activity of these peptidomimetics.

In a different approach, small peptides able to specifically recognize NCp7 RNA targets were identified using a phage-displayed library [119]. This technology provides a large diversity of peptides on the surface of filamentous phages [120]. This strategy has been used for selecting peptides that specifically recognize the ψ encapsidation sequence [119]. All selected peptides are composed of a cluster of Trp residues surrounded by basic residues and bind to the ψ sequence with micromolar affinities. The optimized peptide HKWPWW was found to adopt a symmetric cis-trans equilibrium at the level of the Pro residue where it is structured (Fig. (**8**)) [121]. These two conformations are characterised by a close proximity between Trp5 and 6 in the cis conformation and between Trp 3 and 5 in the trans conformation. The two conformations of the peptide bind both TAR and PBS sequences with low micromolar affinities, mainly through stacking interactions between the Trp residues and the oligonucleotide bases. Moreover, the HKWPWW peptide stabilizes the cTAR secondary structure and inhibits the NC-directed melting of the cTAR sequence. Interestingly, HKWPWW was found to inhibit RNA encapsidation and HIV-1 replication in cellular assays (Dietz *et al.*, submitted), probably due to a competition with NC to its target nucleic sequences. Like RB2121, HKWPWW probably partially mimics the NC hydrophobic plateau, notably the two aromatic residues of this plateau, confirming that the NC hydrophobic plateau is a promising starting point to develop agents with potent antiviral activities.

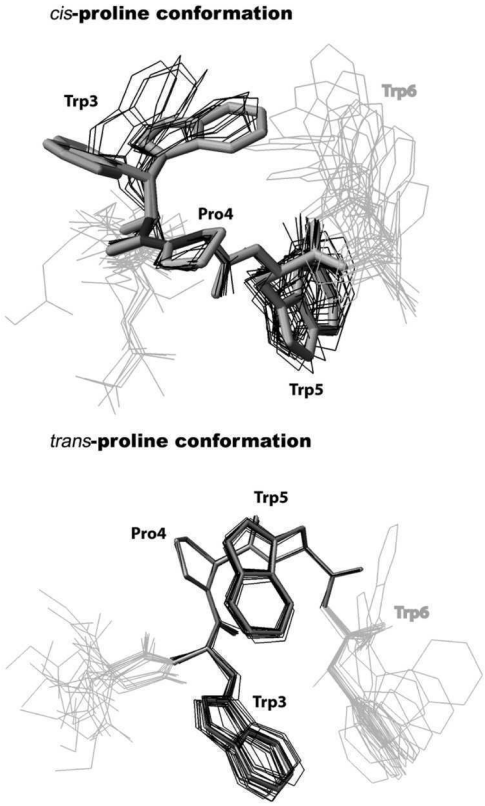

Fig. (8). NMR-derived structures of HKWPWW.

The HKWPWW peptide showed an equilibrium between *cis* and *trans* conformers around the central Pro residue. The *cis*-Pro conformation (top) exhibits a folded structure while the *trans*-Pro conformation (bottom) is more extended. In the *cis* conformation, Trp3 adopts two orientations while Pro4 and Trp5 can be superimposed. In the *trans* conformation, these three moieties adopt a unique conformation. In both conformations, Trp6 shows some preferred conformation and is therefore shaded. In contrast, the side chains of His1 and Lys2 are not represented since they do not exhibit any preferred conformation [121].

VI. APTAMERS

Though the specific recognition of HIV-1 ψ packaging signal by Gag *via* its NC domain has been firmly established [14-16,122,123], the reasons for this specificity are still poorly understood. Indeed, only modest differences in NC affinity were observed between the stem loops of the ψ sequence in comparison with control RNAs. Nevertheless, the direct link between the specific recognition by NC of this region and the production of infectious particles stimulated the search for small RNA aptamers with antiviral activity. Different libraries of RNA were produced using the SELEX method [124], generating aptamers of about 40 nucleotides in length [125,126]. Their secondary structures correspond to stem-loops in which the stems are rich in GC base pairs and the loops contain G and U residues. Several aptamers exhibit a higher affinity (K_d in the low nM range) for NC than the ψ sequence itself and are thus able to fully abolish the binding

of NC to ψ and TAR *in vitro*. The proof of concept to use an RNA aptamer as an inhibitor of NC function was assessed by cotransfecting a plasmid expressing the aptamer and one expressing the HIV-1 DNA. This resulted in a partial inhibition of genomic RNA packaging, without modifying the amount of genomic RNA within transfected cells. Thus, the aptamer probably interferes with the recognition of ψ by NCp7 in HIV-1 producing cells [127]. One possible explanation for this limited decrease of genomic RNA packaging into virions caused by NC-specific RNA aptamers could be that genomic RNA recruitment by the Gag polyprotein could also be under the control of the matrix protein (MA) at the Gag N-terminus. In fact, SELEX carried out using HIV-1 Gag polyprotein has clearly evidenced two classes of aptamers: those directed against NC and those against MA [128] . Binding of a NC ligand to Gag was unable to inhibit the binding of a MA ligand and vice-versa, suggesting that aptamers directed against NC can not prevent the binding of MA to the genomic RNA. More importantly, differences in the binding and chaperone properties of NC alone as compared with Gag-NC have been recently reported [129] Thus, one should be careful when using free NCp7 as opposed to Gag-NC to identify inhibitory ligands capable of disrupting Gag assembly and thus the formation of infectious HIV-1. Accordingly, the proof of concept for the use of aptamers as anti-NC agents still awaits full validation .

CONCLUSIONS

Due to its central role in both the early and late steps of the HIV-1 replication cycle, the nucleocapsid protein should be viewed as a major target for the development of new antiviral agents. This conclusion is further substantiated by the strong conservation of the central zinc finger domain of NC and the inability of the virus to escape from mutations that affect the proper folding of this ZF domain. The importance of the proper folding appears to be related to the role played by the hydrophobic residues at the top of the folded ZF domain. In fact, these residues form a hydrophobic plateau that is required for the proper recognition of the viral nucleic acids by NC and thus for NC functions. Nevertheless, NC exhibits several drawbacks that do not facilitate the search for antiviral agents directed against it. Indeed, NC has no enzymatic activity and therefore HTS assays are not easy to design. In this respect, one should keep in mind that all the drugs used in HAART are directed against the HIV enzymes, except for the T20 agent, which appears to be a moderate inhibitor as compared with anti-RT and anti-PR. Screening for anti-NCs is further complicated by the fact that the early and late functions of NC also rely on the basic residues flanking the ZFs. Due to its large number of basic residues, NC can bind a large array of DNA and RNA molecules in addition to the viral RNA and DNA molecules [11,130,131]. , Moreover, the extensive coating of the genomic RNA by about 1500 copies of NC in the viral particle and during the early steps of the viral cycle (Fig. (**1**); RTC) is thought to generate a very high local concentration of NC and consequently, would need a high local concentration of anti-NC. Last, during virus assembly, NC needs to selectively recruit the genomic RNA among a large excess of cellular RNAs. However, such a selective mechanism is carried out by the NC domain of Gag and not by the free NC protein and is still poorly understood. [129].

In spite of these difficulties, several strategies have already been designed to inhibit NC. Various classes of zinc ejectors have been developed. These molecules covalently react with the Cys ligands of the ZFs, causing zinc ejection and NC unfolding. These compounds are efficient and result in a loss of virus infectivity. However, they suffer from a lack of selectivity but may be promising in inactivating viruses for HIV vaccine trials. More recent strategies are directed at inhibiting the two main functions of NC, namely the chaperoning of RT during viral DNA synthesis and the specific recognition of the ψ packaging signal necessary during virus assembly [73]. These strategies include the use of small molecules (selected by screening), peptidomimetics, DNA binders and intercalators, as well as RNA aptamers. Though promising preliminary results have been obtained, more extensive studies are required to better understand their mechanism and structure activity relationships to improve their bioavailability and demonstrate their potential use in clinical trials against HIV-1 infection and pathogenesis.

ACKNOWLEDGEMENTS

This work has been supported by the EC (TRIoH), INSERM, ANRS and SIDACTION. VS and SA are supported by TRIoH and the FRM, respectively.

REFERENCES

[1] Chen, M. ; Garon, C. F. ; Papas, T. S. *Proc Natl Acad Sci U S A*, **1980**, *77*, 1296.
[2] Pager, J. ; Coulaud, D. ; Delain, E. *J Virol*, **1994**, *68*, 223.
[3] Darlix, J. L. ; Lapadat-Tapolsky, M. ; de Rocquigny, H. ; Roques, B. P. *J Mol Biol*, **1995**, *254*, 523.
[4] Davis, J. ; Scherer, M. ; Tsai, W. P. ; Long, C. *J Virol*, **1976**, *18*, 709.
[5] Dickson, C. ; Eisenman, R. ; Fan, H. ; Hunter, E. ; Reich, N. *in (R. Weiss, N. Teich, H.Varmus, J. Coffin), RNA tumor viruses, part 2, 2nd ed. Cold Spring Harbor Laboratory, Cold Spring Harbor, New York.*, **1985**, p513.
[6] Chazal, N. ; Gerlier, D. *Microbiol Mol Biol Rev*, **2003**, *67*, 226.
[7] Freed, E. O. *Trends Microbiol*, **2003**, *11*, 56.
[8] Freed, E. O. ; Mouland, A. J. *Retrovirology*, **2006**, *3*, 77.
[9] Muriaux, D. ; Darlix, J. L. ; Cimarelli, A. *Curr Pharm Des*, **2004**, *10*, 3725.
[10] Arts, E. J. ; Wainberg, M. A. *Adv Virus Res*, **1996**, *46*, 97.
[11] Levin, J. G. ; Guo, J. ; Rouzina, I. ; Musier-Forsyth, K. *Prog Nucleic Acid Res Mol Biol*, **2005**, *80*, 217.
[12] Rein, A. ; Henderson, L. E. ; Levin, J. G. *Trends Biochem Sci*, **1998**, *23*, 297.
[13] Poljak, L. ; Batson, S. M. ; Ficheux, D. ; Roques, B. P. ; Darlix, J. L. ; Kas, E. *J Mol Biol*, **2003**, *329*, 411.
[14] Clever, J. ; Sassetti, C. ; Parslow, T. G. *J Virol*, **1995**, *69*, 2101.
[15] Clever, J. L. ; Mirandar, D., Jr. ; Parslow, T. G. *J Virol*, **2002**, *76*, 12381.
[16] Dannull, J. ; Surovoy, A. ; Jung, G. ; Moelling, K. *Embo J*, **1994**, *13*, 1525.
[17] Darlix, J. L. ; Garrido, J. L. ; Morellet, N. ; Mély, Y. ; de Rocquigny, H. *Adv Pharmacol*, **2007**, *55*, 297
[18] Demene, H. ; Dong, C. Z. ; Ottmann, M. ; Rouyez, M. C. ; Jullian, N. ; Morellet, N. ; Mely, Y. ; Darlix, J. L. ; Fournie-Zaluski, M. C. ; Saragosti, S. ; *et al. Biochemistry*, **1994**, *33*, 11707.
[19] Dorfman, T. ; Luban, J. ; Goff, S. P. ; Haseltine, W. A. ; Gottlinger, H. G. *J Virol*, **1993**, *67*, 6159.
[20] Gorelick, R. J. ; Fu, W. ; Gagliardi, T. D. ; Bosche, W. J. ; Rein, A. ; Henderson, L. E. ; Arthur, L. O. *J Virol*, **1999**, *73*, 8185.
[21] Gorelick, R. J. ; Nigida, S. M., Jr. ; Bess, J. W., Jr. ; Arthur, L. O. ; Henderson, L. E. ; Rein, A. *J Virol*, **1990**, *64*, 3207.

[22] Berg, J. M. *Science*, **1986**, *232*, 485.
[23] Berg, J. M. ; Shi, Y. *Science*, **1996**, *271*, 1081.
[24] Klug, A. ; Schwabe, J. W. *Faseb J*, **1995**, *9*, 597.
[25] Cox, E. H. ; McLendon, G. L. *Curr Opin Chem Biol*, **2000**, *4*, 162.
[26] Mely, Y. ; Cornille, F. ; Fournie-Zaluski, M. C. ; Darlix, J. L. ; Roques, B. P. ; Gerard, D. *Biopolymers*, **1991**, *31*, 899.
[27] Mely, Y. ; De Rocquigny, H. ; Morellet, N. ; Roques, B. P. ; Gerad, D. *Biochemistry*, **1996**, *35*, 5175.
[28] McLendon, G. ; Hull, H. ; Larkin, K. ; Chang, W. *J Biol Inorg Chem*, **1999**, *4*, 171.
[29] South, T. L. ; Blake, P. R. ; Hare, D. R. ; Summers, M. F. *Biochemistry*, **1991**, *30*, 6342.
[30] Turner, B. G. ; Summers, M. F. *J Mol Biol*, **1999**, *285*, 1.
[31] Aldovini, A. ; Young, R. A. *J Virol*, **1990**, *64*, 1920.
[32] Morellet, N. ; de Rocquigny, H. ; Mely, Y. ; Jullian, N. ; Demene, H. ; Ottmann, M. ; Gerard, D. ; Darlix, J. L. ; Fournie-Zaluski, M. C. ; Roques, B. P. *J Mol Biol*, **1994**, *235*, 287.
[33] Darlix, J. L. ; Cristofari, G. ; Rau, M. ; Pechoux, C. ; Berthoux, L. ; Roques, B. *Adv Pharmacol*, **2000**, *48*, 345.
[34] Rice, W. G. ; Schaeffer, C. A. ; Harten, B. ; Villinger, F. ; South, T. L. ; Summers, M. F. ; Henderson, L. E. ; Bess, J. W., Jr. ; Arthur, L. O. ; McDougal, J. S. ; *et al. Nature*, **1993**, *361*, 473.
[35] Chuang, A. J. ; Killam, K. F., Jr. ; Chuang, R. Y. ; Rice, W. G. ; Schaeffer, C. A. ; Mendeleyev, J. ; Kun, E. *FEBS Lett*, **1993**, *326*, 140.
[36] Rice, W. G. ; Schaeffer, C. A. ; Graham, L. ; Bu, M. ; McDougal, J. S. ; Orloff, S. L. ; Villinger, F. ; Young, M. ; Oroszlan, S. ; Fesen, M. R. ; *et al. Proc Natl Acad Sci U S A*, **1993**, *90*, 9721.
[37] Yu, X. ; Hathout, Y. ; Fenselau, C. ; Sowder, R. C., 2nd ; Henderson, L. E. ; Rice, W. G. ; Mendeleyev, J. ; Kun, E. *Chem Res Toxicol*, **1995**, *8*, 586.
[38] Domagala, J. M. ; Bader, J. P. ; Gogliotti, R. D. ; Sanchez, J. P. ; Stier, M. A. ; Song, Y. ; Prasad, J. V. ; Tummino, P. J. ; Scholten, J. ; Harvey, P. ; Holler, T. ; Gracheck, S. ; Hupe, D. ; Rice, W. G. ; Schultz, R. *Bioorg Med Chem*, **1997**, *5*, 569.
[39] Rice, W. G. ; Supko, J. G. ; Malspeis, L. ; Buckheit, R. W., Jr. ; Clanton, D. ; Bu, M. ; Graham, L. ; Schaeffer, C. A. ; Turpin, J. A. ; Domagala, J. ; Gogliotti, R. ; Bader, J. P. ; Halliday, S. M. ; Coren, L. ; Sowder, R. C., 2nd ; Arthur, L. O. ; Henderson, L. E. *Science*, **1995**, *270*, 1194.
[40] Tummino, P. J. ; Scholten, J. D. ; Harvey, P. J. ; Holler, T. P. ; Maloney, L. ; Gogliotti, R. ; Domagala, J. ; Hupe, D. *Proc Natl Acad Sci U S A*, **1996**, *93*, 969.
[41] Rein, A. ; Ott, D. E. ; Mirro, J. ; Arthur, L. O. ; Rice, W. G. ; Henderson, L. E. *Leukemia*, **1997**, *11 Suppl 3*, 106.
[42] Tummino, P. J. ; Harvey, P. J. ; McQuade, T. ; Domagala, J. ; Gogliotti, R. ; Sanchez, J. ; Song, Y. ; Hupe, D. *Antimicrob Agents Chemother*, **1997**, *41*, 394.
[43] Loo, J. A. ; Holler, T. P. ; Sanchez, J. ; Gogliotti, R. ; Maloney, L. ; Reily, M. D. *J Med Chem*, **1996**, *39*, 4313.
[44] Turpin, J. A. ; Song, Y. ; Inman, J. K. ; Huang, M. ; Wallqvist, A. ; Maynard, A. ; Covell, D. G. ; Rice, W. G. ; Appella, E. *J Med Chem*, **1999**, *42*, 67.
[45] Song, Y. ; Goel, A. ; Basrur, V. ; Roberts, P. E. ; Mikovits, J. A. ; Inman, J. K. ; Turpin, J. A. ; Rice, W. G. ; Appella, E. *Bioorg Med Chem*, **2002**, *10*, 1263.
[46] Srivastava, P. ; Schito, M. ; Fattah, R. J. ; Hara, T. ; Hartman, T. ; Buckheit, R. W., Jr. ; Turpin, J. A. ; Inman, J. K. ; Appella, E. *Bioorg Med Chem*, **2004**, *12*, 6437.
[47] Schito, M. L. ; Goel, A. ; Song, Y. ; Inman, J. K. ; Fattah, R. J. ; Rice, W. G. ; Turpin, J. A. ; Sher, A. ; Appella, E. *AIDS Res Hum Retroviruses*, **2003**, *19*, 91.
[48] Jenkins, L. M. ; Byrd, J. C. ; Hara, T. ; Srivastava, P. ; Mazur, S. J. ; Stahl, S. J. ; Inman, J. K. ; Appella, E. ; Omichinski, J. G. ; Legault, P. *J Med Chem*, **2005**, *48*, 2847.
[49] Rice, W. G. ; Baker, D. C. ; Schaeffer, C. A. ; Graham, L. ; Bu, M. ; Terpening, S. ; Clanton, D. ; Schultz, R. ; Bader, J. P. ; Buckheit, R. W., Jr. ; Field, L. ; Singh, P. K. ; Turpin, J. A. *Antimicrob Agents Chemother*, **1997**, *41*, 419.
[50] Mayasundari, A. ; Rice, W. G. ; Diminnie, J. B. ; Baker, D. C. *Bioorg Med Chem*, **2003**, *11*, 3215.
[51] Vandevelde, M. ; Witvrouw, M. ; Schmit, J. C. ; Sprecher, S. ; De Clercq, E. ; Tassignon, J. P. *AIDS Res Hum Retroviruses*, **1996**, *12*, 567.
[52] Rice, W. G. ; Turpin, J. A. ; Huang, M. ; Clanton, D. ; Buckheit, R. W., Jr. ; Covell, D. G. ; Wallqvist, A. ; McDonnell, N. B. ; De-Guzman, R. N. ; Summers, M. F. ; Zalkow, L. ; Bader, J. P. ; Haugwitz, R. D. ; Sausville, E. A. *Nat Med*, **1997**, *3*, 341.
[53] Turpin, J. A. ; Terpening, S. J. ; Schaeffer, C. A. ; Yu, G. ; Glover, C. J. ; Felsted, R. L. ; Sausville, E. A. ; Rice, W. G. *J Virol*, **1996**, *70*, 6180.
[54] Bombarda, E. ; Cherradi, H. ; Morellet, N. ; Roques, B. P. ; Mely, Y. *Biochemistry*, **2002**, *41*, 4312.
[55] de Rocquigny, H. ; Ficheux, D. ; Gabus, C. ; Fournie-Zaluski, M. C. ; Darlix, J. L. ; Roques, B. P. *Biochem Biophys Res Commun*, **1991**, *180*, 1010.
[56] Chertova, E. N. ; Kane, B. P. ; McGrath, C. ; Johnson, D. G. ; Sowder, R. C., 2nd ; Arthur, L. O. ; Henderson, L. E. *Biochemistry*, **1998**, *37*, 17890.
[57] Basrur, V. ; Song, Y. ; Mazur, S. J. ; Higashimoto, Y. ; Turpin, J. A. ; Rice, W. G. ; Inman, J. K. ; Appella, E. *J Biol Chem*, **2000**, *275*, 14890.
[58] Jenkins, L. M. ; Durell, S. R. ; Maynard, A. T. ; Stahl, S. J. ; Inman, J. K. ; Appella, E. ; Legault, P. ; Omichinski, J. G. *J Am Chem Soc*, **2006**, *128*, 11964.
[59] Maynard, A. T. ; Huang, M. ; Rice, W. G. ; Covell, D. G. *Proc Natl Acad Sci U S A*, **1998**, *95*, 11578.
[60] Huang, M. ; Maynard, A. ; Turpin, J. A. ; Graham, L. ; Janini, G. M. ; Covell, D. G. ; Rice, W. G. *J Med Chem*, **1998**, *41*, 1371.
[61] Whittal, R. M. ; Benz, C. C. ; Scott, G. ; Semyonov, J. ; Burlingame, A. L. ; Baldwin, M. A. *Biochemistry*, **2000**, *39*, 8406.
[62] Wu, X. ; Bishopric, N. H. ; Discher, D. J. ; Murphy, B. J. ; Webster, K. A. *Mol Cell Biol*, **1996**, *16*, 1035.
[63] Wang, L. H. ; Yang, X. Y. ; Zhang, X. ; Mihalic, K. ; Fan, Y. X. ; Xiao, W. ; Howard, O. M. ; Appella, E. ; Maynard, A. T. ; Farrar, W. L. *Nat Med*, **2004**, *10*, 40.
[64] Maynard, A. T. ; Covell, D. G. *J Am Chem Soc*, **2001**, *123*, 1047.
[65] Lever, A. ; Gottlinger, H. ; Haseltine, W. ; Sodroski, J. *J Virol*, **1989**, *63*, 4085.
[66] Berkhout, B. *Prog Nucleic Acid Res Mol Biol*, **1996**, *54*, 1.
[67] Berkhout, B. ; van Wamel, J. L. *Rna*, **2000**, *6*, 282.
[68] Amarasinghe, G. K. ; De Guzman, R. N. ; Turner, R. B. ; Summers, M. F. *J Mol Biol*, **2000**, *299*, 145.
[69] De Guzman, R. N. ; Wu, Z. R. ; Stalling, C. C. ; Pappalardo, L. ; Borer, P. N. ; Summers, M. F. *Science*, **1998**, *279*, 384.
[70] Morellet, N. ; Demene, H. ; Teilleux, V. ; Huynh-Dinh, T. ; de Rocquigny, H. ; Fournie-Zaluski, M. C. ; Roques, B. P. *J Mol Biol*, **1998**, *283*, 419.
[71] Dong, C. Z. ; De Rocquigny, H. ; Remy, E. ; Mellac, S. ; Fournie-Zaluski, M. C. ; Roques, B. P. *J Pept Res*, **1997**, *50*, 269.
[72] Berthoux, L. ; Pechoux, C. ; Darlix, J. L. *J Virol*, **1999**, *73*, 10000.
[73] Grigorov, B. ; Arcanger, F. ; Roingeard, P. ; Darlix, J. L. ; Muriaux, D. *J Mol Biol*, **2006**, *359*, 848.
[74] Lifson, J. D. ; Piatak, M., Jr. ; Rossio, J. L. ; Bess, J., Jr. ; Chertova, E. ; Schneider, D. ; Kiser, R. ; Coalter, V. ; Poore, B. ; Imming, R. ; Desrosiers, R. C. ; Henderson, L. E. ; Arthur, L. O. *J Med Primatol*, **2002**, *31*, 205.
[75] Rossio, J. L. ; Esser, M. T. ; Suryanarayana, K. ; Schneider, D. K. ; Bess, J. W., Jr. ; Vasquez, G. M. ; Wiltrout, T. A. ; Chertova, E. ; Grimes, M. K. ; Sattentau, Q. ; Arthur, L. O. ; Henderson, L. E. ; Lifson, J. D. *J Virol*, **1998**, *72*, 7992.
[76] Beltz, H. ; Clauss, C. ; Piemont, E. ; Ficheux, D. ; Gorelick, R. J. ; Roques, B. ; Gabus, C. ; Darlix, J. L. ; de Rocquigny, H. ; Mely, Y. *J Mol Biol*, **2005**, *348*, 1113.
[77] Druillennec, S. ; Caneparo, A. ; de Rocquigny, H. ; Roques, B. P. *J Biol Chem*, **1999**, *274*, 11283.
[78] Lener, D. ; Tanchou, V. ; Roques, B. P. ; Le Grice, S. F. ; Darlix, J. L. *J Biol Chem*, **1998**, *273*, 33781.
[79] Bampi, C. ; Bibillo, A. ; Wendeler, M. ; Divita, G. ; Gorelick, R. J. ; Le Grice, S. F. ; Darlix, J. L. *J Biol Chem*, **2006**, *281*, 11736.
[80] Morcock, D. R. ; Thomas, J. A. ; Gagliardi, T. D. ; Gorelick, R. J. ; Roser, J. D. ; Chertova, E. N. ; Bess, J. W., Jr. ; Ott, D. E. ; Sattentau, Q. J. ; Frank, I. ; Pope, M. ; Lifson, J. D. ; Henderson, L. E. ; Crise, B. J. *J Virol*, **2005**, *79*, 1533.
[81] Arthur, L. O. ; Bess, J. W., Jr. ; Chertova, E. N. ; Rossio, J. L. ; Esser, M. T. ; Benveniste, R. E. ; Henderson, L. E. ; Lifson, J. D. *AIDS Res Hum Retroviruses*, **1998**, *14 Suppl 3*, S311.
[82] Chertova, E. ; Chertov, O. ; Coren, L. V. ; Roser, J. D. ; Trubey, C. M. ; Bess, J. W., Jr. ; Sowder, R. C., 2nd ; Barsov, E. ; Hood, B. L.

; Fisher, R. J. ; Nagashima, K. ; Conrads, T. P. ; Veenstra, T. D. ; Lifson, J. D. ; Ott, D. E. *J Virol*, **2006**, *80*, 9039.
[83] Lifson, J. D. ; Rossio, J. L. ; Piatak, M., Jr. ; Bess, J., Jr. ; Chertova, E. ; Schneider, D. K. ; Coalter, V. J. ; Poore, B. ; Kiser, R. F. ; Imming, R. J. ; Scarzello, A. J. ; Henderson, L. E. ; Alvord, W. G. ; Hirsch, V. M. ; Benveniste, R. E. ; Arthur, L. O. *AIDS Res Hum Retroviruses*, **2004**, *20*, 772.
[84] Schito, M. L. ; Soloff, A. C. ; Slovitz, D. ; Trichel, A. ; Inman, J. K. ; Appella, E. ; Turpin, J. A. ; Barratt-Boyes, S. M. *Curr HIV Res*, **2006**, *4*, 379.
[85] Tassignon, J. ; Ismaili, J. ; Le Moine, A. ; Van Laethem, F. ; Leo, O. ; Vandevelde, M. ; Goldman, M. *Nat Med*, **1999**, *5*, 947.
[86] Goebel, F. D. ; Hemmer, R. ; Schmit, J. C. ; Bogner, J. R. ; de Clercq, E. ; Witvrouw, M. ; Pannecouque, C. ; Valeyev, R. ; Vandevelde, M. ; Margery, H. ; Tassignon, J. P. *Aids*, **2001**, *15*, 33.
[87] De Clercq, E. *Med Res Rev*, **2002**, *22*, 531.
[88] Stephen, A. G. ; Worthy, K. M. ; Towler, E. ; Mikovits, J. A. ; Sei, S. ; Roberts, P. ; Yang, Q. E. ; Akee, R. K. ; Klausmeyer, P. ; McCloud, T. G. ; Henderson, L. ; Rein, A. ; Covell, D. G. ; Currens, M. ; Shoemaker, R. H. ; Fisher, R. J. *Biochem Biophys Res Commun*, **2002**, *296*, 1228.
[89] Fisher, R. J. ; Rein, A. ; Fivash, M. ; Urbaneja, M. A. ; Casas-Finet, J. R. ; Medaglia, M. ; Henderson, L. E. *J Virol*, **1998**, *72*, 1902.
[90] Vuilleumier, C. ; Bombarda, E. ; Morellet, N. ; Gerard, D. ; Roques, B. P. ; Mely, Y. *Biochemistry*, **1999**, *38*, 16816.
[91] Cruceanu, M. ; Stephen, A. G. ; Beuning, P. J. ; Gorelick, R. J. ; Fisher, R. J. ; Williams, M. C. *Anal Biochem*, **2006**, *358*, 159.
[92] Azoulay, J. ; Clamme, J. P. ; Darlix, J. L. ; Roques, B. P. ; Mely, Y. *J Mol Biol*, **2003**, *326*, 691.
[93] Beltz, H. ; Azoulay, J. ; Bernacchi, S. ; Clamme, J. P. ; Ficheux, D. ; Roques, B. ; Darlix, J. L. ; Mely, Y. *J Mol Biol*, **2003**, *328*, 95.
[94] Bernacchi, S. ; Stoylov, S. ; Piemont, E. ; Ficheux, D. ; Roques, B. P. ; Darlix, J. L. ; Mely, Y. *J Mol Biol*, **2002**, *317*, 385.
[95] Ramstrom, H. ; Bourotte, M. ; Philippe, C. ; Schmitt, M. ; Haiech, J. ; Bourguignon, J. J. *J Med Chem*, **2004**, *47*, 2264.
[96] Hermann, T. ; Westhof, E. *Curr Opin Biotechnol*, **1998**, *9*, 66.
[97] Guo, J. ; Wu, T. ; Bess, J. ; Henderson, L. E. ; Levin, J. G. *J Virol*, **1998**, *72*, 6716.
[98] Davis, W. R. ; Gabbara, S. ; Hupe, D. ; Peliska, J. A. *Biochemistry*, **1998**, *37*, 14213.
[99] Jeeninga, R. E. ; Huthoff, H. T. ; Gultyaev, A. P. ; Berkhout, B. *Nucleic Acids Res*, **1998**, *26*, 5472.
[100] Temin, H. M. *Virology*, **1963**, *20*, 235.
[101] Temin, H. M. *Virology*, **1963**, *20*, 577.
[102] Gerwin, B. I. ; Levin, J. G. *J Virol*, **1977**, *24*, 478.
[103] Gillespie, E. L. ; Kuti, J. L. ; Nicolau, D. P. *Expert Opin Drug Metab Toxicol*, **2005**, *1*, 351.
[104] Turner, K. B. ; Hagan, N. A. ; Fabris, D. *Nucleic Acids Res*, **2006**, *34*, 1305.
[105] Turner, K. B. ; Hagan, N. A. ; Kohlway, A. S. ; Fabris, D. *J Am Soc Mass Spectrom*, **2006**, *17*, 1401.
[106] Fourmy, D. ; Recht, M. I. ; Blanchard, S. C. ; Puglisi, J. D. *Science*, **1996**, *274*, 1367.
[107] Wallis, M. G. ; von Ahsen, U. ; Schroeder, R. ; Famulok, M. *Chem Biol*, **1995**, *2*, 543.
[108] Faber, C. ; Sticht, H. ; Schweimer, K. ; Rosch, P. *J Biol Chem*, **2000**, *275*, 20660.
[109] Kameoka, M. ; Morgan, M. ; Binette, M. ; Russell, R. S. ; Rong, L. ; Guo, X. ; Mouland, A. ; Kleiman, L. ; Liang, C. ; Wainberg, M. A. *J Virol*, **2002**, *76*, 3637.
[110] Summers, M. F. ; Henderson, L. E. ; Chance, M. R. ; Bess, J. W., Jr. ; South, T. L. ; Blake, P. R. ; Sagi, I. ; Perez-Alvarado, G. ; Sowder, R. C., 3rd ; Hare, D. R. ; *et al. Protein Sci*, **1992**, *1*, 563.
[111] Morellet, N. ; Jullian, N. ; De Rocquigny, H. ; Maigret, B. ; Darlix, J. L. ; Roques, B. P. *Embo J*, **1992**, *11*, 3059.
[112] Morellet, N. ; Meudal, H. ; Bouaziz, S. ; Roques, B. P. *Biochem J*, **2006**, *393*, 725.
[113] Schuler, W. ; Dong, C. ; Wecker, K. ; Roques, B. P. *Biochemistry*, **1999**, *38*, 12984.
[114] D'Souza, V. ; Summers, M. F. *Nature*, **2004**, *431*, 586.
[115] Delahunty, M. D. ; South, T. L. ; Summers, M. F. ; Karpel, R. L. *Biochemistry*, **1992**, *31*, 6461.
[116] Ottmann, M. ; Gabus, C. ; Darlix, J. L. *J Virol*, **1995**, *69*, 1778.
[117] Druillennec, S. ; Meudal, H. ; Roques, B. P. ; Fournie-Zaluski, M. C. *Bioorg Med Chem Lett*, **1999**, *9*, 627.
[118] Druillennec, S. ; Roques, B. P. *Drug News Perspect*, **2000**, *13*, 337.
[119] Pustowka, A. ; Dietz, J. ; Ferner, J. ; Baumann, M. ; Landersz, M. ; Konigs, C. ; Schwalbe, H. ; Dietrich, U. *Chembiochem*, **2003**, *4*, 1093.
[120] Azzazy, H. M. ; Highsmith, W. E., Jr. *Clin Biochem*, **2002**, *35*, 425.
[121] Raja, C. ; Ferner, J. ; Dietrich, U. ; Avilov, S. ; Ficheux, D. ; Darlix, J. L. ; de Rocquigny, H. ; Schwalbe, H. ; Mely, Y. *Biochemistry*, **2006**, *45*, 9254.
[122] Sakaguchi, K. ; Zambrano, N. ; Baldwin, E. T. ; Shapiro, B. A. ; Erickson, J. W. ; Omichinski, J. G. ; Clore, G. M. ; Gronenborn, A. M. ; Appella, E. *Proc Natl Acad Sci U S A*, **1993**, *90*, 5219.
[123] McBride, M. S. ; Panganiban, A. T. *J Virol*, **1996**, *70*, 2963.
[124] Tuerk, C. ; Gold, L. *Science*, **1990**, *249*, 505.
[125] Allen, P. ; Collins, B. ; Brown, D. ; Hostomsky, Z. ; Gold, L. *Virology*, **1996**, *225*, 306.
[126] Berglund, J. A. ; Charpentier, B. ; Rosbash, M. *Nucleic Acids Res*, **1997**, *25*, 1042.
[127] Kim, M. Y. ; Jeong, S. *Biochem Biophys Res Commun*, **2004**, *320*, 1181.
[128] Lochrie, M. A. ; Waugh, S. ; Pratt, D. G., Jr. ; Clever, J. ; Parslow, T. G. ; Polisky, B. *Nucleic Acids Res*, **1997**, *25*, 2902.
[129] Cruceanu, M. ; Urbaneja, M. A. ; Hixson, C. V. ; Johnson, D. G. ; Datta, S. A. ; Fivash, M. J. ; Stephen, A. G. ; Fisher, R. J. ; Gorelick, R. J. ; Casas-Finet, J. R. ; Rein, A. ; Rouzina, I. ; Williams, M. C. *Nucleic Acids Res*, **2006**, *34*, 593.
[130] Krishnamoorthy, G. ; Roques, B. ; Darlix, J. L. ; Mely, Y. *Nucleic Acids Res*, **2003**, *31*, 5425.
[131] Lapadat-Tapolsky, M. ; Pernelle, C. ; Borie, C. ; Darlix, J. L. *Nucleic Acids Res*, **1995**, *23*, 2434.

Received: 29 December, 2006 **Revised: 13 July, 2007** **Accepted: 26 July, 2007**

Identification by high throughput screening of small compounds inhibiting the chaperone activity of the HIV-1 nucleocapsid protein

Volodymyr Shvadchak[1], Sarah Sanglier[2], Sandrine Rocle[1], Pascal Villa[3,4], Jacques Haiech[3,4], Marcel Hibert[3], Alain Van Dorsselaer[2], Yves Mély[1] and Hugues de Rocquigny[1,*]

[1] Laboratoire de Biophotonique et Pharmacologie, UMR 7213 CNRS, Université de Strasbourg, Faculté de Pharmacie, 74 route du Rhin, 67401 Illkirch, France
[2] Laboratoire de Spectrométrie de Masse Bio-Organique, IPHC-DSA, ULP, CNRS, UMR7178 CNRS , ECPM 25 rue Becquerel, 67087 Strasbourg, France
[3] Laboratoire d'Innovation Thérapeutique UMR 7200 CNRS-Université de Strasbourg, Faculté de Pharmacie, 74 route du Rhin, 67401 ILLKIRCH
[4] PCBIS (Plate-forme de Chimie Biologique Intégrative de Strasbourg) /IFR85 CNRS/Université Louis Pasteur, ESBS, Parc d'Innovation, Bld Sébastien Brandt, 67401 Illkirch Cedex, France

Acknowledgments: This work was funded by the European Community via TRIoH and by ANRS and SIDACTION. VS was supported by an Eiffel fellowship. We wish to thank ULP, INSERM, CNRS for support and Jean-Jacques Bourguignon for chemical synthesis of active compounds.

* Corresponding author : Hugues de Rocquigny, Laboratoire de Biophotonique et Pharmacologie, UMR 7213 CNRS, Université de Strasbourg, Faculté de Pharmacie, 74 route du Rhin, 67401 Illkirch, France Tel : +33 (0)3 90 24 41 03 Fax : +33 (0)3 90 24 43 12
e-mail: hderocquigny@pharma.u-strasbg.fr

Key words: NCp7, inhibitor, chemical library, fluorescence, HIV, electrospray ionisation mass spectrometry, high throughput screening

Abstract

Due to its highly conserved zinc fingers and its nucleic acid chaperone properties which are critical for HIV-1 replication, the nucleocapsid protein (NC) constitutes a major target in AIDS therapy. Different families of molecules targeting NC zinc fingers and/or inhibiting the binding of NC with its target nucleic acids have been developed. However, their limited specificity and their cellular toxicity prompted us to develop a screening assay to target molecules able to inhibit NC chaperone properties, and more specifically the initial NC-promoted destabilization of nucleic acid secondary structures. Since this destabilization is critically dependent on the properly folded fingers, the developed assay is thought to be highly specific. The assay was based on the use of cTAR DNA, a stem-loop sequence complementary to the transactivation response element, doubly labelled at its 5' and 3' ends by a rhodamine 6G fluorophore and a fluorescence quencher, respectively. Addition of NC(12-55), a peptide corresponding to the zinc finger domain of NC, to this doubly labelled cTAR, led to a partial melting of cTAR stem, which increases the distance between the two labels and thus, restores the rhodamine 6G fluorescence. Thus, positive hits were detected through the decrease of rhodamine 6G fluorescence. An "in-house" chemical library of 4800 molecules was screened and five compounds with IC_{50} values in the low micromolar range have been selected. The hits were shown by mass spectrometry and fluorescence anisotropy titration to prevent binding of NC to cTAR through direct interaction with the NC folded fingers, but without promoting zinc ejection. These non zinc ejecting NC binders are a new series of anti NC molecules that could be used to rationally design molecules with potential antiviral activities.

Introduction

The nucleocapsid protein of HIV (NCp7) is a small and basic protein which contains two highly conserved CCHC boxes folded around two strongly bound zinc atoms[1-3]. NC is critically involved in both the early and late steps of the HIV-1 cycle, mainly through its ability to chaperone nucleic acids toward their most stable conformation [4]. These NC chaperone properties are notably essential during reverse transcription to anneal the primer tRNA to the RNA primer binding site (PBS) and to promote the two obligatory strand transfers (for a review, see [5-9]) are required for copying the HIV-1 RNA genome into double-stranded DNA. Thus, NC appears as an ideal target for the development of new compounds able to inhibit the HIV-1 replication cycle and complement the so-called 'highly active anti-retroviral therapies' (HAART) based on drugs targeting the viral reverse transcriptase (RT) and protease (PR). In addition, since NC is highly conserved in all HIV-1 subtypes [10] anti-NC drugs are expected to provide a sustained replication inhibition of a large panel of HIV-1 strains including those which are resistant to anti-RT and anti-PR drugs.

Several strategies have been already developed against NC [11]. The most popular strategy was based on zinc ejectors such as 3-nitrobenzamide (NOBA), disulfide-substituted benzamides (DIBA) or pyridinioalkanoyl thiolesters derivatives (PATE) [12-15]. These compounds eject the zinc ions from NC and exhibit a broad anti-viral activity towards laboratory and clinical HIV-1 isolates [16-18]. Interestingly, these compounds show some virucidal properties in primate models but their effect on cellular zinc finger proteins leads to toxicity and poor specificity [19-21]. Alternative approaches, using small Trp-containing peptides [22-24] RNA aptamers [25] or gallein-related compounds [26, 27] have been developed to target the interaction of NC with its nucleic acid targets. However, the efficiency of these approaches in therapeutic applications has not been demonstrated yet.

In the present manuscript, we developed a new strategy to select molecules able to inhibit NC nucleic acid chaperone activity. This activity can be divided in three different components, binding of NC to the nucleic acid sequence, destabilization of the nucleic acid secondary structure and promotion of the annealing of the destabilized complementary sequences [7, 8]. Interestingly, the destabilization step is mediated through the specific binding of the hydrophobic platform at the top of the properly folded zinc fingers of NC [28-31]. In this respect, our objective was to develop a highly specific high throughput screening (HTS) assay to select compounds able to block the NC-mediated destabilization of the stem-loop structure of cTAR DNA, the complementary sequence of the transactivation response element, involved in minus strand DNA transfer during reverse transcription [32-35] . An "in house" chemical library containing 4800 molecules with a large diversity of structures [36, 37] was screened on this assay. Five positive hits with low micromolar range K_i were identified. Electrospray ionization mass spectroscopy and fluorescence anisotropy titration data further indicated that the hits prevent the binding of NC to cTAR through direct interaction with the NC folded fingers, but without promoting zinc ejection.

Materials and Methods

Reagents

NC(12-55) was synthesised and purified as reported [38]. To determine the peptide concentration, an extinction coefficient of 5700 M^{-1} cm^{-1} at 280 nm was used. Peptide was lyophilised and stored at -20°C.

Oligonucleotides were synthesised at a 2 µmole scale and HPLC-purified by IBA GmbH Nucleic Acid Product Support Supply (Göttingen, Germany). For HTS, we used cTAR labelled at the 5' and 3' terminus by 6-carboxyrhodamine (Rh6G) and 4-(4'-dimethylaminophenylazo)benzoic acid (DABCYL) (Rh6G-cTAR-DABCYL) while for fluorescence anisotropy experiments, we used cTAR labeled at their 5' end by 5(and 6)-carboxyfluorescein (Fl-cTAR). To calculate the cTAR concentration, an extinction coefficient of 521,900 M^{-1} cm^{-1} at 260 nm was used [33].

Binding experiments were carried out in 25 mM Tris-HCl (pH 7.5), 30 mM NaCl and 0.2 mM $MgCl_2$ (referred to as binding buffer) [34].

High throughput screening

HTS was performed with an "in house" chemical library that contains 4800 molecules with a large diversity of structures such as heterocyclic molecules, small peptides and amino acid derivatives [36, 37]. This library is available in 96-well plates (Costar® 3686) with 80 molecules and 16 empty wells for controls. Each compound was dissolved in DMSO to a concentration of 10 mM and the plates were stored at -20°C. For the screening, each substance from the stock plates was first diluted to 100 µM in the binding buffer, and then added to 0.1 µM cTAR. Finally, 1.1 µM NC(12-55) was added to the mixture and plates were incubated for 15 minutes at room temperature before reading. The final volume in each well was 50 µl. Dilution and mixing of all components was carried out using a Biomek 2000 workstation (Beckman Coulter). Control wells contained the same percentage of DMSO as the wells with the library molecules (one percent v/v). The fluorescent signals were recorded using a microplate reader Victor ^{2} 1420 (Wallac Perkin Elmer) with 485 and 535 nm as excitation and emission wavelengths. On each plate, the controls with labelled cTAR in the absence and in the presence of NC(12-55) were used to calculate the value of the NC(12-55)-induced fluorescence increase. The percentage of inhibition by a given molecule from the library was calculated in comparison to this value. The hit threshold was set at 100% inhibition. From the ratios obtained with the controls on each plate, the Z' factor, a statistical coefficient reflecting the quality of the assay [39] was calculated. This coefficient that integrates a number of parameters such as the signal to noise ratio and data dispersion was used to accept or reject the data of a given plate. The stability of the measured fluorescence was tested as a function of time and no significant change in the fluorescence was observed for 30 min. Confirmation of the primary hits was performed in duplicate at 1 and 10µM.

Inhibition and Competition experiments

Fluorescence intensity and anisotropy measurements were performed on a FluoroMax3 and a SLM 48000 spectrofluorometer, respectively.

Inhibition of NC(12-55)-induced cTAR melting was monitored by adding increasing concentrations (10^{-4}-10^{-7} M) of the selected hit to a mixture of 0.1 µM Rh6G-cTAR-DABCYL and 1.1 µM NC(12-55). Each hit concentration was tested in triplicate. To check the importance of the addition order, each hit was either pre-incubated with the doubly labelled cTAR for ten minutes before addition of NC(12-55) or incubated with pre-formed NC(12-55)-cTAR complex. To calculate the IC50 values, the experimental data were fitted using the Origin software with the equation:

$$I(C_{INH}) = Io + \frac{If - Io}{1 + (IC_{50} / C_{INH})^{P}} \qquad (1)$$

where I_0 and I_f are respectively the initial and final fluorescence, C_{INH} is the concentration of the inhibitor and p is the Hill coefficient. To deduce the inhibition constant, K_i, the Cheng and Prussof equation [40] was used:

$$K_i = \frac{IC_{50}}{1 + [cTAR]/K_d} \qquad (2)$$

with [cTAR] = 100 nM and $K_d = 5.9\times10^{-8}$ M [28].

Dissociation constants of the complexes of NC(12-55) with the inhibitors were obtained from fluorescence anisotropy titrations of 0.1µM Fl-cTAR by NC(12-55) in the presence and in the absence of an excess of inhibitors (30 µM). In a first approach, the titration curves were fitted with:

$$r = r_0 - \frac{(r_0 - r_t)K_{dapp}}{2nN} \cdot \left[(1 + (nN + P)/K_{dapp}) - \sqrt{(1 + (nN + P)/K_{dapp})^2 - 4nPN/K_{dapp}^2}\right] \qquad (3)$$

where r and r_t are the fluorescence anisotropy at a given and a saturating protein concentration, respectively, r_0 is the anisotropy in the absence of NC, N is the total oligonucleotide concentration, P is the total concentration of the protein and n is the number of NC(12-55)-binding sites [41]. In the absence of inhibitor, K_{dapp} is equal to the dissociation constant K_d of the complex of NC(12-55) with cTAR. In the presence of inhibitor, K_{dapp} is equal to $(1+C_{INH}/K_{d'})/K_a$, where C_{INH} is the inhibitor concentration and $K_{d'}$ is the dissociation constant of the NC(12-55)/inhibitor complex. Alternatively, the titration curves were fitted assuming a competitive binding of the peptide to inhibitor and Fl-cTAR using the Dynafit software [42] that allows numerical simulation of equilibrium systems.

Electrospray ionization mass spectrometry

Mass analyses were performed using an ESI-TOF mass spectrometer (LCT, Micromass, Manchester, UK) calibrated with horse heart myoglobin (Sigma Aldrich). Samples were continuously infused into the ESI ion source at a flow rate of 6 µl/minute. Both gas and source temperatures were set at 80°C. ESI-mass spectra were deconvoluted using the MaxEnt3 algorithm provided by the MassLynx software.

Purity and homogeneity of NC(12-55) was verified by mass analysis in denaturing conditions. The protein was diluted to 5 pmol/µL in a 1:1 water–acetonitrile mixture (v/v) acidified with 1% formic acid. In these conditions the noncovalent interactions are suppressed, which allows the measurement of the molecular weight of the apo form of NC (zinc-free protein) with a good precision (better than 0.01%). Mass spectra were recorded in the positive ion mode on the mass range 200–3000 m/z. Accelerating voltage was set to 25 V and the pressure in the interface region of the mass spectrometer was 1.4 mbar. In this condition, a mass of 5009.6 ± 0.1 Da was measured, which is in agreement with the theoretical molecular mass of 5009.8 obtained from the amino acid sequence [38].

For analysis in non-denaturing conditions, NC(12-55) was directly infused in ammonium acetate ($AcNH_4$) 50 mM, pH 7.0, which enables native structure of proteins to be preserved and is compatible with ESI-MS analysis [43]. Samples were diluted to 20 pmol/µL in the previous buffer and continuously infused into the ESI ion source at a flow rate of 5 µL/min.

Interaction of NC(12-55) with hits was performed by adding 5 and 10 molar equivalents of the hits (CO7, HO2, A10, EO3, HO4 and GO8) to a 20 µM NC(12-55) solution diluted in ammonium acetate 50 mM pH 7.0, followed by 30 min incubation at room temperature. Great care was exercised so that the noncovalent interactions survive the ionization/desorption process. To prevent dissociation in the gas phase during the ionization and desorption process,

the cone voltage was optimized to 5–10 V and the pressure in the interface region was optimized to 5 mbar. Pressure and Vc are parameters controlling the energy given to ions in the interface of the mass spectrometer and must be optimized in each case. Mass data were acquired in the positive ion mode on a mass range of 500–3000 m/z. The relative abundance of the different species present on the ESI mass spectra was measured from their respective peak intensities, assuming that the relative intensities displayed by the different species faithfully reflect their actual distribution in solution [44]. The reproducibility of the determination of the relative proportions of the different species was estimated to be ± 2–3%.

Results

Rational design of the screening assay.

FIGURE 1

The assay was based on the use of cTAR labelled at its 5' and 3' ends by a Rh6G fluorophore and a DABCYL fluorescence quencher, respectively (Fig. 1). The NC(12-55) peptide, that corresponds to the finger domain of NC, was preferred to the native NC since it preserves the nucleic acid binding and chaperone properties of the native NC [28, 45] but does not aggregate the oligonucleotides [46]. In the absence of NC(12-55), the proximity of cTAR ends induces a strong fluorescence quenching of Rh6G by the DABCYL group (solid line) [47, 48]. Due to its destabilizing activity, NC(12-55) melts the lower half of the cTAR stem, increasing the distance between the two dyes and thus, eliciting an about six- to seven-fold increase of Rh6G fluorescence (dots). Addition of 1 mM of EDTA, a chelator of divalent ions that fully depletes zinc from NC [2], leads to the restoration of the low initial fluorescence of the doubly labelled cTAR (dashed line). As a consequence, a positive hit able to inhibit the NC chaperone activity will be detected in this assay through the partial or total reversal of the NC(12-55)-induced increase of Rh6G fluorescence. This assay is simple, being based on a one-step mixture of only two partners. Moreover, it is highly sensitive (leading to up to seven-fold decrease in Rh6G fluorescence) and the changes in fluorescence intensities can be read with a basic fluorescence plate-reader.

High-throughput screening results

A library of 4800 substances representing a large range of structures with potential pharmacologic activities [36, 37] was screened on the aforementioned assay. Using a hit threshold of 100% inhibition at 10 µM, five positives were identified (Table 1). The quality of the assay was validated by the average value of 0.854 for the Z' factor [39]. None of these hits was found to affect the fluorescence of the doubly labelled Rh6G-cTAR-DABCYL or the singly labelled Rh6G-cTAR (data not shown), indicating that they do not correspond to false positives that quench the Rh6G fluorescence. The A10, E03 and H04 compounds exhibit a catechol-like moiety with a polar group in the fourth position. CO7 is a pyridazone with an apolar phenyl group. HO2 consists of two phenyl rings connected by a hydrazone spacer.

FIGURE 2, TABLE 1

To compare the inhibitory potency of the selected hits, we determined their inhibition constant K_i (Fig 2). To this end, cTAR was incubated with various hit concentrations under the same experimental conditions as for the screening, prior to the addition of NC(12-55). By plotting the percentage of fluorescence decrease of Rh6G-cTAR-DABCYL as a function of the hit concentration, it was possible to calculate the K_i value of each molecule. All five hits show K_i values in the low µM range. It should be pointed out that, for this calculation, all the compounds were freshly dissolved in DMSO.

FIGURE 3

To explore whether the inhibition of NC chaperone properties was dependent on the order of the addition of the reagents, two different protocols were compared. In one case, the hits were

preincubated with cTAR for ten minutes prior to the addition of NC(12-55) (Fig 3, solid line). In the second case, the hits were added to the pre-formed NC(12-55)- Rh6G-cTAR-DABCYL complex (Fig 3, dotted line). With both protocols, the signal was monitored after 15 minutes. As depicted with CO7 taken as an example, similar inhibition curves were obtained irrespective of the addition order (Fig. 3).
In a next step, we examined the chemical library to find out related compounds and get a preliminary structure activity relationship study. In the case of the thiazolylpyrocatechol (A10), alkylation of the thiazol part induces a complete loss of inhibition, while replacement of the catechol by a phenyl or a fluorophenyl causes a two-fold increase of the K_i value. For the hydroxymethyl phenyl-pyridazone (C07), addition of aminoethylmorpholine or alkylation of the hydroxyl by a β-phenylethyl group results in a strong decrease of the inhibition activity (data not shown).

Binding of the hits to NCp7

To determine the mechanism of NC(12-55) inhibition, electrospray ionization mass spectrometry (ESI-MS) was performed. Using appropriate non-denaturing conditions and carefully controlled instrumental optimization, electrospray ionization (ESI) is able to transfer noncovalent complexes into the gas phase of the mass spectrometer without dissociation [49].
FIGURE 4
Purity and homogeneity of NC(12-55) was first checked by ESI-MS analysis in denaturing conditions (Fig. 4a). The measured molecular mass of 5009.6 ± 0.1 Da was fully consistent with the theoretical mass of the apo-protein (5009.8 Da) deduced from the aminoacid sequence. Under non-denaturing conditions, in ammonium acetate 50 mM, pH 6.8 (Fig 4b), a molecular weight of 5137.4 ± 0.2 Da was measured, which corresponds to the mass of NC(12-55) bound to two zinc ions. At the low accelerating voltages (5-10 V) used in this study, additional TFA adducts (labelled with *) resulting from incomplete ion desolvation are also observed.
Next, using the same conditions, ESI-MS was performed on mixtures of 20 μM NC(12-55) with a 5-fold molar excess of the hits. With CO7 (Fig. 4c), the main species detected (~ 80 %) was the zinc bound NC(12-55), but an additional compound (~ 20 %) with a molecular weight of 5340.2 ± 0.7 Da corresponding to a 1:1 NC(12-55):CO7 noncovalent complex appeared. Raising the concentration of CO7 to 200 μM increased the relative ratio of the NC(12-55):CO7 complexes to ~ 30 % and a peak corresponding to a complex of NC(12-55) with two CO7 appeared (data not shown). Interestingly, no peak with the molecular mass of the apo-protein or its complex with CO7 was observed, indicating that CO7 does not eject zinc.
A direct interaction between NC(12-55) and HO2 was also evidenced from the formation of a 1:1 complex with a measured mass of 5405.2 ± 0.1 Da (Fig.4d). This complex corresponds approximately to 16 % of the species detected on the ESI mass spectrum. Again, raising the HO2 concentration to 200 μM increased the amount of NCp7:HO2 complex to ~23 % and led to a new peak corresponding to the binding of two HO2 molecules per NC(12-55). Similar conclusions were obtained with EO3 (data not shown). In the case of HO4, a more limited interaction was observed since the NC(12-55): HO4 complex represented only about 5 % at 200 μM of the hit (data not shown).
Interestingly, no binding with NC(12-55) was observed using A10 (Fig. 4e), suggesting that this compound binds with only a low affinity or that its complex with the peptide is dissociated in the gas phase. Alternatively, A10 may bind to cTAR or the complex of NC(12-55) with cTAR. Thus, ESI-MS analysis under non-denaturing conditions shows that all the hits with the exception of A10 bind to NC(12-55), forming 1:1 and 1:2 complexes. Since the last complex only appears at the highest tested concentration of the hits, the second binding

site is likely of lower affinity than the first one. Importantly, none of the hits seems to induce zinc ejection.

Competition of the hits with cTAR for binding to NCp7

To determine whether the inhibitory activity of the hits on NC(12-55)-induced cTAR destabilization result from an inhibition of NC(12-55) binding to cTAR, we performed fluorescence anisotropy titrations using fluorescein-labelled cTAR (Fl-cTAR). In the absence of hits, addition of increasing NC(12-55) concentrations leads to a large increase of the fluorescence anisotropy of Fl-cTAR (from 0.06 to 0.18), due to the mass increase of cTAR when it was fully coated with peptides (Fig. 5 squares). Assuming a binding stoichiometry of eight peptides per cTAR, the fit of the titration curve with equation (3) gives a dissociation binding constant $K_d=6\times10^{-6}$ M, in excellent agreement with the literature [28]

FIGURE 5

In the presence of 30 µM CO7 or HO2, the titration curves were strongly shifted to high NC(12-55) concentrations, the strongest effect being seen with the most potent CO7 inhibitor. Using the above mentioned K_d for NC(12-55)/cTAR and assuming that the hits compete with cTAR for the binding to NC(12-55), we could calculate the dissociation constant $K_{d'}$ of the protein-inhibitor complexes, using a numerical simulation method [42] or from the apparent binding constants of NC(12-55) to cTAR in the presence of an excess of inhibitor (equation (3)). With both methods, the obtained $K_{d'}$ values (7.7×10^{-6} M for CO7 and 1.7×10^{-5} M for HO2) were close to the corresponding K_i values calculated from cTAR melting inhibition experiments (Table 1), indicating that the inhibitory activity of these compounds appears to be related to their ability to block the binding sites of NC(12-55) for cTAR .

Discussion

The central role of the nucleocapsid protein during the replication cycle and the inability of the virus to escape from mutations that affect the proper folding of its zinc finger domain explain the sustained effort to develop small inhibitors directed toward this protein. In this work, we screened an 'in house' library using a specific *in vitro* assay based on NC zinc finger-mediated cTAR destabilisation. The developed assay was simple, being based on a one-step mixture, highly sensitive, due to the 6 to 7-fold change in fluorescence that resulted from the inhibition of the NC chaperone activity and highly reproducible, due to the stability of the partners as a function of time. Moreover, this assay appeared more selective than the previously developed assay based on the inhibition of NC binding to a TG-rich oligonucleotide, since it selects compounds inhibiting a NC property directly involved in reverse transcription [27].

Five positive hits with K_i values in the low µM range were selected in this screening. Using the ESI-MS technique in non- denaturing conditions, which has been shown to be appropriate to characterize non covalent complexes with proteins [50-56], including NCp7 [57-60], we found that four out of the five hits can form a stable complex with NC(12-55). Interestingly, none of these compounds was able to eject zinc, in sharp contrast with DIBAs, PATEs, N-ethylmaleimide (NEM) and SAMTs [61]. This lack of zinc ejection by our compounds should avoid the targeting of cellular zinc binding proteins, which caused the toxicity of most anti-NCs based on zinc ejectors.

Non zinc ejecting NC binders have already been identified in previous screenings [26, 27, 62]. These active compounds belong to the family of the gallein derivatives and contain a xanthenyl ring substituted with two hydroxyl groups. Interestingly, two hydroxyl groups are also present in A10, EO3 and HO4, as well as in CO7, taking into account the keto-enol equilibrium of the carbonyl group in the pyridazin ring. By analogy to the gallein derivatives [27], these hydroxyl groups likely play a critical role, since alkylation of one hydroxyl group

of CO7 strongly reduces its ability to bind and inhibit NC. Noticeably, the two hydroxyls are significantly closer in our hits than in the gallein derivatives, being separated only by two or three carbons, while five atoms separated the hydroxyl groups in the gallein derivatives. As a consequence, these hydroxyl groups may not bind to the same NC residues.
Moreover, the hits of our study differ also from the gallein derivatives, by their ability to inhibit NC even when the protein is already bound to cTAR. Indeed, the gallein derivatives exhibit an inhibitory effect against free NC only and can not compete for NC binding with DNAs [26]. In contrast, both the independence of the inhibitory activity of our hits on the addition order of the compounds (Fig. 3) and the NC/cTAR binding experiments in the presence of the hits (Fig. 5) strongly suggested that our hits compete with cTAR for binding to NC. Thus, the gallein derivatives and our hits may have different binding sites on the NC zinc fingers and thus, differ in their inhibition mechanism.
In conclusion, molecules inhibiting NC fraying activity in the low micromolar range were identified. Their inhibitory activity was related to their ability to compete with the nucleic acids for binding to NC zinc fingers. Efforts are currently performed to further characterize their binding site on NC through NMR studies, a critical step to rationally design new compounds with lower K_i values that will be tested for their antiviral activities.

Acknowledgments: This work was funded by the European Community via TRIoH and by ANRS and SIDACTION. VS was supported by an Eiffel fellowship. We wish to thank ULP, INSERM, CNRS for support and Jean-Jacques Bourguignon for chemical synthesis of active compounds.

Abbreviations: HIV, human immunodeficiency virus. NC, nucleocapsid protein. cTAR, complementary DNA sequence of TAR. DABCYL, 4-(4'dimethylaminophenylazo)benzoic acid. 5/6RhG, 5/6carboxyrhodamine. HTS, High Throughput Screening. K_i, inhibition constant. EDTA, ethylene diamine tetraacetic acid, ESI-MS : electrospray ionisation mass spectrometry

References :

[1] E. Bombarda, N. Morellet, H. Cherradi, B. Spiess, S. Bouaziz, E. Grell, B.P. Roques, Y. Mely, Determination of the pK(a) of the four Zn2+-coordinating residues of the distal finger motif of the HIV-1 nucleocapsid protein: consequences on the binding of Zn2+, J Mol Biol 310 (2001) 659-672.
[2] Y. Mely, H. De Rocquigny, N. Morellet, B.P. Roques, D. Gerad, Zinc binding to the HIV-1 nucleocapsid protein: a thermodynamic investigation by fluorescence spectroscopy, Biochemistry 35 (1996) 5175-5182.
[3] M.F. Summers, T.L. South, B. Kim, D.R. Hare, High-resolution structure of an HIV zinc fingerlike domain via a new NMR-based distance geometry approach, Biochemistry 29 (1990) 329-340.
[4] D. Herschlag, RNA chaperones and the RNA folding problem, J Biol Chem 270 (1995) 20871-20874.
[5] P. Barraud, C. Gaudin, F. Dardel, C. Tisne, New insights into the formation of HIV-1 reverse transcription initiation complex, Biochimie 89 (2007) 1204-1210.
[6] J.L. Darlix, G. Cristofari, M. Rau, C. Pechoux, L. Berthoux, B. Roques, Nucleocapsid protein of human immunodeficiency virus as a model protein with chaperoning functions and as a target for antiviral drugs, Adv Pharmacol 48 (2000) 345-372.

[7] J.G. Levin, J. Guo, I. Rouzina, K. Musier-Forsyth, Nucleic acid chaperone activity of HIV-1 nucleocapsid protein: critical role in reverse transcription and molecular mechanism, Prog Nucleic Acid Res Mol Biol 80 (2005) 217-286.
[8] A. Rein, L.E. Henderson, J.G. Levin, Nucleic-acid-chaperone activity of retroviral nucleocapsid proteins: significance for viral replication, Trends Biochem Sci 23 (1998) 297-301.
[9] C. Tisne, B.P. Roques, F. Dardel, The annealing mechanism of HIV-1 reverse transcription primer onto the viral genome, J Biol Chem 279 (2004) 3588-3595.
[10] J.L. Darlix, J.L. Garrido, N. Morellet, Y. Mély, H. de Rocquigny, Properties, Functions, and Drug Targeting of the Multifunctional Nucleocapsid Protein of the Human Immunodeficiency Virus, Adv Pharmacol 55 (2007) 297 - 347.
[11] H. de Rocquigny, V. Shvadchak, S. Avilov, C.Z. Dong, U. Dietrich, J.L. Darlix, Y. Mely, Targeting the viral nucleocapsid protein in anti-HIV-1 therapy, Mini reviews in medicinal chemistry 8 (2008) 24-35.
[12] M. Huang, A. Maynard, J.A. Turpin, L. Graham, G.M. Janini, D.G. Covell, W.G. Rice, Anti-HIV agents that selectively target retroviral nucleocapsid protein zinc fingers without affecting cellular zinc finger proteins, J Med Chem 41 (1998) 1371-1381.
[13] L.M. Jenkins, J.C. Byrd, T. Hara, P. Srivastava, S.J. Mazur, S.J. Stahl, J.K. Inman, E. Appella, J.G. Omichinski, P. Legault, Studies on the mechanism of inactivation of the HIV-1 nucleocapsid protein NCp7 with 2-mercaptobenzamide thioesters, J Med Chem 48 (2005) 2847-2858.
[14] W.G. Rice, J.G. Supko, L. Malspeis, R.W. Buckheit, Jr., D. Clanton, M. Bu, L. Graham, C.A. Schaeffer, J.A. Turpin, J. Domagala, R. Gogliotti, J.P. Bader, S.M. Halliday, L. Coren, R.C. Sowder, 2nd, L.O. Arthur, L.E. Henderson, Inhibitors of HIV nucleocapsid protein zinc fingers as candidates for the treatment of AIDS, Science 270 (1995) 1194-1197.
[15] J.A. Turpin, Y. Song, J.K. Inman, M. Huang, A. Wallqvist, A. Maynard, D.G. Covell, W.G. Rice, E. Appella, Synthesis and biological properties of novel pyridinioalkanoyl thiolesters (PATE) as anti-HIV-1 agents that target the viral nucleocapsid protein zinc fingers, J Med Chem 42 (1999) 67-86.
[16] J.M. Domagala, J.P. Bader, R.D. Gogliotti, J.P. Sanchez, M.A. Stier, Y. Song, J.V. Prasad, P.J. Tummino, J. Scholten, P. Harvey, T. Holler, S. Gracheck, D. Hupe, W.G. Rice, R. Schultz, A new class of anti-HIV-1 agents targeted toward the nucleocapsid protein NCp7: the 2,2'-dithiobisbenzamides, Bioorg Med Chem 5 (1997) 569-579.
[17] W.G. Rice, D.C. Baker, C.A. Schaeffer, L. Graham, M. Bu, S. Terpening, D. Clanton, R. Schultz, J.P. Bader, R.W. Buckheit, Jr., L. Field, P.K. Singh, J.A. Turpin, Inhibition of multiple phases of human immunodeficiency virus type 1 replication by a dithiane compound that attacks the conserved zinc fingers of retroviral nucleocapsid proteins, Antimicrob Agents Chemother 41 (1997) 419-426.
[18] P.J. Tummino, J.D. Scholten, P.J. Harvey, T.P. Holler, L. Maloney, R. Gogliotti, J. Domagala, D. Hupe, The in vitro ejection of zinc from human immunodeficiency virus (HIV) type 1 nucleocapsid protein by disulfide benzamides with cellular anti-HIV activity, Proc Natl Acad Sci U S A 93 (1996) 969-973.
[19] W.G. Rice, J.A. Turpin, M. Huang, D. Clanton, R.W. Buckheit, Jr., D.G. Covell, A. Wallqvist, N.B. McDonnell, R.N. DeGuzman, M.F. Summers, L. Zalkow, J.P. Bader, R.D. Haugwitz, E.A. Sausville, Azodicarbonamide inhibits HIV-1 replication by targeting the nucleocapsid protein, Nat Med 3 (1997) 341-345.
[20] M.L. Schito, A. Goel, Y. Song, J.K. Inman, R.J. Fattah, W.G. Rice, J.A. Turpin, A. Sher, E. Appella, In vivo antiviral activity of novel human immunodeficiency virus type 1 nucleocapsid p7 zinc finger inhibitors in a transgenic murine model, AIDS Res Hum Retroviruses 19 (2003) 91-101.

[21] M.L. Schito, A.C. Soloff, D. Slovitz, A. Trichel, J.K. Inman, E. Appella, J.A. Turpin, S.M. Barratt-Boyes, Preclinical evaluation of a zinc finger inhibitor targeting lentivirus nucleocapsid protein in SIV-infected monkeys, Curr HIV Res 4 (2006) 379-386.
[22] S. Druillennec, C.Z. Dong, S. Escaich, N. Gresh, A. Bousseau, B.P. Roques, M.C. Fournie-Zaluski, A mimic of HIV-1 nucleocapsid protein impairs reverse transcription and displays antiviral activity, Proc Natl Acad Sci U S A 96 (1999) 4886-4891.
[23] C. Raja, J. Ferner, U. Dietrich, S. Avilov, D. Ficheux, J.L. Darlix, H. de Rocquigny, H. Schwalbe, Y. Mely, A Tryptophan-Rich Hexapeptide Inhibits Nucleic Acid Destabilization Chaperoned by the HIV-1 Nucleocapsid Protein, Biochemistry 45 (2006) 9254-9265.
[24] J. Dietz, J. Koch, A. Kaur, C. Raja, S. Stein, M. Grez, A. Pustowka, S. Mensch, J. Ferner, L. Moller, N. Bannert, R. Tampe, G. Divita, Y. Mely, H. Schwalbe, U. Dietrich, Inhibition of HIV-1 by a peptide ligand of the genomic RNA packaging signal Psi, ChemMedChem 3 (2008) 749-755.
[25] S. Druillennec, H. Meudal, B.P. Roques, M.C. Fournie-Zaluski, Nucleomimetic strategy for the inhibition of HIV-1 nucleocapsid protein NCp7 activities, Bioorg Med Chem Lett 9 (1999) 627-632.
[26] M. Cruceanu, A.G. Stephen, P.J. Beuning, R.J. Gorelick, R.J. Fisher, M.C. Williams, Single DNA molecule stretching measures the activity of chemicals that target the HIV-1 nucleocapsid protein, Anal Biochem 358 (2006) 159-170.
[27] A.G. Stephen, K.M. Worthy, E. Towler, J.A. Mikovits, S. Sei, P. Roberts, Q.E. Yang, R.K. Akee, P. Klausmeyer, T.G. McCloud, L. Henderson, A. Rein, D.G. Covell, M. Currens, R.H. Shoemaker, R.J. Fisher, Identification of HIV-1 nucleocapsid protein: nucleic acid antagonists with cellular anti-HIV activity, Biochem Biophys Res Commun 296 (2002) 1228-1237.
[28] H. Beltz, C. Clauss, E. Piemont, D. Ficheux, R.J. Gorelick, B. Roques, C. Gabus, J.L. Darlix, H. de Rocquigny, Y. Mely, Structural determinants of HIV-1 nucleocapsid protein for cTAR DNA binding and destabilization, and correlation with inhibition of self-primed DNA synthesis, J Mol Biol 348 (2005) 1113-1126.
[29] N. Morellet, N. Jullian, H. De Rocquigny, B. Maigret, J.L. Darlix, B.P. Roques, Determination of the structure of the nucleocapsid protein NCp7 from the human immunodeficiency virus type 1 by 1H NMR, Embo J 11 (1992) 3059-3065.
[30] M.F. Summers, L.E. Henderson, M.R. Chance, J.W. Bess, Jr., T.L. South, P.R. Blake, I. Sagi, G. Perez-Alvarado, R.C. Sowder, 3rd, D.R. Hare, et al., Nucleocapsid zinc fingers detected in retroviruses: EXAFS studies of intact viruses and the solution-state structure of the nucleocapsid protein from HIV-1, Protein Sci 1 (1992) 563-574.
[31] S.V. Avilov, E. Piemont, V. Shvadchak, H. de Rocquigny, Y. Mely, Probing dynamics of HIV-1 nucleocapsid protein/target hexanucleotide complexes by 2-aminopurine, Nucleic Acids Res 36 (2008) 885-896.
[32] J. Azoulay, J.P. Clamme, J.L. Darlix, B.P. Roques, Y. Mely, Destabilization of the HIV-1 complementary sequence of TAR by the nucleocapsid protein through activation of conformational fluctuations, J Mol Biol 326 (2003) 691-700.
[33] H. Beltz, J. Azoulay, S. Bernacchi, J.P. Clamme, D. Ficheux, B. Roques, J.L. Darlix, Y. Mely, Impact of the terminal bulges of HIV-1 cTAR DNA on its stability and the destabilizing activity of the nucleocapsid protein NCp7, J Mol Biol 328 (2003) 95-108.
[34] S. Bernacchi, S. Stoylov, E. Piemont, D. Ficheux, B.P. Roques, J.L. Darlix, Y. Mely, HIV-1 nucleocapsid protein activates transient melting of least stable parts of the secondary structure of TAR and its complementary sequence, J Mol Biol 317 (2002) 385-399.
[35] I. Kanevsky, F. Chaminade, D. Ficheux, A. Moumen, R. Gorelick, M. Negroni, J.L. Darlix, P. Fosse, Specific interactions between HIV-1 nucleocapsid protein and the TAR element, J Mol Biol 348 (2005) 1059-1077.

[36] M. Hachet-Haas, N. Converset, O. Marchal, H. Matthes, S. Gioria, J.L. Galzi, S. Lecat, FRET and colocalization analyzer--a method to validate measurements of sensitized emission FRET acquired by confocal microscopy and available as an ImageJ Plug-in, Microscopy research and technique 69 (2006) 941-956.
[37] M. Krier, G. Bret, D. Rognan, Assessing the scaffold diversity of screening libraries, Journal of chemical information and modeling 46 (2006) 512-524.
[38] H. De Rocquigny, C. Gabus, A. Vincent, M.C. Fournie-Zaluski, B. Roques, J.L. Darlix, Viral RNA annealing activities of human immunodeficiency virus type 1 nucleocapsid protein require only peptide domains outside the zinc fingers, Proc Natl Acad Sci U S A 89 (1992) 6472-6476.
[39] J.H. Zhang, T.D. Chung, K.R. Oldenburg, A Simple Statistical Parameter for Use in Evaluation and Validation of High Throughput Screening Assays, J Biomol Screen 4 (1999) 67-73.
[40] Y. Cheng, W.H. Prusoff, Relationship between the inhibition constant (K1) and the concentration of inhibitor which causes 50 per cent inhibition (I50) of an enzymatic reaction, Biochemical pharmacology 22 (1973) 3099-3108.
[41] H. Beltz, E. Piemont, E. Schaub, D. Ficheux, B. Roques, J.L. Darlix, Y. Mely, Role of the structure of the top half of HIV-1 cTAR DNA on the nucleic acid destabilizing activity of the nucleocapsid protein NCp7, J Mol Biol 338 (2004) 711-723.
[42] P. Kuzmic, Program DYNAFIT for the analysis of enzyme kinetic data: application to HIV proteinase, Anal Biochem 237 (1996) 260-273.
[43] B. Ganem, Y. Li, J.D. Henion, Detection of noncovalent receptor-ligand complexes by mass spectrosmetry, J. Am. Chem. Soc 113 (1991) 6294-6296.
[44] M. Peschke, U.H. Verkerk, P. Kebarle, Features of the ESI mechanism that affect the observation of multiply charged noncovalent protein complexes and the determination of the association constant by the titration method, J Am Soc Mass Spectrom 15 (2004) 1424-1434.
[45] J. Godet, H. de Rocquigny, C. Raja, N. Glasser, D. Ficheux, J.L. Darlix, Y. Mely, During the Early Phase of HIV-1 DNA Synthesis, Nucleocapsid Protein Directs Hybridization of the TAR Complementary Sequences via the Ends of their Double-stranded Stem, J Mol Biol 356 (2006) 1180-1192.
[46] S.P. Stoylov, C. Vuilleumier, E. Stoylova, H. De Rocquigny, B.P. Roques, D. Gerard, Y. Mely, Ordered aggregation of ribonucleic acids by the human immunodeficiency virus type 1 nucleocapsid protein, Biopolymers 41 (1997) 301-312.
[47] S. Bernacchi, Y. Mely, Exciton interaction in molecular beacons: a sensitive sensor for short range modifications of the nucleic acid structure, Nucleic Acids Res 29 (2001) E62.
[48] S. Bernacchi, E. Piemont, N. Potier, A. Dorsselaer, Y. Mely, Excitonic heterodimer formation in an HIV-1 oligonucleotide labeled with a donor-acceptor pair used for fluorescence resonance energy transfer, Biophys J 84 (2003) 643-654.
[49] A.J. Heck, R.H. Van Den Heuvel, Investigation of intact protein complexes by mass spectrometry, Mass Spectrom Rev 23 (2004) 368-389.
[50] C. Stehlin-Gaon, D. Willmann, D. Zeyer, S. Sanglier, A. Van Dorsselaer, J.P. Renaud, D. Moras, R. Schule, All-trans retinoic acid is a ligand for the orphan nuclear receptor ROR beta, Nat Struct Biol 10 (2003) 820-825.
[51] S. Sanglier, W. Bourguet, P. Germain, V. Chavant, D. Moras, H. Gronemeyer, N. Potier, A. Van Dorsselaer, Monitoring ligand-mediated nuclear receptor-coregulator interactions by noncovalent mass spectrometry, Eur J Biochem 271 (2004) 4958-4967.
[52] S. Dhe-Paganon, K. Duda, M. Iwamoto, Y.I. Chi, S.E. Shoelson, Crystal structure of the HNF4 alpha ligand binding domain in complex with endogenous fatty acid ligand, J Biol Chem 277 (2002) 37973-37976.

[53] J.A. Kallen, J.M. Schlaeppi, F. Bitsch, S. Geisse, M. Geiser, I. Delhon, B. Fournier, X-ray structure of the hRORalpha LBD at 1.63 A: structural and functional data that cholesterol or a cholesterol derivative is the natural ligand of RORalpha, Structure 10 (2002) 1697-1707.
[54] N. Potier, I.M. Billas, A. Steinmetz, C. Schaeffer, A. van Dorsselaer, D. Moras, J.P. Renaud, Using nondenaturing mass spectrometry to detect fortuitous ligands in orphan nuclear receptors, Protein Sci 12 (2003) 725-733.
[55] T.D. Veenstra, L.M. Benson, T.A. Craig, A.J. Tomlinson, R. Kumar, S. Naylor, Metal mediated sterol receptor-DNA complex association and dissociation determined by electrospray ionization mass spectrometry, Nat Biotechnol 16 (1998) 262-266.
[56] G.B. Wisely, A.B. Miller, R.G. Davis, A.D. Thornquest, Jr., R. Johnson, T. Spitzer, A. Sefler, B. Shearer, J.T. Moore, T.M. Willson, S.P. Williams, Hepatocyte nuclear factor 4 is a transcription factor that constitutively binds fatty acids, Structure 10 (2002) 1225-1234.
[57] E. Yu, D. Fabris, Direct probing of RNA structures and RNA-protein interactions in the HIV-1 packaging signal by chemical modification and electrospray ionization fourier transform mass spectrometry, J Mol Biol 330 (2003) 211-223.
[58] N. Hagan, D. Fabris, Direct mass spectrometric determination of the stoichiometry and binding affinity of the complexes between nucleocapsid protein and RNA stem-loop hairpins of the HIV-1 Psi-recognition element, Biochemistry 42 (2003) 10736-10745.
[59] R.J. Fisher, M.J. Fivash, A.G. Stephen, N.A. Hagan, S.R. Shenoy, M.V. Medaglia, L.R. Smith, K.M. Worthy, J.T. Simpson, R. Shoemaker, K.L. McNitt, D.G. Johnson, C.V. Hixson, R.J. Gorelick, D. Fabris, L.E. Henderson, A. Rein, Complex interactions of HIV-1 nucleocapsid protein with oligonucleotides, Nucleic Acids Res 34 (2006) 472-484.
[60] A.I. Anzellotti, Q. Liu, M.J. Bloemink, J.N. Scarsdale, N. Farrell, Targeting retroviral Zn finger-DNA interactions: a small-molecule approach using the electrophilic nature of trans-platinum-nucleobase compounds, Chem Biol 13 (2006) 539-548.
[61] A. Rein, D.E. Ott, J. Mirro, L.O. Arthur, W.G. Rice, L.E. Henderson, Suppression of retrovirial replication: inactivation of murine leukemia virus by compounds reacting with the zinc finger in the viral nucleocapsid protein, Leukemia 11 Suppl 3 (1997) 106-108.
[62] A.G. Stephen, A. Rein, R.J. Fisher, R.H. Shoemaker, The Nucleocapsid Protein as a Target for Novel Anti-HIV Drugs, Current Drug Discovery (2003) 33-36.

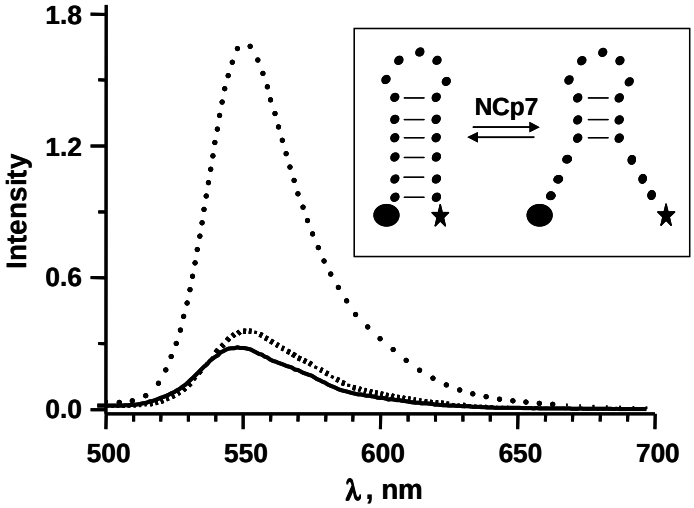

Figure 1: Principle of the assay based on cTAR destabilization by NC(12-55)
Fluorescence spectra of 0.1μM Rh6G-cTAR-DABCYL in the absence (solid line) and the presence of 1.1 μM NC(12-55) (dotted line). The fluorescence increase in the presence of NC(12-55) is due to the increase of the distance between Rh6G and DABCYL that accompanies the destabilization of the lower half of cTAR stem (inset). Addition of 1 mM EDTA (dashed line) that removes zinc from the NC fingers, leads to a complete loss of NC activity. Excitation wavelength was 480 nm. Spectra were corrected for buffer fluorescence.

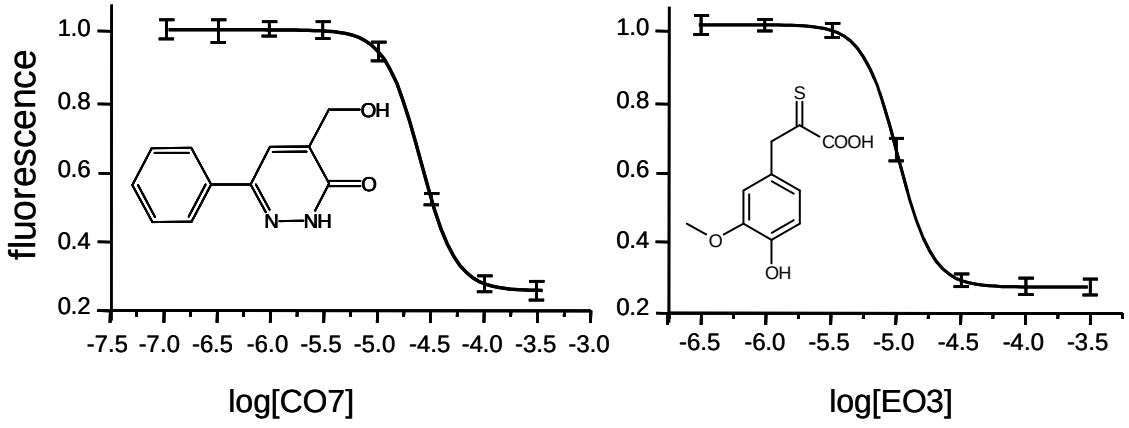

Figure 2: Inhibition of NC(12-55)-induced cTAR melting by C07 and E03 compounds.
The percentage of NC(12-55) activity is plotted as a function of the hit concentration. Data are the result of three independent experiments. The 25% residual fluorescence at high hit concentration corresponds to the fluorescence of closed cTAR.

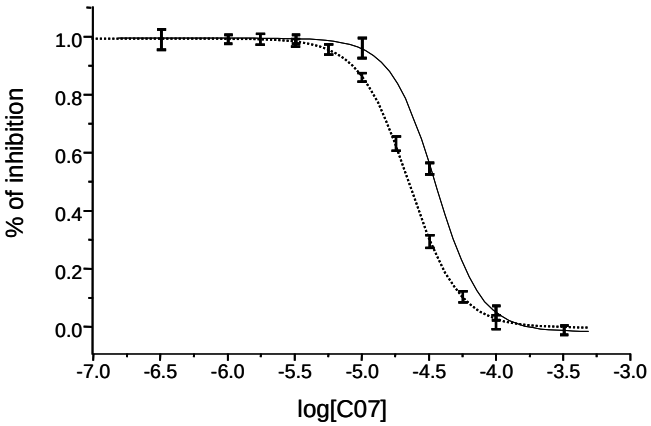

Figure 3: Effect on the pre-incubation protocol on the CO7 inhibition activity.
Rh6G-cTAR-DABCYL was pre-incubated with increasing concentrations of CO7 in the binding buffer for ten minutes followed by addition of NC(12-55) (solid line). Alternatively, cTAR and NC(12-55) were pre-incubated prior to the addition of CO7 (dotted line). K_i values deduced from both curves are 12 μM and 8.5 μM, respectively.

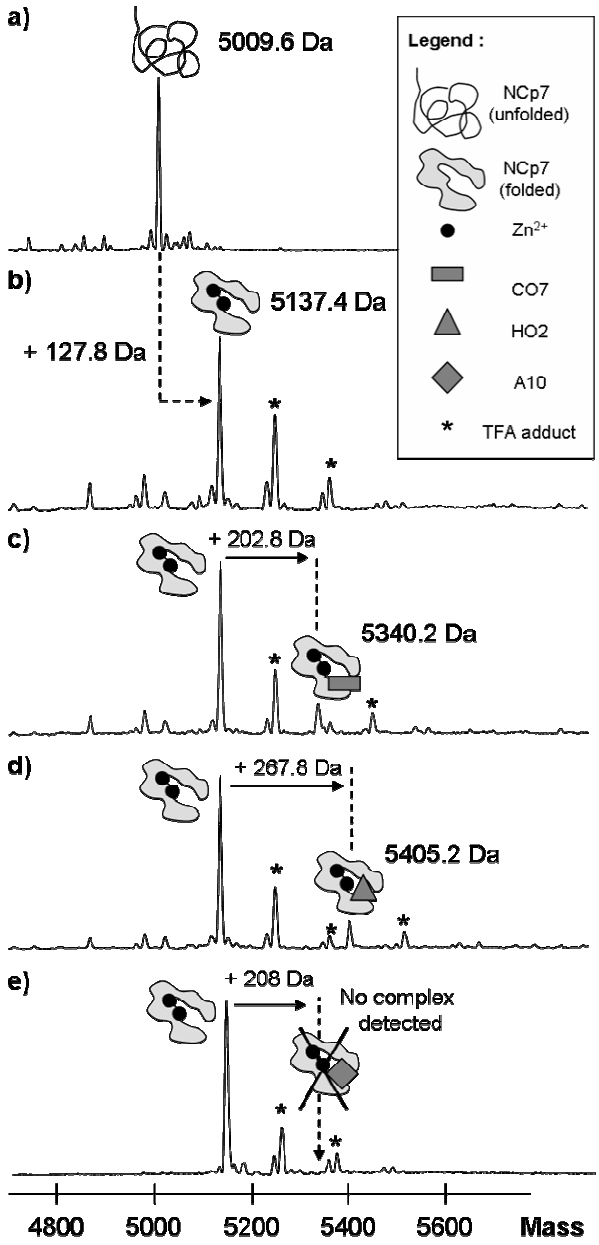

Figure 4: Binding of the hits to NC(12-55) monitored by ESI-MS

The ESI mass spectra were obtained after MaxEnt deconvolution of the multiply charged ions of the different species. a) NC(12-55) alone in denaturing conditions (in water/acetonitrile 50/50 with 1% formic acid) ; b) NC(12-55) alone in non-denaturing conditions (in $AcNH_4$ - 50 mM, pH 7.0). The peak with molecular weight of 5137.4 ± 0.2 Da corresponds to NC(12-55) with two bound zinc ions; c) NC(12-55) after addition of 5 molar equivalents of CO7 (molecular mass = 202.07 Da). The major species (~80%) corresponds to the zinc bound protein. The species (~20%) with a molecular mass of 5340.2 ± 0.7 Da, likely corresponds to a 1:1 NC(12-55):CO7 complex; d) NC(12-55) after addition of 5 molar equivalents of HO2 (268.32 Da). The species (~16%) with a molecular weight of 5405.2 ± 0.1 Da, is in line with a 1:1 NCp7: HO2 complex, (e) NC(12-55) after addition of 5 molar equivalents of A10 (208.24 Da). Only zinc bound NC(12-55) (MW = 5137.4 ± 0.2 Da) is observed but no complex of A10 with the peptide could be detected. Notice that with all hits, no zinc-free NC(12-55) could be perceived, indicating that no zinc ejection occurs.

TFA adducts coming from an incomplete desolvation process are also observed and labelled with (*).

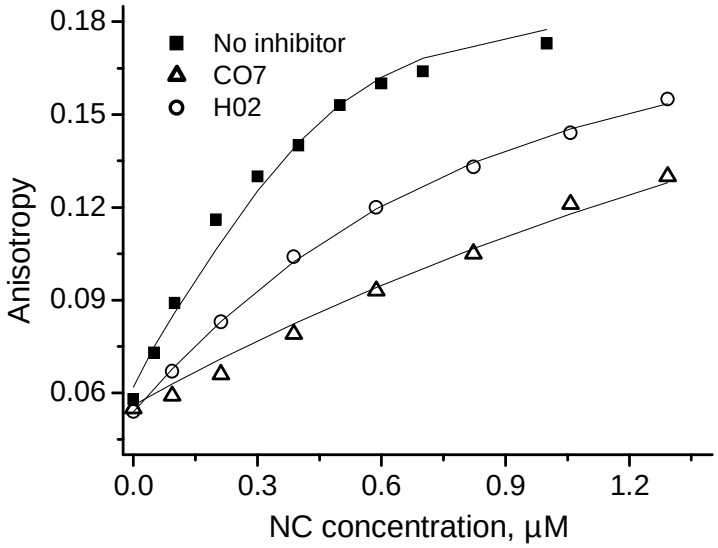

Figure 5: Binding of NC(12-55) to Fl-cTAR in the presence of CO7 and HO2 compounds. The interaction between NC(12-55) and 0.1 µM Fl-cTAR was monitored through the fluorescence anisotropy changes of Fl-cTAR. Titrations were performed either in the absence (squares) or in the presence of 30µM CO7 (triangles) or 30µM HO2 (circles). Solid lines correspond to fits of the experimental data with equation (3)

Table 1 : Structure and K_i values of the positive hits.

Ref	structure	MW	K_i (μM)	
C07	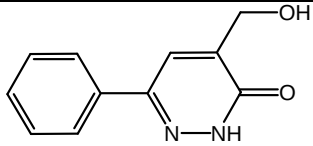	202.07	8.5 ± 0.9	4-(hydroxymethyl)-6-phenyl-2,3-dihydropyridazin-3-one
H02	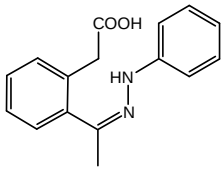	268.32	13 ± 1.0	2-{2-[1-(2-phenylhydrazin-1-ylidene)ethyl]phenyl}acetic acid
A10	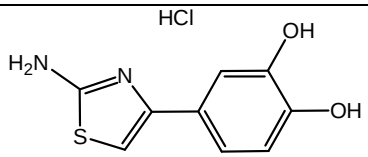	208.24	11 ±1.0	4-(2-amino-1,3-thiazol-4-yl) benzene-1,2-diol
E03	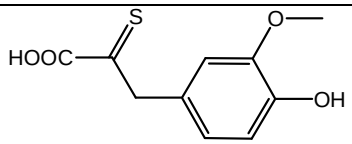	226.20	10.5 ± 0.9	3-(4-hydroxy-3-methoxyphenyl)-2-sulfanylidenepropanoic acid
H04	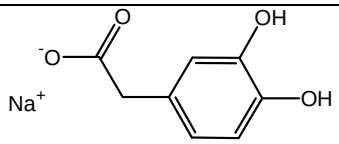	190.02	15 ±1.0	2-(3,4-dihydroxyphenyl)acetic acid

8. REFERENCES

1. Lakowicz, J. R., *New York, Kluwer Academic* **1999**.
2. Ross, J. B.; Szabo, A. G.; Hogue, C. W., *Methods Enzymol* **1997,** *278*, 151-190.
3. Twine, S. M.; Szabo, A. G., *Methods Enzymol* **2003,** *360*, 104-127.
4. Shaner, N. C.; Patterson, G. H.; Davidson, M. W., *J Cell Sci* **2007,** *120*, (Pt 24), 4247-4260.
5. Tsien, R. Y.; Miyawaki, A., *Science* **1998,** *280*, (5371), 1954-1955.
6. Heim, R.; Prasher, D. C.; Tsien, R. Y., *Proc Natl Acad Sci U S A* **1994,** *91*, (26), 12501-12504.
7. Ormo, M.; Cubitt, A. B.; Kallio, K.; Gross, L. A.; Tsien, R. Y.; Remington, S. J., *Science* **1996,** *273*, (5280), 1392-1395.
8. Sapsford, K. E.; Berti, L.; Medintz, I. L., *Angew Chem Int Ed Engl* **2006,** *45*, (28), 4562-4589.
9. Selvin, P. R., *Nat Struct Biol* **2000,** *7*, (9), 730-734.
10. Goncalves, M. S., *Chem Rev* **2009,** *109*, (1), 190-212.
11. Loudet, A.; Burgess, K., *Chem Rev* **2007,** *107*, (11), 4891-4932.
12. Panchuk-Voloshina, N.; Haugland, R. P.; Bishop-Stewart, J.; Bhalgat, M. K.; Millard, P. J.; Mao, F.; Leung, W. Y.; Haugland, R. P., *J Histochem Cytochem* **1999,** *47*, (9), 1179-1188.
13. Didenko, V. V., *Biotechniques* **2001,** *31*, (5), 1106-1116, 1118, 1120-1101.
14. Tan, L.; Li, Y.; Drake, T. J.; Moroz, L.; Wang, K.; Li, J.; Munteanu, A.; Chaoyong, J. Y.; Martinez, K.; Tan, W., *Analyst* **2005,** *130*, (7), 1002-1005.
15. Bernacchi, S.; Mely, Y., *Nucleic Acids Res* **2001,** *29*, (13), E62-62.
16. Qu, Q.; Sharom, F. J., *Biochemistry* **2001,** *40*, (5), 1413-1422.
17. Zhang, J.; Campbell, R. E.; Ting, A. Y.; Tsien, R. Y., *Nat Rev Mol Cell Biol* **2002,** *3*, (12), 906-918.
18. Weber, G.; Farris, F. J., *Biochemistry* **1979,** *18*, (14), 3075-3078.
19. Samanta, A.; Fessenden, R. W., *J Phys Chem A* **2000,** *104*, 8972-8975.
20. Catalan, J.; Perez, P.; Laynez, J.; Blanco, F. G., *J Fluorescence* **1991,** *4*, 215-223.
21. Cerezo, F. M.; Rocafort, S. C.; Sierra, P. S.; Garcia-Blanco, F.; Oliva, C. D.; Sierra, J. C., *Helv Chim Acta* **2001,** *84*, 3306-3312.
22. Chakrabarti, A.; Kelkar, D. A.; Chattopadhyay, A., *Biosci Rep* **2006,** *26*, (6), 369-386.
23. Kaur, Y.; Horowitz, P. M., *Protein J* **2004,** *23*, (7), 475-481.
24. Hiratsuka, T., *Biochemistry* **1998,** *37*, (20), 7167-7176.
25. Baudier, J.; Glasser, N.; Duportail, G., *Biochemistry* **1986,** *25*, (22), 6934-6941.
26. Lehrer, S. S.; Ishii, Y., *Biochemistry* **1988,** *27*, (16), 5899-5906.
27. Harikumar, K. G.; Pinon, D. I.; Wessels, W. S.; Prendergast, F. G.; Miller, L. J., *J Biol Chem* **2002,** *277*, (21), 18552-18560.
28. Hiratsuka, T., *J Biol Chem* **1999,** *274*, (41), 29156-29163.
29. Cohen, B. E.; McAnaney, T. B.; Park, E. S.; Jan, Y. N.; Boxer, S. G.; Jan, L. Y., *Science* **2002,** *296*, (5573), 1700-1703.
30. Nitz, M.; Mezo, A. R.; Ali, M. H.; Imperiali, B., *Chem Commun (Camb)* **2002**, (17), 1912-1913.
31. Chen, H.; Chung, N. N.; Lemieux, C.; Zelent, B.; Vanderkooi, J. M.; Gryczynski, I.; Wilkes, B. C.; Schiller, P. W., *Biopolymers* **2005,** *80*, (2-3), 325-331.
32. Lu, Z.; Lord, S. J.; Wang, H.; Moerner, W. E.; Twieg, R. J., *J Org Chem* **2006,** *71*, (26), 9651-9657.
33. Reichardt, C., *Chemical Reviews* **1994,** *94*, (8), 2319-2358.
34. Summerer, D.; Chen, S.; Wu, N.; Deiters, A.; Chin, J. W.; Schultz, P. G., *Proc Natl Acad Sci U S A* **2006,** *103*, (26), 9785-9789.
35. Cohen, B. E.; Pralle, A.; Yao, X.; Swaminath, G.; Gandhi, C. S.; Jan, Y. N.; Kobilka, B. K.; Isacoff, E. Y.; Jan, L. Y., *Proc Natl Acad Sci U S A* **2005,** *102*, (4), 965-970.
36. Diaz, G.; Melis, M.; Batetta, B.; Angius, F.; Falchi, A., *MICRON* **2008,** *39*, (7), 819-824.
37. Eugenio Vazquez, M.; Rothman, D. M.; Imperiali, B., *Org Biomol Chem* **2004,** *2*, (14), 1965-1966.
38. Vazquez, M. E.; Blanco, J. B.; Imperiali, B., *J Am Chem Soc* **2005,** *127*, (4), 1300-1306.
39. Venkatraman, P.; Nguyen, T. T.; Sainlos, M.; Bilsel, O.; Chitta, S.; Imperiali, B.; Stern, L. J., *Nat Chem Biol* **2007,** *3*, (4), 222-228.

40. Loving, G.; Imperiali, B., *J Am Chem Soc* **2008,** *130*, (41), 13630-13638.
41. Thordarson, P.; Le Droumaguet, B.; Velonia, K., *Appl Microbiol Biotechnol* **2006,** *73*, (2), 243-254.
42. Mujumdar, R. B.; Ernst, L. A.; Mujumdar, S. R.; Lewis, C. J.; Waggoner, A. S., *Bioconjug Chem* **1993,** *4*, (2), 105-111.
43. Haugland, R. P., *Molecular Probes*
2002.
44. Tilley, S. D.; Francis, M. B., *J Am Chem Soc* **2006,** *128*, (4), 1080-1081.
45. Angell, Y. L.; Burgess, K., *Chem Soc Rev* **2007,** *36*, (10), 1674-1689.
46. Agard, N. J.; Baskin, J. M.; Prescher, J. A.; Lo, A.; Bertozzi, C. R., *ACS Chem Biol* **2006,** *1*, (10), 644-648.
47. Baskin, J. M.; Prescher, J. A.; Laughlin, S. T.; Agard, N. J.; Chang, P. V.; Miller, I. A.; Lo, A.; Codelli, J. A.; Bertozzi, C. R., *Proc Natl Acad Sci U S A* **2007,** *104*, (43), 16793-16797.
48. Kohn, M.; Breinbauer, R., *Angew Chem Int Ed Engl* **2004,** *43*, (24), 3106-3116.
49. Kapanidis, A. N.; Ebright, Y. W.; Ebright, R. H., *J Am Chem Soc* **2001,** *123*, (48), 12123-12125.
50. Griffin, B. A.; Adams, S. R.; Tsien, R. Y., *Science* **1998,** *281*, (5374), 269-272.
51. Lin, M. Z.; Wang, L., *Physiology (Bethesda)* **2008,** *23*, 131-141.
52. Merrifield, R. B., *Journal of American Chemical Society* **1963,** *85*, 149-154.
53. Frolov, Y.; Sapoznikov, Y.; Barer, S.; Pogodayev, N.; Tyukavkina, N., *Izv. Akad. Nauk SSSR* **1974,** *10*, 2364-2367.
54. Sengupta, P. K.; Kasha, M., *Chem. Phys. Lett.* **1979,** *68*, (2-3), 382-385.
55. Weller, A., *Z. Elektrochem.* **1956,** *60*, 1144-1147.
56. Ormson, S.; Brown, R., *Progress In Reaction Kinetics* **1994,** *19*, (3), 211-275.
57. Ormson, S.; Brown, R., *Progress In Reaction Kinetics* **1994,** *19*, (1), 45-91.
58. Herek, J. L.; Pedersen, S.; Banares, L.; Zewail, A. H., *J.Chem.Phys.* **1992,** *97*, 9046-9061.
59. Acuna, A. U.; Toribio, F.; Amat-Guerri, F.; Catalan, J., *J Photochem* **1985,** *30*, 339-352.
60. Laemer, F.; Elsaesser, T.; Kaiser, W., *Chem.Phys.Lett.* **1988,** *148*, 119-124.
61. Becker, R. S.; Lenoble, C.; Zein, A., *Chem Phys Lett* **1987,** *91*, 3517-3524.
62. Heller, A.; Williams, D. L., *J Phys Chem* **1970,** *74*, 4473-4480.
63. Grabowska, A.; Mordzinski, A.; Tamai, N.; Yoshihara, K., *Chem Phys Lett* **1990,** *169*, 450-456.
64. Sinha, H. K.; Dogra, S. K., *J.Chem.Phys.* **1986,** *102*, 337-347.
65. Cheng, Y. M.; Pu, S. C.; Hsu, C. J.; Lai, C. H.; Chou, P. T., *Chemphyschem* **2006,** *7*, (6), 1372-1381.
66. Sengupta, P. K.; Kasha, M., *Chem Phys Lett* **1979,** *68*, (2-3), 382-385.
67. Yushchenko, D.; Bilokin', M.; Pyvovarenko, O.; Duportail, G.; Mely, Y.; Pivovarenko, V., *Tetrahedron Letters* **2006,** *47*, (6), 905-908.
68. Yushchenko, D.; Shvadchak, V.; Klymchenko, A.; Duportail, G.; Mely, Y.; Pivovarenko, V., *New Journal Of Chemistry* **2006,** *30*, (5), 774-781.
69. McMorrow, D.; Kasha, M., *J. Phys. Chem.* **1984,** *88*, 2235-2243.
70. Chou, I.-T.; Martinez, M. L.; Clements, H., *J. Phys. Chem.* **1993,** *97*, 2618-2622.
71. Ormson, S. M.; Brown, R. G.; Vollmer, F.; Rettig, W., *J Photochem Photobiol A: Chem* **1994,** *81*, 65-72.
72. Nemkovich, N. A.; Pivovarenko, V. G.; Baumann, W.; Rubinov, A. N.; Sobchuk, A. N., *J Fluoresc* **2005,** *15*, (1), 29-36.
73. Chou, P.-T.; Martinez, M. L.; Clements, J. H., *J Phys Chem* **1993,** *97*, 2618 - 2622.
74. Swiney, T. C.; Kelley, F. D., *J Chem Phys* **1993,** *99*, 211.
75. Ercelen, S.; Klymchenko, A.; Demchenko, A., *Analytica Chimica Acta* **2002,** *464*, 273-287.
76. Ercelen, S.; Roshal, A. D.; Demchenko, A. P.; Klymchenko, A. S., *Polish J Chem* **2002,** *76*, (9), 1287-1299.
77. Klymchenko, A.; Ozturk, T.; Pivovarenko, V. G.; Demchenko, A., *Tetrahedron Lett* **2002,** *43*, 7079-7082.
78. Klymchenko, A. S.; Pivovarenko, V. G.; Demchenko, A. P., *Spectrochim Acta A Mol Biomol Spectrosc* **2003,** *59*, (4), 787-792.
79. Klymchenko, A.; Pivovarenko, V. G.; Demchenko, A., *J Phys Chem* **2003,** *107*, 4211-4216.
80. Klymchenko, A. S.; Demchenko, A. P., *Phys. Chem. Chem. Phys.* **2003,** *5*, 461-468.
81. Klymchenko, A. S.; Pivovarenko, V. G.; Demchenko, A. P., *J Phys Chem A* **2003,** *107*, 4211-4216.

82. Shynkar, V. V.; Klymchenko, A. S.; Piemont, E.; Demchenko, A. P.; Mely, Y., *J Phys Chem A* **2004,** *108*, 8151-8159.
83. Klymchenko, A.; Kenfack, C.; Duportail, G.; Mely, Y., *JOURNAL OF CHEMICAL SCIENCES* **2007,** *119*, (2), 83-89.
84. Itoh, M.; Tanimoto, Y.; Tokumura, K., *J Am Chem Soc* **1983,** *105*, (10), 3339-3340.
85. McMorrow, D.; Dzugan, T. P.; Aartsma, T. J., *Chem Phys Lett* **1984,** *103*, (6), 492-496.
86. Birks, J. B., *Photophysics of aromatic molecules*. Wiley-Interscience: New York, 1970.
87. Laws, W. R.; Brand, L., *J Phys Chem* **1979,** *83*, (7), 795-802.
88. Woolfe, G. J.; Thistlethwaite, P. J., *J Am Chem Soc* **1981,** *103*, 6916-6923.
89. Itoh, M.; Tokumura, K.; Tanimoto, Y.; Okada, Y.; Takeuchi, H.; Obi, K.; Tanaka, I., *J Am Chem Soc* **1982,** *104*, 4146-4150.
90. Swinney, T. C.; Kelley, D. F., *J. Phys. Chem.* **1993,** *99*, (1), 211-221.
91. Marks, D.; Zhang, H.; Glasbeek, M., *Chem Phys Lett* **1997,** *275*, 370-376.
92. Ameer-Beg, S.; Ormson, S. M.; Matousek, P.; Towrie, M.; Nibbering, E. T. J.; Foggi, P.; Neuwahl, F. V. R.; Brown, R. G., *J Phys Chem* **2001,** *105*, 3709-3718.
93. Shynkar, V. V.; Mely, Y.; Duportail, G.; Piemont, E.; Klymchenko, A. S.; Demchenko, A. P., *J Phys Chem A* **2003,** *107*, 9522-9529.
94. Strandjord, A. J. G.; Courtney, S. H.; Friedrich, D. M.; Barbara, P. F., *J Chem Phys* **1983,** *87*, 1125-1133.
95. Strandjord, A. J. G.; Barbara, P. F., *J Chem Phys* **1985,** *89*, 2355-2361.
96. Shynkar, V.; Mely, Y.; Duportail, G.; Piemont, E.; Klymchenko, A.; Demchenko, A., *Journal Of Physical Chemistry A* **2003,** *107*, (45), 9522-9529.
97. Klymchenko, A.; Ozturk, T.; Demchenko, A., *Tetrahedron Letters* **2002,** *43*, (39), 7079-7082.
98. Premvardhan, L. L.; Peteanu, L. A., *J Phys Chem* **1999,** *103*, 7506-7514.
99. Klymchenko, A. S.; Pivovarenko, V. G.; Ozturk, T.; Demchenko, A. P., *New J Chem* **2003,** *27*, 1336-1343.
100. Klymchenko, A. S.; Mely, Y., *Tetrahedron Letters* **2004,** *45*, 8391-8394.
101. Klymchenko, A.; Yushchenko, D.; Mely, Y., *Journal Of Photochemistry And Photobiology A-Chemistry* **2007,** *192*, (2-3), 93-97.
102. Cheng, Y. M.; Pu, S. C.; Yu, Y. C.; Chou, P. T.; Huang, C. H.; Chen, C. T.; Li, T. H.; Hu, W. P., *J Phys Chem A* **2005,** *109*, (51), 11696-11706.
103. Klymchenko, A. S.; Demchenko, A. P., *New J Chem* **2004,** *28*, 687-692.
104. Sytnik, A.; Gormin, D.; Kasha, M., *Proc Natl Acad Sci U S A* **1994,** *91*, (25), 11968-11972.
105. Ercelen, S.; Klymchenko, A. S.; Demchenko, A. P., *FEBS Lett* **2003,** *538*, (1-3), 25-28.
106. Ercelen, S.; Klymchenko, A. S.; Mely, Y.; Demchenko, A. P., *Int J Biol Macromol* **2005,** *35*, (5), 231-242.
107. Sytnik, A.; Litvinyuk, I., *Proc Natl Acad Sci U S A* **1996,** *93*, (23), 12959-12963.
108. Klymchenko, A. S.; Avilov, S. V.; Demchenko, A. P., *Anal Biochem* **2004,** *329*, (1), 43-57.
109. Klymchenko, A. S.; Demchenko, A. P., *J Am Chem Soc* **2002,** *124*, (41), 12372-12379.
110. Klymchenko, A.; Demchenko, A., *SPIE Proceedings* **2002,** *4938*, 323-330.
111. Avilov, S. V.; Bode, C.; Tolgyesi, F. G.; Klymchenko, A. S.; Fidy, J.; Demchenko, A. P., *Biopolymers* **2005,** *78*, (6), 340-348.
112. Avilov, S. V.; Bode, C.; Tolgyesi, F. G.; Klymchenko, A. S.; Fidy, J.; Demchenko, A. P., *Int J Biol Macromol* **2005,** *36*, (5), 290-298.
113. Enander, K.; Choulier, L.; Olsson, A. L.; Yushchenko, D. A.; Kanmert, D.; Klymchenko, A. S.; Demchenko, A. P.; Mely, Y.; Altschuh, D., *Bioconjug Chem* **2008**.
114. Epand, R. M.; Kraayenhof, R., *Chem. Phys. Lipids* **1999,** *101*, 57–64.
115. Klymchenko, A. S.; Duportail, G.; Ozturk, T.; Pivovarenko, V. G.; Mely, Y.; Demchenko, A. P., *Chem Biol* **2002,** *9*, (11), 1199-1208.
116. Klymchenko, A. S.; Duportail, G.; Mely, Y.; Demchenko, A. P., *Proc Natl Acad Sci U S A* **2003,** *100*, (20), 11219-11224.
117. Shynkar, V. V.; Klymchenko, A. S.; Duportail, G.; Demchenko, A. P.; Mely, Y., *Biochim Biophys Acta* **2005,** *1712*, (2), 128-136.
118. Duportail, G.; Klymchenko, A.; Mely, Y.; Demchenko, A., *FEBS Lett* **2001,** *508*, (2), 196-200.
119. Duportail, G.; Klymchenko, A.; Mely, Y.; Demchenko, A., *J Fluorescence* **2002,** *12*, 181-185.

120. Klymchenko, A. S.; Duportail, G.; Demchenko, A. P.; Mely, Y., *Biophys J* **2004,** *86*, (5), 2929-2941.
121. Klymchenko, A. S.; Mely, Y.; Demchenko, A. P.; Duportail, G., *Biochim Biophys Acta* **2004,** *1665*, (1-2), 6-19.
122. Shynkar, V. V.; Klymchenko, A. S.; Kunzelmann, C.; Duportail, G.; Muller, C. D.; Demchenko, A. P.; Freyssinet, J. M.; Mely, Y., *J Am Chem Soc* **2007,** *129*, (7), 2187-2193.
123. Das, R.; Klymchenko, A. S.; Duportail, G.; Mely, Y., *J Phys Chem B* **2008,** *112*, (38), 11929-11935.
124. M'baye, G.; Mely, Y.; Duportail, G.; Klymchenko, A., *Biophysical Journal* **2008,** *95*, (3), 1217-1225.
125. Wapling, J., S. Srivastava, M. Shehu-Xhilaga et G. Tachedjian, *Drug Target Insights* **2007,** *2*, 159-182.
126. Frankel, A. D.; Young, J. A., *Annu Rev Biochem* **1998,** *67*, 1-25.
127. Russell, R. S.; Liang, C.; Wainberg, M. A., *Retrovirology* **2004,** *1*, 23.
128. Gatignol, A.; Kumar, A.; Rabson, A.; Jeang, K. T., *Proc Natl Acad Sci U S A* **1989,** *86*, (20), 7828-7832.
129. Peterlin, B. M.; Luciw, P. A.; Barr, P. J.; Walker, M. D., *Proc Natl Acad Sci U S A* **1986,** *83*, (24), 9734-9738.
130. Prats, A. C.; Sarih, L.; Gabus, C.; Litvak, S.; Keith, G.; Darlix, J. L., *Embo J* **1988,** *7*, (6), 1777-1783.
131. Skripkin, E.; Paillart, J. C.; Marquet, R.; Ehresmann, B.; Ehresmann, C., *Proc Natl Acad Sci U S A* **1994,** *91*, (11), 4945-4949.
132. Ashe, M. P.; Pearson, L. H.; Proudfoot, N. J., *Embo J* **1997,** *16*, (18), 5752-5763.
133. Hayashi, T.; Shioda, T.; Iwakura, Y.; Shibuta, H., *Virology* **1992,** *188*, (2), 590-599.
134. Clever, J. L.; Eckstein, D. A.; Parslow, T. G., *J Virol* **1999,** *73*, (1), 101-109.
135. Helga-Maria, C.; Hammarskjold, M. L.; Rekosh, D., *J Virol* **1999,** *73*, (5), 4127-4135.
136. Sierra, S.; Kupfer, B.; Kaiser, R., *J Clin Virol* **2005,** *34*, (4), 233-244.
137. Ganser-Pornillos, B. K.; Yeager, M.; Sundquist, W. I., *Curr Opin Struct Biol* **2008,** *18*, (2), 203-217.
138. Fiorentini, S.; Marini, E.; Caracciolo, S.; Caruso, A., *New Microbiol* **2006,** *29*, (1), 1-10.
139. Gamble, T. R.; Yoo, S.; Vajdos, F. F.; von Schwedler, U. K.; Worthylake, D. K.; Wang, H.; McCutcheon, J. P.; Sundquist, W. I.; Hill, C. P., *Science* **1997,** *278*, (5339), 849-853.
140. Berthet-Colominas, C.; Monaco, S.; Novelli, A.; Sibai, G.; Mallet, F.; Cusack, S., *Embo J* **1999,** *18*, (5), 1124-1136.
141. Wang, J. Y.; Ling, H.; Yang, W.; Craigie, R., *Embo J* **2001,** *20*, (24), 7333-7343.
142. Delelis, O.; Carayon, K.; Saib, A.; Deprez, E.; Mouscadet, J. F., *Retrovirology* **2008,** *5*, 114.
143. Suzuki, Y.; Craigie, R., *Nat Rev Microbiol* **2007,** *5*, (3), 187-196.
144. Rice, P.; Craigie, R.; Davies, D. R., *Curr Opin Struct Biol* **1996,** *6*, (1), 76-83.
145. Guiot, E.; Carayon, K.; Delelis, O.; Simon, F.; Tauc, P.; Zubin, E.; Gottikh, M.; Mouscadet, J. F.; Brochon, J. C.; Deprez, E., *J Biol Chem* **2006,** *281*, (32), 22707-22719.
146. Delelis, O.; Carayon, K.; Guiot, E.; Leh, H.; Tauc, P.; Brochon, J. C.; Mouscadet, J. F.; Deprez, E., *J Biol Chem* **2008,** *283*, (41), 27838-27849.
147. Jeang, K. T.; Xiao, H.; Rich, E. A., *J Biol Chem* **1999,** *274*, (41), 28837-28840.
148. Cullen, B. R., *Faseb J* **1991,** *5*, (10), 2361-2368.
149. Selby, M. J.; Peterlin, B. M., *Cell* **1990,** *62*, (4), 769-776.
150. Dingwall, C.; Ernberg, I.; Gait, M. J.; Green, S. M.; Heaphy, S.; Karn, J.; Lowe, A. D.; Singh, M.; Skinner, M. A., *Embo J* **1990,** *9*, (12), 4145-4153.
151. Rana, T. M.; Jeang, K. T., *Arch Biochem Biophys* **1999,** *365*, (2), 175-185.
152. Lake, J. A.; Carr, J.; Feng, F.; Mundy, L.; Burrell, C.; Li, P., *J Clin Virol* **2003,** *26*, (2), 143-152.
153. Egele, C.; Barbier, P.; Didier, P.; Piemont, E.; Allegro, D.; Chaloin, O.; Muller, S.; Peyrot, V.; Mely, Y., *Retrovirology* **2008,** *5*, 62.
154. Sheehy, A. M.; Gaddis, N. C.; Choi, J. D.; Malim, M. H., *Nature* **2002,** *418*, (6898), 646-650.
155. Holmes, R. K.; Koning, F. A.; Bishop, K. N.; Malim, M. H., *J Biol Chem* **2007,** *282*, (4), 2587-2595.
156. Bernacchi, S.; Henriet, S.; Dumas, P.; Paillart, J. C.; Marquet, R., *J Biol Chem* **2007,** *282*, (36), 26361-26368.
157. Strebel, K., *Adv Pharmacol* **2007,** *55*, 199-232.
158. Fischer, W. B., *FEBS Lett* **2003,** *552*, (1), 39-46.
159. Das, S. R.; Jameel, S., *Indian J Med Res* **2005,** *121*, (4), 315-332.
160. Schwartz, O.; Marechal, V.; Le Gall, S.; Lemonnier, F.; Heard, J. M., *Nat Med* **1996,** *2*, (3), 338-342.
161. Swigut, T.; Iafrate, A. J.; Muench, J.; Kirchhoff, F.; Skowronski, J., *J Virol* **2000,** *74*, (12), 5691-5701.

162. Pollard, V. W.; Malim, M. H., *Annu Rev Microbiol* **1998,** *52*, 491-532.
163. Thomas, J. A.; Gorelick, R. J., *Virus Res* **2008,** *134*, (1-2), 39-63.
164. Turner, B. G.; Summers, M. F., *J Mol Biol* **1999,** *285*, (1), 1-32.
165. D'Souza, V.; Summers, M. F., *Nat Rev Microbiol* **2005,** *3*, (8), 643-655.
166. Morellet, N.; de Rocquigny, H.; Mely, Y.; Jullian, N.; Demene, H.; Ottmann, M.; Gerard, D.; Darlix, J. L.; Fournie-Zaluski, M. C.; Roques, B. P., *J Mol Biol* **1994,** *235*, (1), 287-301.
167. Morellet, N.; Jullian, N.; De Rocquigny, H.; Maigret, B.; Darlix, J. L.; Roques, B. P., *Embo J* **1992,** *11*, (8), 3059-3065.
168. Summers, M. F.; Henderson, L. E.; Chance, M. R.; Bess, J. W., Jr.; South, T. L.; Blake, P. R.; Sagi, I.; Perez-Alvarado, G.; Sowder, R. C., 3rd; Hare, D. R.; et al., *Protein Sci* **1992,** *1*, (5), 563-574.
169. Lee, B. M.; De Guzman, R. N.; Turner, B. G.; Tjandra, N.; Summers, M. F., *J Mol Biol* **1998,** *279*, (3), 633-649.
170. Bombarda, E.; Morellet, N.; Cherradi, H.; Spiess, B.; Bouaziz, S.; Grell, E.; Roques, B. P.; Mely, Y., *J Mol Biol* **2001,** *310*, (3), 659-672.
171. Mely, Y.; De Rocquigny, H.; Morellet, N.; Roques, B. P.; Gerad, D., *Biochemistry* **1996,** *35*, (16), 5175-5182.
172. Yuan, Y.; Kerwood, D. J.; Paoletti, A. C.; Shubsda, M. F.; Borer, P. N., *Biochemistry* **2003,** *42*, (18), 5259-5269.
173. Krishnamoorthy, G.; Roques, B.; Darlix, J. L.; Mely, Y., *Nucleic Acids Res* **2003,** *31*, (18), 5425-5432.
174. Lapadat-Tapolsky, M.; De Rocquigny, H.; Van Gent, D.; Roques, B.; Plasterk, R.; Darlix, J. L., *Nucleic Acids Res* **1993,** *21*, (4), 831-839.
175. Tanchou, V.; Gabus, C.; Rogemond, V.; Darlix, J. L., *J Mol Biol* **1995,** *252*, (5), 563-571.
176. You, J. C.; McHenry, C. S., *J Biol Chem* **1993,** *268*, (22), 16519-16527.
177. Mely, Y.; de Rocquigny, H.; Sorinas-Jimeno, M.; Keith, G.; Roques, B. P.; Marquet, R.; Gerard, D., *J Biol Chem* **1995,** *270*, (4), 1650-1656.
178. Fisher, R. J.; Rein, A.; Fivash, M.; Urbaneja, M. A.; Casas-Finet, J. R.; Medaglia, M.; Henderson, L. E., *J Virol* **1998,** *72*, (3), 1902-1909.
179. Urbaneja, M. A.; Kane, B. P.; Johnson, D. G.; Gorelick, R. J.; Henderson, L. E.; Casas-Finet, J. R., *J Mol Biol* **1999,** *287*, (1), 59-75.
180. Morellet, N.; Demene, H.; Teilleux, V.; Huynh-Dinh, T.; de Rocquigny, H.; Fournie-Zaluski, M. C.; Roques, B. P., *J Mol Biol* **1998,** *283*, (2), 419-434.
181. Basu, V. P.; Song, M.; Gao, L.; Rigby, S. T.; Hanson, M. N.; Bambara, R. A., *Virus Res* **2008,** *134*, (1-2), 19-38.
182. Vuilleumier, C.; Bombarda, E.; Morellet, N.; Gerard, D.; Roques, B. P.; Mely, Y., *Biochemistry* **1999,** *38*, (51), 16816-16825.
183. Cimarelli, A.; Darlix, J. L., *Cell Mol Life Sci* **2002,** *59*, (7), 1166-1184.
184. Muriaux, D.; Darlix, J. L.; Cimarelli, A., *Curr Pharm Des* **2004,** *10*, (30), 3725-3739.
185. Amarasinghe, G. K.; De Guzman, R. N.; Turner, R. B.; Summers, M. F., *J Mol Biol* **2000,** *299*, (1), 145-156.
186. Shubsda, M. F.; Kirk, C. A.; Goodisman, J.; Dabrowiak, J. C., *Biophys Chem* **2000,** *87*, (2-3), 149-165.
187. Amarasinghe, G. K.; Zhou, J.; Miskimon, M.; Chancellor, K. J.; McDonald, J. A.; Matthews, A. G.; Miller, R. R.; Rouse, M. D.; Summers, M. F., *J Mol Biol* **2001,** *314*, (5), 961-970.
188. De Guzman, R. N.; Wu, Z. R.; Stalling, C. C.; Pappalardo, L.; Borer, P. N.; Summers, M. F., *Science* **1998,** *279*, (5349), 384-388.
189. Amarasinghe, G. K.; De Guzman, R. N.; Turner, R. B.; Chancellor, K. J.; Wu, Z. R.; Summers, M. F., *J Mol Biol* **2000,** *301*, (2), 491-511.
190. Darlix, J. L.; Lapadat-Tapolsky, M.; de Rocquigny, H.; Roques, B. P., *J Mol Biol* **1995,** *254*, (4), 523-537.
191. Berthoux, L.; Pechoux, C.; Ottmann, M.; Morel, G.; Darlix, J. L., *J Virol* **1997,** *71*, (9), 6973-6981.
192. Paillart, J. C.; Shehu-Xhilaga, M.; Marquet, R.; Mak, J., *Nat Rev Microbiol* **2004,** *2*, (6), 461-472.
193. de Rocquigny, H.; Ficheux, D.; Gabus, C.; Fournie-Zaluski, M. C.; Darlix, J. L.; Roques, B. P., *Biochem Biophys Res Commun* **1991,** *180*, (2), 1010-1018.
194. Khan, R.; Giedroc, D. P., *J Biol Chem* **1992,** *267*, (10), 6689-6695.
195. Rein, A.; Henderson, L. E.; Levin, J. G., *Trends Biochem Sci* **1998,** *23*, (8), 297-301.

196. Levin, J. G.; Guo, J.; Rouzina, I.; Musier-Forsyth, K., *Prog Nucleic Acid Res Mol Biol* **2005,** *80*, 217-286.
197. Godet, J.; de Rocquigny, H.; Raja, C.; Glasser, N.; Ficheux, D.; Darlix, J. L.; Mely, Y., *J Mol Biol* **2006,** *356*, (5), 1180-1192.
198. You, J. C.; McHenry, C. S., *J Biol Chem* **1994,** *269*, (50), 31491-31495.
199. Azoulay, J.; Clamme, J. P.; Darlix, J. L.; Roques, B. P.; Mely, Y., *J Mol Biol* **2003,** *326*, (3), 691-700.
200. Beltz, H.; Azoulay, J.; Bernacchi, S.; Clamme, J. P.; Ficheux, D.; Roques, B.; Darlix, J. L.; Mely, Y., *J Mol Biol* **2003,** *328*, (1), 95-108.
201. Bernacchi, S.; Stoylov, S.; Piemont, E.; Ficheux, D.; Roques, B. P.; Darlix, J. L.; Mely, Y., *J Mol Biol* **2002,** *317*, (3), 385-399.
202. Cosa, G.; Harbron, E. J.; Zeng, Y.; Liu, H. W.; O'Connor, D. B.; Eta-Hosokawa, C.; Musier-Forsyth, K.; Barbara, P. F., *Biophys J* **2004,** *87*, (4), 2759-2767.
203. Hong, M. K.; Harbron, E. J.; O'Connor, D. B.; Guo, J.; Barbara, P. F.; Levin, J. G.; Musier-Forsyth, K., *J Mol Biol* **2003,** *325*, (1), 1-10.
204. Beltz, H.; Clauss, C.; Piemont, E.; Ficheux, D.; Gorelick, R. J.; Roques, B.; Gabus, C.; Darlix, J. L.; de Rocquigny, H.; Mely, Y., *J Mol Biol* **2005,** *348*, (5), 1113-1126.
205. Guo, J.; Wu, T.; Kane, B. F.; Johnson, D. G.; Henderson, L. E.; Gorelick, R. J.; Levin, J. G., *J Virol* **2002,** *76*, (9), 4370-4378.
206. Liu, H. W.; Zeng, Y.; Landes, C. F.; Kim, Y. J.; Zhu, Y.; Ma, X.; Vo, M. N.; Musier-Forsyth, K.; Barbara, P. F., *Proc Natl Acad Sci U S A* **2007,** *104*, (13), 5261-5267.
207. Morellet, N.; Bouaziz, S.; Petitjean, P.; Roques, B. P., *J Mol Biol* **2003,** *327*, (1), 215-227.
208. Engler, A.; Stangler, T.; Willbold, D., *Eur J Biochem* **2001,** *268*, (2), 389-395.
209. Wecker, K.; Morellet, N.; Bouaziz, S.; Roques, B. P., *Eur J Biochem* **2002,** *269*, (15), 3779-3788.
210. Schuler, W.; Wecker, K.; de Rocquigny, H.; Baudat, Y.; Sire, J.; Roques, B. P., *J Mol Biol* **1999,** *285*, (5), 2105-2117.
211. Bourbigot, S.; Ramalanjaona, N.; Boudier, C.; Salgado, G. F.; Roques, B. P.; Mely, Y.; Bouaziz, S.; Morellet, N., *J Mol Biol* **2008,** *383*, (5), 1112-1128.
212. Auxilien, S.; Keith, G.; Le Grice, S. F.; Darlix, J. L., *J Biol Chem* **1999,** *274*, (7), 4412-4420.
213. Egele, C.; Schaub, E.; Ramalanjaona, N.; Piemont, E.; Ficheux, D.; Roques, B.; Darlix, J. L.; Mely, Y., *J Mol Biol* **2004,** *342*, (2), 453-466.
214. Johnson, P. E.; Turner, R. B.; Wu, Z. R.; Hairston, L.; Guo, J.; Levin, J. G.; Summers, M. F., *Biochemistry* **2000,** *39*, (31), 9084-9091.
215. Sinha, S.; Grandgenett, D. P., *J Virol* **2005,** *79*, (13), 8208-8216.
216. Thomas, J. A.; Gagliardi, T. D.; Alvord, W. G.; Lubomirski, M.; Bosche, W. J.; Gorelick, R. J., *Virology* **2006,** *353*, (1), 41-51.
217. Gorelick, R. J.; Benveniste, R. E.; Gagliardi, T. D.; Wiltrout, T. A.; Busch, L. K.; Bosche, W. J.; Coren, L. V.; Lifson, J. D.; Bradley, P. J.; Henderson, L. E.; Arthur, L. O., *Virology* **1999,** *253*, (2), 259-270.
218. Druillennec, S.; Caneparo, A.; de Rocquigny, H.; Roques, B. P., *J Biol Chem* **1999,** *274*, (16), 11283-11288.
219. Henklein, P.; Bruns, K.; Sherman, M. P.; Tessmer, U.; Licha, K.; Kopp, J.; de Noronha, C. M.; Greene, W. C.; Wray, V.; Schubert, U., *J Biol Chem* **2000,** *275*, (41), 32016-32026.
220. Zhao, L. J.; Wang, L.; Mukherjee, S.; Narayan, O., *J Biol Chem* **1994,** *269*, (51), 32131-32137.
221. Singh, S. P.; Tomkowicz, B.; Lai, D.; Cartas, M.; Mahalingam, S.; Kalyanaraman, V. S.; Murali, R.; Srinivasan, A., *J Virol* **2000,** *74*, (22), 10650-10657.
222. Bourbigot, S.; Beltz, H.; Denis, J.; Morellet, N.; Roques, B. P.; Mely, Y.; Bouaziz, S., *Biochem J* **2005,** *387*, (Pt 2), 333-341.
223. Yao, X. J.; Subbramanian, R. A.; Rougeau, N.; Boisvert, F.; Bergeron, D.; Cohen, E. A., *J Virol* **1995,** *69*, (11), 7032-7044.
224. Schuler, W.; Wecker, K.; de Rocquigny, H.; Baudat, Y.; Sire, J.; Roques, B. P., *J Mol Biol* **1999,** *285*, (5), 2105-2117.
225. Agostini, I.; Navarro, J. M.; Rey, F.; Bouhamdan, M.; Spire, B.; Vigne, R.; Sire, J., *J Mol Biol* **1996,** *261*, (5), 599-606.
226. Deniaud, A.; Brenner, C.; Kroemer, G., *Mitochondrion* **2004,** *4*, (2-3), 223-233.
227. Kino, T.; Gragerov, A.; Kopp, J. B.; Stauber, R. H.; Pavlakis, G. N.; Chrousos, G. P., *J Exp Med* **1999,** *189*, (1), 51-62.

228. Cohen, E. A.; Terwilliger, E. F.; Jalinoos, Y.; Proulx, J.; Sodroski, J. G.; Haseltine, W. A., *J Acquir Immune Defic Syndr* **1990,** *3*, (1), 11-18.
229. Fritz, J. V.; Didier, P.; Clamme, J. P.; Schaub, E.; Muriaux, D.; Cabanne, C.; Morellet, N.; Bouaziz, S.; Darlix, J. L.; Mely, Y.; de Rocquigny, H., *Retrovirology* **2008,** *5*, 87.
230. Jenkins, Y.; Pornillos, O.; Rich, R. L.; Myszka, D. G.; Sundquist, W. I.; Malim, M. H., *J Virol* **2001,** *75*, (21), 10537-10542.
231. Bachand, F.; Yao, X. J.; Hrimech, M.; Rougeau, N.; Cohen, E. A., *J Biol Chem* **1999,** *274*, (13), 9083-9091.
232. Selig, L.; Pages, J. C.; Tanchou, V.; Preveral, S.; Berlioz-Torrent, C.; Liu, L. X.; Erdtmann, L.; Darlix, J.; Benarous, R.; Benichou, S., *J Virol* **1999,** *73*, (1), 592-600.
233. de Rocquigny, H.; Petitjean, P.; Tanchou, V.; Decimo, D.; Drouot, L.; Delaunay, T.; Darlix, J. L.; Roques, B. P., *J Biol Chem* **1997,** *272*, (49), 30753-30759.
234. Tung, H. Y.; De Rocquigny, H.; Zhao, L. J.; Cayla, X.; Roques, B. P.; Ozon, R., *FEBS Lett* **1997,** *401*, (2-3), 197-201.
235. Li, M. S.; Garcia-Asua, G.; Bhattacharyya, U.; Mascagni, P.; Austen, B. M.; Roberts, M. M., *Biochem Biophys Res Commun* **1996,** *218*, (1), 352-355.
236. Goh, W. C.; Rogel, M. E.; Kinsey, C. M.; Michael, S. F.; Fultz, P. N.; Nowak, M. A.; Hahn, B. H.; Emerman, M., *Nat Med* **1998,** *4*, (1), 65-71.
237. He, J.; Choe, S.; Walker, R.; Di Marzio, P.; Morgan, D. O.; Landau, N. R., *J Virol* **1995,** *69*, (11), 6705-6711.
238. Jowett, J. B.; Planelles, V.; Poon, B.; Shah, N. P.; Chen, M. L.; Chen, I. S., *J Virol* **1995,** *69*, (10), 6304-6313.
239. Zhao, Y.; Elder, R. T., *Front Biosci* **2000,** *5*, D905-916.
240. Li, G.; Elder, R. T.; Qin, K.; Park, H. U.; Liang, D.; Zhao, R. Y., *J Biol Chem* **2007**.
241. Brasey, A.; Lopez-Lastra, M.; Ohlmann, T.; Beerens, N.; Berkhout, B.; Darlix, J. L.; Sonenberg, N., *J Virol* **2003,** *77*, (7), 3939-3949.
242. Herbreteau, C. H.; Weill, L.; Decimo, D.; Prevot, D.; Darlix, J. L.; Sargueil, B.; Ohlmann, T., *Nat Struct Mol Biol* **2005,** *12*, (11), 1001-1007.
243. Nicholson, M. G.; Rue, S. M.; Clements, J. E.; Barber, S. A., *Virology* **2006,** *349*, (2), 325-334.
244. Stewart, S. A.; Poon, B.; Jowett, J. B.; Chen, I. S., *J Virol* **1997,** *71*, (7), 5579-5592.
245. Poon, B.; Jowett, J. B.; Stewart, S. A.; Armstrong, R. W.; Rishton, G. M.; Chen, I. S., *J Virol* **1997,** *71*, (5), 3961-3971.
246. Zhu, Y.; Gelbard, H. A.; Roshal, M.; Pursell, S.; Jamieson, B. D.; Planelles, V., *J Virol* **2001,** *75*, (8), 3791-3801.
247. Popov, S.; Rexach, M.; Ratner, L.; Blobel, G.; Bukrinsky, M., *J Biol Chem* **1998,** *273*, (21), 13347-13352.
248. Vodicka, M. A.; Koepp, D. M.; Silver, P. A.; Emerman, M., *Genes Dev* **1998,** *12*, (2), 175-185.
249. Le Rouzic, E.; Mousnier, A.; Rustum, C.; Stutz, F.; Hallberg, E.; Dargemont, C.; Benichou, S., *J Biol Chem* **2002,** *277*, (47), 45091-45098.
250. Fouchier, R. A.; Meyer, B. E.; Simon, J. H.; Fischer, U.; Albright, A. V.; Gonzalez-Scarano, F.; Malim, M. H., *J Virol* **1998,** *72*, (7), 6004-6013.
251. Waldhuber, M. G.; Bateson, M.; Tan, J.; Greenway, A. L.; McPhee, D. A., *Virology* **2003,** *313*, (1), 91-104.
252. Bukrinsky, M.; Adzhubei, A., *Rev Med Virol* **1999,** *9*, (1), 39-49.
253. Piller, S. C.; Caly, L.; Jans, D. A., *Curr Drug Targets* **2003,** *4*, (5), 409-429.
254. de Noronha, C. M.; Sherman, M. P.; Lin, H. W.; Cavrois, M. V.; Moir, R. D.; Goldman, R. D.; Greene, W. C., *Science* **2001,** *294*, (5544), 1105-1108.
255. Piller, S. C.; Ewart, G. D.; Premkumar, A.; Cox, G. B.; Gage, P. W., *Proc Natl Acad Sci U S A* **1996,** *93*, (1), 111-115.
256. Coeytaux, E.; Coulaud, D.; Le Cam, E.; Danos, O.; Kichler, A., *J Biol Chem* **2003,** *278*, (20), 18110-18116.
257. De Clercq, E., *Nat Rev Drug Discov* **2007,** *6*, (12), 1001-1018.
258. Mitsuya, H.; Weinhold, K. J.; Furman, P. A.; St Clair, M. H.; Lehrman, S. N.; Gallo, R. C.; Bolognesi, D.; Barry, D. W.; Broder, S., *Proc Natl Acad Sci U S A* **1985,** *82*, (20), 7096-7100.

259. Spence, R. A.; Kati, W. M.; Anderson, K. S.; Johnson, K. A., *Science* **1995,** *267*, (5200), 988-993.
260. Haubrich, R.; Gubernick, S.; Yasothan, U.; Kirkpatrick, P., *Nature Reviews Drug Discovery* **2008,** *7*, (4), 287-288.
261. Matthews, T.; Salgo, M.; Greenberg, M.; Chung, J.; DeMasi, R.; Bolognesi, D., *Nat Rev Drug Discov* **2004,** *3*, (3), 215-225.
262. Enander, K.; Choulier, L.; Olsson, A. L.; Yushchenko, D. A.; Kanmert, D.; Klymchenko, A. S.; Demchenko, A. P.; Mely, Y.; Altschuh, D., *Bioconjug Chem* **2008,** *19*, (9), 1864-1870.
263. Sen, S.; Paraggio, N. A.; Gearheart, L. A.; Connor, E. E.; Issa, A.; Coleman, R. S.; Wilson, D. M., 3rd; Wyatt, M. D.; Berg, M. A., *Biophys J* **2005,** *89*, (6), 4129-4138.
264. Okamoto, A.; Tainaka, K.; Saito, I., *Bioconjug Chem* **2005,** *16*, (5), 1105-1111.
265. Piller, S. C., *J Neurovirol* **2001,** *7*, (2), 183-185.
266. Accola, M. A.; Ohagen, A.; Gottlinger, H. G., *J Virol* **2000,** *74*, (13), 6198-6202.
267. Feldherr, C. M.; Dworetzky, S. I., *Cell Biol Int Rep* **1988,** *12*, (9), 791-808.
268. Jacotot, E.; Ravagnan, L.; Loeffler, M.; Ferri, K. F.; Vieira, H. L.; Zamzami, N.; Costantini, P.; Druillennec, S.; Hoebeke, J.; Briand, J. P.; Irinopoulou, T.; Daugas, E.; Susin, S. A.; Cointe, D.; Xie, Z. H.; Reed, J. C.; Roques, B. P.; Kroemer, G., *J Exp Med* **2000,** *191*, (1), 33-46.
269. Sabbah, E. N.; Roques, B. P., *J Neurovirol* **2005,** *11*, (6), 489-502.
270. Klymchenko, A.; Duportail, G.; Ozturk, T.; Pivovarenko, V.; Mely, Y.; Demchenko, A., *Chemistry & Biology* **2002,** *9*, (11), 1199-1208.
271. Valeur, B., *Molecular Fluorescence*. Wiley-VCH: New-York, 2002; p 25-26.
272. Eastman, J. W., *Photochemistry and Photobiology* **1967,** *6*, (1), 55-72.
273. Chou, P.; Martinez, M.; Clements, J., *Chemical Physics Letters* **1993,** *204*, (5-6), 395-399.
274. Livesey, A. K.; Brochon, J.-C., *Biophys J* **1987,** *52*, 693-706.